Heterogeneities in fine-grained slope systems and their impact on seal quality

Thomas Praeger

Submitted in partial fulfilment of the requirements for the degree of Ph.D

Cardiff University

May 2009

UMI Number: U585572

All rights reserved

INFORMATION TO ALL USERS
The quality of this reproduction is dependent upon the quality of the copy submitted.

In the unlikely event that the author did not send a complete manuscript
and there are missing pages, these will be noted. Also, if material had to be removed,
a note will indicate the deletion.

UMI U585572
Published by ProQuest LLC 2013. Copyright in the Dissertation held by the Author.
Microform Edition © ProQuest LLC.
All rights reserved. This work is protected against
unauthorized copying under Title 17, United States Code.

ProQuest LLC
789 East Eisenhower Parkway
P.O. Box 1346
Ann Arbor, MI 48106-1346

Abstract

Fine-grained lithologies control the rates and pathways of migrating fluids in sedimentary basins, and as such, play an important role in the trapping and sealing of hydrocarbons in the subsurface. However, the capacity for mudstones to retain large hydrocarbon column heights is highly variable and closely linked to grain-size distribution. For petroleum explorers, bedding-scale variations in grain-size distributions diminish the potential capacity of seal units and may be instrumental in compromising otherwise effective sealing sequences.

Studies presented here utilise exceptional outcrop exposures and Ocean Drilling Program (ODP) sediment cores to investigate the sedimentology and heterogeneity of mudstone seal analogues. Quantitative data regarding the thickness, interconnectivity and lateral continuity of coarser beds have been collected and evaluated in the context of specific basin settings. Based on these findings, a range of depositional and post-depositional processes which are thought to govern the distribution of coarser material in deep-water environments are discussed. Utilising ODP data archives, the impact of lithological and textural heterogeneities on diagenesis and mechanical compaction of mudstone sequences are also addressed and evaluated from the perspective of seal integrity.

Outcrop studies carried out in the UK and Taranaki, New Zealand, have identified heterogeneous slope mudstone facies containing upto 40% coarse thin-beds. These discrete layers of silt and sand are often laterally continuous, ranging in thickness from millimetre-scale laminations to beds commonly 1-4 cm thick, and are shown to be below the resolution of outcrop gamma-ray spectrometry.

The examination of over 7000 m of hemipelagic slope sediment from the ODP core archives indicates that discrete coarse thin-beds comprise upto 6% of the 24 sequences examined, and that background sediments vary, reflecting differing proportions of clay, silt, sand, and biogenic material.

Data presented from 255 ODP and Integrated Ocean Drilling Program (IODP) wells suggests that lithology - primarily grain-size, plays a significant role in determining the depositional porosities of mudstone sediments and the rates at which they undergo compaction during shallow (<500 m) burial. It is suggested that the use of 'default' initial porosity values for hemipelagic sediments in basin models and decompaction analysis ignores a large range of natural variability, and could lead to significant analytical errors. Porosity profiles of buried slope mudstones also indicate that in shallow sequences, hemipelagic sediments do not

consistently conform to trends of exponentially decreasing porosity values with depth. Deviations from well constrained trends often appear to correlate with shifts in bulk lithology, suggesting that the inherent physical properties of particular intervals are responsible for varying porosity values with depth.

The diagenetic processes associated with the conversion of volcanic ash during burial are also investigated and proposed as a post-depositional mechanism capable of altering the physical properties of mudstone units.

Studies presented here highlight several depositional and post-depositional processes which may be detrimental to mudstone seal quality. This work represents a series of 'pilot studies' which aim to show that a seal evaluation and risking approach which considers these factors, will better predict the character of subsurface mudstone units.

Acknowledgements

I would firstly like to thank my supervisors Joe Cartwright and Andy Aplin for giving me the opportunity to conduct this research and for their continued support, advice, and guidance during the last three and a half years. I am also indebted to colleagues both in Cardiff and the Caprocks Project team for their invaluable input and discussions into all aspects of work and beyond.

I offer my heartfelt thanks and appreciation to friends, family, and loved ones who have never failed to provide support, motivation, and love when I have needed it most.

Thank you to everyone who has made this project possible.

Table of Contents

Abstract i
Acknowledgements iii
Table of contents iv
List of figures viii
List of tables xii

1. Thesis Introduction 1
1.1 Introduction 1
1.2 Seals 1
1.3 The Caprocks Project 9
1.4 Thesis structure 10
1.5 Methodology 12
1.6 Terms used in this thesis 12

2. Grain-size heterogeneities in outcropping slope sequences: Field studies in the Western British Isles and Taranaki basin, New Zealand 14
2.1 General fieldwork introduction 12
2.2 West Wales and Cornwall 17
2.2.1 Aims 17
2.2.2 Basin setting and stratigraphy 18
2.2.2.1 West Wales 18
2.2.2.2 Cornwall 21
2.2.3 Methods 21
2.2.4 Description of lithologies and bedding 23
2.2.4.1 West Wales 24
2.2.4.2 Cornwall 40
2.2.5 Interlayer connectivity 44
2.2.5.1 Sedimentological features 49
2.2.5.2 Structural features 52
2.2.6 Discussion 52
2.2.7 Conclusions 56

2.3 New Zealand 58
2.3.1 Aims of Taranaki field studies 58
2.3.2 Overview of Taranaki Basin and study area 59
2.3.3 Outcrop locations 61
2.3.4 Facies mapping and outcrop logs 63
2.3.4.1 Outcrop gamma-ray spectrometry 63
2.3.4.2 Radioactive elements in sediments 65

2.3.5 Facies mapping....66
2.3.5.1 Lower Weakly Bedded Unit (LWBU)....70
2.3.5.2 Lower Channelled Unit (LCU)....70
2.3.5.3 Middle Weakly Bedded Unit (MWBU)....70
2.3.5.4 Middle Channelled and Interbedded Unit (MCIU)....74
2.3.5.5 Upper Weakly Bedded Unit (UWBU)....78
2.3.5.6 Upper Channelled Unit (UCU)....78
2.3.6 Detailed sedimentary logs and gamma-ray spectrometry....82
2.3.7 Distribution of potential flow units: Sand bodies and thin-beds....90
2.3.8 Physical properties analysis....92
2.3.9 Discussion and implications....93
2.3.10 Conclusions....95

3. Towards a hemipelagite database....97
3.1 Introduction....97
3.1.2 Seal-bypass mechanisms....97
3.1.3 Ocean Drilling Programs....99
3.1.4 Caprocks Hemipelagite Database....102
3.1.5 ODP and petroleum industry data....102
3.1.6 ODP coring techniques....103
3.2 Building the Caprocks Hemipelagite Database....104
3.2.1 Input Data....104
3.3.2 CHD workflow....105
3.3 ODP Site Investigations....105
3.3.1 Location 1: Carolina Slope....108
3.3.2 Location 2: West Africa....112
3.3.3 Location 3: South China Sea....120
3.3.4 Location 4: Nankai Trough....125
3.3.5 Location 5: Cascadia Margin....130
3.3.6 Location 6: Gulf of Mexico....136
3.4 Summary of ODP hemipelagic sites....144
3.5 Discussion....149
3.5.1 Controls on the distribution of thin-beds in hemipelagic sequences....149
3.5.2 Implications for hemipelagite sealing sequences....152
3.6 Conclusions....153

4. Porosity loss in shallow hemipelagic sequences....155
4.1 Introduction....155
4.2 Porosity-loss and compaction....158
4.3 Methods and Data....159
4.3.1 Porosity data....161

4.3.2 Measurement errors....161
4.4 Results....164
4.4.1 Initial porosities in hemipelagic sequences....164
4.4.2 Distribution of porosity with depth in shallow hemipelagic sequences....169
4.4.3 Influence of lithology on porosity....166
4.4.3.1 Porosity-depth plot - ODP Site 717....171
4.4.3.2 Porosity-depth plot - ODP Site 900....171
4.4.3.3 Porosity-depth plot - ODP Sites 931, 935, 936, and 944....171
4.4.3.4 Porosity-depth plot - ODP Site 976....172
4.4.3.5 Porosity-depth plot - ODP Site 977....173
4.4.3.6 Porosity-depth plot - ODP Site 979....173
4.4.3.7 Porosity-depth plot - ODP Site 985....174
4.4.3.8 Porosity-depth plot - ODP Site 1146....174
4.4.3.9 Porosity-depth plot - ODP Site 1148....175
4.4.3.10 Porosity-depth plot - ODP Site 1245....175
4.4.3.11 Porosity-depth plot - IODP Site 1324....176
4.4.4 Summary of porosity-depth plots....193
4.5 Discussion....197
4.5.1 Initial porosities....197
4.5.2 Porosity distributions with depth....200
4.5.3 Porosity distributions and sediment age....201
4.6 Conclusions....201

5. Diagenesis in shallow ash-bearing hemipelagic sequences....203
5.1 Introduction....203
5.2 Distribution of volcanic ash in marine sediments....205
5.3. Introduction to ash diagenesis....209
5.3.1 Silicic ash alteration....209
5.3.2 Basaltic ash alteration....213
5.3.3 Mass balance....213
5.3.4 Summary....215
5.4 Ash diagenesis in natural systems: Observations from the ODP....215
5.4.1 Precipitation of authigenic phases....215
5.4.2 Pore fluid chemistries....224
5.5 Changes to sediment physical properties during ash diagenesis....226
5.6 Conclusion....235

6. Discussion: Heterogeneities in fine-grained slope sequences: Predictability and implications for seal capacity....236
6.1 Introduction....236
6.1.1 Seal capacity of fine-grained slope sequences....236

6.1.2 Global importance of hemipelagite sealing sequences....238
6.1.3 Identification of 'leaky' hemipelagic seals....242
6.2 Quantifying seal capacity: The scale problem....244
6.2.1 Seismic and well-log data....244
6.2.2 Measuring seal capacity directly: MICP analysis....245
6.3 Coarse-grained deposits in deep-water slope environments....247
6.3.1 Introduction....247
6.3.2 Gravity-driven sedimentation processes....247
6.3.3 Contourites....249
6.3.4 Influence of slope morphology....250
6.4 Grain-size heterogeneities in the wider context of seal risking....250
6.4.1 Implications of thin-bed data in seal risking....250
6.5 Towards the better prediction of slope mudstone seal quality ahead of drilling....253
6.5.1 The Caprocks Project seismic genetic units approach....253
6.5.2 A sequence stratigraphic approach....255
6.6 Post-depositional processes: Hemipelagite compaction and ash diagenesis....257
6.6.1 Hemipelagite compaction and overpressure development....257
6.6.2 Effects of ash diagenesis on mudstone physical properties....260

7. Conclusions....264

8. Future research....**266**
8.1 Further characterisation of genetic units....266
8.2 Porosity-loss trends for fine-grained facies....266
8.3 The importance of ash diagenesis in mudstone seals....267

References....**268**

Appendices....**306**
Appendix 1 – Urenui Fm. sample physical properties sheets....307
Appendix 2 – Caprocks Hemipelagite Database (CD-ROM inside back-cover).

List of Figures

Chapter 1. Thesis Introduction

Figure 1.1 Structure of the Caprocks Project....2
Figure 1.2 Schematic illustration of a membrane seal....4
Figure 1.3 Core photographs from a Tertiary mudstone caprock....6
Figure 1.4 Petroleum system data from a Tertiary oilfield imaged at seismic, wireline, and core scales....7

Chapter 2. Grain-size heterogeneities in outcropping slope sequences: Field studies in the Western British Isles and Taranaki basin, New Zealand.

Figure 2.1 Mudstone core and outcrop comparison....16
Figure 2.2 Map showing the geology of the area around Cardigan and Dina Island, West Wales....19
Figure 2.3 Map showing the location of studied outcrop sections from the Cardigan area....19
Figure 2.4 Map showing the location of outcrop sites examined around the town of Bude, Cornwall....22
Figure 2.5 Bude Formation exposured just north of Upton Cross....22
Figure 2.6 Thin section micrographs showing grain-size heterogeneity in mudstone from Aber....25
Figure 2.7 Aerial photograph showing Aber Rhigian wave-cut platform....25
Figure 2.8a Outcrop lithofacies correlation panel at Aber Rhigian....26
Figure 2.8b High-resolution sedimentary logs taken at Aber Rhigian exposure....27
Figure 2.9 Outcrop photographs from Aber Rhigian....28
Figure 2.10 Photo-panels of mudstone facies outcropping at Newport Sands....30
Figure 2.11 Aerial photograph of coastal inlet outcrop examined at Gwbert....31
Figure 2.12 Photo-panel of extensive mudstone outcrop at Gwbert, West Wales....31
Figure 2.13 Outcrop photographs of Nantmel Mudstones Fm. exposed at Gwbert....32
Figure 2.14 High-resolution sedimentary logs through Nantmel Mudstones Fm. exposed at Gwbert....33
Figure 2.15 Outcrop photograph of Nantmel Mudstones Fm. exposed in a beach section at Aberporth....35
Figure 2.16 High-resolution sedimentary log from Aberporth....35
Figure 2.17 Aerial photograph of exposures examined at Tresaith....36
Figure 2.18 Outcrop photograph of Nantmel Mudstones Fm. from Tresaith....36
Figure 2.19 High-resolution sedimentary logs taken from Nantmel Mudstones Fm. exposed in Tresaith....37
Figure 2.20 Aerial photography showing the location of beach sections examined at Llangrannog....38
Figure 2.21 Beach exposure of intensely deformed mudstones, Llangrannog....38
Figure 2.22 High-resolution sedimentary logs taken at Llangranog....39
Figure 2.23 Outcrop photographs of Yr Allt Fm. mudstones from Llangrannog....39
Figure 2.24 Aerial photograph showing exposures at Sandymouth Bay examined during this study....41
Figure 2.25 Bude Fm. mudstones exposed at Sandymouth Bay....41
Figure 2.26 Thinly bedded mudstones at Sandymouth bay....42
Figure 2.27 High-resolution sedimentary logs taken from Bude Fm. mudstones exposed at Sandymouth Bay....43
Figure 2.28 Aerial photograph of Bude Fm. mudstones exposed in beach sections, Upton, Cornwall....45
Figure 2.29 Bude Fm. mudstones exposed at Upton....45
Figure 2.30 High-resolution sedimentary logs taken from Bude Fm. mudstones exposed at Upton....46
Figure 2.31 Histogram plots comparing bed thickness data from outcrop studies and core....47

Figure 2.32 Sedimentological interbed connectivity mechanisms as observed from UK outcrops....51
Figure 2.33 Cartoon illustrating the potential importance of thin-beds in unfractured sequences....53
Figure 2.34 Cartoon illustrating the juxtaposition of coarser horizons in response to fracture and fault offsets....53
Figure 2.35 Structural map of the Taranaki Basin....60
Figure 2.36 Simplified geology of the North Taranaki coastal region....62
Figure 2.37 Urenui Fm. exposed in cliffs approximately 1.5km southwest of Wai-iti....64
Figure 2.38 View looking southwest at the White Cliffs of the Mt. Messenger Fm....64
Figure 2.39 Schematic stratigraphy of the Urenui Fm. as it outcrops on the North Taranaki coast....67
Figure 2.40 Schematic lithofacies transect of the Urenui Fm. from the northern Taranaki coast....68
Figure 2.40 (*cont.*) Orientation map and legend to Urenui Fm. schematic coastal transect....69
Figure 2.41 Siltstones of the lower weakly bedded unit, Urenui Fm....71
Figure 2.42 Panoramas imaging the Urenui Fm....72
Figure 2.43 Close-up image of the Whakarewa Conglomerate outcropping NE of Wai-iti Beach....73
Figure 2.44 Close-up image of thin sand laminations interbedded with siltstones of the LWBU....73
Figure 2.45 Panoramas imaging the Urenui Fm....75
Figure 2.46 Outcrop images of the middle channelled and interbedded unit outcropping at Urenui Beach....76
Figure 2.47 Onshore seismic profile showing a 2km wide channel feature within the Urenui Fm....77
Figure 2.48 Siltstones of the upper weakly bedded unit exposed in coastal section NW of Onaero Beach....79
Figure 2.49 3m high concretion found in siltstones of the upper weakly bedded unit, Urenui Fm....79
Figure 2.50 Okoki Conglomerate as it outcrops close to the base of the upper channelled unit....80
Figure 2.51 Outcrop images of a series of stacked channels above and adjacent to the Okoki conglomerate....81
Figure 2.52 Sedimentary logs and accompanying gamma-ray curves from the outcropping Urenui Fm....84
Figure 2.53 Illustrations of three common gamma-ray motifs indicative of changes in sediment grain-size....89
Figure 2.54 Sedimentary logs and gamma-ray curves taken from thinly interbedded sequences, Urenui Fm....89
Figure 2.55 Histogram plot of coarser grained thin-bed thicknesses from the Urenui Fm....91

Chapter 3. Towards a hemipelagite database

Figure 3.1 Workflow outline for the Caprocks Project Phase II genetic units study....98
Figure 3.2 Seismic profile from a major delta system, provided by industry sponsors....98
Figure 3.3 Seismic profiles taken from Cartwright et al (2007) showing bypass systems....100
Figure 3.4 Map showing the locations of Ocean Drilling Program Legs 100-210....101
Figure 3.5 Example of a thin-bed distribution plot from ODP Site 1244 on the Cascadia Margin....106
Figure 3.6 ODP core description with corresponding core photographs form Site 1244....107
Figure 3.7 Map showing the location of sites drilled during Leg 172 of the ODP....109
Figure 3.8 Seismic profiles from Carolina Slope ODP Sites 1057, 1060, and 1054....110
Figure 3.9 Thin-bed distribution plots for OPD Leg 172 on the Carolina Slope and Sohm Abyssal Plain....111
Figure 3.10 Map of the North Atlantic showing an approximate path of the Deep Western Boundary Current....113
Figure 3.11 Photographs contourites from cores recovered during ODP Leg 172....113
Figure 3.12 Map showing the location of ODP Sites 1075, 1076, and 1077 drilled in the Lower Congo Basin....115
Figure 3.13 Seismic profiles from ODP Leg 175 Sites drilled in the Lower Congo Basin....116
Figure 3.14 Map showing the location of ODP Leg 175 Sites 1078 and 1079 drilled in the Mid-Angola Basin....117
Figure 3.15 Seismic profile showing the slope position of ODP Sites 1078 and 1079 in the Mid-Angola Basin..117
Figure 3.16 Thin-bed distribution plots for OPD Leg 175 drilled in the Mid-Angola Basin, west Africa....119
Figure 3.17 Regional map of the South China Sea showing the location of the Pearl River Mouth Basin....121

Figure 3.18a Seismic profile from ODP Site 1144 in the South China Sea....121
Figure 3.18b Seismic profile from ODP Site 1146 in the South China Sea....122
Figure 3.19 Map showing the location of ODP Site 1143 in the southern South China Sea....122
Figure 3.20 Seismic image showing the hemipelagic seismic facies recorded from sediments at Site 1143....122
Figure 3.21 Thin-bed distribution plots for OPD Leg 184 in the South China Sea....124
Figure 3.22 Map showing the tectonic setting of the Nankai Trough and the Shikoku Basin....126
Figure 3.23a Stratigraphy recorded from ODP Site 1177 at the Nankai Trough....127
Figure 3.23b Seismic profile showing the location of ODP Site 1177 in the Shikoku Basin....127
Figure 3.24 Thin-bed distribution plots for OPD Leg 190 in the Nankai Trough region....129
Figure 3.25 Maps showing the tectonic setting and bathymetry of ODP Leg 204 drill sites....131
Figure 3.26 East-west 3D seismic slice showing the structural and stratigraphic setting of Leg 204 Sites....132
Figure 3.27 East-west 3D seismic slice showing the structural and stratigraphic setting of Sites 1251....132
Figure 3.28 Thin-bed distribution plots for OPD Leg 204 drilled on the Cascadia Margin....134
Figure 3.29 Map of the northern Gulf of Mexico showing the Brazos-Trinity and Mars-Ursa regions....137
Figure 3.30 SW-NE orientated 3D seismic image showing the locations of IODP Sites 1319 and 1320....137
Figure 3.31 Detailed 3D seismic image showing the structural and stratigraphic setting of Site 1319....138
Figure 3.32 Detailed seismic image showing the stratigraphy at Site 1320....138
Figure 3.33 Map showing the location of Sites 1322, 1323, and 1324 in the Mars-Ursa region, Gulf of Mexico..139
Figure 3.34 Seismic profile showing the location and stratigraphy of Mars-Ursa Sites 1322 and 1324....141
Figure 3.35 Seismic images through IODP Sites 1322 and 1324, Gulf of Mexico....141
Figure 3.36 Thin-bed distribution plots for IODP Leg 308 Sites 1319 and 1320 in the Gulf of Mexico....142
Figure 3.37 Thin-bed distribution plots for IODP Leg 308 Sites 1322 and 1324 in the Gulf of Mexico....143
Figure 3.38 Histogram plots of thin-bed measurements at the six ODP locations examined....145
Figure 3.39 Plots showing bed spacings and bed thicknesses recorded from 23 hemipelagic sequences....147
Figure 3.40 Plots of total bed number and net-to-gross for the 23 hemipelagic sequences examined here....150

Chapter 4. Porosity loss in shallow hemipelagic sequences

Figure 4.1 Relationship between porosity and depth for shales and argillaceous sediments....157
Figure 4.2 Ternary diagram used by the Ocean Drilling Program in the classification of siliciclastic sediments..163
Figure 4.3 Initial porosity values from 255 ODP and IODP drill sites, categorised by facies type....165
Figure 4.4 Distribution of initial porosity values, displayed as a histogram....167
Figure 4.5 Grouping of facies based on initial porosity values....168
Figure 4.6 Plot containing porosity-depth data from 16 hemipelagic sequences drilled by the ODP and IODP...170
Figure 4.7 Porosity-depth plots 1-13....177
Figure 4.8 Porosity-depth plots from four ODP sites which reveal trends of non-exponential porosity loss....194
Figure 4.9 Porosity-depth plots from four ODP sites which reveal trends of exponential porosity loss....195
Figure 4.10 Porosity-depth relationship for sediments at ODP Site 976 in the western Mediterranean....196
Figure 4.11 Illustrative graph decompacting a 1m column of sediment using a range of initial porosity values...198

Chapter 5. Diagenesis in shallow ash-bearing hemipelagic sequences

Figure 5.1 Thin ash beds in cored hemipelagic sediments from ODP Leg 190 at the Nankai Trough....206
Figure 5.2 Ash beds in core recovered from ODP Leg 190 - Site 1173....207
Figure 5.3 Images of bentonite layers in outcrop....208

Figure 5.4 Thin section photo showing hydration layer in rhyolitic glass sample from Japan....210
Figure 5.5 Perlitic fracturing of volcanic glass....212
Figure 5.6 Thin-section micrographs of palagonite....214
Figure 5.7 Some important publications concerning the alteration of volcanic material....216
Figure 5.8 Locations of Ocean Drilling Program drill sites examined in this work....218
Figure 5.9 Stratigraphy from Site 833 in the North Aoba Basin (New Hebrides margin, Leg 134)....219
Figure 5.10 Stratigraphy from Site 1173 in the Shikoku Basin (Nankai Trough, Leg 190)....220
Figure 5.11 Core recovered from Site 793 showing gypsum-filled fractures in a fine-sandstone interval....222
Figure 5.12 Plot showing the volume of ash material plotted against downhole depth from Site 999....223
Figure 5.13 Depth profile showing the distribution of discrete ash layer recorded at Site 998....223
Figure 5.14 Depth plot from ODP Site 1173 showing the total volume of clay minerals and dissolved silica....225
Figure 5.15 Pore water silica concentration from Site 792, Izu-Bonin Arc....225
Figure 5.16 Plot from ODP Site 832 showing concentrations of Na, K and Ca in pore-fluids....227
Figure 5.17 Depth plot showing gas permeability data from ODP Site 1173 at the Nankai Trough....229
Figure 5.18 Seismic profiles across Hydrate Ridge on the Cascadia Margin....230
Figure 5.19 Core photograph from Site 832, New Hebrides Arc....233
Figure 5.20 Photograph of normal fault surfaces from core recovered at Site 832....233
Figure 5.21 Seismic profiles from the Nankai Trough....234

Chapter 6. Discussion: Heterogeneities in fine-grained slope sequences: Predictability and implications for seal capacity

Figure 6.1 Plot showing the distribution of top seal lithologies....237
Figure 6.2 Schematic cross-section through the Balmoral Field, North Sea....239
Figure 6.3 Cross-plots comparing seal thicknesses with field hydrocarbon volumes....241
Figure 6.4 Location map and cross-section for the North Rankin field, NW Australia....243
Figure 6.5 Considerations for those making preliminary top seal evaluations....252
Figure 6.6 Seismic profile from West Africa showing hemipelagic drape deposits....254
Figure 6.7 Seismic profile from North Africa showing a channel-levee complex....254
Figure 6.8 Seismic profile from West Africa showing mass-transport complexes....256
Figure 6.9 Seismic profile interpreted using the Caprocks Project genetic units methodology....256
Figure 6.10 Schematic idealised sequence stratigraphic framework....258
Figure 6.11 Stratigraphic column and porosity-depth profile from ODP Site 1173, Nankai Tough....261

List of Tables

Table 2.1 General information regarding the outcrop exposures studied in west Wales and Cornwall.....20

Table 2.2 Measured characteristic of thin-beds from mudstone examined in West Wales and Cornwall.....48

Table 4.1 Location information for the 16 hemipelagic sequences examined in chapter 4.....160

Table 6.1 Data from 20 oilfields where hemipelagic top seals are present.....240

Chapter 1

Chapter 1

Introduction: Thesis aims and rationale

1.1 Introduction

The work presented in this thesis was carried out as part of the ongoing Caprocks Project, a multidisciplinary collaboration between international petroleum companies and researchers at Newcastle, Cardiff and Heriot Watt Universities. The Caprocks Project focuses on the fine-grained section of sedimentary basins, developing insight into the related process of petroleum trapage and leakage. The objective of the Caprocks Project is to develop methodologies with which to quantify seal risk and to define the rates, mechanisms and pathways by which petroleum migrates through kilometre thick sequences of fine-grained sediment.

The Caprocks Project academic research team comprises scientists with a range of expertise including sedimentologists, structural geologists, geochemists, mathematicians, and geo-modellers. Utilising this array of skills, the Caprocks Project has undertaken the task of integrating geological, geophysical and petrophysical data from both industrial and academic sources with the aim of developing our understanding of fluid-flow in mudstones (Fig. 1.1).

1.2 Seals

Sealing rocks or 'caprocks' are an essential element of any hydrocarbon system, providing a barrier to migrating oil and gas. Rock units can act as effective hydrocarbon seals providing the minimum displacement pressure, or capillary entry pressure (CEP), of the unit is greater than the buoyancy pressure exerted by the hydrocarbon column beneath (e.g. Watts, 1987). The CEP of a rock is largely governed by pore-throat size, which is a function of the grain-size distribution (e.g. Downey, 1994). Fine-grained clastic rocks dominated by silt and clay sized particles (<4μm) generally exhibit high capillary entry pressures, and are therefore among the most commonly encountered caprock lithologies, along with evaporites and organic-rich rocks (Downey, 1994; Schlomer and Krooss, 1997).

While the physical properties of mudstones are known to be well suited to retarding the flow of migrating phases, the huge volumes of petroleum accumulated above thick sequences of

Figure 1.1 Structure of the Caprocks Project. The project relies on close collaboration between institutions and scientists to develop ideas and to conduct multidisciplinary research.

fine-grained sediment in most petroleum systems are a testament to the capacity of caprock sequences to transmit petroleum on geological timescales (Macgregor, 1996; Weber, 1997). Seal leakage is commonly identified (Caillet, 1993; Leith et al., 1993; Leith and Fallick, 1997; Losh et al., 1999; O'Brien et al., 1999; Gartrell et al., 2002; Nordgard Bolas and Hermanrud, 2003; Boles et al., 2004) although it remains poorly quantified (Brown, 2000). Failure of unfaulted sealing intervals can occur in one of two ways, as outlined by Watts (1987). Membrane leakage, or capillary leakage, occurs when the CEP of the seal is equalled or exceeded by the hydrocarbon column, allowing phases to enter the sealing rock, displacing formation fluids and migrate through pathways of connected permeability, shown schematically in Figure 1.2. In instances where the CEP of a unit is extremely high, such as in some evaporites and tight shales, pore pressures at the reservoir-seal interface may increase to a point where the effective minimum stress of the seal rock is exceed before the CEP is met, leading to hydraulic fracturing (e.g. Gullfaks Field, North Sea (Løseth et al. 2008). The term 'hydraulic seal' is given to caprocks which fail under these conditions (Watts, 1987).

During hydrocarbon exploration and seal risking, assumptions regarding the probability of seal failure, or seal capacity, of a caprock will significantly influence the estimated trap volume (Bishop, 1983). Evaluations of the likely minimum CEP of a unit, as well as the range and distribution of permeability values throughout the sealing sequence, are key considerations for those calculating hydrocarbon column heights and risking potential assets. Despite their economic importance as seals, our understanding of the physical and fluid-flow properties of fine-grained clastic sediments lags far behind that for other sedimentary rock types, and the physical processes of leakage through these rocks remain poorly understood (Watts, 1987; Dewhurst et al., 1999b; Slatt, 2003).

A growing database of measured and modelled fluid-flow properties of mudstones is becoming available, highlighting the significant range of permeabilities and CEP values that can be expected for mudstones and shales (e.g. Neuzil, 1994; Dewhurst et al., 1998). Permeabilities reported by Yang and Aplin (2007) indicate that mudstones dominated by silt-sized grains may have permeabilities three orders of magnitude higher than those of clay-dominated mudstones at similar porosities. This work highlights the need for a better understanding of the distribution of grain-size heterogeneities in mudstone units and that where the degree of heterogeneity is unknown, that making accurate predictions as to the sealing capacity of a caprock unit is difficult.

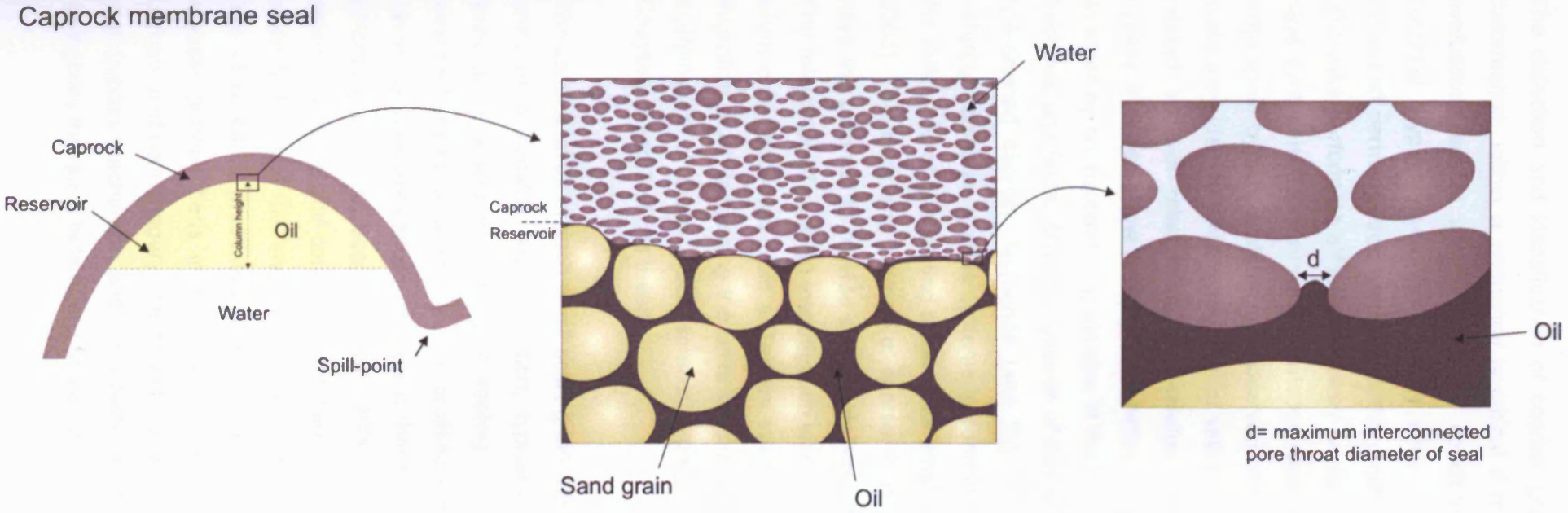

Figure 1.2 schematic illustrations of a membrane or capillary seal. The migration of oil from the reservoir into the overlying seal requires the capillary entry pressure (CEP) of the seal unit be equalled or exceeded by the buoyancy pressure of the hydrocarbon column. If this occurs, hydrocarbons may migrate into the seal unit by displacing formation fluids. A units CEP is strongly influenced by the pore-throat size, which is related to grain-size distribution. Figure adapted and redrawn from Watts (1987).

The detection and identification of coarser grained units, as well as zones of structural deformation, within a sequence is critical if modelled fluid-flow simulations and seal risk evaluations are to accurately reflect conditions in the subsurface. Such features offer potential 'bypass' systems, creating entry points and pathways of reduced CEP and increased permeabilities which have the potential to transmit fluids across units which may otherwise perform as effective capillary seals. In their recent paper, Cartwright et al. (2007) have synthesised the current knowledge regarding the identification and potential impact of large-scale bypass systems, as observed from outcrop and seismic imagery. At this large-scale they identify three categories of seismically resolvable bypass systems, namely fault-related, intrusion-related, and pipe-related systems. Such features are seen to allow the bypass of a seal's low porosity pore-network by providing pathways of higher permeability, whether by an increase in grain-size in the case of sand injections, or through transmissive fractures and faults. Bypass systems of this scale have the potential to span kilometres of fine-grained caprock sequence (*see* Fig. 3.3). Investigations into centimetric grain-size heterogeneities as bypass systems in contrast, have not received the same attention given the difficulties of interpreting small-scale amplitude anomalies in seismic data (Løseth et al., 2008). Thin-beds and laminae of coarser material interspersed within a high CEP lithology have the potential to provide a relatively high permeability/low CEP fluid migration pathway. The relevance of such an investigation was brought to the attention of the Caprocks Project when core recovered from a Tertiary sealing sequence revealed thin-beds facilitating the migration of oil, bypassing the units low porosity pore-network, shown in Figure 1.3. It is the examination of these much smaller bypass features which forms the central theme of Chapters 2 and 3 of this thesis.

The consideration of such small scale grain-size heterogeneities requires evaluation of these units at a suitably high-resolution, typically not carried out during petroleum system exploration, where the coring of sealing lithologies is extremely rare. The resolution of wireline logging tools and seismic profiling critically limits the detection of heterogeneities within caprock sequences, rendering these features essentially invisible to explorationists (Worthington, 2000; Scaglioni et al., 2006). This rationale is illustrated in Figure 1.4 where seismic, wireline and core data, sourced from a sponsor company, have been integrated in order to highlight the 'invisibility' of four intervals of thinly bedded mudstone caprocks. The aim of research presented here is therefore to document and quantify the existence of coarser grained beds in fine-grained clastic successions from detailed examinations of outcrop and core imagery. It is hoped these investigations will aid evaluations of this potential seal bypass mechanism and allow better informed seal risk analyses where there is a high probability that such heterogeneities exist.

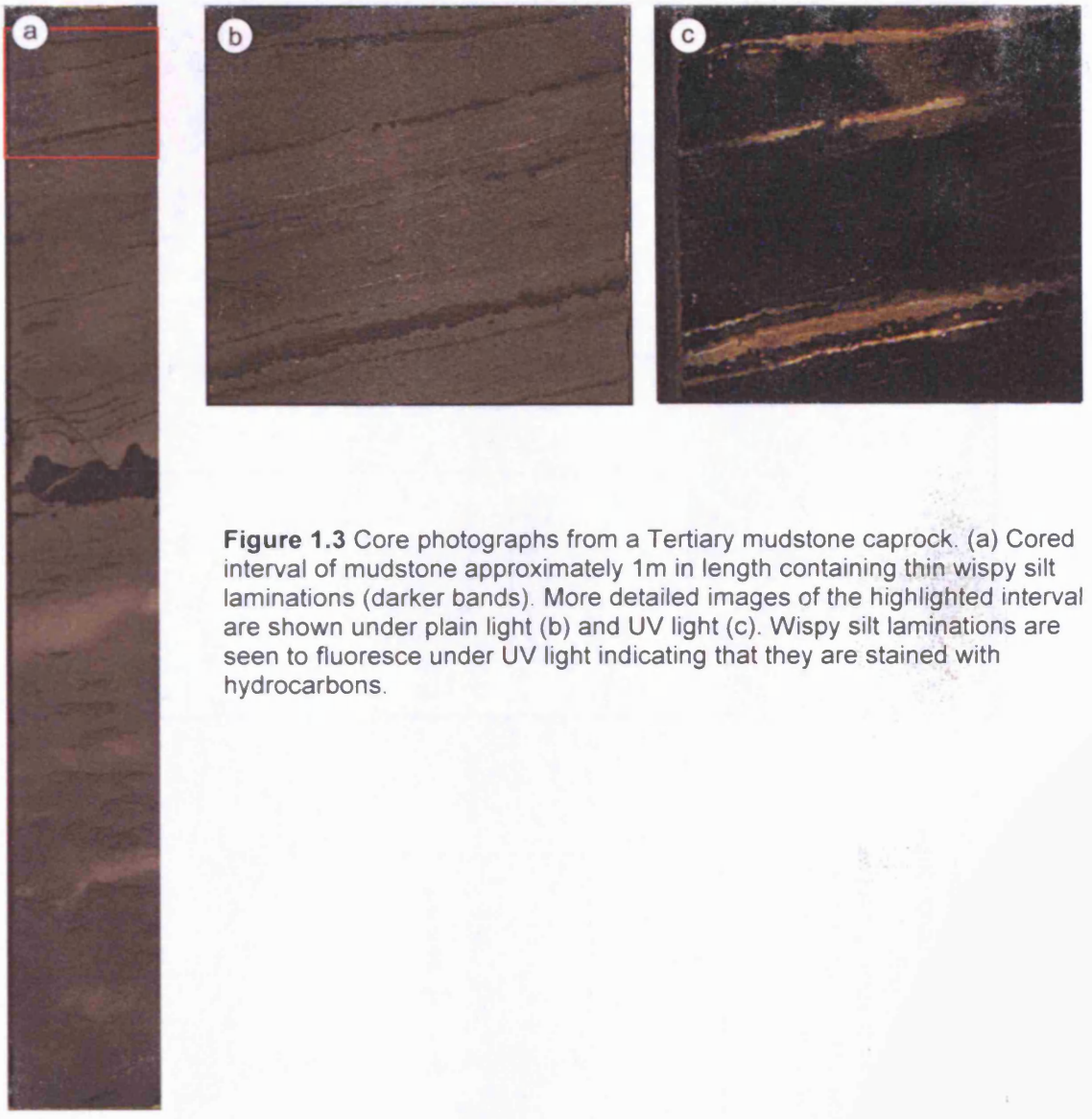

Figure 1.3 Core photographs from a Tertiary mudstone caprock. (a) Cored interval of mudstone approximately 1m in length containing thin wispy silt laminations (darker bands). More detailed images of the highlighted interval are shown under plain light (b) and UV light (c). Wispy silt laminations are seen to fluoresce under UV light indicating that they are stained with hydrocarbons.

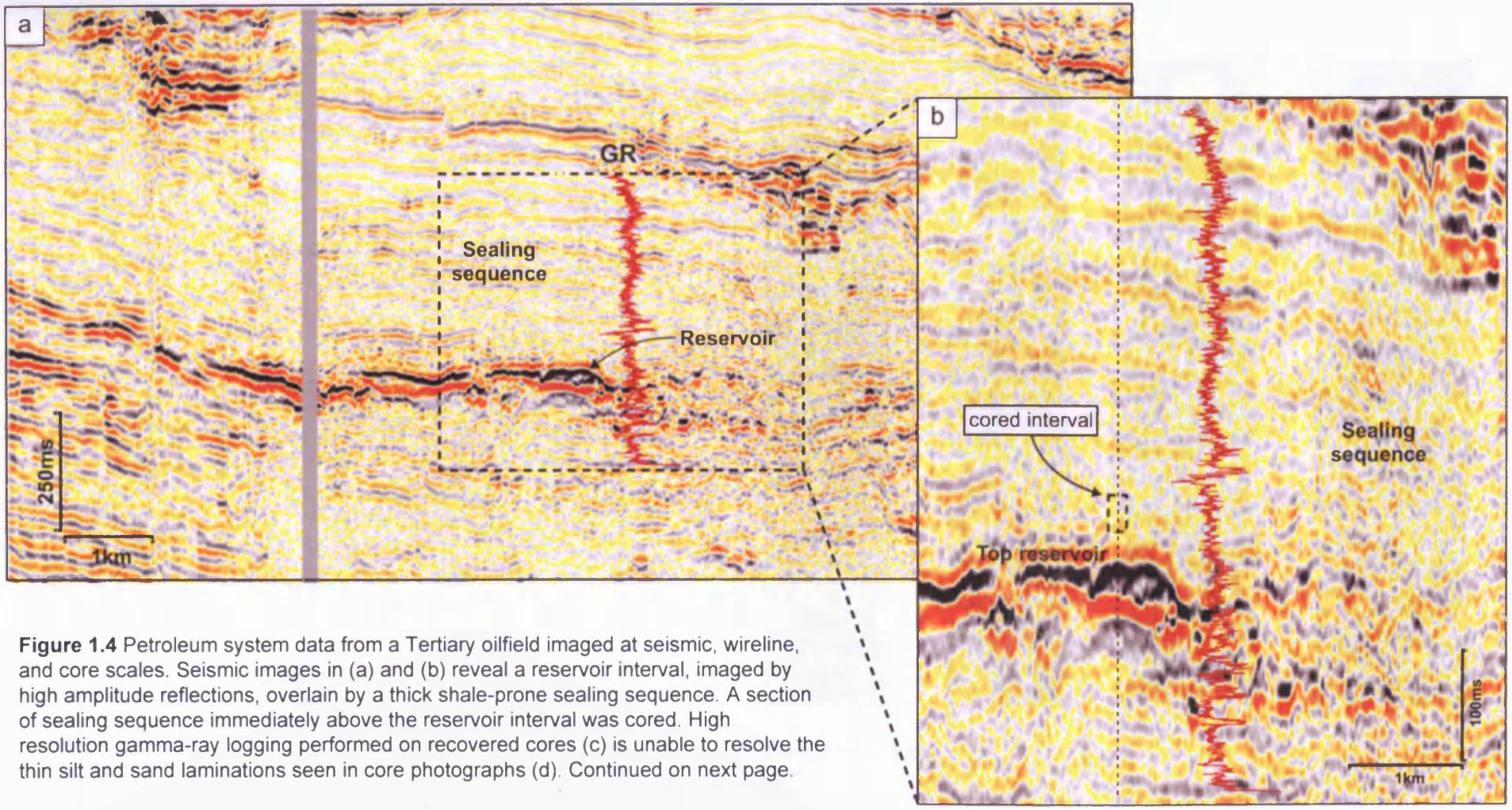

Figure 1.4 Petroleum system data from a Tertiary oilfield imaged at seismic, wireline, and core scales. Seismic images in (a) and (b) reveal a reservoir interval, imaged by high amplitude reflections, overlain by a thick shale-prone sealing sequence. A section of sealing sequence immediately above the reservoir interval was cored. High resolution gamma-ray logging performed on recovered cores (c) is unable to resolve the thin silt and sand laminations seen in core photographs (d). Continued on next page.

Fig. 1.4 *cont*

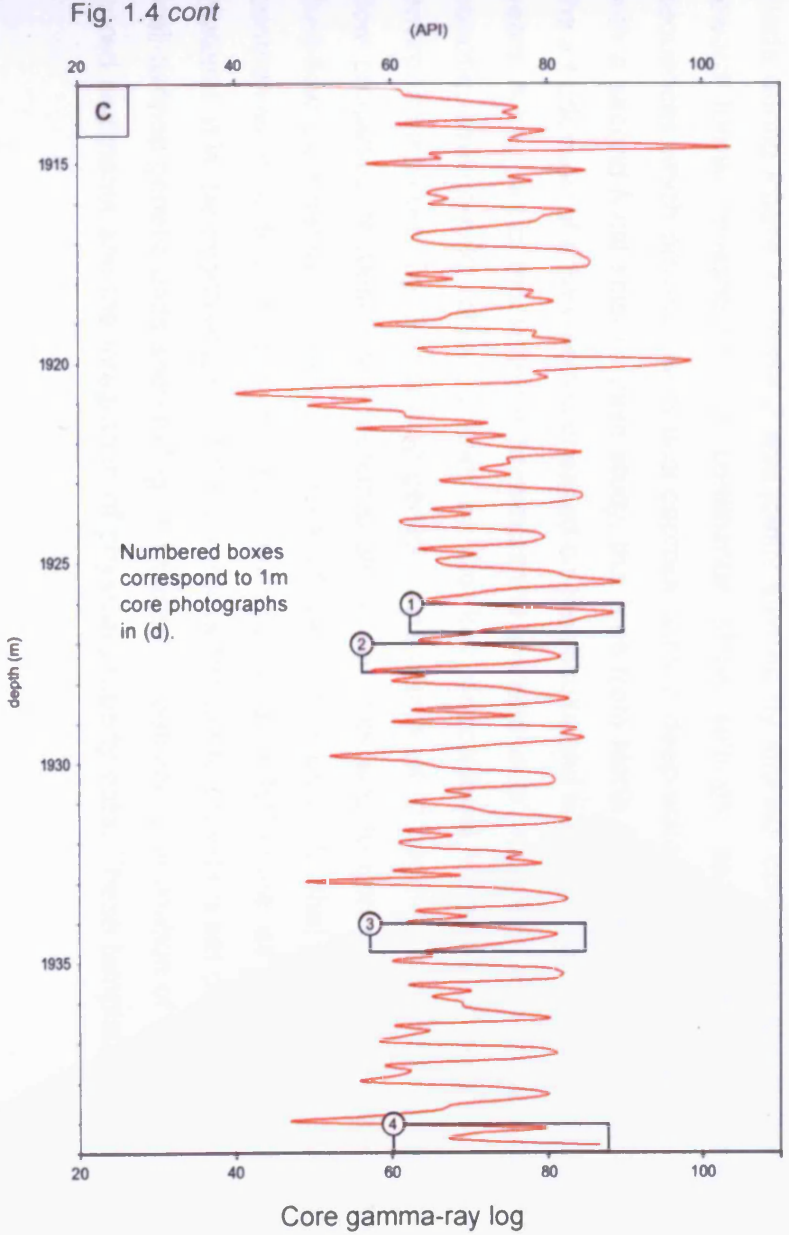
(API)
20
40
60
80
100
c
1915
1920
1925
1930
1935
depth (m)
Numbered boxes correspond to 1m core photographs in (d).
1
2
3
4
20
40
60
80
100
Core gamma-ray log

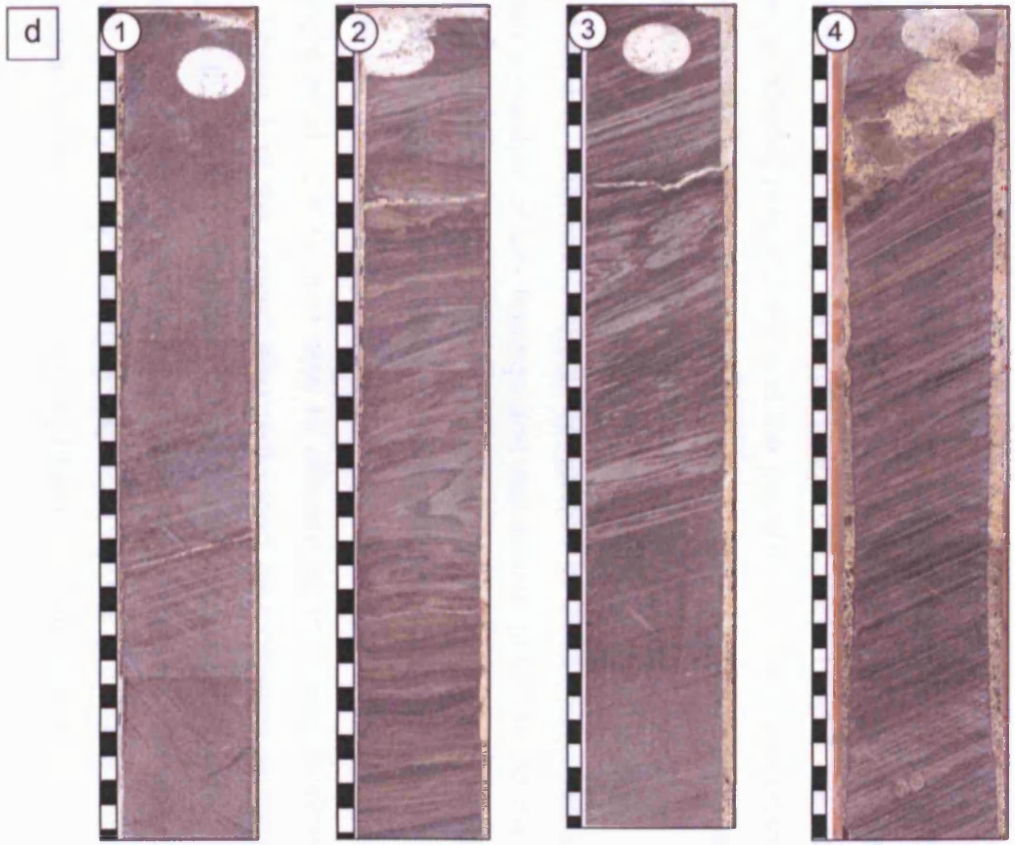
d
1
2
3
4
Core photographs

1.3 The Caprocks Project

Research presented in this thesis was conducted during Phase 2 of the Caprocks Project as a direct response to the results and outcomes of Phase 1. An important factor in determining the direction of continuing research in the Caprocks Project are collaborative discussions between academic researchers and the petroleum company sponsor group. Through these discussions, the project is able to deliver results-based research that can be fed directly to operational staff in petroleum companies.

Phase 1 of the Caprocks Project, completed in 2006, was ongoing for three years and produced a number of key findings and deliverable products. At the centre of Phase 1 was work undertaken to integrate rock properties, wireline, and seismic data from a west African case study, supplied by a sponsor company. This work helped to define and identity potential flow units and fluid escape structures within the caprock sequence as previously mentioned (Cartwright et al., 2007), and also to allocate seismic and wireline attributes to caprocks facies. Phase 1 of the project also performed petrophysical analysis on caprock samples, adding to the limited database of mudstone physical properties, while also providing a classification of mudstones based on grain-size distribution (Moore, 2005). Several areas of research, namely the upscaling of caprock physical properties and the generation of fluid-flow models, have been continued into Phase 2 of the project.

Phase 2 of the Caprocks Project began in 2007 and has set out to build on the advances made during Phase 1. Phase 2 was jointly steered by sponsor companies and researchers toward further investigation of continental slope settings, as it is these fine-grained sequences which provide the typical caprock units in deep-water petroliferous basins. Along with a second focal seismic case study, this time from North Africa, Caprocks Phase 2 saw the introduction of a new workflow based on the results and learnings from the previous three years. A key part of this scheme, known as the 'genetic units' approach, aims to evaluate the specific sealing-risks of a number of the key depositional units which exist in slope environments (*see* Fig. 3.1). Using genetic units allows us to begin to define the likely fluid-flow properties of seismically recognisable slope units and to consider fitting quantitative fluid-flow parameters to them. Sources of data, in addition to that supplied by sponsor companies, include outcrop and Ocean Drilling Program (ODP) data, as well as open source material. It is the eventual goal of the Caprocks Project to provide a set of templates for the well-defined genetic units seen in Fig. 3.1 based on detailed examination of outcropping and cored sediments and the integration of physical property data. These templates will provide

the basic building-blocks with which to populate slope sequences in basin models and fluid-flow simulations.

1.4 Thesis structure

Work presented in Chapters 2 and 3 of this thesis centres on the sedimentological evaluation of heterogeneous slope sediments and the distribution and geometries of potential fluid flow pathways. Initial outcrop studies presented in Chapter 2 were necessary to construct a quantitative dataset regarding the scale, distribution and connectivity of coarser layers within slope sediments. This stage of enquiry represents an important phase of data collection and feeds directly into mathematical modelling and fluid-flow simulations being developed by the Caprock Project team. Initial examinations also provided a testing ground for data collection techniques and allow the development of an outcrop workflow methodology which can be applied to future field studies of any of the Caprocks Project genetic units. Importantly, data extracted from outcrop sequences also validates the existence of thinly bedded heterogeneous slope sequences, quantitative investigations of which have seldom been published (e.g. Revil et al., 1998; Lash, 2006).

Building on knowledge gained from outcrops, the Caprocks Hemipelagite Database, presented in Chapter 3, aims to utilise the extensive data archives amassed by the ODP to provide further quantitative data regarding the physical properties of slope mudstones and the nature and distribution of any coarser horizons present. A workflow, modified from that developed for outcrop studies, has been used to efficiently mine ODP data repositories allowing for the meticulous yet focussed collection of data from over 7000m of cored Tertiary sediment. An advantage of employing this global dataset over outcrop based investigations is that the basin context of ODP case studies is far better constrained, allowing the importance of likely controls on the grain-size distribution and sediment properties to be evaluated (i.e. sources, distribution network, sediment/current interactions). Quantitative insights into the distribution of thin-beds in generic slope sequences presented in Chapters 2 and 3 represent important Caprocks Project deliverables. This work forms part of a much larger body of collaborative research by Caprocks Project scientists during Phase 2 which aims to develop geologically realistic fluid-flow simulations based on the mapping and quantification of outcropping and cored sediments, thus building towards the goals of the genetic units model.

In addition to the largely sedimentological research aimed at populating a genetic units model with geologically grounded data (Chapters 2 & 3), investigations were also undertaken

to examine post-depositional changes to mudstone sequences during shallow burial by utilising the extensive ODP digital archives (Chapters 4 & 5).

Work presented in Chapter 4 explores the degree to which grain-size and sedimentary composition controls the depositional and burial porosities of fine-grained marine sediments. The rationale for this work stems from the importance of understanding the evolution of porosity/depth relationships in the development of accurate basin models and decompaction analysis. While mudstone depositional porosity values presented in Chapter 4 are spread over a range of 60%, it remains common practice for mudstones to be allocated a generic depositional porosity value during calculations (Sclater & Christie, 1980; Mann & Mackenzie, 1990). The accuracy of depositional porosity values will determine, to an extent, the validity of resulting calculations, and may lead to significant inaccuracies (*see* Fig. 4.12). Work suggests that subtle changes in grain-size and lithology play an important role in determining the depositional porosity, and to an extent the porosity/depth relationship, of fine-grained sediments.

During ODP site investigations, carried out to develop the Caprocks Hemipelagite Database (Chapter 2) as well as porosity studies presented in Chapter 4, it became apparent that the physical properties of clay-dominated intervals at a number of ODP drill sites had been significantly influenced by diagenetic processes. One diagenetic process of particular interest was the conversion of volcanic ash to clay minerals at relatively shallow depths (<500m). Investigations into the impact of ash conversion on the physical and mechanical properties of fine-grained sediments are rare (e.g. Ninkovich and Heezen, 1967; Nelson and Anderson, 1992; Flint and Selker, 2003), although chemical processes associated with ash alteration are known to significantly alter the composition of pore-fluids and the grain structure of ash-bearing intervals (e.g. Leckie et al., 2000; Schacht et al., 2008). Work presented in Chapter 5 uses ash conversion as an example of how shallow diagenetic processes have the potential to alter the physical properties of fine-grained sediments, and potentially impact their ability to retard the flow of fluids in the subsurface.

Work presented in this thesis explores a number of topics pertinent to caprock research and feeds into the central theme of the Caprocks Project. The range of topics examined, from outcrop-based mudstone sedimentology, to investigations of mudstone physical properties, compaction, and shallow diagenesis reflects both the development of ideas within the Caprocks Project and the steering of sponsor companies.

1.5 Methodology

Data presented in this thesis was acquired through a range of methods ranging from fieldwork studies to database 'data mining'. Outcrop locations used in this study were identified from literature and preliminary reconnaissance was conducted where possible. Data collection in the field was conducted principally using sedimentary logging techniques and manually acquired bed thicknesses measurements (*see* sections 2.2.3 and 2.3.4. Bed continuities were also examined at outcrop using a number of techniques which are also described in section 2.2.3. The geophysical examination of outcrops in New Zealand using a portable gamma-ray spectrometer was also conducted (*see* section 2.3.4.1). This method of investigation provided data regarding the resolvability of thinly bedded sequences and was considered the most suitable and practical geophysical investigation of these siliciclastic sediments.

Data presented in Chapters 3, 4, and 5 represents existing data which was 'mined' from a number of databases and literature. ODP and IODP borehole data was extensively used in Chapter 3 and 4 to build a picture of sediment deposition and compaction in continental slope settings. This data is in the public domain and is easily accessible, however some of the limitations of this dataset are discussed in section 3.1.5. Methods used to extract data from the ODP and IODP database are described in section 3.2.

The ODP and IODP databases were also used extensively when investigating the impact of diagenesis on mudstone sediments presented in Chapter 5. In addition to borehole data, the literature examining volcanic ash diagenesis was also reviewed in order to develop a wider perspective of the mechanisms and physical processes which accompany ash alteration.

1.6 Terms used in this thesis

- Fine-grained and coarse-grained

Grain-size classifications in this thesis are based on the Udden-Wentworth grain-size scheme (Wentworth, 1922). 'Fine-grained' is used throughout the thesis to describe sediments, generally siliciclastic, which comprise of grains which are predominately of clay- and silt-size (<63μm). 'Coarse-grained' is used throughout to describe sediments, generally siliciclastic, which are dominated by grains lager than <63μm. Unless otherwise stated, 'coarse-grained' refers to sediments comprising predominately of sand-size particles.

- Thin-bed

Beds are separated by bedding planes, most of which represent planes of non-deposition, an abrupt change in composition or grain-size, or an erosional surface (Campbell, 1967). The term 'thin-bed' is used extensively throughout this thesis to describe sedimentary beds which are generally less than 10 cm thick, unless specific thicknesses are otherwise stated.

- Laminae/Lamination

The term 'laminae' or 'lamination' is used here to describe discrete units of sediment which are less than 1 cm in thickness.

- Hemipelagite/Hemipelagic

The term 'hemipelagitic' is used in this thesis to describe the deposition of fine-grained sediment through the combination of vertical 'pelagic' settling and the slow lateral advection of material, after Stow and Tabrez (1998). Stow and Tabrez (1998) also provide a concise sedimentological definition of 'hemipelagites' stating "[Hemipelagites] generally comprise an admixture of >10% biogenic pelagic material and >10% terrigenous or volcanigenic material, in which >40% of the terrigenous (volcanigenic) fraction is silt size or greater (i.e. >4 pm)". This definition obviously categorises a broad variety of fine-grained sediments under the term 'hemipelagite', encompassing muddy oozes, siliceous and calcareous muds, as well as glacigenic-rich and volcanigenic-rich muds.

For the purpose of sedimentological descriptions presented in this work, the term 'hemipelagite' is used, in alignment with Stow and Tabrez (1998), to describe fine-grained sediments which comprise a mixture of terrigenous and biogenic material thought to have been deposited through vertical setting and slow lateral advection.

In addition to the use of 'hemipelagite' as a sedimentological term, the term is also used separately to describe seismic facies which exhibit particular reflection attributes (*see* section 6.5.1). When used in this context, the term 'hemipelagite' is not based on direct sedimentological evidence of hemipelagic deposition, but rather the 'hemipelagic' nature of sequences is inferred from intervals with specific acoustic attributes (e.g. Bertrand et al., 2003; Madof et al., 2009). These units are therefore referred to as 'hemipelagic seismic facies'.

Chapter 2

Chapter 2

Grain-size heterogeneities in outcropping slope sequences: Field studies in the western British Isles and Taranaki Basin, New Zealand.

2.1 General fieldwork introduction

Field-based investigations into the detailed sedimentology and internal geometries of continental slope mudstones are reported in this chapter. Outcrop investigations form a critical component of sedimentary basin analysis, allowing investigators to evaluate empirically, the physical, mechanical and structural properties of rocks at varying stages of induration and deformation. Real rock studies underpin our knowledge of sedimentary systems and are required to calibrate geophysical tools used to make interpretations about subsurface geology. Quantitative data collected from outcropping rocks are also used to populate increasingly sophisticated basin models and represent an incredibly valuable dataset with which to interpret proxy data.

Fieldwork investigations documented in this chapter were conducted as part of a wider investigation of slope sequences by the Caprocks Project (*see* Fig. 1.2). The examination of fine-grained lithologies in outcrop presented here have formed part of a more holistic investigation of the sealing capacity of slope sediments undertaken by Caprocks Project scientists, involving the analysis and integration of seismic, well-log, outcrop, and petrophysical data (*see* Chapter 1). Integration of data from such a wide range of scales (e.g. micron-scale pore measurements to kilometre-scale seismic profiles) presents a significant challenge. Outcrop investigations allow physical property data such as porosity, permeability, and grain-size information to be placed into a sedimentological context and provide an important scale of investigation between the scope of petrophysical and wireline data. Critically however, the centimetric scale of sedimentary features addressed in this study, places them beneath the resolution of commonly used wireline logging tools (e.g. Worthington, 2000; Scaglioni et al., 2006), making them essentially invisible to those making assessments as to sealing capacity of mudstone sequences, as illustrated in Fig. 1.4. The fundamental objective of field investigations has therefore been to investigate the existence of centimetre scale heterogeneities within clay-rich sequences which are likely to impact the migration of fluids and are therefore pertinent to the evaluation of a unit's seal capacity. This outcrop-based probabilistic approach, coupled with further work carried out on cored

sediments (*see* Chapter 3), allows us to better predict the likely distribution of grain-size heterogeneities within buried slope mudstone sequences.

Facies examined in outcrop during this study, which are dominated by hemipelagites, fine-grained turbidites, channel-levee sediments and mass-transport deposits, form the building blocks of slope sequences in many petroliferous basins. Evidence from core photographs confirms the similarities between clay-rich sediments exposed in studied outcrops and lithologies which make up subsurface sealing units (Fig. 2.1). Here, four core photographs of a top seal unit display strikingly similar sedimentological characteristics to thinly bedded mudstones examined at outcrops. The potential importance of thin-beds as a seal bypass system in these fine-grained successions is clearly illustrated in Fig.1.3. where thinly bedded mudstone facies recovered from a Tertiary top seal unit are seen here to be oil stained, suggesting that hydrocarbons are actively migrating through a connected network of coarser layers.

Fieldwork campaigns in the western British Isles and Taranaki Basin have provided data regarding the sedimentology, connectivity and spatial distribution of relatively coarse, centimetre scale grain-size heterogeneities within Palaeozoic and Neogene slope sediments, respectively. Heterogeneities, in the form of silt and sand horizons, have relatively high permeabilities compared to typical clay-rich hemipelagic sediments, and as a result, may offer a means of compromising an otherwise effective capillary seal by providing a pathway of increased permeability and reduced capillary entry pressure (Schlomer and Krooss, 1997; Dewhurst et al., 1999b; Yang and Aplin, 2007). Studied exposures of slope sediments indicate that thin (0.1-3cm) layers of silt and/or sand grains punctuate, at a range of frequencies, relatively homogeneous, fine-grained 'background' sediments.

To date, very little consideration has been given in the published literature regarding the importance of these centimetre scale 'thin-beds' in the evaluation of top seals (Revil et al., 1998; Lash, 2006). Field investigations carried out on both 'classic' and previously unstudied exposures in West Wales, Cornwall and the northern Taranaki Peninsula in New Zealand facilitate the first known attempt to quantify the distribution of this type of grain-size heterogeneity. This work, as well as data reported from ocean drilling campaigns presented in Chapter 3, suggests that thin-beds of more permeable material will be commonly encountered in fine-grained slope sequences, bringing into question the widely held view that fine-grained hemipelagic slope sediments will always represent high quality sealing lithologies.

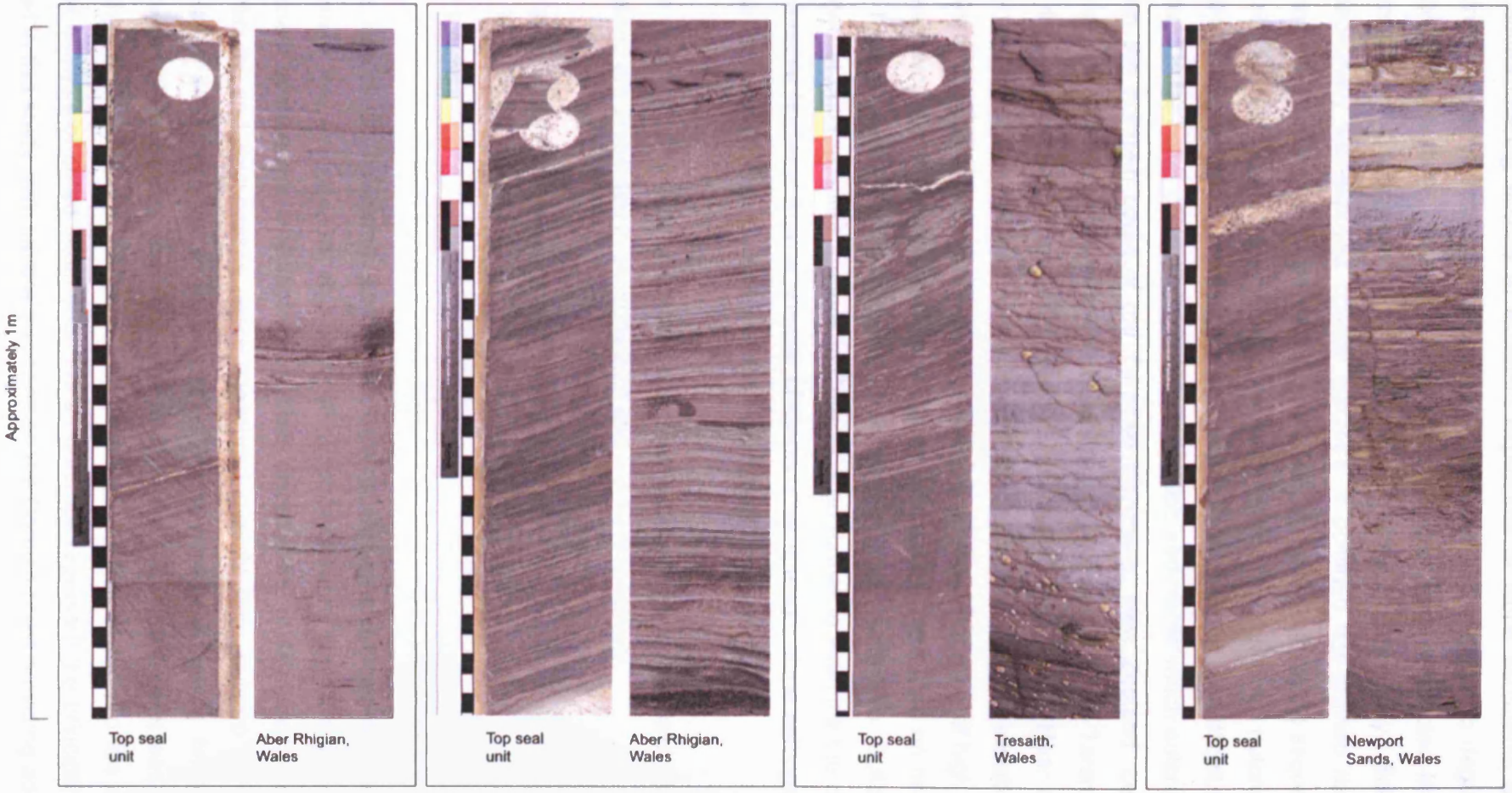

Figure 2.1 Core photographs of four intervals of top-seal mudstone recovered from a Tertiary sealing sequence. These images have been matched with photographs of outcropping mudstone facies from west Wales which show similar internal structures and thin-bed configuration.

Locations offering access to excellent exposures of slope sediments are rare. The fine-grained nature of such outcrops makes them highly susceptible to degradation, permitting limited preservation. Detailed outcrop investigations were conducted in West Wales and Cornwall on Ordovician and Carboniferous strata, respectively. Both locations offer exceptionally well-exposed coastal outcrops of polished fine-grained rocks from which to quantify the existence of coarse thin-beds. Whilst these Palaeozoic sequences allow for the detailed examination of sedimentary features and structures at an outcrop-scale, the basin setting and depositional context for individual exposures is more difficult to ascertain. Basin context is far better constrained in Miocene slope sediments which outcrop for almost 17km along the northern coast of the Taranaki Peninsula, New Zealand. Less indurated than Welsh and Cornish exposures, continental margin sediments of the Taranaki Basin lie within an extensively studied, petroliferous Neogene basin (see 2.2.3). Near continuous coastal exposures were examined here to investigate the distribution and variability of fine-grained facies from a continental slope system and to map the distribution of high permeability units. These two field study datasets complement one another and form an essential first-step in the high-resolution investigation of thinly bedded slope sediments. Building on knowledge gained at outcrop, investigations in Chapter 3 go further to examine the distribution of more permeable horizons from a number of modern hemipelagic slope settings by utilising cored sediments recovered during ocean drilling projects.

The major finding and conclusions for fieldwork studies conducted in the UK and New Zealand are presented in sections 2.27 and 2.3.10 respectively.

2.2 West Wales and Cornwall

2.2.1 Aims

The key aims of fieldwork carried out in West Wales and Cornwall were to examine and quantify the existence of thin-beds of more permeable sediment which punctuate fine-grained sequences. Specific measurable parameters of thin-beds, namely their lateral continuity and thicknesses, were measured directly from outcrop to allow us to make tentative predictions as to the impact of more permeable layers on sediment fluid-flow. Mapping of the outcrop-scale distribution and frequency of thin-beds was also undertaken to add to our current knowledge of mudstone facies types and to provide a reference for the later analysis of cored sediments. Welsh outcrops represent the principal British field areas used in this study, with several locations on the Cornish coast providing additional data.

2.2.2 Basin setting and stratigraphy

2.2.2.1 West Wales

Fieldwork conducted in West Wales was centred around the town of Cardigan, utilising the exposures of Ordovician (~450-440 Mya) mudstones which outcrop along the north Pembrokeshire and Ceredigion coasts. The geology of this region is dominated by Palaeozoic strata, much of which comprises hemipelagic and turbiditic mudstones, cut by a WSW-ENE trending fault zone known as the Fishguard-Cardigan Fault Belt (FCFB) (Fig. 2.2). The FCFB formed the southern margin of a fault-bounded trough or graben at the southern edge of the Palaeozoic Welsh Basin (Kokelaar, 1988). Recent publications by the British Geological Survey (Davies et al., 2003) have incorporated new formation names and boundaries, largely discarding those presented in previous works by James (1975; 1997) and McCann (1992). To aid simple description of the regional geology, classifications proposed by Davies et al. (2003) are used here.

The oldest rocks recorded in the region are lavas and tuffs of the Fishguard Volcanic Group, deposited across the margin during the Llanvirn (Davies et al., 2003). Subsequent uplift along the FCFB led to mass-wasting of margin deposits and the deposition of slumped mudstones and debrites north-eastward into the basin, forming the lowermost ~200m of the Penyraber Mudstone Fm. (Castle Point and Saddle Point Members of Davies et al., 2003). The remaining ~500m of the Penyraber Mudstone Fm. and the overlying Cwm-yr-Eglwys Mudstone Fm. are dominated by hemipelagic and turbiditic silty mudstones which now outcrop north of the Aber Richard Fault (Fig. 2.2). The late Caradoc Dinas Island Fm., which outcrops along much of the coast between Dinas Island and Cardigan, overlies, and is laterally equivalent to, mudstones of the Cwm-yr-Eglwys Fm. The Dinas Island Fm. records a thick sequence (1300m) of alternating hemipelagic mudstones and sandstone turbidites as well as local debrites and channel features. The remaining Ordovician strata preserved in the region comprise the Nantmel Mudstones and Yr Allt Formations, both of Ashgillian age, which outcrop extensively to the south and east of Cardigan (Davies et al., 2003) (Fig. 2.2). Fine-grained rocks of the Nantmel Mudstones Formation form a thick sequence (1300m) of hemipelagic sediments thought to have blanketed the region at the beginning of the Ashgill, possibly in response to polar cooling ahead of the initiation of a deep thermohaline circulation (Armstrong and Coe, 1997). Overlying this unit are hemipelagic and turbiditic sediments of the Yr Allt Formation which record an increase in the rate and volume of material supplied to the margin, thought to be in response to a major fall in sea-level (Davies et al., 2006). The entire Ordovician sequence underwent significant deformation during the Acadian Orogeny

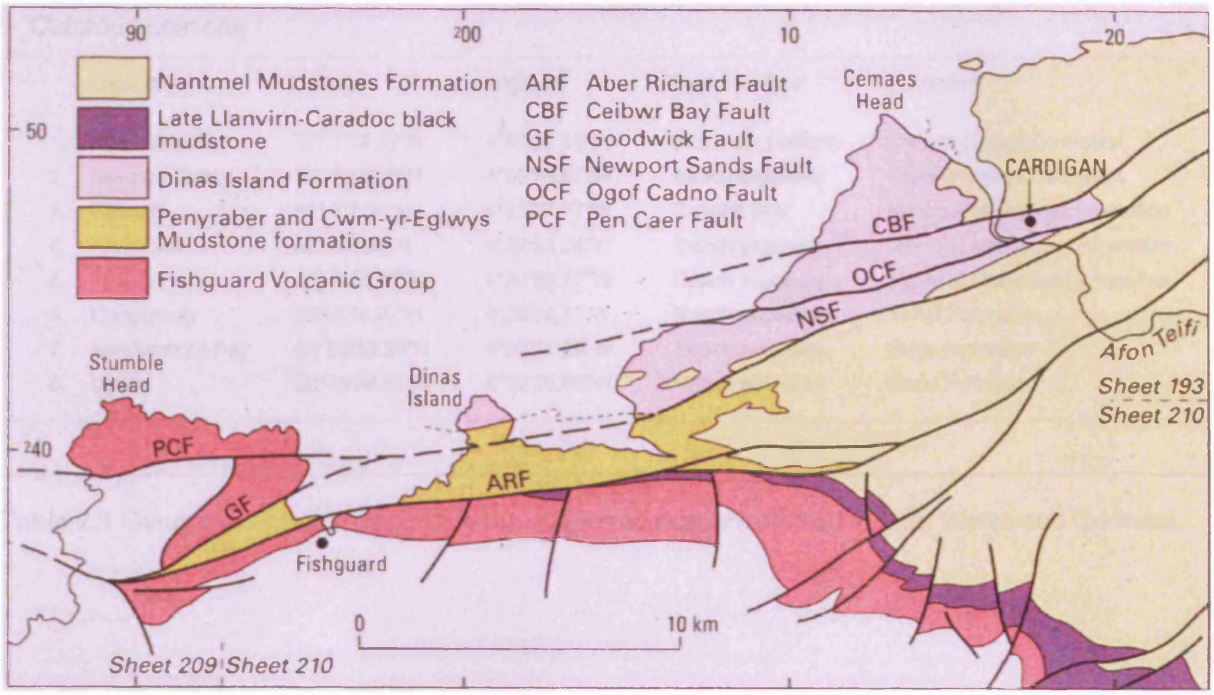

Figure 2.2 Map showing the geology of the area around Cardigan and Dina Island, west Wales. See text for formation descriptions. Image taken from Davies et al, 2003.

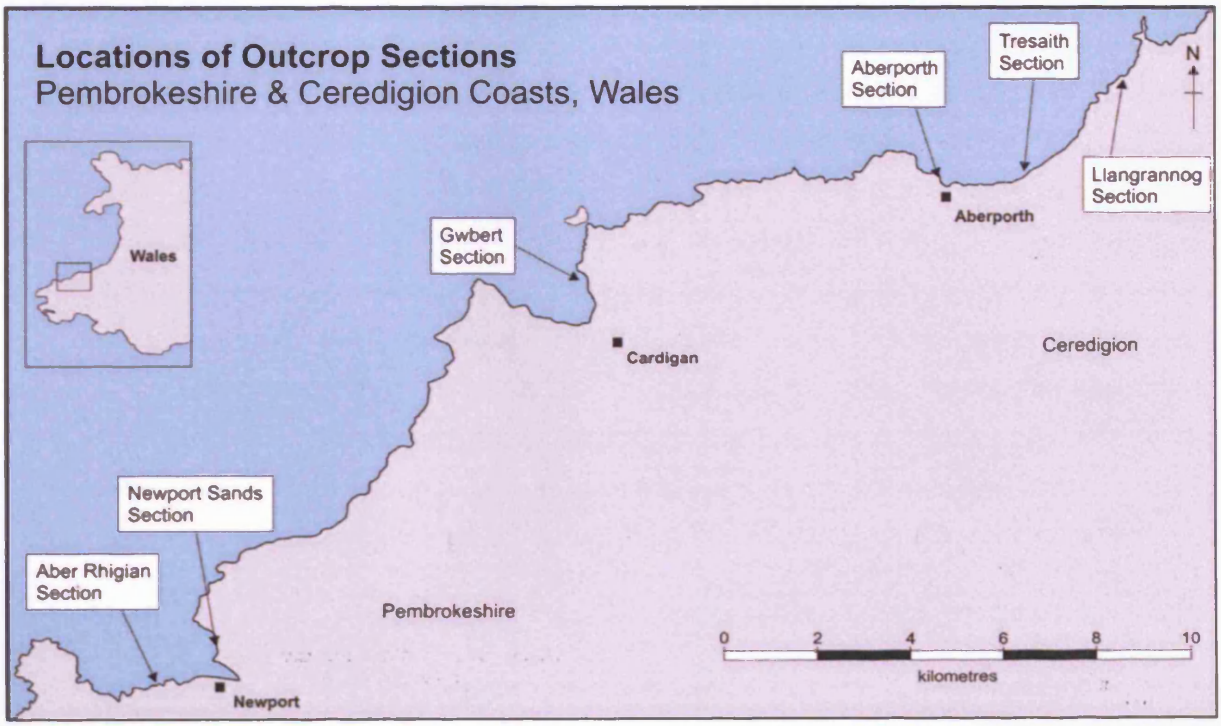

Figure 2.3 Map showing the location of studied outcrop sections from the Cardigan area.

Outcrop Locations

	Location	Latitude	Longitude	Exposure type	Formation
1.	Aber Rhigian	52° 1'14.17"N	4°51'56.45"W	Wave-cut platform	Cwm-yr-Egwys Formation
2.	Newport Sands	52° 1'54.28"N	4°50'18.57"W	Beach exposure	Cwm-yr-Egwys Formation
3.	Gwbert	52° 7'7.34"N	4°41'27.77"W	Coastal inlet	Nantmel Mudstones Formation
4.	Aberporth	52° 8'8.53"N	4°32'53.24"W	Beach exposure	Nantmel Mudstones Formation
5.	Tresaith	52° 8'10.44"N	4°30'59.72"W	Beach exposure	Nantmel Mudstones Formation
6.	Llangranog	52° 9'40.07"N	4°28'16.11"W	Beach exposure	Yr Allt Formation
7.	Sandymouth Bay	50°50'38.30"N	4°33'24.29"W	Beach exposure	Bude Formation
8.	Upton	50°48'56.60"N	4°33'26.99"W	Beach exposure	Bude Formation

Table 2.1 General information regarding the outcrop exposures studied in west Wales and Cornwall.

(400Ma), leading to considerable folding of strata and the development of a slaty cleavage in mudstone lithologies. Some portions of the FCFB also underwent compression and inversion during this phase resulting in some faults now being downthrown to the south (Davies et al., 2003).

A total of six exposures were chosen for detailed investigations largely on the basis of outcrop extent and accessibility (Fig. 2.3), a summary of locations is shown in Table 2.1. Outcrops at Aber Rhigian and Newport Sands are within the Cwm-Yr-Eglwys Formation, while Gwbert, Aberporth and Tresaith sections are located in the Nantmel Mudstones Formation. The most northern outcrop investigated, at Llangranog, lies within the lowermost units of the 600m thick Yr Allt Formation.

2.2.2.2 Cornwall

In addition to fine-grained sediments found in West Wales, coastal exposures of the Bude Formation were also studied. The Bude Fm. also outcrops in coastal cliffs; north and south of the town of Bude, on the north Cornish coast (Fig. 2.4). Rocks are dominated by alternating, well indurated mudstones and sandstones of Upper Carboniferous (Westphalian) age, deposited as part of the Culm Basin sequence (Higgs, 1991). Sediments conformably overlie similar units of the older Crackington Fm., all of which have undergone Variscan deformation (Fig. 2.5). Bude Fm. strata outcrop for roughly 15km in coastal sections between Morwenstow to the north of Bude, and Widemouth Bay in the south, recording over 1200m of stratigraphy (Higgs, 2004). The sedimentology and basin setting of the Bude formation has been discussed extensively for over 40 years (e.g. Reading, 1963; Higgs, 2004). However, there remains some disagreement as to the exact setting of deposition, with some authors favouring a deep-sea fan environment (Melvin, 1987; Burne, 1995, 1998) while others propose a foreland basin lake margin fed by turbidites (Higgs, 1994, 1998). The occurrence of slumped units and the deposition of sand units by turbidity currents suggest that the margin was sloping, but it remains unclear as to the water depth during deposition.

2.2.3 Methods

A number of data collection techniques were developed during the course of field campaigns to aid the collection of detailed and accurate data regarding the physical characteristics of thinly bedded coarse layers. As previously mentioned, the collection of specific data was needed to enable us to build a picture of how the distribution of thin-beds might impact fluid-flow in mudstones. Where thinly bedded mudstones outcrop, a suite of measurements was

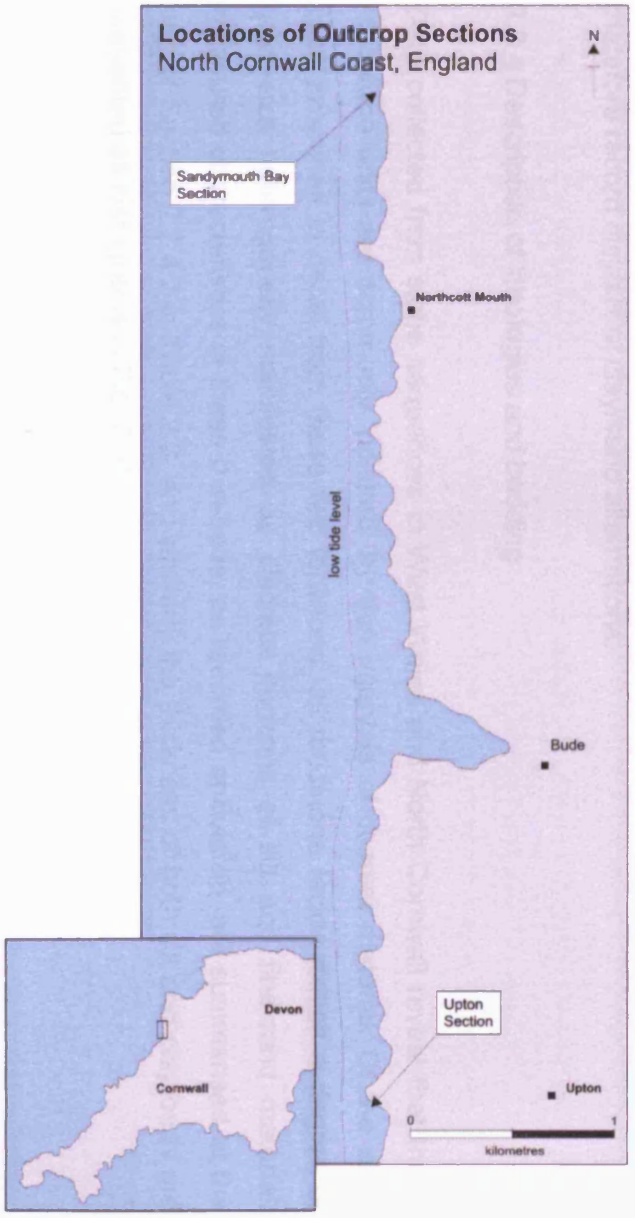

Figure 2.4 (left) Map showing the location of outcrop sites examined around the town of Bude, Cornwall.

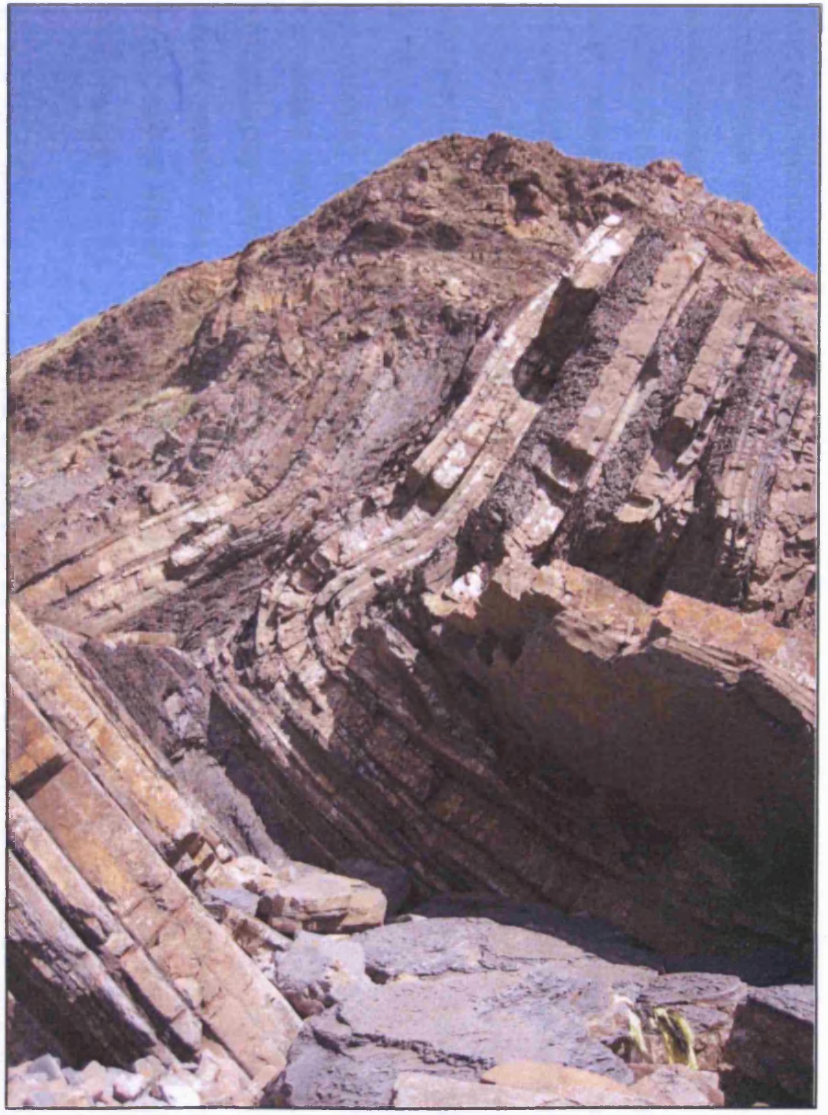

Figure 2.5 (right) Cliff section from the Bude Formation exposured just north of Upton Cross showing characteristically deformed sand/shale alternations.

collected focusing on the lateral continuity, thickness, and sedimentology of any coarser grained intervals. At larger outcrops (i.e. Aber Rhigian), initial facies mapping at the metre-scale allowed us to document the lateral and vertical variability in mudstone lithotypes, based largely on the occurrence and dimensions of silt layers (*see* Fig. 2.8a). Identified facies were then subject to high-resolution (centimetre-scale) sedimentary logging in order to characterise the distribution and dimensions of thin-beds. The exact thickness of each individual horizon was collected manually and data is presented as high-resolution sedimentary logs, each typically covering roughly 2m of stratigraphy (e.g. Figs. 2.8b, 2.14, 2.16). In order to ascertain the lateral continuity of these measured layers, a number of micro-logs, generally separated by 3m were collected and individual thin-beds were correlated laterally. Techniques involving the lateral tracing of beds using panoramic photography were also incorporated at some locations (*see* Fig. 2.10). Preliminary investigations into the inter-connectivity of more permeable horizons were undertaken, principally at Welsh locations, allowing us to catalogue potential connective structures and features (*see* 2.5.5).

In the vast majority of outcrops examined, background sediments were dominated by clay-rich mudrocks of varying colour. These units were often seen to be punctuated by the deposition of coarser sediments, generally silt grade material in West Wales, and silt/fine-sand mixtures in Cornwall. At outcrop, distinctions between clay-dominated background and the paler, coarser silt/sand layers can be made by visual inspection, however petrographic analyses were performed in order to confirm inferred grain-size variations (Fig. 2.6). Recognition of these distinct grain-size units using an essentially binary method, allowed for time effective data collection and simple comparisons between sites. Sedimentary logs therefore record clay/silt or clay/sand alternations.

2.2.4 Description of lithologies and bedding

Data collected from slope sequences in West Wales and North Cornwall reveal that these mudstone units are commonly 'polluted' by thin intervals of coarser material. Of the eight sites examined in detail from these two locations, all mudstone facies exhibit a degree of grain-size heterogeneity manifested as discrete horizons of silt and fine-sand material. Measured characteristics of these thin-beds, as recorded at outcrop, are summarised at the end of Section 2.2.4.2 in Table 2.2, and similarly the thickness of both silt and clay beds are presented as histograms in Fig. 2.31.

2.2.4.1 West Wales

Aber Rhigian

Mudstones outcropping in the wave-cut platform just east of Aber Rhigian represent the largest single outcrop exposure examined. Here, mudstones of the Cwm-yr-Eglwys Formation are exposed and provide an exceptional opportunity to gauge the lateral continuity of coarser-grained thin-beds (Fig. 2.7). Strata here dip steeply to the north providing a cross-sectional view through roughly 40m of mudstone stratigraphy. The platform, exposing roughly 7000m^2 of rock, was mapped and divided into several separate lithofacies based on the distribution and volume of silt material present. The distribution and stratigraphy of these lithofacies is shown graphically in Figure 2.8a and described in the text below. High-resolution sedimentary logs, shown in Fig. 2.8b, were used to quantitatively characterise the thickness and spacings of silt beds for each of the lithofacies.

At the base of the exposed sequence lies a largely homogeneous unit comprising medium to dark grey claystone (lithofacies A in Fig. 2.8). This unit is roughly 10m thick in outcrop and records internally deformed sediments with common recumbent folding and internal truncations. Rare thin-beds of coarser material were recorded, although these rarely exceed 5mm in thickness and show poor lateral continuity. Lithofacies B appears to lie conformably above lithofacies A and records a 10-15m thick sequence of alternating clays and silts (Fig. 2.9a). Thin-beds of medium grained silt comprise approximately 40% of this unit, record a mean thickness of 10mm, and are traceable over large portions of the outcrop (>100m). Lithofacies C differs from the underlying lithofacies B in that coarse layers occur more frequently and are generally thinner, with a mean thickness value of just 3mm (Fig. 2.9b). Beds are also highly laterally continuous with occasional beds traceable across the entire outcrop despite maximum thicknesses of ~10mm. Lithofacies C, as exposed, records approximately 10m of stratigraphy, 35% of which comprises discrete thin-beds of silt material. Thin units comprising discontinuous mudstone lenses, silty clasts and a largely homogenised clayey matrix are interpreted as thin debris-flow deposits. These are classified as lithofacies D in Fig. 2.8, are recorded from seven stratigraphic levels within lithofacies B. Deposits range in thickness from several centimetres to 25cm (Fig. 2.9c). They conform to descriptions of debris flow deposits given by Tucholke et al. (2004) and Tripsanas et al. (2008). Of the seven deposits identified, only two could be correlated across the full width of the outcrop (Fig. 2.8). The lateral continuity of silty beds does not show a clear relationship with bed thickness or bed frequency. Thinly bedded units at Aber Rhigian, for example,

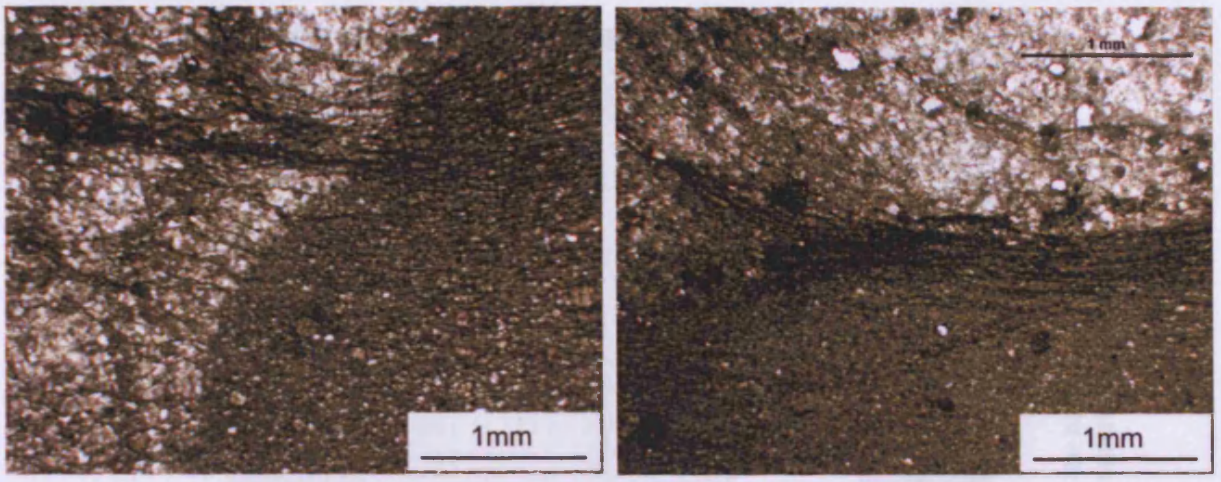

Figure 2.6 Thin section micrographs showing grain-size heterogeneity in mudstone from Aber Rhigian. Both images are taken at the contact between silt- (white) and clay-dominated (dark green) thin-beds.

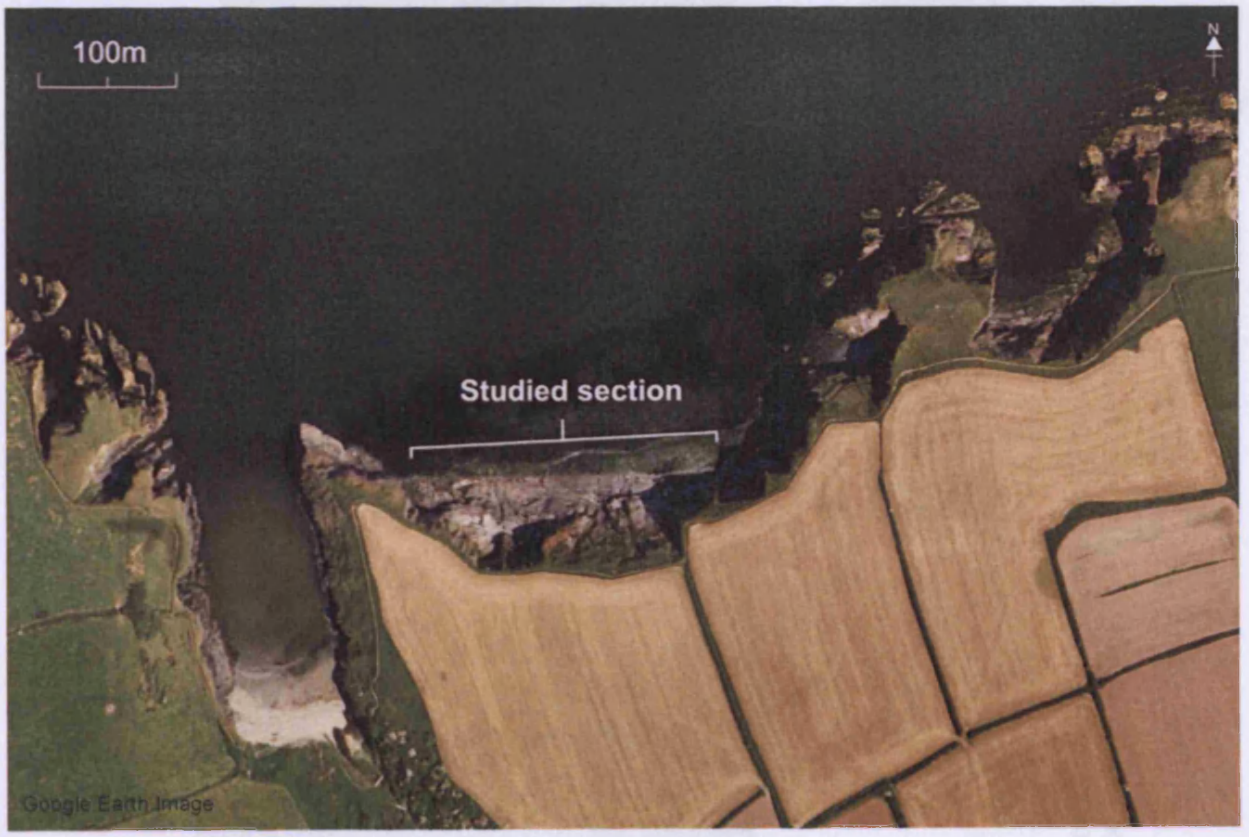

Figure 2.7 Aerial photograph showing Aber Rhigian wave-cut platform exposed beneath sea-cliffs east of Dinas Island. Rocks strike roughly east-west and dip steeply northward (80°) meaning that a cross-section of stratigraphy can be studied.

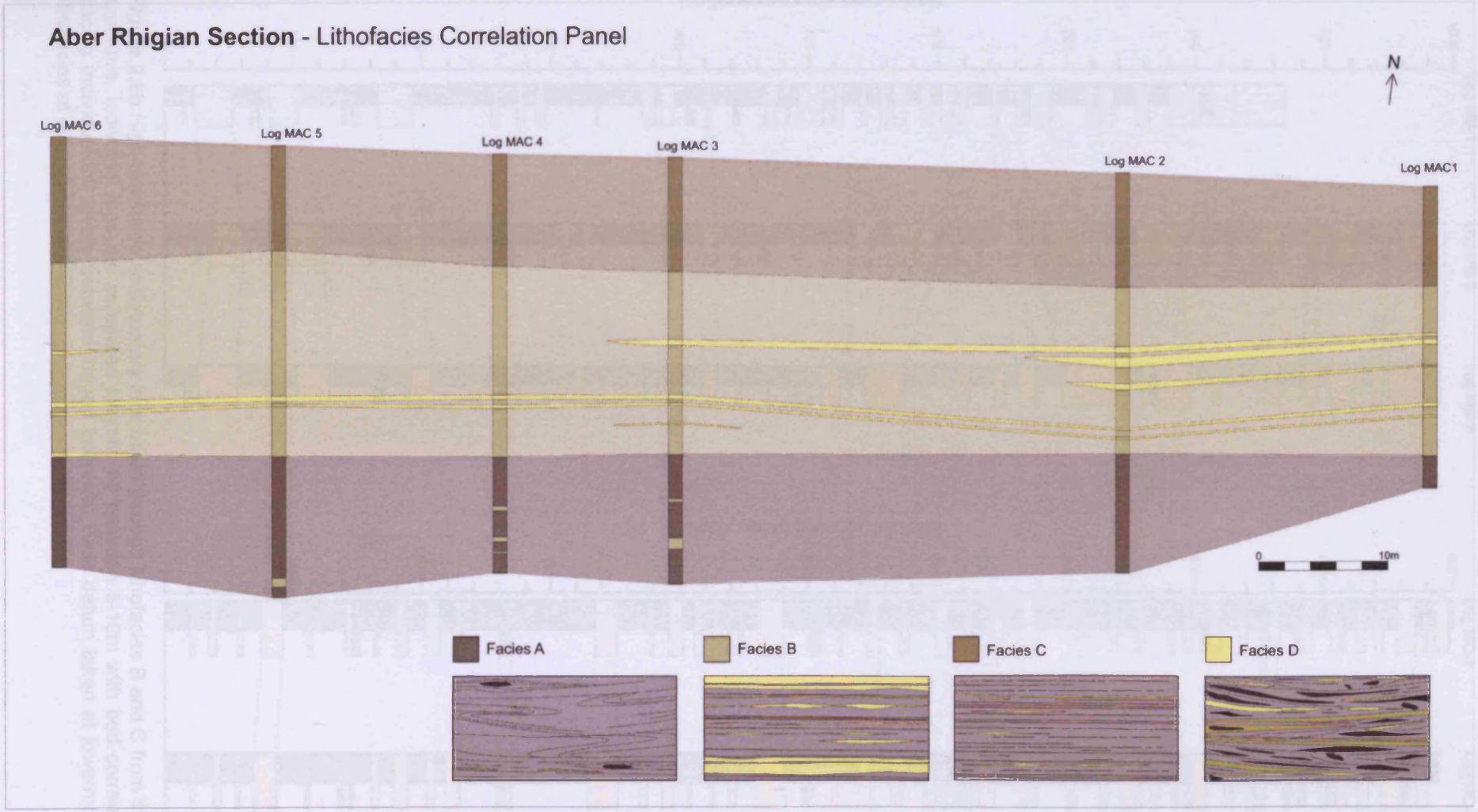

Figure 2.8a Outcrop lithofacies correlation at Aber Rhigian. Three distinct mudstone lithofacies were identified on the basis of the distribution of volume and coarser grained material (Facies A, B, C). Facies D represents thin debris flow deposits. See text for detailed description of individual lithofacies.

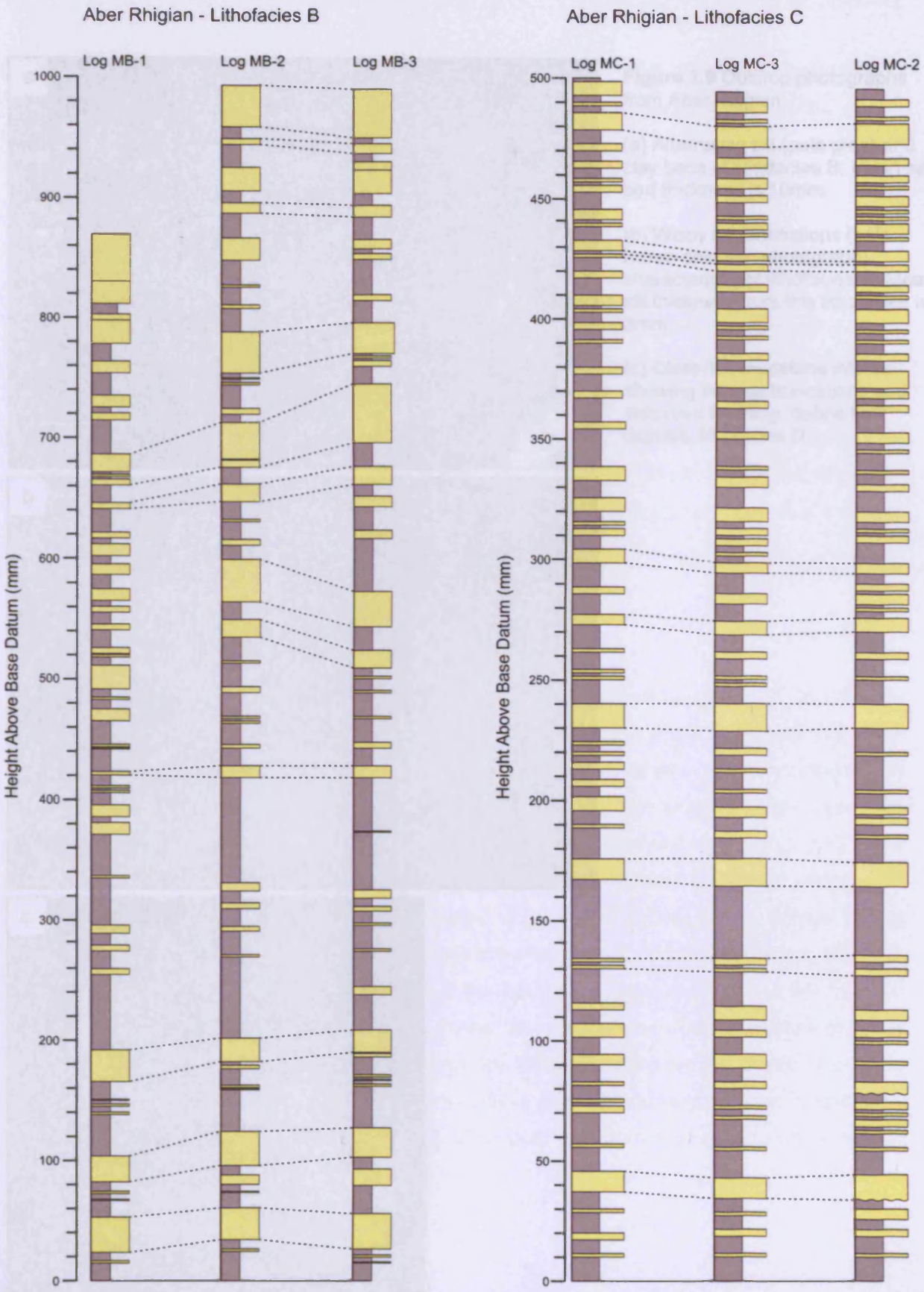

Figure 2.8b High-resolution sedimentary logs taken through lithofacies B and C from the Aber Rhigian exposure. Individual logs are separated laterally by between 5-10m with bed correlations made by tracing individual silt layers between logged intervals. Base datum taken at lowermost exposure of lithofacies at outcrop (*see* fig. 2.8a).

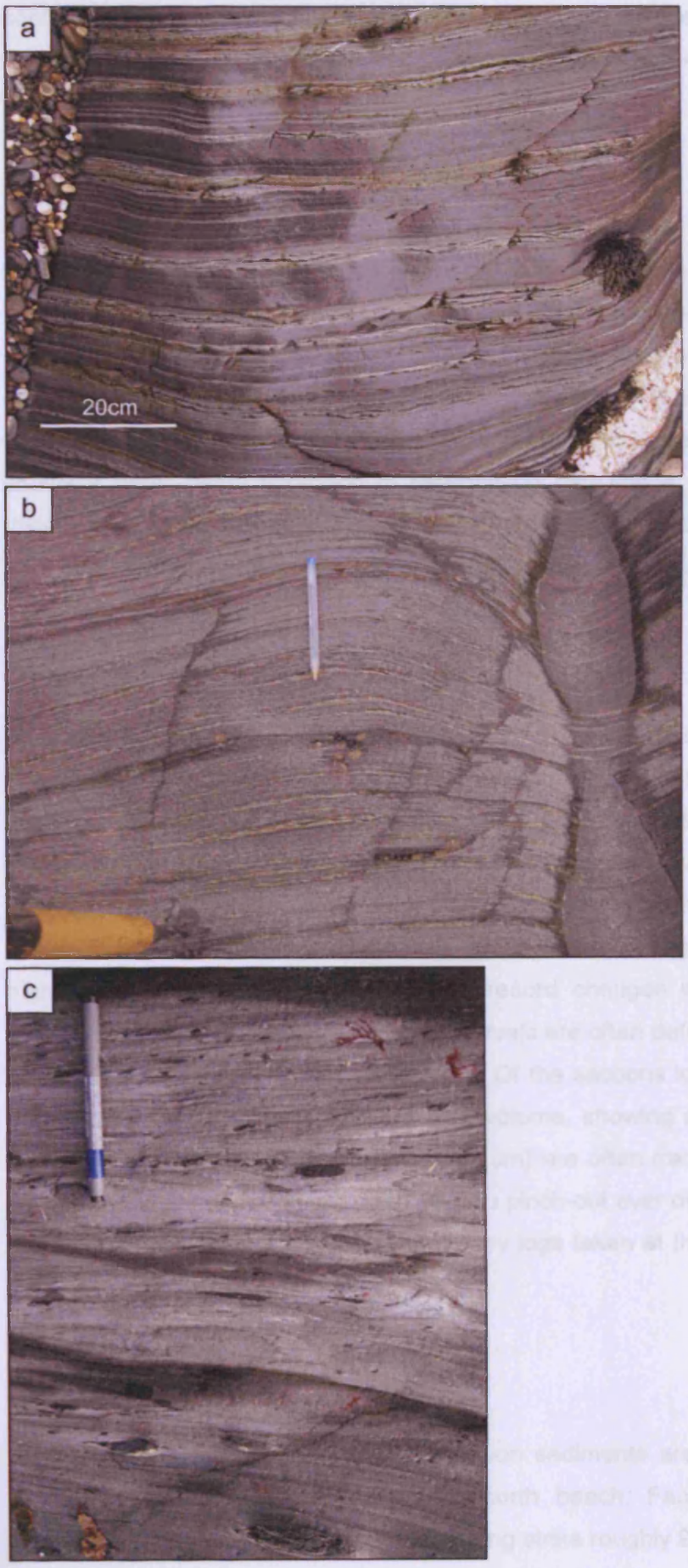

Figure 2.9 Outcrop photographs from Aber Rhigian.

(a) Alternating silt (pale grey) and clay beds of lithofacies B. Mean silt bed thickness is 10mm.

(b) Wispy silt laminations (pale brown colour in photograph) characteristic of lithofacies C. Mean silt thickness from this lithofacies is 3mm.

(c) Clast-rich mudstone interval showing internal truncations and disturbed bedding, debris flow deposit, lithofacies D.

contain silts of 4-5mm thickness which are correlatable for over 50m laterally while thicker, 1-3cm silt layers at Newport, discussed below, rarely show continuities exceeding 20m.

Newport Sands

Cwm-yr-Eglwys mudstones outcropping in beach exposures at Newport Sands record similarly heterolithic units to those of lithofacies B and C from Aber Rhigian. Rocks comprise alternating clay-rich intervals interspersed with abundant thin-beds of coarser material which exhibit a mean thickness of 18mm (Table 2.2). Estimations of lateral continuity are hindered by relatively limited exposure compared to Aber Rhigian, however occasional beds can be traced for 25m, while many are seen to pinch-out or become truncated at <5m. Figure 2.10 shows a photo-panel approach to determining bed lateral continuity over relatively short distances. Coarse intervals, typically dominated by silt grade material, comprise between 13% and 17% of the total rock volume at the locations logged.

Gwbert

This coastal inlet location provides another exceptional location at which to assess the continuity of coarser units with continuous exposure for up to 90m (Figs. 2.11and 2.12). Fine-grained sediments of the Nantmel Mudstones Fm. are exposed as colour banded mudstones interbedded with bioturbated intervals and thin silt layers. Background, clay-rich layers are generally 3-4cm thick and often show diffuse contacts with underlying layers (Fig. 2.13). The colour of these layers varies from pale green to medium grey and is thought, along with highly variable levels of bioturbation, to record changes in bottom water anoxia during deposition (Potter et al., 2005). Coarse intervals are often deformed by bioturbation, although rarely does complete dissemination occur. Of the sections logged, thin-beds of silt material account for roughly 12% of the total rock volume, showing a mean bed thickness of 7mm. Beds of higher than average thickness (>1cm) are often traceable for the length of outcrop (~90m), while thinner beds are often seen to pinch-out over distances of between 5 and 50m. Examples of the high resolution sedimentary logs taken at the Gwbert section are shown in Fig. 2.14.

Aberporth

Exposures of Nantmel Mudstones Formation sediments are also found in beach and cliff exposures at the western end of Aberporth beach. Facies are very similar to those encountered at Gwbert, located broadly along strike roughly 9km to the southwest.

Figure 2.10 (a) Photo-panel of mudstone facies outcropping at Newport Sands. Stitching together outcrop photographs allows the lateral continuity of coarser beds to be traced digitally. Once beds have been traced (b), the photograph can be removed and bed lengths measured (c).

Figure 2.11 (left) Aerial photograph of coastal inlet outcrop examined at Gwbert. Image courtesy of Google Earth.

Figure 2.12 (below) Photo-panel of extensive mudstone outcrop at Gwbert which allowed the tracing of beds laterally for upto 90m. Data was collected from the lower portion of these 8m high cliffs.

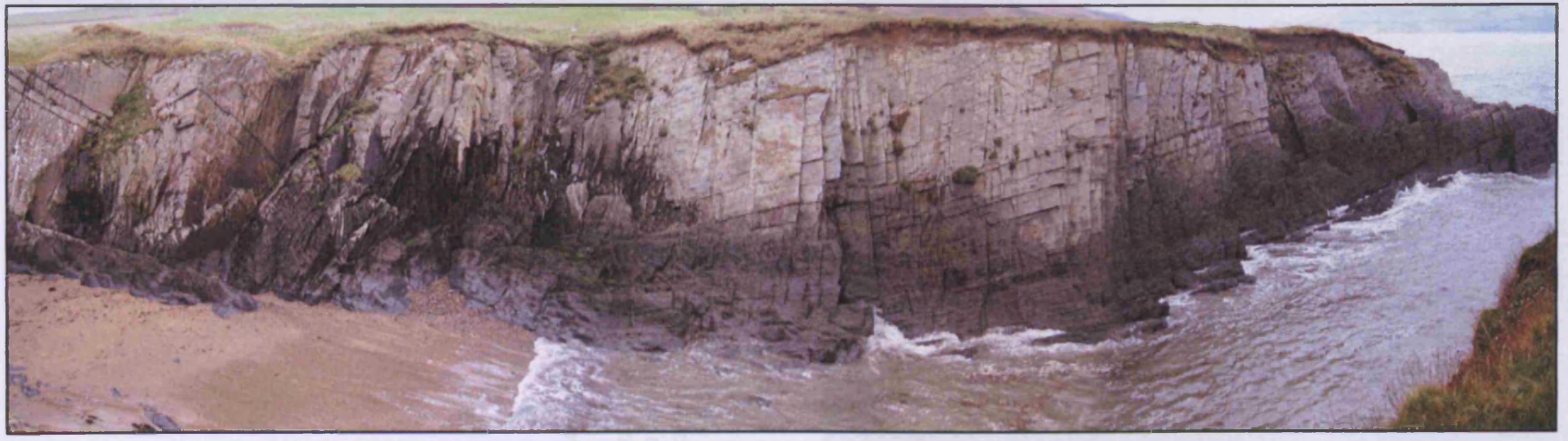

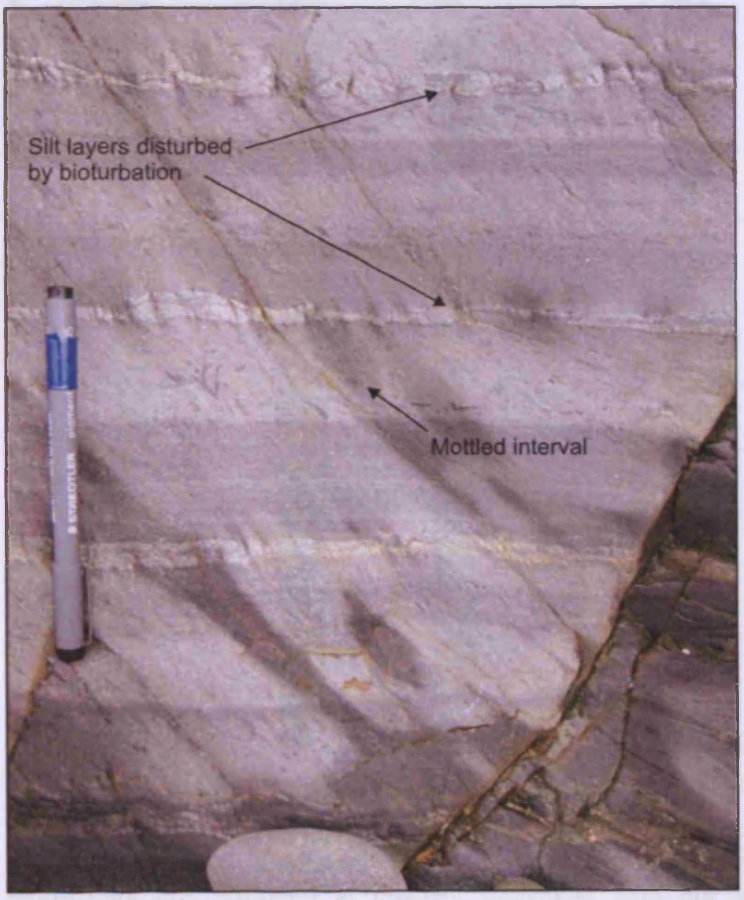

Figure 2.13 Outcrop photographs of Nantmel Mudstones Fm. exposed at Gwbert. The characteristic colour banding of this formation is produced by alternating layers of mottled and weakly laminated mudstones. Thin silt layers, generally <1cm thick, punctuate the sequence and are often disrupted by bioturbation.

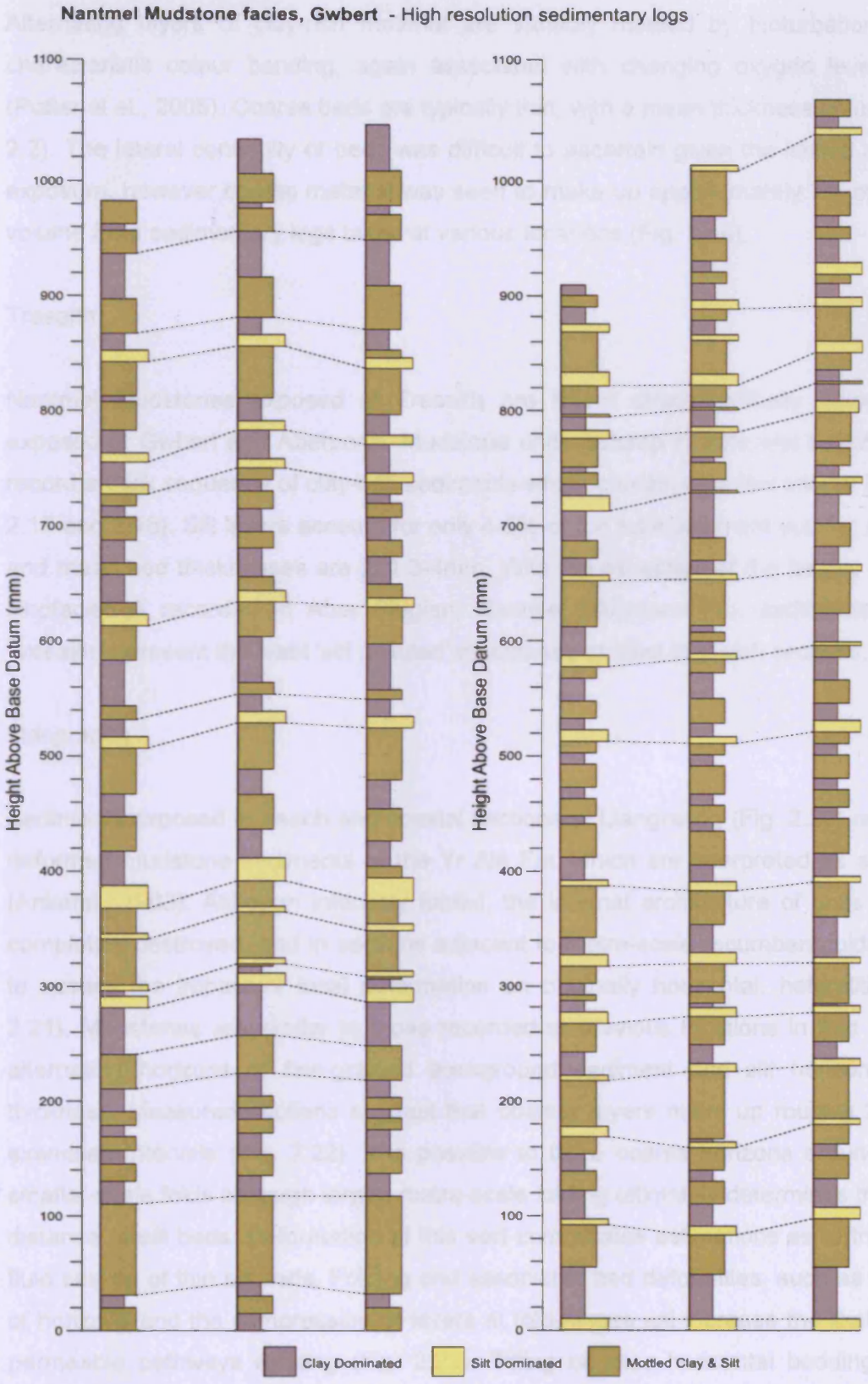

Figure 2.14 Two examples of correlated high-resolution sedimentary logs through Nantmel Mudstones Fm. exposed at Gwbert. Individual logs are separated laterally by 8-12m with bed correlations made by tracing individual silt layers between logged intervals. Base datum equal to beach level.

Alternating layers of clay-rich material are variably mottled by bioturbation and display characteristic colour banding, again associated with changing oxygen levels (Fig. 2.15) (Potter et al., 2005). Coarse beds are typically thin, with a mean thickness of just 5mm (Table 2.2). The lateral continuity of beds was difficult to ascertain given the limited accessibility of exposure, however coarse material was seen to make up approximately 7% of the total rock volume from sedimentary logs taken at various locations (Fig. 2.16).

Tresaith

Nantmel Mudstones exposed at Tresaith are found stratigraphically below those units exposed at Gwbert and Aberporth. Mudstone units outcrop in cliffs and beach sections and record a thick sequence of clay-rich sediments which contain very few coarse horizons (Figs. 2.17 and 2.18). Silt layers account for only 4-5% of the total sediment volume at logged sites and mean bed thicknesses are just 3-4mm. With the exception of the largely homogeneous lithofacies A recorded at Aber Rhigian, Nantmel Mudstone Fm. sediments examined at Tresaith represent the least 'silt polluted' mudstones studied in Welsh sections.

Llangranog

Sediments exposed in beach and coastal sections at Llangranog (Fig. 2.20) reveal intensely deformed mudstone sediments of the Yr Allt Fm. which are interpreted as slump deposits (Anketell, 1963). Although intensely folded, the internal architecture of units has not been completely destroyed, and in sections adjacent to metre-scale recumbent folds it is possible to assess the impact of local deformation on originally horizontal, heterolithic units (Fig. 2.21). Mudstones are similar to those recorded at previous locations in that they comprise alternating horizons of fine-grained background sediment and silt horizons of 5-10mm thickness. Measured sections suggest that coarser layers make up roughly 20-25% of the examined intervals (Fig. 2.22). It is possible to trace coarse horizons around the limbs of smaller-scale folds although larger, metre-scale folding ultimately determines the correlatable distance of silt beds. Deformation of this sort complicates estimations as to the likely risk to fluid sealing of thin silt beds. Folding and associated bed deformities, such as the elongation of horizons and the compression of layers at fold-hinges will increase the likelihood of more permeable pathways existing (Fig. 2.23). Tilting of once horizontal bedding also creates vertical or sub-vertical pathways of increased permeability which may extend through significant intervals of stratigraphy.

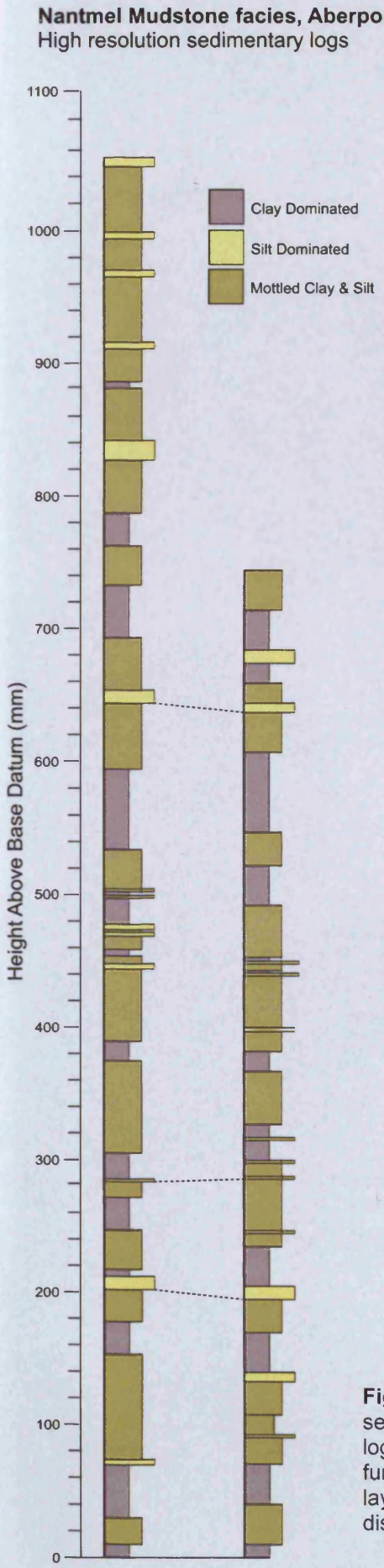

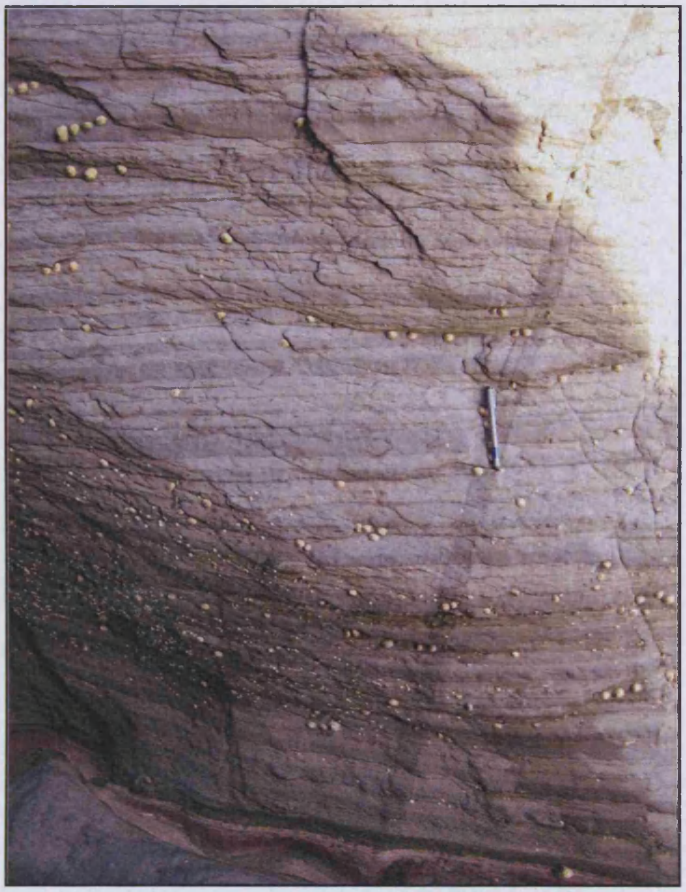

Figure 2.15 (above) Outcrop photograph of Nantmel Mudstones Fm. exposed in a beach section at Aberporth. Mudstone facies are similar to those exposed at Gwbert, comprising occasional silt layers interbedded with varyingly mottled clay-dominated sediments.

Figure 2.16 (left) High-resolution sedimentary log from Aberporth. Individual logs are 4m apart, however exposure limits further investigation of lateral continuity. Silt layers >5mm are correlatable over this distance. Base datum equal to beach level.

Figure 2.17 Aerial photograph showing the location of Nantmel Mudstones Fm. coastal exposures examined at Tresaith.

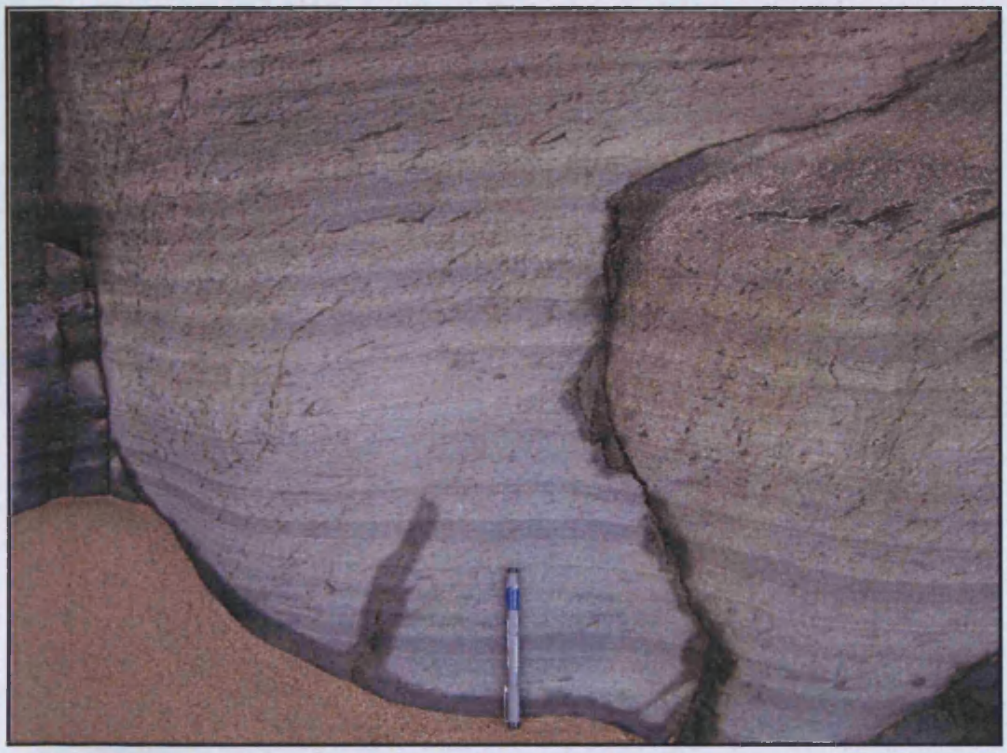

Figure 2.18 Outcrop photograph of Nantmel Mudstones Fm. from Tresaith. Facies are clay-dominated with occasional silt horizons generally less than 1cm thick. Bed contacts often show evidence of bioturbation.

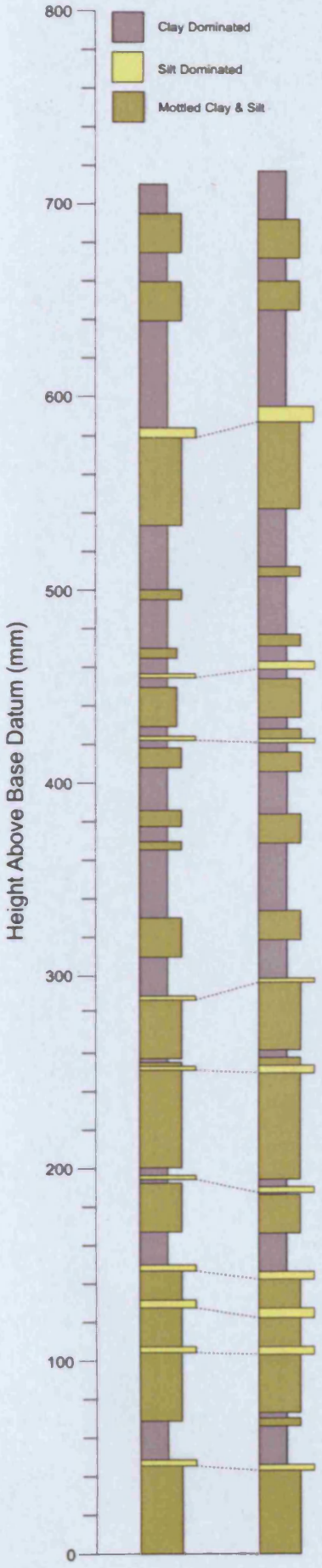

Figure 2.19 High-resolution sedimentary logs taken from Nantmel Mudstones Fm. exposed in Tresaith coastal outcrop. Two logs are separated by 4m with bed correlations made by tracing individual silt layers between logged intervals. Discrete silt layers are rare accounting for only 4-5% of the total mudstone volume. Base datum equal to beach level.

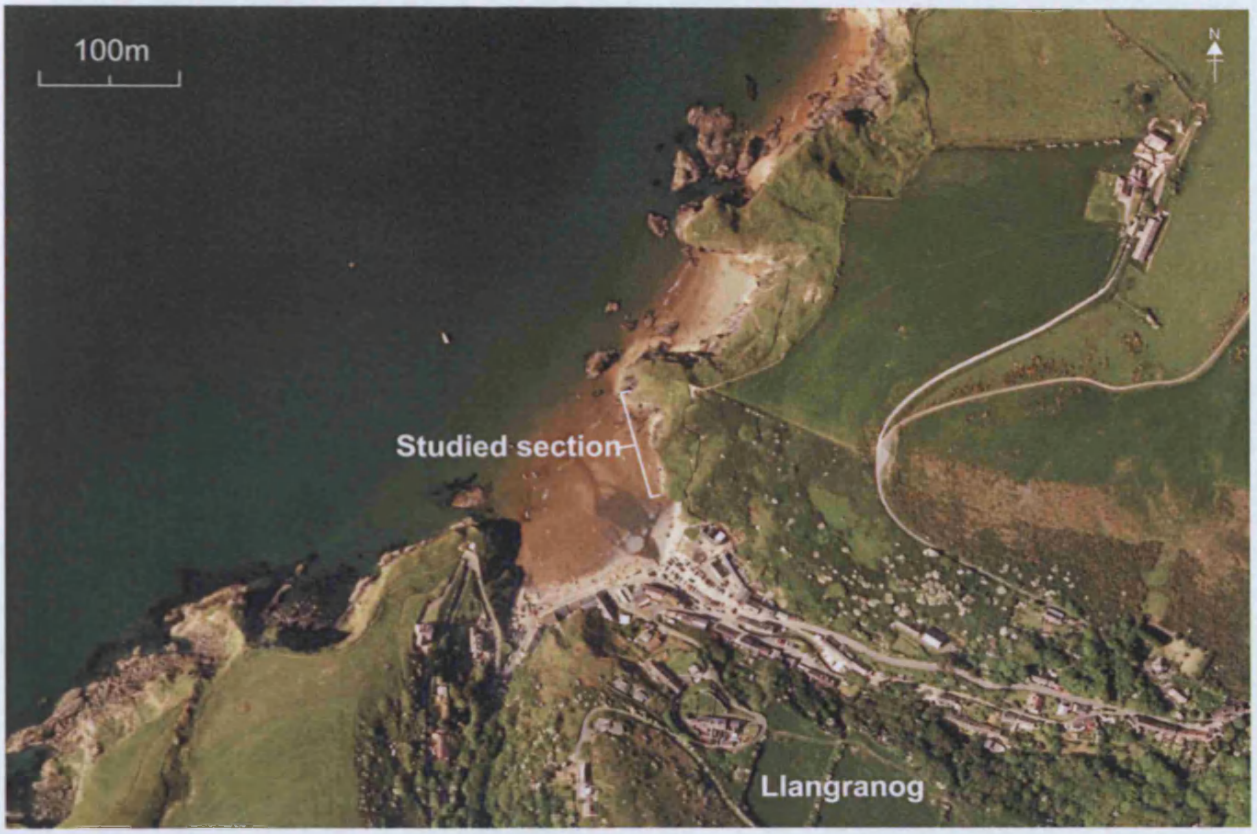

Figure 2.20 Aerial photography showing the location of Yr Allt mudstone beach sections examined at Llangrannog, west Wales.

Figure 2.21 Beach exposure of intensely deformed mudstones, Llangrannog. Camera case 7x10cm.

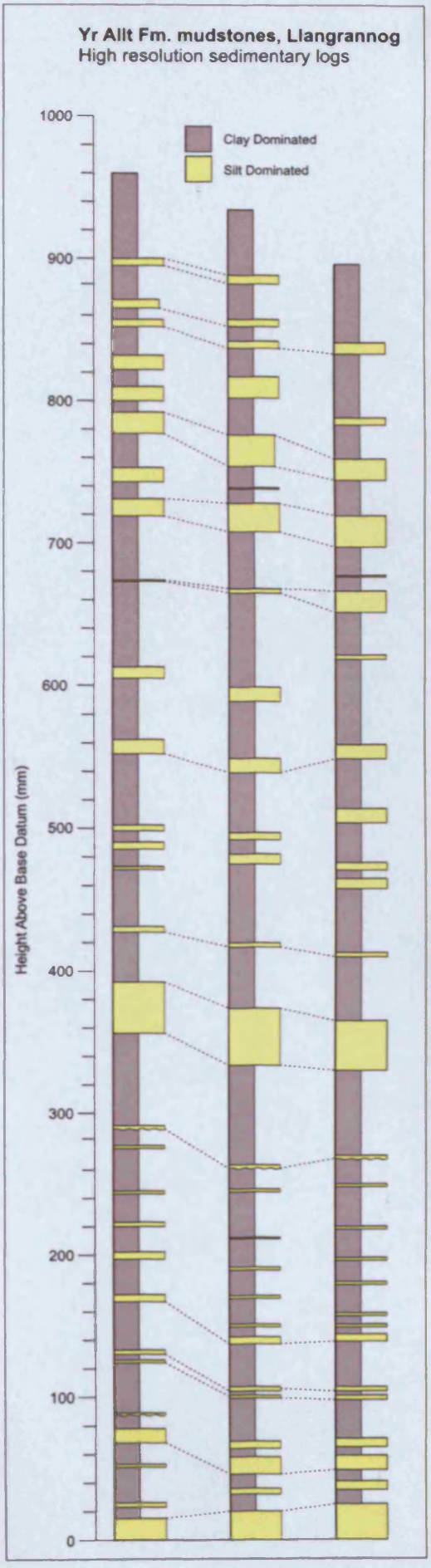

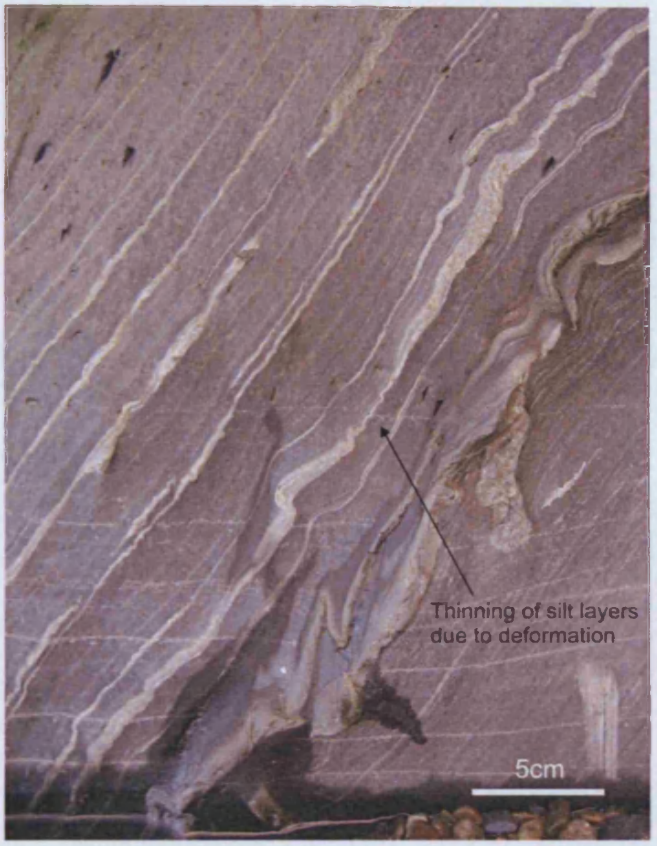

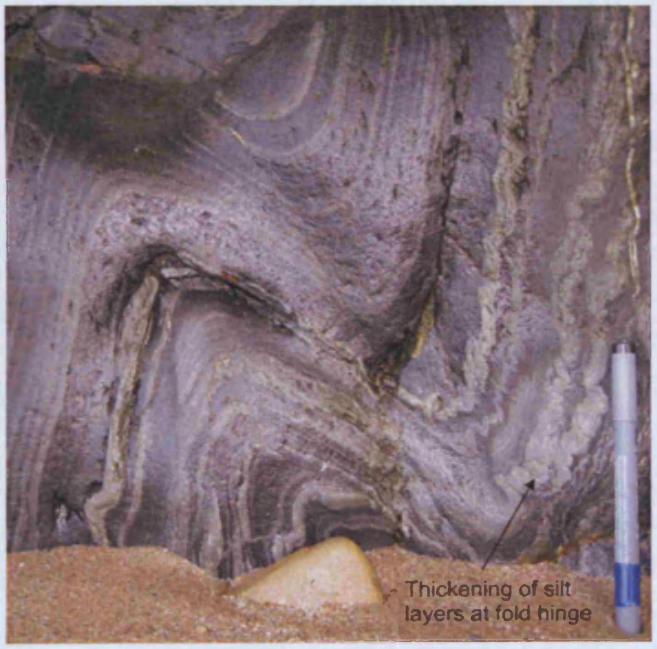

Figure 2.23 (above) Outcrop photographs of Yr Allt Fm. mudstones from Llangrannog. Internal deformation has altered the distribution of coarser layers away from their depositional orientations.

Figure 2.22 (left) High-resolution sedimentary logs taken at Llangranog. Logged intervals were separated laterally by 2-3m, however bed lengths were much greater due to folding. Correlations were possible for many thin-beds. Base datum equal to beach level.

2.2.4.2 Cornwall

Sediments examined at Upton and Sandymouth Bay belong to the Westphalian-aged Bude Formation and record a thick sequence of alternating grained sands interbedded with mudstones and occasional thick mudstone units (Freshney et al., 1979). Thick sandy packages (>1m), which are largely absent from Ordovician sequences examined in West Wales, are common in cliff exposures of the Bude Fm., attesting to considerable gravity-driven sediment delivery. Mud-rich units, which range from 10cm to over 5m in thickness, are thought to record periods of relatively high clay and silt input and relative basin quiescence during which muddy turbidites and hemipelagic sedimentation are thought to have persisted (e.g. Burne, 1995). Bude Fm. sediments were chosen to complement sequences examined in West Wales by allowing the examination of muddy facies deposited within a more dynamic, sand-rich depositional setting. Measured characteristics of thin-beds from Cornish locations are summarised in Table 2.2.

Sandymouth Bay

Mudstone dominated units, known locally as the Sandy Mouth Shale (Freshney et al., 1979), were examined in beach and cliff exposures roughly 1km north of Northcott Mouth (Fig. 2.24). Sediments are characterised by pale-grey mudstones interbedded with thin silt and fine-sand horizons (Fig. 2.25). Sedimentary structures are exceptionally well preserved in coarser layers where ripples and load structures are commonly observed (Fig. 2.26). Mudstones are typically largely structureless and occur as laterally continuous layers at the outcrop scale (maximum 60m continuous exposure). Thinly bedded coarse layers, which account for approximately 24% of the examined sequence, are also often traceable for upto 20m with a mean thickness of ~1cm. Examples of high-resolution sedimentary logs used to quantify bed characteristics at Sandymouth Bay are shown in Fig. 2.27.

Upton

Sediments examined in beach exposures directly west of Upton record alternating mudstones and sands contained within the steeply dipping northern limb of a small syncline (Fig. 2.28). Locally, facies record a mudstone dominated sequence which is punctuated with intervals of fine-sand and silt grade material. Coarser horizons range in thickness from 2-3mm thick laminae, to 10cm thick fine-sandstone beds. Coarser layers, interpreted as turbidite deposits, are regularly graded and show erosive bases where fine-sands contact underlying clay-rich mudstones, which are themselves typically structureless. Lateral tracing

Figure 2.24 Aerial photograph showing the location of Bude Fm. beach exposures at Sandymouth Bay examined during this study.

Figure 2.25 Bude Fm. mudstones exposed at Sandymouth Bay. Clay-rich layers are interspersed with silt and sand dominated horizons. Two ripple laminated beds are visible in the centre of the picture.

Figure 2.26 Thinly bedded mudstones at Sandymouth bay. Coarser layers (lighter grey) display ripple laminations and loaded basal contacts.

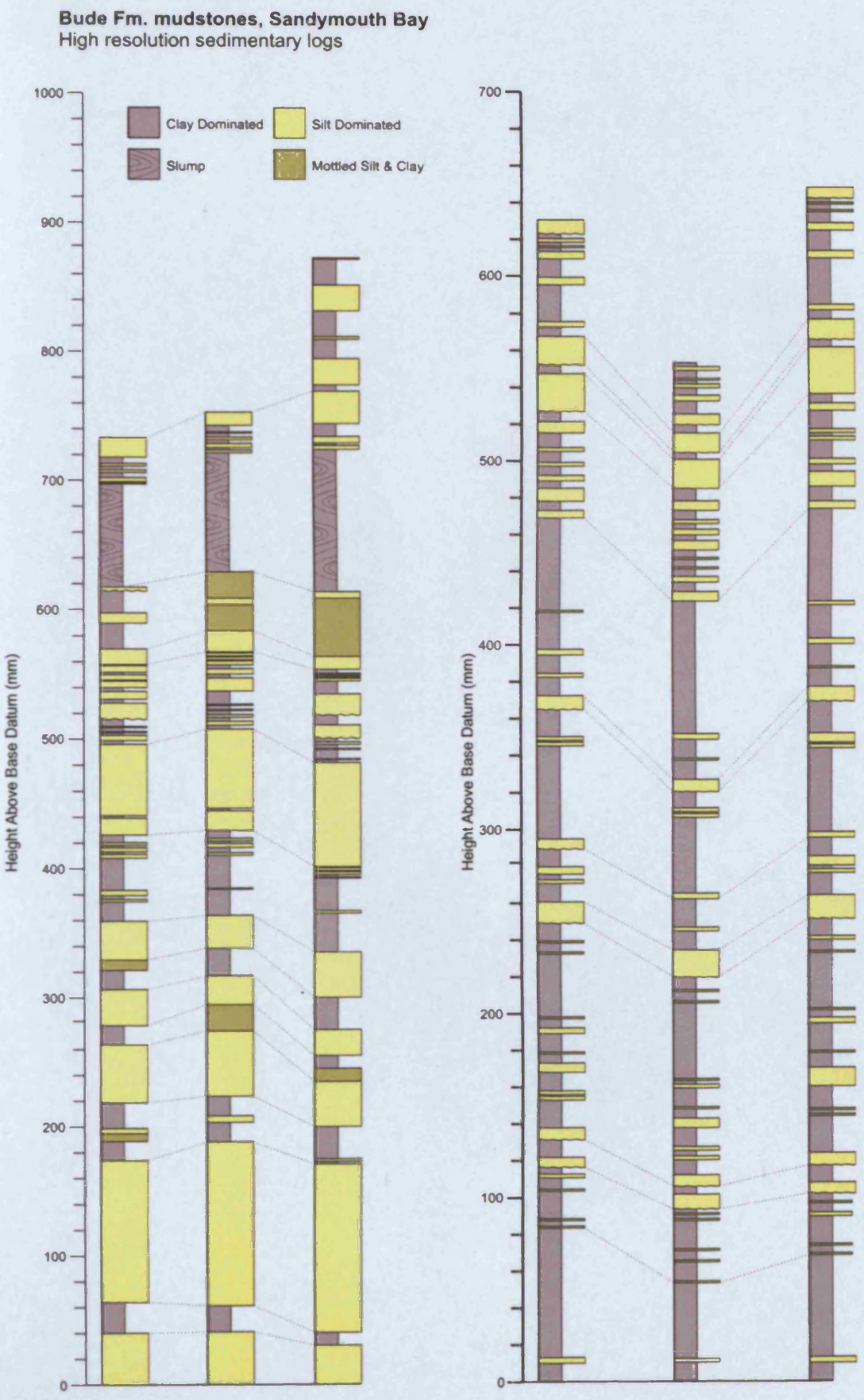

Figure 2.27 High-resolution sedimentary logs taken from Bude Fm. mudstones exposed at Sandymouth Bay. Each set of three logs above shows thin-bed correlations over >15m, although lateral correlations of >40m have been recorded. Base datum equal to beach level.

of both fine and coarser interbeds reveals that bed thicknesses vary very little over distances approaching 60m, producing a distinctive colour-banding appearance to the exposure (Fig. 2.29). High-resolution sedimentary logs taken at Upton are shown in Fig. 2.30. Within the mud-dominated facies examined at Upton, roughly 25% of the total rock volume is made up of discrete silt and fine-sand intervals, mirroring that of similar muddy facies examined at Sandymouth Bay.

Thinly bedded mudstones from west Wales and Cornwall have provided quantifiable information regarding the distribution, thickness, and lateral continuity of coarser grained beds within predominately fine-grained sequences. The overall coarser-grained nature of Bude Fm. deposits compared to mudstones from west Wales is reflected in the mean thickness of thin-beds in Table 2.2. Histogram plots in Fig. 2.31 also show the detailed distribution of bed thicknesses from outcrops examined in Wales and Cornwall and from core examined from a Caprocks Project petroleum industry case study. Core from this case study comprises a Tertiary slope-drape mudstone sealing sequence from North Africa and is presented here for comparison purposes (*see* Fig. 2.1). Plots reveal that the bed thicknesses and spacings of coarser, more permeable layers, are similar for Wales and Cornwall, with mean values varying by less than 1cm. Outcrop data also shows close similarities to the bed distribution recorded for the Tertiary mudstone seal, which appears comparable in this sense to the turbidite-rich sediments examined from the Bude Formation. Visual comparisons made from Fig. 2.1 and bed thickness data (Fig. 2.31) indicate that sedimentological studies made at outcrop may act as useful analogues for making predictions regarding the permeability distribution in subsurface mudstone sealing units.

2.2.5 Interlayer connectivity

Slope mudstone units examined from West Wales and Cornwall reveal that thin layers of coarser, potentially more permeable material exist within otherwise clay-rich, fine-grained sequences. In their original depositional arrangement, these coarse horizons will create a degree of permeability anisotropy by offering bedding-parallel zones of higher permeability and lower capillary entry pressure (Yang and Aplin, 2007). Layers of clay-rich sediment which lie between horizons of more permeable material can be thought of as thin, intraformational seals. Features or structures which allow permeable 'connections' between more permeable horizontal layers represent instances where vertical, as well as lateral permeability may be increased. In both West Wales and Cornwall, tectonic forces have since folded stratigraphy, however the original depositional relationship between more permeable and less permeable layers has been largely preserved (i.e. characteristic 'striped'

Figure 2.28 Aerial photograph of Bude Fm. mudstones exposed in beach sections, Upton, Cornwall. Studied interval indicated.

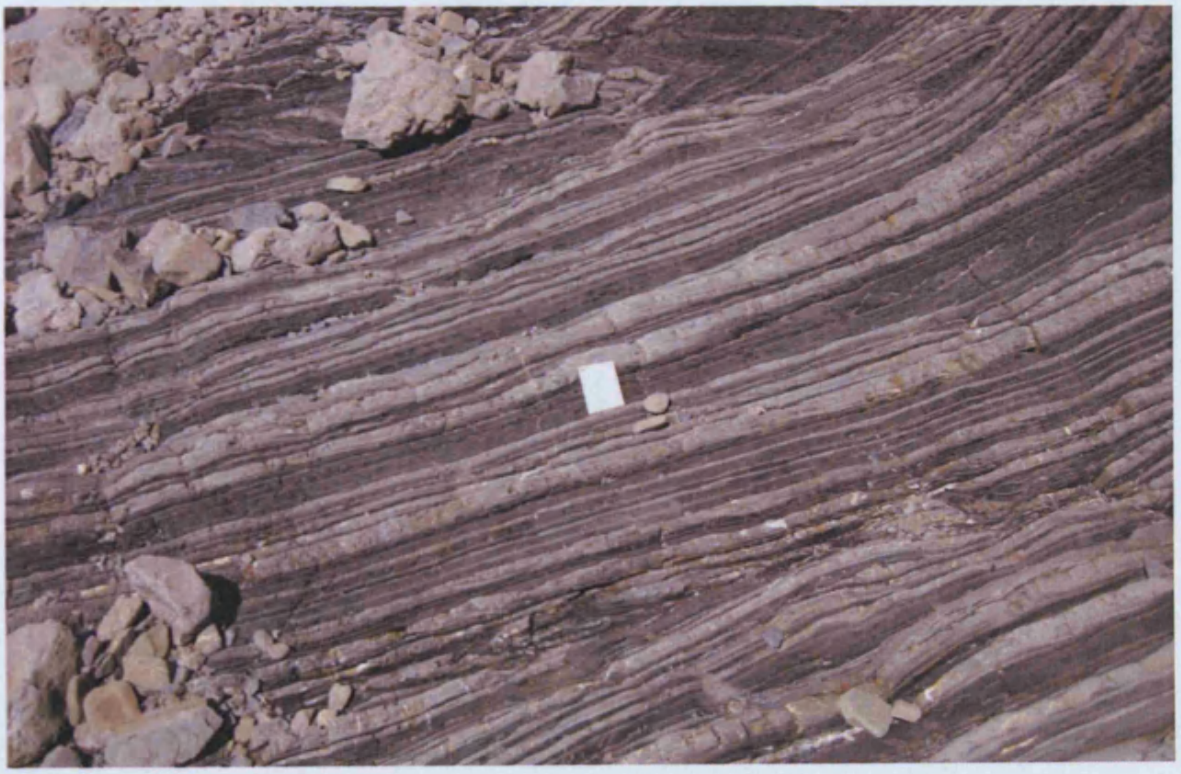

Figure 2.29 Bude Fm. mudstones exposed at Upton. Clay-rich beds are interspersed with lighter coloured silt and sand dominated beds producing the characteristic 'banded' appearance.

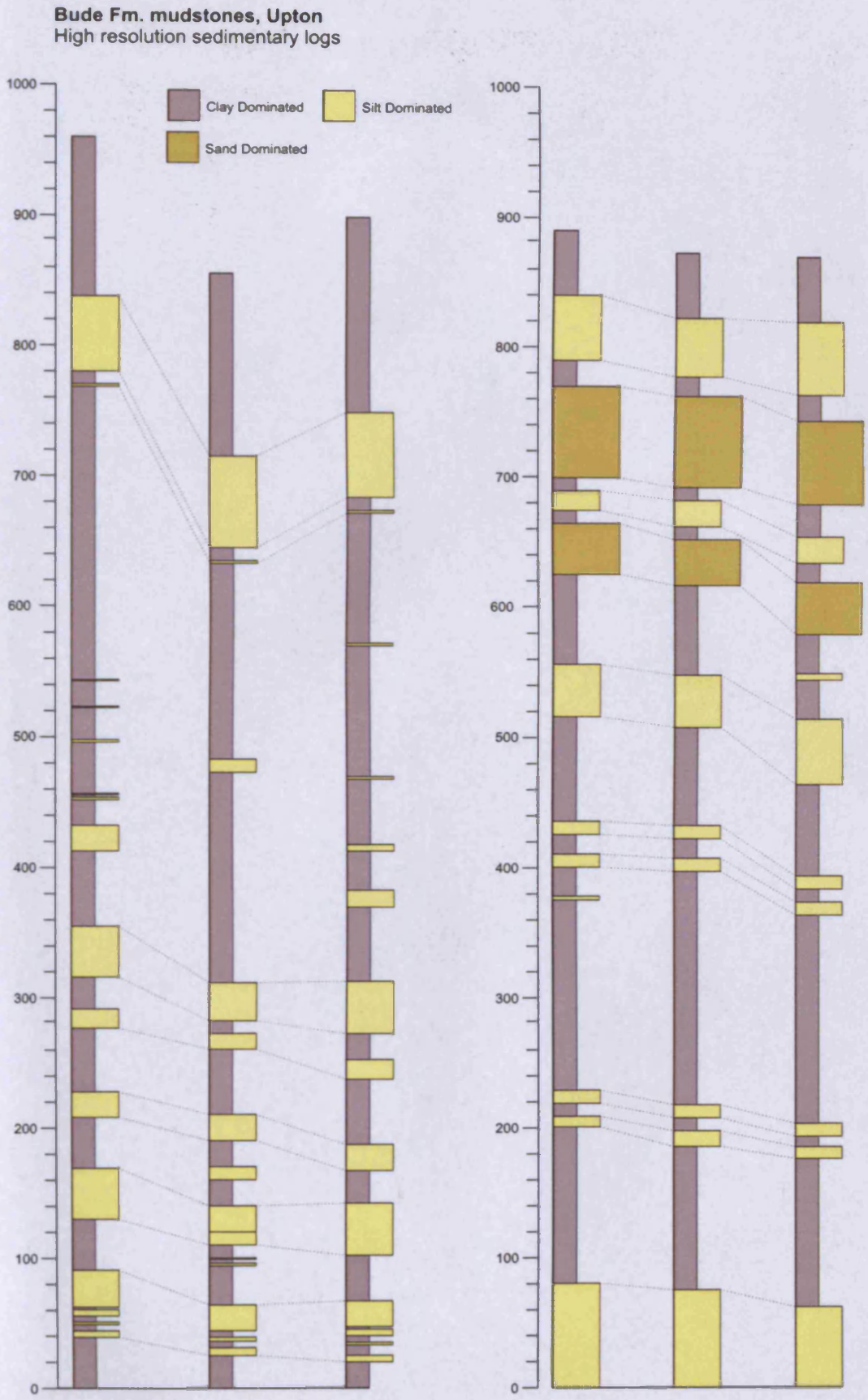

Figure 2.30 High-resolution sedimentary logs taken from Bude Fm. mudstones exposed at Upton. Each set of three logs above shows thin-bed correlations over >15m, although lateral correlations of >50m have been recorded. Base datum equal to beach level.

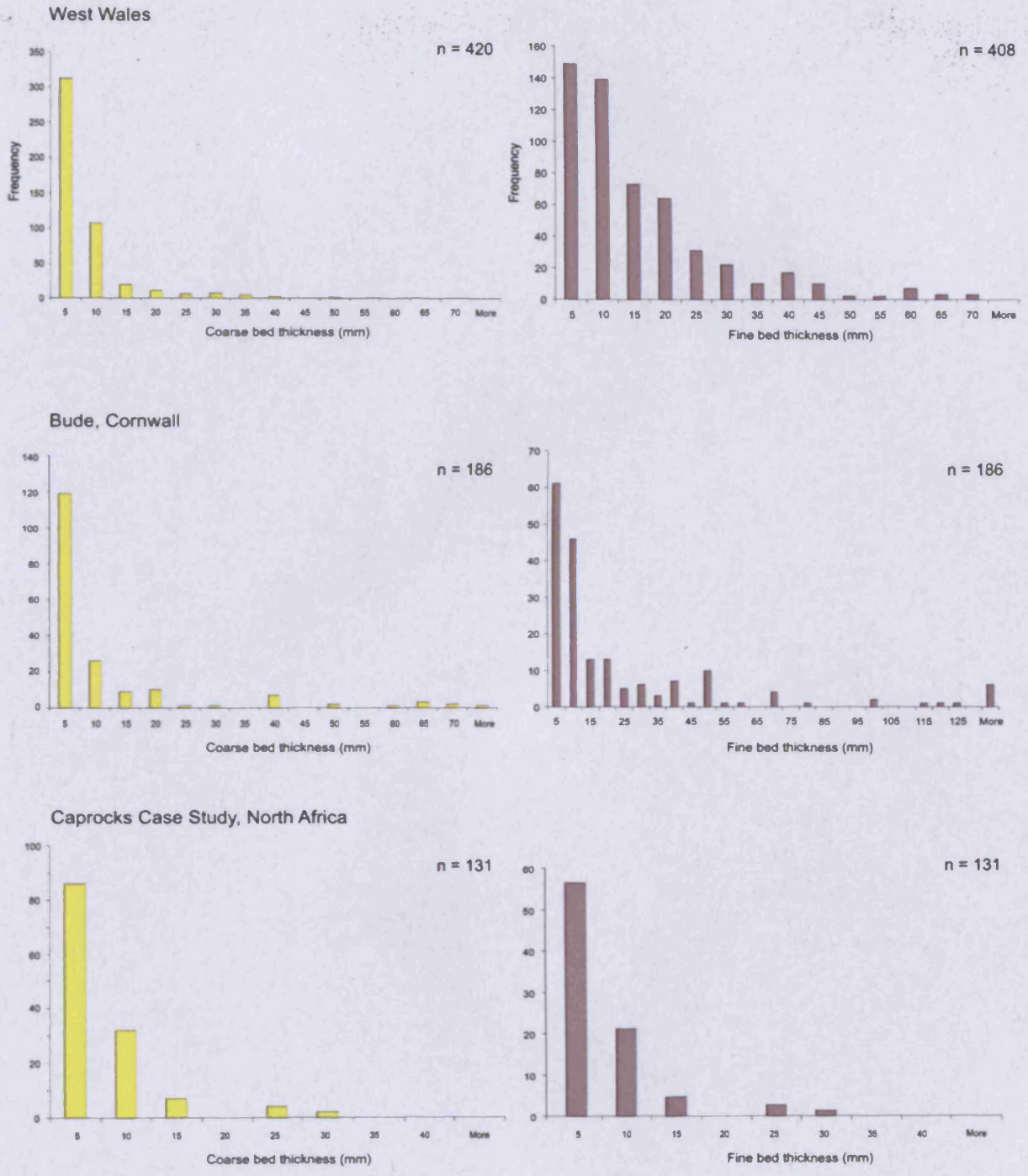

Figure 2.31 Histogram plots comparing bed thickness data collected from outcrop studies (Wales and Cornwall) and from core recovered from a Tertiary sealing sequence. More permeable layers, dominated by silts and fine-sand (yellow), are most commonly <1cm thick from all examples examined, while the thickness of clay-dominated layers separating them are commonly up to 2-3cm thick.

Thin-bed Data Summary

	Number of locations examined	Mean coarse bed thickness (cm)	Mean fine bed thickness (cm)	Total volume of coarse layers (%) (Range/mean)	Max thin-bed lateral continuity	Interlayer connectivity
West Wales	6	0.6	1.4	4-40/20	+100m	Limited to fracture networks, no sedimentary connections observed.
Cornwall	2	1.0	2.3	20-25/23	+50m	Rare sedimentary connections; load structures and bed truncations. Small fractures common.

Table 2.2 Summary of measured characteristic of thin beds from mudstone sequences examined in west Wales and Cornwall (n=606).

alternations, Fig. 2.29). Close inspection of outcrops reveals that a range of connection mechanisms exist, although they are relatively uncommon at the studied locations. Features observed fall into two broad categories (1) sedimentological features, and (2), structural features. The range of features observed in the field is outlined below.

2.2.5.1 Sedimentological features

Load structures

Load structures occur when the rapid deposition of a layer generates a density inversion with the layer below leading to soft-sediment deformation (Allen, 1982). Generally, these features are seen at the base of thicker silt and sand layers where coarser material has settled into the underlying mudstone. Where material becomes completely detached from its parent layer, features are known as load-balls. Where two more permeable horizons of silt or fine-sand are separated by only a thin interval of mudstone, load structures originating in the upper layer have been seen to create links with underlying layers (Fig. 2.32a). Load structures were recorded at many of the Welsh locations examined, particularly Yr Allt Fm. rocks at Llangranog, but were rare in Bude Fm. sediments. Of the load structures observed, very few show sufficient syn-sedimentary deformation to allow interbed connections to be made, and as a result, it is thought to be unlikely that this particular mechanism will represent a common method of interstratal connectivity.

Sediment ripples

Sediment ripples are formed where transporting currents interact with unconsolidated sediment creating undulating upper surfaces in silt and sand layers (Collinson and Thompson, 1989). The morphology and extent of ripples depends on the nature and volume of sediment being mobilised and the specific hydrodynamic conditions at the seabed. The most commonly observed features in Sandymouth Bay and Upton sections are starved ripples, formed where silt or sand material is limited such that grains are eroded from the stoss side and deposited on the lee side of the ripple (Nichols, 1999). A characteristic feature of the starved ripples observed in outcrop is a reduction in the concentration of coarser grains within the arcuate upper portion of individual ripples, producing a wispy, feather-like feature (Fig. 2.32b). Where such ripple sets exist, the vertical distance between the upper surface of ripples and the bottom surface of overlying silt/sand layers is reduced, and on rare occasions, completely bridged. Compared to the largely parallel, and uniformly thick coarser intervals observed in West Wales exposures, heterolithic units from Upton and Sandymouth

Bay contain frequent intervals of starved ripples, increasingly the probability that vertical connections may be made through contacts between coarser, more permeable horizons.

Bed terminations and truncations

Measurements of lateral continuity at many of the locations studied indicate that coarser beds are often continuous over distances in excess of 100m. Where beds are seen to pinch-out or become truncated bed spacings are modified from the uniform banded alternation of fine and coarser layers which dominate the majority of outcrops. Departures from this uniformly layered bed configuration lead to increased instances of coarser horizons being in vertical contact with one another. Bed truncations are more common in sediments which show signs of higher energy conditions during deposition. Current action and soft sediment deformation may juxtapose coarser layers (Fig. 2.32c), creating a unbroken pathway of increased permeability.

Bioturbation

Evidence for the bioturbation of sediments is relatively rare in the majority of Welsh and Cornish sections examined. Many outcrops preserve relatively undisturbed depositional structures, particularly in Bude Fm. sediments, which show very little evidence of bioturbation. Bioturbation is seen at several Welsh locations, namely Gwbert and Aberporth, where thinly bedded mudstones of the Nantmel Mudstones Fm. show a degree of homogenisation, thought to represent the action of burrowing organisms in a weakly oxic environment (Davies et al., 2003). Where sediment mixing has occurred, bed contacts become diffuse and sedimentary structures are destroyed, producing zones of homogenised sediment with a characteristic mottled appearance (Fig. 2.32d). Investigations by Lash (2006) suggest that thinly bedded mudstones which have been disrupted by bioturbation will preserve larger voids and pore-throats during mechanical compaction resulting from the poor alignment and angularity of silt grains. Thinly bedded mudstones which are not bioturbated are thought to undergo relatively rapid mechanical compaction, producing a planar, bedding parallel microfabric in clay-dominated intervals, resulting in lower permeabilities (Lash, 2006). Pervasive homogenisation of thinly bedded heterolithic mudstones therefore may decrease a unit's ability to act as an effective capillary seal to migrating fluids.

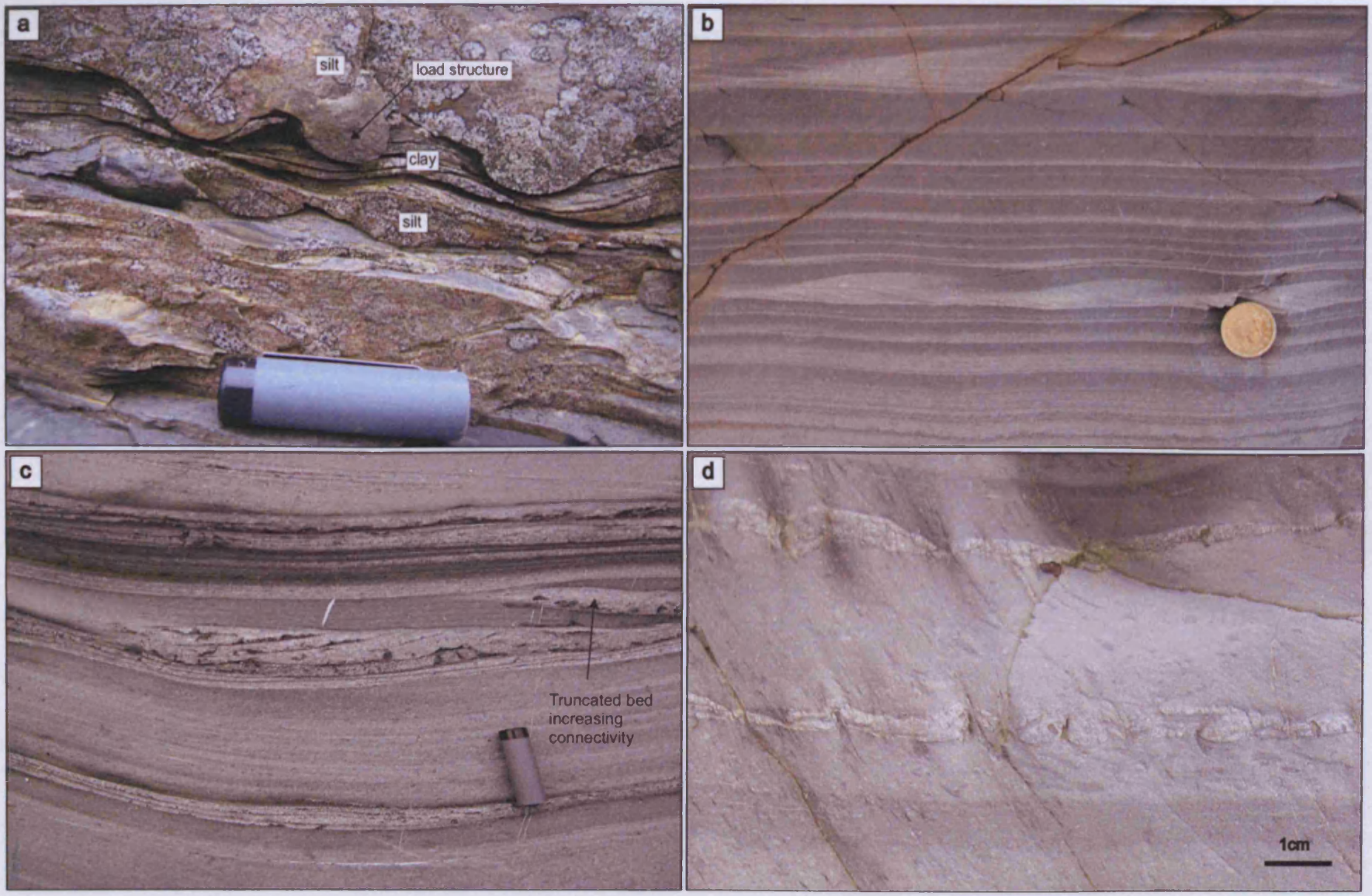

Figure 2.32 Sedimentological interbed connectivity mechanisms as observed from west Wales and Cornwall outcrops. (a) Load structures (b) Sediment ripples (c) Bed truncations (d) Bioturbation. See text for explanations.

2.2.5.2 Structural features

Fractures

Vertical (mode 1) fractures and fracture networks are known under certain circumstances to provide conduits of increased permeability in fine-grained sedimentary sequences (e.g. Mandl and Harkness, 1987; Watts, 1987; Long et al., 1996). Transmissive fractures which 'link' layers of higher permeability offer a mechanism with which to promote cross stratal fluid migration in thinly bedded mudstone facies. Unlike homogeneous mudstone units, fractures in thinly bedded units need only provide relatively short vertical pathways between coarser horizons, negating the need for large, unit bypassing fractures or faults as shown schematically in Fig. 2.33. Outcrop investigations carried out here reveal widely developed fracture networks at all of the locations examined (e.g. Fig. 2.25), most likely linked to post-depositional folding of sequences. Instances where tectonic or natural hydraulic fracture networks have developed in thinly bedded mudstones are likely to represent the most common and effective mechanism for producing inter-layer connectivity.

Bed juxtaposition

Another mechanism with which to form interconnected porosity is through post-depositional juxtaposition of more permeable layers. Displacements on fractures and faults, which generate small vertical offsets, could bring coarser horizons into or closer to, physical contact (Fig. 2.34). In addition to the juxtaposition of centimetre-scale coarser layers, larger scale displacements generated by faults may shift thinly bedded mudstone units into juxtaposition with more permeable units, such as channelised sand-bodies (e.g. Friedmann and Nummedal, 2003).

2.2.6 Discussion

Predominately fine-grained, clay-rich, marine sediments have been examined at coastal exposures along the Pembrokeshire and Ceredigion coasts in Wales and the around the town of Bude in Cornwall. Investigations have aimed to add to our knowledge regarding the existence and dimensions of thinly bedded silt and fine-sand layers which are seen to punctuate otherwise clay-rich submarine mudstone deposits. Where coarser horizons exist, modification of a unit's bulk grain-size distribution occurs, altering fluid-flow properties with potentially significant consequences for sealing capacity. Detailed field investigations at eight

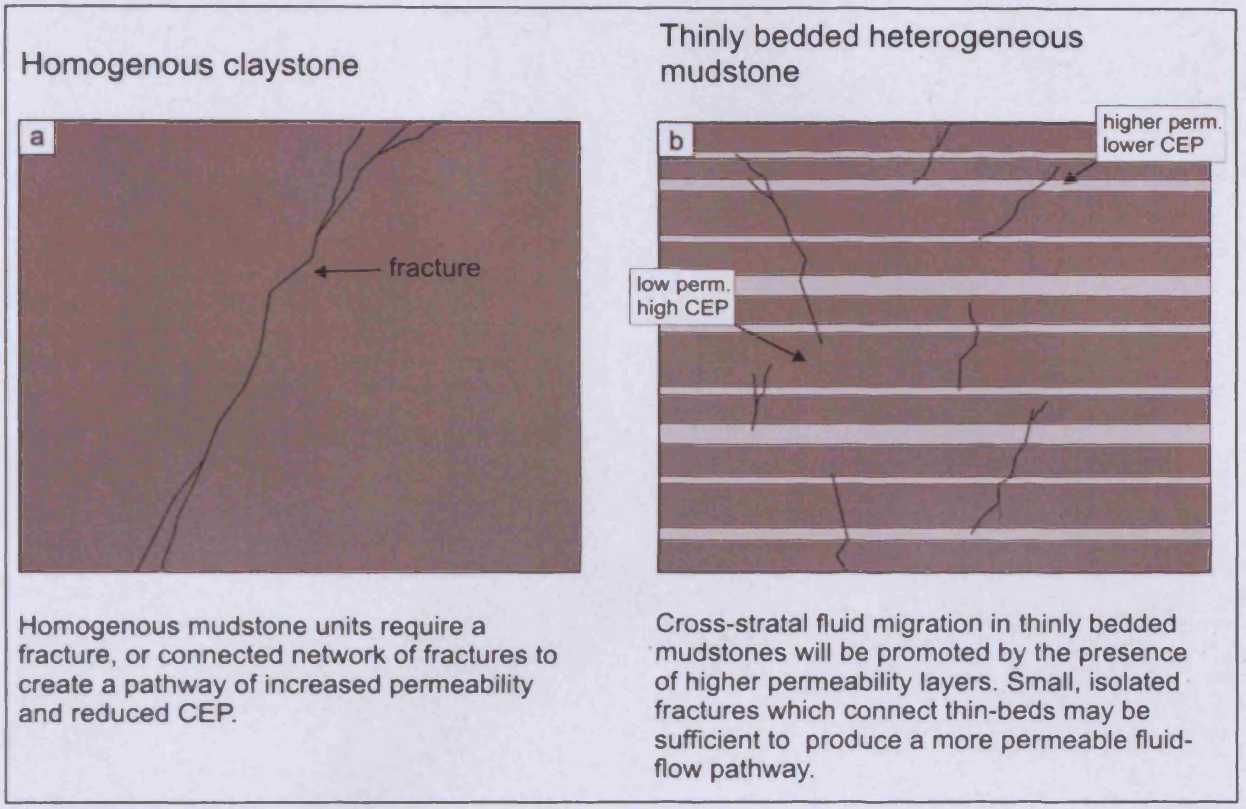

Figure 2.33 Cartoon illustrating the potential importance of thin-beds in establishing a vertically connected pathway of increased permeability in sequences lacking cross-stratal fractures.

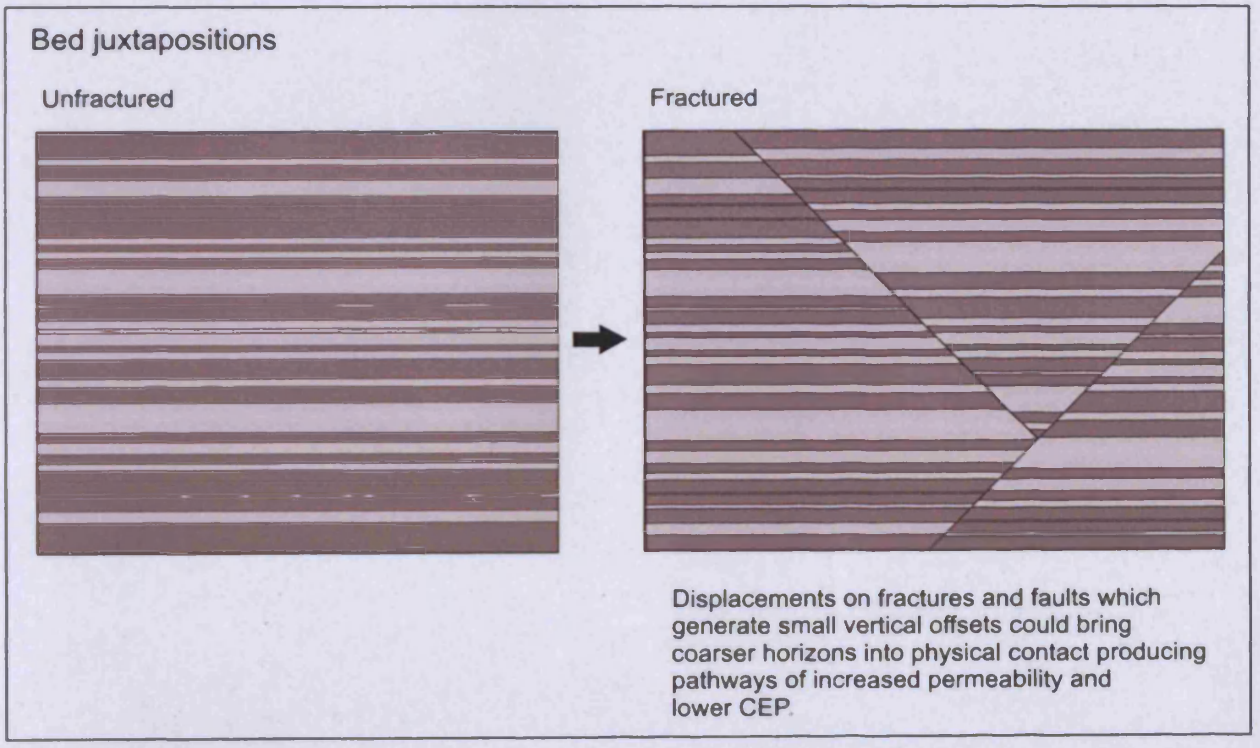

Figure 2.34 Cartoon illustrating the development of more permeable fluid-flow pathways through the juxtaposition of coarser horizons in response to fracture and fault offsets.

localities have provided quantitative data regarding the dimensions of thinly bedded slope mudstone successions, which to our knowledge, represents a largely unique dataset.

Coastal outcrops of Ordovician mudstones examined in West Wales reveal that thin-beds of silt-dominated material are commonly found interspersed with clay-rich background sediments, where they may comprise anywhere between 5% and 40% of the total rock volume. Locations sampling approximately 1500m of stratigraphy are dominated by largely structureless grey to green mudstones thought to represent largely background sedimentation onto a sloping basin margin. Punctuating these units in a range of configurations are pale grey silty horizons, generally less than 2cm thick, which are seen to preserve structures indicative of flow or current deposition (i.e. sediment ripples, laminations, or grading). The distribution and dimensions of these coarser horizons are found to vary between outcrops, presumably recording changes in the volume of coarse material delivered to the basin margin, or shifts in the way material was transported down-slope (i.e. confined or unconfined flows). The highest volumes of silt material were recorded within mudstones of the Cwm-yr-Eglwys Fm. exposed at Aber Rhigian and Newport are thought to represent channel-levee deposits. Thick sand turbidites and submarine channel features of the Dinas Island Fm. lie stratigraphically adjacent to the Cwm-yr-Eglwys Fm. (Davies et al., 2003) and may have provided these frequent pulses of silty material. Coarser layers are likely to represent deposition from largely unconfined turbidity flows originating upslope, or more confined flows which have subsequently over-spilled channel margins (e.g. Pirmez et al., 1997; Hiscott et al., 1997; Keevil et al., 2006). Mudstone units examined higher in the sequence record less frequent and generally thinner intervals of silt material belonging to the Nantmel and Yr Allt Formations, which are thought to have blanketed the slope (Davies et al., 2003). Exposures of these formations at Gwbert, Aberporth, Tresaith and Llangranog record an average of 10% silt found as discrete beds, indicating a pronounced shift in the depositional regime.

The frequency, thickness and volume of coarser material recorded from Bude Fm. units is in keeping with their interpretation as a higher energy facies compared to those examined in West Wales. The more pronounced activity of turbidity currents has increased the likelihood of vertical bed connections by creating ripples and bed truncations but has also reduced the lateral continuity of coarser grained layers. In general, the greater volume of coarser material and the increased chance of establishing connected layers indicate that this type of thinly bedded facies would likely act as a less effective capillary seal than the majority of those examined in West Wales.

The scale of outcrop limits the lateral tracing of coarser grained beds to roughly 100m at even the largest exposures, however their lateral persistence and often uniform thickness over these distances implies that they may be far more extensive than the limits of outcrop i.e. Aber Rhigian. The winnowing of coarser horizons during deposition appears to be the primary process affecting the lateral continuity of thin-beds, although the action of burrowing organisms and soft-sediment deformation are also seen to disturb bedding.

The often laterally continuous silt beds examined at outcrop offer horizons of high permeability and lower capillary entry pressure; however their ability to promote the vertical migration of fluids is reliant on a degree of connectivity between layers. Evidence from the mudstone units studied suggests that connectivity facilitated by sedimentological features will be sporadic and unpredictable. Depositional conditions do not appear to have been sufficiently energetic to promote a greater level of disruption to otherwise horizontal bedding contacts, limiting potential 'primary' connections (sediment ripples, load structures etc). Deformation of the Palaeozoic rocks examined in West Wales and Cornwall has produced sequences which are highly faulted and pervasively fractured. Networks of small (<1m) fractures are found throughout the examined exposures, and were similar fractures to be present in modern slope mudstone sequences, would represent the most likely mechanism by which linkage of more permeable horizons may occur (Aydin, 2000).

The usefulness of these outcrop investigations relies on the ability to draw analogies between the facies studied and sequences thought to be actively functioning as barriers or baffles to fluid migration. Investigations put forward in Chapter 3 indicate that heterolithic mudstone units are indeed found in the majority of fine-grained continental slope successions, though they generally record fewer discrete thin layers than the studied outcrops (*see* Chapter 3.) When coupled with data gathered from outcrops, this information brings into question the widely held notion that clay-rich slope deposits can always be considered as high quality capillary seals.

While seismic-scale seal-bypass systems such as sandstone injection networks and fluid pipes are receiving increasing attention (Cartwright et al., 2007), the rarity of recovered sediment core from sealing lithologies, and the sub-logging tool resolution of thinly bedded units means that very little attention has been paid to the potential for thin-beds to act as a "stratigraphic" bypass mechanism. Evidence of top seal leakage is commonly confirmed by oil shows within the sealing unit itself (Fig. 1.3) or the existence of stratigraphically separated reservoirs (Dewhurst and Hennig, 2003). In such instances, capillary leakage is often not considered as a contributory factor to leakage based on the typically low permeabilities

associated with clay-rich sequences. In the absence of an evident large-scale bypass system (i.e. charged, fault-linked reservoirs), networks of conductive fractures are commonly suggested to have contributed to leakage (Leith et al., 1993; Aydin, 2000; Dewhurst and Hennig, 2003). Fracture networks, which allow fluids to bypass the pore-network of a seal unit, are generally below the resolvability of seismic data and are often difficult to predict spatially. In settings where pre-existing fracture networks occur or where hydraulically induced fractures have developed, the presence of thinly bedded mudstones will promote further leakage through the sediment pore-network enhancing the overall rate of hydrocarbon escape.

The potential significance of thin-beds in dominantly fine-grained clastic sequences also goes beyond their function as seals to oil and gas accumulations. Hydrocarbons reservoired within units which are classically considered as 'shale-prone', are themselves becoming increasingly favourable exploration targets (Shew et al., 1995). Thinly bedded channel-levee sediments in the Gulf of Mexico are one example of heterolithic sand/shale sequences which are under investigation as potential petroleum reservoirs (Darling and Sneider, 1992; Felt et al., 2004). Assessing the distribution of these units from an oil producing perspective presents the same difficulties as investigations from a sealing capacity standpoint. Increasingly, examinations of slope and channel-levee deposits at outcrop are providing vital information regarding the distribution and likely connectivity of coarser units (e.g. Khan et al., 1996). An aim of the Caprocks Project has been to embed high-resolution outcrop data concerning the distribution of more permeable beds into fluid-flow simulations with the eventual aim of being able to up-scale effective properties to a suitable scale for use in standard basin modelling packages.

2.2.7 Conclusions

1. Field investigations carried out as part of the Caprocks Project have revealed that well exposed mudstones, likely to represent a mixture of hemipelagitic and channel-levee deposits, outcropping around the town of Cardigan in Wales and Bude in Cornwall comprise up to 40% discrete coarse beds.

2. Mean net-to-gross values for mudstone facies examined in Welsh locations reveal a value of 20% while Cornish exposures reveal a mean value of 23%.

3. Coarser beds have a mean thickness of 6mm from Welsh locations, and 10mm from Cornish locations, while interbedded clay layers have mean values of 14mm and 23mm, respectively.

4. Coarser horizons of a few centimetres thickness may be laterally continuous for distance in excess of 100m. Continuity appears to be largely dependent on hydrodynamic conditions and syn-depositional disruption to bedding.

5. Hydraulic conductivity between sub-horizontal layering is likely to be limited, with transmissive fracture networks representing the most likely method of creating pressure communication between coarser layers.

6. Thin-beds offer a sub-log scale bypass mechanism which may be responsible for compromising otherwise effective capillary seals by providing a connected network of more permeable sediment.

2.3 New Zealand

2.3.1 Aims of Taranaki field studies

Building on outcrop data collected in the western British Isles, field studies in New Zealand's Taranaki region utilised world-class exposures to examine the spatial relationships of various continental slope facies and the existence of coarser grained lithologies. As discussed in the fieldwork introduction (section 2.1), real rock studies such as this are invaluable, providing grounding for remote subsurface investigations and adding to the overall knowledge of mudstone sedimentology. This work complements the high-resolution mudstone outcrop studies from West Wales and Cornwall by examining near continuous exposure of 850m of Miocene continental slope stratigraphy. Mapping of lithological units at the facies-scale allowed us to capture the distribution of varying sediment types and to highlight the presence of coarser lithologies, likely to act as less effective capillary seals. The northern Taranaki coast exposures also provide an opportunity to assess the kilometre-scale distribution of characteristic slope 'genetic' depositional units such as submarine channels, mass-transport complexes and hemipelagic units, something that is typically only possible to estimate using seismic profiling. This information feeds into the Caprocks Project genetic units modelling approach and provides geological grounded data regarding the genetic building-blocks of a continental slope succession.

Also under investigation was the resolvability of thin-intervals of coarser grained lithologies using a portable gamma-ray spectrometry. Identifying coarser grained bodies, tens of meters wide, and estimating their dimensions and internal character is possible using seismic data and wireline logging, however detection of thinly bedded mudstones may be at the resolution limit of these tools. Using this geophysical technique allowed us to assess the likely response of this universally employed exploration tool to small-scale grain-size heterogeneities in the subsurface.

Laboratory analyses were carried out on a range of samples providing quantitative physical properties data with which to evaluate the likely fluid-flow properties of finer portions of this slope depositional system.

In summary, the keys aims of the Taranaki fieldwork were to;

- Map the distribution and spatial relationships of different slope lithofacies
- Produce detailed sedimentary logs of heterolithic and thinly bedded facies

- Evaluate the resolvability of heterolithic units using portable gamma-ray spectrometry
- Sample sediments to determine grain-size distribution and hydraulic properties

2.3.2 Overview of Taranaki Basin and study area

The Taranaki Basin occupies an area of approximately 100,000km² along the western margin of New Zealand's North Island, and in places, records close to 9 km of Cenozoic sediment (King and Thrasher, 1996). The majority of the basin is located offshore beneath the modern continental shelf, whilst onshore portions of the basin form the Taranaki Peninsula and north-western South Island. The contemporary Taranaki Basin (Fig. 2.35) lies to the west of the major east-dipping Taranaki Fault Zone which denotes its eastern margin (Cope and Reed, 1967). To the west and northwest the basin deepens and merges with the New Caledonia Basin (Pilaar and Wakefield, 1978). The basins arbitrary southern limit is generally taken as Nelson in the northern South Island (Knox, 1982). The Taranaki Basin is the largest petroliferous basin in New Zealand, currently producing 14 millions barrels of oil and 650,000 barrels of LPG per year (Crown Minerals, 2009a). Many of the formations which outcrop in the Taranaki Peninsula (e.g. Urenui and Mt. Messenger) are also important units in subsurface plays, making detailed field investigations extremely useful when interpreting petroleum system data.

The evolution of the Taranaki Basin has been extensively studied since the early Twentieth Century when the region's hydrocarbon prospects were becoming apparent (e.g. Henry, 1911; Henderson, 1937; van der Klugt et al., 1959; Cope, 1965). More recent publications have made use of a growing volume of open access petroleum industry reports and seismic data to interpret the regional subsurface structure (e.g. Knox, 1982; Thrasher and Cahill, 1990; King and Thrasher, 1996; Hansen and Kamp, 2004).

The early evolution of the Taranaki Basin is thought to be represented by a period of intracontinental rifting associated with seafloor spreading in the Tasman Sea during the Mid-Late Cretaceous. This led to a series of north- and northeast-striking half-grabens and sub-basins (King and Thrasher, 1996; Laird, 1980). Subsequent deposition during Pliocene-Eocene post-rift regional subsidence records a gradual transgression and a transition from terrestrial, to marginal marine, to fully marine environments (Holt and Stern, 1994; King and Thrasher, 1996). Following the inundation of rift topography created during the Cretaceous, the Taranaki Basin developed as a passive margin with regional sedimentation patterns and continued transgression. Waning terrigenous input to the basin during the Late Oligocene coupled with rapid subsidence, particularly in the east, led to an under-filling of the basin and

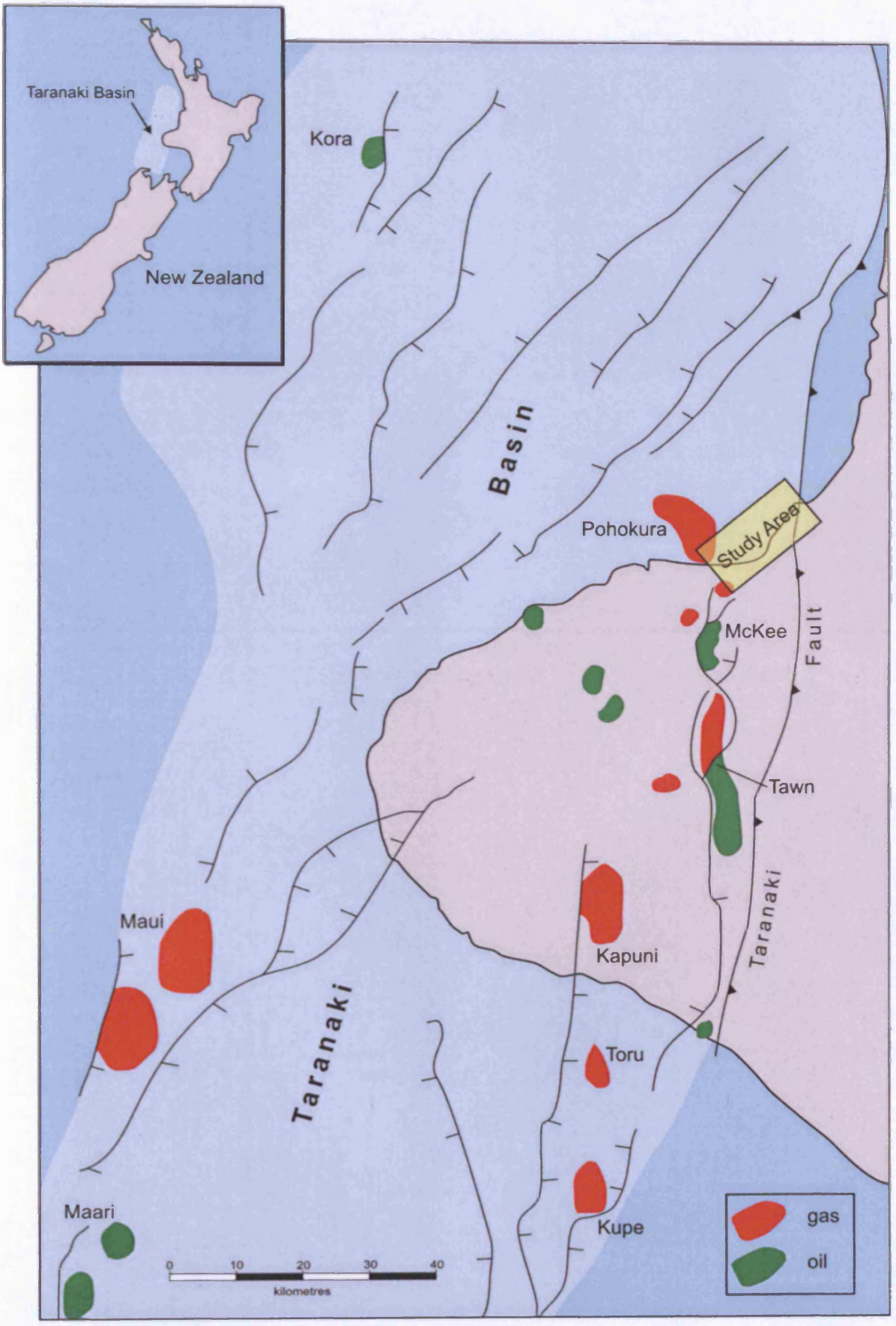

Figure 2.35 Structural map of the Taranaki Basin showing the location of major faults and oil and gas fields. Study area on the northern Taranaki coast is shown. Redrawn from Hart (2001).

a shift from siliciclastic to carbonate dominated sedimentation (King and Thrasher, 1996). The earliest Miocene marked a shift from extensional to compressional tectonism at the eastern margin of the basin, resulting from the clockwise rotation of the Australia-Pacific plate boundary (Knox, 1982). Subsequent crustal thickening and westward thrusting of basement rocks along the Taranaki Fault Zone (Knox, 1982) caused further loading of the lithosphere and expanded the developing foredeep westward (Holt and Stern, 1994). This foredeep remained under-filled until ~17Ma when a marked increase in sedimentation is interpreted by Holt and Stern (1994) to reflect the change from submarine to subaerial topography at the thrust belt. During the middle Miocene - Pliocene contractional forces waned in the north of the basin and shifted southward as a result of rotation of the Hikurangi Trench (King and Thrasher, 1996). This shift led to inversion of Cretaceous-Paleocene grabens in the southern Taranaki Basin and the creation of new NE-SW trending extension grabens in the northern and central regions (Hansen and Kamp, 2004; King and Thrasher, 1996). These tectonically controlled depocentres were rapidly infilled with sediment sourced from the erosion of uplifted regions to the southeast of the basin and record a rapid north-westward progradation of the sedimentary wedge (King and Thrasher, 1996). Urenui Formation sediments, examined in outcrop for this study, were deposited as part of this phase of rapid outbuilding. Following a widespread base Pliocene unconformity, rapid uplift and erosion of the Southern Alps to the south provided renewed sediment input and facilitated the progradation of sediments onto the Western Stable Platform (King and Thrasher, 1996). Large volumes of sediment delivered to the Taranaki Basin margin during the Plio-Pleistocene, depositing the Giant Foresets Fm., resulted in an overall acceleration of the regression initiated during the Miocene (Kamp et al., 2004).

2.3.3 Outcrop locations

The study area encompasses the type section of the Urenui Formation as established by Glennie (1958). Hay (1967) later used the name Urenui Siltstone, but here we favour the Urenui Fm. (*sensu* King, 1988).The Urenui Fm. comprises a thick sequence of largely fine-grained slope sediments punctuated at several stratigraphic levels by coarser channelised facies. The formation was deposited during the late-Miocene (~10 Ma), a period when large volumes of clastic sediment were delivered to the NE-SW trending continental margin and developing sediment wedge (Kamp et al., 2004).

Coastal sections examined during this study extend south-westward from Pariokariwa Point to just northeast of Motunui, providing almost continuous exposure of the gently dipping Urenui Fm. (Fig. 2.36). The northern limit of the study area marks the gradational contact

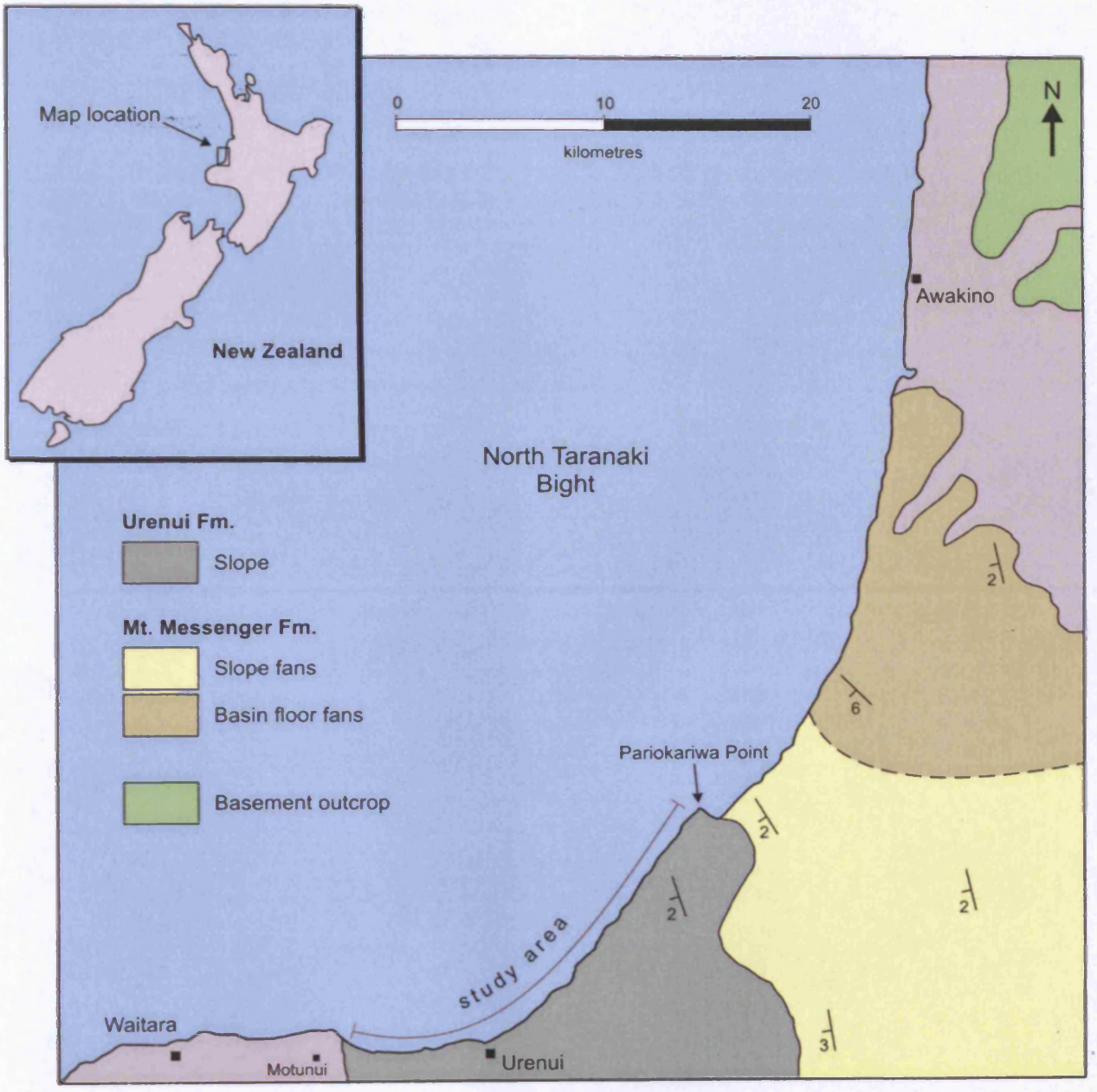

Figure 2.36 Simplified geology of the North Taranaki coastal region. Modified and redrawn from Nelson et al (2004).

between the Urenui Fm. and the underlying sand-dominated Mt. Messenger Fm. as seen in outcrop. The Urenui Fm. is exposed south of Pariokariwa Point for approximately 20 km as the coastline swings westward, recording roughly 850m of vertical stratigraphy (King et al., 1993). Miocene strata dip to the southwest at between 5-10 ° and are generally confined to the lower half of sea-cliffs throughout the area, although less well-exposed inland outcrops exist. Relief along the coast is typically between 10 and 25m, although high ground gives way to areas of lower lying topography where rivers intercept the coast. Pleistocene cover deposits overlie and truncate the Urenui Fm. throughout the area, and are commonly exposed in the upper portions of cliffs (Fig. 2.37).

Throughout the region, the Urenui Fm overlies the middle-late Miocene deepwater Mt. Messenger Fm (King et al., 1993). This formation is best exposed in the north-west of the Taranaki Peninsula, directly north of our study area, where an 850m thick section is exposed in coastal cliffs (Fig. 2.38). The formation is first exposed at the Mokau River and extends south, at an average dip of ~5°, until Pariokariwa Point where it dips towards the offshore. The section comprises mainly thinly bedded fine- to very-fine sandstones, interbedded with silts and mud. Thick bedded sandstones at the base of the unit are interpreted by King et al. (1994) to represent basin floor-fan deposits which give way to thinly interbedded deposits indicative of slope-fan deposits higher in the section. For a detailed description of lithologies the reader is referred to King et al. (1993).

2.3.4 Facies mapping and outcrop logs

In addition to mapping the distribution of slope facies from the outcropping Urenui Fm., detailed sedimentary logging was carried out at select locations throughout the study area, utilising beach-level exposures. A total of 20 detailed sedimentary logs were acquired, many with accompanying gamma-ray spectrometry. Log locations were chosen within intervals of interest based on sedimentological character, the condition and suitability of the outcrop, and the accessibility of the site. Where appropriate, samples were removed for laboratory grain-size and porosity analysis.

2.3.4.1 Outcrop gamma-ray spectrometry

Spectral gamma-ray spectrometers are commonly employed as a means of recording the natural gamma-ray spectra emitted by decaying radioactive isotopes present in most sedimentary rocks. The application of such tools conventionally focuses on the use of gamma-ray emissions as a tentative proxy for grain-size variations in sedimentary

Figure 2.37 Urenui Fm. exposed in cliffs approximately 1.5km southwest of Wai-iti (view looking southwest). Here, weakly bedded siltstones are overlain and truncated by Quaternary volcanoclastic deposits.

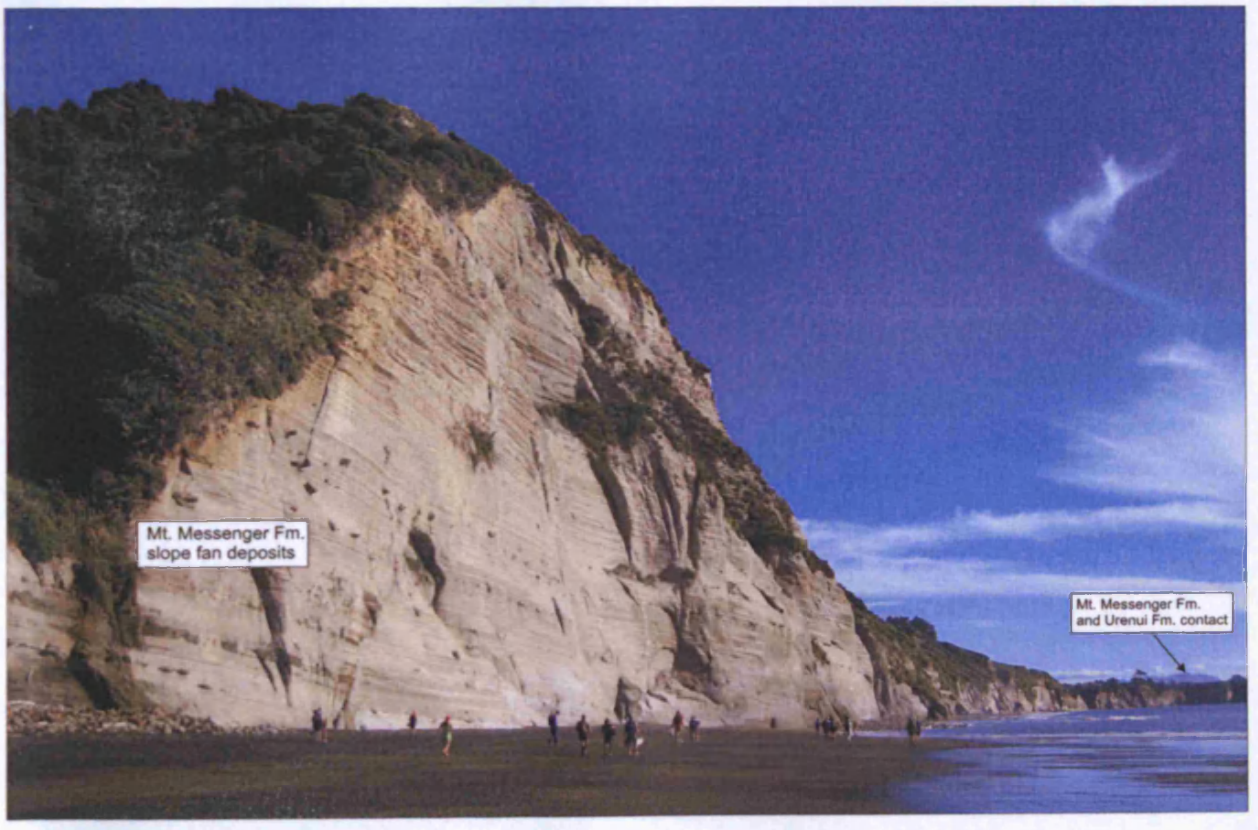

Figure 2.38 View looking southwest at the White Cliffs of the Mt. Messenger Fm. The formation dips beneath the Urenui Fm. at Pariokariwa Point.

sequences, with the technique routinely employed in subsurface hydrocarbon exploration (Selley, 1998). Outcrop studies which employ portable gamma-ray spectrometer to investigate the natural radioactivity of siliciclastic dominated sediments are far rarer. Published studies often emphasize the value of outcrop gamma-ray curves in helping to improve correlations between wireline gamma-ray curves and sedimentary sequences as well as wireline facies identification (Myers, 1989; Aigner et al., 1995; Martinius et al., 2002). However, others are quick to highlight the limitations and potential pitfalls of such methods (i.e. North and Boering, 1999; Andersson and Worden, 2004; Evans et al., 2007), views which are often shared in the broader literature on wireline gamma-ray spectrometry (i.e. Hurst, 1990; Rider, 1990). Gamma-ray spectrometry data collected during this study was designed to evaluate the resolvability of more or less radioactive layers relative to one another, rather than address absolute gamma emission values.

2.3.4.2 Radioactive elements in sediments

The presence of naturally occurring uranium (U), potassium (K), and thorium (Th) varies within sediments depending on the chemical composition of constituent grains. Major sources of K in clastic sediments include feldspars, mica grains and to a lesser extent, illite clay. Detrital clay minerals may also continue to adsorb K from solution during transport and upon deposition in marine environments (Myers and Wignall, 1987). Thorium is largely insoluble and is typically present either in accessory minerals or adsorbed onto the surface of detrital clays such as kaolinite and montmorillonite. Uranium may also be associated with the detrital clay fraction however its solubility and inherent mobility means its presence is more ambiguous and high concentrations may represent 'authigenic' or leached U deposits (Myers and Wignall, 1987). Fine-grained intervals of the Urenui Formation likely adhere to Potter et al.'s (1980) description of fine-grained marine sediments as being generally composed of mixtures of clay minerals and silt-grade quartz with minor feldspar, carbonate, and organic matter. In the absence of coarser material containing abundant feldspars and micas, it is expected that clay minerals represent the main source of K and Th. Conversely, coarser grained lithofacies within the Urenui Formation, which represent channelised bodies, can be broadly characterised as having larger grain-sizes and are likely to contain a higher concentration of feldspathic and micaeous grains. It should be noted however that due to the level of ambiguity regarding the sources of K, Th, and U elements in sedimentary rocks, care must be taken when making grain-size interpretations from gamma profiles alone (Rider, 1990). Profile motifs are here analysed and interpreted in conjunction with high resolution sedimentary logs in order to help constrain the likely mineralogical sources of radioactive elements.

Gamma-ray measurements were generally taken at spacings of between 5-20 cm based on the specific sediments, and the instrument was allowed to record naturally emitted radiation for a total of 180 seconds. The majority of gamma-ray profiles are roughly 2m in height and contain between 15 and 40 discrete measurements.

2.3.5 Facies mapping

Lithofacies mapping aimed to characterise an outcropping slope succession with respect to the volume and distribution of coarser grained lithologies which are likely to alter the fluid-flow properties of a predominately fine-grained depositional system.

The Urenui Formation, as exposed at the north Taranaki Coast, comprises a roughly 850 m thick section of pale grey siltstones with three exposed channelised sandstone bodies and rarer coarser intervals of conglomeratic material. The section is dominated by three thick sequences of heavily bioturbated siltstones which are capped at three stratigraphic levels by coarser, channelled intervals. This led King et al. (1993) to informally subdivide the section into six units, namely the lower, middle, and upper weakly bedded units, upper and lower channelled units, and a middle channelled and interbedded unit. These subdivisions provide a practical framework with which to study the outcrop, and were therefore used in this study. This broad stratigraphy of the Urenui Fm. from outcrop is shown schematically in Fig. 2.39.

Four lithofacies were encountered during the mapping of the Urenui Fm. on the northern Taranaki Peninsula;

- Weakly bedded to massive siltstones and clayey siltstones.
- Thin-bedded siltstones and fine to medium grained sandstones
- Thickly bedded channelised and tabular sandstones
- Rare conglomerates

The distribution of these lithofacies is given schematically in Fig. 2.40. Here, a series of filled panels, representing the 20.5 km of Urenui Fm. exposure, illustrate the bulk lithofacies at a given location. The following descriptions provide a brief summary of the sub-units of the Urenui Fm. slope sequence.

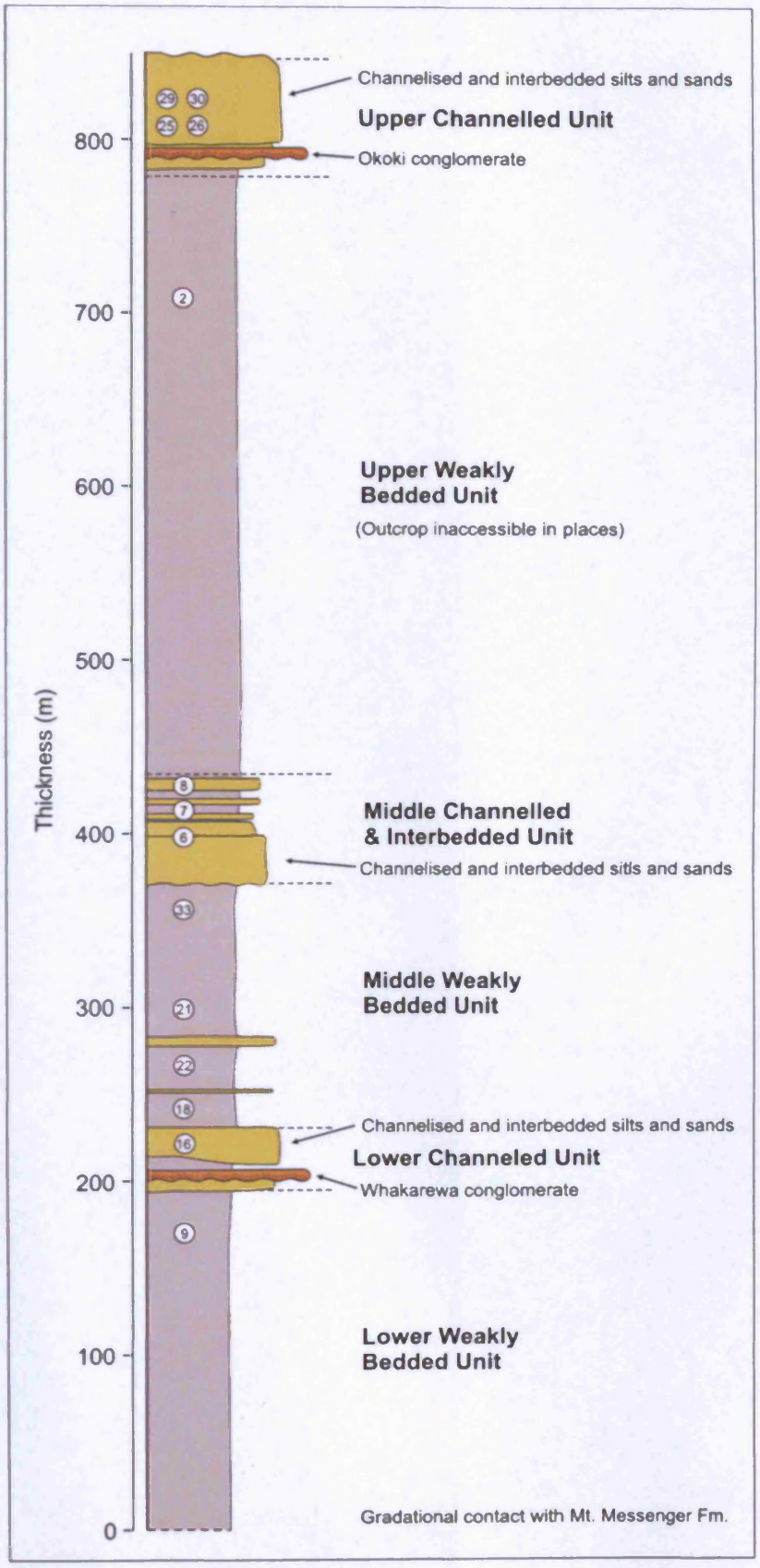

Figure 2.39 Schematic stratigraphy of the Urenui Fm. as it outcrops on the North Taranaki coast. Nomenclature and the position of several subdivisions based on King et al (1993). Circled numbers indicate the position of analysed samples.

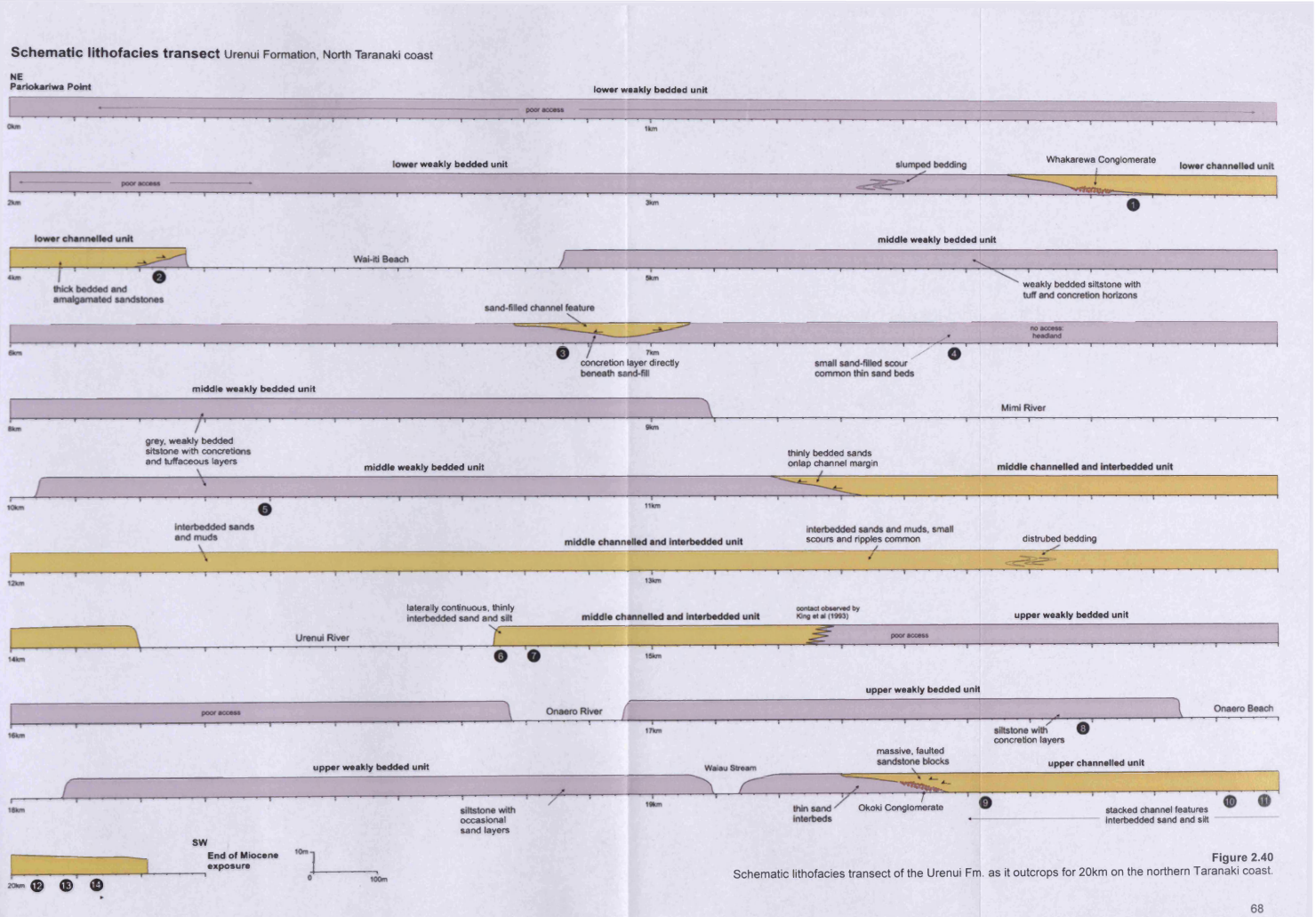

Figure 2.40
Schematic lithofacies transect of the Urenui Fm. as it outcrops for 20km on the northern Taranaki coast.

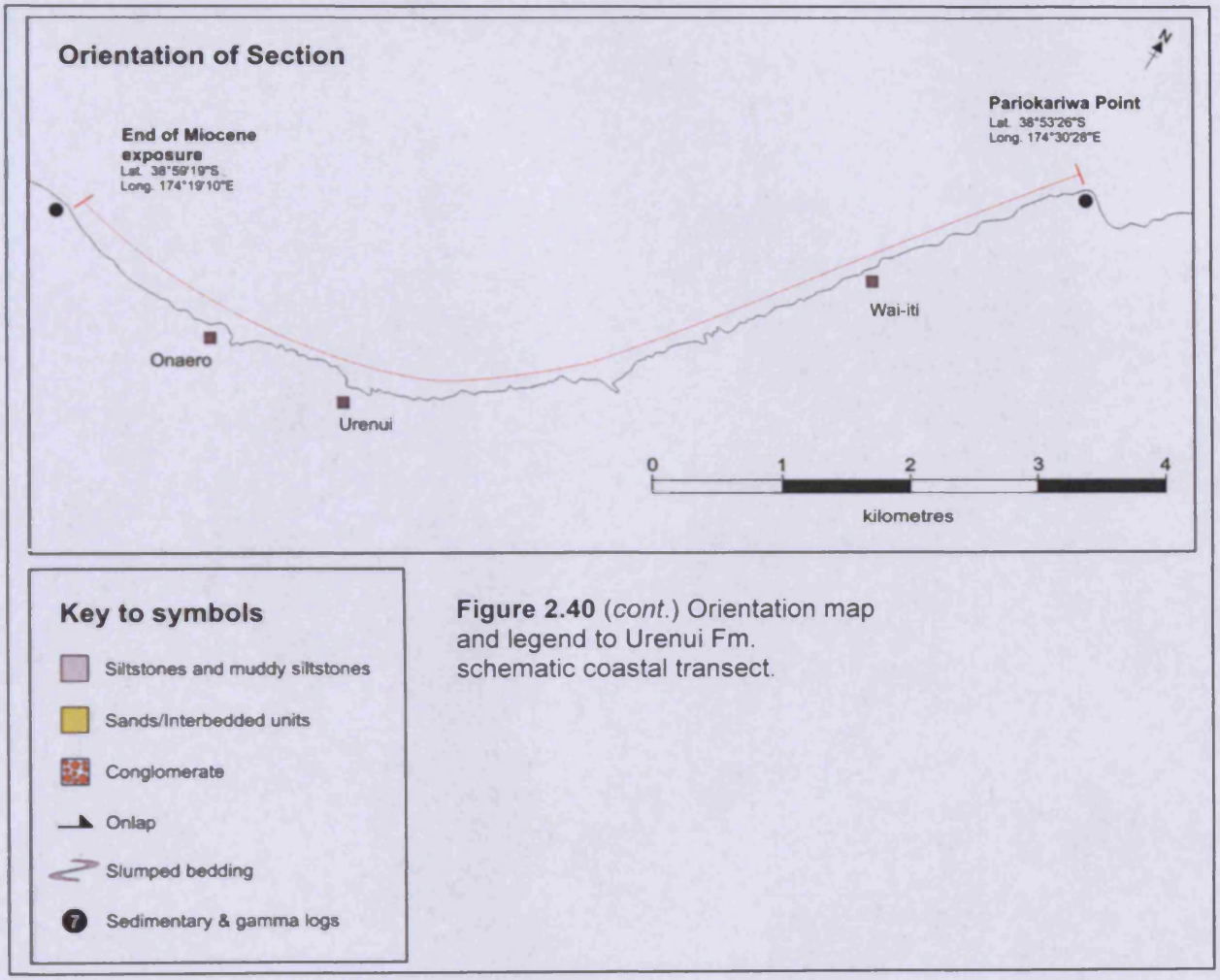

Figure 2.40 (*cont.*) Orientation map and legend to Urenui Fm. schematic coastal transect.

2.3.5.1 Lower Weakly Bedded Unit (LWBU)

This unit directly overlies the uppermost sandstone unit of the Mt. Messenger Fm. and outcrops largely in inaccessible cliffs directly east and to the south of Pariokariwa Point. The lower weakly bedded unit is dominated by approximately 200m of olive grey, weakly bedded siltstones with occasional tuff horizons (Fig. 2.41) (King et al., 1993). Sediments are generally heavily bioturbated, contain bivalve fragments and are slightly calcareous. Stacked concretions which are typically vertical or sub-vertical are common throughout section (Fig. 2.41) measuring up to 5m long and 50cm wide. The unit contains rare discrete sand horizons, although sandy material is seen to commonly fill burrows. The deposition of this unit marks a significant change in the depositional regime to that operating during the deposition of the underlying Mt. Messenger Fm. units, although a gradational contact is observed in cliff sections at Pariokariwa Point (King et al., 1993). The transition from the Mt. Messenger Fm. to homogeneous silt-grade deposits of the LWBU records a shift from deep-water fan to slope depositional system receiving considerable less coarse material.

2.3.5.2 Lower Channelled Unit (LCU)

The lowermost channelled unit outcrops just north of Whakarewa Point where it overlies and incises siltstones of the lower weakly bedded unit (Fig. 2.42a). This ~50m thick unit is characterised by the inversely graded Whakarewa Conglomerate (King et al., 1993) at its base which contains abundant pebbles, mudstone clasts and reworked concretions (Fig. 2.43). The conglomeratic fill is flanked by thickly bedded, channelised sandstones which can also be seen cutting underlying siltstones containing thin sand layers (Fig. 2.44). Sandstones which persist above this interval are sheet-like and often amalgamated, containing occasional finer horizons and silt stringers. The western margin of the lower channelled unit, as exposed at the eastern end of Wai-iti Beach (Fig. 2.42b), again records the incision of weakly bedded siltstones by thickly bedded sandstones. The LCU represents the lowermost sand-dominated interval in the outcropping Urenui Fm., and represents focussed transport of coarser material across the slope.

2.3.5.3 Middle Weakly Bedded Unit (MWBU)

The middle weakly bedded unit is exposed for roughly 7 km west of Wai-iti Beach recording approximately 140m of stratigraphy; the shallow dip (~4°) of beds and the orientation of the coast makes for some along-strike repetition of stratigraphy (King et al., 1993). The unit comprises a monotonous sequence of pale grey muddy siltstones displaying weak or absent

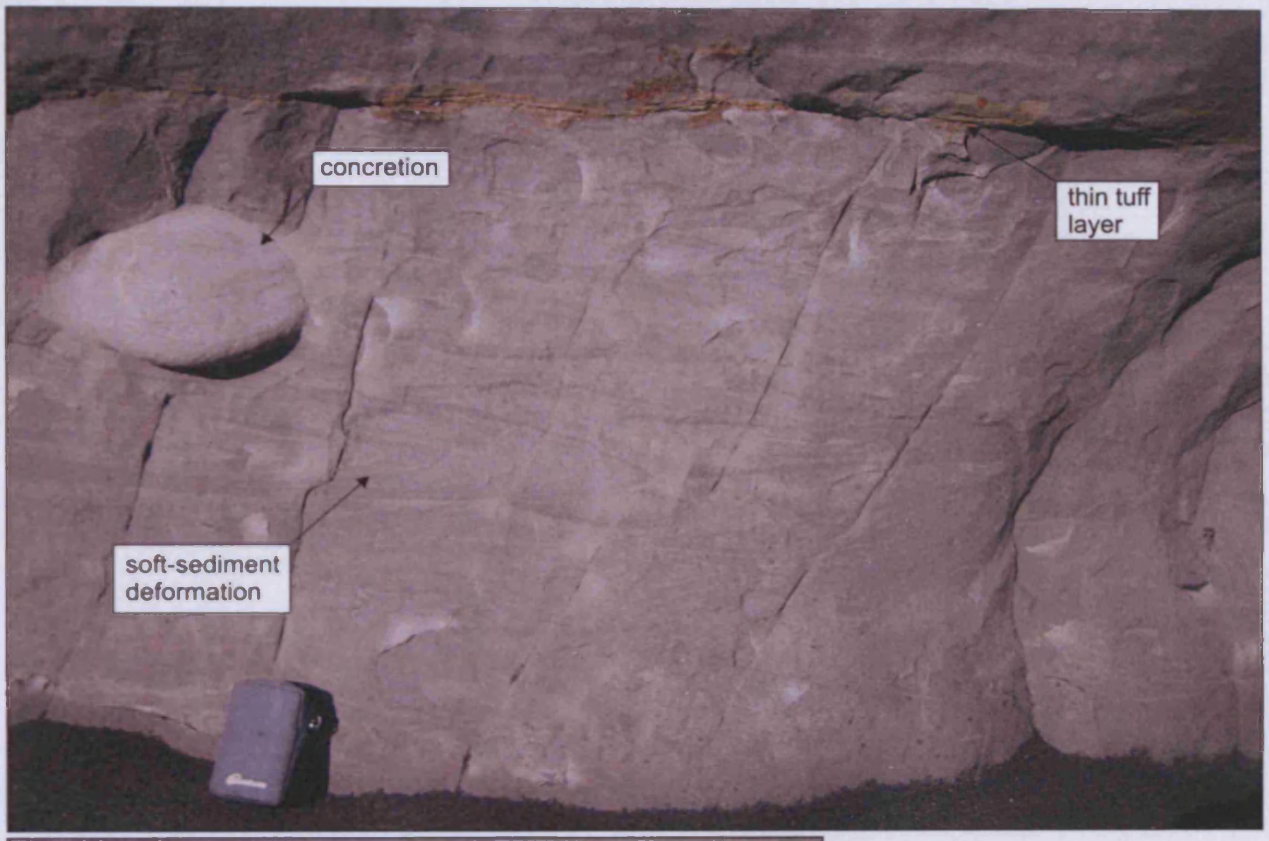

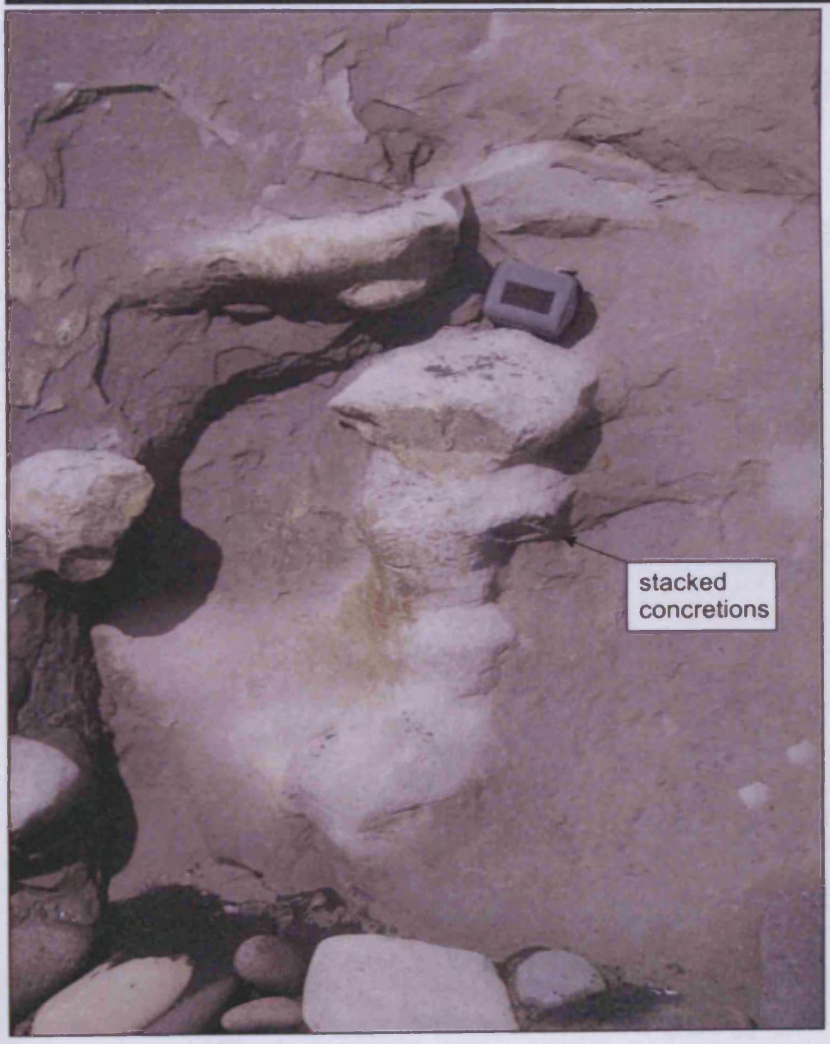

Figure 2.41 Siltstones of the lower weakly bedded unit, Urenui Fm. Top image reveals soft-sediment deformation preserved in rocks NE of the Whakarewa Conglomerate. Thin tuff layers are also common. Concretions (left) are found throughout siltstone units of the Urenui Fm. The stacked concretion shown in this image is approximately 1m high, however chimney-like features 4-5m high have also been observed.

Figure 2.42 (a) Panorama looking SE at the Whakarewa Conglomerate overlying and incising siltstones of the lower weakly bedded unit. Conglomerate facies grades southwest (right in figure) into thick and often amalgamated sand beds. Person for scale. (b) Panorama taken at the NE end of Wai-iti Beach showing the southern most coastal outcrop of the lower channelled unit. Thick sands, seen here overlying pale grey siltstones, are the lateral equivalent of tabular sands seen in (a). A 1-2m thick unit of thinly interbedded silt and sand beds is present immediately above the channel base, which is overlain by thick, typically massive sand beds. Stitching of images in (a) has produced some perspective distortion giving an arcuate view of what is a linear outcrop.

Figure 2.43 (above) Close-up image of the Whakarewa Conglomerate outcropping NE of Wai-iti Beach. Fallen blocks are seen in the foreground.

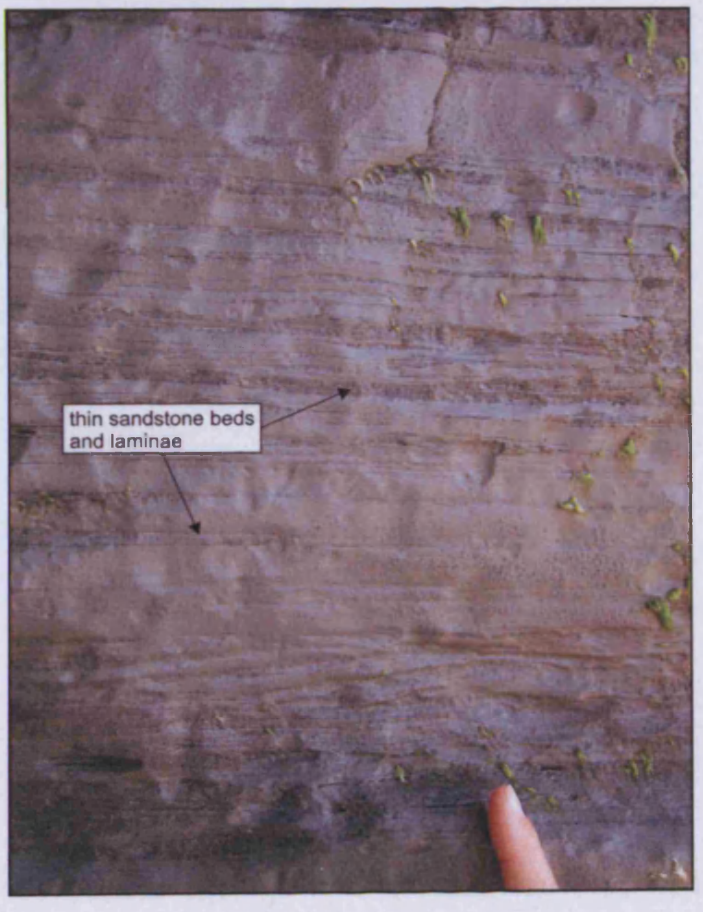

Figure 2.44 (right) Close-up image of thin sand laminations interbedded with siltstones of the LWBU underlying the Whakarewa Conglomerate.

bedding with occasional silt and tuff stringers (Fig. 2.45a). Bioturbation is intense throughout the unit with burrows commonly infilled with coarser tuffaceous material. Concretions are particularly abundant in this unit and form large, often sinuous vertical features up to 5m in height. Approximately 2km west of Wai-iti Beach siltstones are cut by a 40m wide channel feature (Fig. 2.45b). This feature displays classic channel geometry and is filled with laterally aggrading sand packages. The base of the channel is marked by a layer of boulder sized concretions within the underlying siltstones. Directly west of this channel, the unit is once again dominated by weakly bedded muddy siltstones although direct access to the outcrops is restricted. The unit is well exposed in 20m high cliffs directly to the east of the Mimi River mouth, before giving way to low lying fluvial and beach deposits. The middle weakly bedded unit continues to outcrop west of the Mimi River for roughly 0.5km. The unit remains fine-grained with largely unrecognisable bedding surfaces and abundant concretions. A distinct, but not sharp, contact is recorded by King et al. (1993) between the middle weakly bedded unit and the overlying middle channelled and interbedded unit.

2.3.5.4 Middle Channelled and Interbedded Unit (MCIU)

The middle channelled and interbedded unit outcrops from roughly 1km west of the Mimi River Mouth for approximately 5km west along the coast to just east of the Onaero River Mouth. The base of this ~140m thick channelled and interbedded unit is spectacularly exposed where a 30m wide channel incises underlying siltstones of the underlying middle weakly bedded unit. The basal section of the unit differs from the lower and upper channelled units by the absence of a basal conglomerate. This channel is unconformably overlain and onlapped by laterally continuous thickly bedded sand packages which frequently display centimetre scale ripples and cross-stratification. Small-scale scour surfaces can be seen in units above the main channel incision and are often filled with cross-stratified material. Higher in the unit, sediments become less sand-dominated giving way to packages of thinly bedded silts and sandstones (Fig. 2.46a). Thinly bedded sandstones outcropping at Urenui Beach sections contain intervals of starved ripples as well as heavily bioturbated horizons (Fig. 2.46b and 2.46c). Interbedded silt layers are largely structureless and variably bioturbated, exhibiting a similar character to siltstones of the MWBU. King et al. (1993) suggested that the MCIU is the outcropping equivalent of 1-2km wide channel features imaged in nearby seismic profiles which occur at the same stratigraphic level (Fig. 2.47).

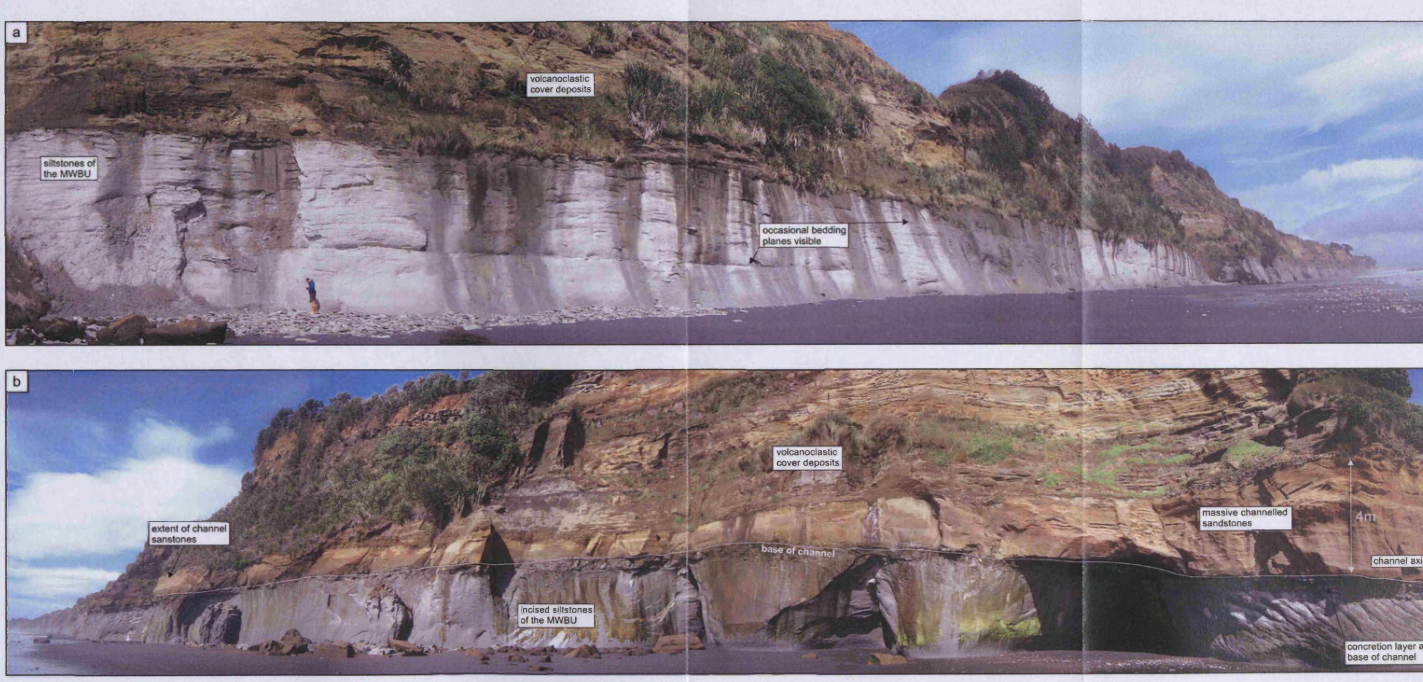

Figure 2.45 (a) Panorama looking SW along the outcropping middle weakly bedded unit southwest of Wai-iti Beach. Light grey siltstones are overlain by volcanoclastic deposits. (b) Panorama looking NE back along the middle weakly bedded unit towards (a). Here siltstones of the MWBU are incised by a small sand-filled channel. Features such as these are likely to have significantly different physical properties compared to the surrounding fine-grained siltstones and will be at the lower limit of seismic resolvability.

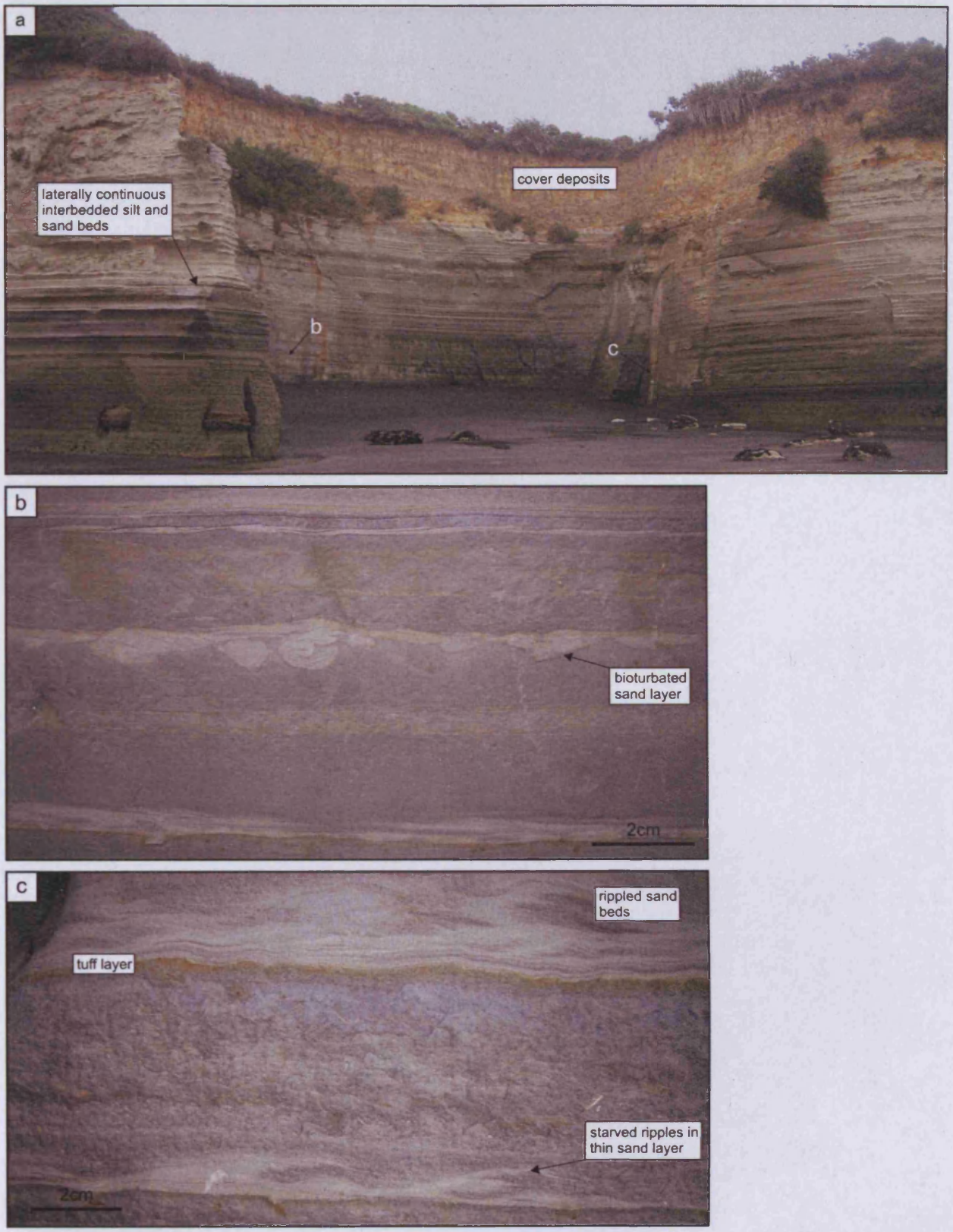

Figure 2.46(a) Middle channelled and interbedded unit outcropping at Urenui Beach. Laterally continuous thin silt and sand beds seen here are thought to be deposited in broad channel features. The locations of images (b) and (c) are shown; **(b)** Sand layers are bioturbated thin sand layer interbedded with darker grey silty material; **(c)** Sand ripples within a silt-dominated interval.

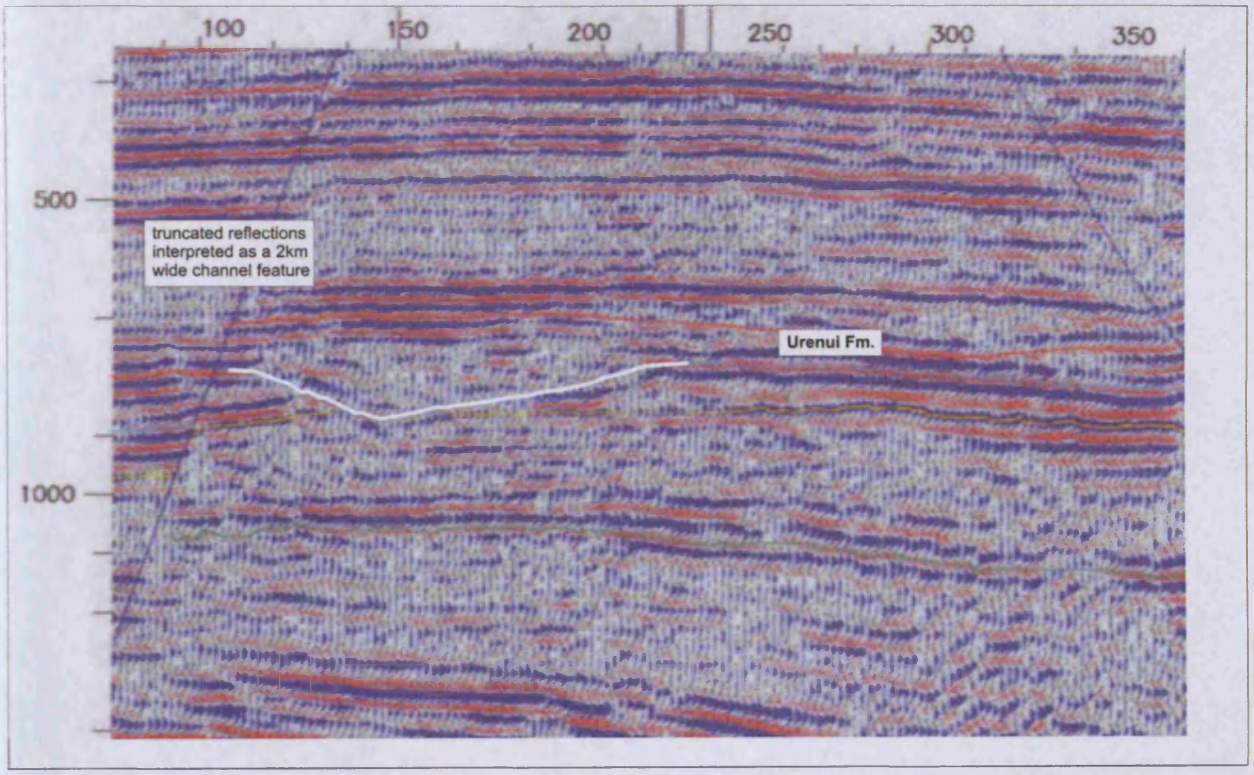

Figure 2.47 Onshore seismic profile showing a 2km wide channel feature within the Urenui Fm. (image from Marabella Enterprises Ltd., 2001).

2.3.5.5 Upper Weakly Bedded Unit (UWBU)

Interbedded lithologies of the middle channelled and interbedded unit display a gradational contact with the overlying upper weakly bedded unit. The latter comprises a ~325m sequence of monotonous siltstones, mudstones and occasional fine-sand bodies exposed from the east of the Onaero River mouth for approximately 3 km, to just west of the Waiau Stream (Fig. 2.48). Vertical concretions occur throughout the unit but are more concentrated in lower portions (Fig. 2.49). The unit shows a broad fining from predominately siltstones towards its base to more clay-rich intervals in upper sections. Appreciable volumes of sand grade material are limited to a small scour feature exposed at the western end of Onaero Beach and occasional discontinuous fine-sand bands interbedded with siltstones. The top of the unit is marked by an unconformable contact with the upper channelled unit 200m west of the Waiau Stream mouth.

2.3.5.6 Upper Channelled Unit (UCU)

This unit represents the uppermost unit of the Urenui Formation exposed in the north Taranaki coastal section. The unit is exposed for roughly 1.5km westward from its contact with the upper weakly bedded unit until is dips beneath quaternary volcanoclastic sediments just northeast of Motunui, close to the end of Turangi Road (Fig. 2.40). The base of this ~70m thick unit comprises medium grey siltstones with abundant bed-parallel concretion horizons, which are erosively overlain by a stacked channel complex. Lower channelled sandstones are themselves incised by a relatively narrow conglomerate-filled channel feature. This, the Okoki Conglomerate of King et al. (1993), comprises largely cobble and boulder size intraformational siltstone and fine-sandstone clasts. The margin of this channel is progressively onlapped by adjacent channel sandstones, as are the tilted and slumped blocks of intraformational material which lie on top of the conglomerate (Fig. 2.50). Laterally adjacent and stratigraphically above the Okoki conglomerate channel scours show a progressive truncation of older channels westward, an example of which is given in Fig. 2.51. Channel fills are commonly thinly interbedded fine-sands and siltstones displaying a variety of features including shelly lenses, rip-up clasts, and gravel/shell lags (Fig. 2.51). Thin sandstone beds often contain wavy laminations and cross-stratification indicative of turbiditic deposition (Bouma, 1962).

The informal stratigraphy of the Urenui Fm. as described above provides an insight into the depositional architecture of a slope sequence. The Urenui Fm. at outcrop can be characterised, as proposed by King et al. (1993), by the broad distinction between weakly

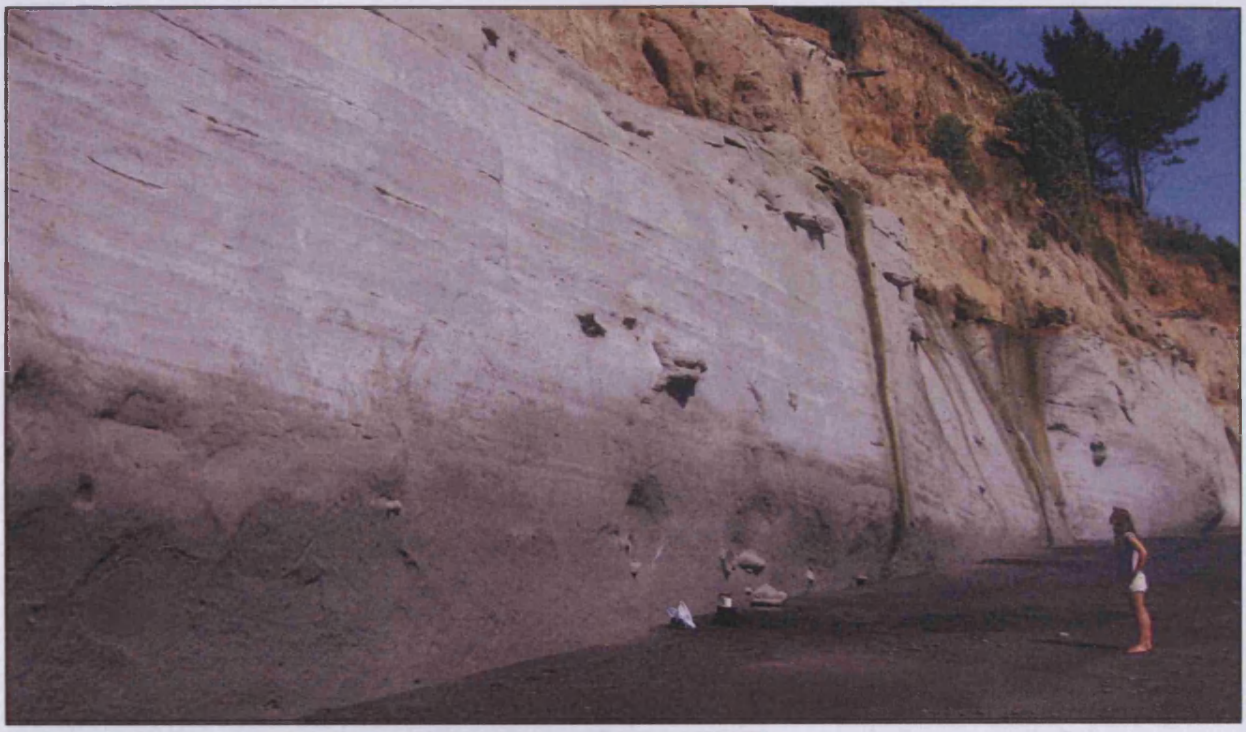

Figure 2.48 (above) Siltstones of the upper weakly bedded unit exposed in coastal section immediately NW of Onaero Beach.

Figure 2.49 (left) 3m high concretion found in siltstones of the upper weakly bedded unit. These features are common throughout siltstone units of the Urenui Fm.

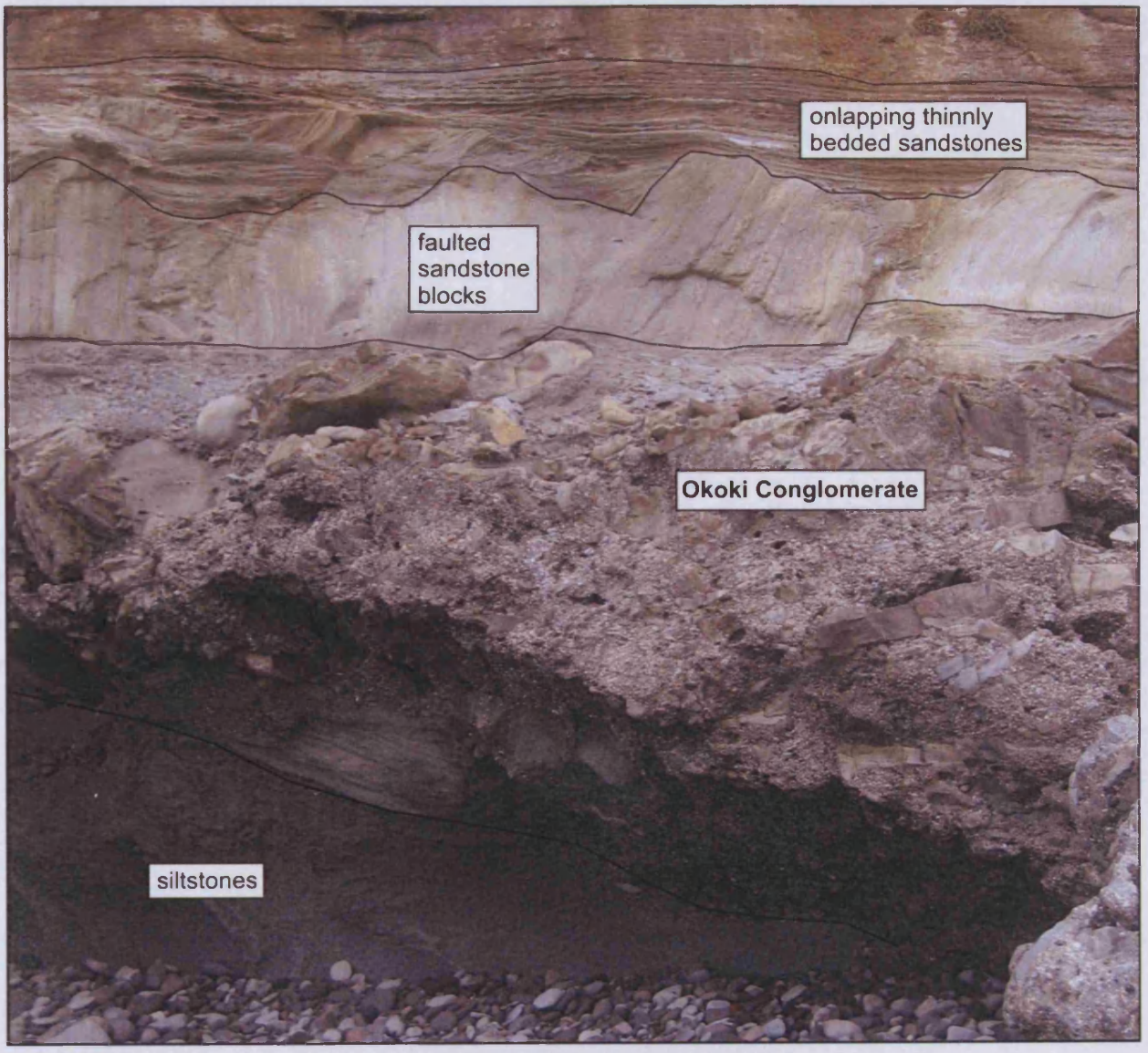

Figure 2.50 Okoki Conglomerate as it outcrops close to the base of the upper channelled unit, 400m NW of Waiau stream mouth. Conglomerate incises underlying siltstones and is overlain by faulted sandstone blocks. A unit of thinly bedded sandstones onlaps these faulted blocks and can be traced laterally into a shallow channel feature.

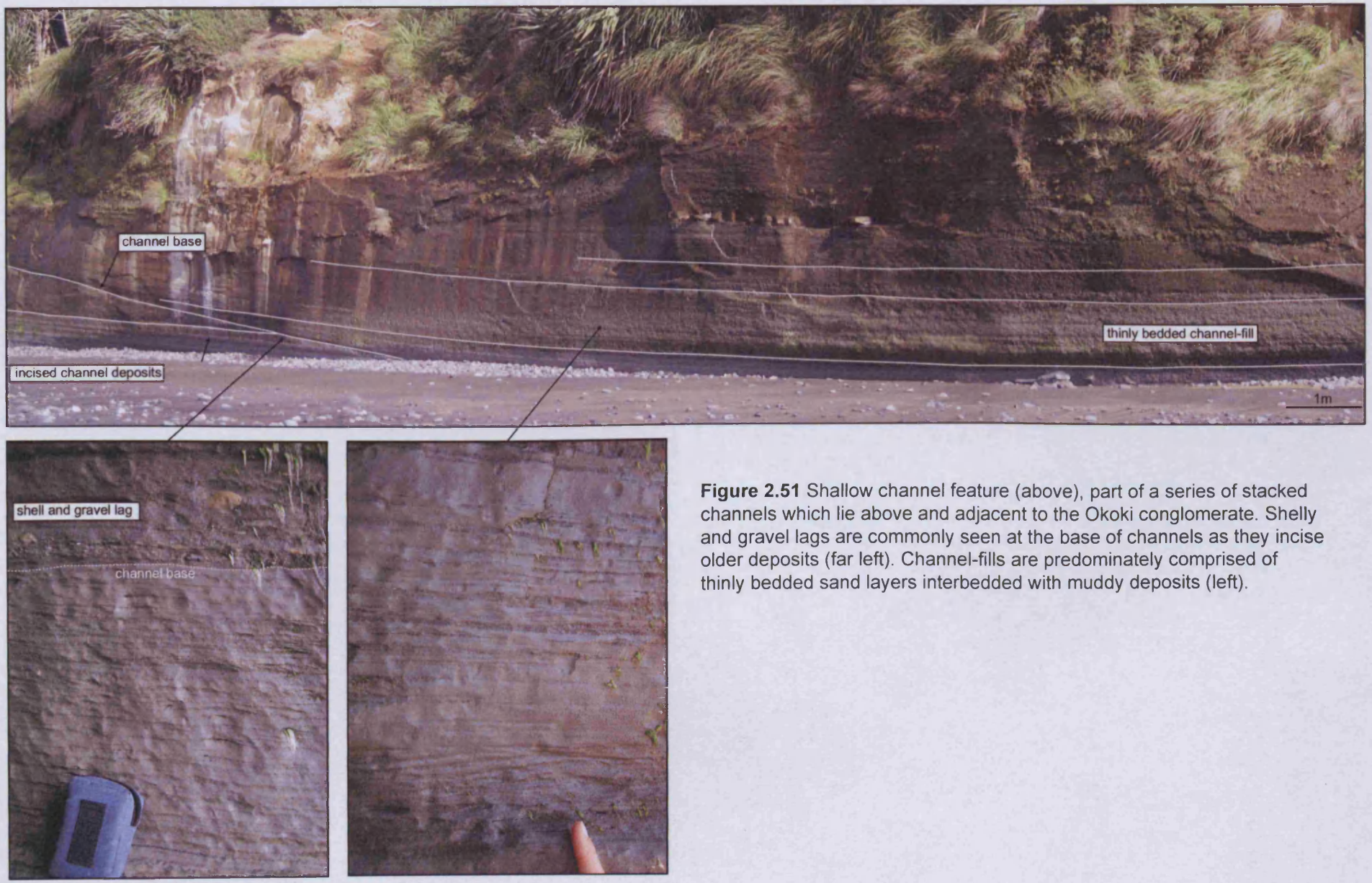

Figure 2.51 Shallow channel feature (above), part of a series of stacked channels which lie above and adjacent to the Okoki conglomerate. Shelly and gravel lags are commonly seen at the base of channels as they incise older deposits (far left). Channel-fills are predominately comprised of thinly bedded sand layers interbedded with muddy deposits (left).

bedded units of homogeneous siltstone and sand-rich channelised intervals. Conglomeratic deposits are limited to just two channel axis intervals, while heterogeneous deposits are also largely restricted to inter-channel deposits.

2.3.6 Detailed sedimentary logs and gamma-ray spectrometry

Gamma-ray spectrometry was performed on all of the lithotypes examined at Urenui Fm. outcrops. In addition to intervals of thinly bedded heterolithic sediment which were identified deposited adjacent to channel features or within channel margins, homogeneous siltstones and sand bodies were also examined. Fig. 2.52 shows a selection of the logs collected along with corresponding radioactive signatures as recorded using a Exploranium GR-256 gamma-ray spectrometer. Gamma-ray curves are described here in terms of 'motifs', as used by Martinius et al. (2002) and defined by Serra and Sulpice (1975). Figure 2.53 shows motifs which are commonly used to describe shifting levels of gamma emissions interpreted as a response to changes in sediment type, typically grain-size. 'Bell' shaped motifs characterise a broad upward increase in natural gamma-ray emissions and may point to a sequence of fining-upwards sediments. Conversely, 'funnel' shaped motifs are created by an upward decrease in gamma emissions and are thought to represent broadly coarsening-upwards intervals. Where profiles show little deviation, a 'cylinder' motif refers to an interval of broadly stable gamma-ray emissions.

Logs 3, 5, and 8 in Fig. 2.52 all record largely uniform sequences of weakly bedded siltstones which are seen to dominate Urenui Fm. facies. Corresponding gamma-ray curves do not however appear to reflect this degree of uniformity. Gamma-ray curve 3 records a broad cylinder motif, with characteristically high gamma emissions, while curves 5 and 8 record a far greater degree of variability. Shifts in the gamma-ray values in curve 8 lie within a relatively narrow field (range is 45-50 counts per second) compared to curve 5, which records extreme values close to the maximum and minimum values recorded for all gamma-ray curves. The source of these shifts in radiation is unclear, although the visually uniform nature of the sediment suggests that changes in mineralogy may be producing the spiky values recorded in curves 5 and 8.

Logs 1, 2 and 14 record the vertical transition from largely silt and clay dominated sediments into sandstones, which is seen wherever weakly bedded units are punctuated by channelised sediments. Gamma-ray curve 2 records such a transition very clearly with a 'bell' motif in the upper third of the sequence corresponding with an increase in the bulk grain-size and a reduction in fines. Gamma-ray curves from the remaining two profiles are somewhat more

ambiguous. Although an overall reduction in gamma-ray emissions is recorded in curve 1 corresponds with the metre scale lithological changes, the higher frequency variability of this facies is not represented in the gamma-ray curve. Only very minor shifts are recorded in curve 14 despite the sedimentary log recording gradation into a thick sandstone bed from a unit of finer grained material. The strength of gamma-ray emissions appear, at least in this case, to be insufficiently varied so as to produce a pronounced curve in the gamma-ray signature.

The remaining gamma-ray curves (4, 6, 7, 9, 10, 11, 12, and 13) were all acquired in sequences recording a high level of heterogeneity, often with very thinly bedded sediments and high frequency vertical grain-size changes. Thinly bedded sand layers represent turbidity current deposits which are interbedded with silty deposits recording less energetic sedimentation. Examining these gamma-ray curves against the corresponding lithology indicates that shifts in the amount of emitted radiation can often be tentatively linked to broad changes in the sedimentology of the logged units. Curve 7 provides a good example of this where a clear 'funnel' motif corresponds to an interval of gradually fining sediments. This 'funnel' motif is capped by an interval of slightly reduced radiation, which is likely to record the existence of the thick sandstone bed recorded in the sedimentary log at 25cm depth (Fig. 2.52). Other gamma-ray curves are not so revealing, and offer very little information regarding any changes in sediment type or grain-size (i.e. curves 10 and 13). Gamma-ray profiling has failed to resolve thinly bedded layers (below 15-20cm) in any of the curves. Logged intervals containing a high number of thin-beds are seen to often record the most uniform and smooth curves (e.g. 10, 12, 13, and 14), likely resulting from the radioactive signatures of discrete layers 'overlapping', giving a composite value for any measured point.

Varying the spacing of the spectrometer sensor to 5cm during data collection did not improve the resolvability of thin-beds (Fig. 2.54). An important result is that the resolvability of beds below 20cm is not possible using common portable gamma-ray spectrometers, given the resolution of the instrument sensor. Gamma-ray values measured in sequences where bed thicknesses are below this size will not record discrete beds, but the composite gamma-ray levels emitted by sediments within range of the sensor. Shifts in the relative proportion of coarse and fine material within a thinly bedded sequence will influence the overall shape of the gamma-ray curve, but the position and thickness of coarser layers are undetectable using this particular technique. This has implications for the recognition of thinly bedded units using the typically lower resolution wireline logs as heterogeneity is likely to be unresolved.

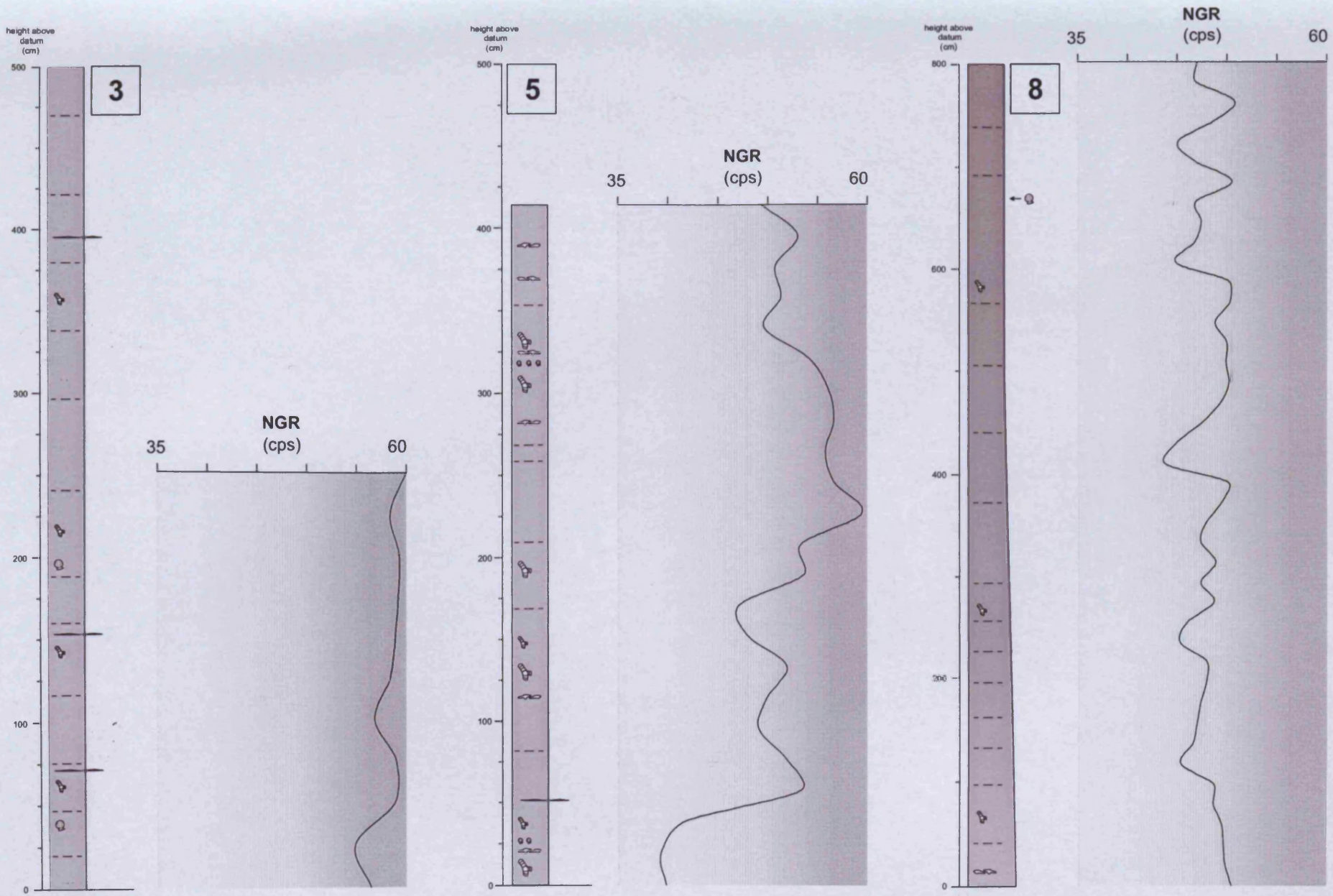

Figure 2.52 Sedimentary logs and accompanying gamma-ray curves from the outcropping Urenui Fm. Datum equal to beach level. Gamma ray units in counts-per-second (CPS)

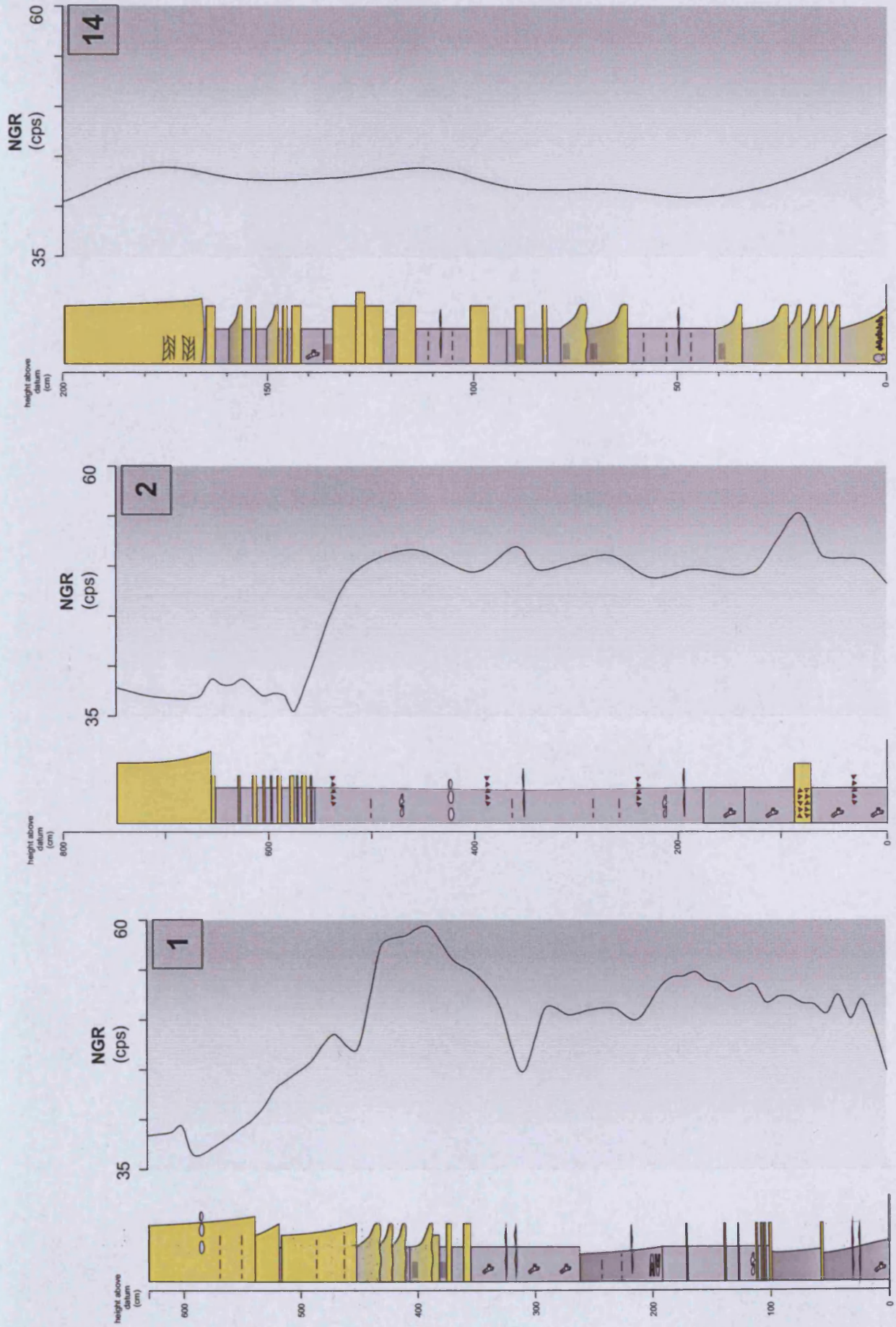

Figure 2.52 *cont.*

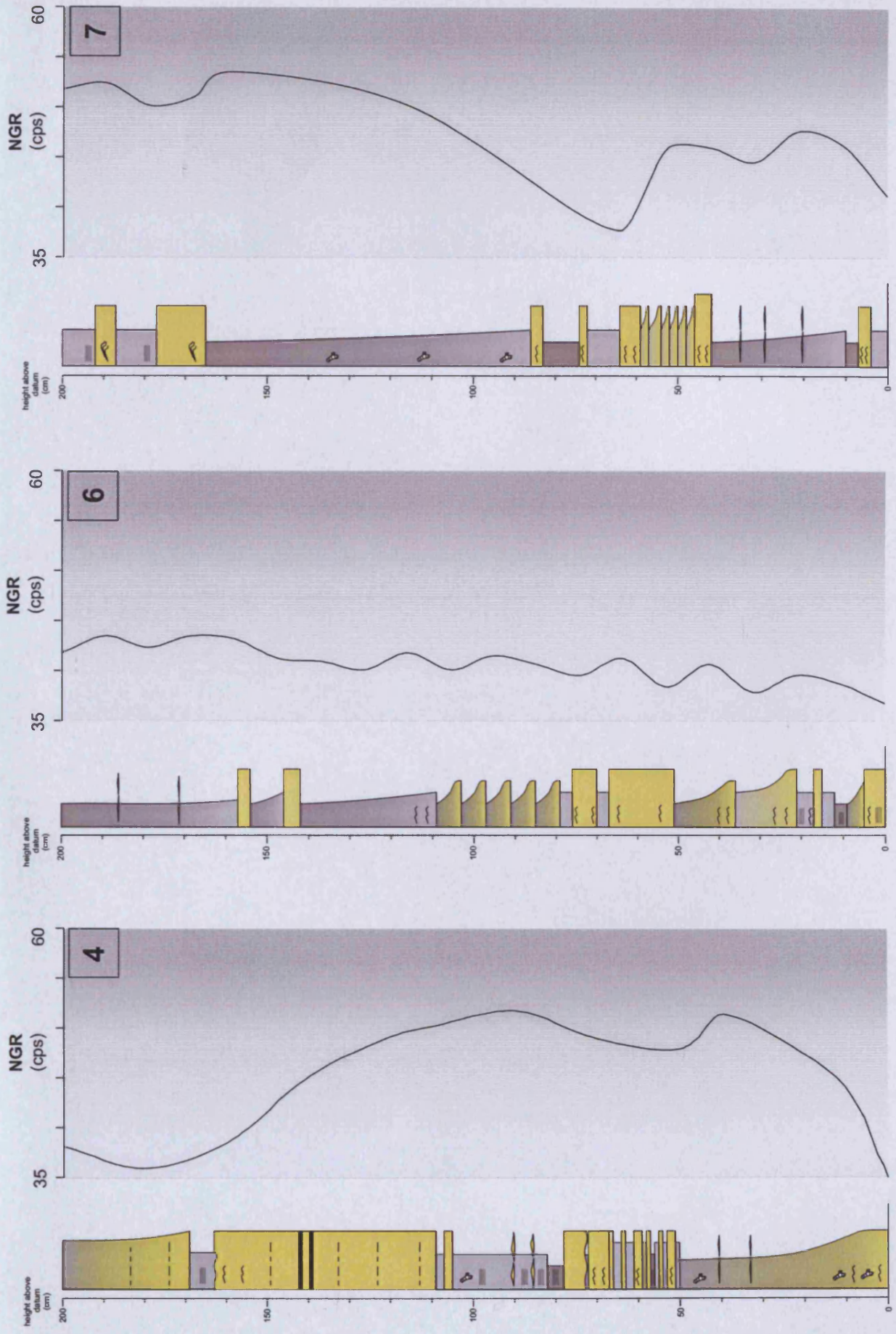

Figure 2.52 *cont.*

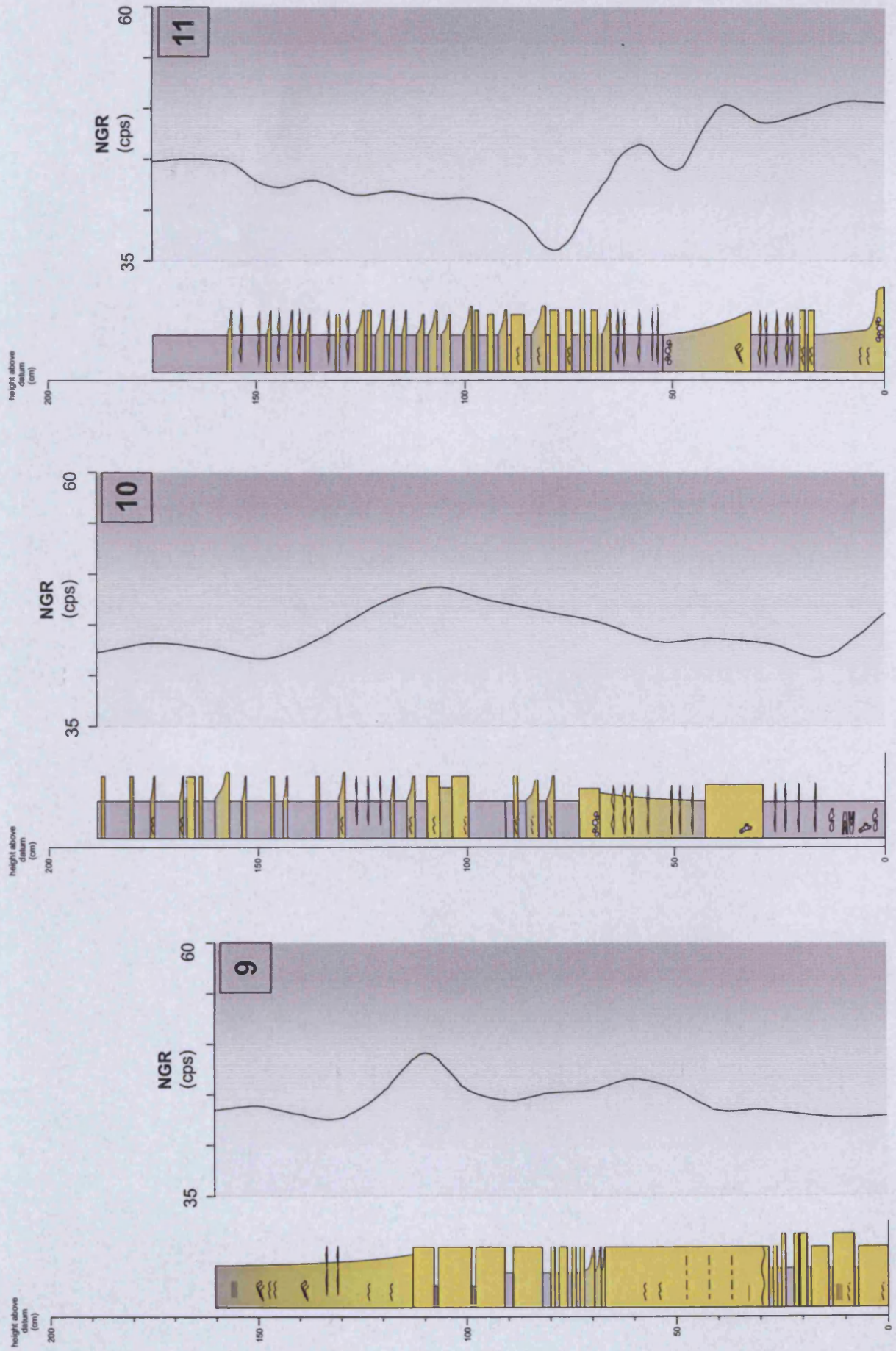

Figure 2.52 *cont.*

Figure 2.52 *cont.*

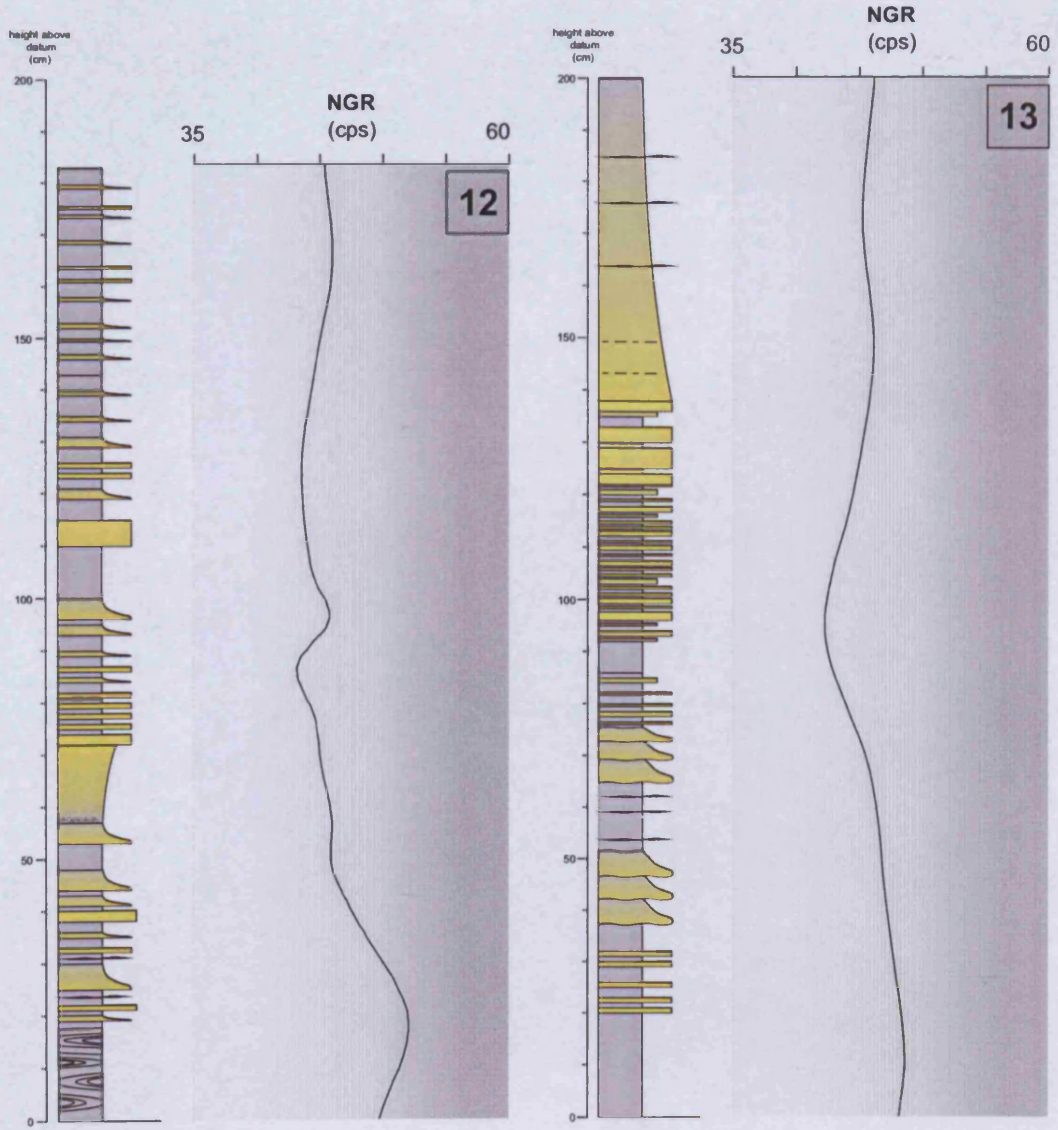

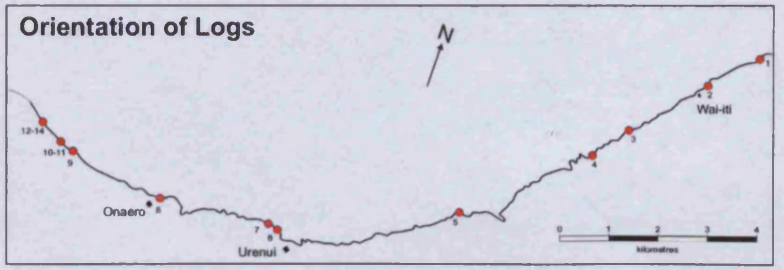

Lithologies

- Fine and medium sand
- Fine sand and silt
- Silt
- Muddy silt
- Graded

Symbols

- Laminations
- Deformed interval
- Burrow marks
- Shelly fragments
- Ripples

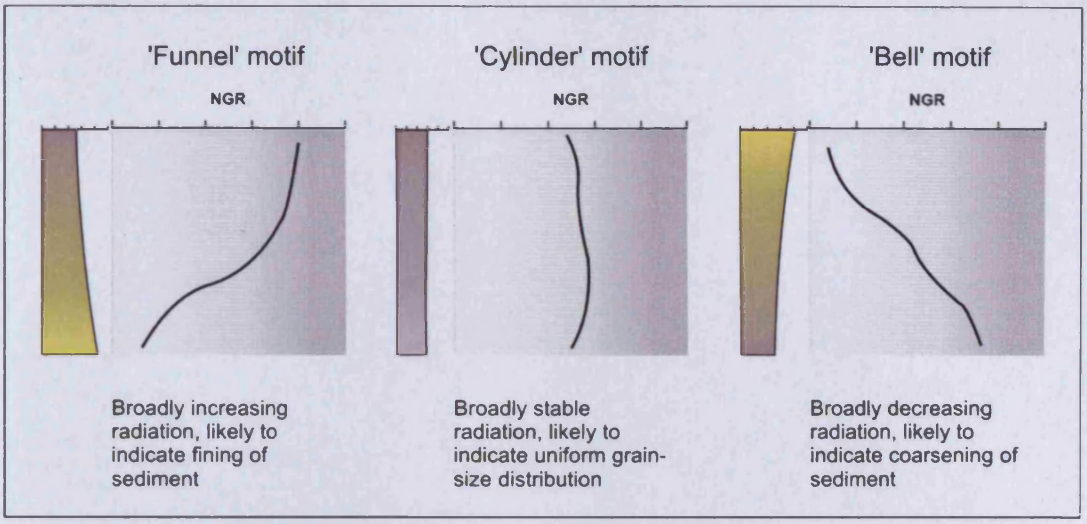

Figure 2.53 (above) Illustrations of three common gamma-ray motifs indicative of changes in sediment grain-size.

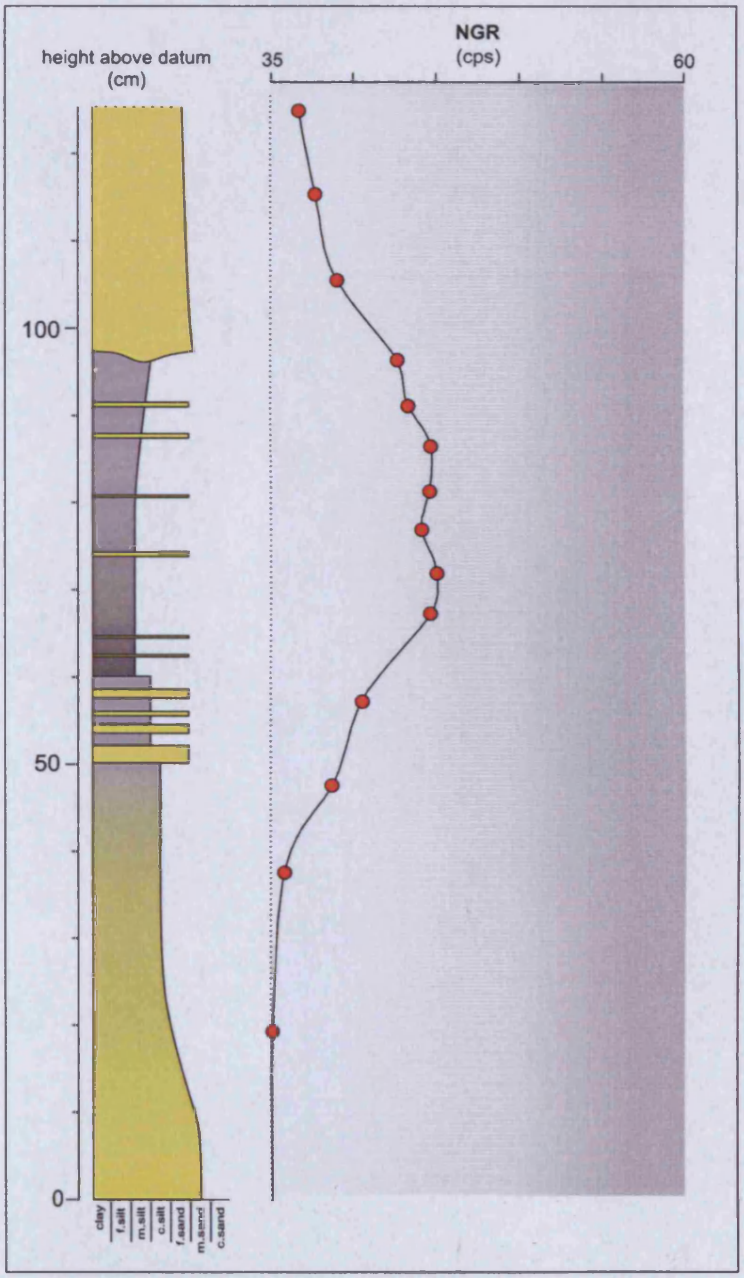

Figure 2.54 (left) Sedimentary log and gamma-ray curve taken from thinly interbedded sand/mud sequence, Urenui Fm. Gamma-ray emissions measured every 5cm (red dots) is insufficient to highlight the presence of thin sand layers. Datum equal to beach level, gamma-ray emissions measured in counts-per-second.

2.3.7 Distribution of potential flow units: Sand bodies and thin-beds

One of the principle aims of this field study was to evaluate the distribution of more permeable lithologies within this slope sequence. When viewed from a sealing perspective, sand-rich intervals, both channel features and thinly bedded deposits, are likely to offer zones of the higher permeability, and therefore can be viewed as the greatest risk to sealing.

The outcropping Urenui Fm. comprises approximately 850m of late Miocene slope sediments, of which roughly 200m, or 20%, comprises dominantly coarser grained channelised sands. Channelised intervals are however largely isolated and are separated stratigraphically by thick units of typically homogeneous siltstone and clayey siltstone. Three-dimensionally, sand packages associated with channel-fills are likely to offer increased lateral permeabilities, but may not significantly increase the chances of vertical fluid migration.

Units comprising thinly bedded deposits are not distributed throughout the formation, but rather are found in close association with larger channelised units. Thin-beds are most commonly deposited as early interbedded channel-fills, particularly in the UCU, and as later abandonment channel-fills, such as shown in Fig. 2.46a from the MCIU. The lateral continuity of thin-beds is therefore determined by the width of channel scours, onto which beds onlap. The widest scours are associated with the abandonment phase of the MCIU where beds are traceable for over 80m in beach sections to the west of Urenui Beach. Exposure limits further correlations, but beds are thought to be continuous over much greater distance than visually recorded. Conversely, beds are confined to much narrower, 40-50m wide, scours in stacked channels features of the UCU (Fig. 2.51). Figure 2.55 shows a histogram plot of sand bed thicknesses collected from all thinly bedded intervals of the outcropping Urenui Fm. Thin-beds recorded represent pulses of coarser sediment delivered to the slope during periods of channel filling or abandonment, most likely by low-density turbidity currents (King et al., 1993). A mean bed thickness value of 2.7cm is recorded from the data gathered. Mean bed thicknesses from the fine-grained Palaeozoic sequences examined in Wales and Cornwall are less than from Urenui Fm. at <1cm. Channelised intervals studied at outcrop suggest that the lateral continuity of thin-beds and the thickness of thinly bedded units are controlled by the dimensions of channel scours into which they are deposited.

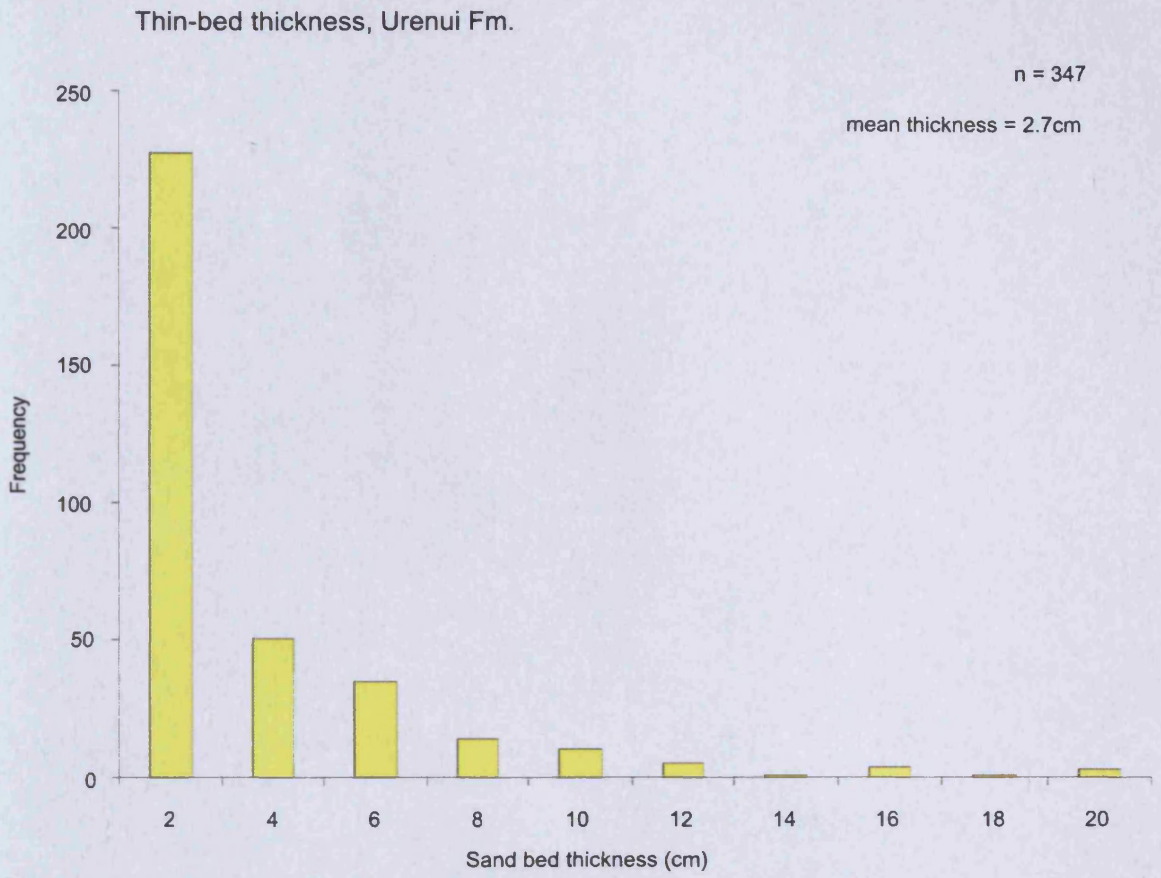

Figure 2.55 Histogram plot of coarser grained thin-bed thicknesses from the Urenui Fm. Bed thickness data has been compiled from all logged intervals to provide information regarding the typical thickness of thin sand beds which are found interbedded with background siltstone deposits.

2.3.8 Physical properties analysis

Grain-size analysis was performed on a total of 14 samples, for which the stratigraphic positions are shown schematically in Fig. 2.39. Fine-grained intervals were preferentially sampled to allow evaluation of the grain-size distribution and porosity of silty slope sediments. Sheets containing detailed information and images relevant to each of the 14 measured samples can be found in the appendix. All grain-size analysis was conducted at Newcastle University.

All samples from fine-grained (non-sand) intervals of the Urenui Fm. reveal broadly similar grain-size distributions. Fourteen tested samples show a mean clay sized fraction (<4μm) of 20% (range 15-30%) and a mean silt fraction (<63μm) of 76% (range 70-81%), classifying samples as siltstones and clayey-siltstones (Shepard, 1954; Fig. 4.2). Sand sized grains (>63μm) are rare, with a maximum sand fraction of 9% (Sample 26).

Porosity values, measured using mercury injection capillary pressure (MICP), are similar for the 14 samples tested, with a mean value of 28% (range 25% -35%). Similar silty mudstones compiled within the Caprocks Project Mudstone Database reveal comparable porosities at depths exceeding 2000m. Given this, and the limited degree of induration exhibited by sampled sediments, it is unlikely that the outcropping Urenui Fm. section has undergone post-depositional burial exceeding several kilometres.

Using the known values of clay content, porosity, and mean pore-size, modelled permeabilities have also been derived, based on work by Yang and Aplin (1998). Permeabilities for the 14 samples examined range between 9.4×10^{-21} m^2 and 4.5×10^{-18} m^2 (roughly 10-4600 nanodarcies (nD)). These values are in-keeping with published data for silt-rich sediments (e.g. Bryant et al., 1975; Young et al., 1964), and add to the rather limited published database of mudstone physical properties.

Although grain-sizes were not measured from channelled sandstone units within the outcropping Urenui Fm., these intervals have been the target of several exploration wells onshore. Well Cheal-1, located roughly 50km south of the outcropping Urenui Fm., recorded porosities of 15% and permeabilities of several hundred millidarcies (mD) from intra-Urenui Fm. channel sands at a depth of 1310m (Crown Minerals Website, 2009b; NZOG, 1995), indicating that these coarser grained intervals do indeed constitute more permeable intervals than the silt dominated units examined here. In addition to subsurface data, measured porosity and permeabilities from thinly bedded sands in the outcropping Mt. Messenger Fm.,

immediately beneath the lowermost Urenui Fm., record values of 20-35% and $1.97x10^{-14}$ m^2 - $5.9x10^{-13}$ m^2 (20-600mD) respectively (Browne et al., 2000).

Further comparisons can be made between the permeabilities of outcropping siltstones and various mudstone types contained within the Caprocks Project Mudstone Database. Data compiled by the Caprocks Project indicate that siltstones (>75% silt) have measured and modelled permeabilities of between 1.30×10^{-21} m^2 to 2.90×10^{-20} m^2 (roughly 1-30nD) at an average porosity of 14%. These values are as much as three orders of magnitude less than those measured from Urenui Fm. sediments, however this is likely a result of the different compaction states of the two data sets (Caprocks Project Mudstone Database siltstone samples average depth = 3000m).

2.3.9 Discussion and implications

Sediments of the Urenui Fm. represent a prograding slope sequence. Exceptional outcrop exposure has allowed us to assess the spatial distribution of grain-size heterogeneities, which occur at several scales. Thin-beds of coarser material, similar to those found at studied UK locations, produce heterogeneities on a centimetre scale, while sand-rich channelised intervals represent a coarsening of the sequence's bulk grain-size over tens of metres. Thin-beds of coarser grained material interspersed with background sediment were found to be rare, and were only recorded in close proximity to channelised intervals, commonly as channel-fill deposits. Contrasting with slope sequences examined in the UK, thinly bedded units, produced by frequent alternations in sediment grain-size, were not volumetrically significant within the outcropping Urenui Fm. Where thinly interbedded units do exist, they are found immediately adjacent to, or often interspersed with, thickly bedded sandstone units. Thinly bedded channel-fill deposits record bed thickness averaging 2.7cm, although the lateral continuity of beds is largely determined by the width of the infilled channel scours onto which they onlap (Fig. 2.51). Thinly bedded units belonging to the MCIU are less confined than those of the lower and upper channelised units, and may have significant lateral continuity. In the case of the Urenui Fm. however, the potential impact of thin-beds on cross-stratal fluid migration is to some degree negated by their clear proximity to sand bodies, which will themselves ultimately control the passage of fluids by offering the greatest permeabilities.

Coastal outcrops offering near continuous exposure have allowed us to identify the exact stratigraphic positions of coarser grained intervals within a slope succession. In the case of the Urenui Fm., thin-beds are unlikely to significantly increase vertical permeabilities due to

their scarcity and widely spaced distribution. Where they were found to occur in outcrop, examinations of these units has provided useful information regarding the detectability of thin-beds in the subsurface. Portable gamma-ray spectrometry data collected from intervals of thin-beds reveal that alternations in sediment grain-size which are less than 20cm thick are undetectable. That is not to say that the specific level of gamma radiation emitted by thin-beds is not picked up by the instrument's sensor, rather it appears that the sensor's field of investigation is too large to resolve the discrete radioactive signature of individual beds. Where thin-beds are not associated with larger, and more easily detectable sand bodies in the subsurface, their detection using widely employed wireline tools, such as gamma-ray logging, will be extremely difficult.

Fine-grained background sediment, which constitutes roughly 80% of the 850m thick Urenui Fm., reveals a surprisingly uniform grain-size distribution. Samples from fine-grained intervals distributed throughout the formation are dominated by silt-sized material (minimum of 70%), with only minor amounts of clay-and sand-sized material detected. Inspection of mudstone physical property data held in the Caprocks Mudstone Database and the Ocean Drilling Program archives indicate that 'clean' siltstones of this nature are rare, and that fine-grained slope sediments typically contain higher proportions of < 4μm grains. This low clay-sized fraction suggests that hemipelagic sedimentation was out paced by clastic sediment input during the progradation of the slope, with sediment thought to have been sourced through the winnowing of shelf material (King et al., 1993). The low volume of sand-sized material within background sediments indicates that deposition of coarser material supplied to the shelf edge has been confined within slope channels, or may have bypassed the slope altogether. Similar slope bypass is recorded in the modern Congo Basin, West Africa (*see* section 3.3.2), where coarse grained sediment is channelled directly to the base of slope via the deeply incised Congo Canyon, such that upper portions of the slope are starved of coarser material (Wefer et al., 1998). The Congo Canyon is far wider than erosional channels of the Lower and Upper Channelised Units of the Urenui Fm., with a channel width of 3-7km at the mid-slope, corresponding to roughly 2000m water depth (Babonneau et al., 2002). Despite this difference in scale, these two channel systems share several similar morphological characteristics. Shallow seismic profiles from the upper portion of the Congo Canyon indicate that this deeply incised channel erodes pre-channel hemipelagites and that no significant levee or overbank deposition has occurred (Babonneau et al., 2002). Similarly, the steep margins and confined nature of the Upper and Lower Channelised Units of the Urenui Fm. suggest that they were also highly erosional and provided a conduit for coarse sediment bypass. This confinement and bypass of coarse material appears also to have limited levee deposition adjacent to channels such that thinly bedded levee units are not well

developed. Background hemipelagic sediments of the Urenui Fm. and those from the upper reaches of the Congo slope are among the most homogeneous slope sediments examined during the course of my investigations. In both examples, the lack of coarser grained thin-beds is controlled by the development of channel systems which allow coarse material to efficiently bypass the slope, and thus restrict the 'pollution' of adjacent hemipelagites with coarser material.

As previously mentioned, background sediments are nonetheless coarser grained than clay-rich hemipelagites commonly deposited in slope settings (e.g. Congo Basin, Gulf of Mexico; *see* Chapter 3). The impact on the fluid-flow of this increased grain-size is evident from measured and modelled fluid-flow characteristics. Calculations for the sampled intervals indicate that background fine-grained sediments of the Urenui Fm. have vertical permeability values spanning three orders of magnitude from roughly $9x10^{-21}$ m^2 - $4.6x10^{-18}$ m^2 (9-4600nD) at 25-30% porosity. Permeabilities in slope sediments with higher proportions of clay-sized particles are likely to be considerably lower. Clay-dominated (>60%) samples from the Caprocks Mudstone Database record an average permeability of just $7x10^{-21}$ m^2 (7nD) at porosities between 25-30%, compared to $9x10^{-19}$ m^2 (900nD) for Urenui Fm. sediments at the same porosity.

Complementing the examinations of slope deposits from West Wales, Urenui Fm. units have provided the Caprocks Project with important information regarding the distribution and resolvability of potential flow-units within a channelised slope system, which has experienced coarse sediment bypass.

2.3.10 Conclusions

1. Field investigations carried out as part of the Caprocks Project have confirm that the Urenui Fm. slope sequence outcropping as part of the late Miocene Taranaki Basin consists of three channelised intervals separated spatially, and stratigraphically, by thick sequences of largely homogeneous siltstone.

2. Thin-beds of coarse sediment are not found within fine-grained facies but are limited predominately to channel-fill deposits where there are found interspersed and adjacent to thickly bedded sandstones deposits.

3. Thin-beds which are below ~20cm in thickness are not resolvable using a standard portable gamma-ray spectrometer. Detection of such heterogeneities in the

subsurface is highly unlikely unless high resolution instruments are employed, e.g. formation micro-scanner (FMS).

4. Hemipelagic sedimentation onto the Taranaki Basin slope during the late Miocene was dominated by silt-grade material which record permeabilities of up to three orders of magnitude greater than clay-rich slope sediments analysed for the Caprocks Mudstone Database from West Africa and the North Sea.

Chapter 3

Chapter 3

Towards a hemipelagite database

3.1 Introduction

The Caprocks Project is a multidisciplinary joint industry project (JIP) which aims to define the rates, mechanisms, and pathways by which petroleum is able to migrate through kilometre-scale sequences of fine-grained rock. For the investigation of continental slope sequences, the Caprocks Project has employed a genetic units approach to evaluate the specific sealing-risks of a number of the key depositional units which exist in slope environments. The separation of the main elements of slope deposition into four genetic units, namely; hemipelagic sediments, mass-transport deposits, contourite deposits and channel-levee systems allows for detailed evaluation of the deposit-specific physical characteristics which are likely to impact the sealing capacity of a particular genetic unit (Fig. 3.1). A typical slope sequence is unlikely to be homogeneous, but rather can be thought of as a collection of genetic units, the exact stacking pattern and distribution of which has a profound effect on the sealing capacity of the sequence as a whole. In reality, the exact configuration of depositional bodies is often difficult to predict accurately, but approximations can be made using seismic analysis, coupled with available well information (Fig. 3.2). Using a genetic units approach allows us to begin to define the likely fluid-flow properties of recognisable slope units and to consider fitting quantitative fluid-flow parameters to them. It is the eventual goal of the Caprocks Project to provide a set of templates for well-defined genetic units which provide the basic building-blocks with which to populate slope sequences in basin models and fluid-flow simulations. My role in the development of the Caprocks Group genetic units model involved the evaluation of hemipelagic sediments in modern slope sequences, with the aim of parameterizing the previously undetermined physical characteristics of coarser grained heterogeneities which may impact the sealing capacity of these units, using data from the huge Ocean Drilling Program (ODP) repository.

3.1.2 Seal-bypass mechanisms

While huge volumes of hydrocarbons reservoired in slope sequences are a testament to the high capillary entry pressures and sealing capacity of hemipelagite-dominated successions, under-filled structures and dry exploration boreholes also testify to the effectiveness of sealing bypass and leakage mechanisms in certain settings. Structural elements such as

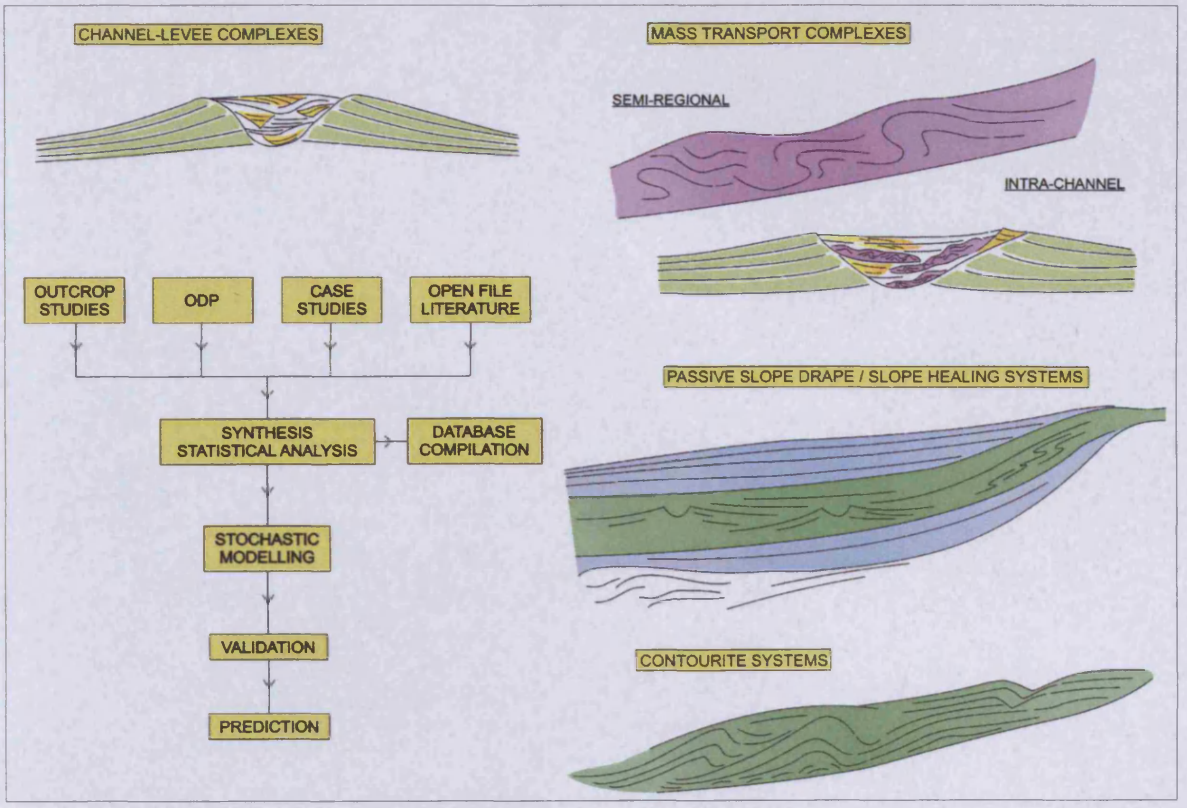

Figure 3.1 Workflow outline for the Caprocks Phase II genetic units study indicating the four key genetic slope depositional features. The characterisation of hemipelagic sediments as part of the genetic units approach has been conducted through outcrop studies (*see* Chapter 2) and through the examination of Ocean Drilling Program data presented in this chapter.

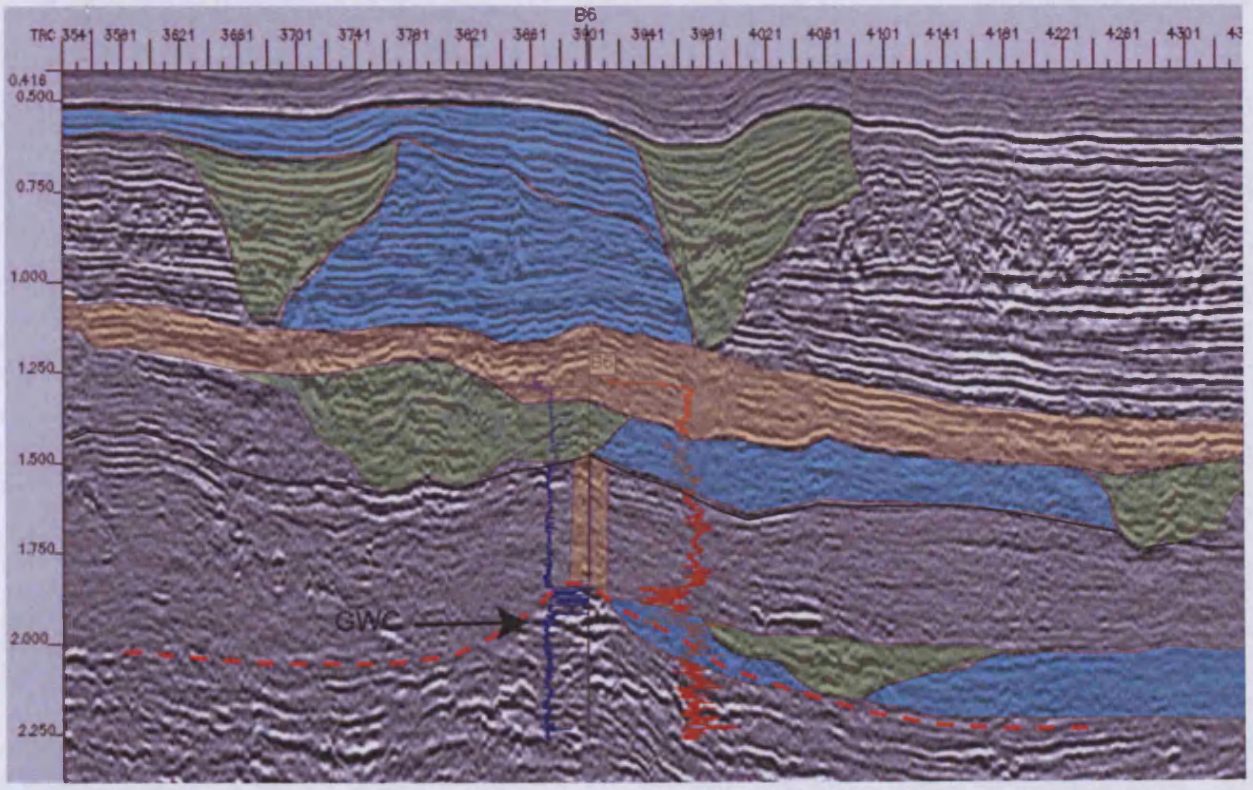

Figure 3.2 Seismic profile from a major delta system, provided by industry sponsors. Coloured panels correspond to specific genetic units interpreted on the basis of seismic facies, gross architecture and wireline responses. Work conducted by Caprocks Project scientist, Aggeliki Georgiopoulou. Further explanation regarding this method of genetic units facies interpretation are given in section 6.5.1.

faults and hydraulically induced fracture networks have been widely cited as potential fluid-flow conduits affecting the sealing capacity of fine-grained sealing units (Grauls and Cassignol, 1992; Caillet, 1993; Esch and Hanor, 1995). In their recent paper, Cartwright et al. (2007) review mechanisms which offer potential fluid-migration pathways through fine-grained sealing sequences, which they list in three main groups; fault-related, intrusion-related, and pipe-related systems. Cross-stratal features of this kind are thought to essentially allow the bypass of a seal's low porosity pore-network by providing pathways of higher lateral and vertical permeability (Sibson, 1981; Ingram and Urai, 1999; Aydin, 2000; Hurst, 2003; Løseth et al. 2003; Boles et al., 2004; Aplin and Larter, 2005; Cartwright et al., 2007). Unlike the centimetre-scale lithological heterogeneities focused on in this study, the bypass mechanisms outlined by Cartwright et al. (2007) represent much larger-scale features, potentially offering permeable pathways across kilometres of sealing sequence, and are therefore often recognisable in high-resolution seismic data (Fig. 3.3). Bypass features represent an important aspect of seal-risk analysis, and while seismic-scale bypass features are receiving increasing attention, detailed investigations of thinly bedded grain-size heterogeneities in sealing sequences have not been previously conducted. The scarcity of information evaluating the possible impact of core-scale heterogeneities can be attributed to the difficulties of recognising these elements in commonly acquired geophysical and petrophysical petroleum system data. The unparalleled sediment core archive of the ODP and other ocean drilling projects offers the best resource with which to investigate this potentially significant seal-bypass system.

3.1.3 Ocean Drilling Programs

Archives of the IODP and it predecessors, the ODP and the older Deep Sea Drilling Project (DSDP), hold the single largest repository of data collected from continuously cored fine-grained sediment. Since the late 1960's, ocean drilling projects have visited more than 1300 sites worldwide, recovering over 400,000m of rock and sediment core (Fig. 3.4). Data used in the development of the Caprocks Hemipelagite Database (CHD) were mined largely from a range of ODP sources, including published volumes, online image-banks and the ODP's web-based database, known as Janus. The ODP specialises in the drilling and coring of relatively shallow (<1000m) drill sites, where wireline logging is performed over the entire depth of the well and continuous core recovery is a priority. This is in contrast to petroleum industry drilling campaigns where wireline logging is often restricted to reservoir intervals and core recovery is rare, especially in the finer grained portions of the sequence.

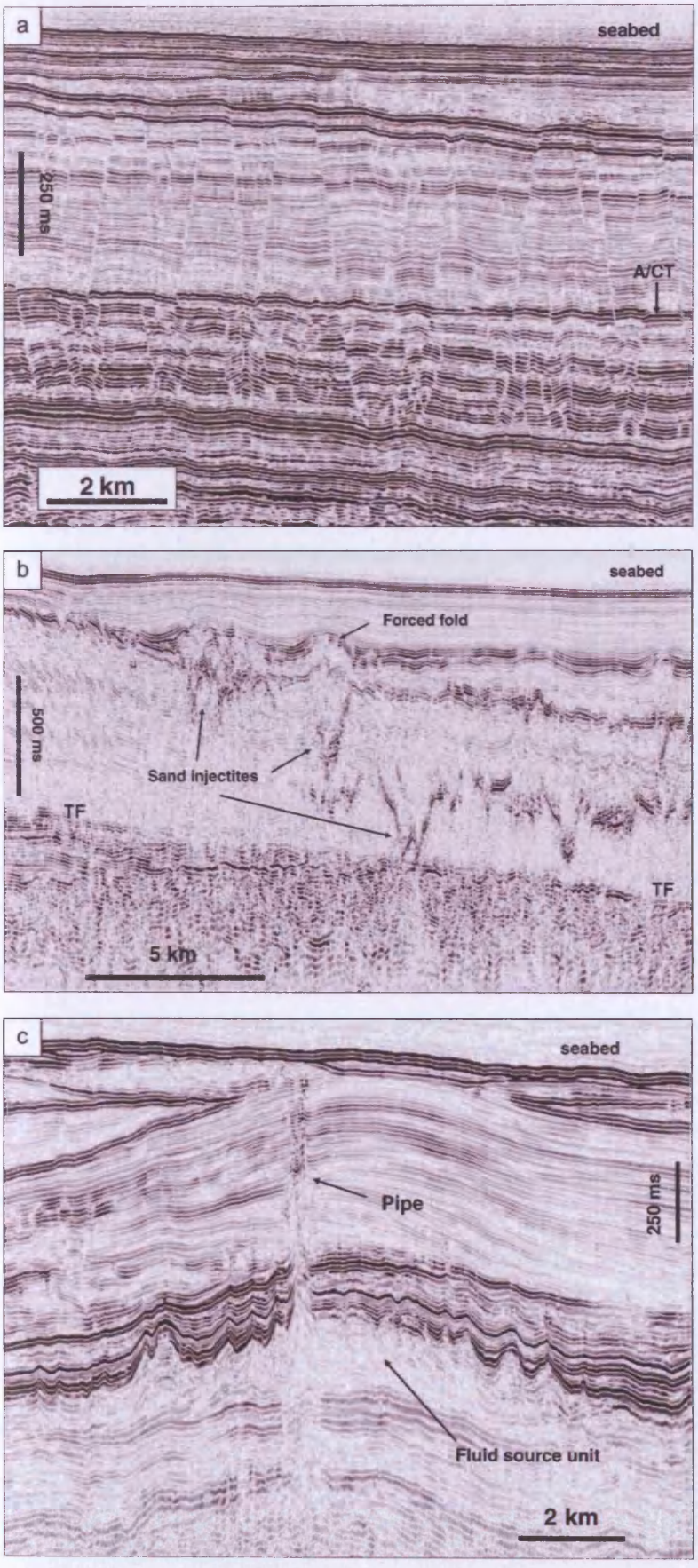

Figure 3.3 Seismic profiles taken from Cartwright et al (2007) showing examples of potential topseal bypass systems from fine-grained sealing sequences
(a) Polygonally faulted sealing interval from offshore Norway
(b) Seismic profile imaging sand intrusions from the Faroe-Shetland Basin.
(c) Seismic profile imaging what is thought to be a pipe acting as a conduit for vertical fluid migration.

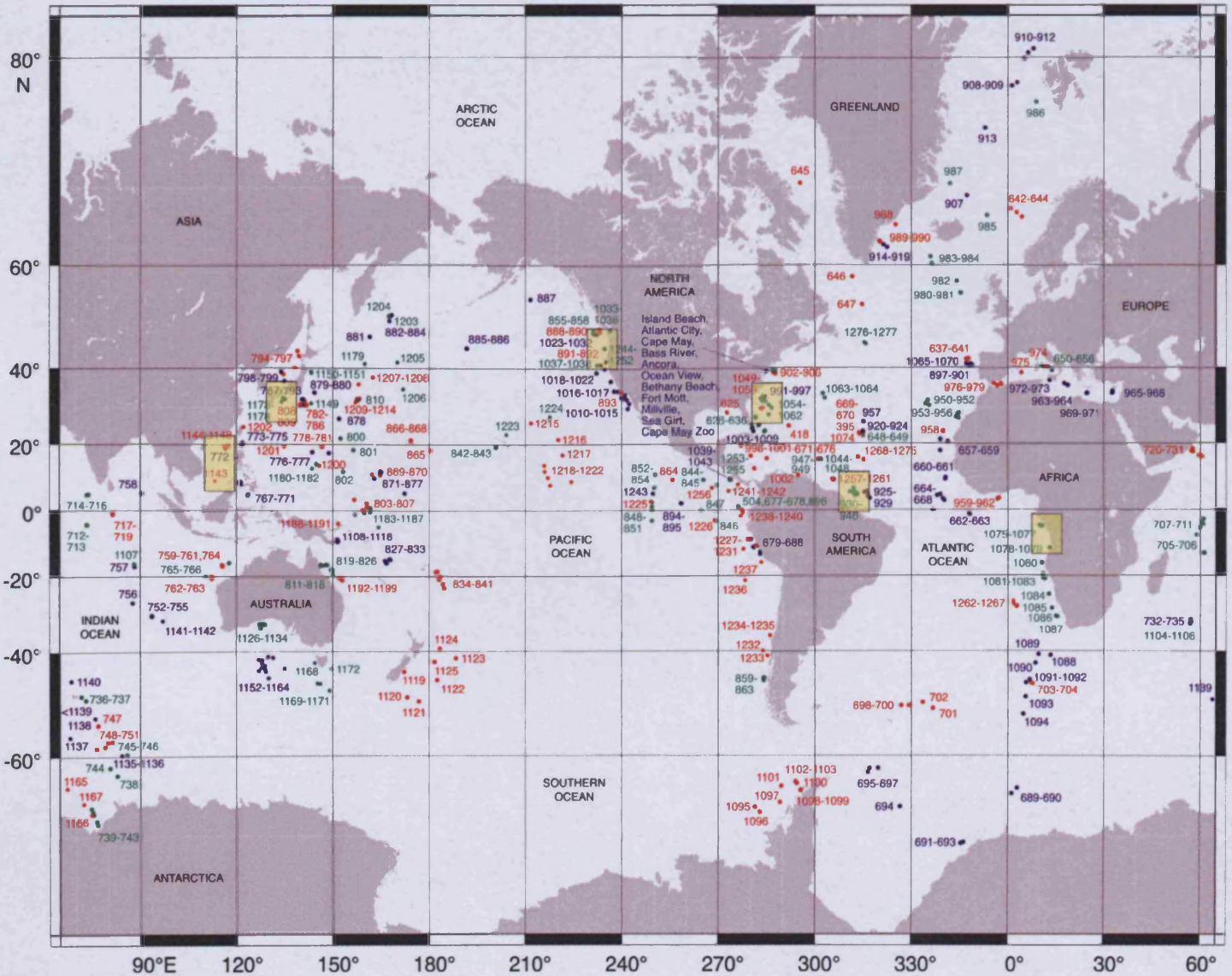

Figure 3.4 Map showing the locations of Ocean Drilling Program Legs 100-210 (Sites 625-1277) drilled between 1985 and 2003. Sites examined in detail in this chapter are highlighted. Note that Leg 310 (Gulf of Mexico) was drilled by the later Integrated Ocean Drilling Program in 2006, and is not shown on this map.

3.1.4 Caprocks Hemipelagite Database

The main objective of the CHD was to bring together information pertinent to the evaluation of hemipelagic sequences as sealing lithologies. The focal aim was to identify and quantify the nature and distribution of more permeable intervals within hemipelagic sequences. The existence of thin-beds consisting of silt and fine-sand have been well documented from field investigations (*see* Chapter 2) and core imagery, where they are commonly seen punctuating monotonous sequences of clay-dominated hemipelagic sediment. However, a fundamental limitation of outcrop studies is that of scale, with the best field exposures only providing information specific to a very limited sediment interval. While outcrops do not provide sufficient scale to document the distribution of thin-beds, the centimetric thicknesses of these heterogeneities leave them unresolved by all but the highest-resolution geophysical tools. A principal aim of the CHD was therefore to mine the huge repository of cored hemipelagic sediment to answer questions regarding the probability of encountering thin-beds of coarse material in slope hemipelagite successions.

3.1.5 ODP and petroleum industry data

Ocean drilling programs collect lithological, biological, and geophysical data which reflect the scientific objectives of the particular drilling campaign. Petroleum industry drilling in contrast tends to penetrate sediments at much greater depths, recording only data important to investigations of the petroleum system. Recovery of sediment core and detailed analysis of samples forms an important part of ODP investigations, which contrasts with the limited recovery commonly made from oil and gas exploration wells. Certain tools which are widely used in oil and gas exploration, such as high-resolution three-dimensional (3D) seismic profiling, have remained largely absent from the regular suite of tools employed by the ODP and IODP until recently.

Making direct comparisons between shallow ODP wells and much deeper petroleum wells is made difficult by the very different pressure and temperature conditions experienced by the sediments. Physical properties such as porosity and permeability are greatly affected by burial depth and associated compaction of sediment grains *(see* Chapter 4), while chemical diagenesis becomes increasingly important at depths exceeding several kilometres (Powers, 1967). The effects on hemipelagic sediments of chemical processes such as cementation, clay-mineral transformations, and hydrocarbon generation are rarely observed from ODP wells, but will feature significantly in petroleum industry wells drilled to greater depth. The principal focus of the CHD is to document the existence of thin-beds of coarse material in

hemipelagic sequences, the broad distribution of which will not change during burial. Although the impacts of certain pressure/temperature dependent processes cannot be examined in shallow ODP cores, ocean drilling data undoubtedly remains an extremely useful, and largely unique, data repository for the examination of marine sediments. For the purposes of this study, the ODP represents the only open source resource available which is capable of providing the required data.

3.1.6 ODP Coring techniques

ODP and IODP coring operations typically employ different coring methods depending on the required depth of the cored interval and the lithology being drilled. Advanced Piston Corers (APC) and Extended Core Barrel coring (XCB) can be used to core to depths of approximately 500 mbsf (metres below sea-floor), and are widely used to core soft to firm sedimentary rocks (Graber et al., 2002) . The APC method envelopes the cored sediment as it is drilled and therefore provide excellent rock core recovery, while the XCB tool is only expected to provide core-recoveries of 55-75% in granular rocks (Graber et al., 2002). To core sediment deeper than 500 mbsf, the ODP employ a Rotary Coring Bit (RCB) which uses a hollow drill bit to recover sections of cored rock. This tool is capable of coring any type of formation to depths where bottom-hole temperatures reach 230°C (Graber et al., 2002).

The principal limitations, with regards to core, of the RCB method is that unconsolidated granular sediments (i.e. sand and gravels) are often poorly recovered, and cored sections of soft formation are prone to damage from fluids. While the majority of ODP Sites examined here were cored using the APC techniques, deeper cored sections from the South China Sea (Leg 184) were drilled using the RCB, and coring in the Nankai Trough also employed the XCB tool. These two tools are likely to give poor recovery of sandy intervals, and therefore the net-to-gross values from these two particular sites, as calculated from thin-bed distribution, should be considered as minimum values.

It should also be noted that data from ODP and IODP boreholes is commonly spliced together from a number of closely spaced drill sites (labelled alphabetically) to form a composite section. When this technique is employed, there is the possibility that errors may occur in depth data as a result of the splice. No spliced borehole data was used in this study. ODP and IODP Sites cited in this Chapter refer to a single borehole, typically the first well spudded (e.g. Site 1075 Hole A). For the purpose of this study, this uncertainty associated with the splicing of borehole data would not have significantly impacted the results presented here.

3.2 Building the Caprocks Hemipelagite Database

3.2.1 Input Data

ODP sites chosen for inclusion in the CHD were selected on the basis of a number of criteria, principally depositional setting, dominant lithology, and data availability. Strict filtering of drill sites was necessary in order to compile data regarding the character of clay-dominated sequences while eliminating the influence of other lithologies and their associated physical characteristics.

- Depositional setting

For the purpose of drawing close analogies with current deepwater petroleum exploration, sites selected for inclusion in the CHD all represent deepwater continental slope settings, drilled in water depths ranging from 427m to 4844m. Sites represent both passive and active basin margins and display widely ranging sedimentation rates, sediment input sources and provenance, as well as slope morphologies. Investigating hemipelagite sequences from a range of basin settings allowed us to evaluate the influence of external parameters such as sediment source and slope morphology on the nature of recently deposited sediments.

- Dominant lithology

For sites to be selected for inclusion in the CHD certain lithological criteria had to be met. Sites had to record a sequence of clay-dominated hemipelagic sediments without significant coarse-grained siliciclastic material (i.e. submarine slope channel deposits). Sites dominated by calcareous and biosiliceous material were also excluded. Dominant grain-size and bulk sediment compositions were determined from shipboard analysis of samples using qualitative methods.

- Data availability

Data extraction followed a common work-flow, and as such, certain prerequisite data was required from all sites. Continuous core recovery and associated core descriptions and photography were used to build a picture of the distribution of coarser layers, while seismic profiles and physical property data were also used to characterise the depositional regime at each location.

3.2.2 CHD workflow

A work-flow was established in order to effectively extract the relevant data from a combination of visual and descriptive media. Site selection, based initially on depositional setting, was followed by closer examination of lithological facies using core descriptions, physical properties data and seismic profiles. While many sites fulfilled certain CHD criteria, for example, depositional setting, further essential data was often not available thus rendering the location unusable for our purposes. Sites, which met all criteria, were then selected for inclusion in the CHD.

The principal component of the CHD is quantitative data regarding the down-hole distribution of thin-beds of silt- and sand-grade material. An example of this data is represented graphically in Fig. 3.5 where the thickness and position of beds for a specific ODP site are shown against well depth. In order to produce such plots it was necessary to record the exact thickness and position of every discrete silt and sand horizon within a cored sequence. Thin-beds were identified from core descriptions and cross-referenced against corresponding core photographs (Fig. 3.6). Facies information was also extracted for each 10m section of core in order to evaluate shifts in background facies. Well depths varied considerably between sites ranging from 121 mbsf to 624 mbsf, with 23 ODP and IODP sites allowing roughly 7000m of hemipelagic core to be examined at a centimetre resolution.

As well as producing graphic representation of thin-bed distribution, the CHD also contains tabulated numerical data from each site, recording values for the total thickness, number and average spacing of thin-beds, as well as net-to-gross values for the sequences examined (*see* Caprocks Hemipelagite Database, CD-ROM inside back cover).

3.3 ODP Site Investigations

Sites chosen for investigation during this study are outlined in this section. A general setting is provided for locations examined, followed by a brief description of the facies distribution and the distribution of coarser beds as recorded from recovered cores. The likely controls on this facies distribution are also discussed with particular reference to local conditions such as sediment sources and sediment transport networks.

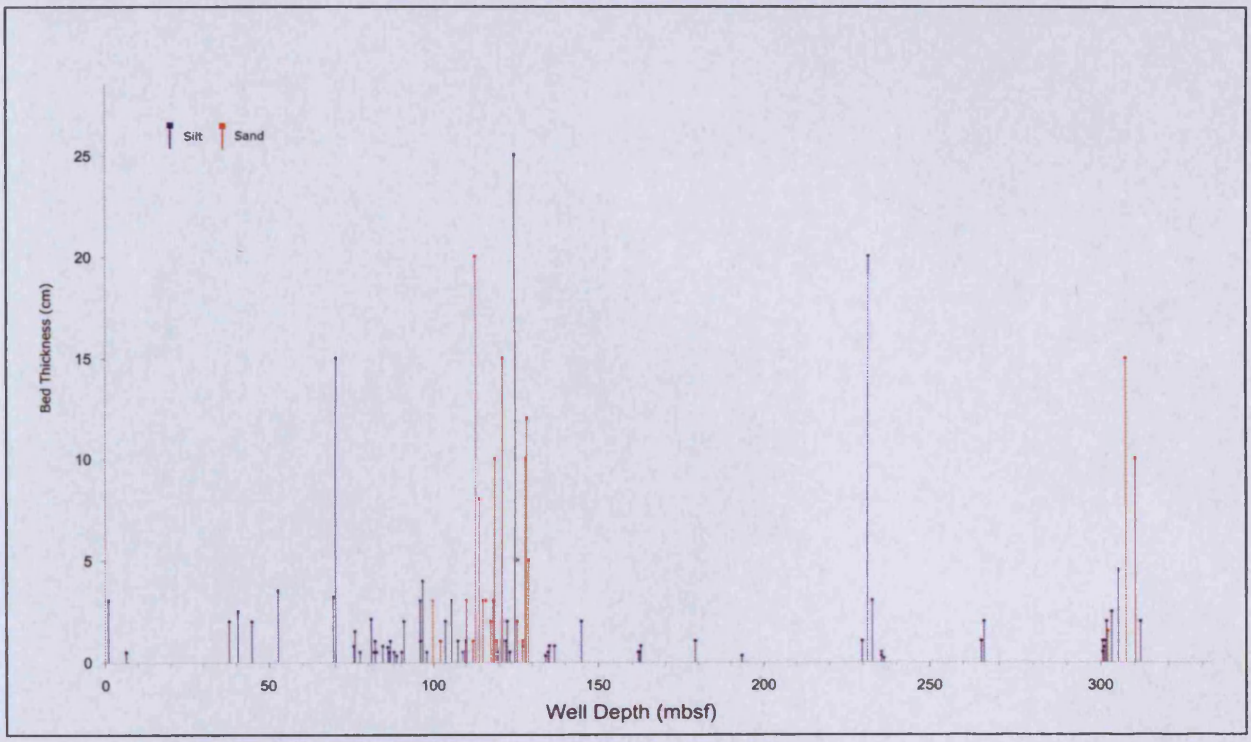

Figure 3.5 Example of a thin-bed distribution plot from ODP Site 1244 on the Cascadia Margin, northeast Pacific. This plot indicates the thickness and position of silt and sand beds recorded from cores as a function of depth. In this particular example, 87 coarse layers were recorded within clay-rich background sediments, constituting approximately 1% of the total sediment recovery.

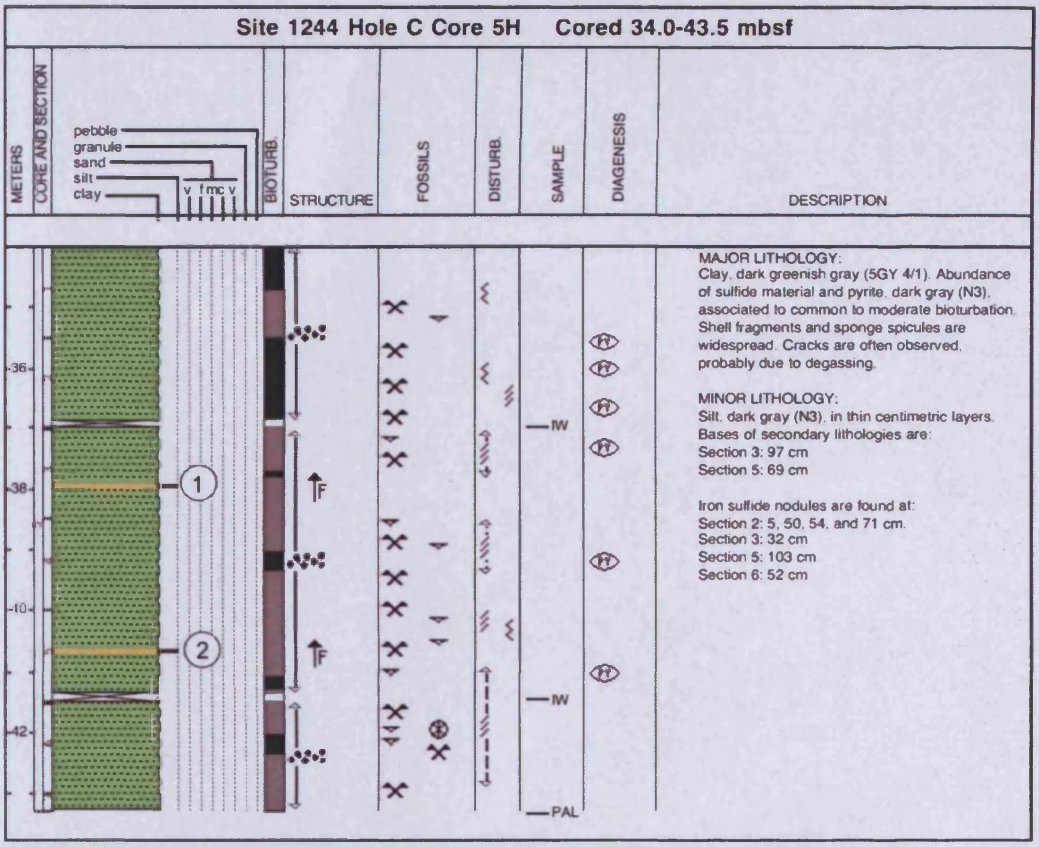

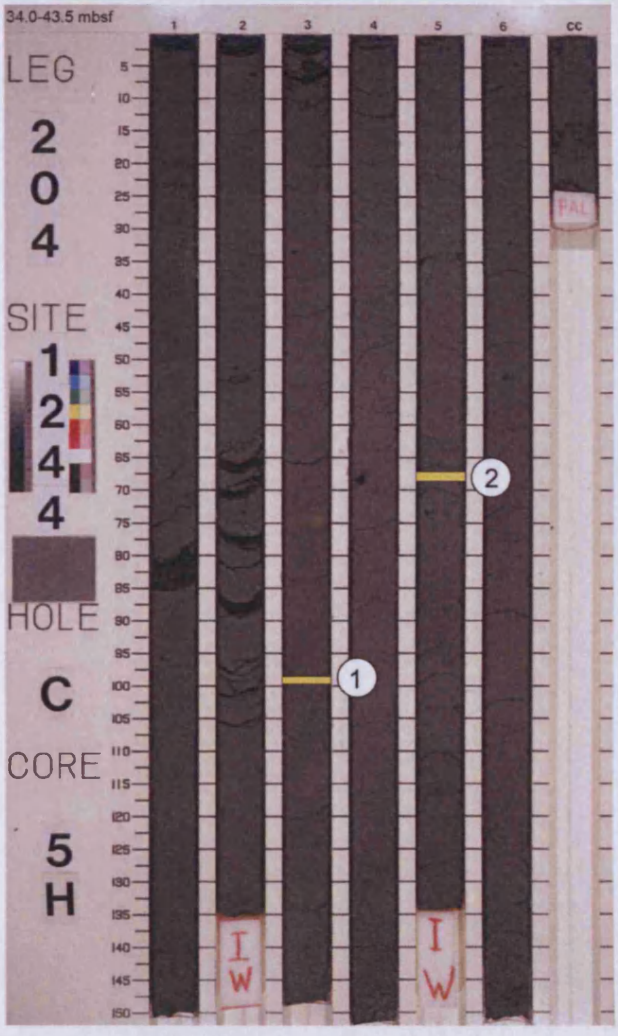

Figure 3.6 ODP core description (above) with corresponding core photographs (left) form Site 1244 on the Cascadia Margin. Yellow intervals indicate the position of two fine-sand thin-beds.

3.3.1 Location 1: Carolina Slope

Setting

The Carolina Slope and Blake-Bahama Outer Ridge (BBOR) lie in the western North Atlantic, offshore United States, and were the targets for drilling during ODP Leg 172. The Carolina Slope lies seaward of a broad 200km-wide shelf fed by several small point-sources, while the BBOR represents a large sediment drift which extends south-eastward from the Carolina Slope into abyssal waters. Four of the eight wells drilled during Leg 172 were included in the CHD, recording high sedimentation rates in the region during the Pleistocene (Keigwin et al., 1998). Sites 1054 and 1055 represent the shallowest sites located on the Carolina Slope in water depths of 1300m and 1800m respectively, while Sites 1057 and 1060 were drilled along the crest of the BBOR in waters depths of 2584m and 3481m respectively (Fig. 3.7) (Keigwin et al., 1998). Sites form a NW-SE depth transect with drilling locations located at 5km (Site 1054), 17km (Site 1055), 70km (Site 1057) and 270km (Site 1060) southeast of the shelf-slope break. Seismic profiles from Sites 1055, 1057, and 1060 reveal a single seismic facies of stacked parallel reflections which are typically low-amplitude and highly laterally continuous (Fig. 3.8a,b), indicative of low-energy hemipelagic sedimentation (Brown and Fisher, 1977). Seismic reflectors recorded from the uppermost ~70m of sediment at Site 1054 are similar to those recorded from deeper sites, however beneath this depth, reflections become less continuous and show clear truncations (Fig. 3.8c).

Thin-Bed Distribution

Hemipelagic sediments recovered from Leg 172 sites reveal a broad decrease in the volume and grain-size of relatively coarse material with increasing distance offshore (Yokokawa & Franz, 2002), both in background sediments and as discrete thin-beds (Fig. 3.9). Silty-clay background sediments, which are common on the upper slope at Site 1054, are progressively replaced by clays with appreciable amounts of nannofossils towards the more distal Sites 1057 and 1060. Site 1054 records approximately 25 thin-beds which range in thickness from thick bio-clastic turbidites of >100cm to thinner silty beds measuring several centimetres. Discrete coarse beds represent approximately 6% of the total core recovered at Site 1054, a figure which decreases to 2.5% 13km further downslope at Site 1055. Interestingly, although Site 1055 records less total volume of coarse material, the total number of thin-beds is over twice that of Site 1054, at 62. Thin-beds at Site 1057 located at the base of slope, constitute just 1% of the total sediment and are dominated by thin silt layers 1-10cm thick, evenly distributed throughout 131m of core. Finally, just three discrete

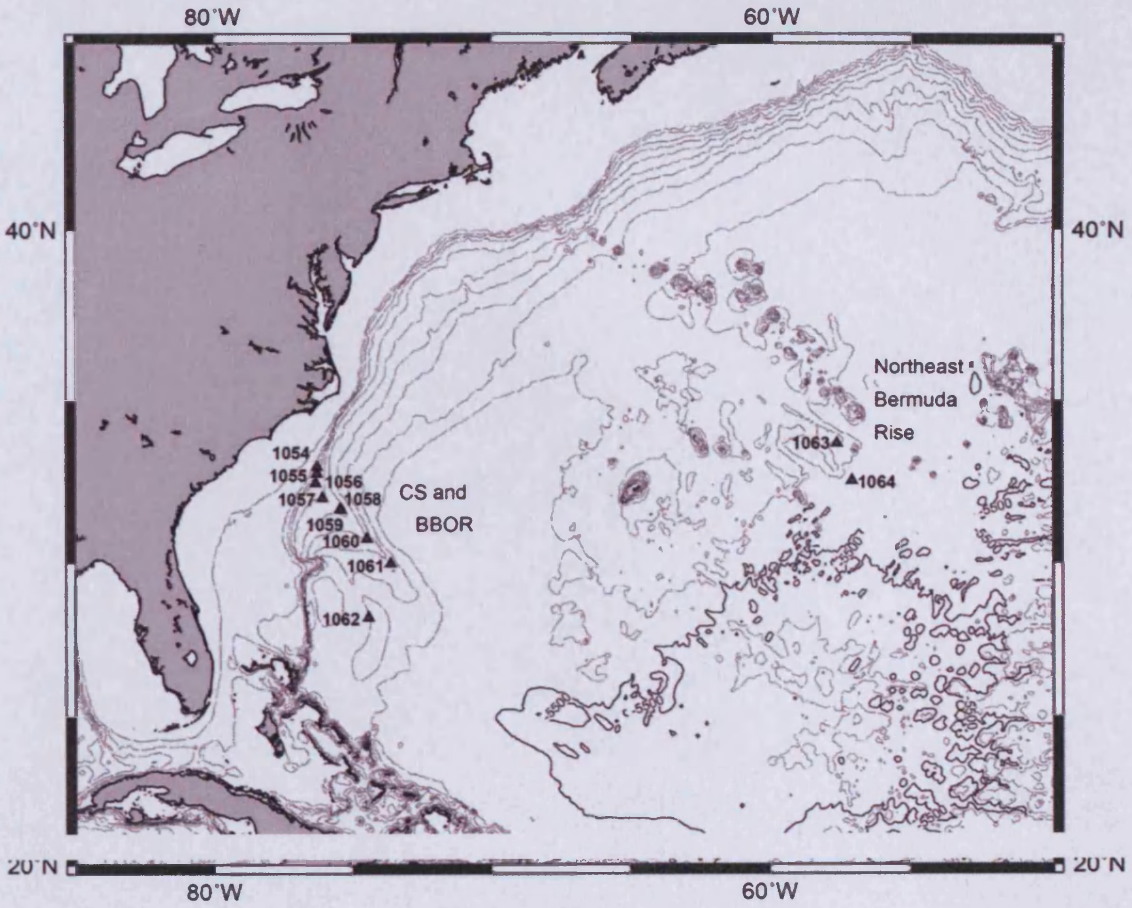

Figure 3.7 Map showing the location of sites drilled during Leg 172 of the ODP on the Carolina Slope and Sohm Abyssal Plain (taken from Keigwin et al, 1998).

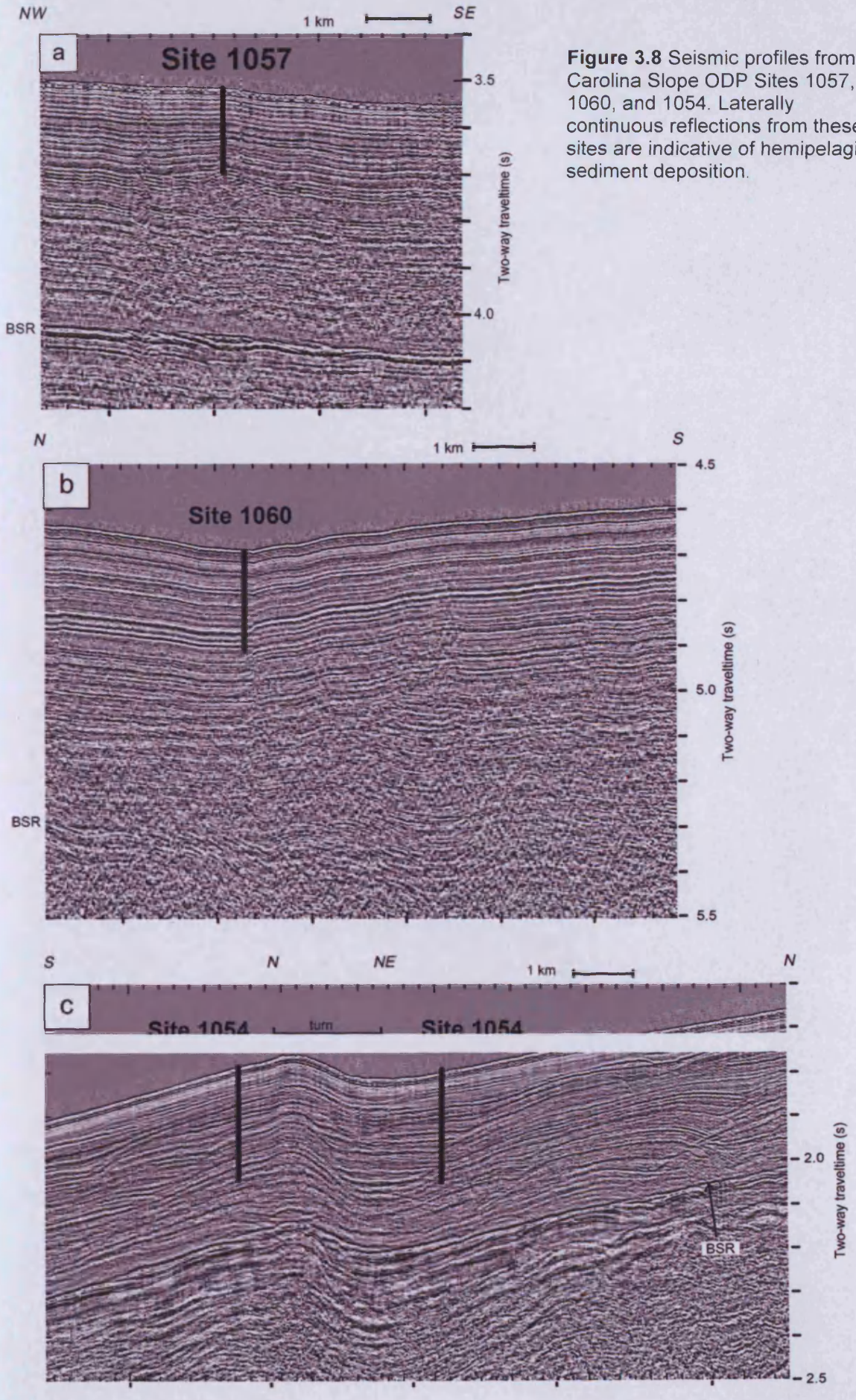

Figure 3.8 Seismic profiles from Carolina Slope ODP Sites 1057, 1060, and 1054. Laterally continuous reflections from these sites are indicative of hemipelagic sediment deposition.

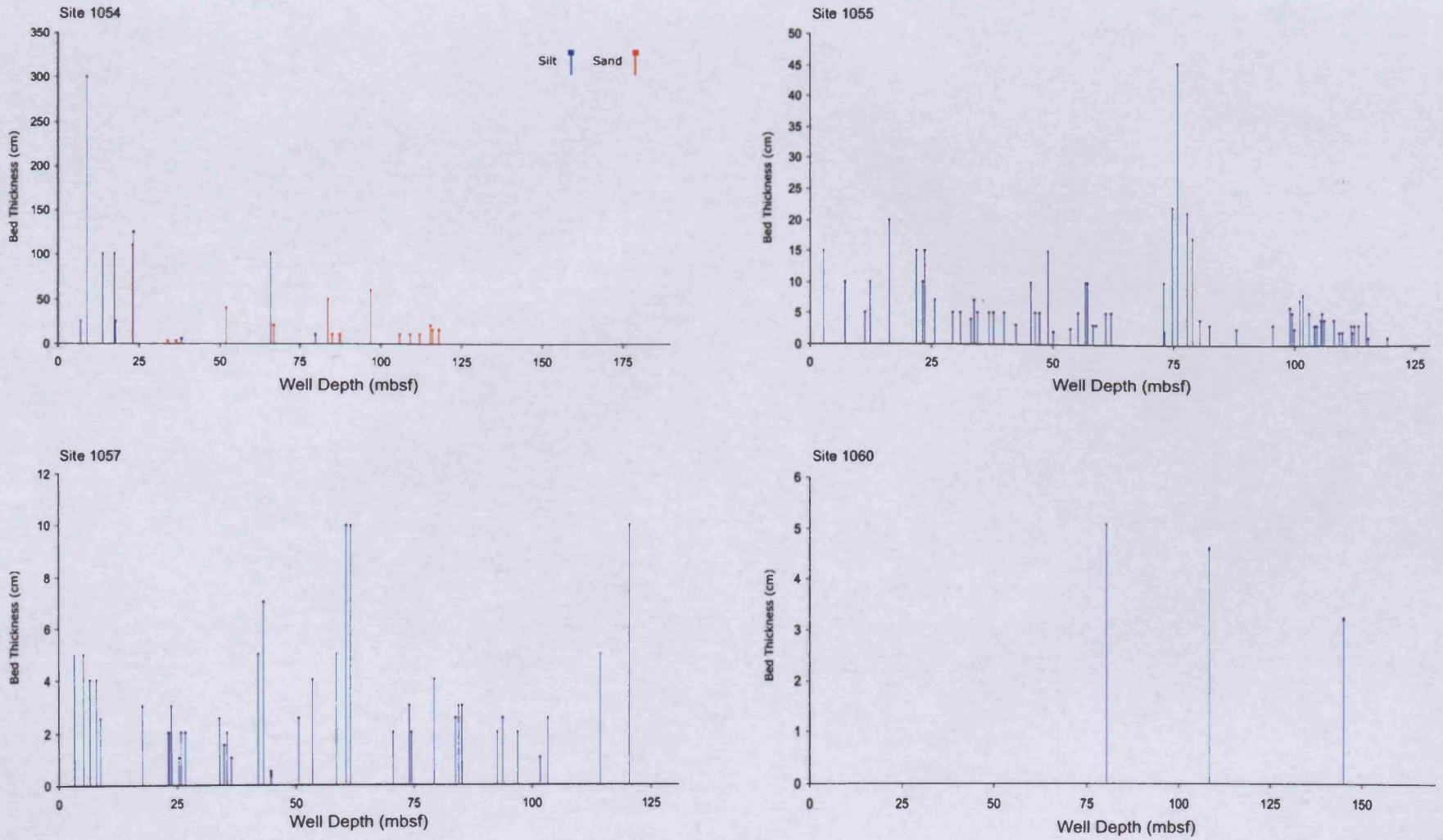

Figure 3.9 Plots showing the distribution and thickness of discrete silt and sand beds against depth for the four Sites examined from OPD Leg 172 on the Carolina Slope and Sohm Abyssal Plain. See Fig. 3.7 for locations.

silt beds are recorded from the Site 1060, constituting less than 1% of the 170m of sediment recovered.

Controls on sedimentation

Unlike the majority of passive margin slopes which receive large quantities of sediment from the shelf, the majority of material deposited at Carolina Slope and BBOR sites is thought to be derived from the Canadian continental margin and transported southward by the Deep Western Boundary Current (Fig. 3.10) (Haskell et al., 1991; Laine et al., 1994). Hemipelagic sedimentation rates for Pleistocene sediments at Leg 172 sites have been shown to increase downslope from an average of 6.5 cm/k.y. at Site 1054 to 19 cm/k.y at Site 1060, reflecting the influence and sediment input of the DWBC (Keigwin et al., 1998). Thin, normally graded coarse beds recorded from Site 1054 are indicative of waning current flows and suggest that sediment is also sourced from shelf regions, probably introduced by turbidity currents. Coarse thin-beds which are recorded downslope at Site 1055 show sharp sediment contacts and often appear massive (Fig. 3.11), features which Stow & Holbrook (1984) associate with deposition from contourite currents. High resolution X-radiograph images reveal that structures such as cross-laminations, fining-up sequences, and erosive surfaces are found at water depths in excess of 5500m, attesting to the combined influence of turbidity and contourite currents in the region (Yokokawa, 2001). The dominant influence of either turbidity currents or contourite currents on coarse material distribution at Leg 172 sites is unclear, however the structure of thin-beds can provide clues as to the processes controlling their deposition. It is likely that the deposition and distribution of coarser horizons will become increasingly influenced by contourite currents, associated with the DWBC, below a specific depth. Hemipelagic sediments examined from the Carolina Slope and BBOR reveal relatively few individual beds of coarse material compared to other locations included in the CHD (i.e. Gulf of Mexico), largely owing to the dominant along-slope input of relatively fine-grained material and the lack of local sediment point-sources to deliver coarse terrigenous sediments directly to the slope.

3.3.2 Location 2: West Africa

Setting

The scientific objectives of Leg 175 were to reconstruct the late Neogene history of the Benguela Current and associated upwelling systems along the western coast of Africa (Wefer et al., 1998). A total of five sites were selected for inclusion in the CHD from the

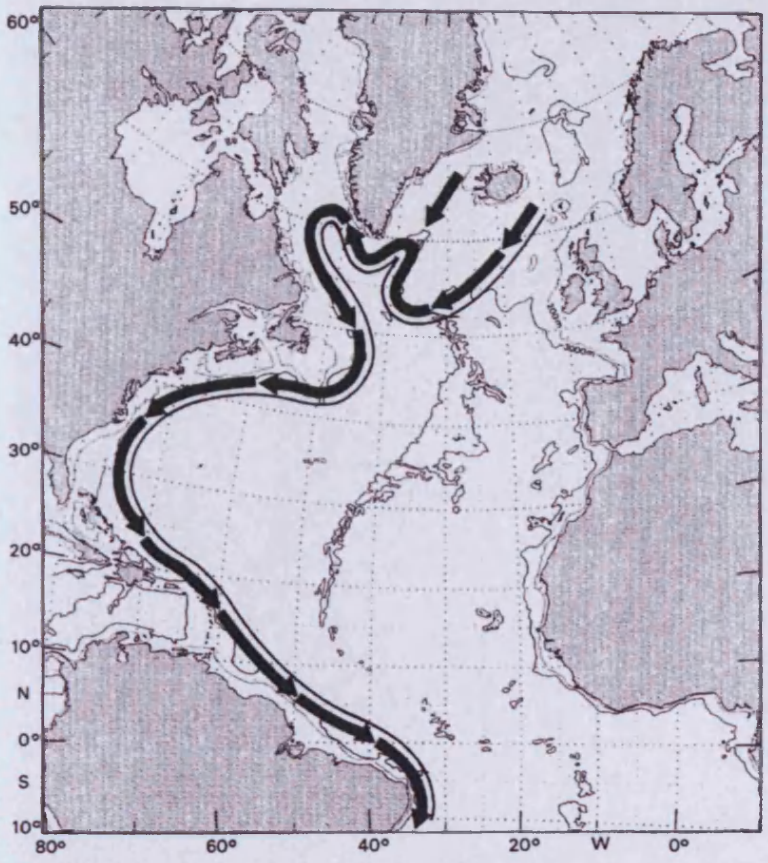

Figure 3.10 Map of the North Atlantic showing an approximate path of the Deep Western Boundary Current, from Rhein (1994). Sediment is transported south by this current along the eastern US continental slope and rise.

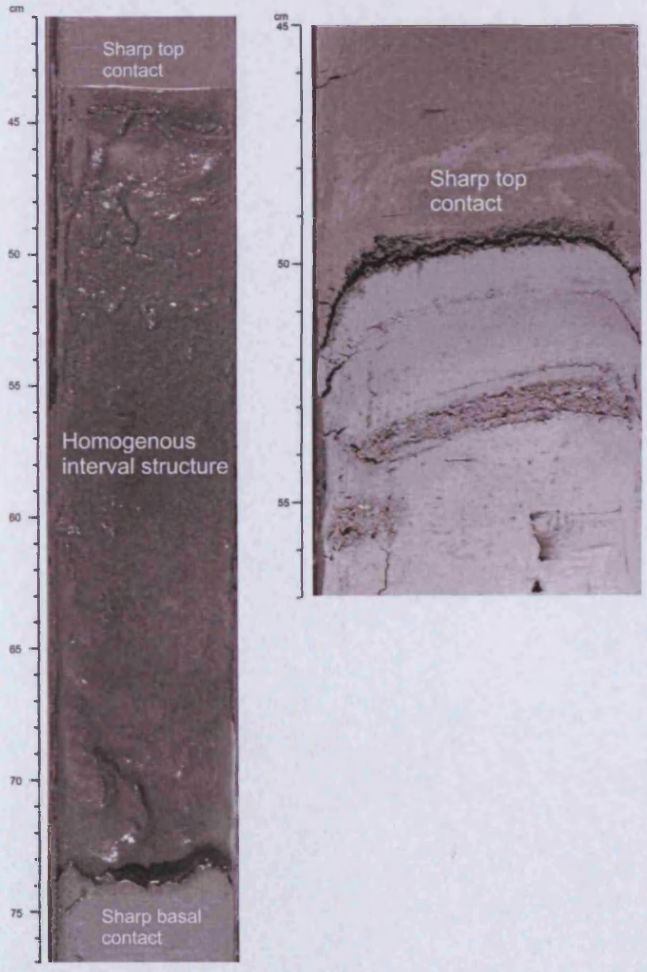

Figure 3.11 Photographs of cored interval recovered during Leg 172 showing intervals of coarser grained material with sharp upper and lower contacts and largely homogenous internal structure. These features have been interpreted as being deposited from long-shore contourite currents. Images from Keigwin et al (1998).

thirteen drilled during Leg 175. Sites 1075, 1076, and 1077 are located in the Lower Congo Basin, directly north-west of the Congo River mouth (Fig. 3.12). These locations form a depth transect of the Congo slope at water depths from 1404m to 2995m (Wefer et al., 1998) and were selected in order to investigate the influence of major point-source terrigenous sediment input on the distribution of coarse thin-beds. Site 1076 represents the most proximal location, drilled roughly 180km northwest of the Congo River mouth, while Sites 1077 and 1075 lie a further 50km and 100km to the northwest respectively.

Seismic reflection data from the Lower Congo Basin document similar seismic facies corresponding to the drilled intervals of Sites 1075, 1076, and 1077 (Fig 3.13). Site 1076 reveals an uppermost, thin (40ms two-way travel time (TWT)) packet of relatively high amplitude and laterally continuous reflections. Reflections below this are of lower amplitude and show less coherency, with common sub-vertical transparent zones interpreted as faults (Wefer et al., 1998). Site 1077 also shows strong reflections at, and just below, the seabed, beneath which lies a 150ms (TWT) low amplitude interval containing only two prominent and laterally continuous reflections. The lowermost 100ms TWT of seismic data corresponding to cored sediments at Site 1077 reveals an increase in the amplitude and continuity of reflections and these show a degree of undulation not seen in reflections above. The configuration of seismic facies at Site 1075 is very similar to that of Site 1077, although higher amplitude reflections towards the base of the drilled interval, also seen at Site 1077, show a lesser degree of lateral continuity.

In addition to sites from the Lower Congo Basin, two sites from the Angola Basin were also included in the CHD. Sites 1078 and 1079 were drilled roughly 800km to the south of the Lower Congo Basin sites in the upper slope of the Mid-Angola Basin in water depths of 427m and 737m respectively (Fig. 3.14) (Wefer et al., 1998). Seismic profiles from Site 1078 reveal a familiar 'tram-line' configuration of stacked parallel reflections of relatively high amplitude, showing considerable lateral continuity (Fig. 3.15). Seismic facies from Site 1079 document similar, laterally continuous, parallel reflections of slightly higher amplitude. When compared to seismic facies of Congo Basin sites, these profiles show an overall increase in reflection coherency, continuity and amplitude.

Thin-bed distribution

Sediment in the Lower Congo Basin almost entirely comprises of diatomaceous clays. Remarkably, not a single coarse bed was recorded from over 600m of recovered core from the three sites examined, a fact made more notable by the proximity of the sites to the Congo

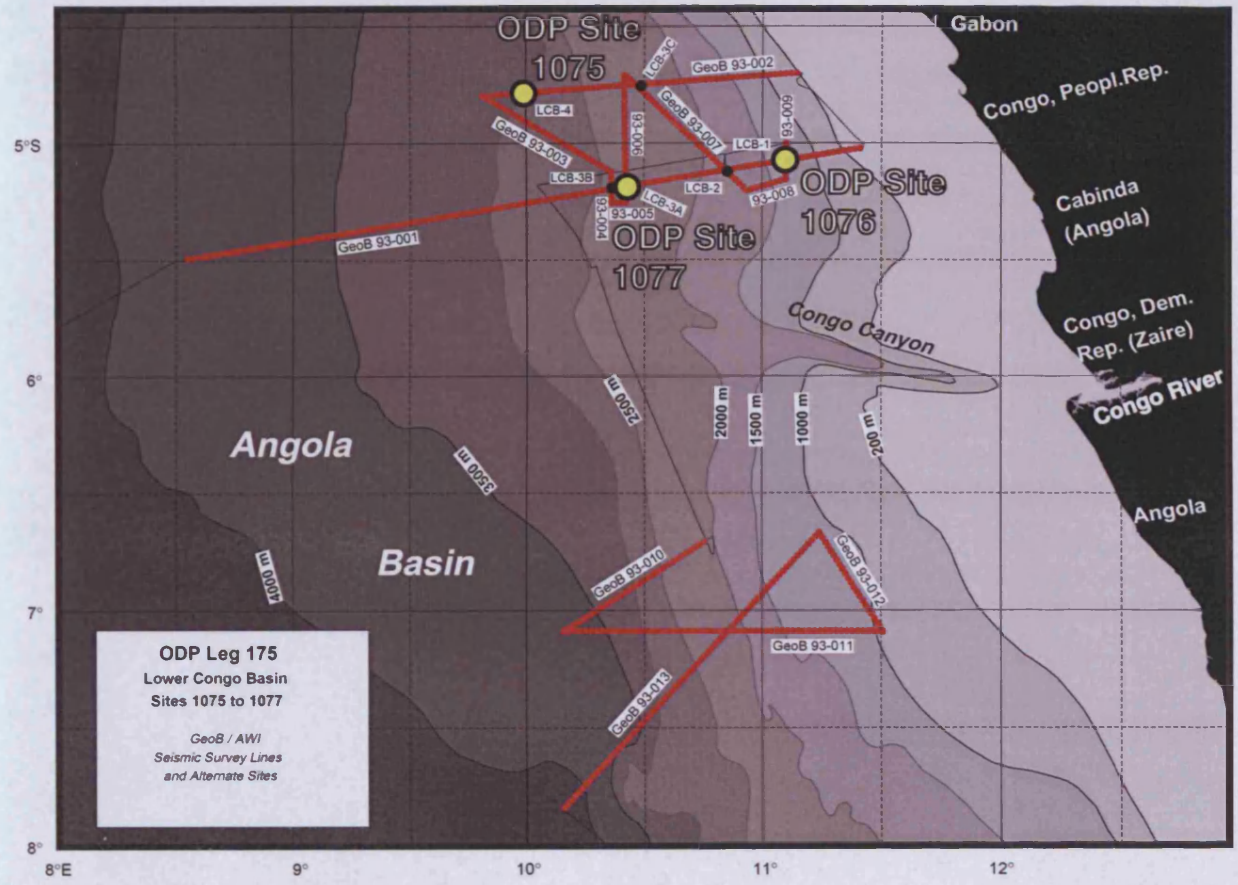

Figure 3.12 Map showing the location of ODP Sites 1075, 1076, and 1077 drilled in the Lower Congo Basin during Leg 175. From Wefer et al (1998).

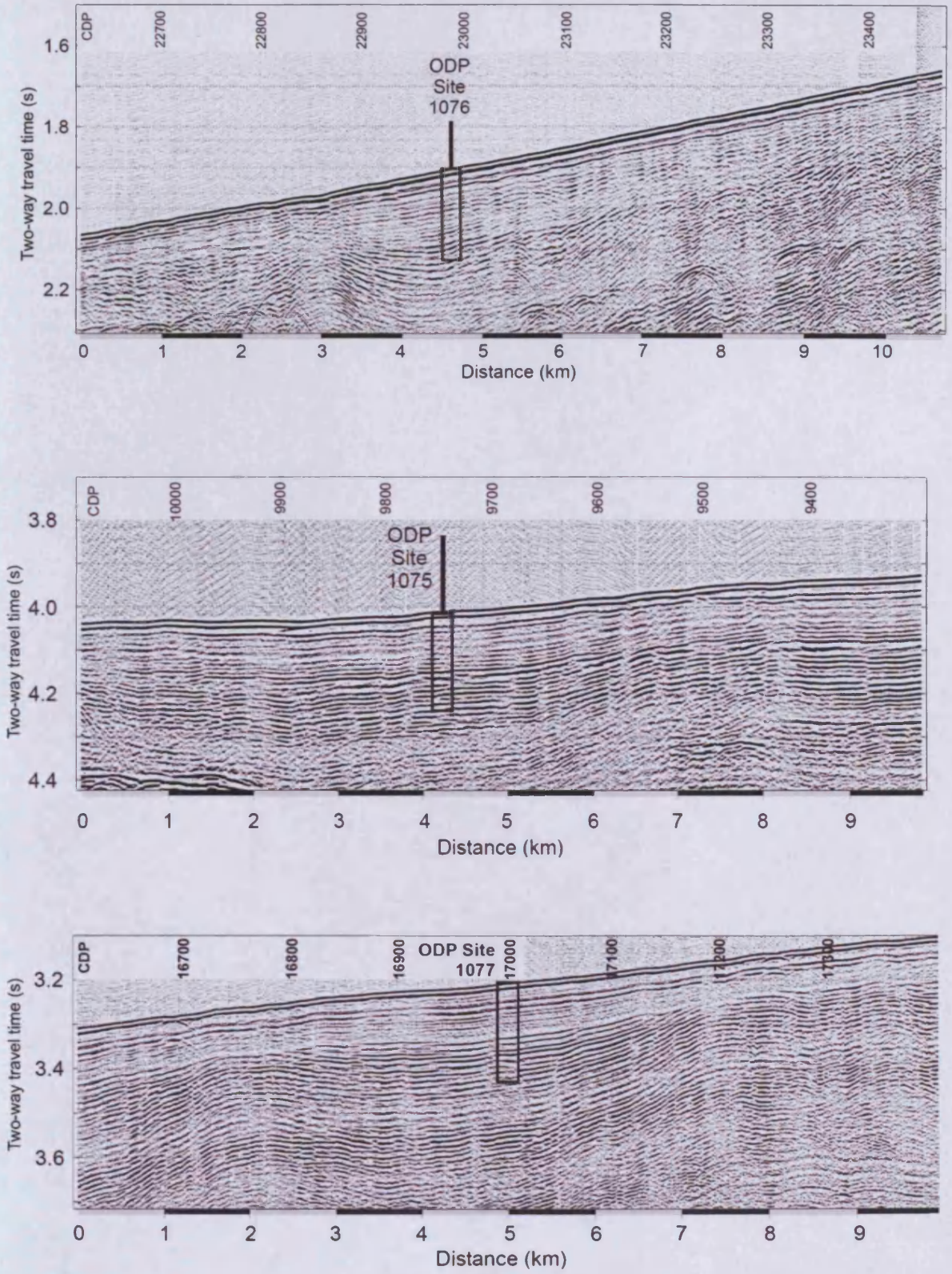

Figure 3.13 Seismic profiles from ODP Leg 175 Sites 1075, 1076, and 1077 drilled in the Lower Congo Basin. Laterally continuous high amplitude reflectors are indicative of hemipelagic sedimentation at these locations. Images from Wefer et al (1998).

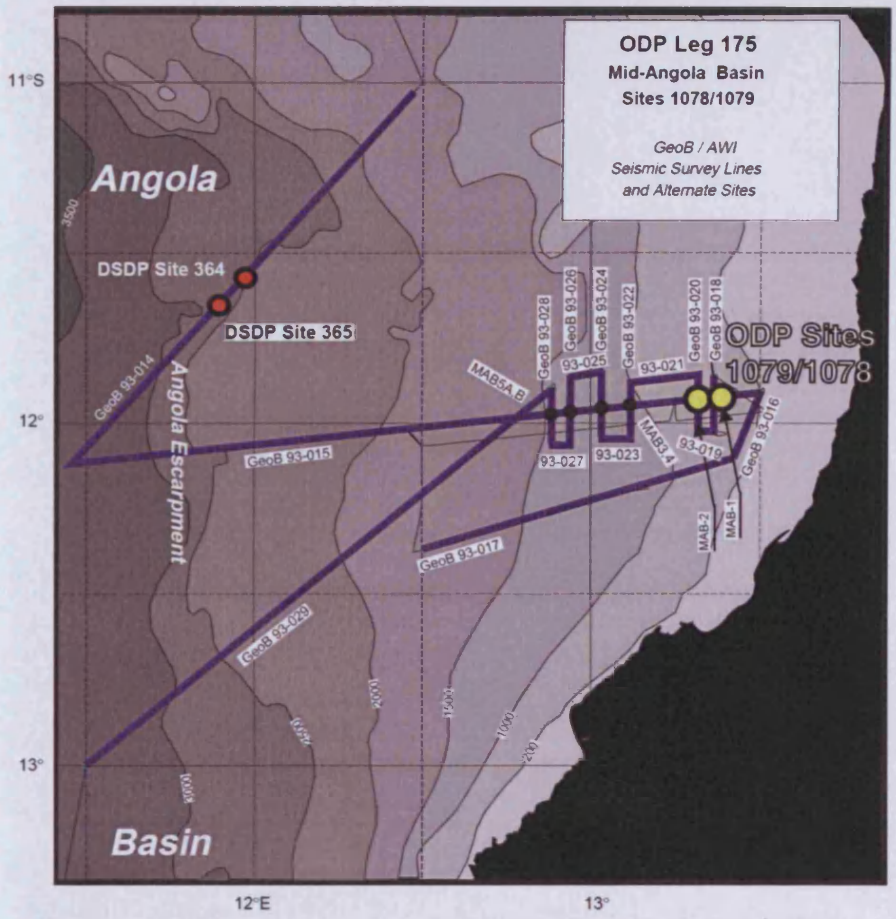

Figure 3.14 Map showing the location of ODP Leg 175 Sites 1078 and 1079 drilled in the Mid-Angola Basin. Image from Wefer et al (1998).

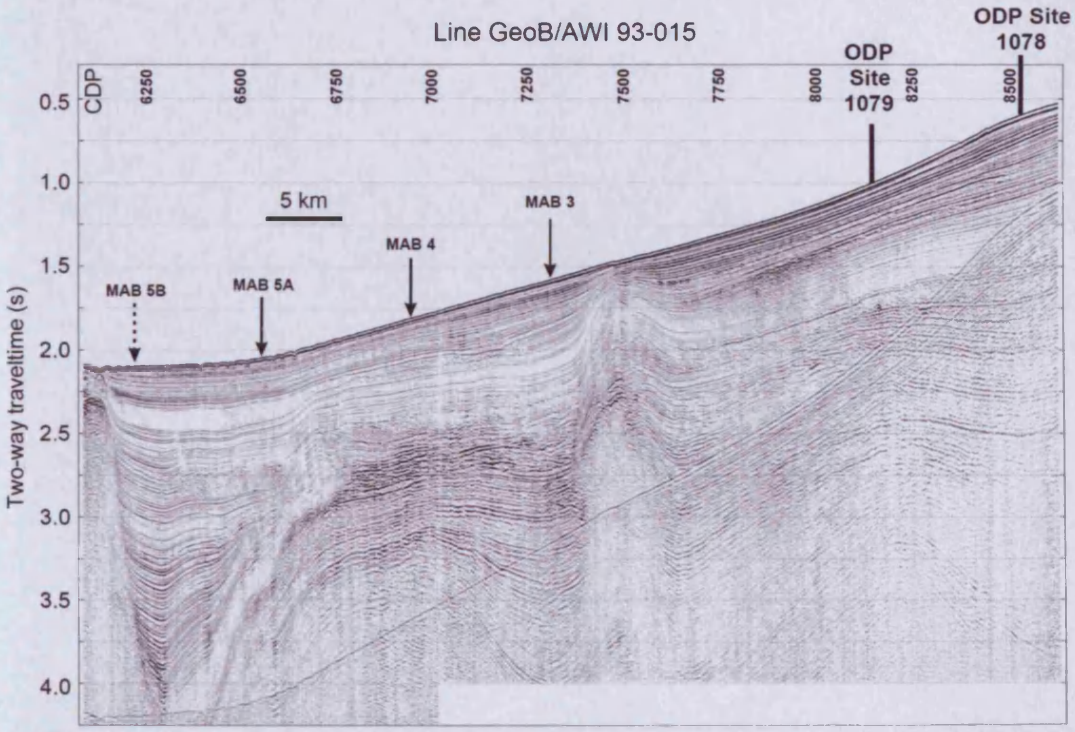

Figure 3.15 Seismic profile showing the slope position of ODP Sites 1078 and 1079 in the Mid-Angola Basin. The profile shows a similar hemipelagic seismic facies to that recorded from the Lower Congo Basin (Fig. 3.13). Position of seismic line is shown in Fig. 3.14. Image from Wefer et al (1998).

River mouth. Sediments recovered from Angola Basin sites 1078 and 1079 record a total of 247m of nannofossil-rich silty clay, punctuated by a total of 20 coarse thin-beds. In the case of Site 1079, thin coarse deposits constitute just over 2% of the total sediment volume, a figure reduced to <1% at Site 1078 (Fig 3.16).

Controls on sedimentation

The absence of appreciable volumes of coarse-grained material in hemipelagic sediments deposited at Sites 1075, 1076, and 1077 is thought to be the result of effective sediment bypass (Wefer et al., 1998). Sediments recovered from these sites are indeed largely sourced from the Congo River, attested to by abundant freshwater diatom taxa and terrigenously derived lipids (Wefer et al., 1998; Schefuss et al., 2001); however coarse detrital material is thought to be channelled directly to deeper water via the Congo Canyon (Wefer et al., 1998). Sediment bypass of this nature has essentially starved the continental slope adjacent to the canyon of coarser material, allowing the deposition of largely uninterrupted hemipelagic clays and biogenic sediments.

Sediments recovered from Sites 1078 and 1079 from the Angola Basin reveal elevated levels of coarse detrital material compared to sites from the Congo Basin, despite only limited proximal terrigenous sediment point sources. Coarse material has been shown to have likely origins in igneous provinces of southern Africa, fed to the Atlantic by the Kunene River and transported roughly 600km northward to the Angola Basin by the Benguela Current (Wefer et al., 1998). Terrigenous silt- and sand-grade material may also be introduced from coastal erosion in the area, linked to the rapidly uplifting shoreline in the region (Wefer et al., 1998).

Hemipelagic sediments recovered from Leg 175 sites, like those of Leg 172, highlight the importance of sediment input and sediment distribution on the nature and frequency of coarse thin-beds. Lower Congo Basin sites reveal that proximity to a major point-source is not necessarily a prerequisite for elevated terrigenous material and that slope sediment bypass can be extremely effective. This particular depositional setting provides an interesting analogue to deeply incised passive margin successions that develop during sea-level low-stands and represent potential targets for petroleum exploration. Like sites examined at the Carolina Slope and BBOR, Angola Basin sites from Leg 175 (Sites 1078 and 1079) draw attention to the importance of ocean currents in the lateral transport and remobilisation of slope sediments.

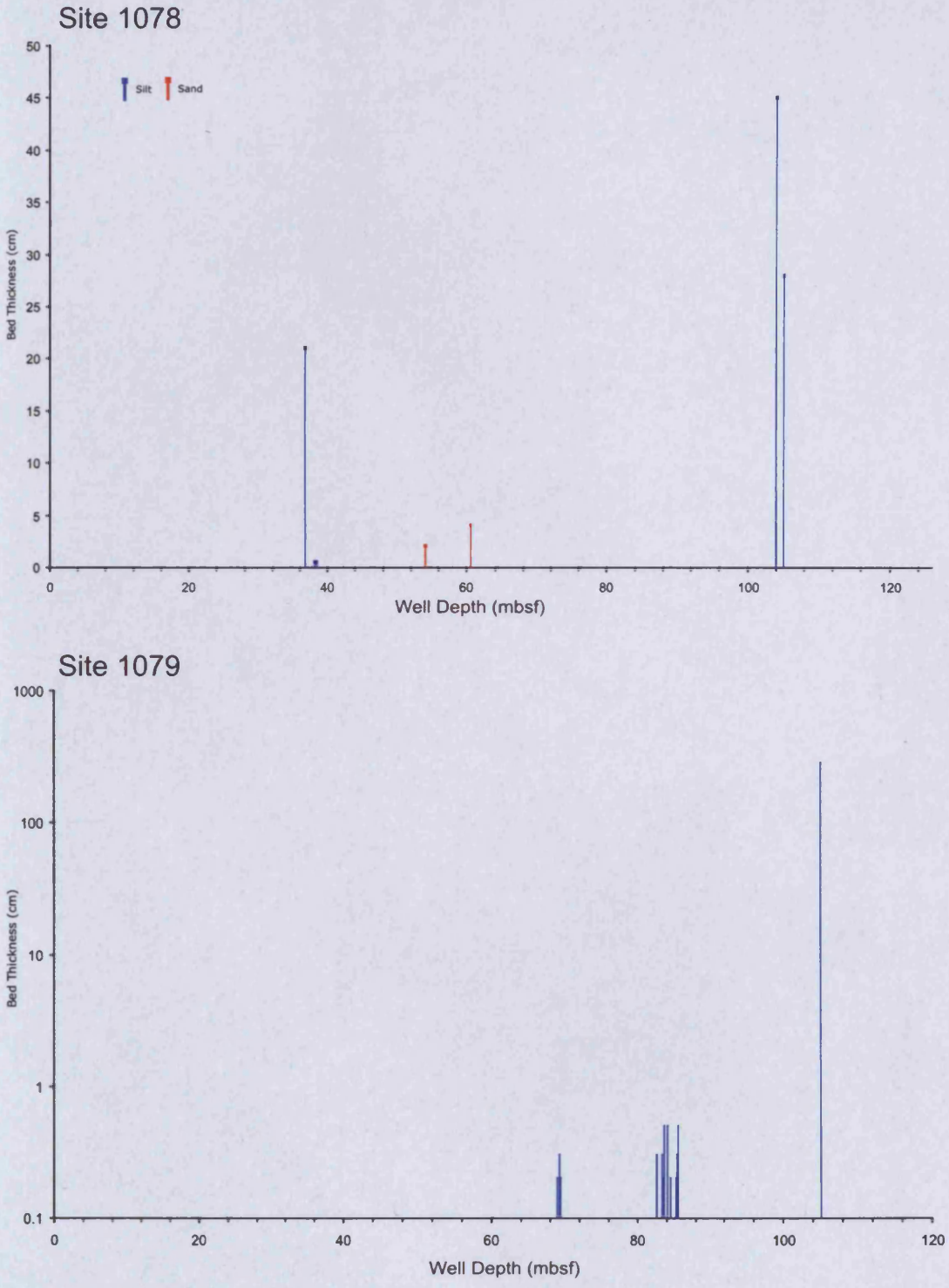

Figure 3.16 Plots showing the distribution and thickness of discrete silt and sand plotted beds against depth for ODP Sites 1078 and 1079 drilled in the Mid-Angola Basin, west Africa.

3.3.3 Location 3: South China Sea

Setting

The South China Sea Basin has emerged in recent years as an important petroleum producing province with active oil production in both the northern and southern areas of the region (Zhang et al., 2007; Yao et al., 2008). A total of 6 sites were drilled during ODP Leg 184, of which three have been chosen for inclusion in the CHD. Sites 1144 and 1146 were drilled in slope sediments on the basin's northern margin seaward of a broad (upto 350km wide) continental shelf containing the petroliferous Pearl River Mouth Basin (Fig. 3.17a,b). These sites record thick sequences of hemipelagic sediment characterised by high terrigenous sediment inputs from the Pearl and Red Rivers, which has led to extremely high sedimentation rates at Site 1144 of between 310-930 centimetres per thousand years (cm/k.y.) over the last million years (Wang et al., 2000). Site 1146 occupies a slope position 140km to the southwest of Site 1144 and in contrast has experienced much lower sedimentation rates, in the region of 60 cm/k.y. Seismic profiles from Site 1144 reveal a thick series of stacked reflections with high lateral continuity, seen to converge downdip at an increasing angle, forming a wedge-shaped geometry (Fig. 3.18a) (Wang et al., 2000). This feature is interpreted as a prograding slope-wedge created as a result of the extremely high volume of sediment delivered to the area. Seismic facies from Site 1146 record reflections which are similar in amplitude and lateral continuity to those at Site 1144, but are largely parallel and delineate a gentle slope-gradient, a configuration indicative of hemipelagic slope deposition (Fig 3.18b) (Brown and Fisher, 1977).

A third site, 1143, was drilled in deep water (2772m) off the Nansha Island area, 1200km SSW of Site 1144, east of the Gulf of Thailand (Fig 3.19) (Wang et al., 2000). The seismic record for Site 1143 is of poor quality, and records a sequence of discontinuous and sometimes chaotic reflections (Fig. 3.20). The sequence drilled at Site 1143 constitutes the topmost 500m of a fault-bound sediment filled basin thought to be several kilometres thick (Wang et al., 2000). Sedimentation rates since the late Miocene at Site 1143 are in the region of 50 cm/k.y., recording terrigenous input from the Mekong River which enters the South China Sea through Vietnam some 700km to the east (Wang et al., 2000).

Thin-beds

Sites 1144 and 1146, located on the northern margin of the South China Sea basin, record very similar configurations of coarser grained beds. Both sites reveal roughly 10 discrete

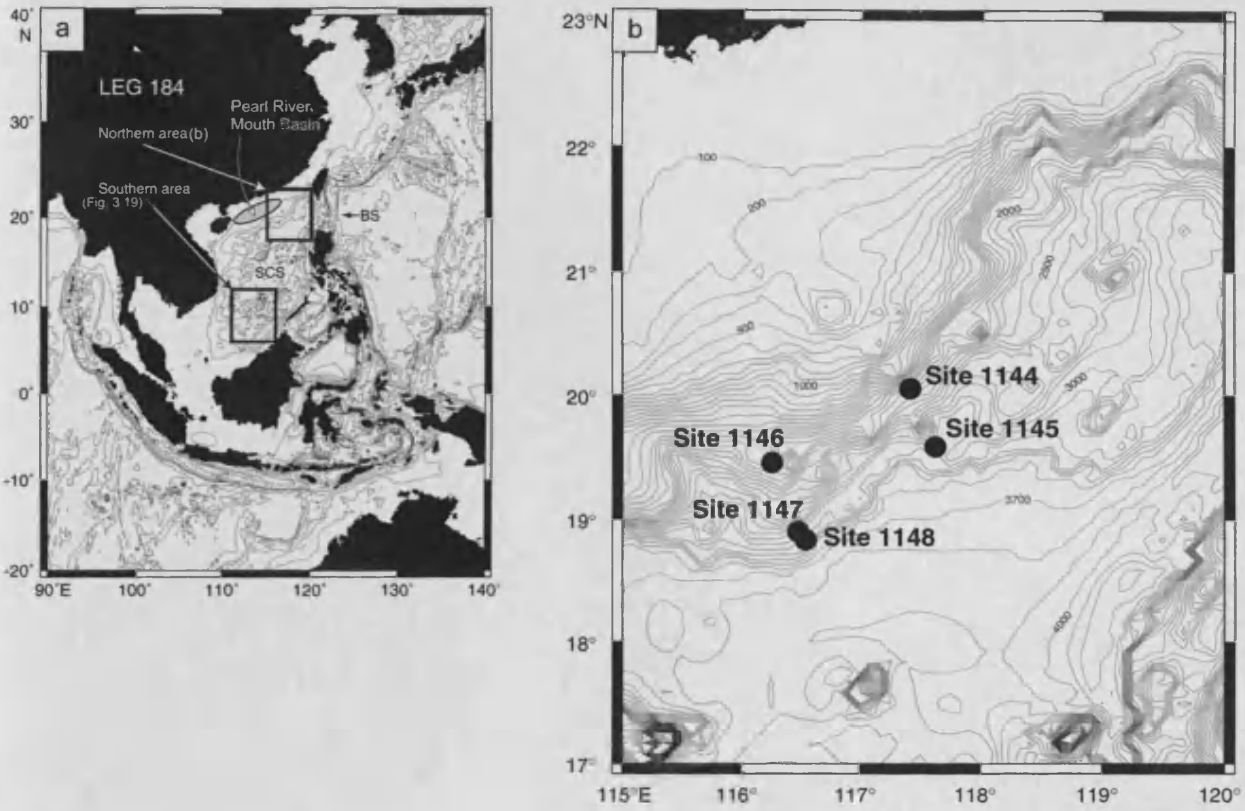

Figure 3.17 (a) Regional map of the South China Sea showing the location of the Pearl River Mouth Basin and the general position of northern drill sites, shown in more detail in (b). Images in Figs 3.17-3.20 adapted from Wang et al (2000).

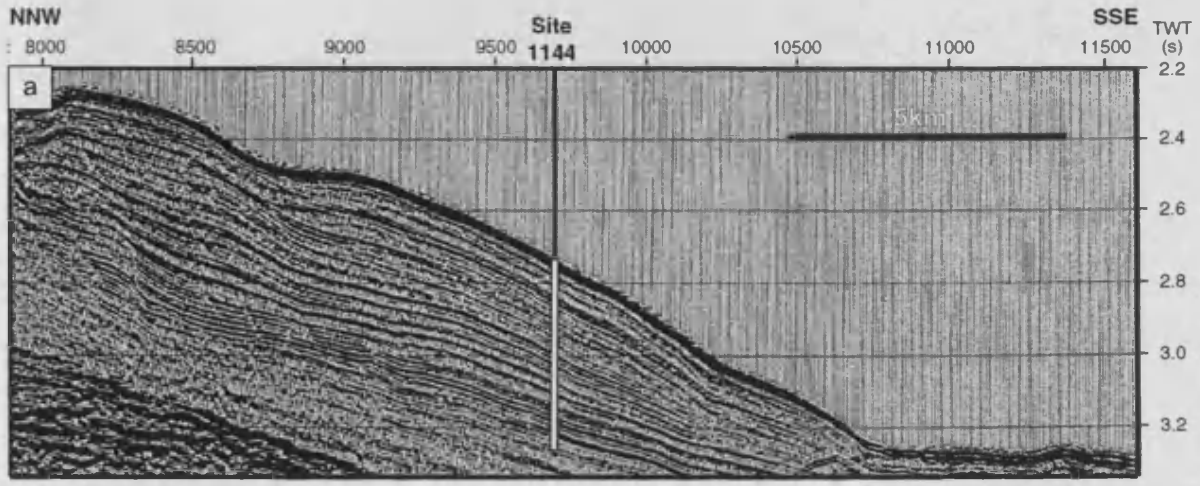

Figure 3.18a Seismic profile from ODP Site 1144 in the South China Sea. The thick slope sediment wedge imaged in this seismic data is the result of extremely high sedimentation rates.

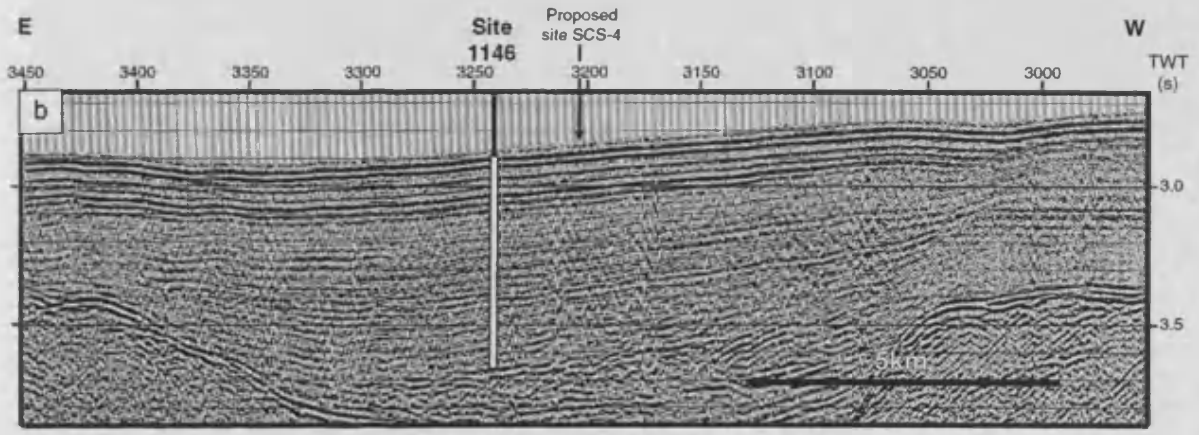

Figure 3.18b Seismic profile from ODP Site 1146 in the South China Sea. High amplitude and laterally continuous reflections are indicative of hemipelagic sedimentation.

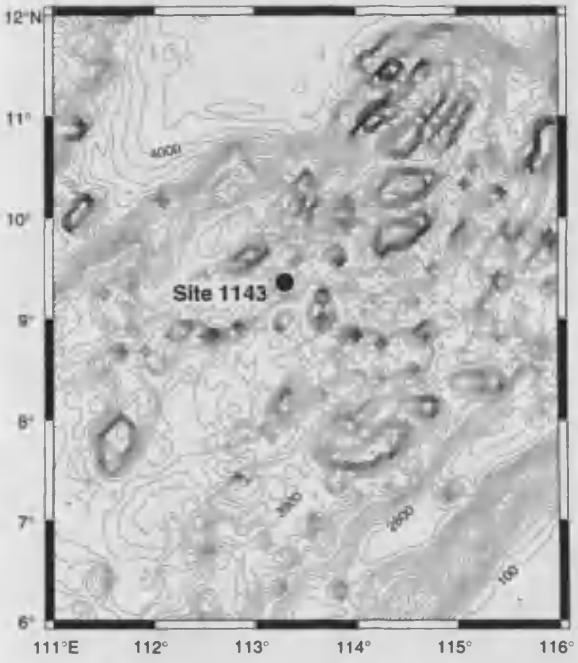

Figure 3.19 Map showing the location of ODP Site 1143 in the southern South China Sea (see regional map for regional context, Fig. 3.17a).

Figure 3.20 (below) Seismic image showing the discontinuous and sometimes chaotic seismic facies recorded from hemipelagic sediments at Site 1143.

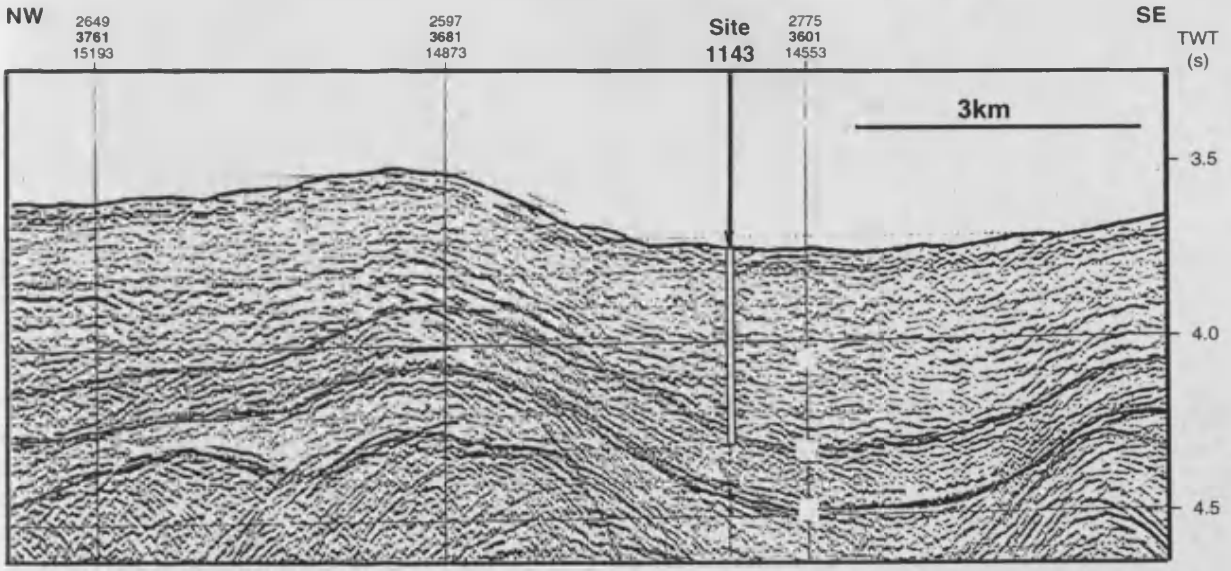

beds of silt and sand grade material which are evenly distributed throughout the recovered cores. Beds are upto 10cm thick, but average 2-3cm, constituting just 0.1% of the total sediment column at both sites (Fig 3.21). Despite the similarities in the distribution of discrete silt and sand accumulations, background sediments are markedly different. Site 1144 is dominated by silty-clay facies while Site 1146 records a thick sequence of nannofossil-rich clays.

Hemipelagic sediments at Site 1143 are dominated by nannofossil-rich clays punctuated by roughly 60 thin-beds of coarser material which comprise approximately 1% of the 500m cored (Fig. 3.21). Thin-beds are typically thicker than at sites located on the northern margin of the basin reaching a maximum thickness of 70cm. Coarse beds are often graded, likely to reflect deposition by turbidity currents which become more prevalent in deeper portion of the well below ~300m, suggesting a shift in either sediment supply or local depositional conditions.

Controls on sedimentation

Preferential deposition of terrigenously sourced coarse material in the region of Site 1144 has formed the prominent prograding wedge imaged in seismic data (Fig. 3.18a). Site 1146 lies outside of this high-sedimentation zone, 135km to the SW, and records a sequence largely devoid of significant coarse terrigenous material. Both areas however reveal similar clay mineral assemblages which have been shown to be sourced predominantly from the Pearl River to the north (Boulay et al., 2005), suggesting that elevated silt and sand fractions found at Site 1144 are the result of local sediment pathways, and not differing sediment inputs.

Unlike many hemipelagic sequences (i.e. Gulf of Mexico), coarse material at Site 1144 exists largely as dispersed grains within the background sediment. This notable absence of discrete coarse thin-beds is thought to be indicative of the overall efficiency of sediment delivery system to this portion of the northern South China Sea slope. The dispersed nature of silt and sand grade material may also be linked to the introduction of eolian dust originating from surrounding landmasses, which may represent a significant source of detrital grain mass (Wang et al., 1999).

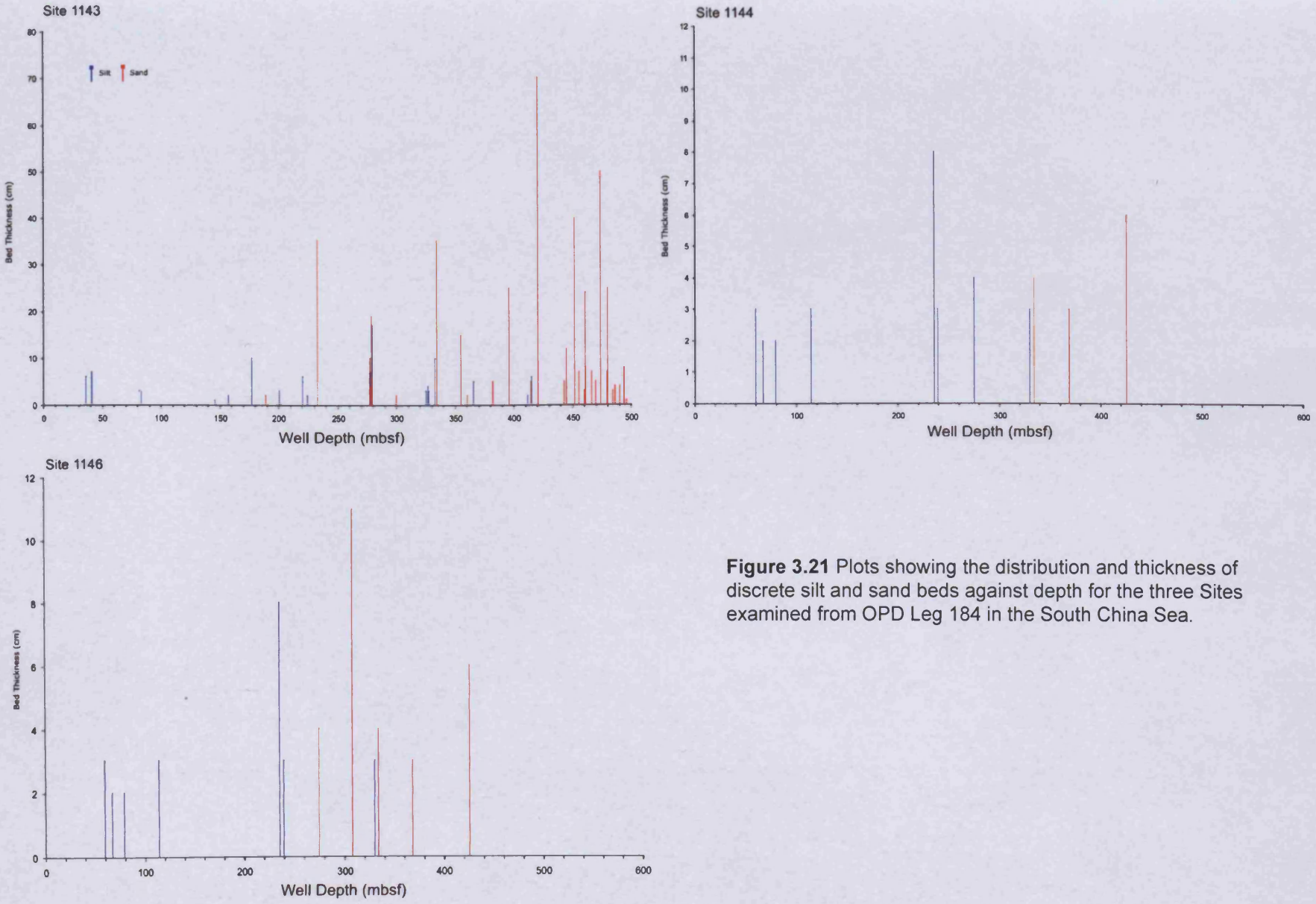

Figure 3.21 Plots showing the distribution and thickness of discrete silt and sand beds against depth for the three Sites examined from OPD Leg 184 in the South China Sea.

3.3.4 Location 4: Nankai Trough

Setting

Drill-sites from ODP Leg 190 flank a zone of active subduction at the Nankai Trough, offshore Shikoku Island (Japan) where sediments of the Shikoku Basin (Philippine Plate) are obliquely subducted beneath the Japan Arc (Eurasian Plate) at rates of ~4cm/yr (*see* Fig 5.21) (Karig & Angevine, 1986). The Shikoku Basin is a narrow, fan shaped basin which extends south-eastward from the Nankai Trough, bound to the east by the Izu-Bonin Arc, and the Kyushu-Palau Ridge to the west (Fig. 3.22). Three sites were chosen from the six drilled during Leg 190 for inclusion in the CHD. Site 1173 is located in the Shikoku Basin, southeast of the Nankai Trough, and records an undeformed sequence of Neogene hemipelagic sediments overlain by a trenchward thickening package of Quaternary turbidite deposits (*see* Fig 5.10) (Moore et al., 2001). Site 1174 lies 13km trenchward of Site 1173, in a zone of proto-thrusts related to the accretion and deformation of sediments at the subduction zone (*see* Fig. 5.21). Intervals of hemipelagic sediment included in the CHD at Sites 1173 and 1174 correspond to the Shikoku Basin facies, consisting of an Upper Shikoku Basin facies (USBF) characterised by abundant volcanic ash beds, and a Lower Shikoku Basin facies (LSBF) containing rare siliceous clay layers (Moore et al., 2001). Site 1177 was drilled 116km southwest of Site 1173, also in undeformed sediments of the Shikoku Basin. Hemipelagic sediments were recovered between depths of 300 and 450m, while lower portions of the sequence are seen to be dominated by coarser material and were therefore not included in the CHD (Fig. 3.23a) (Moore et al., 2001).

The seismic profile in Fig. 5.21 images both Sites 1173 and 1174 revealing distinct seismic facies above and below a level interpreted by Moore et al. (2001) as a décollement layer. The USBF at Site 1173 is represented by a stacked sequence of low-amplitude reflections displaying a degree of lateral continuity, below which, sediments of the LSBF are characterised by an interval of higher amplitude reflectors. The interval directly below the décollement layer shows few coherent reflections. Seismic facies recorded at Site 1174 reveals a similar configuration to those at Site 1173, although overall reflection amplitudes are markedly lower, expected to be a function of the greater depth of sediments. Fine-grained sediments recovered from Site 1177 reveal two distinct seismic facies; an overlying transparent interval with very few coherent reflections, and a lower interval comprising a stacked sequence of low-amplitude, laterally continuous reflectors which can be traced below the protothrust zone (Fig. 3.23b) (Moore et al., 2001).

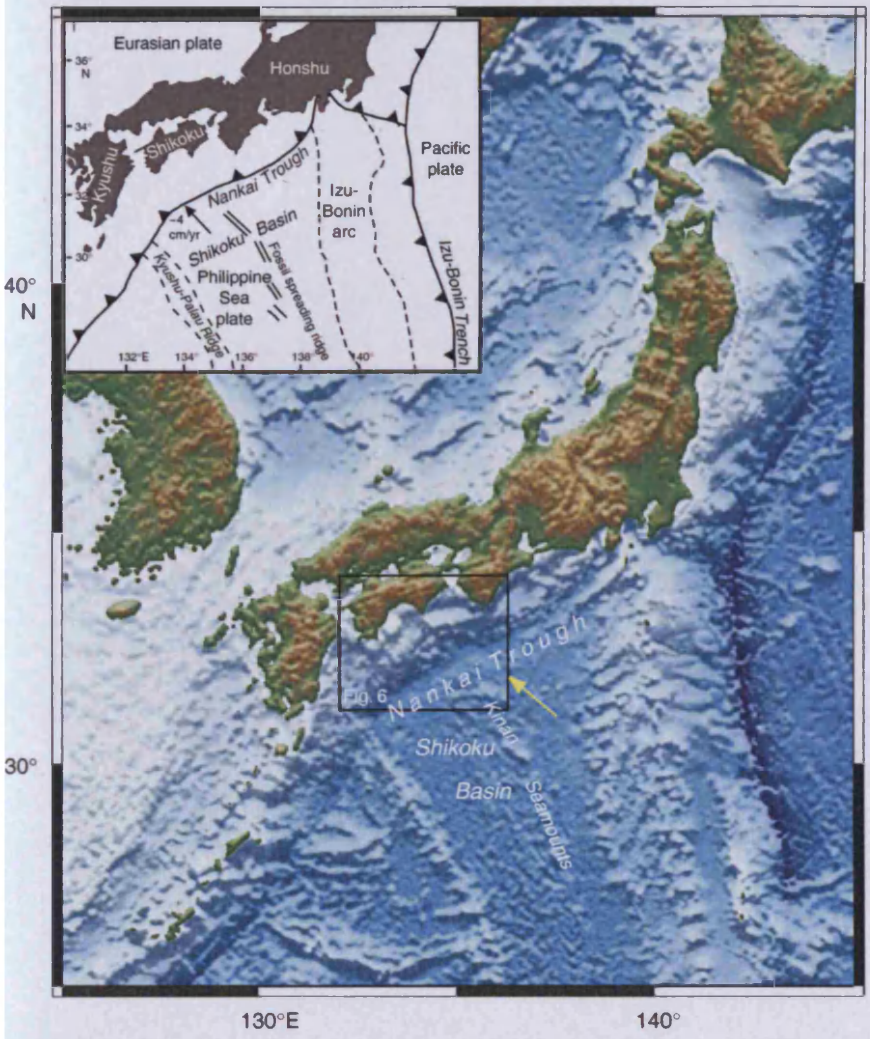

Figure 3.22 Map showing the tectonic setting of the Nankai Trough and the Shikoku Basin. Image from Moore et al (2001).

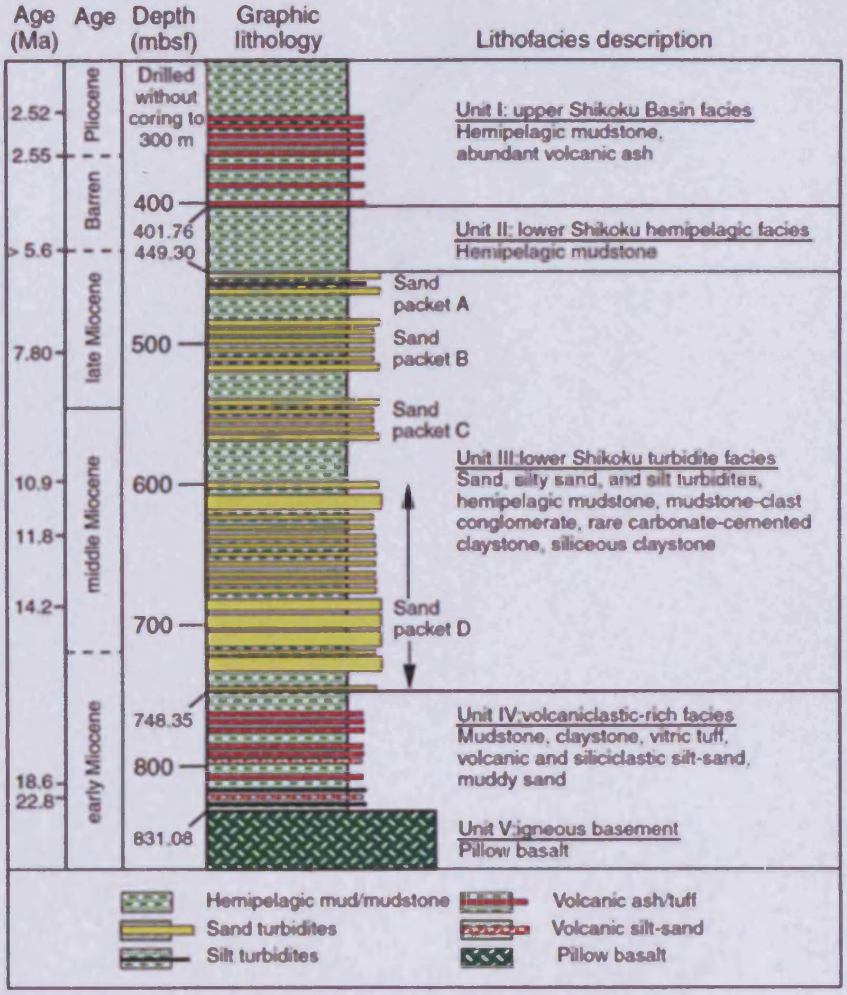

Figure 3.23a Stratigraphy recorded from ODP Site 1177 at the Nankai Trough. Only data from the hemipelagic interval (300-450m depth) was used in this study. Image from Moore et al (2001).

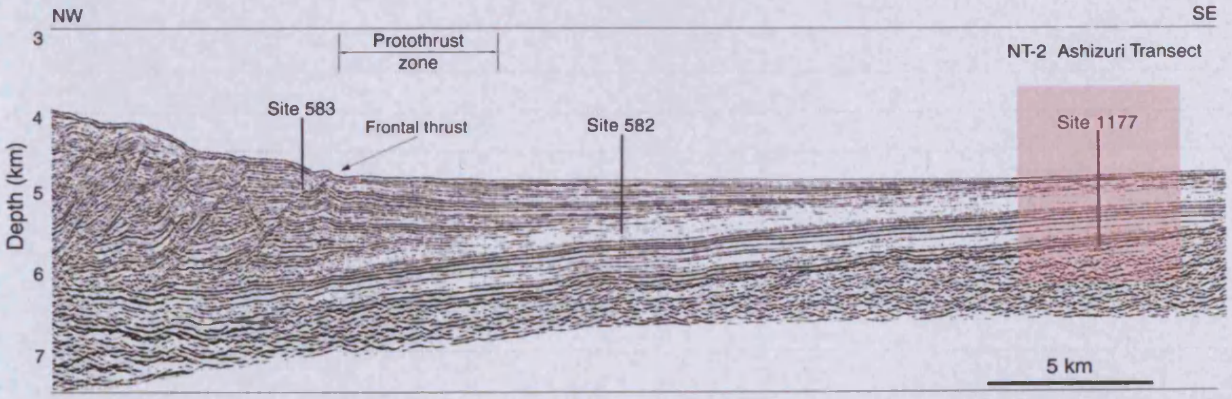

Figure 3.23b Seismic profile showing the location of ODP Site 1177 in the Shikoku Basin. Image from Moore et al (2001).

Thin-beds

Sites 1173 and 1174 both record thick sequences of hemipelagic sediments of the Shikoku Basin facies, overlain by a sequence of coarser, turbidite deposits. Only the clay-dominated sediments of the Shikoku Basin facies were examined here. Shikoku Basin facies are predominately silty clays, with occasional intervals of clayey-silt. Sediments recovered from Sites 1173 and 1174 reveal a complex distribution of coarser horizons, which are dominated by thin layers of silt and sand sized volcanic ash and glass particles (*see* Chapter 5). A total of 93 discrete layers were recorded from Site 1173, recording a total thickness of 4.9m and constituting ~1% of the total sediment column (Fig. 3.24). Coarse layers are dominated by volcanic ash and are generally <10cm thick and comprise angular shards of rhyolitic glass with various amounts of quartz, plagioclase, amphibole, opaque minerals and pumice (Moore et al., 2001). The down-hole distribution of these ash layers appears to be controlled by diagenesis, with unaltered volcanic ash layers being largely absent in the LSBF, below a depth of 343m. A similar distribution of ash layers is recorded at Site 1174 (Fig. 3.24), where a transition from unaltered to altered ash occurs at approximately 660m depth, marking the boundary between the upper and lower Shikoku Basin facies. Volcanic ash layers which have undergone alteration become increasingly dominated by clays, opal C/T, siliceous clay minerals and zeolites (Wilson et al., 2003). The frequency of these clay layers within the LSBF, thought to correspond to altered volcanic ash layers, is relatively low compared to the number of unaltered ash layers in the USBF. This disparity would suggest that either ash falls during deposition of the LSBF were less frequent, introducing less material to undergo alteration, or that pervasively altered glass has gone undetected during core inspections. Site 1177, located 120km southeast of Site 1173, records 150m of Upper Shikoku Basin facies. Similar to Sites 1173 and 1174, coarse horizons at Site 1177 are dominated by volcanic ash layers of silt to coarse-sand grade, and occasionally gravel grade. Diagenesis controls the boundary between the USBF and LSBF, which is again denoted by the deepest recorded unaltered ash layer, which in the case of Site 1177 lies at 401mbsf (Fig. 3.24).

Controls on sedimentation

The Shikoku Basin facies is dominated by silty-clay hemipelagic sediments, similar to those recovered from Site 1144 in the South China Sea. The majority of coarse grained thin-beds recorded Sites 1173 and 1174 represent thin volcanic ash horizons, while deposits from turbidity currents and other down-slope sediment transport processes are rare. The alteration of ash layers by shallow diagenetic processes leads to the development of siliceous clay layers, defining the boundary between the USBF and LSBF at Nankai Trough sites. Thus the

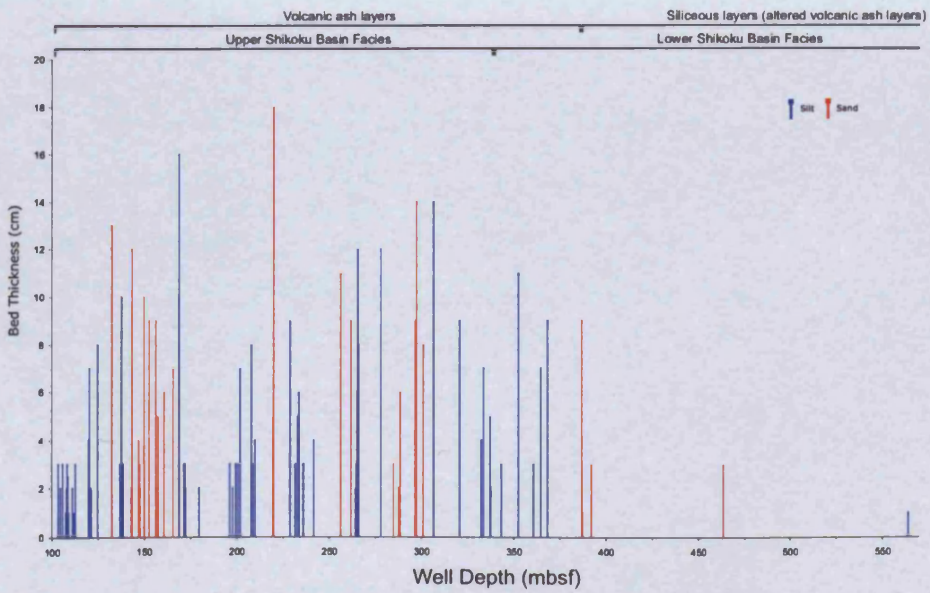

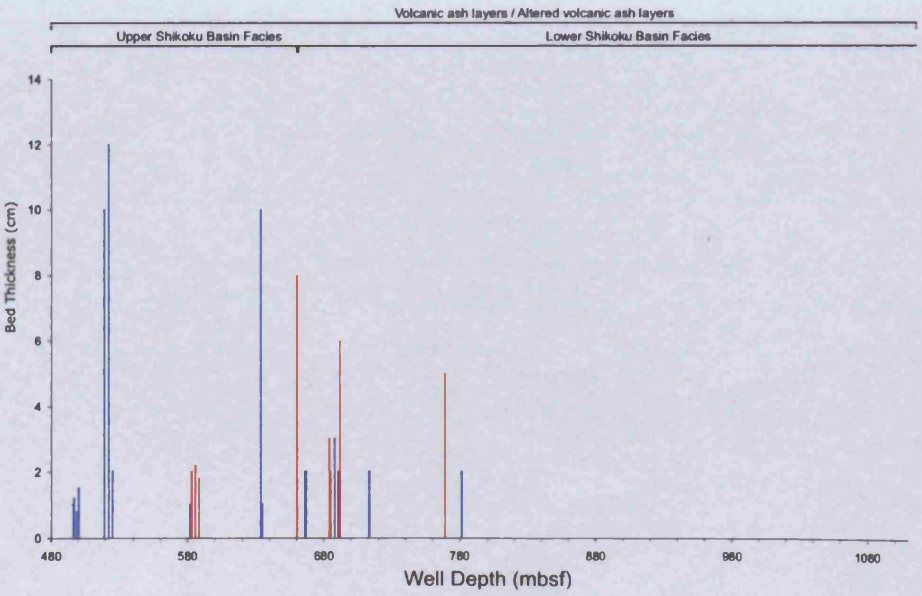

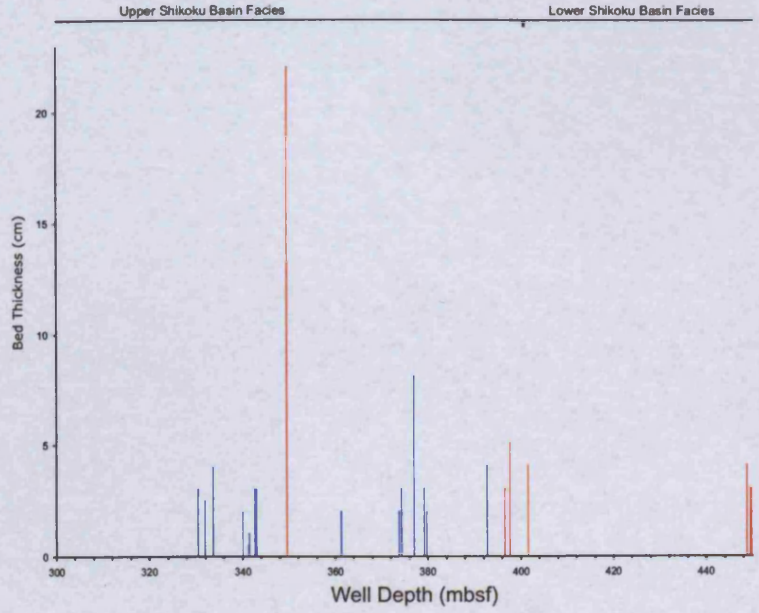

Figure 3.24 Plots showing the distribution and thickness of discrete silt and sand beds against depth for the three Sites examined from OPD Leg 190 in the Nankai Trough region.

physical properties of thermodynamically unstable ash horizons are largely dependent on temperature sensitive reactions, which are in turn largely a function of burial depth. Further, detailed discussion of the reaction kinetics and alteration products of shallow ash diagenesis at the Nankai Trough can be found in Chapter 5. In volcanically active regions, such as the Nankai area, the distribution of ash falls constitutes an important consideration with regards to predictions as to the likely distribution of porosity and permeability in hemipelagic host sequences.

3.3.5 Location 5: Cascadia Margin

ODP Leg 204 targeted the Southern Hydrate Ridge (SHR), a series of small anticlines, located in the accretionary complex of the Cascadia subduction zone, offshore Oregon, USA (Fig. 3.25a-c) (Gràcia et al., 2006). Leg 204 sites were aimed at investigating the nature of shallow gas hydrate deposits, identified from seismic data by a high-amplitude bottom-simulating reflector (BSR), indicative of the base of the gas hydrate stability field (Fig. 3.26) (Tréhu et al., 2003). Unlike passive margin hemipelagic sequences examined from western Africa and the South China Sea, Plio-Pleistocene sediment of the Cascadia Margin have been deposited in varying, and often structurally-complex depocentres, recording the continual deformation of the margin. Seismic profiles shot perpendicular to the roughly N-S striking SHR reveal a relatively thin succession of Plio-Pleistocene sediments draped over faulted-blocks associated with the accretionary complex (Fig. 3.26). Early sediments onlap the footwalls of major extensional faults on the western flank of the SHR creating wedge-shaped growth packages (Fig. 3.26). Recent extensional collapse and subsidence of the eastern flank of the SHR (200 k.y.) has shifted the main focus of deposition towards intraslope basins east of the ridge (Tréhu et al., 2003). ODP Sites 1144, 1145, 1151, and 1152 transect the SHR, and provide an opportunity to examine the distribution of coarse material in an actively deforming hemipelagic succession.

Site 1251 represents the most landward of the four sites examined, drilled in 1210m of water within a linear depression to the east of SHR, and records 445m of clay-dominated sediment with occasional intervals of silty-clay and coarse thin-beds (Fig. 3.28) (Tréhu et al., 2003). Seismic profiles reveal that drilling is likely to have penetrated the accretionary complex beneath a locally thick, wedge-shaped package which is thought to represent early sedimentation onlapping the eastern flank of the SHR. This package is itself unconformably overlain by two eastward thickening basin-fill units which represent sedimentation associated with the later subsidence on the eastern flank of the SHR (Fig. 3.27). Deformed sediments recovered between 20-35 mbsf indicate that Site 1251 also penetrates the tapered updip

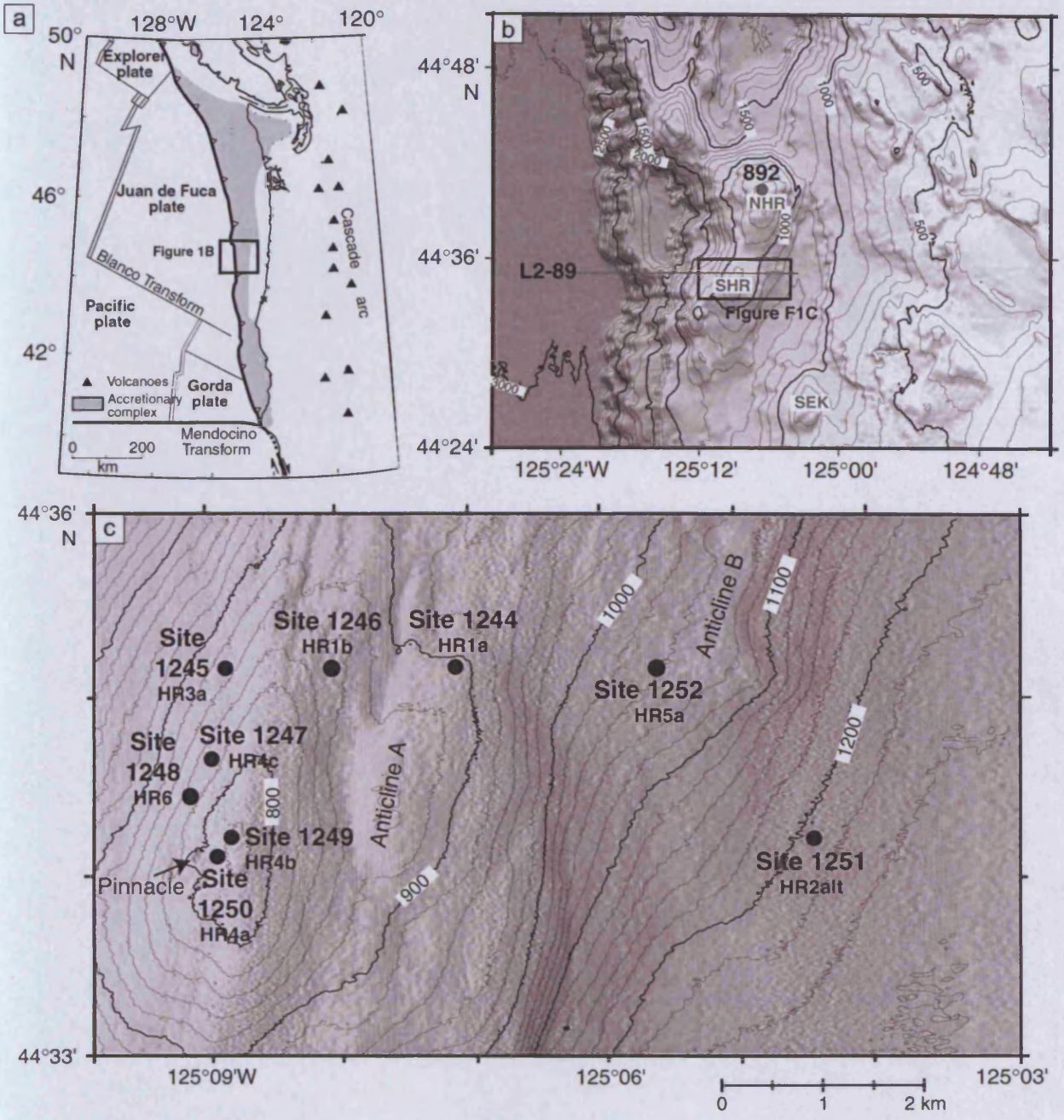

Figure 3.25 (a) Map showing the tectonic setting of ODP Leg 204 drill sites. (b) Bathymetric map showing the slope position of Hydrate Ridge and the complex relief of the Cascadia continental slope. (c) Detailed bathymetric map showing the locations of Leg 204 Sites. Images modified from Tréhu et al (2003).

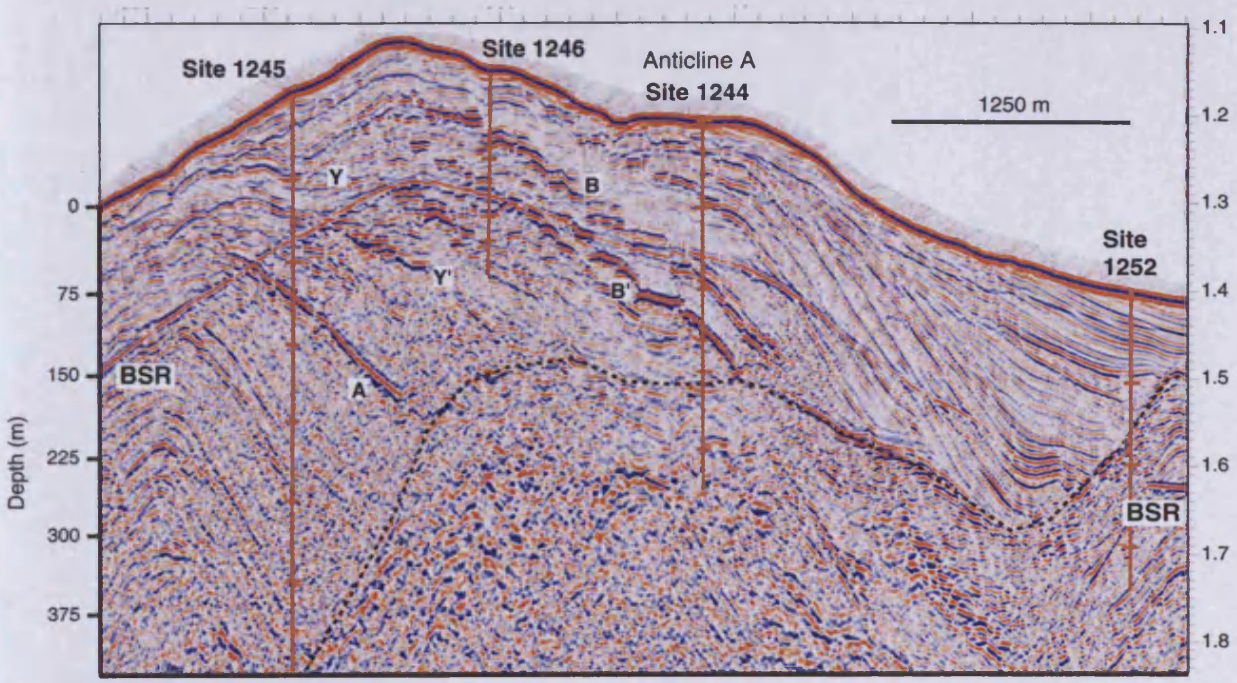

Figure 3.26 East-west 3D seismic slice showing the structural and stratigraphic setting of Leg 204 Sites 1244, 1245, 1246, and 1252. Bottom simulating reflector (BSR) is labelled (Modified from Tréhu et al (2003).

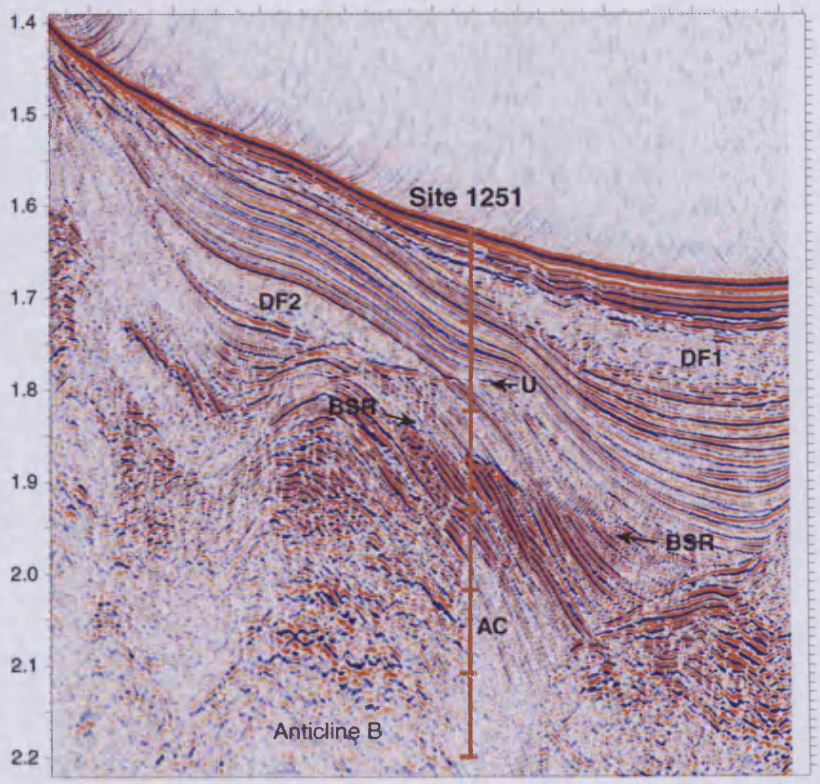

Figure 3.27 East-west 3D seismic slice showing the structural and stratigraphic setting of Sites 1251. Intervals interpreted as debris flows Tréhu et al (2003) are indicated (DF). Image modified from Tréhu et al (2003).

extremity of a debris flow which is imaged down-dip as a wedge shaped, internally chaotic, feature on seismic data (Fig. 3.27) (Tréhu et al., 2003).

Site 1252 is located 2.5km northwest of Site 1251, on the western flank a small anticline. Sediments record a 260m thick sequence dominated by silty-clay facies containing few discrete beds, with the exception of an interval between 90-115 mbsf which shows a high concentration of thin silt and sand turbidites (Fig. 3.28). Above sediments of the accretionary complex at Site 1152, seismic data reveals a stacked series of divergent reflections which onlap the western flank of the anticline, unconformably overlain by thin package of sub-parallel reflections thought to image the most recent basin-fill deposits. Both of these units represent down-slope sediment deposition resulting from the uplift and erosion of the main SHR anticline to the west.

Site 1244 was drilled 2km east of Site 1252 on the eastern flank of the main SHR anticline, while Site 1245 was drilled in a similar water depth on the western flank of the same broad anticline (Fig. 3.26). Sediments of the accretionary complex form a prominent 'dome' beneath the main SHR anticline, over which lie several thick units of eastward dipping sediments thought to have been deposited prior to the main period of SHR uplift (Chevallier et al., 2006). Sediments at both sites are dominated by Pleistocene aged silty-clay and clayey sediments (Tréhu et al., 2003).

Thin-beds

The distribution of thin-beds at Leg 204 sites reflects the complex structural history, and shifting depocentres on the Cascadia Margin slope over the last 1.5 Ma (Chevallier et al., 2006). Coarse thin-beds recorded from Leg 204 sites are dominated by the coarse lower portions of turbidites and are generally of silt or sand grade, with a mean thickness of <10cm Fig. 3.28). Discrete coarse layers constitute <1% of the total sediment volume at all of the sites investigated, however background facies are dominated by silty-clay sediments and are seen to contain up to 40% silt grade material. Sites located on the flanks of the main SHR anticline (Sites 1144 and 1145) record the highest frequency of thin turbidites, with over 200 recorded. These two sites penetrate older sedimentary units associated with deposition to the west of the SHR prior to the period of major ridge uplift (Chevallier et al., 2006). A number of prominent, high-amplitude reflections drilled at these sites correspond to intervals of turbidite and volcanic ash deposits shown to be acting as conduits for methane migrating vertically to the seafloor (labelled 'A', 'Y', and 'B' in Fig. 3.26). In this instance, recovered sediments suggest that both lithological heterogeneities and deformational features have

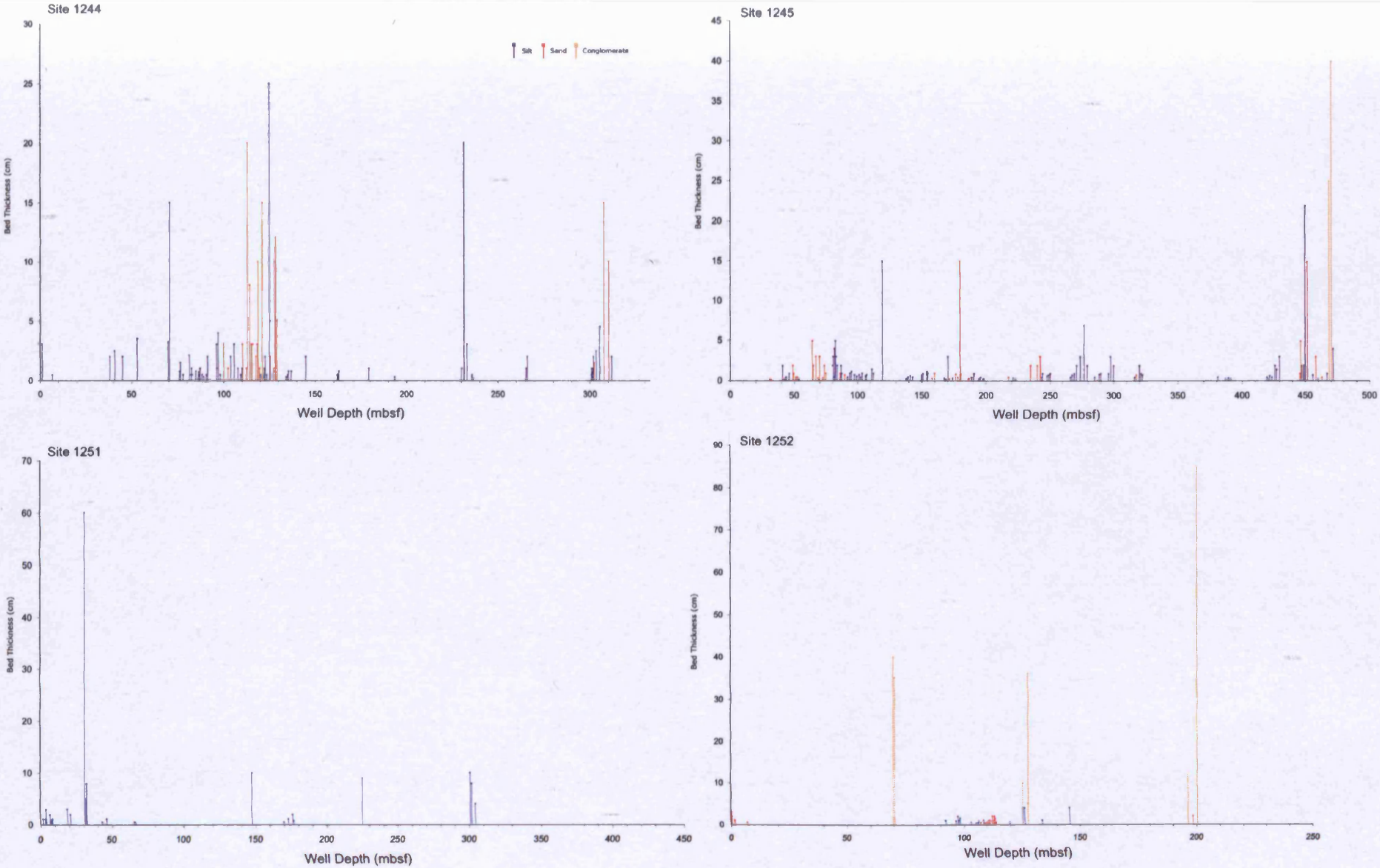

Figure 3.28 Plots showing the distribution and thickness of discrete coarse grained beds against depth for the four Sites examined from OPD Leg 204 on the Cascadia Margin.

created a pathway of connected permeability for gas to migrate through fine-grained sediments, ultimately to the seabed (Tréhu et al., 2004). The most recent sedimentation at Sites 1144 and 1145 is characterised by clay-dominated drape across much of the main SHR anticline containing very few coarse horizons.

Sites 1151 and 1152 record sedimentation in basins created by the extensional faulting and subsidence of the SHR's eastern margin (Chevallier et al., 2006). Discrete thin-beds are rare at both locations, with a total of ~70 recorded (Fig. 3.28). Several coarse turbidite beds are associated with a thin mass-transport deposits found between 20-45 mbsf at Site 1251, below this however, discrete beds are infrequent and sediments are dominated by hemipelagic silty-clays seen on seismic data to drape the eastern flank of the main SHR anticline (Figs. 3.26 and 3.27). Site 1152 sediments show similar lithological characteristics; two thick (~40cm) turbidites are associated with a separate mass-transport deposit at 70 mbsf, below which a 20m thick interval is seen to onlap a structural high in the underlying accretionary complex recording a high concentration of thin turbidite deposits. The uppermost 70m of sediments at Site 1252 record hemipelagic seismic facies and comprise silty-clay material with very occasional thin-beds.

Controls on sedimentation

Investigation of a structurally complex hemipelagic sequence provides clues to the controls on thin-bed deposition within a setting with changing input sources and transport pathways. Structurally deformed hemipelagic units such as those recorded from Leg 204 contrasts with the largely undeformed hemipelagic sequences seen at passive margins (e.g. Lower Congo Basin, Leg 175). Sedimentary sequences at Leg 204 sites reflect the tectonic uplift and denudation of the SHR and the surrounding region. In complex regions such as this, careful structural reconstruction is needed to assess the likely bathymetry, slope architecture and sediment distribution pathways active during periods of hemipelagic sedimentation. For example, late Pliocene sediments found towards the base of Sites 1144 and 1145 were originally deposited in basins west of the modern SHR, prior to the major period of uplift and deformation, and record sedimentation from the axially sourced Astoria Fan (Chevallier et al., 2006). These sediments contain a concentration of thin coarse beds reflecting their submarine fan source and have since been uplifted and incorporated into the main SHR anticline (Chevallier et al., 2006). The tectonically active nature of the margin has meant that only those sediments imaged on seismic data as the most recent hemipelagic drape deposits reflect the current deposition regime in the area. This thin sedimentary drape unit reveals the absence of coarse material at the main SHR structural high (Sites 1144 and 1145), and the

existence of thin turbidite deposits at the intraslope basin Site 1151 to the east, thought to indicate the role of bathymetry in directing and ponding present day sediments at the SHR.

3.3.6 Location 6: Gulf of Mexico

The final wells chosen for inclusion in the CHD were drilled during the recent Integrated Ocean Drilling Program (IODP) Leg 308 in the Gulf of Mexico (GOM). Two sites from the Brazos-Trinity region in the western GOM are investigated along with two further sites from the Mars-Ursa region 530km to the east (Fig. 3.29) (Flemings et al., 2006).

The Brazos-Trinity region comprises a series of intraslope basins which lie roughly 250km south of Galveston, Texas. A network of slope channels link these basins with upper-slope and shelf sediment sources. Site 1319 records a 157m thick Pleistocene hemipelagic sequence from a location on the southern slope of the bowl-shaped Brazos-Trinity basin IV in a water depth of 1440m (Figs. 3.30 and 3.31) (Flemings et al., 2006). Background sediments are dominated by silty-clay and nannofossil-rich facies, imaged in Figures 3.30 and 3.31 as relatively low-amplitude, parallel reflections. Site 1320 is situated 4km to the northwest of Site 1319, at the centre of the Brazos-Trinity basin IV, in 1470m of water (Flemings et al., 2006). The top 175m of sediment at Site 1320 contains abundant, thick sand-turbidites which represent late Pleistocene basin-fill facies, and were not included in the CHD. An interval of clay-dominated hemipelagic sediment between 175-295 mbsf depth, which correlates with sediments recovered from Site 1319, was examined (Fig. 3.30). The seismic image in Figure 3.32 from Site 1320 reveals several thick packages of relatively weak, semi-continuous reflections beneath much higher amplitude packages related to the younger, sand-prone basin-fill.

Sites 1322 and 1324 lie roughly 530km to the west of the Brazos-Trinity region within the Mars-Ursa region (Fig. 3.33). The two sites are located on a gentle (<1% gradient) eastward dipping slope at the seaward termination of the Mars Ridge, to the east of the Mississippi Canyon (Fig. 3.34) (Flemings et al., 2006). Sites 1322 and 1324 record late Pleistocene sequences of hemipelagic clays imaged on seismic data as thick packages of parallel, laterally continuous reflections, separated by several intervals of wavy, semi-continuous reflections interpreted as redeposited hemipelagic sediments (Flemings et al., 2006). Seismic facies in Figures 3.34 and 3.35 suggest that sediments recovered from Sites 1322 and 1324 record hemipelagic drape units overlying thick wedges of sediment which have been interpreted as distal levee deposits; although distinguishing these two units based on either lithological or seismic data alone is difficult.

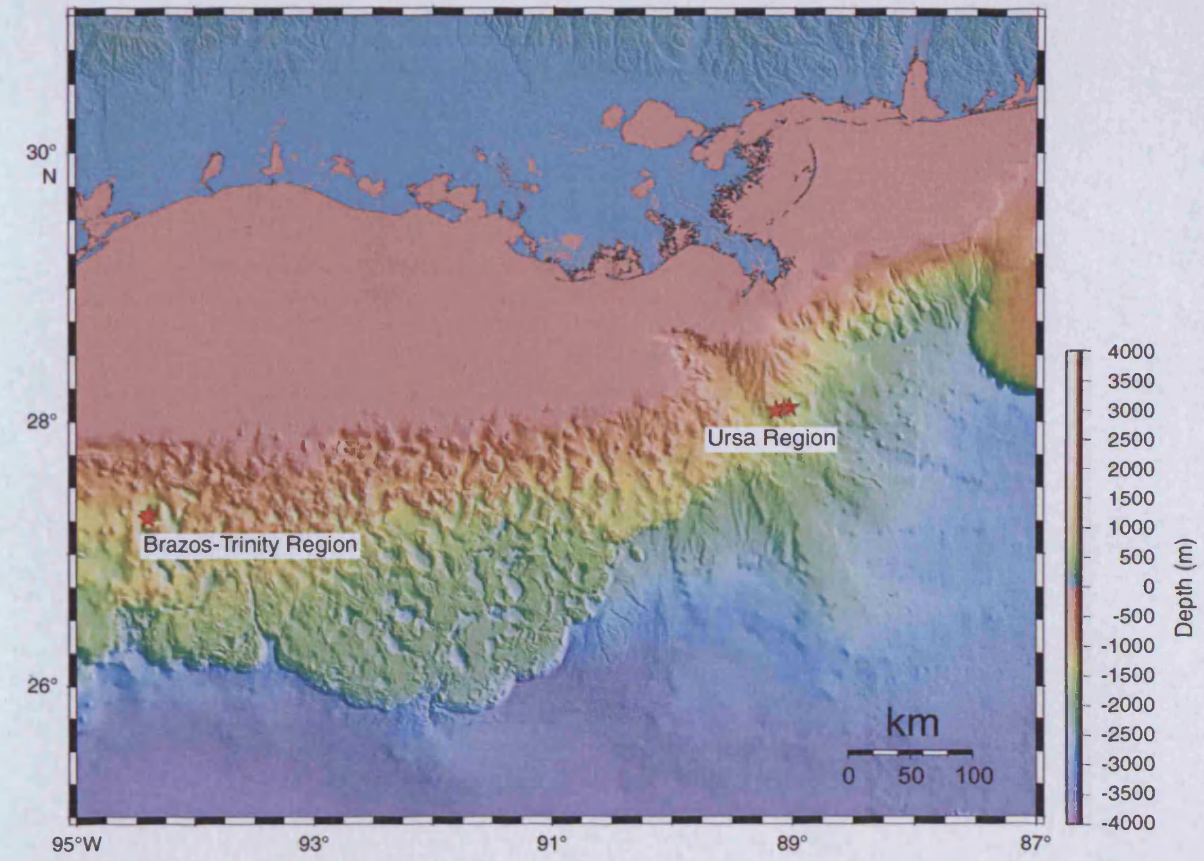

Figure 3.29 Map of the northern Gulf of Mexico showing the position of the Brazos-Trinity Region and the Mars-Ursa Region.

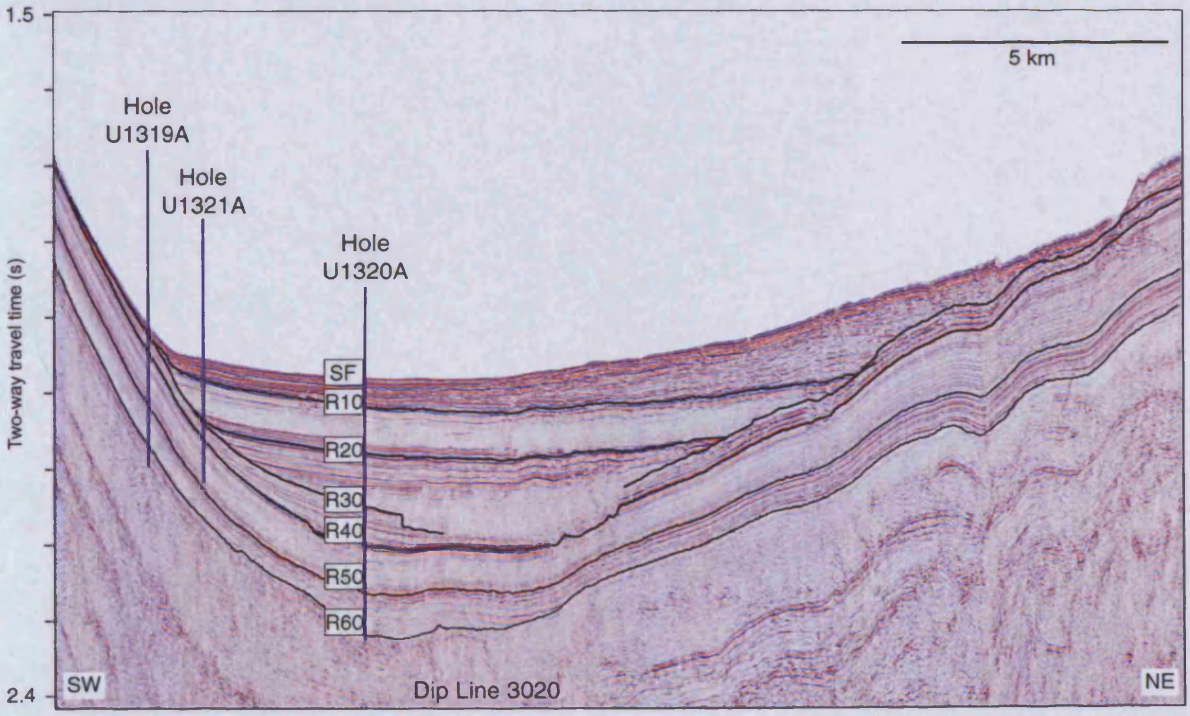

Figure 3.30 SW-NE orientated 3D seismic image showing the locations of Sites 1319 and 1320. Sand-prone basin-fill facies (Seafloor – R40) are imaged onlapping a package of hemipelagic drape (R40 – R60).

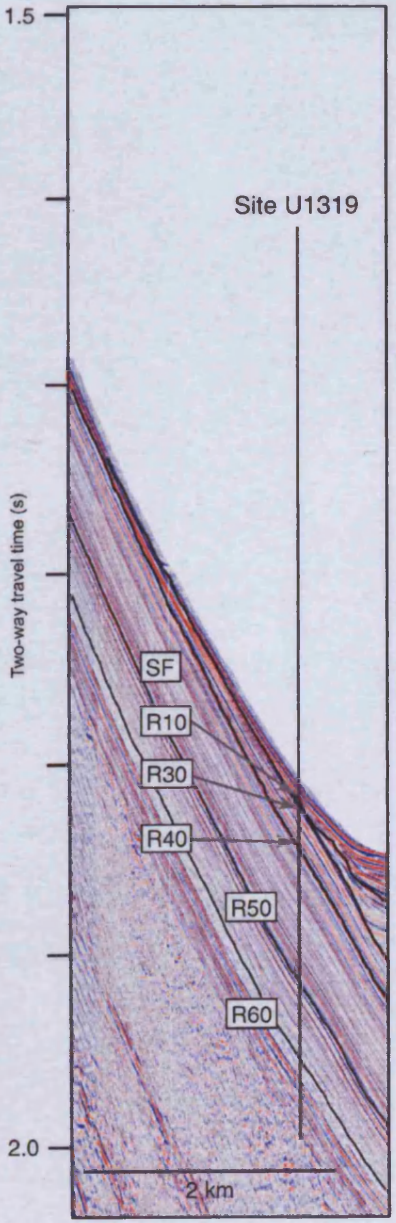

Figure 3.31 Detailed 3D seismic image showing the structural and stratigraphic setting of Site 1319. Image taken from Flemings et al (2006).

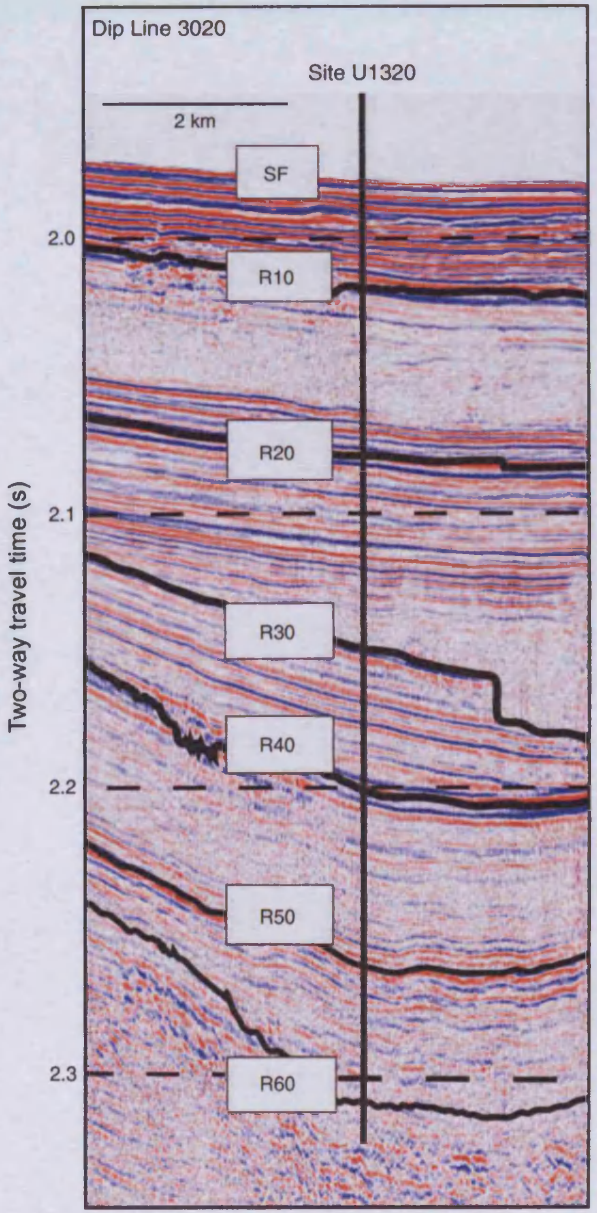

Figure 3.32 Detailed seismic image showing the stratigraphy at Site 1320. Hemipelagic sediments, included in this study, were drilled between R40 and R60. Image taken from Flemings et al (2006).

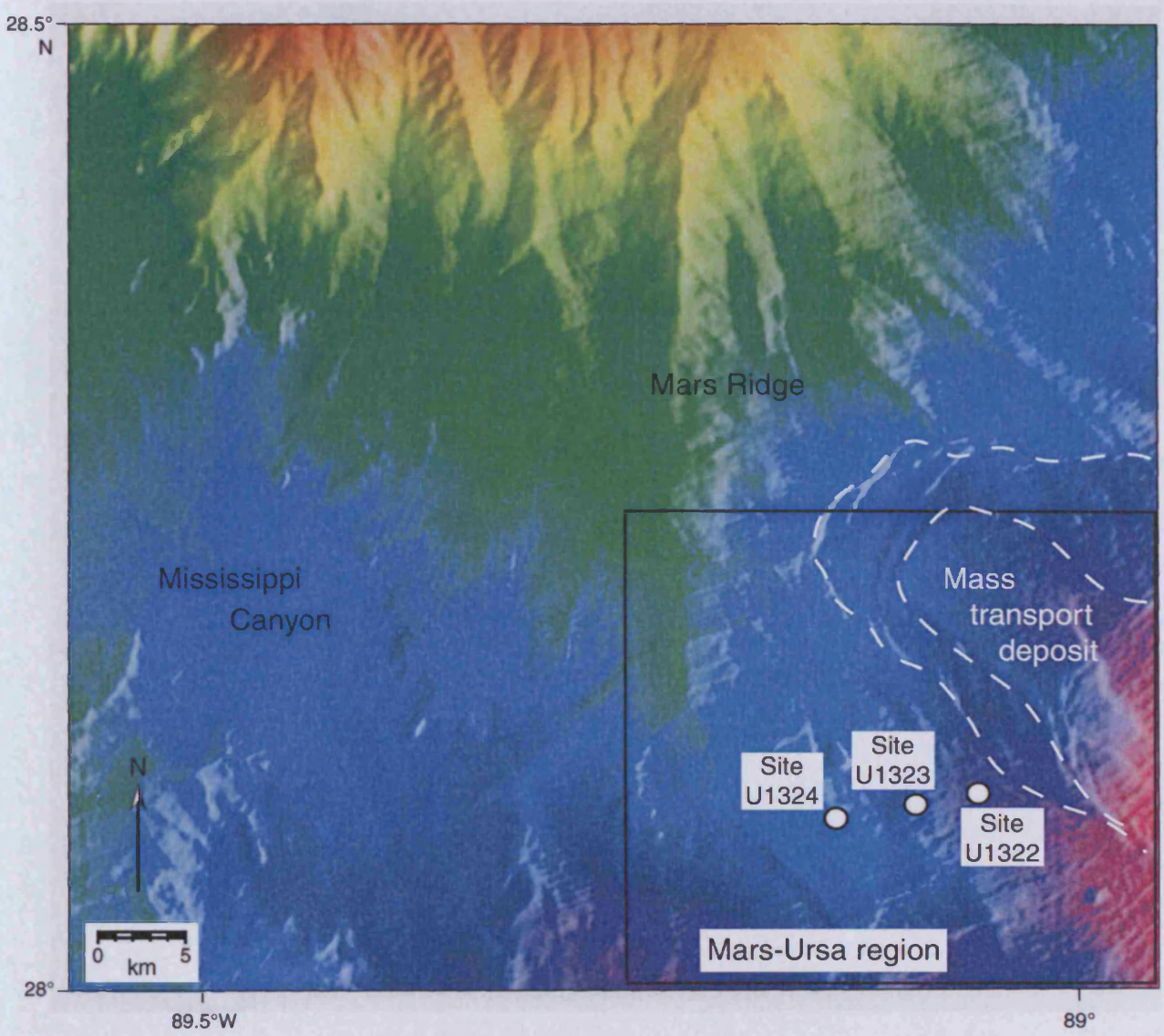

Figure 3.33 Map showing the location of Sites 1322, 1323, and 1324 in the Mars-Ursa region, Gulf of Mexico. Image taken from Flemings et al (2006).

Thin-beds

The majority of the ~70 discrete coarse beds recorded from Site 1319 are located within the uppermost 30m of sediment, a unit which represents the southern distal edge of the basin-fill sequence which overlies hemipelagic sediments in the centre of the Brazos-Trinity basin IV. Coarse horizons are rare throughout the remaining 130m of hemipelagic sediment, and are commonly less than 1cm thick. A similar distribution of coarse layers is recorded from Site 1320 where ~20 coarse layers are thought to represent low density turbidity currents or river plume deposits (Fig. 3.36) (Flemings et al., 2006).

Thin-beds of silt and sand material are commonly encountered in sediments recovered from the Mars-Ursa region. Site 1322 records a total of 140 coarse horizons, the majority of which are believed to represent thin turbidite deposits which are generally <1cm thick (Fig. 3.37). No apparent distribution of thin-beds is found to correspond to either hemipelagic or levee deposits, however high concentrations of thin (<1cm) silt layers are found within intervals characterised by incoherent seismic reflections which have been interpreted as units of redeposited slope sediment (*see* Fig. 3.37) (Flemings et al., 2006). Sediments found at depths between 150-350 mbsf at Site 1324 are interpreted as distal-levee deposits from seismic data, constituting the eastern levee of the Southwest Pass Canyon (Flemings et al., 2006). This interval contains surprisingly few discrete thin-beds, with the exception of a 20m interval at its base which containing more than 30 thin turbidites and marks a transition from clay-dominated levee sediments above, to the more sand-prone facies beneath which have been interpreted as unconfined channel deposits (Fig. 3.37) (Flemings et al., 2006).

Controls on sedimentation

Thin-beds recorded from hemipelagic intervals within the intra-slope Brazos-Trinity basin IV likely represent infrequent down-slope transport of low-density turbidites. Later sand-rich basin-fill deposits which overlie hemipelagic sediments attest to the rapid accumulation of terrigenous material in the basin and reflect a major shift in either the volume or source of material entering the Brazos-Trinity slope. In contrast, the slope sediments recovered from the Mars-Ursa region sites show a close relationship between evolving submarine channels, slope-instabilities and hemipelagic sedimentation. All clay-dominated intervals from Sites 1322 and 1324 were examined despite having been interpreted as representing deposition from a variety of slope processes (i.e. levee deposition, mass-transport deposits, and hemipelagic sedimentation). Regarding the distribution of discrete coarse horizons, little variation is noted between hemipelagic and distal levee depositional facies, while

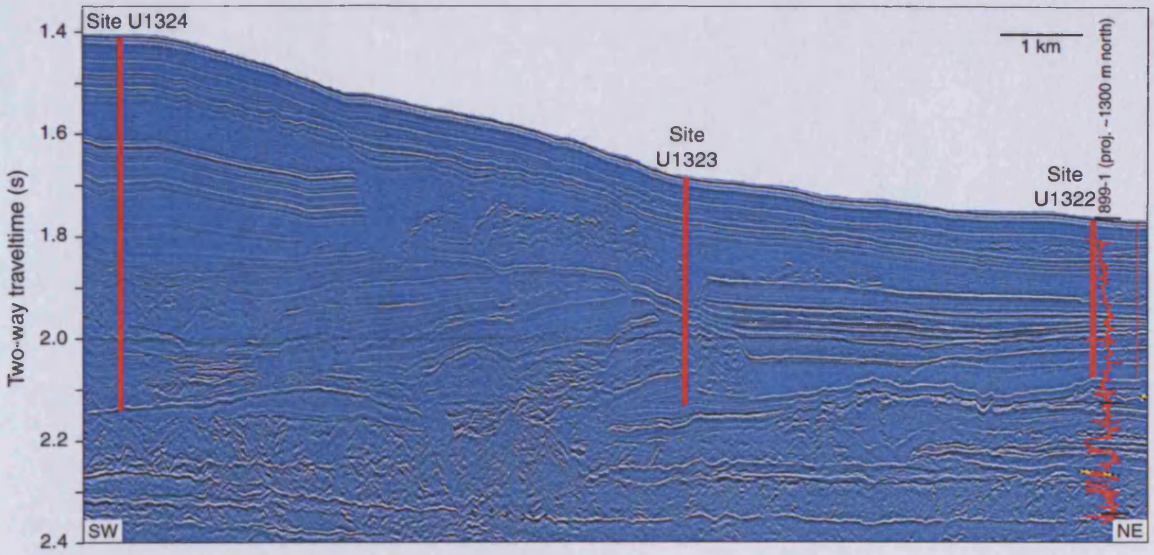

Figure 3.34 Seismic profile showing the location and stratigraphy of Mars-Ursa Sites 1322 and 1324 examined in this study. Image from Flemings et al (2006).

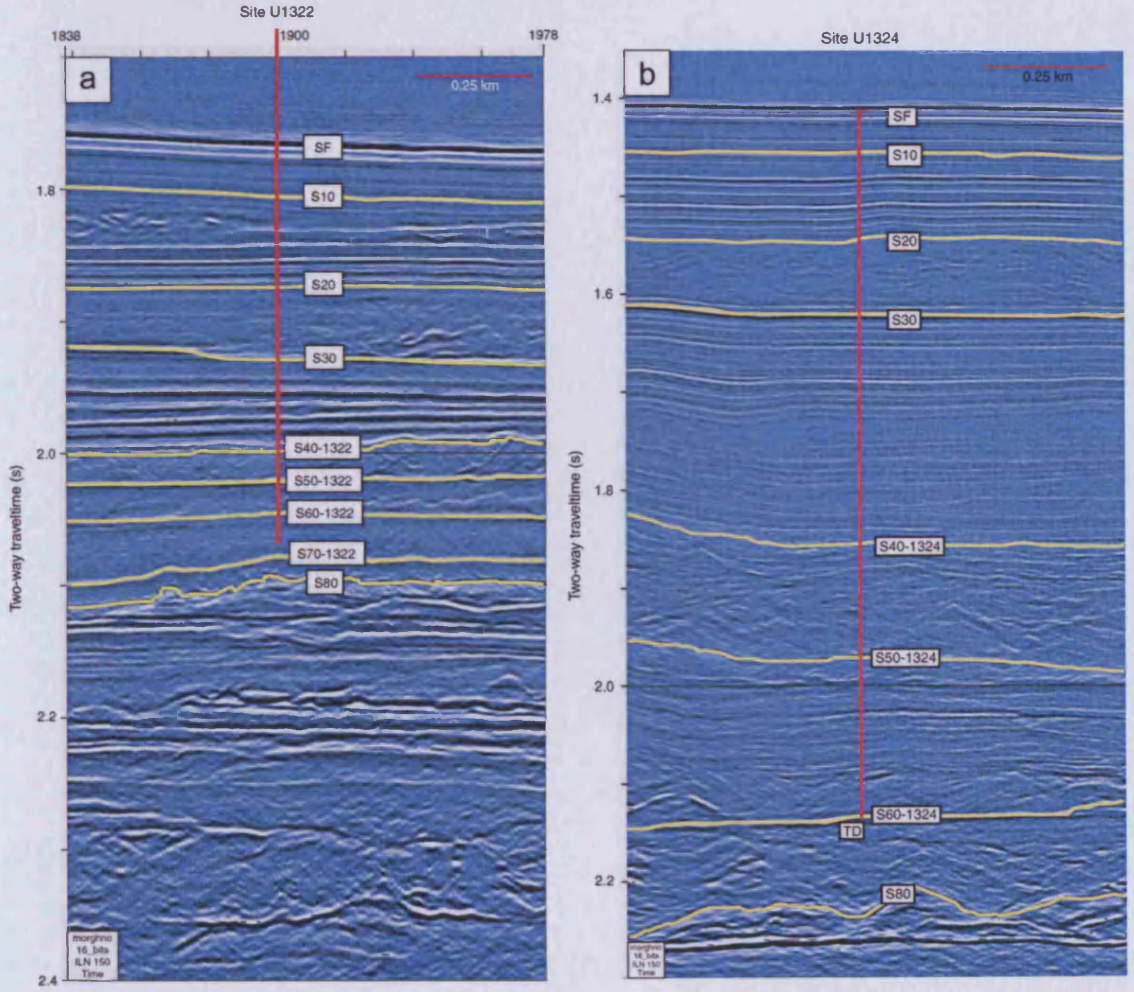

Figure 3.35 (a) Detailed seismic image from Site 1322, hemipelagic intervals are interspersed with mass-transport complexes and channel-levee deposits. (b) Detailed seismic image from Site 1324, discontinuous seismic facies seen between S20 and S30 represents an interval of mass-transport complexes. Images from Flemings et al (2006).

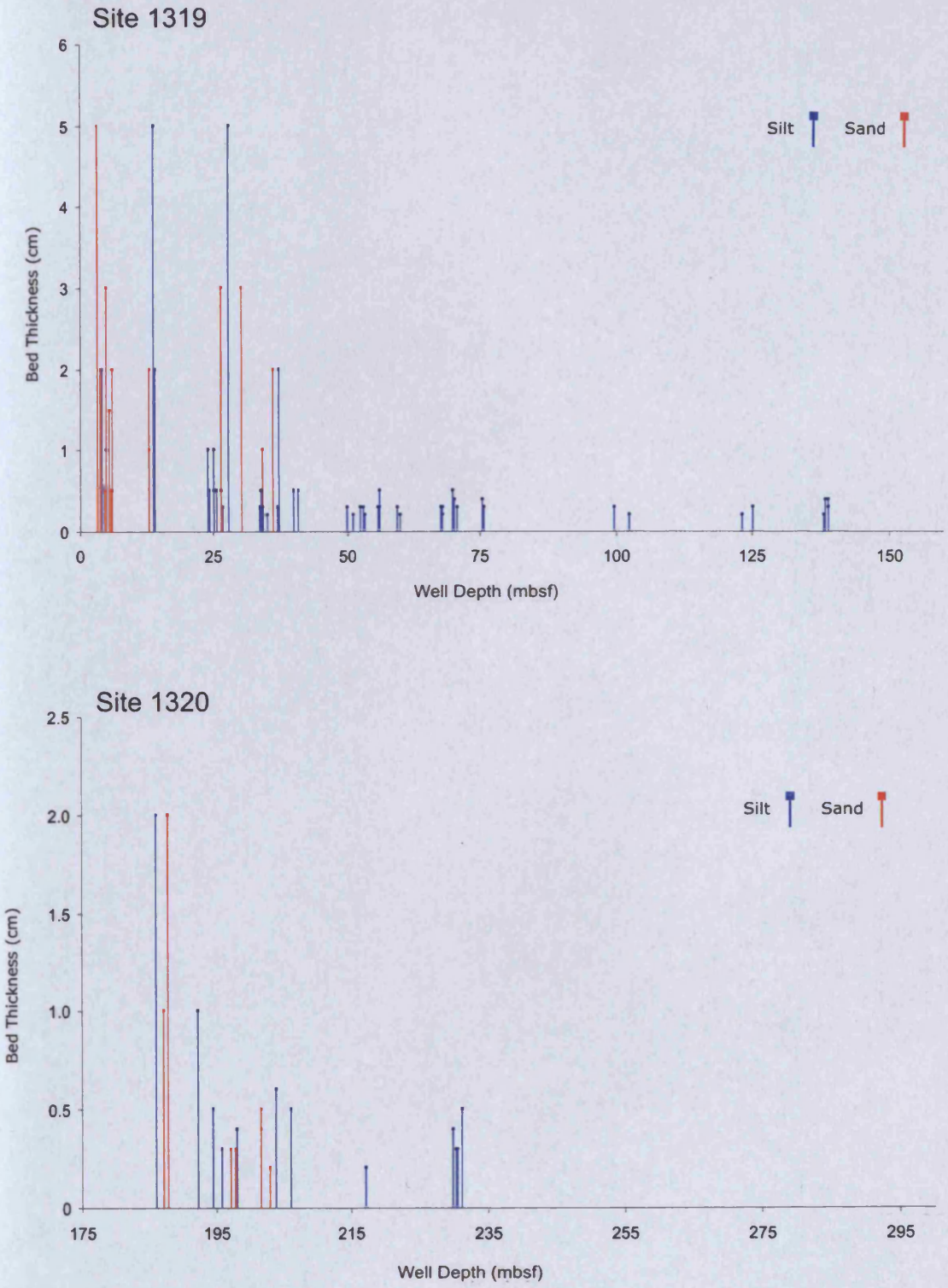

Figure 3.36 Plots showing the distribution and thickness of discrete coarse grained beds against depth for Sites 1319 and 1320 examined from IODP Leg 308 in the Gulf of Mexico.

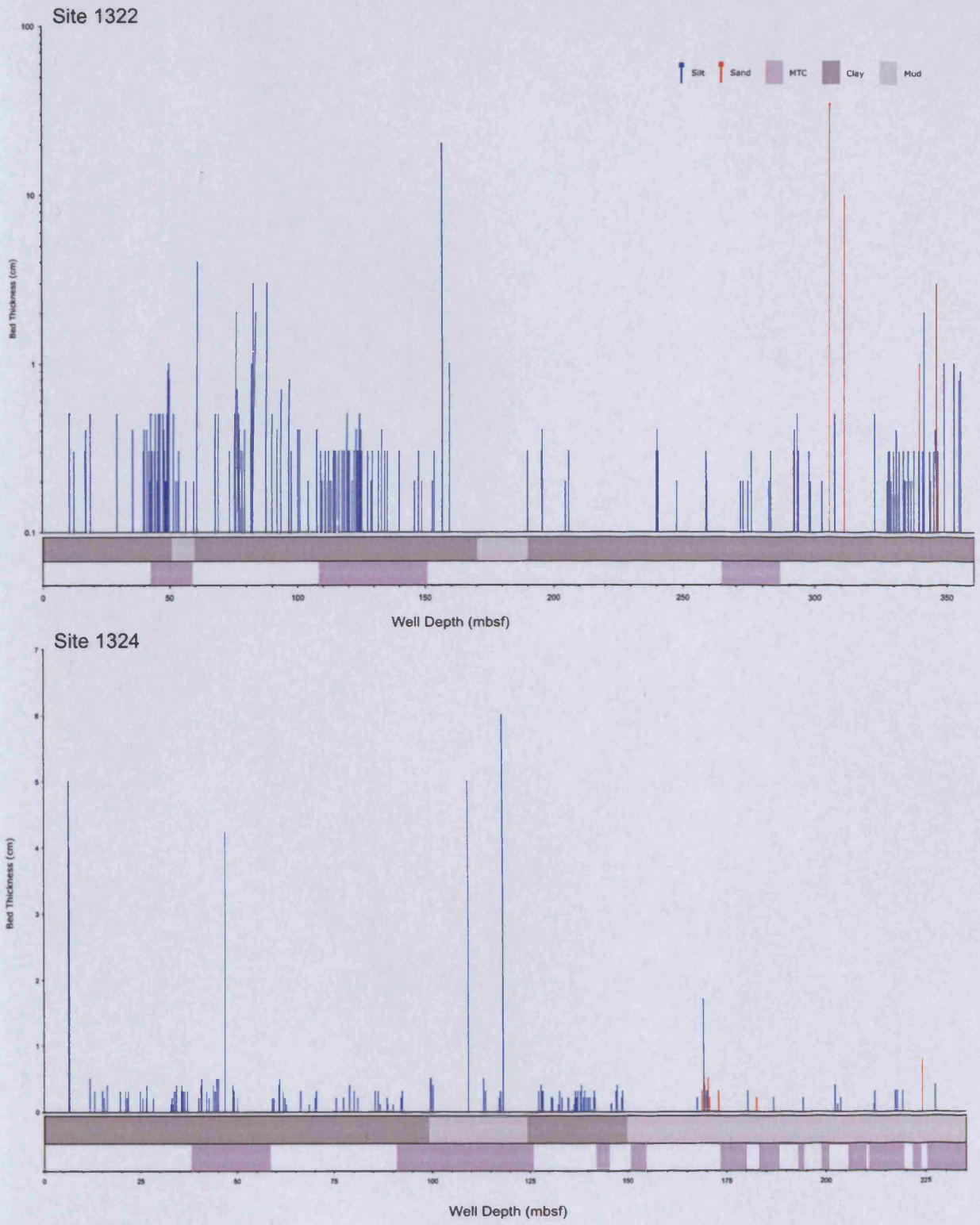

Figure 3.37 Plots showing the distribution and thickness of discrete coarse grained beds against depth for Sites 1322 and 1324 examined from IODP Leg 308 in the Gulf of Mexico. The position of mass-transport complexes within the cored sequences are indicated in purple.

redeposited units show a higher concentration of thin silt, and occasionally sand beds. Discrete coarse horizons constitute less than 1% of the total volume of sediment at all Gulf of Mexico sites examined.

3.4 Summary of ODP hemipelagic sites

Thin-beds have been identified from hemipelagic sequences on the basis that they represent a grain-size contrast with surrounding background sediments. With the exception of three sites examined from the Congo Basin, all hemipelagic sequences investigated revealed the existence of thin-beds of relatively coarse material, comprising predominately of silt- and sand-sized clastic grains. Plots in Figure 3.38 summarise the thickness and spacing of coarser layers at each of the settings examined here. Coarser bed thicknesses are seen to range from laminations of just a few millimetres to turbidites over a metre thick, while the vertical distance between coarser horizons is seen to be typically less than 10m, but as much as 50m. Thin-bed spacing varies enormously between ODP sites, ranging from closely spaced, high-frequency distal turbidite deposits such as those recorded at Site 1324, to isolated thin-beds separated by tens of metres of background sediment, as seen at Site 1144. Core measurements from all six margin locations examined have been amalgamated in Figure 3.39 producing a more general characterisation of the likely thickness and spacing of coarse grained beds in hemipelagic sequences. Figure 3.39a and 3.39b illustrate that from a range of basin settings, with varying water depths and sedimentation regimes, the mean thickness of the ~900 thin-beds recorded, is 2.7cm, with an average spacing of 3m. Figure 3.39c shows a plot of coarse bed thickness against the vertical, up-core distance to the next coarse layer. The data scatter recorded would suggest that no clear relationship exists between these variables, and that bed spacing, or the hiatus between periods of coarse sediment deposition, is not a factor which determines bed thickness.

Plots examining the relationship between thin-bed distribution and the cumulative volume of coarser material (net-to-gross or N/G) are shown in Figure 3.40. Net-to-gross is plotted against total thin-bed number in Fig. 3.40a. This plot reveals that while the total volume of coarser material remains less than 1% for Sites from the Gulf of Mexico, Cascadia Margin, Nankai Trough and South China Sea, the number of discrete beds recorded varies by as much as an order of magnitude. Net-to-gross is plotted against mean bed thickness in Figure 3.40b. This plot appears to show a relationship between increasing mean thickness of beds, and an increase in the overall net-to-gross at several locations; however this correlation does not extend to all sites examined.

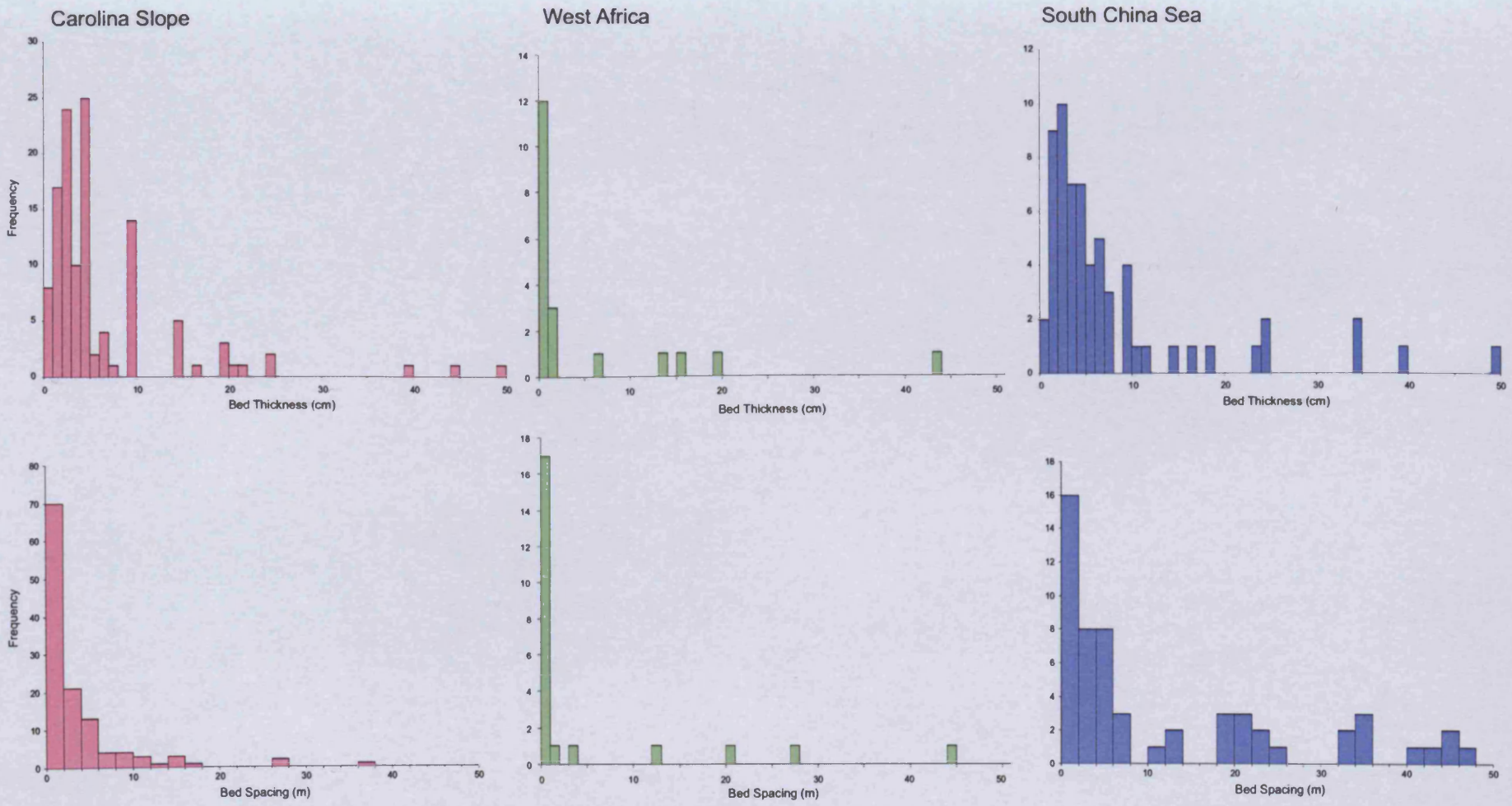

Figure 3.38 Histogram plots of the spacing and thickness of coarse-grained beds recorded from cores at the six ODP locations examined. Continued on next page.

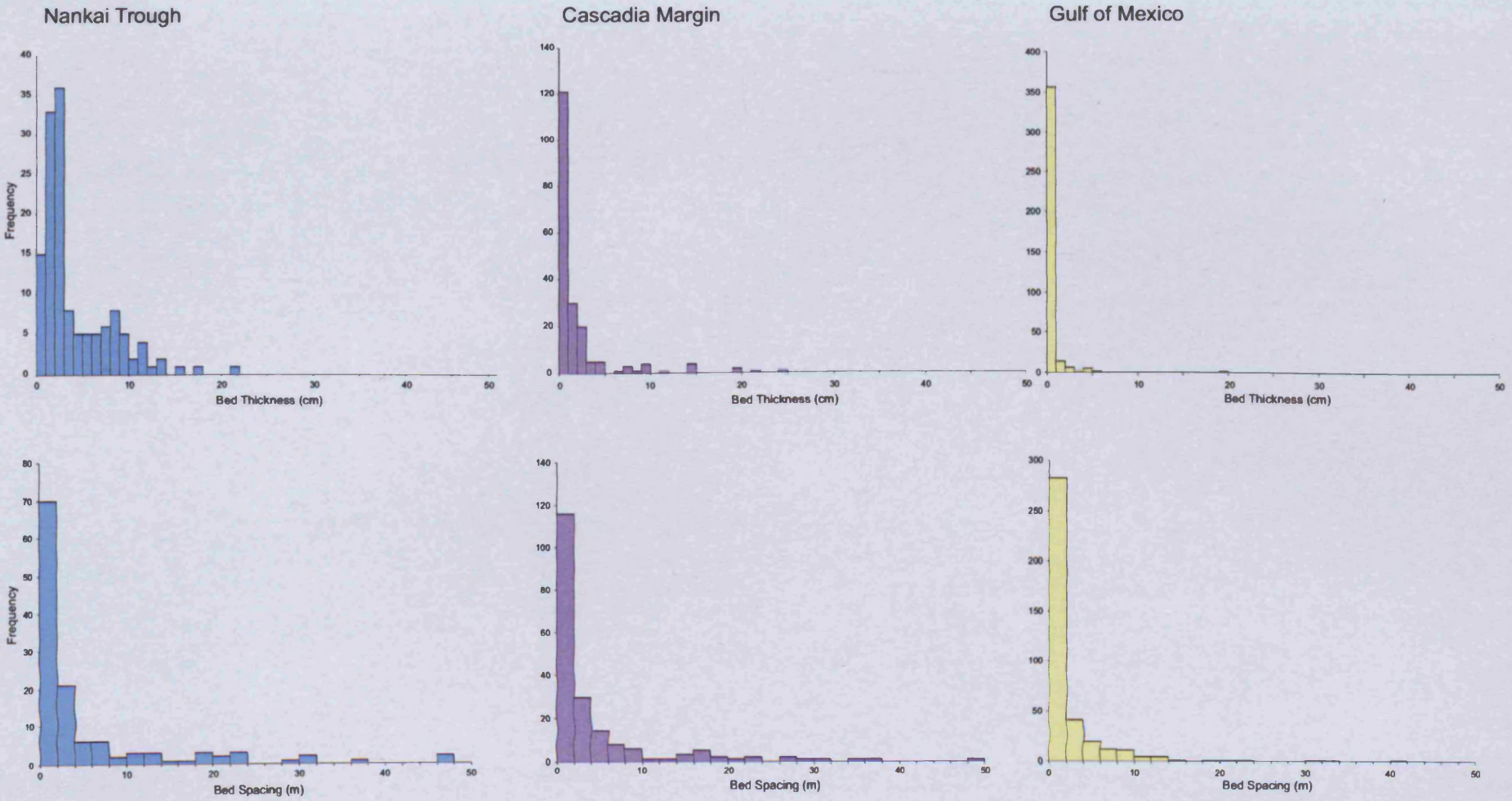

Figure 3.38 *cont.*

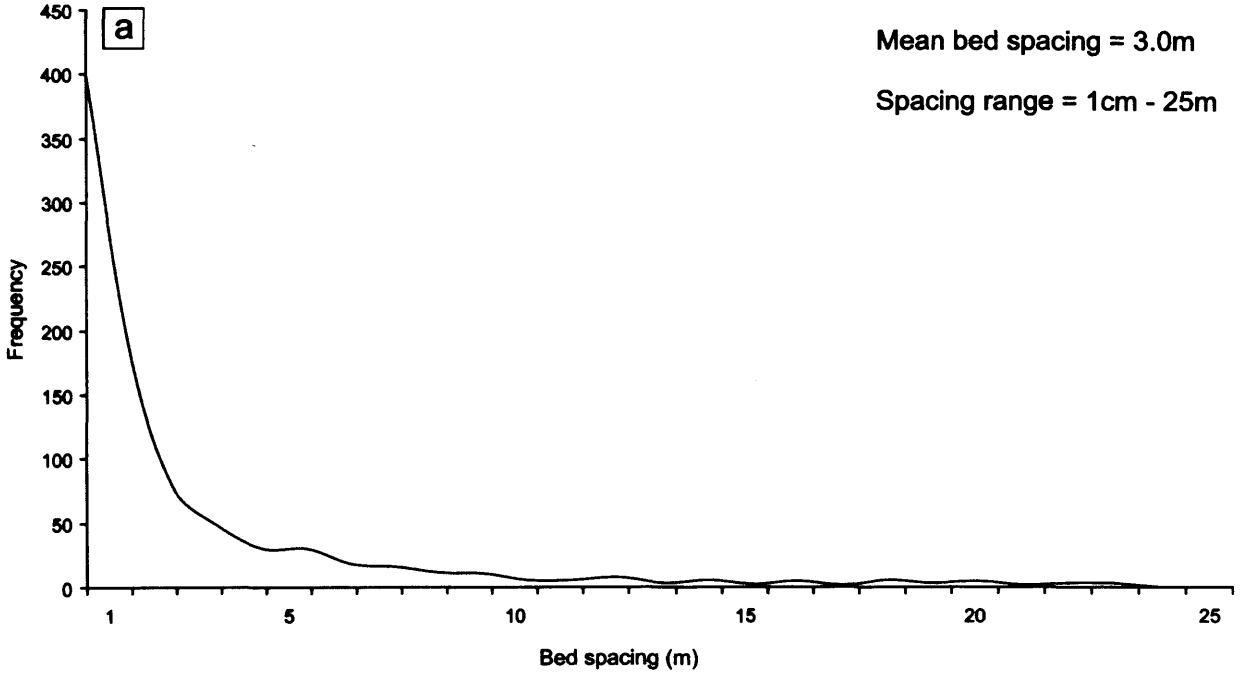

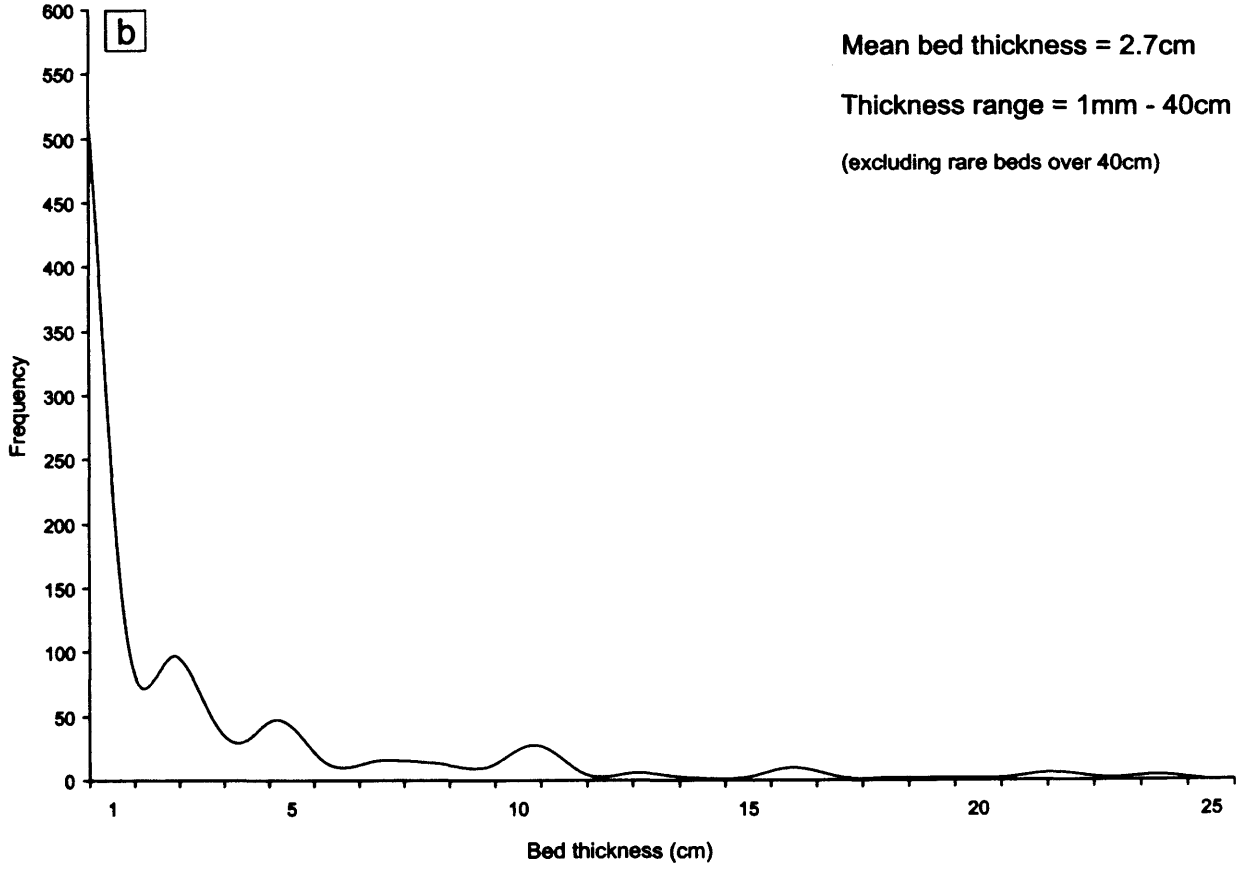

Fig. 3.39 *See next page for caption*

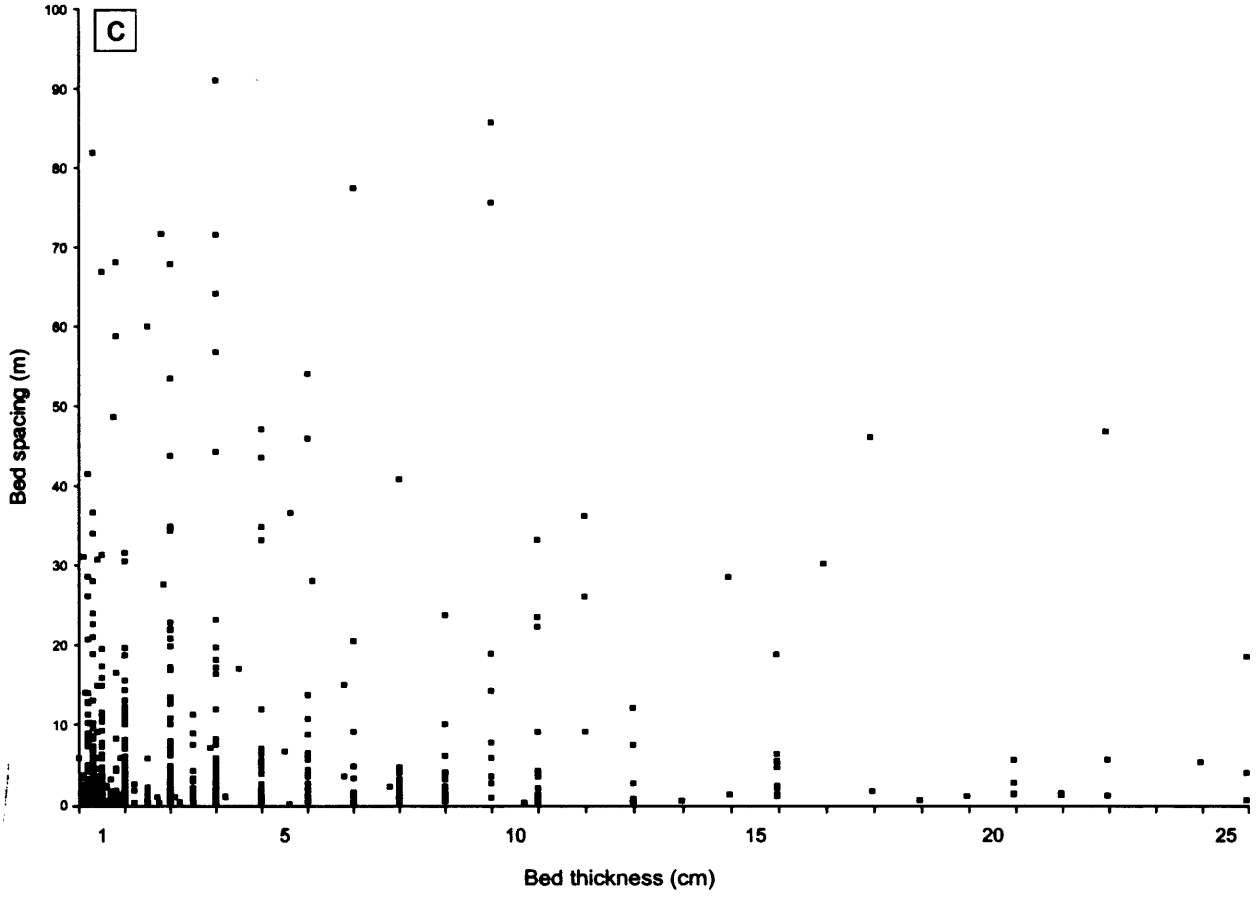

Figure 3.39 (a) Plot showing the distribution of bed spacings recorded from 23 hemipelagic sequences. (b) Plot showing the distribution of bed thicknesses recorded from 23 hemipelagic sequences. (c) Graph plotting the thickness of individual coarse beds against the vertical, up-core distance to the next coarse bed.

Several important geometrical parameters regarding the distribution of thin-beds in hemipelagic sequences are not constrained in the Caprocks Hemipelagite Database. Core-derived data does not allow for either the examination of lateral continuity, or the inter-connectivity of thin-beds. Based on outcrop studies presented in Chapter 2, it is expected that thin-beds will be locally laterally continuous on the scale of tens to hundreds of metres. Interconnectivity of beds, by means of a relatively high-permeability conduit, becomes increasingly statistically unlikely with increasing bed spacings, however fieldwork studies have identified a number of sedimentological and mechanical mechanisms which may allow layers to be in pressure communication with one another (*see* Chapter 2). Quantifying the frequency and distribution of inter-bed connections is extremely difficult given the limited availability of suitable outcrop areas, however the most important vertical connections are likely to be related to structural deformation such as faults and fractures, rather than sedimentological features.

3.5 Discussion

3.5.1 Controls on the distribution of thin-beds in hemipelagic sequences

Slope environments in which hemipelagic sedimentation dominates are inherently relatively low-energy deposition settings (e.g. Reading, 1996). Basin margins where large volumes of coarse terrigenous material is introduced to the shelf and slope environments typically develop efficient sediment transport systems such as submarine channels and submarine canyon systems (e.g. Shepard and Emery, 1973; Posamentier and Vail, 1988). Thin-beds of coarse material deposited away from confined sediment conduits (e.g. submarine channel-levee systems and slope canyons), such as those examined in the CHD, are thought to be introduced principally by low-density turbidity flows and ocean-currents. Evidence from examined cores reveals that thin-beds are commonly graded or show signs of current action and sediment winnowing, processes indicative of turbiditic and contouritic deposition (*see* Fig. 3.6 and 3.11) (Stow and Mayall, 2000).

From data examined here, the distribution of thin-beds of potentially more permeable material in hemipelagic sequences is seen to be controlled, at least in part, by the complex interaction of several important location specific factors. These include sediment input sources, sediment transport pathways, sediment redistribution, and post-depositional alterations. The relative influence of each of these processes is likely to vary between locations and will be unique to a particular setting. Making predictions as to the likely

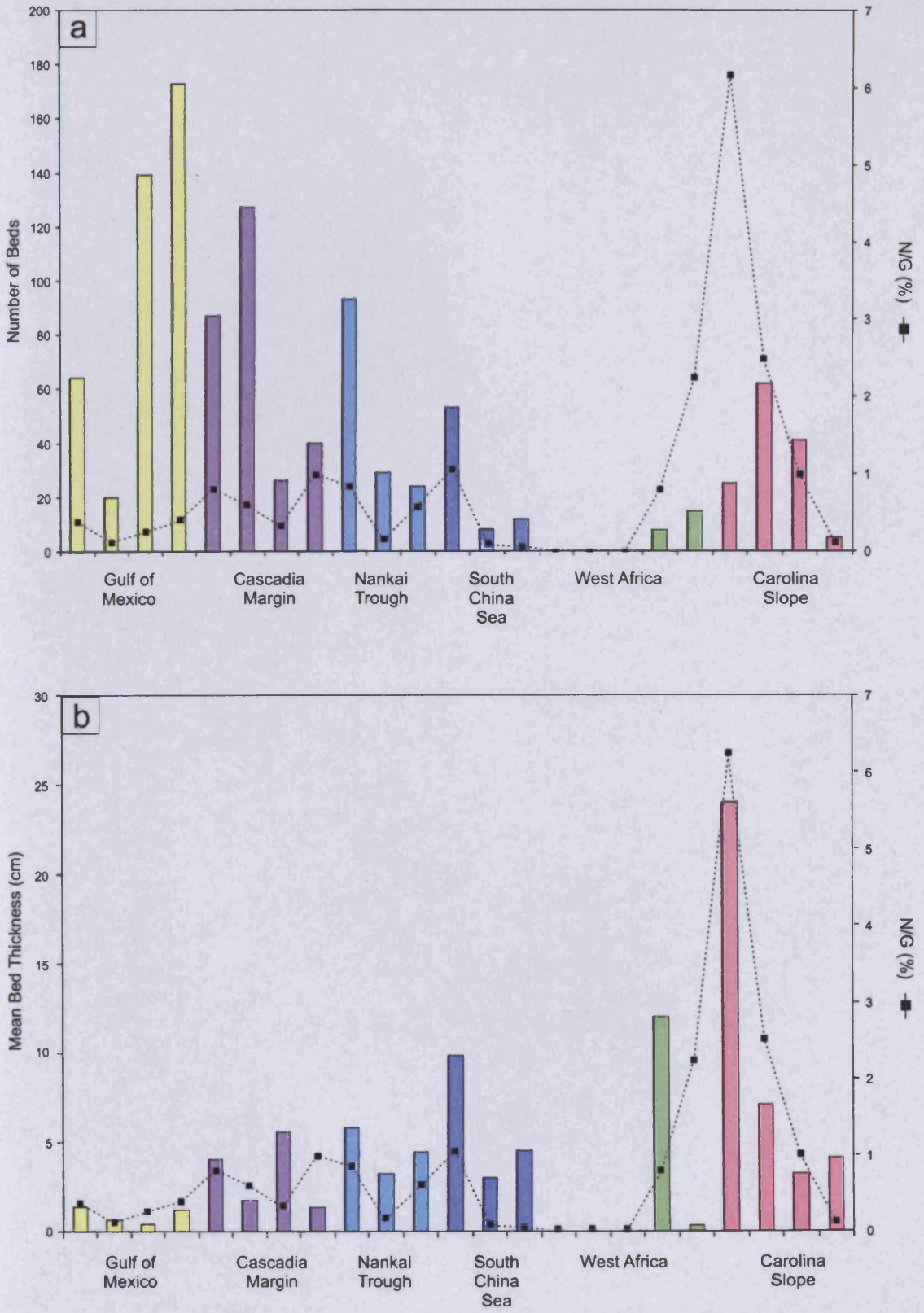

Figure 3.40 **(a)** Plot showing the relationship between the number of beds recorded (bars) and the net-to-gross for the 23 hemipelagic sequences examined here. **(b)** Plot showing the relationship between the mean thickness of coarse beds (bars) and the net-to-gross for the 23 hemipelagic sequences examined here.

frequency and distribution of coarse layers within a hemipelagic sequence therefore requires the probable influence of each of these factors to be considered for a specific basin location.

This study would suggest that no single parameter can be used to estimate the thickness or specific distribution of coarser layers within hemipelagic sequences, for example water-depth, or distance from sediment source. It can be argued that location specific conditions exert the strongest influence over the depositional regime in a particular location, and that this regime may vary regionally. For example, the proximity of ODP Sites from the Lower Congo Basin (1075-1077) to the Congo River has not resulted in a high occurrence of coarser thin-beds being deposited, despite the river representing a major local sediment point source. The northern margin of the South China Sea provides another example of where the depositional regime at a particular location is not necessarily governed by its position relative to a particular point source. Here, the silt content of hemipelagic sediments deposited on the slope varies laterally as a result of the position of the primary depocentre of the region, imaged in seismic data as a sediment wedge (Fig. 3.18a). Sites 1044 and 1046 were drilled in similar water depths an equal distance from the margin's major sediment source, the Pearl River. However, the contrasting character of the hemipelagic sediment deposited at these locations could not be accurately predicted without specific knowledge of sediment transport pathways and the depositional architecture of the slope.

Locations examined from the Angola Basin and Carolina Slope are without significant proximal sources of clastic sediment. However, both locations record the deposition of coarser grained sediment layers within hemipelagic sediments. In the case of Carolina Slope Site 1054, these are up to 300cm thick. Alongslope bottom water currents, thought to be responsible for these grain-size heterogeities, are known to have a significant impact on the mobilisation and depositional character of sediments on continental margins (Heezen and Hollister, 1964; Stow and Holbrook, 1984; Bluck et al., 2007). Depositional settings which are affected by contouritic and hemipelagic sedimentation processes will record grain-size distributions which reflect the relative influence of both regimes (Pudsey, 2002; Maldonado et al., 2003). Predicting the distribution of higher permeability facies in such settings will require the probable grain-size distribution of laterally transported and hemipelagic sediment to be evaluated.

Data examined from the Cascadia Margin and the Gulf of Mexico indicate that local bathymetry and slope structure are also important in determining the deposition of coarser grained lithologies by influencing downslope transport pathways. Salt-withdrawal mini-basins found in the Brazos-Trinity region of the Gulf of Mexico are depocentres for gravity-driven

deposits (Smith, 2004), while the distribution of coarse grained beds recorded from the Cascadia Margin is thought to reflect the interaction of down-slope sediment transport and the complex bathymetry of what is an actively deforming margin (Alexander and Morris,1994; Kneller, 1995; Kneller and Buckee, 2000).

3.5.2 Implications for hemipelagite sealing sequences

From the data examined here, it has not been possible to identity a 'generic' hemipelagite facies or to quantify the most common configuration of thin coarse beds. It appears that the conditions of a particular basin setting exert a major control over the grain-size distributions of hemipelagic sediments and that facies variability can be accounted for by evaluating the range of possible external controls at a particular location. From a hydrocarbon sealing perspective is it also important to note that although thin-beds have been found in the vast majority of hemipelagic intervals examined in the CHD, they do not form a significant portion of the total sediment column, typically representing less than 1%. For these thin-beds to act as potential fluid-flow conduits within hemipelagic sequences will also depend critically on their connectivity. Connective elements observed from outcrop studies (*see* Chapter 2) allow bed connections over centimetre-scales, while typical bed spacings recorded from ODP sites are in the region of 5-10m. The isolation of higher permeability layers may render them far less likely to act as conduits for fluid-flow and will significantly reduce their impact on seal integrity. One possible mechanism where widely spaced thin-beds may aid leakage is where the development of fractures and faults brings silt and sand layers into pressure communication with one another. Fault leakage and hydraulic fracturing have themselves been documented by a number of authors as posing a risk to seal integrity in fine-grained sediments (Grauls and Cassignol, 1992; Caillet, 1993; Esch and Hanor, 1995), although the possibility of additional lateral transfer and the expansion of a pore-scale leakage network through more permeable thin-beds is rarely discussed (e.g. Lash, 2006).

A key learning from this extensive examination of ODP data is that the classical notion of hemipelagic slope sediments as uniformly fine-grained units cannot be applied ubiquitously. In particular settings examined, the distribution of discrete coarser grained horizons may not significantly alter the overall sealing properties of the host unit (e.g. Lower Congo Basin sites), however in other locations, the closely spaced and regular occurrence of thin-beds may impact vertical and horizontal fluid-flow (e.g. Mars-Ursa region, Gulf of Mexico, Sites 1322 and 1324). Hemipelagic sequences examined also reveal a significant range of grain-size distributions present in what are considered as 'background' sedimentary units. The grain-size distribution and lithology of background sediments and the volumes of dispersed

silt and sand grade will impact a unit's capillary sealing properties. Diatomaceous clays from Lower Congo Basin sites for example exhibit shallow porosities of between 75-90% compared to values of between 50-70% for silty clays and clayey silts recovered from the Cascadia Margin (*see* Caprocks Hemipelagite Database, CD-ROM, inside back cover). Other physical properties which will also govern the capillary sealing capacity of bulk hemipelagic sediments, such as permeabilities, clay mineral assemblages, and mean pore-throat sizes will similarly be influenced by the variability observed in background hemipelagic facies (Meade, 1964; Yang and Aplin, 1998; Dewhurst et al., 1999b).

The specific grain-size and lithological properties of predominately fine-grained hemipelagic slope sequences will inevitability govern the sealing capacity of these units. Coarser grained material deposited as either discrete thin-beds, as examined here, or as dispersed grains will influence fluid-flow by altering sediment physical properties. Controls on the likely grain-size distribution of hemipelagic sequences has been shown to be strongly influenced by a number of factors (*see* section 3.5.1). Considerations as to the likely influence of local and regional forces on sediment input, transport and deposition/reworking will allow a more accurate classification of hemipelagic sediments to be made at a particular location of interest. Petroleum systems modelling and subsequent seal risk evaluations based on location-specific hemipelagite physical properties will more accurately reflect the sub-surface geology and the probability of capillary leakage.

3.6 Conclusions

1. The Caprocks Hemipelagite Database contains data regarding the frequency, distribution, and dimensions of more permeable lithologies from the examination of over 7000m of cored hemipelagic sediment.

2. No generic hemipelagite lithofacies has been observed. Discrete coarse grained intervals comprise between 0-6% of the total sediment cored at the sites examined, while background facies show a range of lithologies and grain-sizes reflecting varying proportions of clay, silt, sand, and biogenic material.

3. Thin-bed thicknesses range from 1mm silt and sand laminations upto beds 40cm thick, with a mean value of 2.7cm recorded from the ~1000 beds measured.

4. Vertical spacings between thin-beds range from 1cm - 25m, with a mean distance of 3m recorded from the ~1000 beds measured.

5. Sediment input sources, transport pathways, and remobilization processes are thought to govern the distribution and deposition of coarser material in hemipelagic slope settings. Location specific evaluations of the likely influence of these controls are therefore essential to accurately predict the character of hemipelagic sediments.

Chapter 4

Chapter 4

Porosity loss in shallow hemipelagic sequences

4.1 Introduction

The rates and mechanisms by which hemipelagic sediments lose porosity during shallow burial represent key questions for those considering the evolution of sedimentary basins. An increasing level of interest from the petroleum industry into the porosity of shallow hemipelagic sequences has arisen in recent years, driven by the existence of abnormally pressured sediments at relatively shallow depths, and the increasing exploration of shallow gas accumulations (Flemings et al., 2008; Ostermeier et al., 2001; Rollet et al., 2009). Knowledge of the likely relationship between porosity and depth/effective stress in hemipelagic sequences is a key input for decompaction analysis and sediment back-stripping (e.g. Baldwin, 1971; Watts et al., 1982; Lawrence et al., 1990; Springer, 1993), and is also fundamental to any appraisal of hydrocarbon sealing capacity (e.g. Schowalter, 1979).

Hemipelagic sequences are common in many passive margin settings, often deposited as thick, regionally extensive units comprising mixtures of terrigenous, biogenic and authigenic material which are seen to drape slope bathymetry, for example in the Gulf of Mexico (Bouma, 1981) and South China Sea (Wang et al., 2000). The loss of porosity during burial in these shallow sequences is likely to be dominated by mechanical compaction and subsequent grain rearrangement rather than chemical processes such as cementation, which are more prevalent at depths exceeding 1000 metres where temperatures are elevated (Powers, 1967; Velde, 1996). In response to increasing overburden stress experienced during burial, fine-grained hemipelagic sediments experience rapid porosity loss and dewatering and as a result can contribute significantly to the redistribution of pressure and fluid migration in basin margin sequences (Dugan and Flemings, 2000; Broichhausen et al., 2005). A common feature of thick hemipelagic sequences is the development of overpressured pore-fluids created when expelled fluids are unable to escape and assume a portion of the vertical stress (Hart et al., 1995). For a sequence to remain hydrostatically pressured, fluids expelled from pores during the rearrangement of grains must be able to escape, ultimately to the seafloor.

Early works addressing the relationship between porosity and depth in porous media include Terzaghi (1925) and Hedberg (1926, 1936), with the most commonly used porosity-depth function being that of Athy (1930)

$$\phi = \phi_0 e^{cz} \qquad (1)$$

where ϕ is the porosity at depth z [m], ϕ_0 is the initial porosity, and the compaction coefficient c is a constant value for a given lithology. Terzaghi and Peck (1948) describe compaction by porosity loss as a function of effective stress in soils, which was later applied to fine-grained sediments by Rubey and Hubbert (1959). These models assumes that grains are incompressible and that compaction of the sediment is caused exclusively by the reduction in the volume of water-filled pores, such that

$$\sigma = ob - p \qquad (2)$$

where σ is the effective stress, ob is the overburden load and p is the formation pressure in MPa. According to this, the weight of overburden is partly borne by the rock matrix and partly by the formation fluid. A number of authors have subsequently developed porosity/effective stress functions building on these early principles, these include Rieke and Chilingarian (1974), Sharp (1976), Gibson et al. (1981), and Lerche (1990). A plot showing various early 'compaction curves' for fine-grained sediments is shown in Fig. 4.1. Yang and Aplin (2004) more recently examined the relationship between effective stress and porosity specific to mudstones. They concluded that the effective stress/porosity functions established in soil mechanics literature (i.e. Terzaghi, 1943; Skempton, 1970; Burland, 1990) adequately described that of the one-dimensional mechanical compaction of natural and artificial mudstones.

Another important process intrinsically linked to the burial of fine-grained sediments is differential compaction (Bjørlykke and Hoeg, 1997). Commonly this involves the creation of structure within sequences where sedimentary units experience differing compaction rates. Folds located above basement highs are commonly seen accommodating differential compaction where clay-rich sediments drape bathymetry, e.g. Forties field, North Sea (Glennie, 1998), while more complex relief can develop where hemipelagic sediments grade laterally into less compressible, more sand-rich lithologies such as those existing in channel-levee systems (e.g. Mayall et al., 2006)

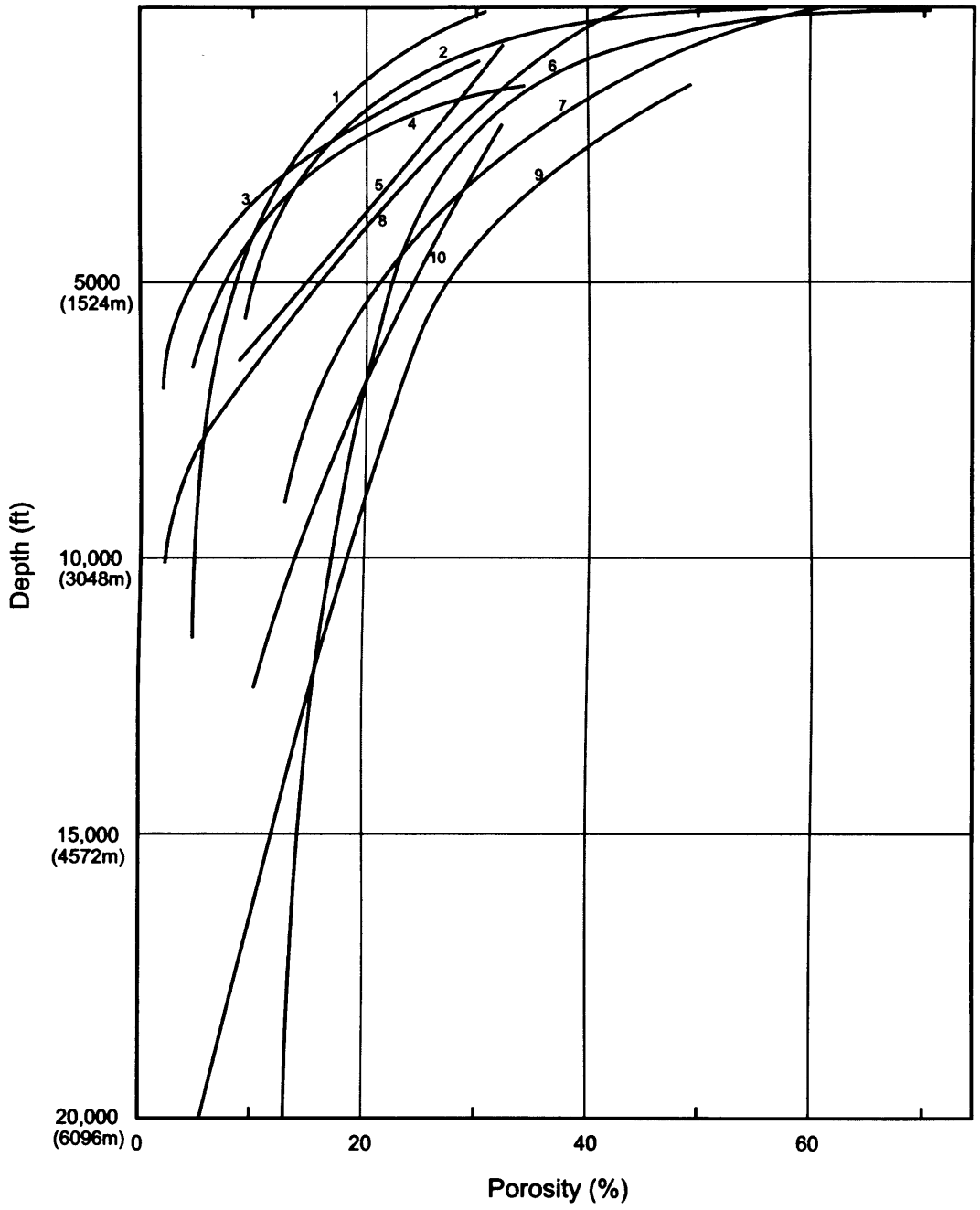

Figure 4.1 Relationship between porosity and depth for shales and argillaceous sediments, redrawn from Rieke and Chilingarian (1974). 1 = Proshlyakov (1960); 2 = Meade (1966); 3 = Athy (1930); 4 = Hosoi (1963); 5 = Hedberg (1936); 6 = Dickinson (1953); 7 = Magara (1968); 8 = Weller (1959); 9 = Ham (1966); 10 = Foster and Whalen (1966).

Following the work of Velde (1996), porosity data from ODP and IODP wells are used here to aid discussions of porosity loss in shallow (~500m thick) hemipelagic sequences. Initial porosity values, representing those at or close to the seabed, are discussed as they form a key input to basin modelling and decompaction calculations, but are often assumed. Using lithologically calibrated porosity data from over 250 boreholes we are able to show that a huge range of initial porosity values exist in naturally occurring hemipelagic sediments, and show the sensitivity of these values to changes in facies. We also present distributions of porosity with depth for 16 shallow hemipelagite sequences in order to investigate the distribution and trends in porosity values with depth, as well as the impact of facies variability on compacted porosity values.

4.2 Porosity loss and compaction

Compaction can be essentially thought of a continuous process which begins soon after sediments are deposited. In order to understand the evolution of compaction as a function of depth or effective stress many published studies provide 'compaction curves' which aim to describe a generalised trend in porosity or bulk density measurements through a sediment column (e.g. Dickinson, 1953; Baldwin, 1971; Rieke and Chilingarian, 1974; Sclater and Christie, 1980; Baldwin and Butler, 1985). The common use of depth as a proxy for effective stress stems from the difficulties of acquiring in situ stress measurements in natural systems. The major drawback of this approach is that while in normally pressured sequences effective stress correlates very strongly with depth, this is not the case in overpressured zones. A common feature of normally pressured hemipelagic sequences is an exponential reduction in porosity values with increasing depth, as was first recognised by Athy (1930), see equation (1), and subsequently documented by many authors (*see* Baldwin and Butler, 1985, and references therein).

Depth (mbsf) is used here as a proxy for effective stress in the absence of effective stress data. ODP drilling campaigns generally avoid regions where overpressured sediments are likely, being ill-equipped to control significant well blow-outs created when overpressured zones are drilled. Data used here in porosity-depth plots were collected on successful drilling campaigns with no reported blow-outs or shallow pressure hazards encountered, with the exception of a single plot from the Gulf of Mexico where overpressures were under investigation.

In order to investigate the rates and mechanisms by which compaction proceeds under known effective stresses, numerous studies have also experimentally compacted natural

clay-rich materials (e.g. Dewhurst et al., 1998) as well as remoulded silty-clays and clays (e.g. Skempton, 1970; Karig and Hou, 1992) and pure clays (e.g. Meade, 1964; Vasseur et al., 1995). The advantage of laboratory compaction studies is that pressures and lithologies are well constrained and the compaction of sediment can be measured at a range of effective stresses. However, Velde (1996) points out that experiments routinely record higher compaction states than those seen in naturally compressed sediments, suggesting higher compressibilities, most likely owing to the difficulties of recreating artificially the structure and arrangement of flocculated material (Burland, 1990; Vasseur et al., 1995). Meade (1964) also notes that compaction experiments often involve a single grain-size fraction or simple pore-fluid chemistry making direct correlations with complex natural systems difficult.

In our analysis of porosity data, distributions of values plotted against increasing depth are not discussed in terms of compaction trends, but rather simply as porosity versus depth plots. The notion of a 'compaction-curve', such as those in Fig. 4.1 would suggest that the state of a discrete interval has some intrinsic relation to that of other intervals stratigraphically above or below, which is perhaps misleading. In reality, the particular porosity/effective-stress pathway a sample has taken to arrive at the point at which its porosity is measured will never be known, as alluded to by Giles (1997).

4.3 Methods and Data

The ODP and IODP archives represent a huge and easily accessible source of data that permit investigation of many aspects of marine sedimentology. The relatively shallow wells investigated by ocean drilling programs are well suited to the purpose of this study, contrasting with those commonly drilled by the petroleum industry, which tend to focus on deeper intervals. This study uses published porosity data from ODP and IODP sites drilled between 1985 and 2005 (Table 4.1). For the purpose of this study, sixteen sites were chosen to provide porosity data of shallow-buried (<500m), clay-rich (>50%) hemipelagic sequences with low carbonate and biogenic silica fractions. Sediments recovered are referred to as claystones and silty-claystones interspersed with various amounts of calcareous nannofossils. For the investigation of initial porosities, a total of 255 values were extracted from drilled sites covering a range of water-depths and marine settings which include the Iberia margin, Indian Ocean, Amazon Fan, Mediterranean Sea, Northeast Atlantic, Cascadia margin, Philippine Sea, and the Gulf of Mexico. These data have been categorised by specific lithological facies using published ODP core-descriptions and literature (Proceedings of the Ocean Drilling Program 1983-2003, available at [http://www.odplegacy.org/])

Porosity-depth plot	Leg	Site	Latitude	Longtitude	Location	Date
1	116	717	0° 56'S	81° 23'E	Indian Ocean	1987
2	149	900	40° 41'N	11° 36'W	North Atlantic - Iberia margin	1993
3a	155	931	5° 9'N	46° 38'W	Atlantic - Amazon Fan	1994
3b	155	935	5° 26'N	47° 34'W	Atlantic - Amazon Fan	1994
3c	155	936	5° 38'N	47° 44'W	Atlantic - Amazon Fan	1994
3d	155	944	5° 56'N	47° 45'W	Atlantic - Amazon Fan	1994
4	161	976	36° 12'N	4° 19'W	Mediterranian	1995
5	161	977	36° 2'N	1° 57'W	Mediterranian	1995
6	161	979	35° 43'N	3° 12'W	Mediterranian	1995
7	162	985	66° 56'N	6° 27'W	North Atlantic	1995
8	162	986	77° 20'N	9° 5'E	North Atlantic	1995
9	175	1079	11° 56'S	13° 19'E	Atlantic - West Africa	1997
10	184	1146	19° 27'N	116° 16'E	South China Sea	1999
11	184	1148	18° 50'N	116° 34'E	South China Sea	1999
12	204	1245	44° 35'N	125°9'W	Pacific - Cascadia margin	2002
13	308	1324	28° 04'N	89°08'W	Gulf of Mexico	2005

Table 4.1 Location information for the 16 hemipelagic sequences examined in this chapter.

4.3.1 Porosity data

Porosity determinations made shipboard were downloaded from the ODP's online data repository, the Janus Web Database, and used to construct porosity versus depth plots. The ODP routinely employ several laboratory-based methods to determine porosity values at drill sites (Blum, 1997). Gamma-ray Attenuation Porosity Evaluation (GRAPE) is a method used to estimate density by comparing the attenuation of gamma-rays through core sections to that of calibration standards, typically aluminium rods of varying diameters surrounded by a water-filled core-liner (Blum, 1997). An advantage of the GRAPE method is that it allows a high-resolution record of density to be easily collected. However the GRAPE method is based on core unit volume and as such, gas expansion cracks and microfractures present in the core are recorded as porosity (Blum, 1997). Boyce (1973) noted that only minimum porosity values recorded using the GRAPE method are likely to be valid. However, porosity determinations used in this study were made using a single standardised measurement technique, referred to as ODP MAD Method C (moisture and density). This technique uses gas pycnometry to determine the volume of interstitial fluid of a given sample by measuring its mass and volume before and after drying, with corrections being made for the volume of evaporated salt (Blum, 1997). Raw data shows samples measured every 1-2m, although greater sampling intervals are seen at a number of the sites studied. This method is carried out in shipboard laboratories and is thought to provide the best density (and subsequent porosity) determinations (Hamilton, 1976). The use of a standardised method for the determination of porosity also allows for straightforward comparisons between data without the need for manipulation or correction.

4.3.2 Measurement errors

Buried sediment samples which are brought to the surface for analysis undergo a significant reduction in stress. A number of studies have investigated the phenomena of 'porosity rebound', thought to occur as samples expand in response to greatly reduced confining stresses (Hamilton, 1976; Nobes et al., 1991; Marsters and Manghnani, 1993; Blum, 1997). Consolidation tests carried out by Hamilton (1976) using sediment samples collected by the DSDP suggest that the porosity of pelagic clays may 'rebound' by as much as 6.9% from burial depths of just 300m, while porosity-rebound within calcareous oozes and terrigenous sediments from the same depths are likely to be 4.4% and 5.2% respectively. Consolidation tests carried out on calcareous sediments by Marsters and Manghnani (1993) from the Ontong Java Plateau reveal porosity rebounds of 1-4% from sediments buried to depths of 1200mbsf. They go on to suggest that 'rebound corrections' can be employed to correct

shipboard measurements to more accurately represent in situ porosity values (Marsters and Manghnani, 1993). Meanwhile, Blum (1997) argues that the expansion of solids is not important when considering the exhumation of sediment samples and that pore-fluid expansion from the majority of ODP cores is in the region of 1% and is therefore negligible compared to analytical errors. Similarly, Nobes et al. (1991) found no significant differences between those porosity values acquired by the MAD method shipboard and those measured using neutron porosity and lithodensity down-hole tools and concluded that laboratory measurements, at least in the sediments studied, were representative of in situ porosities and that porosity-rebound was not significant. Porosity values used here in the investigation of initial porosities have not undergone any significant burial and therefore require no rebound correction. Porosity data from the 16 hemipelagic sequences studied here share both common maximum burial depths and bulk lithologies and would therefore be likely to experience any porosity-rebound to a similar degree. In light of the references and discussions mentioned, no corrections have been applied to porosity measurements used in this study made via the MAD-C method.

Lithological descriptions published in ODP volumes follow a well established methodology and are based primarily on smear-slide analysis performed by shipboard scientists. This method takes into account composition and texture to define lithology, with no generic terms, such as 'pelagic', 'hemipelagic', or 'turbiditic' used. For non-biogenic sediments (>60% non-biogenic material), the principal sediment name is determined by the relative proportion of silt, sand, and clay sized grains when plotted on a modified Shepard (1954) classification diagram (Fig. 4.2). Major and minor modifiers are listed in order of decreasing abundance to the left of the principal name. For example, a sediment classified as a nannofossil-bearing foraminifer-rich clay contains >60% clay-grade, non-biogenic material, 5%–10% nannofossils, and 10%-30% foraminifer (e.g. Sigurdsson et al., 1997).

Lithologies described in this study are based on only semi-quantitative grain-size analysis, obtained using the above methods. Lithologies and lithological boundaries must be interpreted with a degree of caution owing to the uncertainties concerning the exact grain-size distribution and texture of sediments. While exact absolute grain-size data of sediments is unknown, the relative proportion of different grain-sizes and lithologies are constrained using a detailed and standardised analytical workflow.

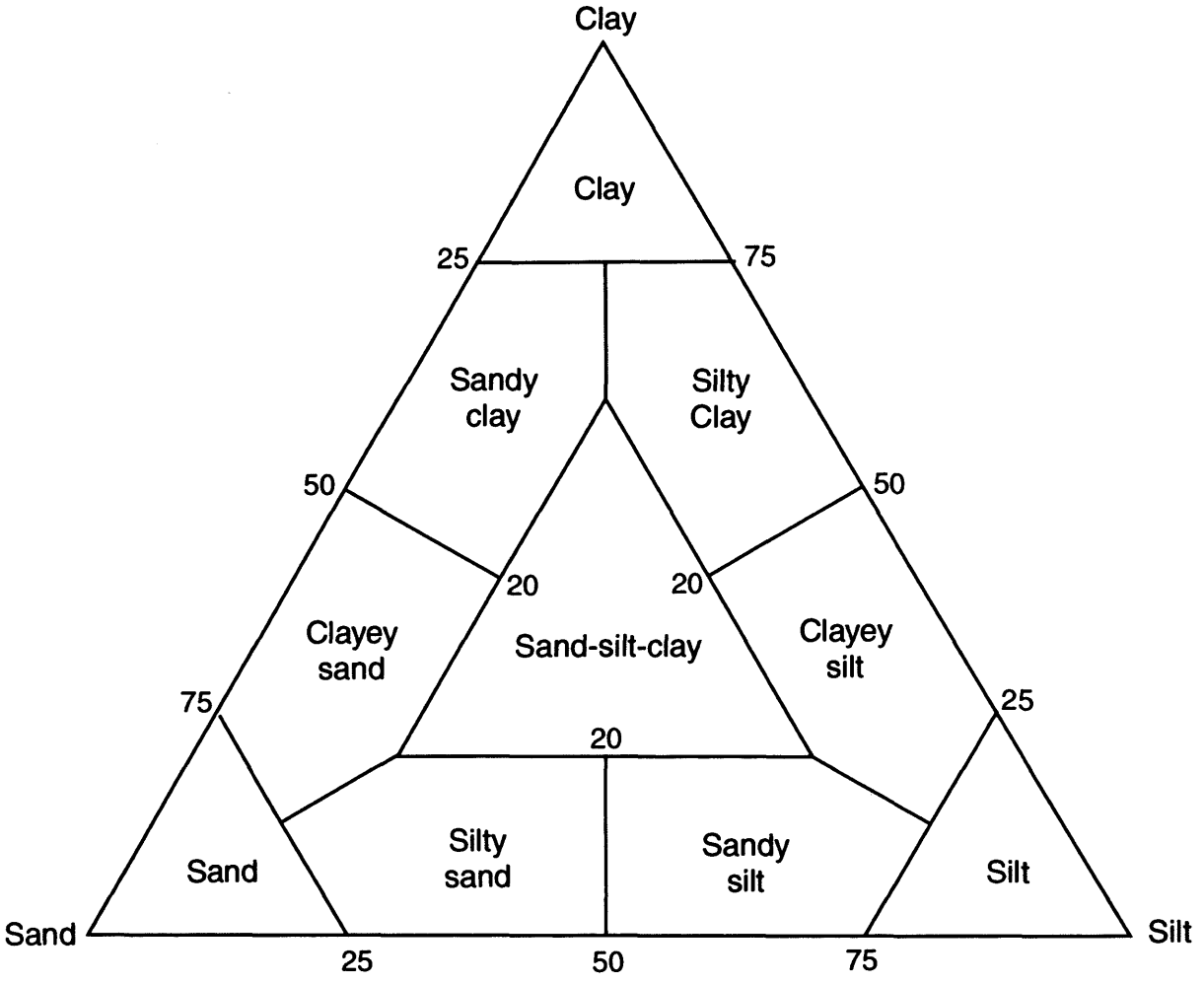

Figure 4.2 Ternary diagram used by the Ocean Drilling Program in the classification of siliciclastic sediments, modified after Shepard (1954).

4.4 Results

In the introduction we touched on the notion of porosity versus depth distributions as 'compaction curves'. In the following descriptions, porosity data are considered as the distribution of porosity values with depth, rather than in terms of sediment compaction.

4.4.1 Initial porosities in hemipelagic sequences

Porosity loss in hemipelagic sediments begins soon after deposition, as grains begin to rearrange into a more efficient configuration in response to the increasing weight of overburden. Initial porosities represent a key input of decompaction calculations used in basin models and subsidence history enquiries (Giles, 1997, equation 10.12). The accuracy of so-called 'compaction curves' extrapolated from discrete porosity determinations depend on the assignment of well-defined initial porosities to specific facies within a sediment column. Traditionally, generic initial porosity values for clay-rich hemipelagic facies are commonly defined as roughly 63%, after work by Sclater and Christie (1980) on North Sea shales, with little or no distinction made for specific facies (e.g. Mann and Mackenzie, 1990).

Fig. 4.3 shows a plot containing initial porosity determinations from 255 Sites from the Atlantic and Pacific Ocean margins, South China Sea, Indian Ocean, Mediterranean Sea, Southern Ocean and the North Sea. Porosity values in each case were determined within the top 50cm of solid sediment recovered, using the MAD C method (see section 4.3), and categorised by facies, using detailed core descriptions made shipboard. The distribution of data in Fig. 4.3 represents the range of depositional porosities as recorded, categorised by specific facies.

Perhaps the most striking feature of Fig. 4.3 is the sheer range of porosities recorded. With the exception of the lowermost two facies in Fig. 4.3, assigned to sandy and silty units, facies are dominated by clay-grade material and can be characterised as 'clay-rich hemipelagic' sediments. The generally lower initial porosity values recorded for the coarser two facies compared to the more clay-rich units are in good agreement with well known initial porosity values for sandy sediments, which are generally <50% (e.g. Allen and Allen, 1990). It is likely that higher porosity values recorded within these silty and sandy sediments represent the impact of increased clay fraction, for example between a sand and a clayey-sand. The remaining facies classifications are based on the proportions of constituent lithologies with the term 'clay' or 'ooze' signifying a dominance (>60%) of either siliciclastic, or biogenic grains respectively, and the terms 'siliceous' and 'calcareous' simply denote the nature of the

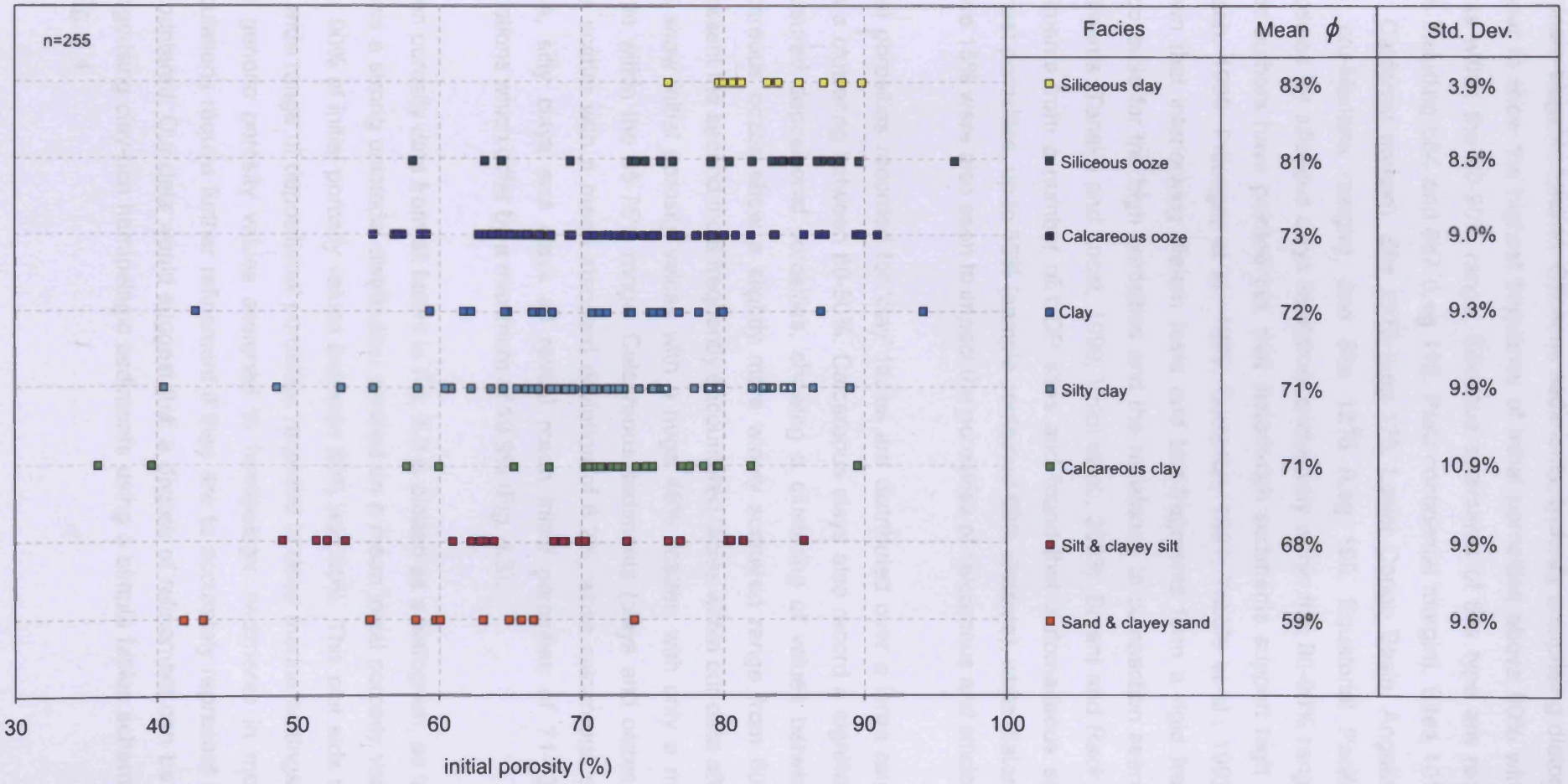

Figure 4.3 Initial porosity values from 255 ODP and IODP drill sites, categorised by facies type.

dominate biogenic fraction. Siliceous sediments, typically comprising diatomaceous material, appear to show the highest frequency of initial porosities above 80% with clusters of data points within the 80-90% range. Siliceous sediments of this type are recorded from ODP sites including 684 and 687 (Leg 112, Peru continental margin), Sites 1018 and 1022 (Leg 167, California margin), Site 1075 (Leg 175, Lower Congo Basin, Angola), Site 1149 (Leg 185, Izu-Mariana margin), and Site 1218 (Leg 199, Equatorial Pacific Ocean). Initial porosities for siliceous clays lie almost exclusively within this 80-90% range, suggesting, as other authors have pointed out, that diatom-rich sediments support high levels of porosity (Busch, 1989; Pittenger et al., 1989; Compton, 1991; Tribble et al., 1992). It is has been shown that interlocking diatom tests and test-fragments form a rigid framework which is responsible for the high porosities and the resistance to compaction seen in diatomaceous sediments (Tanaka and Locat, 1999; Volpi et al., 2003). Bryant and Rack (1990) examined sediments from a number of ODP sites and found that diatomaceous sediments had the highest porosities, up to 85% (sample contained 88% diatoms), while diatomaceous fractions above 15% were also seen to impact the porosities of calcareous and siliciclastic sediments.

Initial porosities recorded for 'clay' facies are distributed over a large range from 43-94%, with a clustering between 60-80%. Calcareous clays also record a significant range in their measured depositional porosities, showing a clustering of values between 70-80% while calcareous oozes show a slightly more widely scattered range from 60-80%. Silty clays represent the second most frequently encountered facies within our data after the clay facies, and show initial porosity values with a huge 48% scatter, with only a minor clustering of points within the 65-75% range. Calcareous sediments (clays and oozes) reveal the least data scatter with a mean standard deviation of 6.2%, while calcareous oozes, calcareous clays, silty clays and clays all reveal mean initial porosities of 71-73% and standard deviations which differ by a maximum of 10.9% (Fig. 4.3).

When porosity data from all facies in Fig. 4.3 is plotted as a histogram, as in Fig. 4.4, the plot shows a strong unimodal distribution centred on a mean initial porosity value of 72.5%, with over 90% of initial porosity values between 60% and 90%. This plot aids to further highlight the wide range of depositional porosities recorded in deep marine settings, and would imply that generic porosity values assigned to hemipelagic sediments in modelling tools and calculations require further refinement if they are to accurately represent the various facies encountered. Our data would suggest that a degree of refinement can be achieved through categorising clay-rich hemipelagic sediments using a simple facies scheme such as is used in Fig. 4.4.

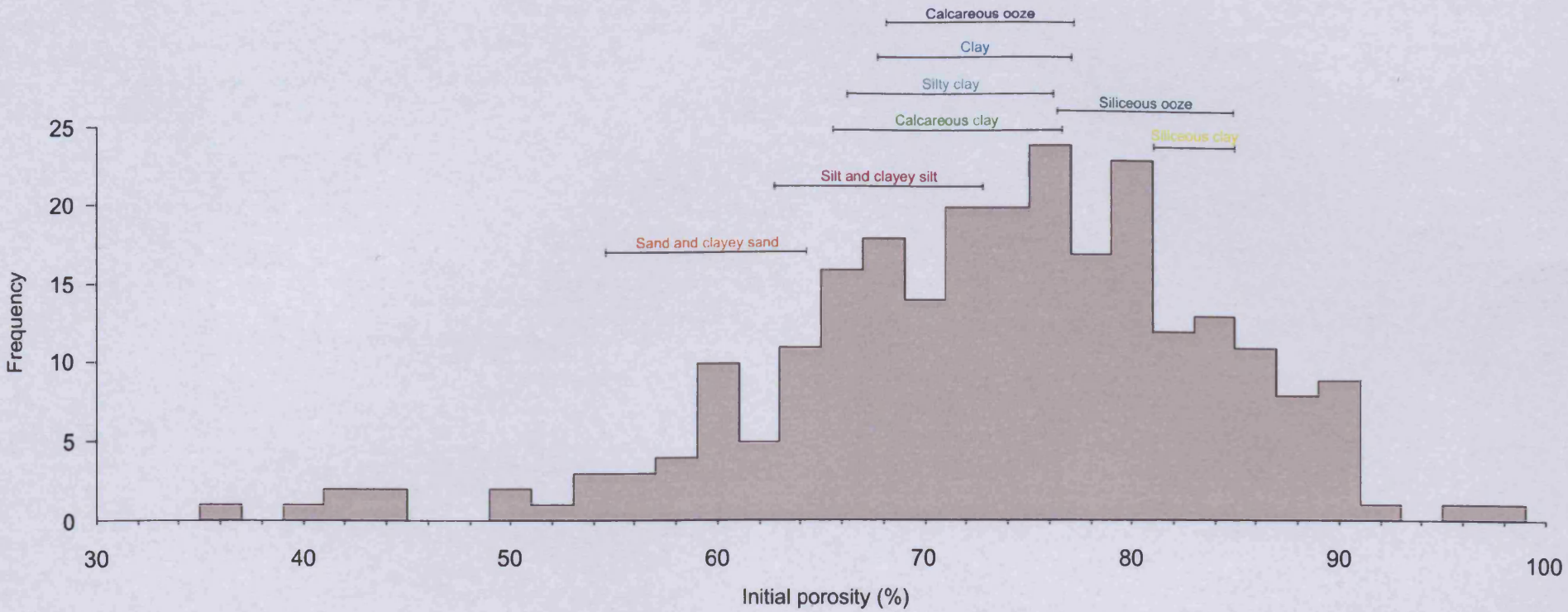

Figure 4.4 Distribution of initial porosity values, displayed as a histogram. Horizontal bars denote standard deviations from mean porosity values for the eight facies described (see Fig. 4.3 for values)

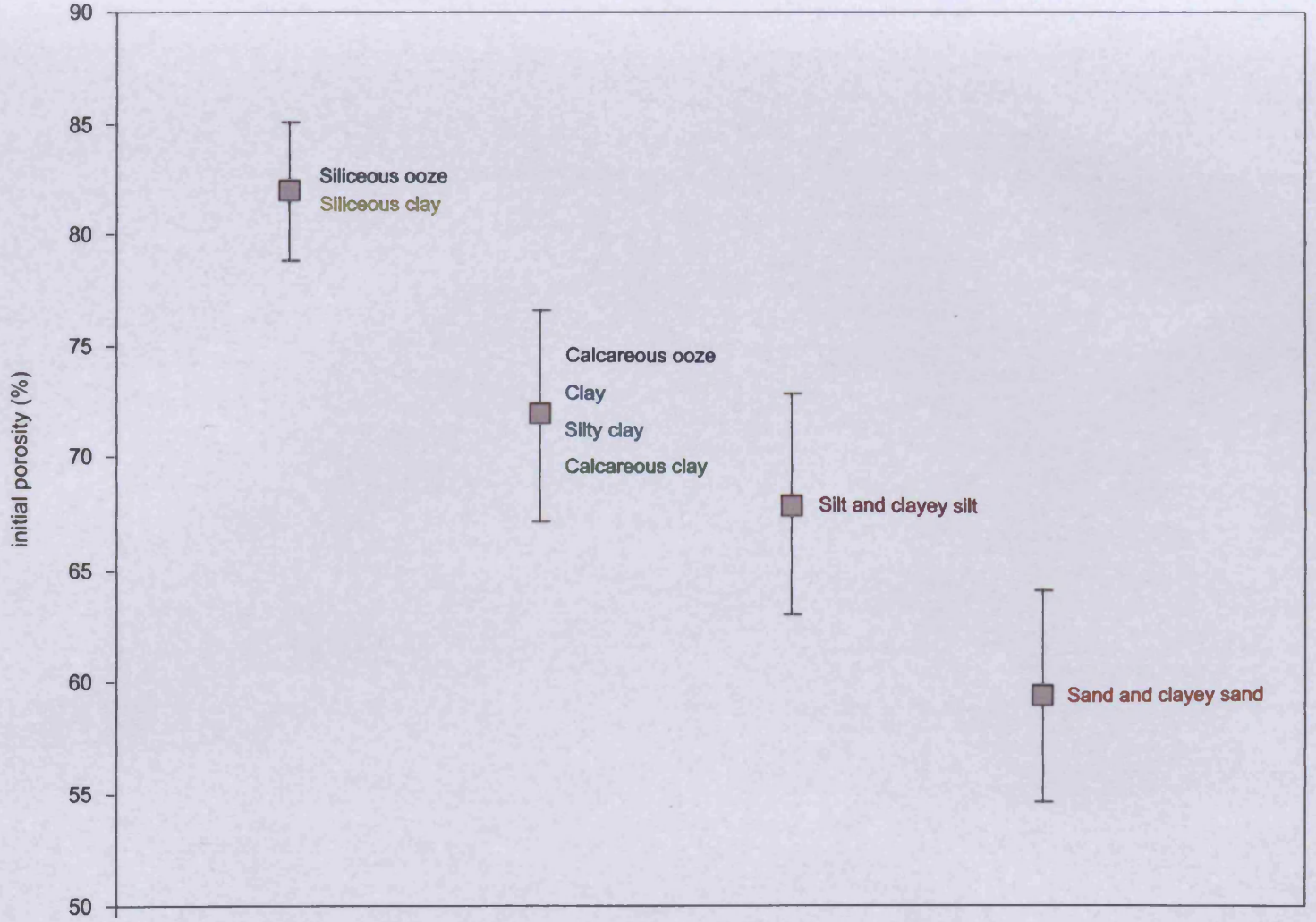

Figure 4.5 Grouping of facies based on initial porosity values (grey squares = mean, vertical bar = mean standard deviation). This style of grouping allows refinement of generic initial porosity values assigned to fine-grained sediments.

An example of a practical usage of such a classification is shown in Fig. 4.5. Initial porosity values are here refined by grouping the eight facies examined into four groups based on their mean initial porosity values and standard deviation. Using such a scheme would allow analysts to allocate one of four mean porosity values to fine-grained sequences, depending on local facies type, and also to apply error margins based on mean standard deviations.

4.4.2 Distribution of porosity with depth in shallow hemipelagic sequences

In addition to initial porosity data, sixteen shallow clay-rich hemipelagite sequences drilled by the ODP were selected for further detailed investigation regarding the relationship between porosity and depth. A key aim of this work was to establish the range of scatter for absolute porosity values with increasing depth and to characterise trends in these porosity distributions.

Porosity determinations for 16 clay-rich hemipelagic sequences are shown in Fig. 4.6 plotted against depth down-hole on the vertical axis. Broadly speaking, the data show a considerable range of measured porosity values at a given depth, up to almost 50% in some intervals. However, a concentration of data points within this general scatter forms a much narrower field of values, typically with a range of 10-15% (Fig. 4.6). This field maintains a scatter of 10-15% with remarkably consistency to depths of 500m, with only porosities at or close to the seafloor showing a significantly larger range of values. This general trend is similar to many published porosity distributions from equivalent sequences, showing a trend of exponentially decreasing values with increasing depth (e.g. Velde, 1996; Bahr et al., 2001). Plots such as that in Fig. 4.6 should however be viewed with caution, as while an exponential trend is observed, data have been compiled from 16 largely unrelated drill sites. When viewed individually, as in Fig. 4.7, it becomes clear that it is difficult to allocate a common trend to all of the hemipelagic sequences examined here.

4.4.3 Influence of lithology on porosity

Porosity-depth data from the sixteen hemipelagic sequences shown in Fig. 4.6 have been individually plotted along with their corresponding lithologies in Fig. 4.7. These plots provide an opportunity to cross-reference shallow porosity trends against detailed lithological records. Porosity-depth plots reveal the distribution of porosity with depth, although the exact mechanisms responsible for trends are sometimes rather ambiguous given the absence of effective stress data. Brief descriptions of many of these plots with regards the relationship between hemipelagite facies and porosity values are given below.

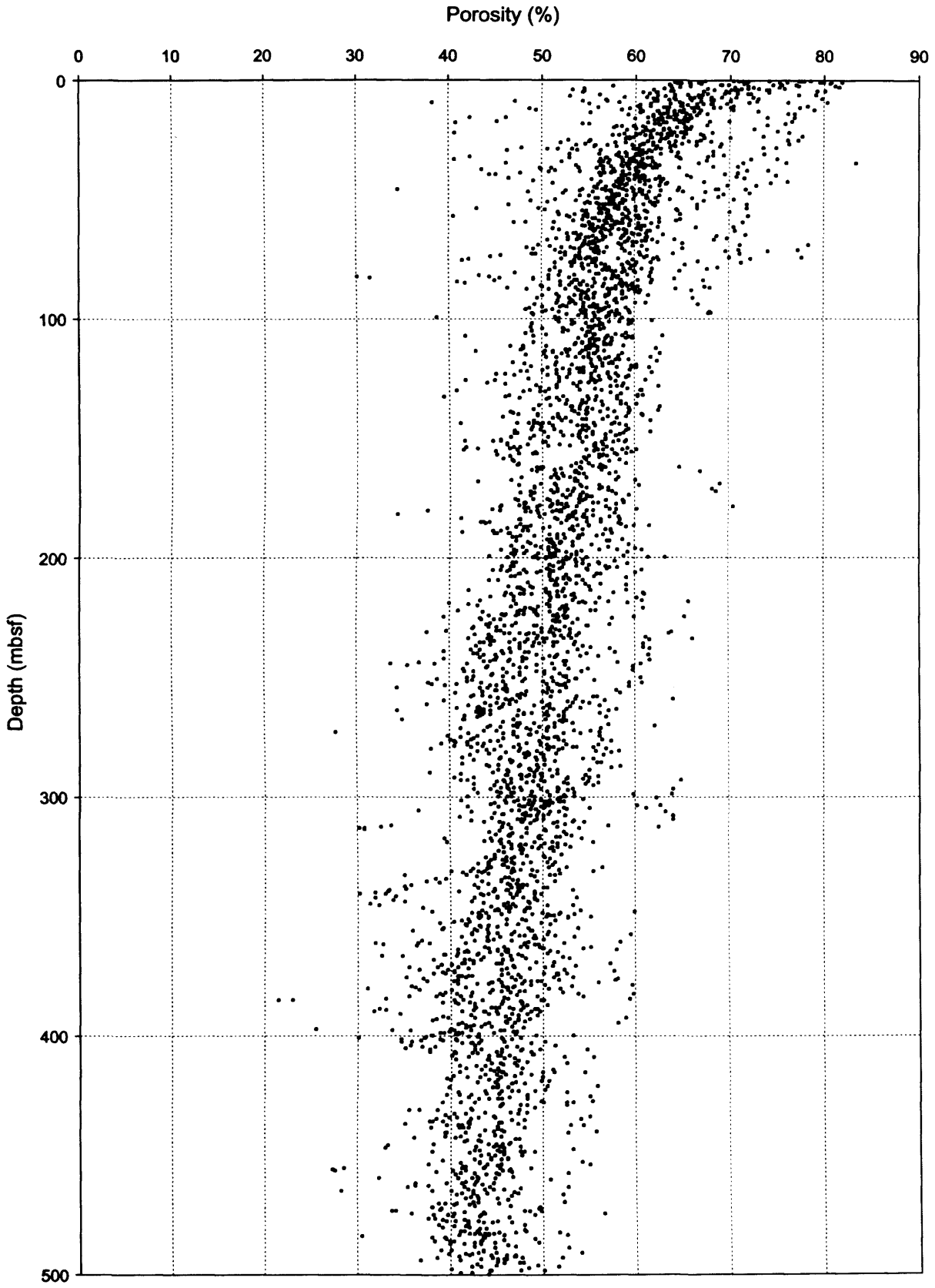

Figure 4.6 Plot containing porosity-depth data from 16 hemipelagic sequences drilled by the ODP and IODP.

4.4.3.1 Porosity-depth plot 1 – ODP Site 717

Porosity-depth plot 1 (Fig. 4.7) records hemipelagic deposition since the Miocene in the distal Bengal Fan, 750km south of Sri Lanka, and roughly 2500km south of the Ganges-Brahmaputra Rivers, the principal terrigenous sediment source to the area (Cochran et al., 1988). Porosity data from porosity-depth plot 1 reveals a trend of decreasing porosity with depth. Values determined for the first 150 m of sediment show a significant range of values from ~40-75%. This interval corresponds to a unit of variable lithology which includes coarser grained silty turbidites. Silt- and sand-rich sediments are seen in Fig. 4.3 to have lower initial porosities than clay-dominated sediments, and are thought to be the likely cause of this data scatter in this interval. Below 150 mbsf, sediments switch to largely uniform silty-clay facies, a shift which is clearly reflected in the better constrained distribution of porosity values of typically only 15-20%.

4.4.3.2 Porosity-depth plot 2 - ODP Site 900

Porosity-depth plot 2 (Fig. 4.7) records porosity and lithology data from Site 900 on the Iberia Margin, located approximately 175km seaward of the shelf-slope break in 5036m of water. Biostatigraphic data provide well-constrained ages for this sequence, with the lowermost units dated to early Miocene age (Sawyer, et al., 1994). Relatively high-frequency lithological variability (1-5m scale) is noted from core-descriptions at this site and may be responsible for shifts in the distribution of porosity seen in porosity-depth plot 2. This 500m thick sequence of nannofossil-rich clayey facies shows porosity values of around 65% in the first 25m of sediment corresponding to an interval of largely clay dominated sediment. Porosity loss within the shallowest part of the sequence follows a linear trend (*see* Fig. 4.8) contrasting with the exponentially decreasing trend of other plots. This trend continues to a depth of 500 mbsf where values of 35-45% are recorded. The distribution of porosity values with depth is reasonably well constrained for the entire sequence within a range of approximately 10%, however shifts in this general trend may correspond to changes in bulk lithology, such as that seen at 250 mbsf depth.

4.4.3.3 Porosity-depth plot 3a - 3d - ODP Sites 931, 935, 936, and 944

Porosity-depth distributions for four individual sequences drilled in the south Atlantic, and separated by distances of upto 160km, are shown in Porosity-depth plots 3a-3d (Fig. 4.7). All four sequences record Pleistocene age sediment columns of between 375 mbsf and 425 mbsf, each displaying laminated silt-rich facies in various configurations (Flood et al., 1995).

Porosity values close to the seafloor are between 70-80% for all four sequences, correlating to intervals of laminated silty-clay or silty-clay facies. The distribution of porosity values within the initial 75-100 m of three of the sediment columns appear to lie within ranges which can be well described by exponential trends (Fig. 4.9). Within this interval, porosity scatter is limited to ~5% suggesting that measured samples from at least three of the sites may have experienced a similar porosity loss history. Below depths of ~100 mbsf, all four sequences reveal an interval of more significant porosity scatter. Porosity-depth plot 3a records a subtle shift in the trend of porosity values from a depth of 250 mbsf where values increase steadily with depth down to 425 mbsf. This depth range corresponds with an interval of finer facies and the disappearance of sand intervals present above 250 mbsf. This porosity trend may be recording undercompaction resulting from overpressured pore fluids unable to escape from this clay-rich portion of the sequence. Porosity-depth plot 3b also reveals an increase in porosity values within the interval from 270-320 mbsf, coinciding with a zone of lithological variability. Increased volumes of calcareous material in the interval 275-295 mbsf may have retained higher porosities than the surrounding sediments, producing the trend seen in porosity-depth plot 3b, or similarly, these increased values may record an overpressured compartment. Porosity-depth plot 3c records a steady decline in porosity values from 50-30 mbsf. At 300 mbsf a pronounced increase in values corresponds with a clear shift towards a siltier facies at the same depth. It is possible that this lithological boundary may be acting as an upper seal to a compartment of moderately overpressured pore fluids below 300 mbsf. Porosity-depth plot 3d records an interval of rapidly decreasing porosity from 180-240 mbsf, followed by interval of increasing porosity values from 240-310 mbsf. This pattern of data might be expected if the rapid compaction of the interval from 180-240 mbsf has limited the escape of fluids from the interval directly beneath leading to the development of a zone of overpressure below 240 mbsf.

4.4.3.4 Porosity-depth plot 4 – ODP Site 976

Porosity-depth plot 4 (Fig. 4.7) corresponds to Site 976 which was drilled 60km south of Malaga in slope sediments of the western Mediterranean, in a water depth of 1107m. The first 350m of porosity-depth plot 4 is dominated by a mixture of Plio-Pleistocene aged nannofossil-rich clay and more silty-clay facies (Comas et al., 1996). Porosity values within this unit are distributed over a range of 10-15% at any single depth and show absolute values of ~70% at the seafloor. The general distribution of porosity values decreases with depth however the uppermost 150m of sediment do not follow either to an exponential or linear trend (Fig. 4.7). Below this depth however, the data is adequately described by a linear trend. A number of measured porosities lie above this general scatter of values at depths

ranging from 60-300 mbsf. These points may represent either the existence of coarser grained facies, or the existence of thin intervals of underconsolidated sediment. Porosity data is limited below 360 mbsf owing to poor core recovery; however measurements made below this depth show a marked reduction in porosity compared to values from the finer grained units deposited above. Late Pliocene sediments below 360 mbsf contain elevated levels of silt and sand, and it is these sediments which are likely to be responsible for the lower porosities seen. These sediments will have developed very different depositional porosities to those of the more clay-rich rocks above and are expected to have experienced markedly different compactional histories. This plot is reproduced again in Fig. 4.10 where hypothetical 'compactions curves' have been added to show the possible effect on porosity trends of a more uniform sedimentary sequence without the pronounced lithology shift at 300 mbsf.

4.4.3.5 Porosity-depth plot 5 – ODP Site 977

Porosity-depth plot 5 (Fig. 4.7) was drilled 210km east of porosity-depth plot 4 in the western Mediterranean roughly 80km south of the Spanish mainland. The plot shows the distribution of porosity from a 500m thick, apparently relatively homogeneous, hemipelagic sequence of clays and nannofossil oozes recording sedimentation since the early Miocene (Comas et al., 1996). Porosity values at the seafloor show absolute values of ~70-75% with relatively little scatter compared to other sequences. Values experience a marked reduction with depth over the first 150m of sediment, falling rapidly to values of 50-60% at 150 mbsf. A stronger degree of scatter exists between 150-200 mbsf, which does not appear to correlate with any significant lithological heterogeneity, however subtle shifts in the proportion of silt and biogenic material may be capable of producing such trends.

4.4.3.6 Porosity-depth plot 6 – ODP Site 979

Porosity-depth plot 6 (Fig. 4.7) was also drilled in the western Mediterranean half way between porosity-depth plot 4 and porosity-depth plot 5. The drill-site is located in a small, elongate, intraslope basin lying 50km north of the northern Moroccan coastline. Porosity-depth plot 6 records a porosity distribution very similar to that of porosity-depth plot 5, albeit with a slightly increased degree of scatter, through comparable sediments of Plio-Pleistocene age (Comas et al., 1996). Porosity values at, or close to, the seafloor are ~70% and show a largely linear reduction with increasing depth (Fig. 4.8). Again, in the absence of any recorded shifts in lithology, it seems feasible that the scatter of values seen in porosity-depth plot 5 is either a result of unresolved changes in grain-size distribution, or the effect of other mechanisms such as cementation or localised undercompaction.

4.4.3.7 Porosity-depth plot 7 – ODP Site 985

Porosity-depth plot 7 (Fig. 4.7) was drilled in 2788m of water on the gentle northern slope of the Iceland Plateau, 250km northeast of the Icelandic shelf in the southern Norwegian Basin. Data in porosity-depth plot 7 reveal an excellent example of how lithology likely influences the loss of porosity with depth within a hemipelagic sequence. Within the top 100m of sediment (Plio-Pleistocene), silty-clays record porosity values with a range of up to 30% at a single depth (Jansen et al., 1996). Given the shallow depth of this interval it seems likely that this scatter of porosity values has been inherited from a wide range of depositional porosities, expected to be strongly influenced by the nature of deposited lithologies (*see* Fig. 4.3). Below this interval of scatter, sediments record a thick sequence of Miocene sediments in which the distribution of porosity values at a given depth becomes better constrained, dispersed over a range of only 10-15% (Jansen et al., 1996). However, there are several significant shifts in the trend of this distribution which correlate well with distinct lithological changes. The most prominent of these is an interval between 250 mbsf and 300 mbsf, where high porosity values remain relatively constant within a rare interval of diatomaceous clay. Porosity measurements from this interval record high porosity values upto 80%, exceeding those measured within even the top 100m of the sediment column. This preservation of porosity is somewhat ambiguous, and may be in response to a number of mechanisms. One possibility is that this trend reflects the resistance of the interval to pore-collapse perhaps resulting from the framework strength of its biosiliceous diatom fraction, as discussed in section 4.4.1. Other possibilities include the development of overpressured pore-fluids leading to undercompaction, or simply that a graded sequence of sediments has reached a similar state of porosity at a range of depths. The lowermost portion of the sequence shows a more familiar linear reduction in porosity with depth through a 200m interval of clay-rich facies, suggesting that either heterogeneities are not present, or that they have been smoothed out of the sequence by the increased degree of vertical load, inducing strain. Porosity-depth plots 8 and 9 are not discussed in any detail in the text.

4.4.3.8 Porosity-depth plot 10 – ODP Site 1146

Porosity-depth plot 10 (Fig. 4.7) was drilled in upper slope sediments of the northern South China Sea margin, roughly 400km southeast of the Pearl River mouth, which supplies much of the areas terrigenous material. The upper 300m of sequence correspond to Plio-Pleistocene deposition, underlain by late Miocene units (Wang et al., 2000). Like that of porosity-depth plot 7, the general trend of porosity distribution with depth for porosity-depth plot 10 shows a correlation with changing lithology. The 500m thick sequence is dominated

by mixtures of nannofossil-rich clay facies and nannofossil oozes for which porosity values show a much smaller degree of scatter than many of the previously described porosity-depth plots (e.g. porosity-depth plot 1, porosity-depth plot 6). Measured porosity values at the seafloor are in the region of 80%, but fall away linearly throughout the top 150m of sediment (Fig. 4.8). Sediment buried to a depth of between 150 mbsf and 250 mbsf shows porosity values which increase slightly with depth suggesting that increasing values represent sediment that has either undergone a slower rate of porosity loss over the period of burial, or which began with a higher depositional porosity than immediately overlying sediments. Below this interval, the distribution of porosity once again follows a familiar trend of decreasing values with depth, marked by a shift in dominant lithology towards a more carbonate-rich facies, containing a higher proportion of foraminifers.

4.4.3.9 Porosity-depth plot 11 – ODP Site 1148

Porosity-depth plot 11 (Fig. 4.7) corresponds to ODP Site 1148, also drilled on the northern margin of the South China Sea, located 80km down-slope of porosity-depth plot 10 in 3291m of water. The lowermost sediments of porosity-depth plot 11 are of late Oligocene age making it one of the oldest sequences studied here, however the distribution of porosity with depth is similar to a number of the previously described Plio-Pleistocene aged sequences (porosity-depth plot 5, and porosity-depth plot 13) (Wang et al., 2000). The relationship between porosity distribution and age is discussed in section 4.5.3. Initial porosity values of approximately 80% fall-away rapidly to a depth of 225-250 mbsf. This trend ends rather abruptly just below 250 mbsf, but with no clear corresponding shift in lithology or bulk grain-size distribution. Down to a depth of 350 mbsf, porosity values then remain remarkably constant showing only a very slight range of scatter. Given the uniformity of the lithological sequence and the absence of diatomaceous sediments, this apparent 'preservation' of porosity may simply signify that this particular interval has not been significantly influenced by the addition of 100m of overburden or, as in porosity-depth plot 7, it may indicate the development of overpressured pore fluids.

4.4.3.10 Porosity-depth plot 12 – ODP Site 1245

Sediments investigated in porosity-depth plot 12 (Fig. 4.7) were drilled in 875m of water, 85km west of the Oregon coastline. The sequence records Pleistocene sedimentation towards the base of the continental slope, on the western flank of Hydrate Ridge (Tréhu et al., 2003). Porosity values for porosity-depth plot 12 are distributed over a fairly small range at any particular depth interval, with only a small number of measured points lying outside of

this range. From the seabed to 150 mbsf a linear trend of decreasing porosity with increasing depth exists (Fig. 4.8). Between the depths of 75 mbsf and 200 mbsf there are a number of intervals where porosity values deviate from this largely linear 'best-fit'. The top of this 125m interval coincides with a shift in lithology from a mixture of silty-clay with thin sand layers, to a much more clay-dominated facies. Perhaps unsurprisingly, porosity values within the underlying clay-dominated facies remain higher than those in the overlying coarser grained unit producing the observed increase in porosity values with depth. A similar distribution of porosity values is seen at 200 mbsf where values again appear to increase with depth, possibly as a result of a shift in the bulk lithology. Although in this case, this shift is more subtle, with sediments showing only an overall minor increase in silt content, which is perhaps insufficient to explain the observed trend.

4.4.3.11 Porosity-depth plot 13 – IODP Site 1324

Porosity-depth plot 13 (Fig. 4.7) represents a portion of the Pleistocene sequence drilled at IODP Site 1324 in the Mars-Ursa Basin, Gulf of Mexico (Flemings et al., 2006). The sequence records a relatively heterogeneous succession of predominately siliciclastic sediments dominated by clays and silts with subordinate thin-sands. The porosity values from this particular sequence display a trend which is perhaps closest to the classic 'compactional' trends inferred by many authors. Values are highest at the seafloor, becoming progressively lower with increasing depth. Porosity data show a relatively small scatter of 5-10% for given depths and appear to fit well to an exponentially decreasing trend (Fig. 4.9). Shifts in lithology within the upper 300m are subtle and are not clearly registered in the general distribution of porosity values. A single porosity measurement at 305 mbsf correlates with a 1m thick sand unit and records a porosity value significantly removed from surrounding measurements. Below roughly 300 mbsf, facies become coarser grained and are dominated by silty-clays, silts, and silty-sands. Porosity values below 300 mbsf decrease linearly.

Investigations by Flemings et al. (2008) found that the uppermost 200m of clay-dominated sediment at this location are overpressured. Pore fluid pressures in this clay-dominated interval are at 70% of the hydrostatic effective stress, indicating that they are overpressured by up to 2 MPa (Flemings et al., 2008). Below 200 mbsf, pore fluid pressure begins to fall to 60% of the hydrostatic effective stress, coinciding with the coarser grained sediments found below these depths. High sedimentation rates are thought to be responsible for overpressures, by not allowing fluids to escape from clay-dominated low-permeability

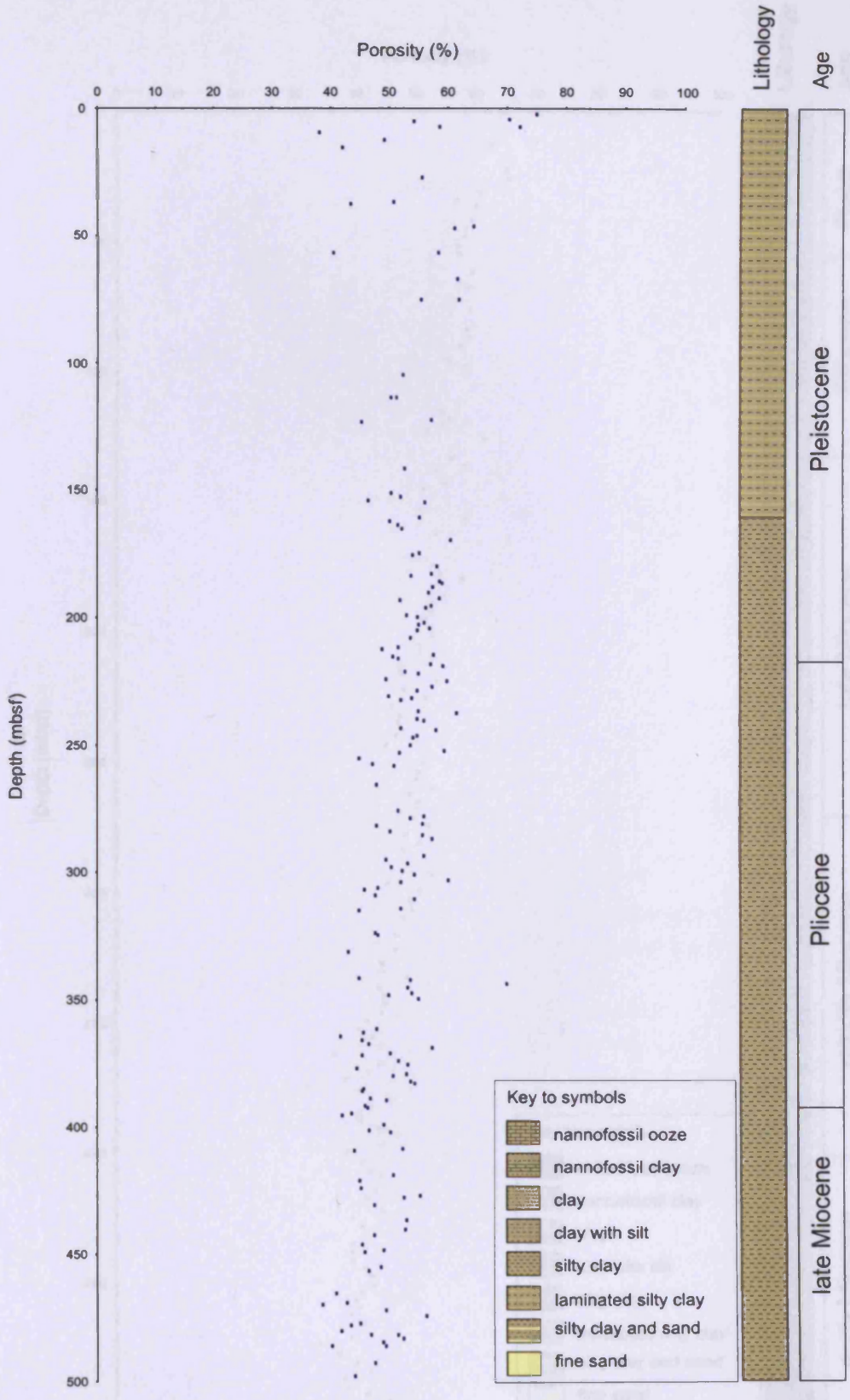

Figure 4.7
Porosity-depth plot 1 from ODP Site 717, Indian Ocean.

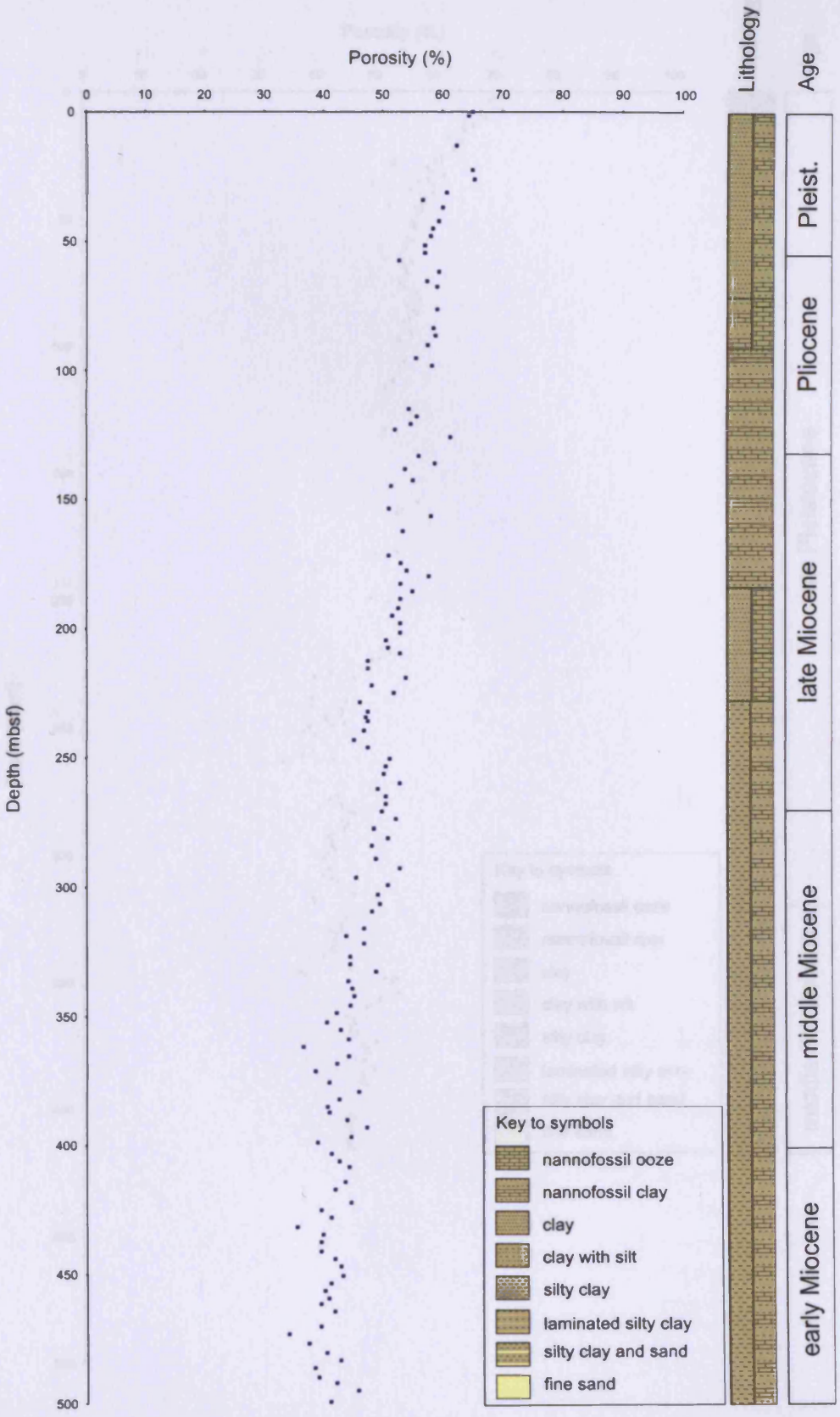

Figure 4.7 *cont.*
Porosity-depth plot 2 from ODP Site 900, Iberia margin.

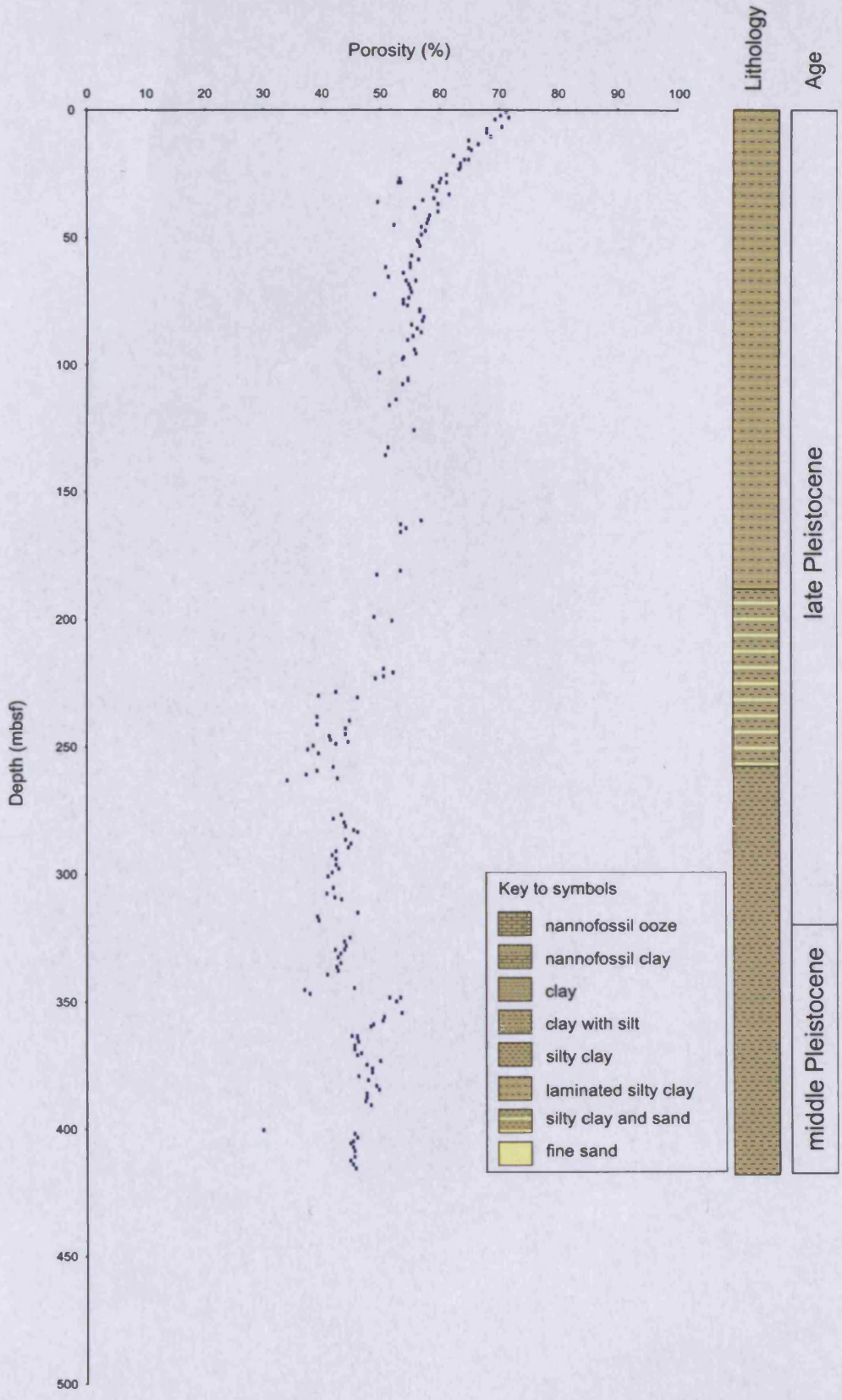

Figure 4.7 *cont.*
Porosity-depth plot 3a from ODP Site 931, Amazon Fan.

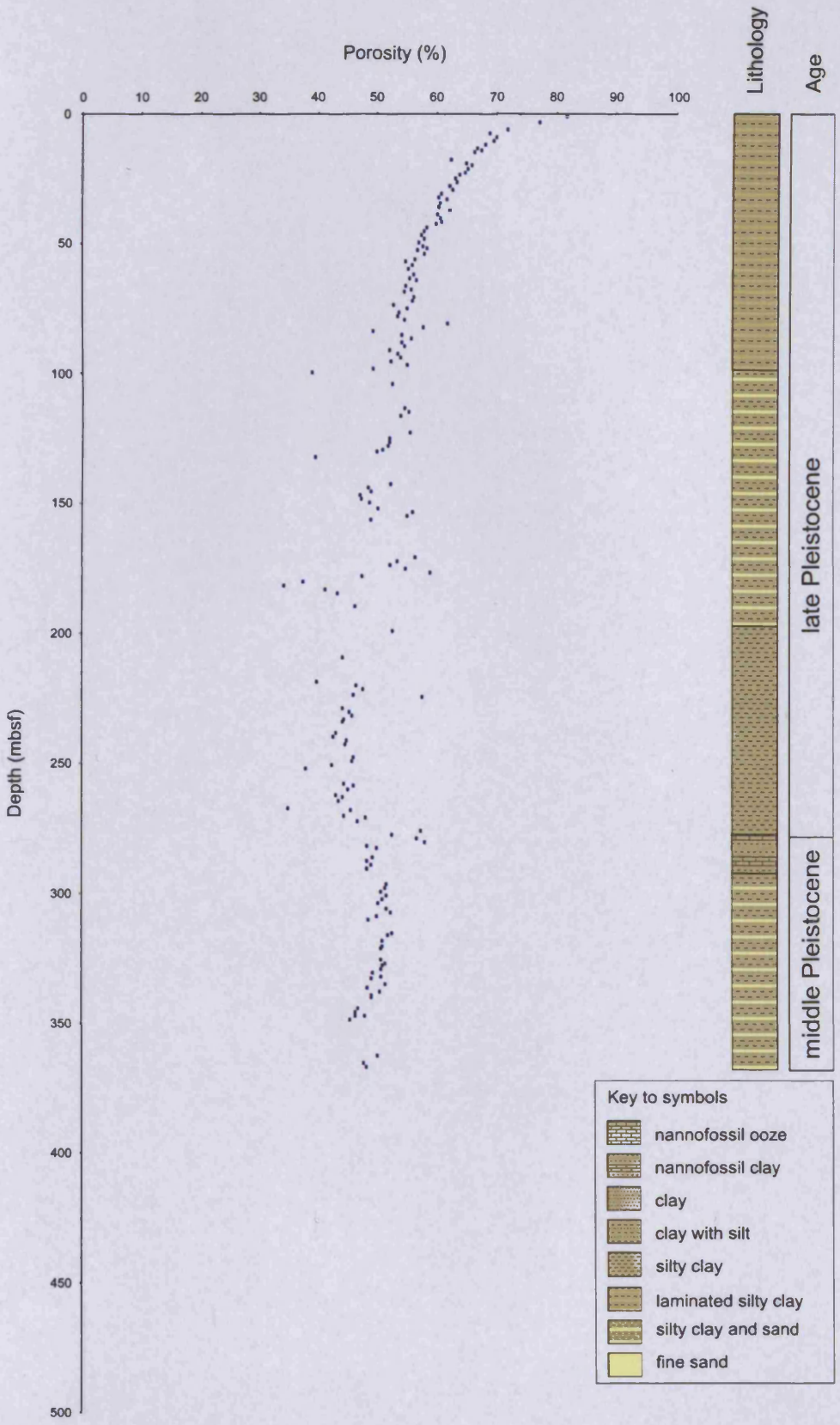

Figure 4.7 *cont.*
Porosity-depth plot 3b from ODP Site 935, Amazon Fan.

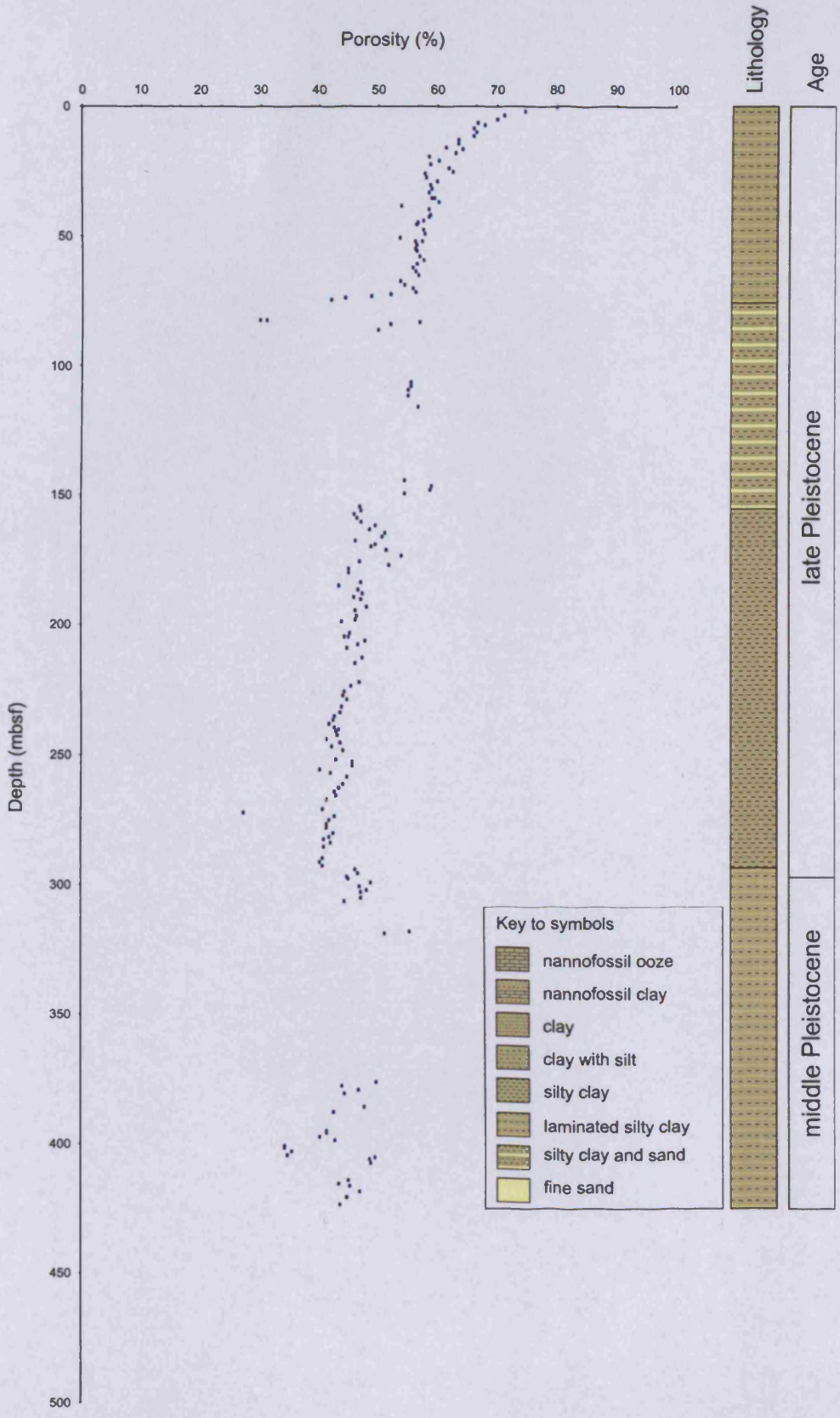

Figure 4.7 *cont.*
Porosity-depth plot 3c from ODP Site 936, Amazon Fan.

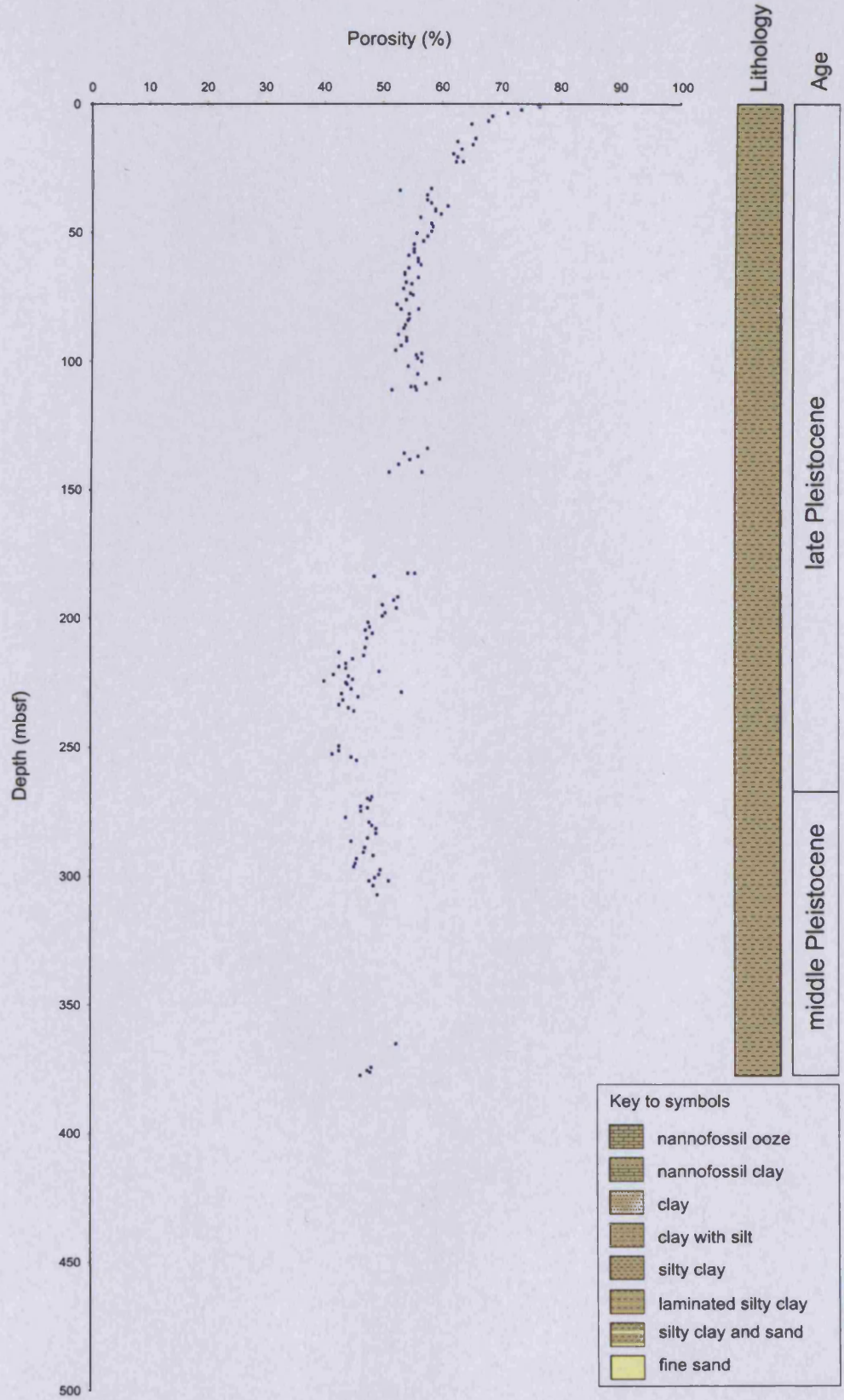

Figure 4.7 *cont.*
Porosity-depth plot 3d from ODP Site 944, Amazon Fan.

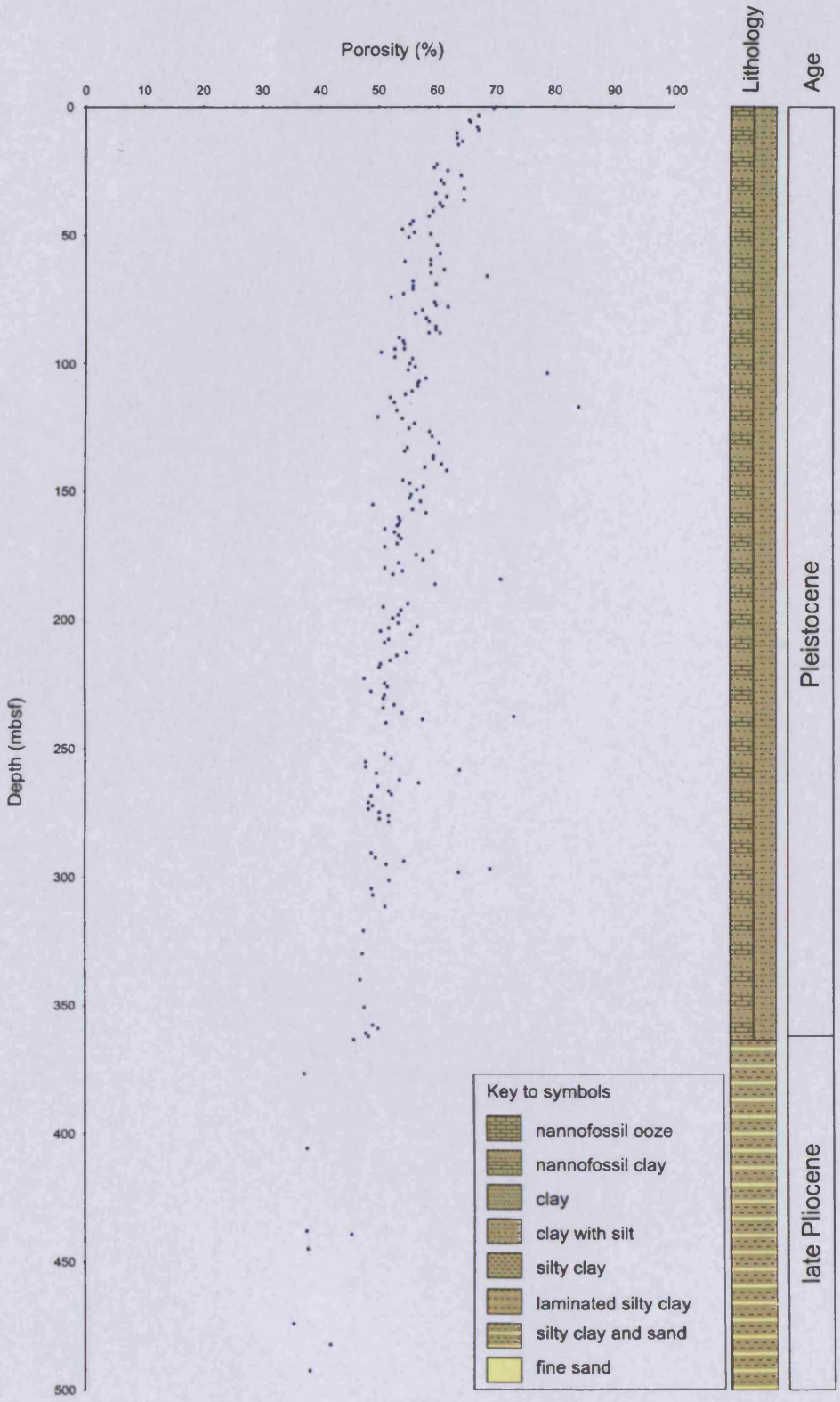

Figure 4.7 *cont.*
Porosity-depth plot 4 from ODP Site 976, western Mediterranean.

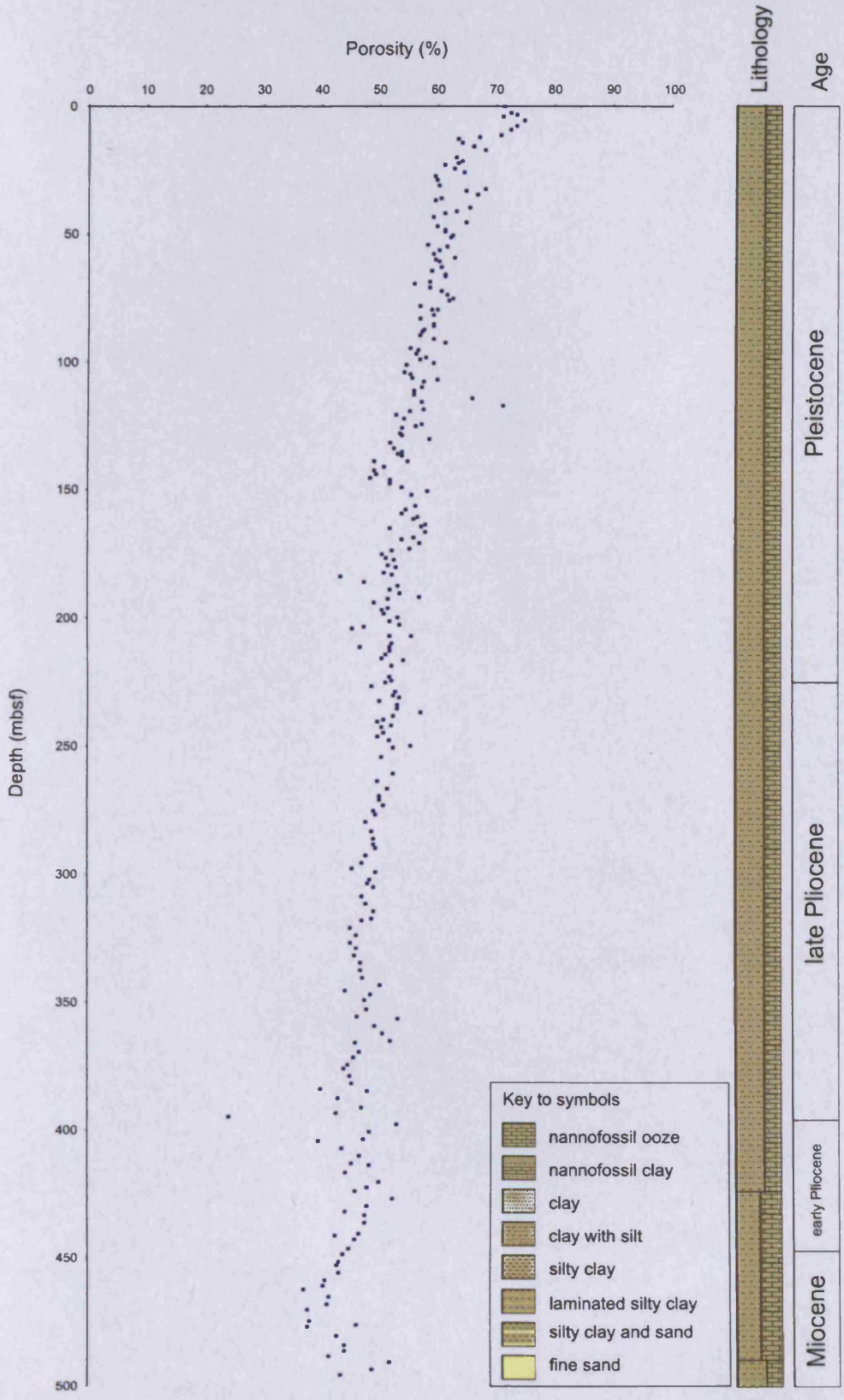

Figure 4.7 *cont.*
Porosity-depth plot 5 from ODP Site 977, western Mediterranean.

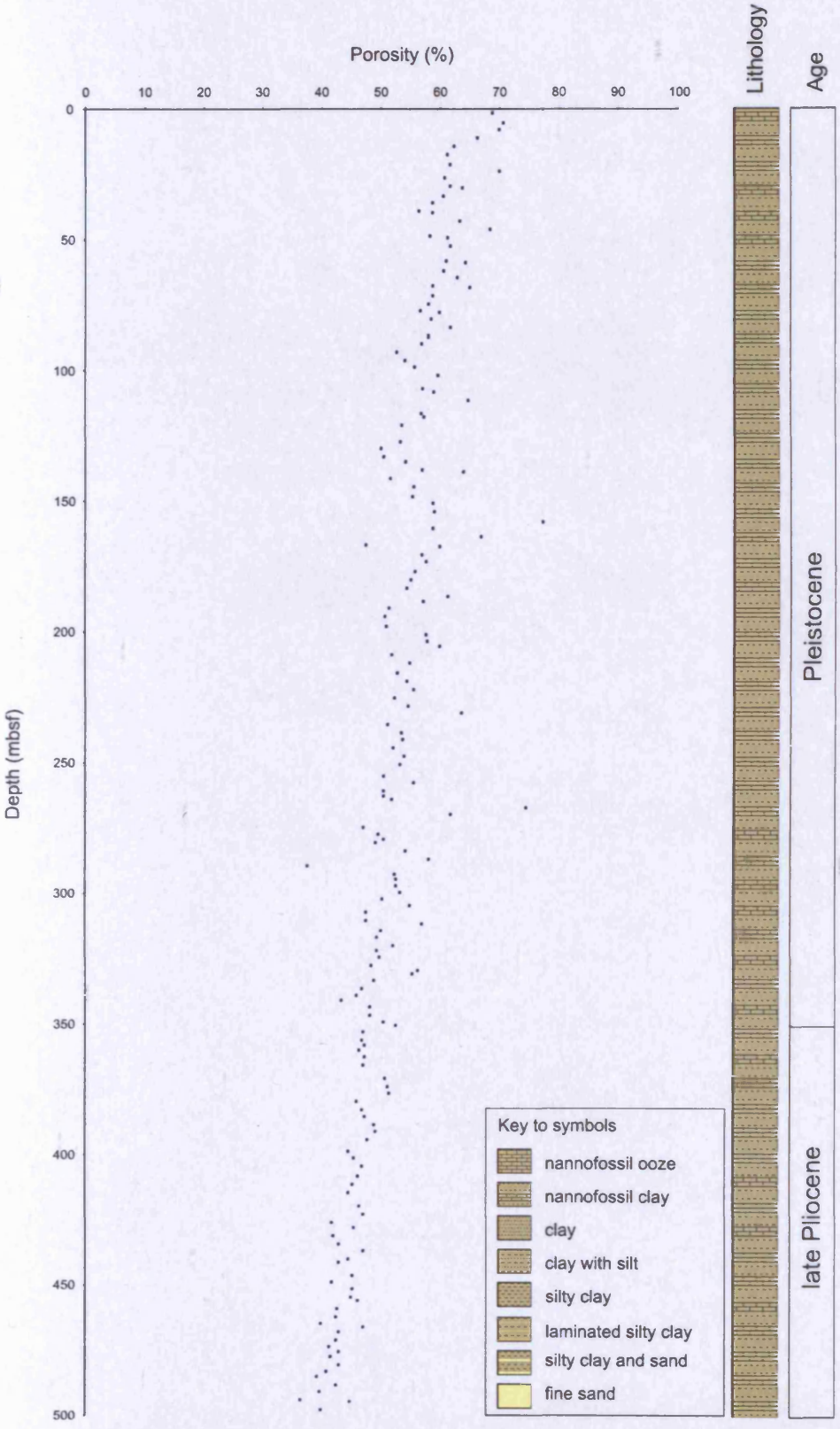

Figure 4.7 *cont.*
Porosity-depth plot 6 from ODP Site 979, western Mediterranean.

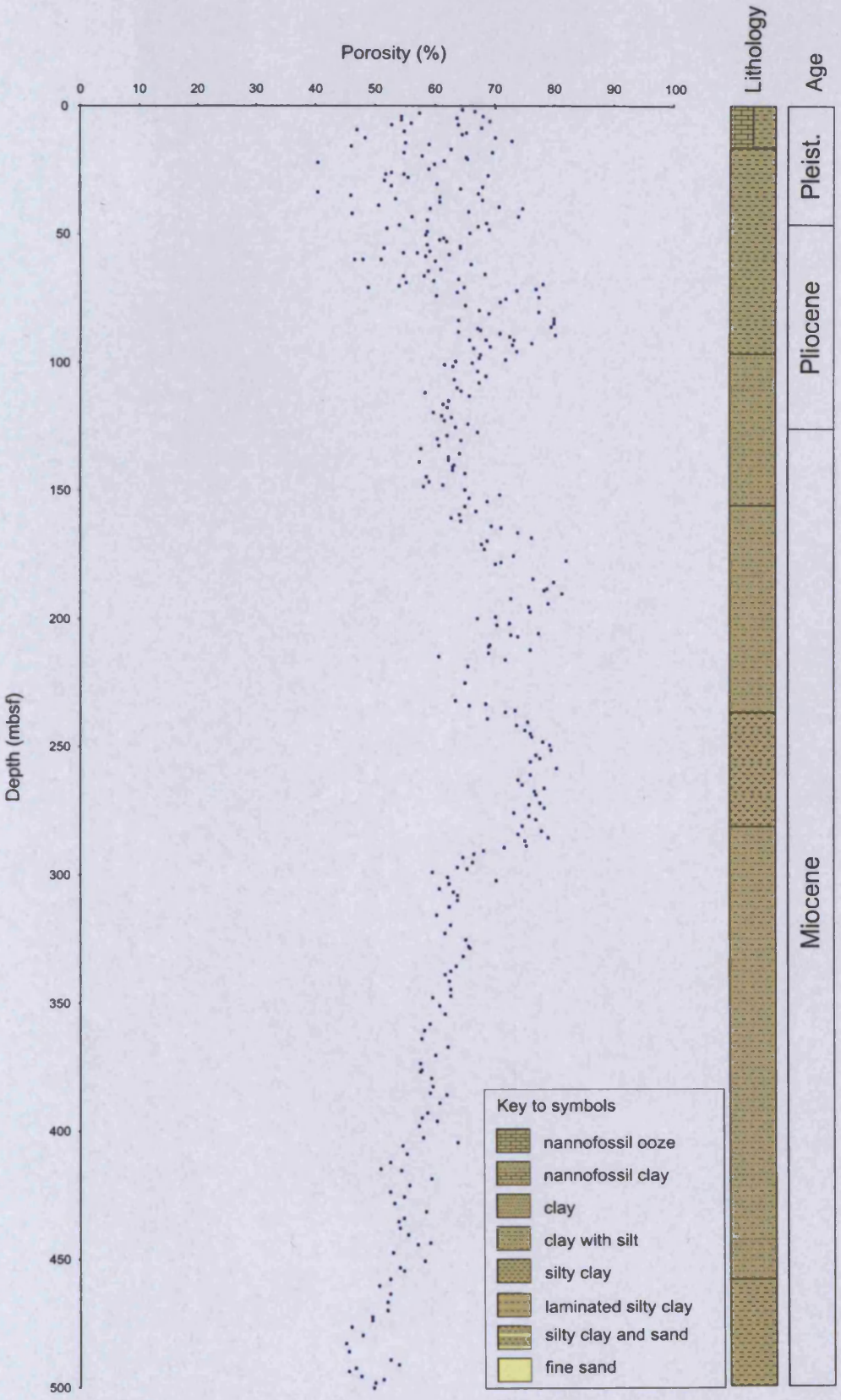

Figure 4.7 *cont.*
Porosity-depth plot 7 from ODP Site 985, North Atlantic.

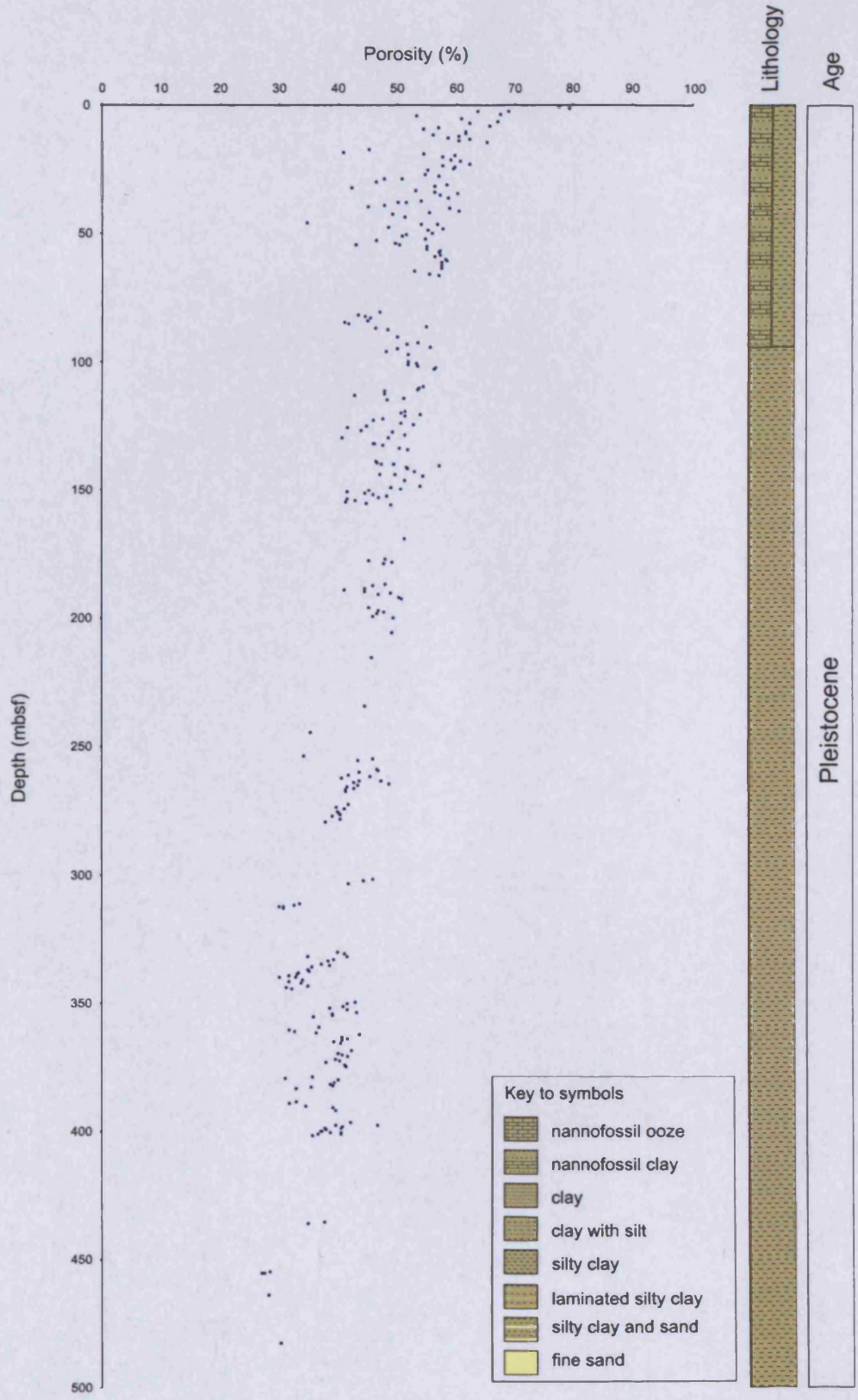

Figure 4.7 *cont.*
Porosity-depth plot 8 from ODP Site 986, North Atlantic.

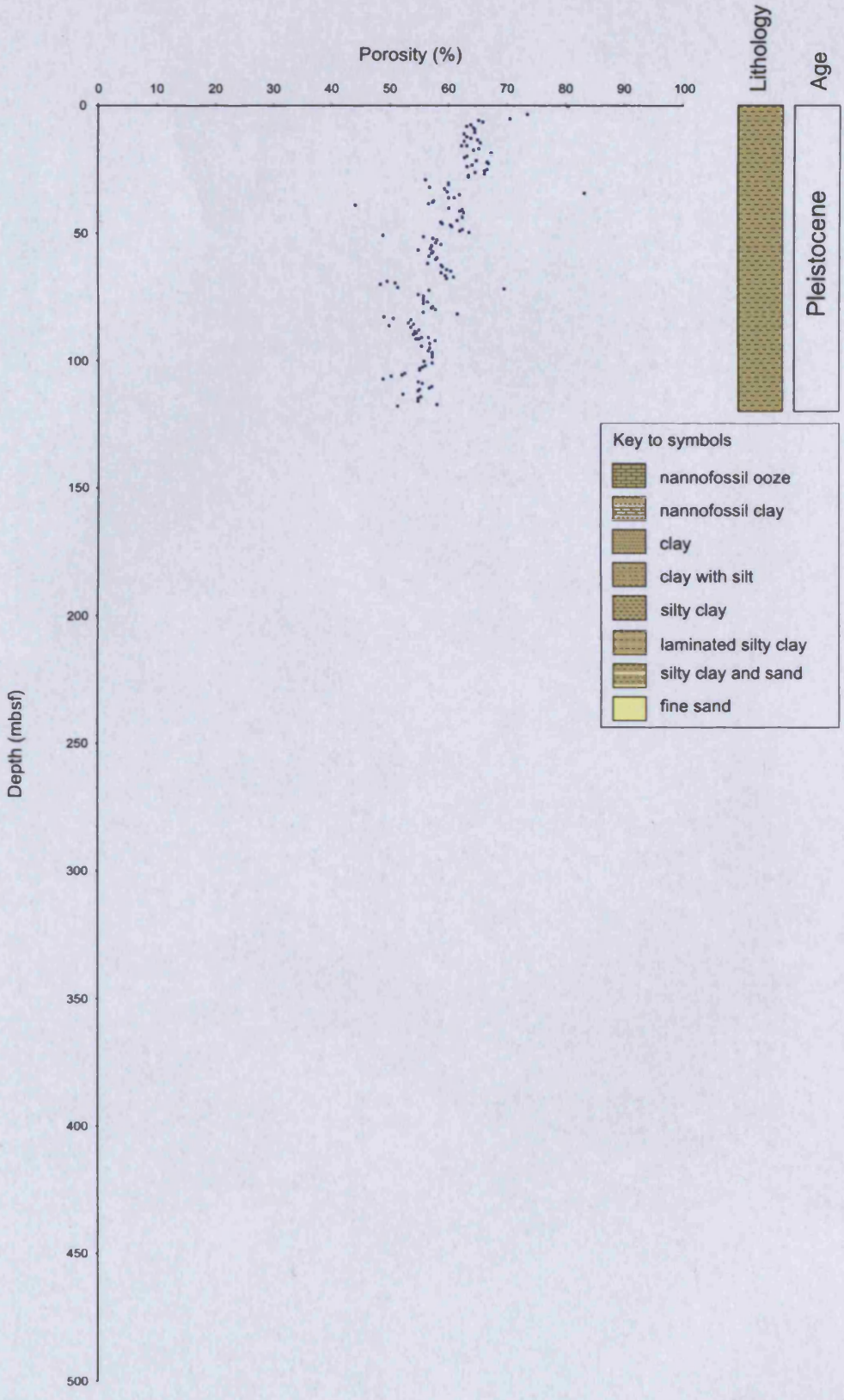

Figure 4.7 *cont.*
Porosity-depth plot 9 from ODP Site 1079, West Africa.

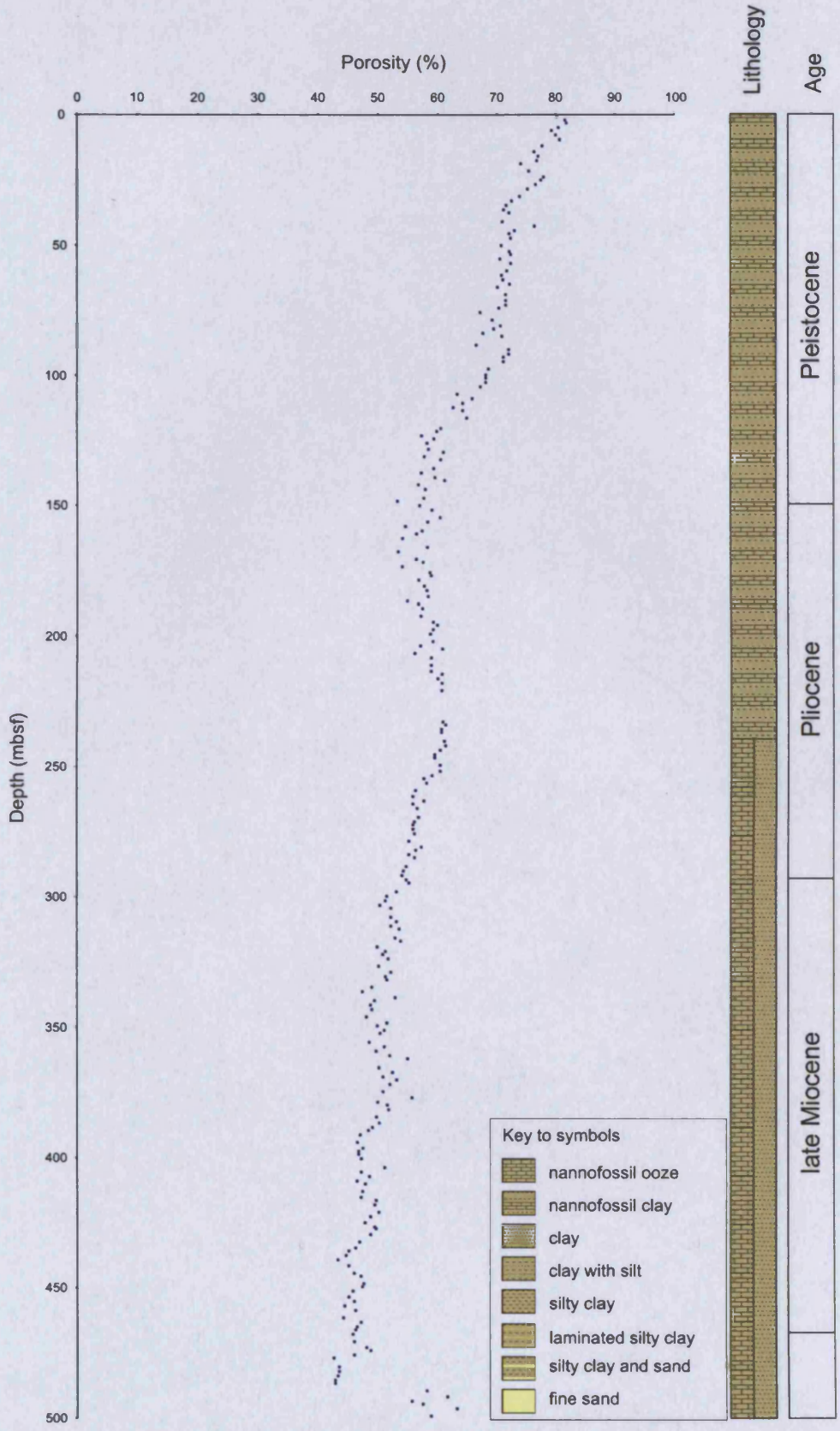

Figure 4.7 *cont.*
Porosity-depth plot 10 from ODP Site 1146, South China Sea.

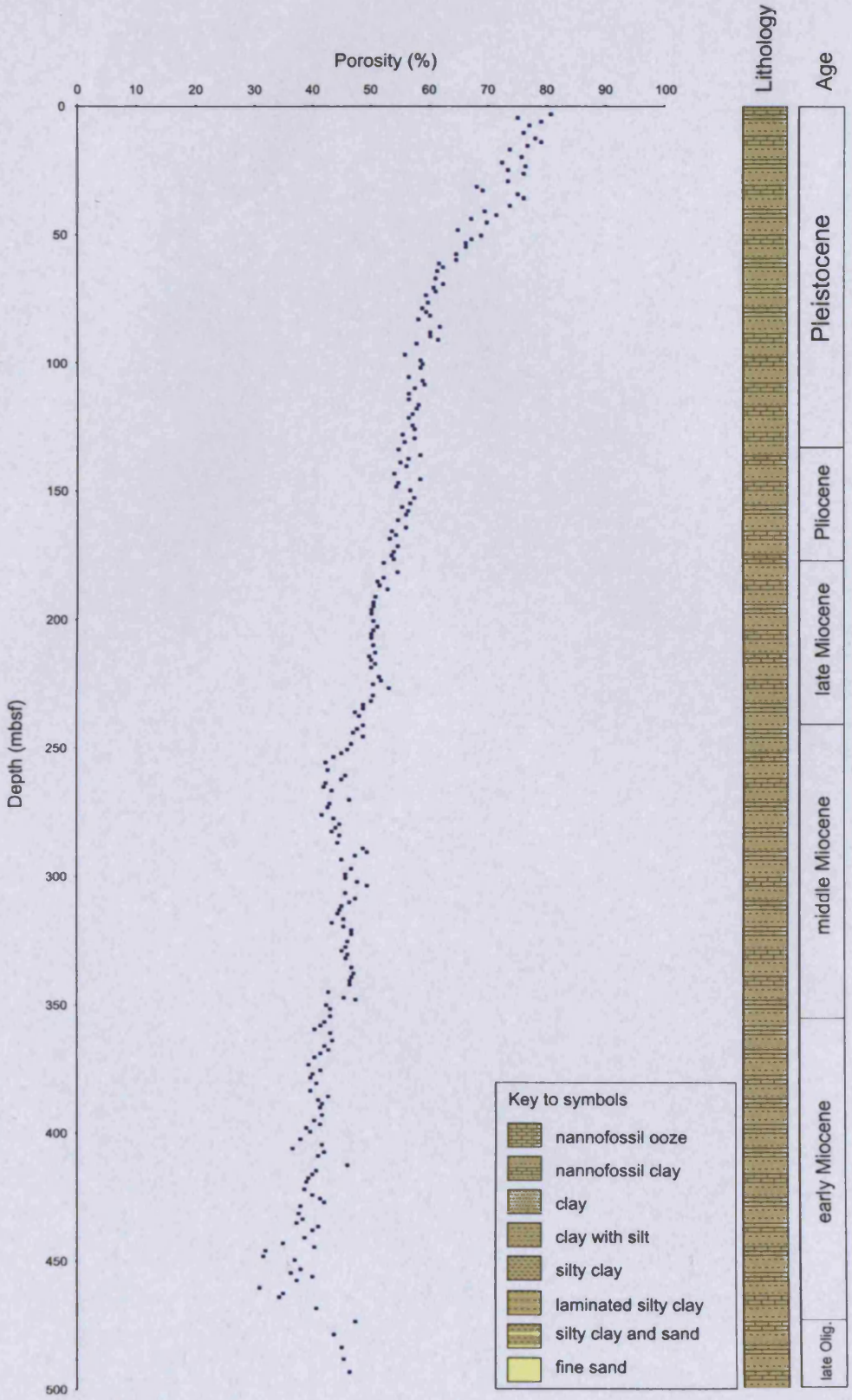

Figure 4.7 *cont.*
Porosity-depth plot 11 from ODP Site 1148, South China Sea.

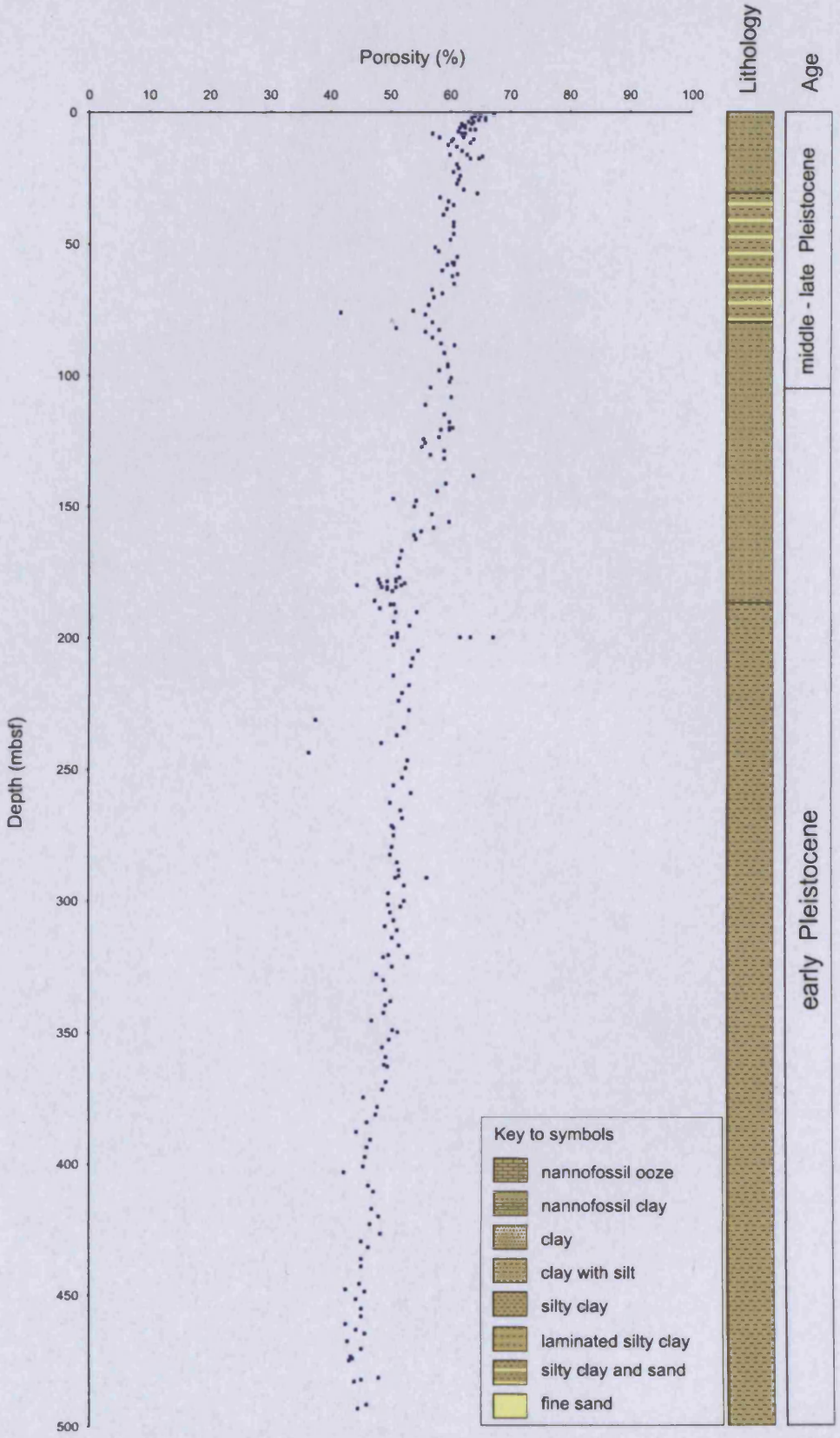

Figure 4.7 *cont.*
Porosity-depth plot 12 from ODP Site 1245, Cascadia margin.

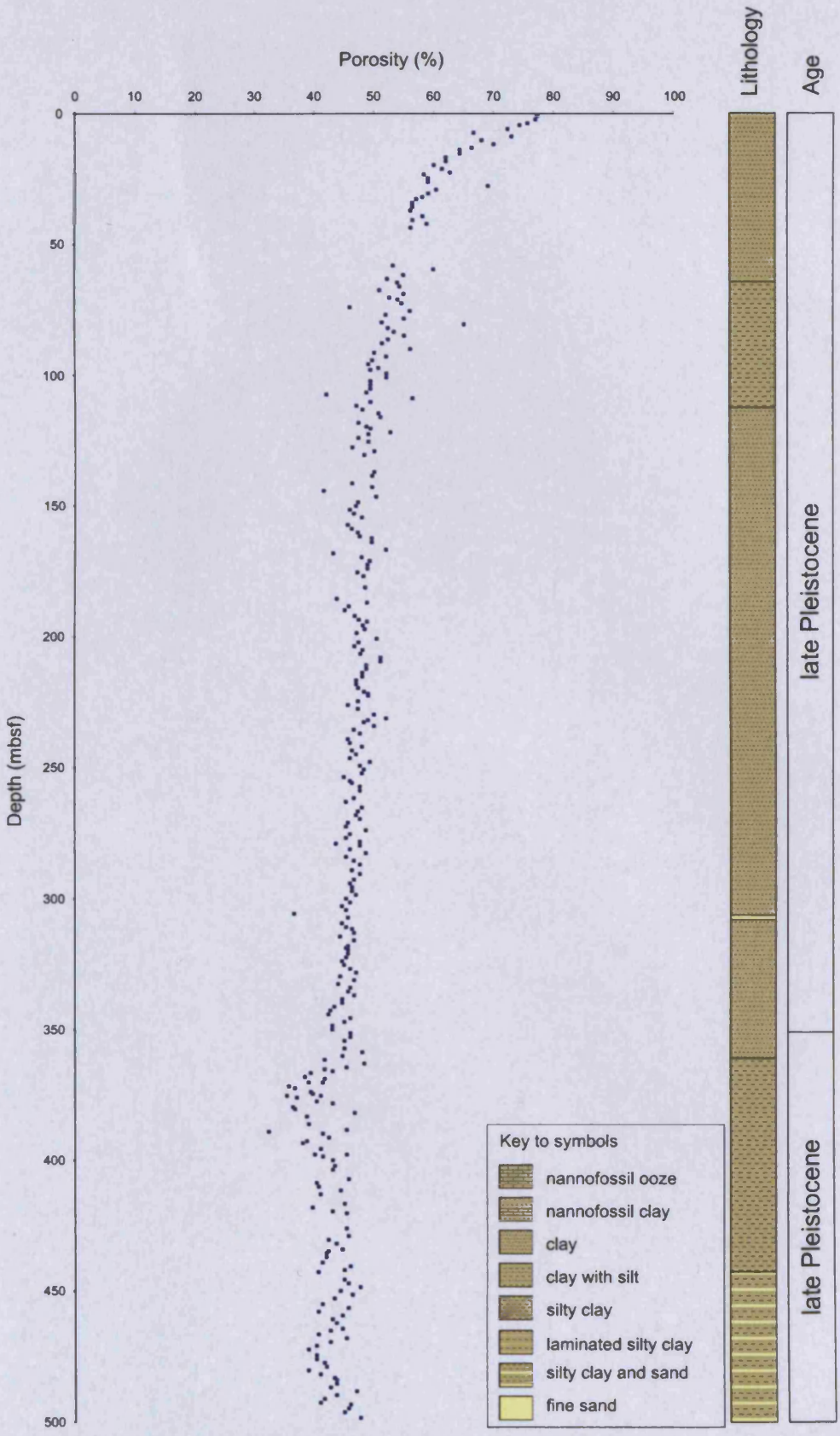

Figure 4.7 *cont.*
Porosity-depth plot 13 from IODP Site 1324, Gulf of Mexico.

hemipelagic sediment. Porosity-depth plot 13 is a rare example of a marine borehole where insitu effective stress and pore fluid pressure measurements have been acquired. Unlike previous porosity-depth plots, where such data is available, much better informed evaluations of porosity/depth/effective stress relationships can be made.

4.4.4 Summary of porosity-depth plots

From the sixteen hemipelagic sequences described above and shown in Fig. 4.7 (Plots 1-13) it is reasonable to conclude that at the shallow depths investigated here, clay-rich hemipelagic sediments typically experience a reduction in porosity with depth. A number of clay-dominated sites show rapid decreases in porosity within the first 100m of burial which are well described by exponential trends (Fig. 4.9), as noted by many authors for compactional trends in fine-grained sediments (e.g. Skempton, 1970; Baldwin and Butler, 1985; Velde, 1996; Bahr et al., 2001). Other plots reveal a more linear trend to falling porosity values within the first 100-200m of burial (Fig. 4.8). In a number of cases, porosity values go against the general trend of decreasing values with depth, and are seen to increase with increasing burial. In some examples, such deviations begin to occur in the same depth interval as changes in the sequences bulk facies type e.g. Porosity-depth plots 3a (250 mbsf), 3b (270 mbsf), 3c (75 mbsf and 300 mbsf), 4 (360 mbsf), 7 (240 mbsf and 300 mbsf), 10 (240 mbsf), 12 (80 mbsf), and 13 (360 mbsf). Where this correlation can be made, increases in the trend of porosity values may be as a result of contrasting facies having different depositional porosities (e.g. siliceous clay and silty clay), and subsequently having undergone different porosity-depth pathways. Similarly, where facies characterised by high porosity values (e.g. clay) is underlain by coarser-grained sediments, the reverse is seen, producing a pronounced fall in porosity, as is sometimes observed (Fig. 4.10, Plot 10).

Trends of increasing or stable porosity values with increasing depth are also recorded within apparently uniform sedimentary sequences where facies changes are not documented e.g. Porosity-depth plot 3d (240m), 5 (150m), and 6 (130m). It is possible that high-frequency or subtle variations in facies type have not been detected or recorded from the sequence, if this were the case, discussions in the preceding paragraph would apply. However, intervals of overpressured pore fluids may also produce undercompacted sediment, and in the absence of facies variability, may more adequately account for the three examples mentioned above.

The absence of effective-stress data makes it difficult to differentiate between the effect of lithological heterogeneities and abnormal fluid-pressures even when facies changes clearly correlate with shifts in porosity-depth trends. It is possible that trends reflect the joint

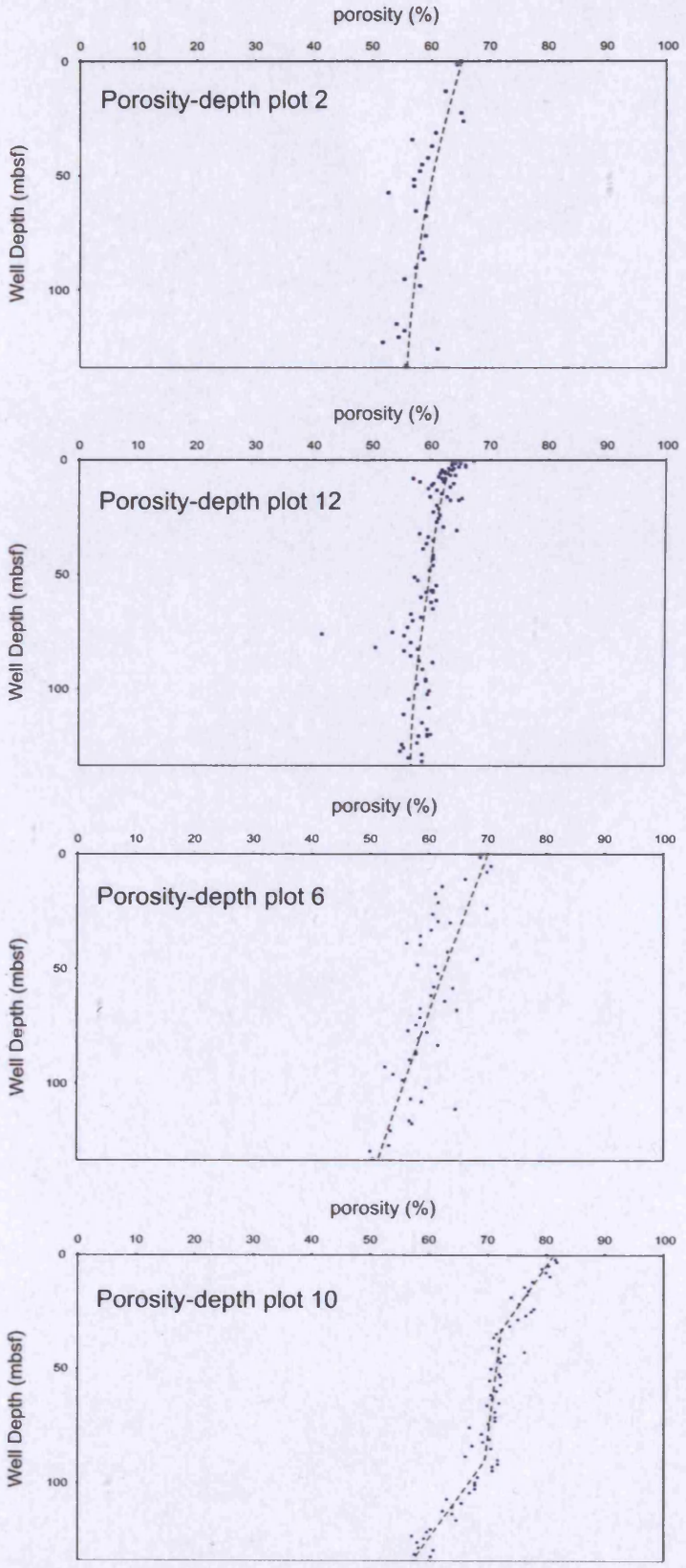

Figure 4.8 Porosity-depth plots from four ODP sites which reveal trends of non-exponential porosity loss at shallow depths. Trend lines added manually.

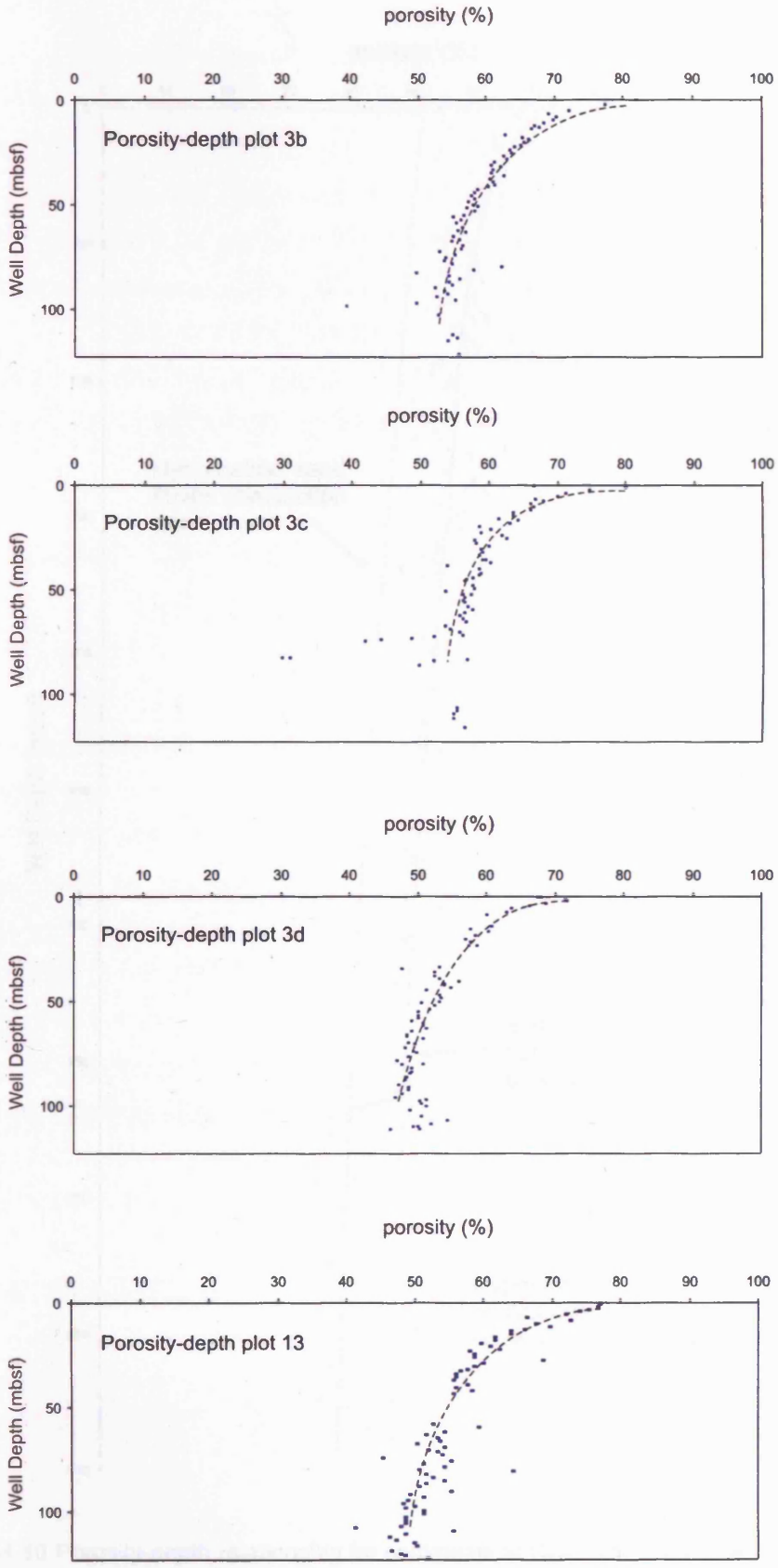

Figure 4.9 Porosity-depth plots from four ODP sites which reveal trends of exponential porosity loss at shallow depths. Trend lines added manually.

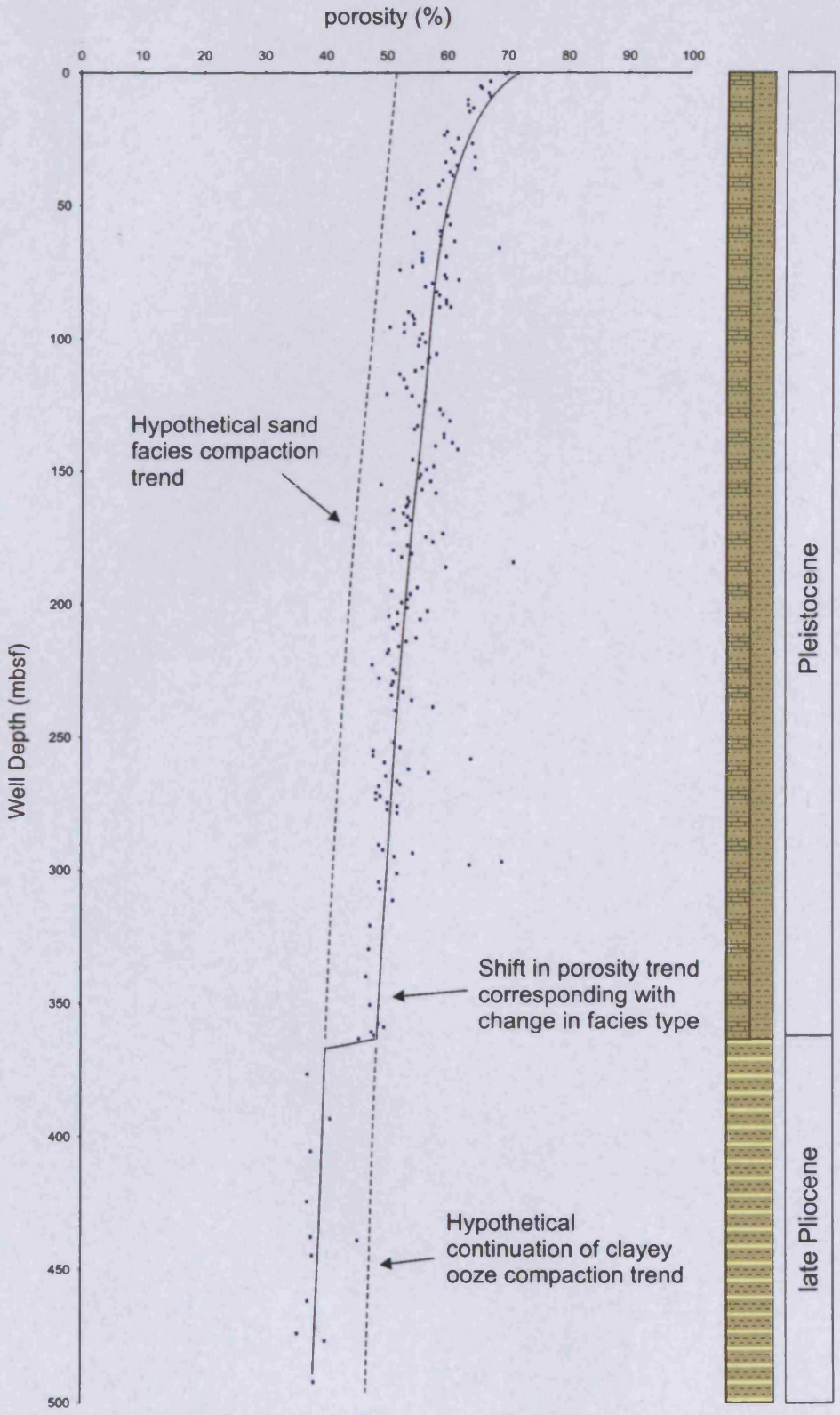

Figure 4.10 Porosity-depth relationship for sediments at ODP Site 976 in the western Mediterranean. A shift in the trend of porosity loss with depth (solid line) at 360m depth correlates with a change in facies from nannofossil clay to silt and sand. Dashed lines represent hypothetical 'compaction curves' for these two lithologically distinct units (*see* page 185 for lithology symbols).

influence of abnormal pore-fluids on sediments which have experienced varying porosity-trends. Porosity-depth plot 13 from the Gulf of Mexico is the only example here of a sequence which is known to be entirely overpressured (Flemings et al., 2008). Without pore pressure data, the low degree of data scatter and the lithological homogeneity of this sequence provide few clues as to the pressure state of pore fluids, highlighting the difficulties of differentiating porosity shifts resulting from facies changes and overpressure. Although the exact cause of many of these porosity trend shifts remains ambiguous, it seems reasonable to assume that the physical properties (i.e. grain-size and fluid flow properties) of juxtaposed fine-grained facies represent an important control on the observed trends in porosity with depth.

4.5 Discussion

4.5.1 Initial porosities

Initial or 'depositional' porosity values are a critical input for basin analysis calculations examining basin histories and the prediction of overpressure and fluid-flow (Schneider et al., 1996; Gutierrez and Wangen, 2005; Bernaud et al., 2006). Commonly used 'default' initial porosity values for fine-grained sediments in decompaction calculations may, or may not accurately describe the sediments under investigation. Sclater and Christie (1980) used a value of 63% to parameterise the initial porosity of North Sea shales, reporting that "we are confident that the shales of the North Sea have a porosity of close to 63% near the surface". Similarly, modelling parameters set out by Mann and Mackenzie (1990) for the investigation of pore-fluid pressures uses 62.9% as an initial porosity value for shales, silty shales, shaley silts, as well as silts. Giles et al. (1998) and Avseth et al. (2005) both note the potential pitfalls of generic initial porosity values in modelling calculations.

Figure 4.11 shows the theoretical decompaction thicknesses of sediments based on a very simple model. In this example a 1m column of sediment buried to depth, with a porosity of 50% (therefore 50% solid grains and 50% fluid), has been 'decompacted' to a range of different initial porosity values. In each case the solid grain component, in this case 50cm thick, remains constant, while the volume of pore-water is seen to increase non-linearly with increasing initial porosities. Figure 4.11 illustrates that decompaction to an initial porosity value of 70% results in an expansion of this 1m of sediment to an original thickness of 1.6m. Importantly however, if an initial porosity of 80% is used, the original thickness of this 1m thick interval increases to 2.5m, and likewise for an initial porosity of 90%, this value increases markedly to 5m. Given the range of initial porosity values recorded from genuine

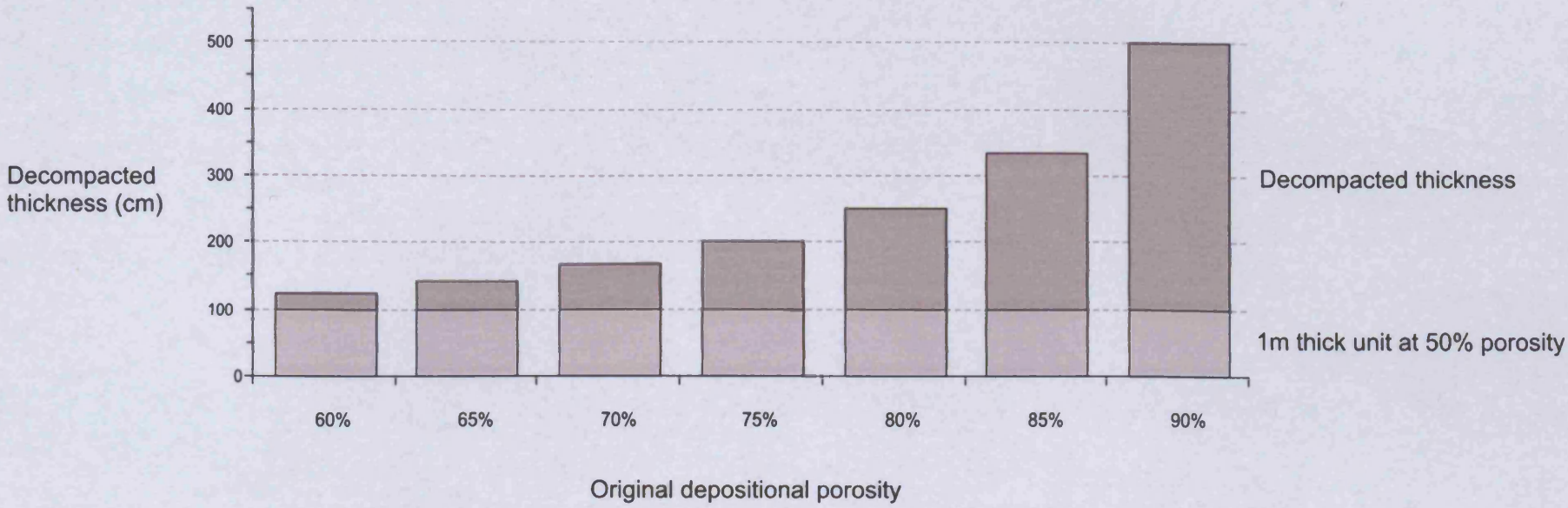

Figure 4.11 Illustrative graph to show the hypothetical effect of decompacting a 1m column of sediment with a porosity of 50% back to its original thickness using a range of initial porosity values.

hemipelagic facies in Fig. 4.3, it seems that significant errors are likely when decompacting entire hemipelagic sediments without either very detailed lithological information, or in situ porosity measurements (Giles et al., 1998). Consequently, the use of default initial porosity values in numerical modelling and those in-built into commercial basin modelling software packages such as TEMIS 3D and BasinMod, can yield large numerical errors.

Lithology, or more specifically the particular component grains of a sediment, will have a significant influence on initial porosity given the known differences in the pore-scale character of clay-, silt- and sand-dominated sediments (Chilingar, 1964; Skempton, 1970; Burland, 1990). Facies categories in Fig. 4.3 suggest that both the likely range and absolute values of initial porosities are governed to a certain degree by the nature of dominant grains. The most striking example of this is seen in data from clays with a biosiliceous component which show a very narrow range of initial porosities and high absolute values (Fig. 4.3). The compaction of deep-marine biosiliceous sediments is discussed in section 4.4.1 and suggests that interlocking skeletal material is responsible for the increased rigidity and subsequent resistance to compaction. Conversely, silt and sandy sediments show noticeably lower initial porosities in Fig. 4.3, contrasting clearly with the clay-dominated facies, which is in-keeping with studies examining the packing arrangements of silt and sand grade sediments. Sediments which are described as containing a mixture of silt and clay display the greatest range of initial porosities. In the absence of quantitative grain-size data, distinctions between facies are made on the basis of approximate proportions of major grain-size components based on the ODP's standardised practises.

Based on experimental studies, Meade (1964) suggests that other factors likely to affect the depositional porosity of clay-rich sediments include the chemistry and the electrolyte concentrations of pore-fluids. Meade (1964) also reports work regarding the specific surface areas for pure clays, which suggest that montmorillonite is capable of retaining significantly more water at a range of pressures than either illite or kaolinite. The type of clay mineral assemblage present, which is strongly influenced by sediment provenance, has also been shown to influence the structure and porosity of clay floccules (Olson and Mitronovas, 1962). Velde (1996) points out that floccules are largely responsible for the high initial porosities observed in clay-rich sediments by creating open networks of electrostatically bonded clay minerals with large void-ratios.

In light of the relationships between initial porosity and facies illustrated in Fig. 4.3 and 4.5 and aforementioned discussions, I suggest that initial porosity values of fine-grained marine sediments are strongly influenced by sediment type, particularly the distribution of clastic

grain-sizes, and volumes of biosiliceous material, as noted previously by authors including Meade (1964), Chilingar (1964), Skempton (1970), Busch (1989), Pittenger et al. (1989), Burland (1990), and Compton (1991).

4.5.2 Porosity distributions with depth

As well as initial porosities from 255 ODP sites, 16 clay-dominated hemipelagic sequences were examined in order to assess the relationship between porosity loss and burial depth. These trends are discussed here in terms of porosity loss with depth rather than in compaction curves. Compaction curves are often used to make predictions regarding the former compaction states of buried samples within a sequence. The predicted compaction history of a sample buried at say, 100m depth is therefore based on the porosity values measured from shallower samples in the sequence. Giles (1997) points out that it is impossible to know with any certainty the actual compaction history of a particular sample prior to its porosity being measured at a given depth. In reality, the exact compactional 'curve' of any one measured sample is largely independent of any other point with a given sediment column. Two similar porosity determinations for example, separated by just a few metres stratigraphically, may well have reached that state from (a) very different depositional (initial) porosities and (b) by markedly different porosity loss with depth trends. With this in mind, the commonly held notion (Dickinson, 1953; Baldwin, 1971; Rieke and Chilingarian, 1974; Sclater and Christie, 1980; Baldwin and Butler, 1985) that a single trend-line or "compaction curve" extrapolated through discrete porosity measurements can, with any certainty, describe the compactional history of a sedimentary sequence is mistaken. However, there is undoubtedly useful information to be gained from porosity/depth data which appear to fall into relatively ordered arrays (Figs. 4.6, 4.8, and 4.9). It is unlikely, although possible, that data which lie along, or close to, superimposed linear or exponential fit lines achieved their respective compaction states as a result of widely varying rates of pore-collapse. It does not seem possible to assign a single fit or trend to all of the sequences examined here. Rather factors such as grain-size distribution and the sequence of lithologies appear to play a role in how sequences compact, such that location specific, as opposed to generic, 'compaction curves' will provide the most accurate tool for assessments of the subsurface in a particular locality, as suggested by Giles et al. (1998). It is suggested therefore that within shallow hemipelagic sequences where neither fluid-pressure nor detailed lithologies are known, only tentative assumptions can be made about the compactional history of the sequence as a whole based on a trend-line delineating discrete porosity measurements.

4.5.3 Porosity distributions and sediment age

Porosity distributions plotted against depth in Fig. 4.7 indicate that within our data, no clear relationship exists between porosity values and sediment age. Initial porosities, considered to represent 'zero' age, show a considerable range of values as described in section 4.4.1 which are thought to be influenced by lithology and grain-size (Fig. 4.3). Shallow hemipelagic sequences examined in Fig. 4.7 record maximum ages ranging from Pleistocene to late Oligocene, with 11 of those 16 sequences examined recording a 500m thick sediment column. Porosities recorded at 500m depth in these sequences reveal values can be similar for sediments of markedly different ages. Porosity-depth plot 11, drilled in the South China Sea, records a porosity of 47% at 500m depth in sediments of late Oligocene age, while porosity-depth plot 12 (Cascadia Margin) records the same porosity at 500m, but from sediments of early Pleistocene age. Similarly, porosity-depth plot 2 records a porosity of 40% at 500m depth in early Miocene sediments, while porosity-depth plot 6 records porosity of 41% from the same depth, in late Pliocene aged sediments. It would appear that at the shallow depths studied here, the influence of time on mechanical porosity loss is not significant and that burial depth is the main factor controlling porosity loss. The rate at which sediments are buried however will be determined by sedimentation rate. It is differences in the sedimentation rates which allow the aforementioned sediments of different ages to exhibit similar porosities. Sediment age is likely to play a more significant role in determining porosity in sediments buried to depths where cementation and pressure-solution are prevalent (Dzevanshir et al., 1986; Giles, 1997).

4.6 Conclusions

This study adds to the current knowledge base concerning the shallow porosity loss trends of clay-rich sequences. Porosity determinations in natural systems offer basin-modellers the opportunity to develop and refine more accurate predictive tools for basin analysis.

1. We have presented evidence from 255 ODP and IODP wells to suggest that lithology, primarily grain-size, plays a significant role in determining the range and absolute values of initial porosities in hemipelagic sediment. It has also been shown that the use of single default values to characterise the initial porosities of hemipelagic sediments ignores a large range of natural variability, and could lead to significant analytical errors when default values are used in basin models and decompaction analysis (Fig. 12).

2. Porosity-depth plots in shallow hemipelagic sequences do not habitually reveal trends of exponentially decreasing porosity values with depth, as suggested by some authors (e.g. Baldwin and Butler, 1985; Bahr et al., 2001).

3. Deviations from exponential or linear porosity loss trends are often seen to correlate with shifts in bulk lithology, however differentiating between the effect of lithology and overpressured pore-fluids on porosity shifts is difficult without data regarding effective stresses, as noted by MarcussenØ et al. (2009).

4. Sediments comprising upwards of 30-40% biosiliceous material reveal very high initial porosities of 80-90% and tend to show a considerably slower reduction in porosity with depth than other hemipelagic facies. This is thought to be characteristic of diatomaceous sediments where the structure of interlocking biosiliceous material offers increased resistance to sediment compaction (Busch, 1989; Pittenger et al., 1989; Compton, 1991).

Chapter 5

Chapter 5

Diagenesis in shallow ash-bearing hemipelagic sequences

5.1 Introduction

The aim of this chapter is to highlight the potential impact of shallow ash alteration on the physical properties of fine-grained marine sediments and suggest how this may influence the fluid-flow and mechanical properties of ash-bearing sequences. Although the chemical and physical processes by which volcanic material undergoes alteration have been extensively studied (e.g. Friedman et al., 1966; Friedman and Long, 1976; Jezek and Noble, 1978; Scheidegger et al., 1978; Ninkovich, 1979; Gieskes and Lawrence, 1981; Staudigel and Hart, 1983; Furnes, 1984; Crovisier et al., 1987; Berger et al., 1994; Fiore et al., 2001; Techer et al., 2001; Stroncik and Schmincke, 2002), investigations into the impact of these reactions on the physical and mechanical properties of fine-grained sediments are far less common (e.g. Ninkovich and Heezen, 1967; Carlson et al., 1980; Dadey and Klaus, 1992; Nelson and Anderson, 1992).

My work aims to summarise the current knowledge regarding the chemical and physical processes which accompany ash alteration, and also to utilise data from Ocean Drilling Program (ODP) campaigns to investigate changes to the physical properties of ash-bearing sequences during alteration. This work is not intended to constitute an exhaustive review of ash diagenesis, but rather to highlight the potential for shallow diagenetic processes to alter the properties of fine-grained host sediments.

Fine-grained sequences, such as those examine in chapters 2 and 3 of this thesis, are dominated by clay-rich facies, the physical properties of which are significantly altered during shallow (<1000m) burial in response to diagenesis. Diagenetic processes evolve as sediments are buried to greater depths where increasing pressure and temperature conditions force progressive physical and chemical changes (Giles, 1997). The most pronounced diagenetic changes in shallow clay-dominated sequences are driven principally by mechanical compaction and the rearrangement of particles in response to burial and dewatering (Meade, 1964; Skempton, 1970; Rieke and Chilingarian, 1974; Velde, 1996; Bjørlykke, 1999). Changes to other physical properties such as sediment density, permeability and velocity will also be linked to a reduction in porosity during compaction (Rieke and Chilingarian, 1974; Dewhurst et al., 1998; Yang and Aplin, 1998). Generally

speaking, significant chemical diagenesis in hemipelagic sequences is only prevalent at depths exceeding 1-2km where temperatures are sufficient to promote the alteration of clay-minerals and quartz dissolution-precipitation reactions (Powers, 1967; Peltonen et al., 2008). That said, lithological heterogeneities which punctuate otherwise homogeneous clay-dominated sequences may respond differently to both mechanical and chemical diagenesis, impacting the bulk physical properties of entire sequences.

Volcanic ash layers represent a common heterogeneity and are of particular significance in the study of shallow hemipelagite diagenesis. Volcanic ash layers are seen to undergo a particularly rapid and chemically complex diagenetic evolution which contrasts with that of the majority of siliciclastic sediments, especially at shallow depths (Powers, 1967; Gieskes and Lawrence, 1981; Hodder et al., 1993). While porosities and permeabilities of fresh (unaltered) ash material are expected to resemble those of clastic material of a similar grain-size (e.g. silt and sand grade), other physical properties, such as mineralogy and strength, will differ. Unlike siliciclastic material, volcanic sediments undergo both mechanical compaction and chemical exchanges during shallow burial. These chemical exchanges involve the dissolution of glass and the precipitation of authigenic phases, typically smectites and zeolites (Fisher and Schmincke, 1984). The impact of these dissolution-precipitation reactions on the bulk physical properties of ash-bearing hemipelagic sediments has received little attention.

Changes to sediment physical properties as a result of ash alteration are of particular interest in petroliferous basins where diagenetic processes may alter the way in which fluids are able to migrate or be sealed. The following discussion highlights some of the important alterations to ash material during shallow diagenesis and considers the likely implications for sediment physical properties such as hydraulic conductivity and sediment stability. Sequences in petroliferous basins known to contain volumes of volcanic ash at varying states of alteration include Lower Tertiary mudstone of the North Sea basin (Huggett, 1992), and the Pearl River Basin of the northern South China Sea (Yan et al., 2006). Ocean drilling campaigns have also documented the existence of altered, or partly altered, ash material from locations including the Columbia Basin, southern Caribbean (Sigurdsson et al., 1997), the Izu-Bonin (Taylor et al., 1990) and Nankai convergent margins (Moore et al., 2001) offshore Japan, and the New Hebrides margin, close to Vanuatu (Collot et al., 1992). The diagenetic state of glassy volcanic material in these settings will strongly influence the physical state of ash horizons and may also impact the physical properties of surrounding host sediment. This data collected by ocean drilling programs on shallow ash-bearing sequences provides

valuable information regarding the processes and products of ash conversion in fine-grained marine sediments, and constitutes the primary dataset examined here.

5.2 Distribution of volcanic ash in marine sediments

Cored ocean sediments reveal that thin horizons of volcanic ash are commonly found interbedded with hemipelagic sediments in active, or formerly active volcanic regions. Ash layers represent thin, often laterally continuous beds of volcanogenic material which when deposited, generally comprise silt and sand sized glass shards and pumice fragments (Fisher and Schmincke, 1984) (Fig. 5.1). Ash deposited in ocean basins originates from both the wind-blown fallout of ash following subaerial eruptions and from material erupted subaqueously. The distribution of ash ejected from terrestrial volcanoes is largely governed by eruption column heights and prevailing wind conditions. Isopach maps constraining the distribution of ash fallout from modern land eruptions would suggest material can be dispersed over huge areas of several thousand km^2 (e.g. Carey and Sigurdsson, 1980; Kataoka et al., 2001). Correlations have been made between grain-size and distance from origin, suggesting that wind-blown ash deposits fine with increasing distance from source (Fisher and Schmincke, 1984). The distribution of wind-blown volcanic material once introduced to the ocean is ultimately controlled by the direction and velocity of marine currents and the influence of any subsequent sediment reworking and remobilisation processes. Ash beds deposited on the seafloor by fallout through the water column are typically less than 10cm thick and rarely exceed 50cm (Fisher and Schmincke, 1984). Beds generally display sharp basal contacts with underlying sediment but show diffuse upper boundaries which are commonly the result of post-depositional reworking by bottom currents or the activity of organisms (Fisher and Schmincke, 1984) (Fig. 5.1 and 5.2). Ash layers may also exhibit graded bedding resulting from grain-size segregation and flocculation during settling.

Volcaniclastic material is well known to be a contributor to the world's sediment budget, with estimates suggesting that on average between 4 and 8 km^3 of material has been introduced annually over the last 180 m.a. (Nakamura, 1974; Fujii, 1975; Crisp, 1984). However, it is likely that volumes of altered volcanic ash in the rock record are widely underestimated. Ash layers which have undergone significant alteration are preserved in the rock record as thin, areally extensive clay horizons, or bentonites (Fig. 5.3). Bentonites have been documented from many exposed marine sequences, however the identification of bentonitic layers in fine-grained sequences can be difficult, often only made possible by the presence of relict glass

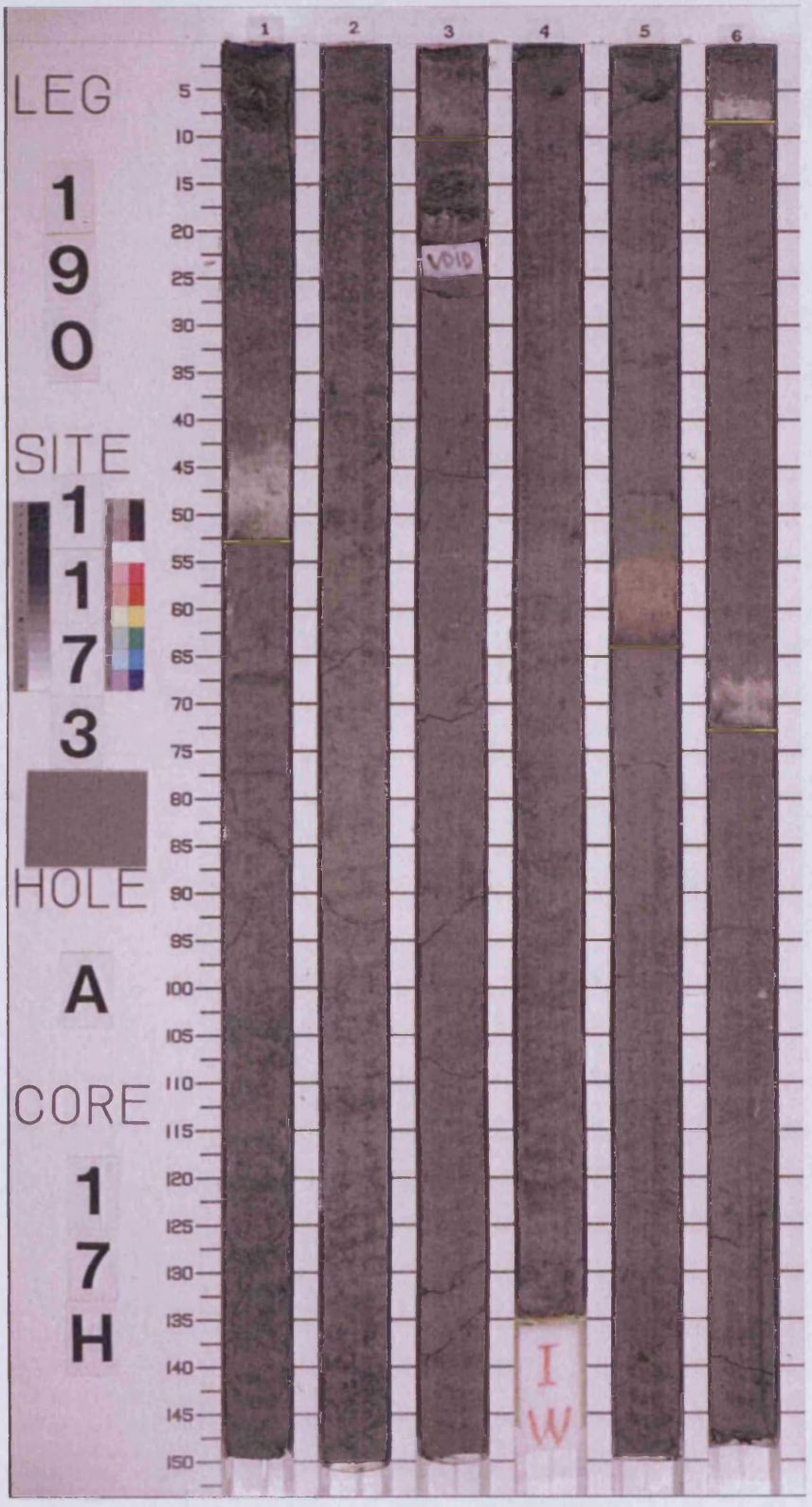

Figure 5.1 Thin ash beds in cored hemipelagic sediments from ODP Leg 190 at the Nankai Trough. Yellow lines mark the bases of five discrete ash beds identified. Image taken from Moore et al (2001).

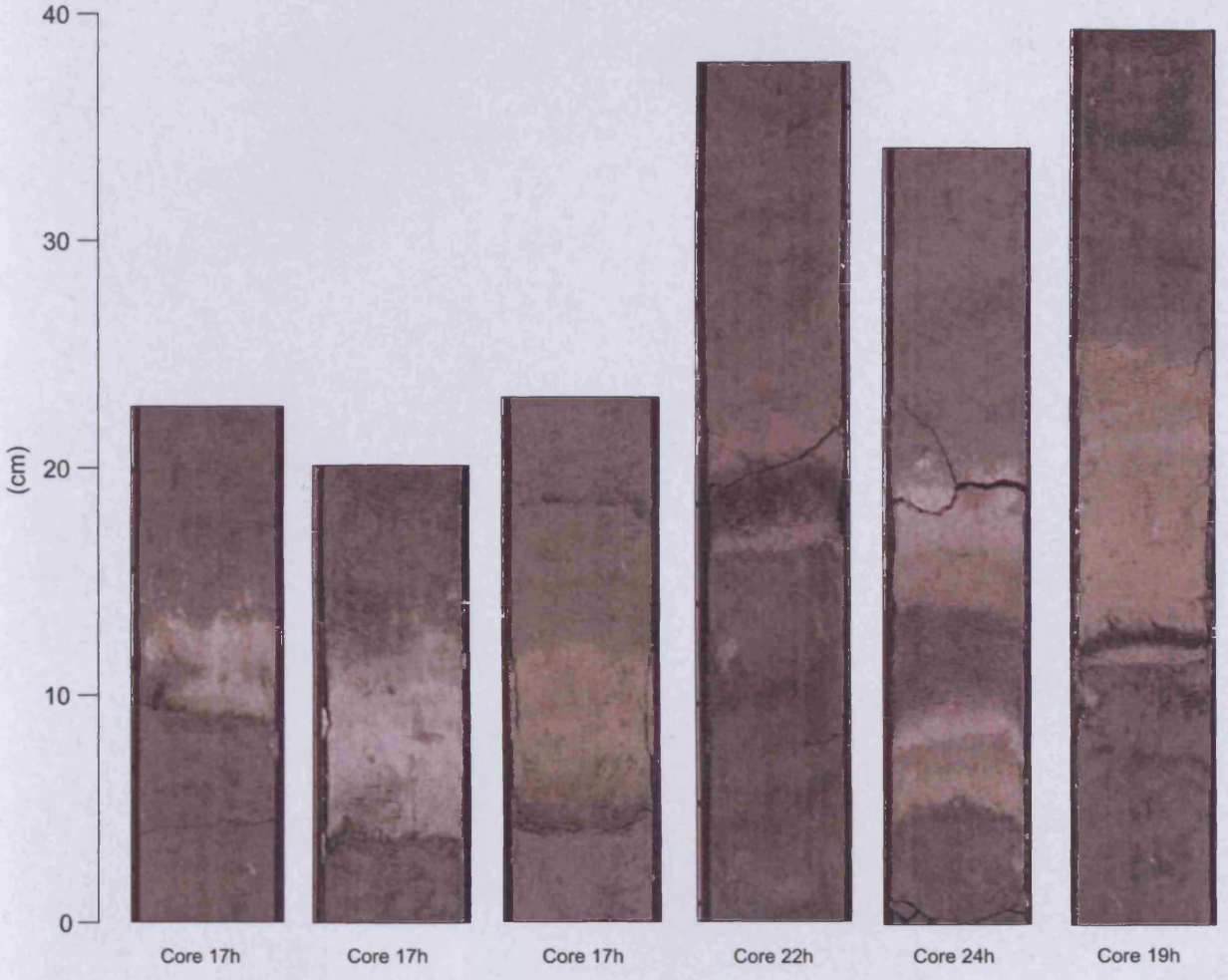

Figure 5.2 Ash beds in core recovered from ODP Leg 190 - Site 1173 (lighter grey intervals) showing characteristic sharp lower contacts and diffuse upper contacts. Images taken from Moore et al (2001).

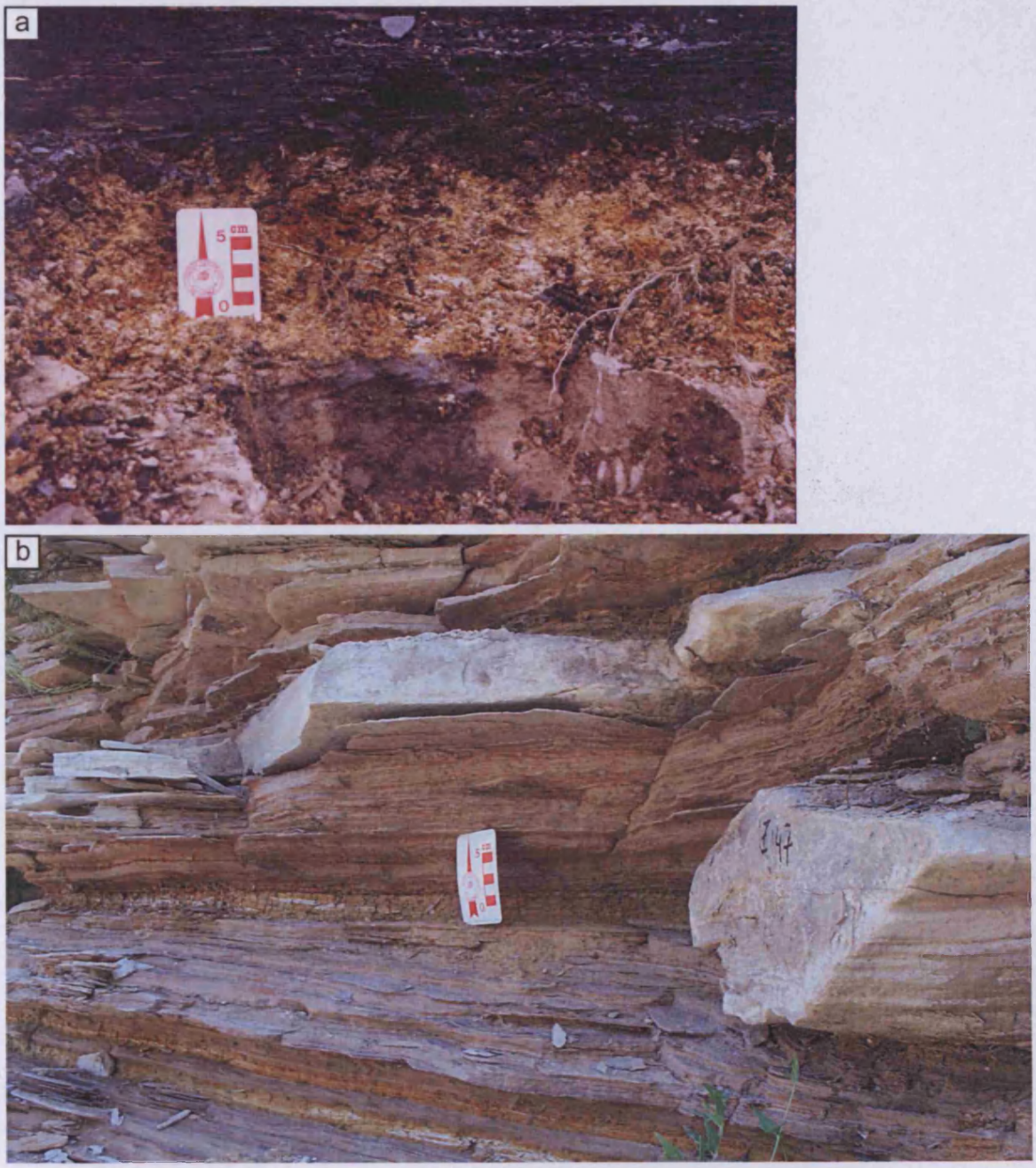

Figure 5.3 Images of bentonite layers in outcrop. Image (a) shows a 10cm thick bentonite layer from Kansas, (b) shows a thin bentonite layer within the Bridge Creek Limestones, Texas (images and descriptions taken from Desmares, 2005).

shards and the characteristic low abundances of detrital grains (Grim and Güven, 1978; Fisher and Schmincke, 1984; Wilson et al., 2003).

5.3. Introduction to ash diagenesis

Volcanic glass is thermodynamically unstable, and as a result, is readily altered to secondary phases and authigenic minerals by low temperature diagenetic reactions. These processes have been documented for over 150 years (von Waltershausen, 1845), though studies in recent years are beginning to unravel the complexities of processes associated with ash and volcanic glass alteration. Fisher and Schmincke (1984) have suggested that ash and pore-fluid chemistry, as well as physical parameters such as temperature and grain-size, play an important role in determining the rates and products of alteration reactions. The mineralogy and texture of fresh volcanic ash varies according to the petrography of the parent magma and its interaction with the atmosphere and aqueous phases after eruption. Basaltic ash commonly consists of complete or fragmented droplets of sideromelane and tachylite glass with variable volumes of mafic phenocrysts, whilst ash from andesitic and rhyolitic melts contains large amounts of vitric grains (glass and pumice), with variable quantities of phenocrysts and lithic fragments (Heiken, 1974). The incipient alteration of both basaltic and rhyolitic volcanic glass typically involves the addition of water and the subsequent hydration of glass shard surfaces (Fig. 5.4). This is followed by reactions involving the dissolution and breakdown of glass and the precipitation of authigenic phases (Ross and Smith, 1955; Staudigel and Hart, 1983; Stroncik and Schmincke, 2001). The alteration of basaltic and rhyolitic ashes are governed by different reaction kinetics and produce a variety of authigenic products. This variability may influence how diagenesis affects the physical properties of host sediments, and for that reason, each is outlined separately in the following sections.

5.3.1 Silicic ash alteration

Incipient hydration of silica-rich volcanic glass (obsidian) under natural conditions results in the development of perlite, a phase characterised by 'perlitic' cracks and produced by initial diffusion-controlled hydration of glass (Ross and Smith, 1955; Fisher and Schmincke, 1984). Friedman and Smith (1958) demonstrated that high water contents in perlites, compared to fresh obsidian, were the result of secondary hydration of glass by molecular H_2O. While unaltered obsidian typically contains between 0.1-0.9 % water, naturally hydrated perlite may contain as much as 6% water (Ross and Smith, 1955; Federman, 1984). Perlite commonly surrounds unaltered glass and is characterised by networks of concentric 'onion skin' and tension fractures which develop in response to the volumetric expansion of surface layers

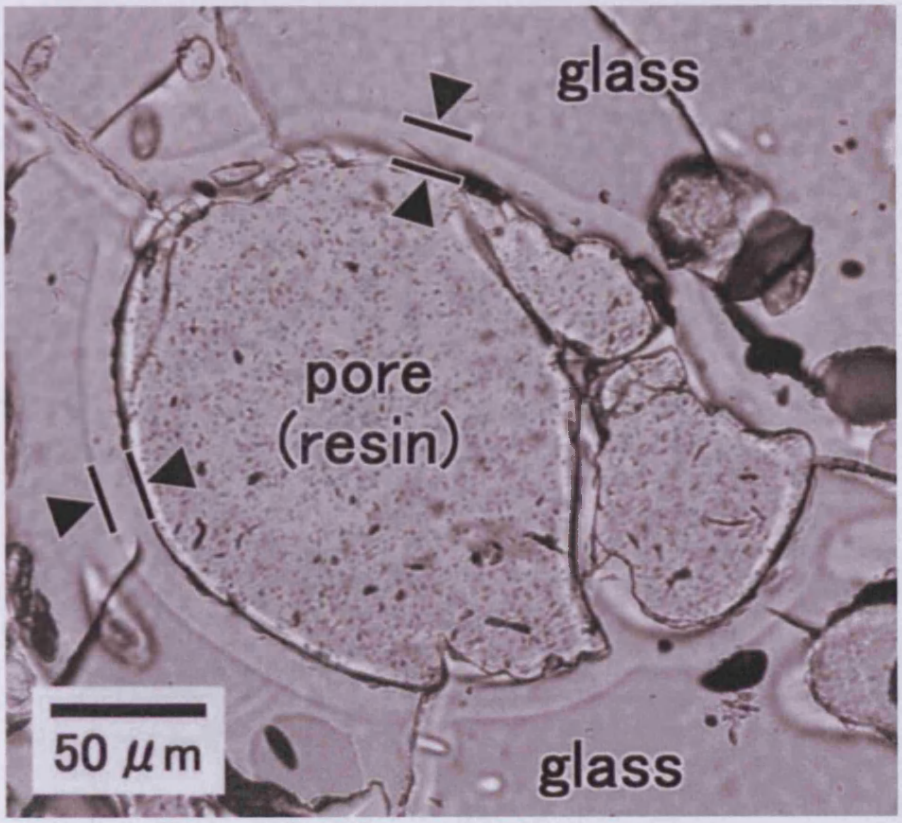

Figure 5.4 Thin section photo showing hydration layer in rhyolitic glass sample from Japan. The hydration layer (arrowed) develops along the reactive surface of the glass. Image from Yokoyama and Banfield (2002).

associated with hydration (Friedman and Smith, 1958) (Fig. 5.5). These fractures facilitate the movement of water further into the unaltered obsidian thus progressing the alteration process. The rate at which obsidian alters to this initial secondary phase in the presence of water is largely dependent on temperature and chemical composition of the glass (Friedman and Long, 1976). Terrestrially deposited glasses exposed to permafrost conditions have been shown to hydrate considerably slower than those from tropical regions (Friedman and Smith, 1960).

Hydration and the development of perlitic fractures represent the first stage of low temperature silicic glass alteration. More advanced diagenesis involves the dissolution of hydrated glass and the formation of smectite (montmorillonite), as well as the precipitation of appreciable amounts of authigenic products, commonly clay minerals and zeolites (e.g. Fiore et al., 2001). Although this process is poorly understood, the exchange of cations between glass and pore fluids has been investigated with reference to naturally and artificially altered glasses (Fisher and Schmincke, 1984). The most commonly observed cation exchanges involve mobility of alkalis such as Na and K as well as network forming Si. Several studies have shown that glass which has undergone secondary hydration contains significantly less NaO_2 and SiO_2 than unaltered coexisting samples suggesting a leaching of cations out of glass and into pore fluids (Lipman, 1965; and Aramaki and Lipman, 1965; Noble, 1967). Lipman et al. (1969) also noted a significant increase in the K content of hydrated glass relative to coexisting unaltered obsidian. Jezek and Noble (1978) studied naturally occurring obsidian-perlite pairs and observed that appreciable cation exchange was confined to fine fractures within perlitic samples, where Na was found to be depleted relative to unaltered obsidian while K content had increased. More recently, Fiore et al. (1999) conducted experimental studies investigating elemental mobility during obsidian alteration in water at 82°C / pH=5.5. Over the course of the experiment the leaching of major elements left the obsidian increasingly depleted in Mg, Ca, Fe, Si, O, K, and Na, while water was taken up by the glass. Under higher experimental temperatures (150°C – 200°C) Kawano et al. (1993) observed similar element mobility and the development of authigenic smectite. Despite elevated temperatures, cation exchanges observed during experimental studies are generally in agreement with those measured in natural systems. More advanced stages of alteration, involving the precipitation of authigenic minerals and the complete transformation of glass to smectites, are reported from marine settings under natural geothermal gradients (Taylor et al., 1990; Collot et al., 1992; Sigurdsson et al., 1997; Moore et al., 2001).

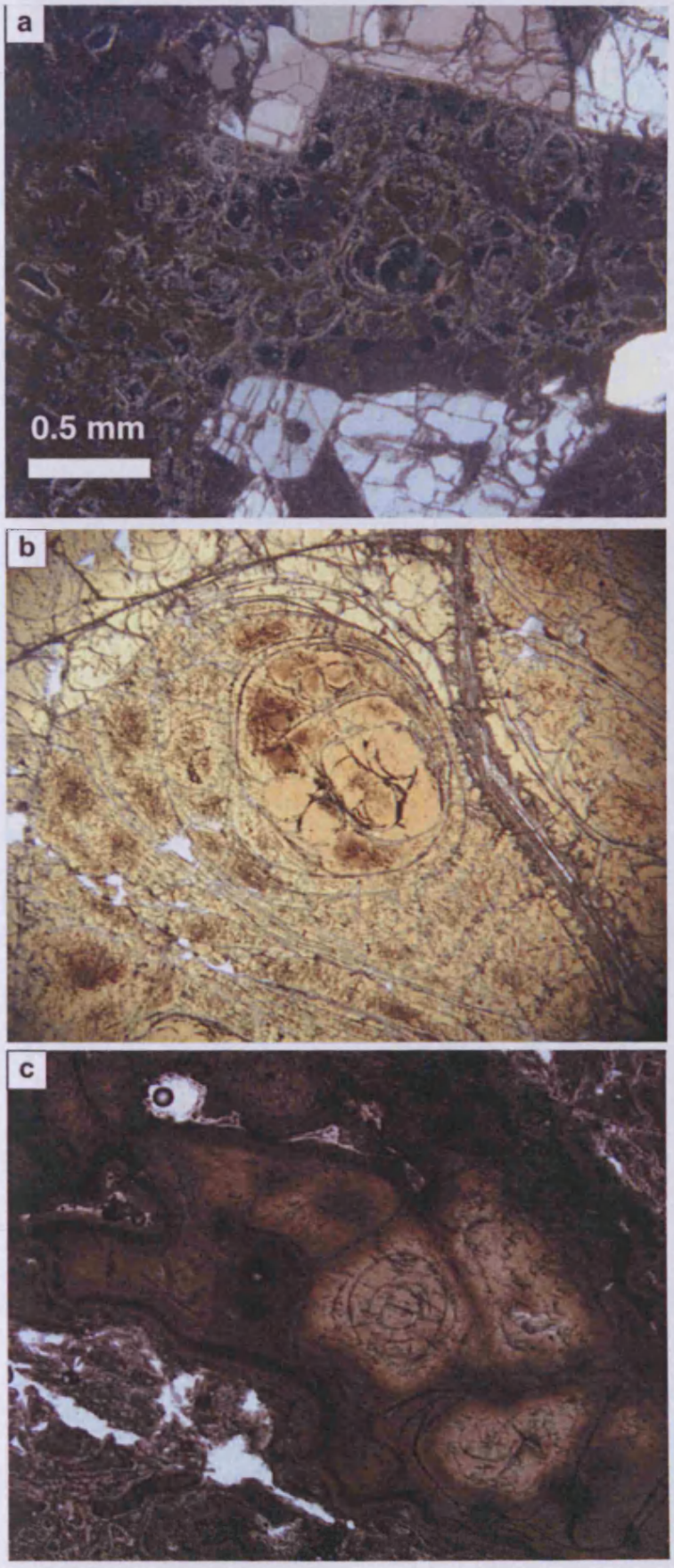

Figure 5.5. Perlitic fracturing of volcanic glass.

(a) Photomicrograph showing concentric 'onion-skin' fracturing of glassy groundmass from ODP Site 1139 (Binns et al, 2002)

(b) Photomicrograph showing concentric perlitic fracturing of altered felsic glass, ODP Site 1139. Field of view = 5.5mm (Coffin et al, 2000).

(c) Thin section photograph of perlitic texture in altered volcanic glass, ODP Site 1188. Field of view = 2.75mm (Binns et al, 2002).

5.3.2 Basaltic ash alteration

The low temperature alteration of basaltic volcanic glass (sideromelane) differs from that of obsidian glass in that the initial hydration of sideromelane is often accompanied by the development of palagonite, an amorphous gel-like phase (Stroncik and Schmincke, 2001). Palagonite itself is a wax-like substance which is thermodynamically unstable and is eventually altered to stable crystalline phases, typically smectite clays (Fig. 5.6). The exact mineralogical nature of palagonite remains poorly defined. Numerous authors have proposed compositions which include montmorillonite, illite, mixed-layer clays, zeolites, and mixtures of altered, hydrated, and oxidised glasses (e.g. Hay and Iijima, 1968b; Furnes, 1984). Stroncik and Schmincke (2001) studied palagonite samples ranging in age from 10 ka – 30 Ma, which have undergone alteration at very low temperatures (0-15 °C) and suggests that the palagonisation of sideromelane glass occurs in two distinct stages. Firstly, the initial stage involves the dissolution of glass and the contemporaneous precipitation of fresh palagonite. This is followed by a stage of progressive aging or evolution, where palagonite is altered to smectites through ion exchanges with surrounding pore fluids. Although the exact mechanisms of palagonite formation and evolution are not fully understood, it is generally accepted that palagonite forms initially from a dissolution-precipitation process (Fisher and Schmincke, 1984; Stroncik and Schmincke, 2001).

5.3.3 Mass balance

Similar to chemical exchanges reported from altering obsidian, the alteration of basaltic glass and the development of palagonite are driven by chemical exchanges between glass and solution. Studies have shown that the alteration of glass results in the loss of many elements into pore fluids. Staudigel and Hart (1983) studied the results of submarine palagonisation and reported significant losses of SiO_2, Al2O_3, MnO, MgO, CaO, Na_2O, Zn, Cu, and Ni from altered sideromelane into pore fluids, significant increases in water and K_2O in the resulting palagonite, as well as the passive accumulation FeO and TiO_2. Stroncik and Schmincke (2001) report very similar elemental losses during the first stage of palagonite formation to that of Staudigel and Hart (1983). However, they also observe an uptake of Si, Al., Mg, and K out of solution during the later stage evolution of palagonites and the precipitation of smectite clays. Andrew (1977) also reported similar increases in potassium during the development of palagonite. Elemental losses during palagonite formation by as much as 65 wt% where recorded by Stroncik and Schmincke (2001), however the overall element loss, when one includes subsequent precipitation of authigenic phases, was in the region of 25 wt%.

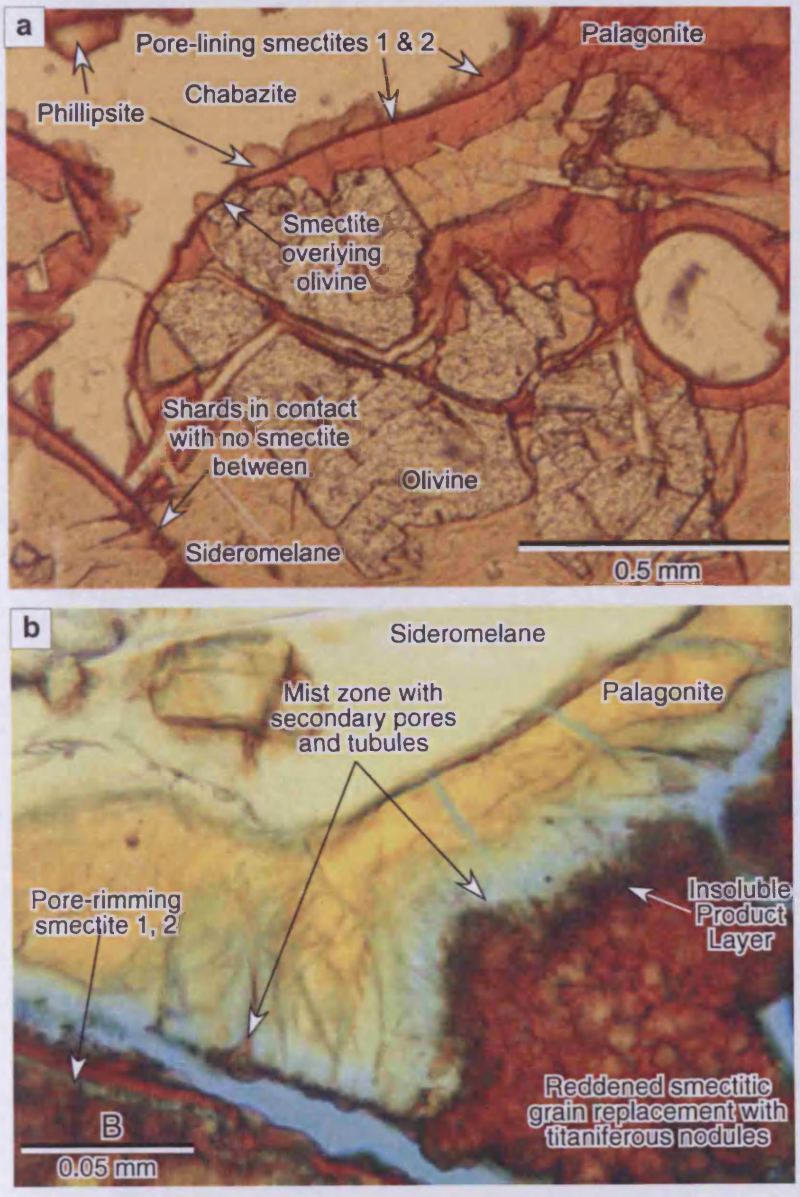

Figure 5.6. Palagonite

(a) and (b) Thin section images showing alteration and palagonisation of sideromelane glass, images taken from Walton and Schiffman (2003)

(c) Thin section micrograph of submarine palagonite alteration layers around unaltered glass (1.95x2.44cm). Image from Stroncik and Schmincke (2001).

Authigenic crystalline phases are the major sink for elements recovered from pore fluids during the later stages of ash diagenesis.

Considerations of the elemental mass balance during ash diagenesis are important when evaluating the likely impact of alteration reactions on sediment physical properties. For example, if ion exchanges during glass alteration are not isovolumetric, as suggested by Crovisier et al. (1987) and Stroncik and Schmincke (2001), a reduction in bulk sediment volume resulting from a removal of mass into solution may have implications for the development of fractures in fine-grained sediments, a topic discussed in more detail in section 5.5.

5.3.4 Summary

Studies of artificially and naturally altered ashes discussed in preceding sections indicate that volcanic ash is capable of undergoing significant diagenetic alteration at relatively low temperatures (Fig. 5.7). They also suggest that ash layers can be completely altered to smectite clays and other authigenic phases through a process of initial glass hydration, followed by complex dissolution-precipitation reactions between glass, pore fluids and authigenic phases. The evolution of pore fluid chemistries and sediment mineralogy as a result of these processes will inevitably alter the physical properties of the ash layer themselves, and potentially the characteristics of surrounding host sediments.

5.4 Ash diagenesis in natural systems: Observations from the ODP

5.4.1 Precipitation of authigenic phases

The precipitation of authigenic phases attests to the progress of chemical diagenesis and provides clues as to the depths and conditions under which ash layers may begin to be significantly altered. Generally speaking, the first authigenic materials observed in the cores examined here are zeolites and smectite precursors, such as palagonite, followed at greater depth by the presence of authigenic smectites (Taylor et al., 1990; Collot et al., 1992; Sigurdsson et al., 1997; Moore et al., 2001). These observations regarding the alteration of ash and glass are in keeping with those made during experimental studies cited in section 5.3, and suggest that ash undergoes a similar diagenetic evolution in natural systems.

Four previously mentioned ODP drilling campaigns, which have all targeted ash-bearing submarine sediments, are used here to illustrate the authigenic products produced during

Volcanic glass and ash diagenesis - Chronological list of some key studies

Palagonite and basaltic glass

von Waltershausen (1845)	Described a yellow to brown waxy substance in marine basaltic tuffs from Palagonia, Sicily. He named this palagonite.
Bunsen (1847)	Recognised that Icelandic palagonite was similar to basalt but for the addition of water and the loss of Ca and Na.
Penck (1879)	First to show that palagonite is not a mineral and employed palagonite as a general term for any hydrous, altered basaltic glass.
Peacock (1926)	First comprehensive petrographic study of palagonite, identifying two main varieties.
Hay and Iijima (1968)	Proposed that palagonite is composed of montmorillonite and mixed-layer mica montmorillonite. However the exact mineralogy of palagonite has never been fully agreed upon.
Staudigel and Hart (1982)	Studied submarine basaltic glass and found the development of palagonite is associated with a loss of SiO_2, $Al2O_3$, MnO, MgO, CaO, Na_2O and others, and is replaced by H_2O and K_2O.
Gieskes and Lawrence (1981)	Reported pore-fluid chemistries from a series of ocean drilling sites and suggests that changes to the concentrations of calcium, magnesium and potassium where primarily the result of ash alteration with the sediment column.
Crovisier et al (1987)	Documented results from experimental alterations of volcanic glass in seawater, reporting that secondary minerals were precipitated in alternation layers after the complete breakdown of the glassy network. They also report that the transformation from glass to palagonite is unlikely to be systematically isovolumetric.
Stroncik and Schmincke (2001)	Report results from an extensive study of palagonitic samples. They conclude that palagonite 'ages' with time until it is eventually completely transformed to smectite clays.
Stroncik and Schmincke (2002)	Authors provide a comprehensive review of literature regarding palagonite and basaltic glass alteration up until 2002.

Perlite and obsidian glass

Ross & Smith (1955)	Concluded that secondary hydration gave rise to a perlitic layer around unaltered obsidian samples. They also observed a volume change and stressed surface of the obsidian as a result of hydration.
Friedman & Smith (1958)	Examined coexisting obsidian and perlite samples and concluded, using deuterium levels, that secondary hydration had occurred from meteoric waters.
Friedman & Smith (1960)	Dating method for obsidian artefacts. Marked difference in rates of hydration from samples from Alaskan permafrost and the tropics. (0.36 μm^2/k.y. compared with 11 μm^2/k.y.)
Aramaki and Lipman (1965)	Studied altered and unaltered obsidian samples from the same volcanic mass and reported leaching of SiO2 and Na2O from the altered samples.
Friedman et al (1966)	Record temperatures as low as 5 °C for the effective hydration of obsidian samples from coastal Alaska. They also provide a rate equation, based on the thickness of perlitic layers for use in the dating of obsidian artefacts.
Noble (1967)	Studied the effects of hydration on natural samples of obsidian, and reports the leaching of Na_2O from samples which have undergone hydration (initial alteration), and an increase in K.
Jezek & Noble (1978)	Studied obsidian pairs and noted that secondary hydration of ~ 3% was common. Although this hydration was associated with only minor elemental losses or gains.

Figure 5.7 Table containing a chronological list of some important publications concerning the alteration of volcanic material.

shallow ash diagenesis and the changes to pore fluid chemistries which accompany these reactions. These four locations are the Izu-Bonin Arc (Taylor et al., 1990), Nankai Trough (Moore et al., 2001), New Hebrides Islands (Collot et al., 1992), and the Caribbean Columbia Basin (Sigurdsson et al., 1997) (Fig. 5.8). Marine sediments recovered from these locations contain varying amounts of volcanogenic material in the form of ash and pumice, interspersed with clay, silt and sand grade sediments. Unaltered submarine volcanic deposits recovered at these sites are dominated by silt and sand sized glass shards and pumice fragments as well as crystalline minerals and clay-sized matrix material. All four locations studied are unique with respect to the distribution of ash in studied cores, the specific lithology of background sediments, and the specific basin conditions under which ash alteration occurs. Sites do however share a similar regional tectonic setting, with all sites located in basins at, or close to, zones of active plate subduction and island arc volcanism. New Hebrides sites (832 and 833) and Izu-Bonin sites (792 and 793) record background sedimentary sequences of silty clays, silts, ash material, and vitric sands (Fig. 5.9) while Caribbean sites (998 and 999) from the Columbia Basin are largely biogenic oozes punctuated by hundreds of ash layers. Ash-bearing mudstone units recovered from the Shikoku Basin (Site 1173) offshore Japan are capped by a more recent sand-rich turbidite dominated basin-fill package (Fig. 5.10).

Sediments recovered from Site 833 in North Aoba Basin (New Hebrides margin) record the presence of zeolites in ash layers from sediments buried to just 146 mbsf, whilst authigenic smectites first appear, in the same core, at a depth of 270 mbsf (Collot et al., 1992). Authigenic phases which have been precipitated in the uppermost occur ~400 mbsf at Site 833, and neighbouring site 832, lie within ash-bearing biogenic sediments and silts which contain volcanic ash as discrete layers and dispersed grains. Intervals of volcanic breccia which lie directly beneath these ash-bearing units extend to depths of between 600-700 mbsf at the North Aoba Basin Sites (832 and 833) and contain zeolites as well as authigenic smectites. Temperatures at the bases of these breccia intervals remain relatively low, reaching a maximum of 35 °C at Site 833 (Martin, 1994) indicating active chemical diagenesis is taking place at relatively low temperatures.

Ash-bearing fine-grained sediments recovered from the Izu-Bonin fore-arc basin, reveal a significant influence of diagenetic processes below 150-200 mbsf. Below this depth, at Site 792, there is a significant reduction in the volume of volcanic glass identified from cores, and a concurrent increase in the occurrence of palagonite and zeolites (Taylor et al., 1990). The volume of smectite clay is also seen to broadly increase with increasing depth at Site 792, exhibiting several peaks in concentration below a depth of 400 mbsf (Tazaki and Fyfe, 1992).

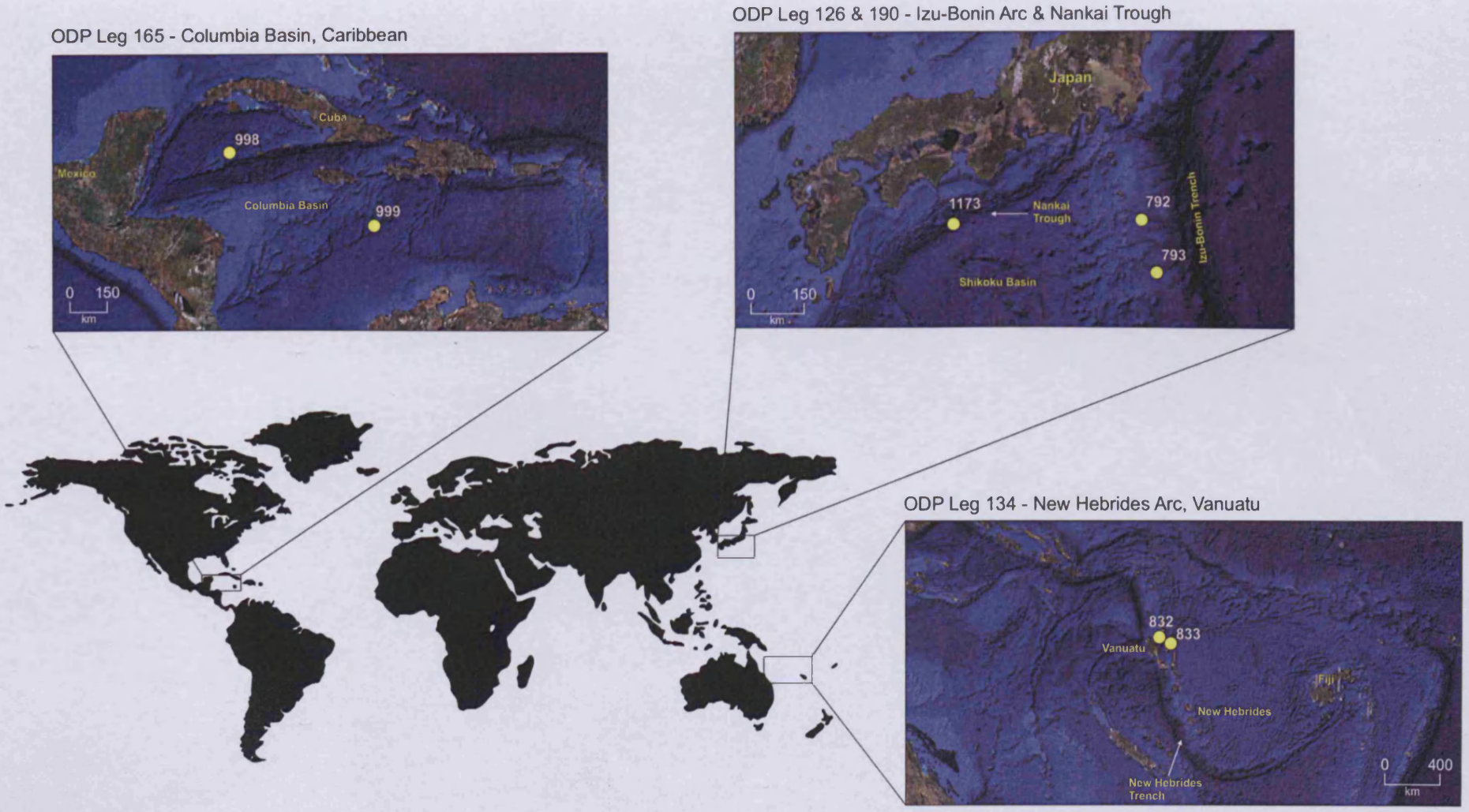

Figure 5.8 Locations of Ocean Drilling Program drill sites examined in this work. Bathymetry maps sourced from Google Earth [http://earth.google.com/]

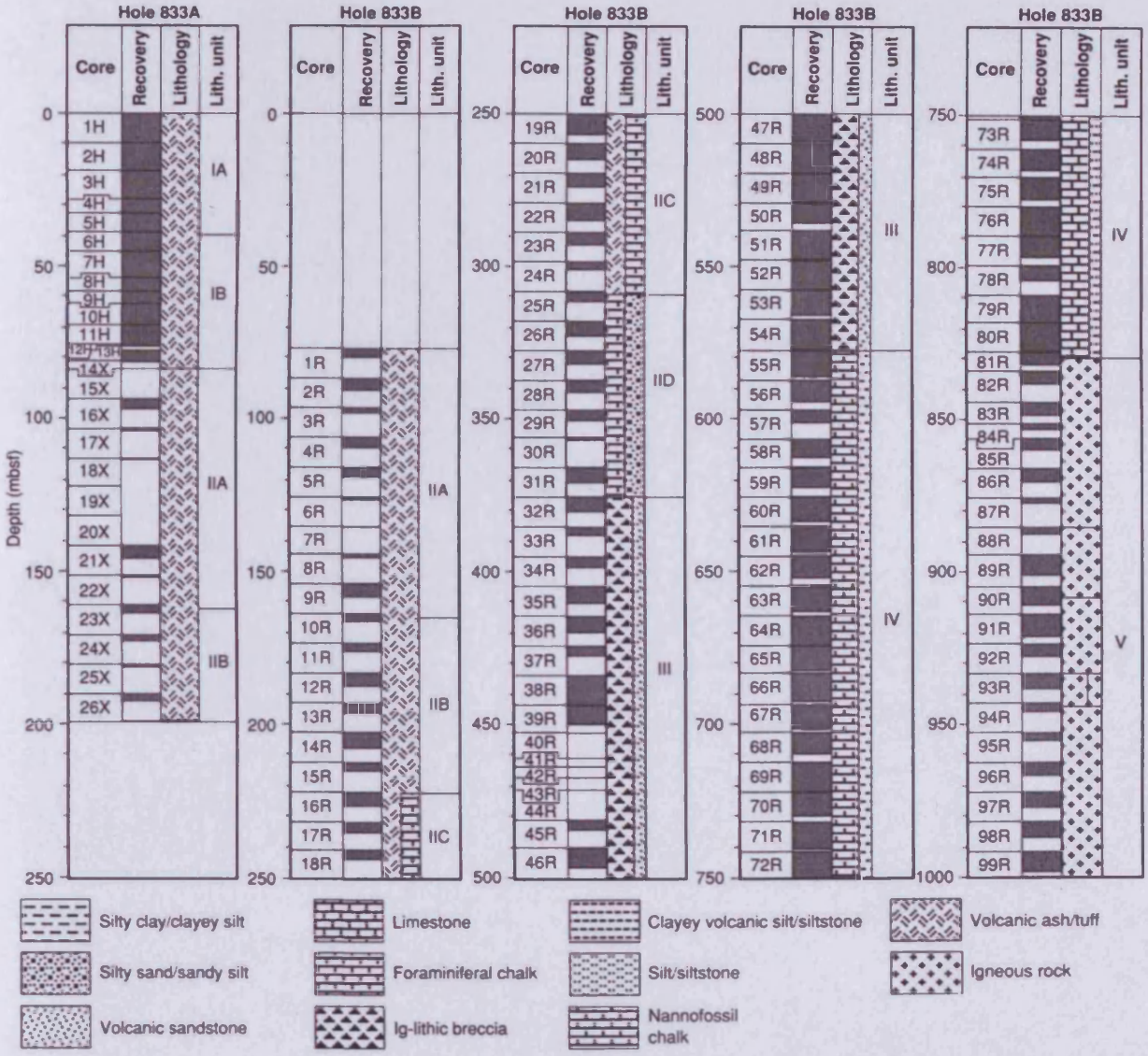

Figure 5.9 Stratigraphy from Site 833 in the North Aoba Basin (New Hebrides margin, Leg 134). Image from Collot et al (1992).

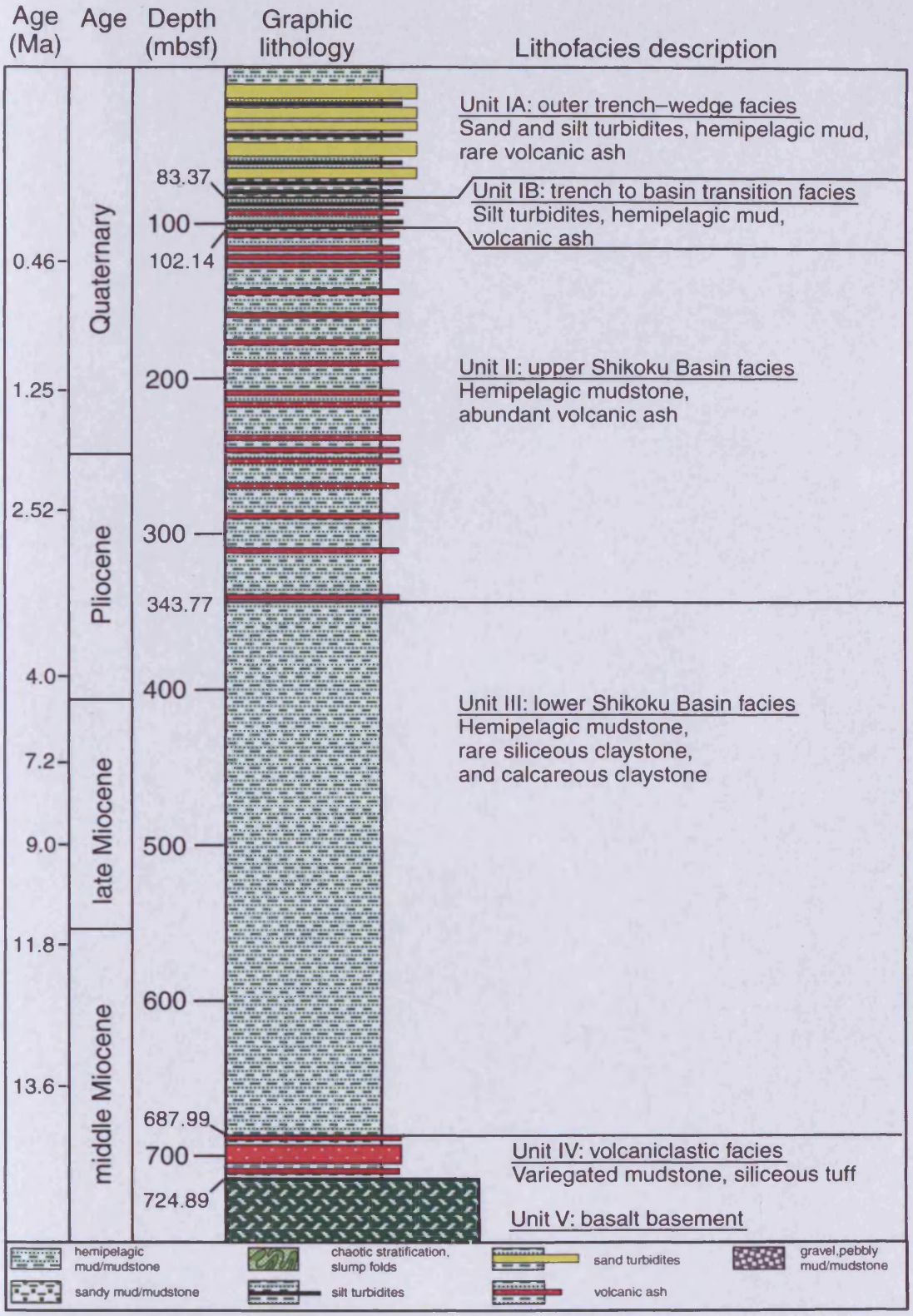

Figure 5.10 Stratigraphy from Site 1173 in the Shikoku Basin (Nankai Trough, Leg 190). Image from Moore et al (2001).

Dissolved silica, which may have been liberated during ash diagenesis, is precipitated as authigenic Ca-bearing silicate cements at Site 792 and 793 (Egeberg et al., 1990). This process is thought to occur at temperatures as low as 25 °C at Site 792, and at roughly 40 °C at Site 793, 150km to the south (Egeberg et al., 1990). Chemical reactions active below a depth of 500 mbsf at Site 792 lead to the precipitation of gypsum and smectites (Fig. 5.11) at temperatures not thought to exceed 80 °C (Egeberg et al., 1990; Tazaki and Fyfe, 1992).

Ash layers first appear in significant numbers below depths of approximately 100-150 mbsf at Sites 998 and 999 from the Columbia Basin (Sigurdsson et al., 1997) (Fig. 5.12). Thick sequences of oozes and biogenic-rich clays are punctuated by frequent ash horizons which first record alteration products, in this case authigenic smectite, at 140 mbsf at Site 998, and at a similar depth of 150 mbsf at Site 999 (Sigurdsson et al., 1997). Chert accumulations below a depth of 350m are also thought to be linked to ash diagenesis, providing a sink for silica released by altering glass material (Lyons et al., 2000) (Fig. 5.13). This process of chert formation thus provides an alternative to the more conventional interpretation of a silica diagenetic pathway from a biogenic opaline starting material to the microcrystalline cherts via opal C-T (Williams and Crerar, 1985).

Ash-bearing hemipelagic sediments of the Shikoku Basin offshore Japan also appear to undergo chemically driven ash-diagenesis at relatively shallow depths and low temperatures (Masuda et al., 1996; Spinelli et al., 2007). Authigenic smectites are first reported from Site 1173 at a depth of roughly 200 mbsf where temperatures are approximately 40 °C (Moore et al., 2001). A stepped increase in the volume of clay minerals is also seen below a depth of ~340 mbsf, coinciding with the lowermost identified unequivocal ash layer (Fig. 5.14). Below 340 mbsf, ash layers are not preserved. This depth interval also coincides with a significant reduction in the concentration of dissolved silica in pore fluids from approximately 1200μM to 200 μM (Moore et al., 2001) (Fig. 5.14). Concentrations of dissolved silica increase steadily to a depth of 340 mbsf depth coinciding with a unit of increasingly deeply buried volcanic ash-bearing mudstones. The pronounced fall in silica values at 340 mbsf is thought to result from the precipitation of smectite and other authigenic phases acting as sinks to dissolved silica (Spinelli et al., 2007).

The precipitation of authigenic phases in the seven ODP Sites mentioned above indicate that as suggested by experimental investigations, the conversion of ash and glass can occur at relatively low temperatures, and at correspondingly shallow depths. Zeolites and palagonites are first seen at depths approaching 150 mbsf depth, while the first instances of authigenic smectite have been recorded at depths of 140 mbsf and 270 mbsf at two of the sites

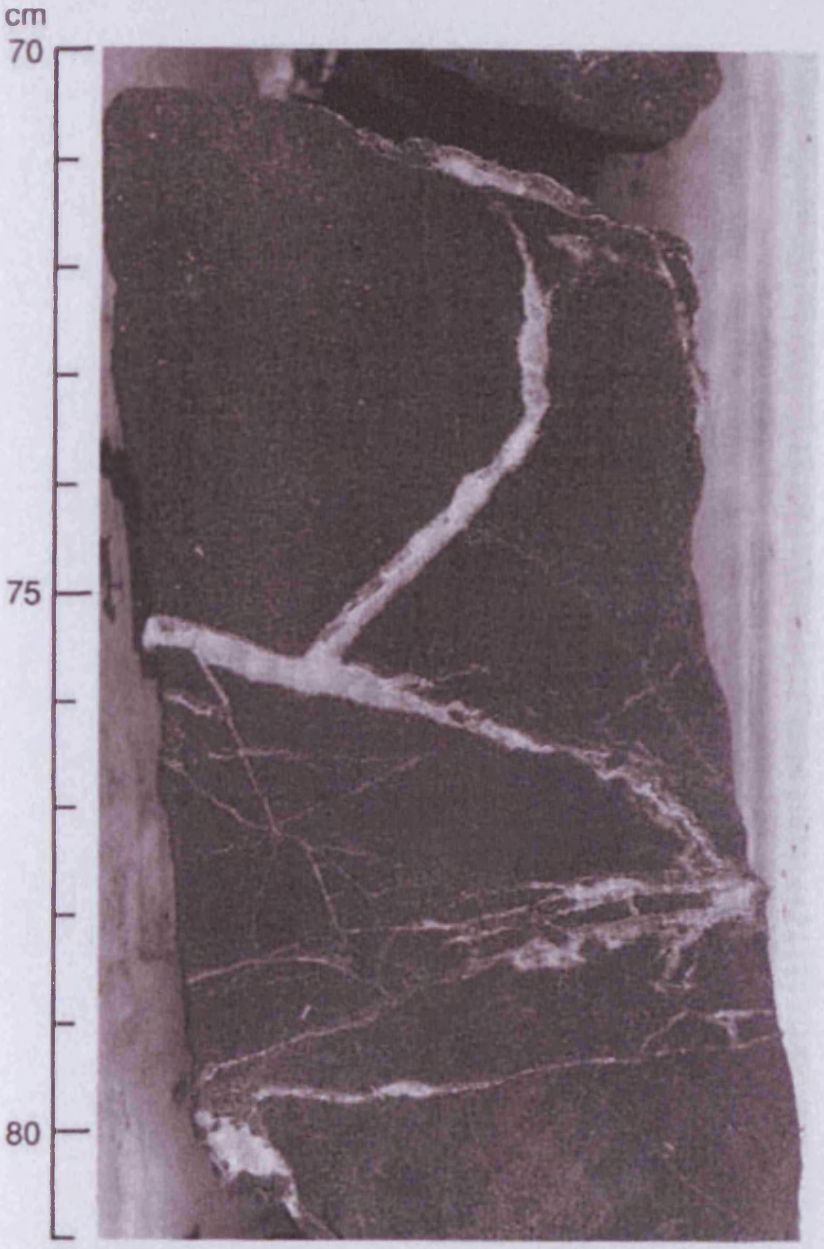

Figure 5.11 Core recovered from Site 793 (Core 27R-3, 70-81cm) showing gypsum-filled fractures in a fine-grained sandstone interval.

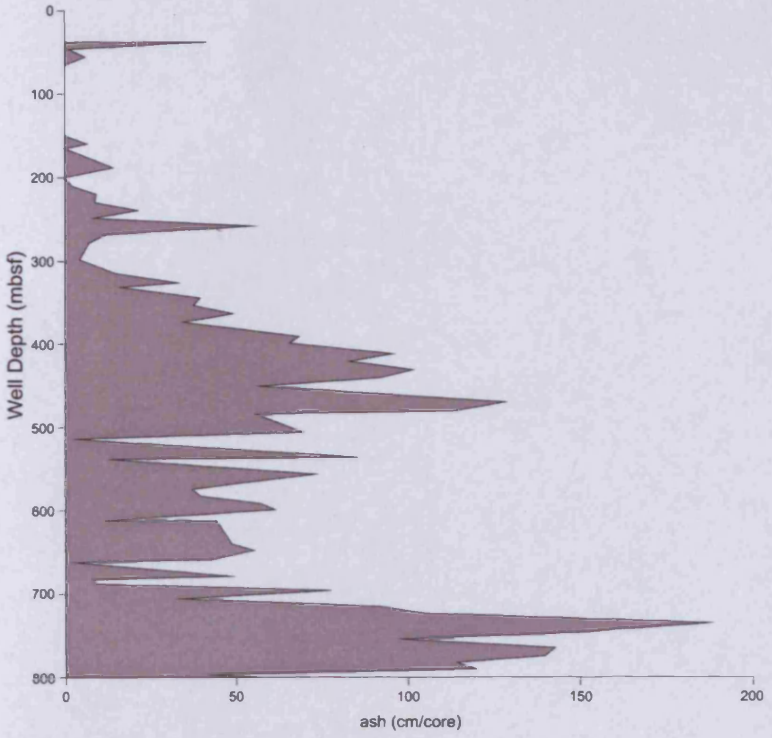

Figure 5.12 Plot showing the volume of ash material plotted against downhole depth from Site 999, Columbia Basin (Caribbean). Redrawn from Lyons et al (2000).

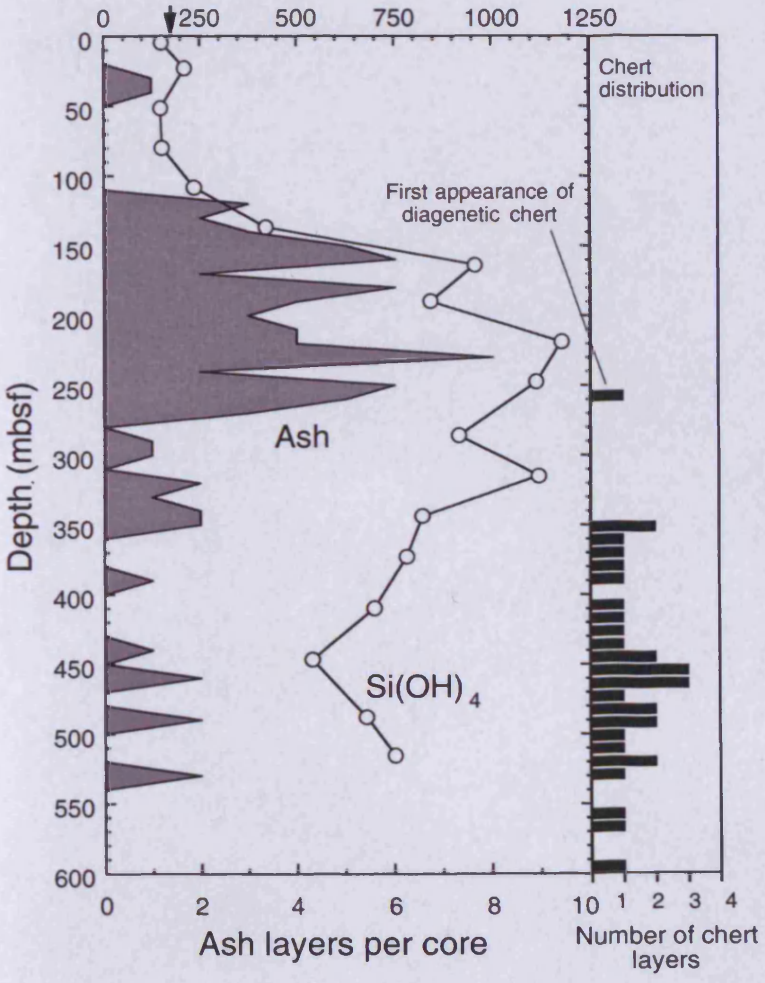

Figure 5.13 Depth profile showing the distribution of discrete ash layer recorded at Site 998 and the frequency of chert layers. Interstitial silica concentrations is also shown (arrow indicates mean ocean bottom-water silica concentration). From Lyons et al (2000).

examined. At depths exceeding 500 mbsf cherts and gypsum have been reportedly precipitated from evolved pore fluids which are directly influenced by ash alteration reactions (Egeberg et al., 1990).

5.4.2 Pore fluid chemistries

Alterations to original pore fluid chemistries occur during ash alteration resulting from the liberation of elements during grain dissolution and their subsequent uptake during authigenic mineral precipitation. Changes in pore fluid chemistries are therefore often seen to coincide with appearances of authigenic minerals which provide a sink for pore fluid cations (e.g. Egeberg et al., 1990; Moore et al., 2001). The shallow chemical alteration of ash material is seen to play an important role in the precipitation of phases such as zeolites, clay minerals, quartz, and gypsum at the ODP sites examined (Egeberg, 1992; Gérard and Person, 1994; Lyons et al., 2000).

In particular, pore fluid concentrations of elements including Si, Ca, K, and Na are seen to be strongly influenced by the distribution and diagenetic state of ash material in the volcaniclastic sequences studied. Dissolved silica concentrations measured from Site 998 in the Columbia basin for example, are seen to increase with increasing ash content until falling sharply at ~350 mbsf where authigenic smectite and chert are thought to provide a sink for these leached cations (Fig. 5.13) (Lyons et al., 2000). A similar relationship is seen at Site 1173 from the Shikoku Basin where silica concentrations in pore fluid fall sharply, by over 80%, at a depth of 340 mbsf, an interval which also correlates exactly with an increase in the volume of clay minerals (Fig. 5.14). Pore fluid silica concentrations from Izu-Bonin Site 792 reveal a pronounced drop at approximately 400 mbsf, below which depth smectites and gypsum begin to be precipitated (Fig. 5.15).

Perhaps the most significant alteration to pore fluids in response to ash conversion is the development of $CaCl_2$ brines, reported from both Izu-Bonin and New Hebrides sites. Egeberg et al. (1990) report extreme Ca concentration in pore fluid from Izu-Bonin sediment cores recovered during ODP Leg 126. Pore fluids enriched in Ca are thought to have developed through the dissolution of volcanogenic material. It is suggested that hugely elevated Cl concentrations develop because of the uptake of water during ash hydrolysis (Egeberg et al., 1990). Mass balance considerations suggest that up to 25% of the rock matrix has been converted to low temperature secondary products such as smectites, zeolites and gypsum (Egeberg et al., 1990). Very similar Ca-rich brines have also been reported from fine-grained sediments from the New Hebrides margin, which are also thought to be linked to exchanges

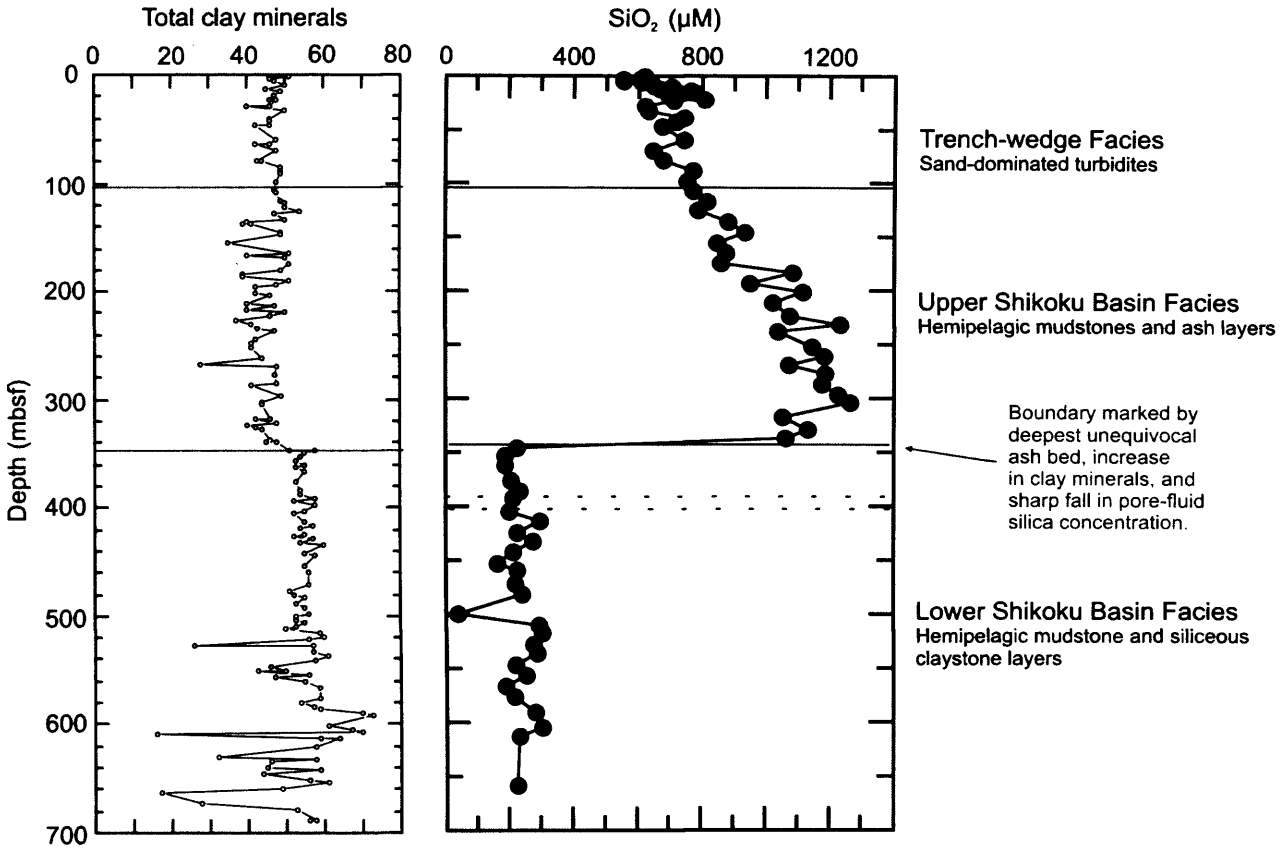

Figure 5.14 Depth plot from ODP Site 1173 (Nankai Trough) showing the total volume of clay minerals and the concentration of dissolved silica from interstitial fluids. An increase in the volume of clay minerals and a marked fall in the concentration of dissolved silica coincide with the depth of the lowermost unequivocal ash bed at 340m depth (adapted from Moore et al, 2001).

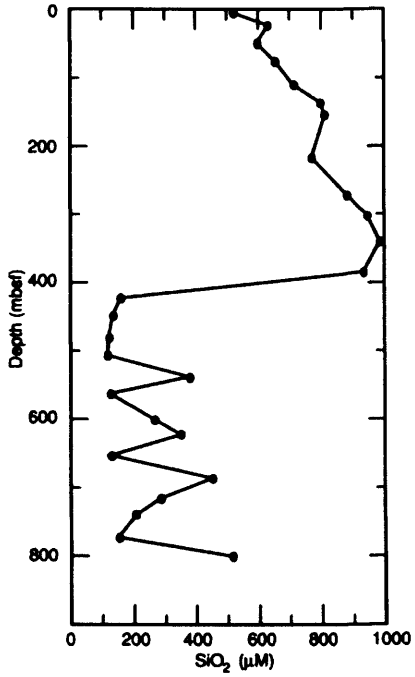

Figure 5.15 Pore water silica concentration from Site 792, Izu-Bonin Arc. Below a depth of 400m, smectites and gypsum begin to be precipitated (adapted from Taylor et al, 1990).

between ash and pore waters (Martin, 1994). Insights into the mobility of particular elements in pore fluid chemical changes resulting from ash diagenesis also come from a range of experimental studies. In addition to Ca and Cl, exchanges of other cations such as K and Na are documented from the experimental dissolution of synthetic glass (e.g. Techer et al., 2001) and comparisons of fresh and altered glass samples (e.g. Noble, 1967; Lipman et al., 1969; Staudigel and Hart, 1983). These experiments indicate that glass undergoing alteration is generally depleted in Na compared to fresh glass, whilst K may be either enriched or depleted. Pore fluid compositions recorded from ash-bearing marine sediment also illustrate the mobility of K and Na during ash alteration. Data collected from Izu-Bonin sites indicates that pore fluid concentrations of Na and K experience a pronounced reduction at the top of the major altered ash-bearing sequence. It is suggested that at this depth, Na and K released during the early hydrolysis of volcanic material is recovered from pore fluids by precipitating authigenic phases, most likely zeolites (Egeberg et al., 1990). Cations recovered from pore fluids at Site 792 are almost entirely replaced by Ca producing the $CaCl_2$ brines mentioned previously (Egeberg et al., 1990). A similar pattern is seen in sediments from the New Hebrides margin where pore fluids show initial Na and K enrichment with respect to seawater, before a marked reduction, corresponding with a unit containing large volumes of ash (Lithological Unit II, Collot et al., 1992) at 400m depth (Fig. 5.16). This reduction in pore fluid Na and K again coincides with a significant increase in the concentration of dissolved Ca (Martin, 1994) (Fig. 5.16). Concentration of dissolved Na and K from Shikoku Basin sediments (ODP Leg 190) also show a marked reduction, in this case at a depth of 340 mbsf, coinciding with the first interval of pervasively altered ash (Moore et al., 2001). The precipitation of zeolites, particularly phillipsite, is thought to provide the most significant sink for Na and K which are liberated from altering ash (Egeberg, 1992).

5.5 Changes to sediment physical properties during ash diagenesis

Very little work has been published examining the physical properties of submarine ash deposits (i.e. Bouma and Moore, 1975; Carlson et al., 1980; Carlson, 1981; Dadey and Klaus, 1992), while even less is known about changes to their physical properties during diagenesis (e.g. Tribble and Wilkens, 1994). Information collected by the Ocean Drilling Program in ash-bearing sequences allows the investigation of shallow diagenesis in natural systems and for changes in the physical properties of ash layers and surrounding sediments to be evaluated. These multifaceted datasets, which include sample analysis and continuous wireline logging, provide pore fluid chemistry and mineralogy data from ash-bearing units and host sediments, providing information regarding active chemical diagenesis (*see* section 5.4). They also provide the majority of what little quantitative data exists regarding the physical

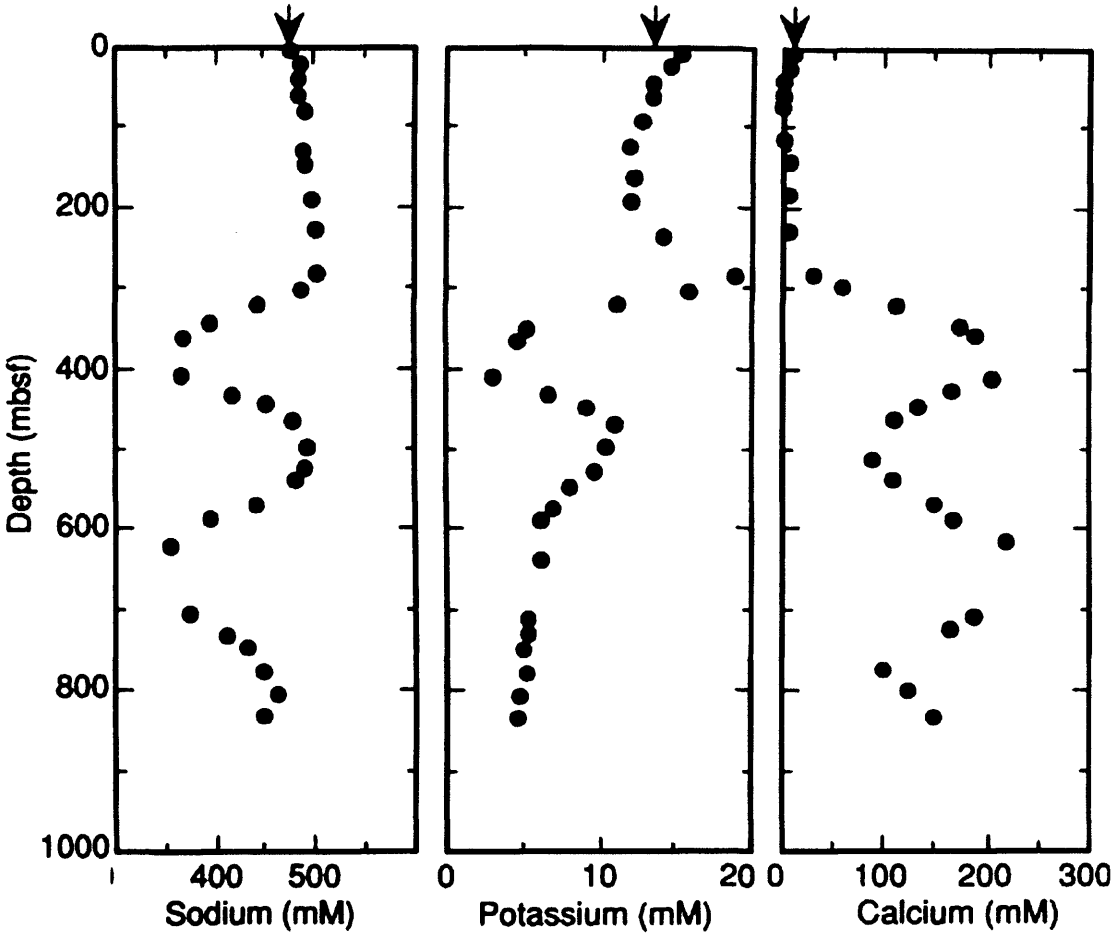

Figure 5.16 Depth plot from ODP Site 832 showing concentrations of sodium, potassium and calcium in pore-fluids. Reductions in the concentrations of sodium and potassium at 350-400m and again at 500-600m depth correlate with maximum values seen in the concentration of calcium.

properties of submarine ash units (e.g. porosity, permeability, grain-size distribution, density etc).

A significant change in the physical properties of ash layers must inevitably accompany the progressive alteration of glass and pumice to smectite clays. Porosity and permeabilities of ash-layers will be influenced by the progressive physical replacement of original glass shards and pumice by clays during diagenesis (Tribble and Wilkens, 1994). Although no data exists for the hydraulic properties of marine ash deposits at the point of deposition, permeability measurements from largely unaltered ash layers were recorded from shallow Shikoku Basin facies in the Nankai Trough and indicate that values are as much as five orders of magnitude greater than those of background clay-rich sediments (Moore et al., 2001) (Fig. 5.17). Shallow buried ash layers which are thought to have undergone little alteration have also been identified the Cascadia margin, and offshore from the Andaman Islands, in the Bay of Bengal. In both of these cases, intervals dominated by volcanogenic sediments act as reservoirs and migration pathways for shallow gas hydrates, exhibiting higher hydraulic conductivities than surrounding fine-grained marine sediments (Tréhu et al., 2003; Collett et al., 2008) (Fig. 5.18). In petroliferous basins, unaltered ash-rich units may exhibit very different fluid-flow characteristics to those of fine-grained host sequences, with implications for seal and trap integrity.

The porosity and permeabilities of ash units which undergo shallow diagenesis will be altered in response to diagenetic reactions and mechanical compaction because of the fundamental change in grain-size distribution (increased volume of clay minerals), specific surface area of particles and electrochemistry (van Olphen, 1977). The precipitation of authigenic phases will progressively infill pore volume with crystalline material while silt- and sand-sized glass shards are increasingly dissolved and replaced. However, the relationship between ash fluid-flow properties and its degree of alteration is likely to be a complex system. Observations of Dadey and Klaus (1992) highlight some of the complexities of these processes from ODP data acquired from the Izu-Bonin sites. Porosity and velocity data collected at Sites 788, 790, 792, and 793 suggest that some buried ash and pumice layers have relatively high porosities (up to 70%), despite in some cases also exhibiting high sonic velocities. They go on to suggest that original intragranular porosity in pumice material and poorly connected porosity, formed by the early cementation of grain contacts, is responsible for high porosities coinciding with increasing sediment rigidity, and hence velocity values. In this case, diagenesis has complicated the normal one-dimensional compaction of sediments.

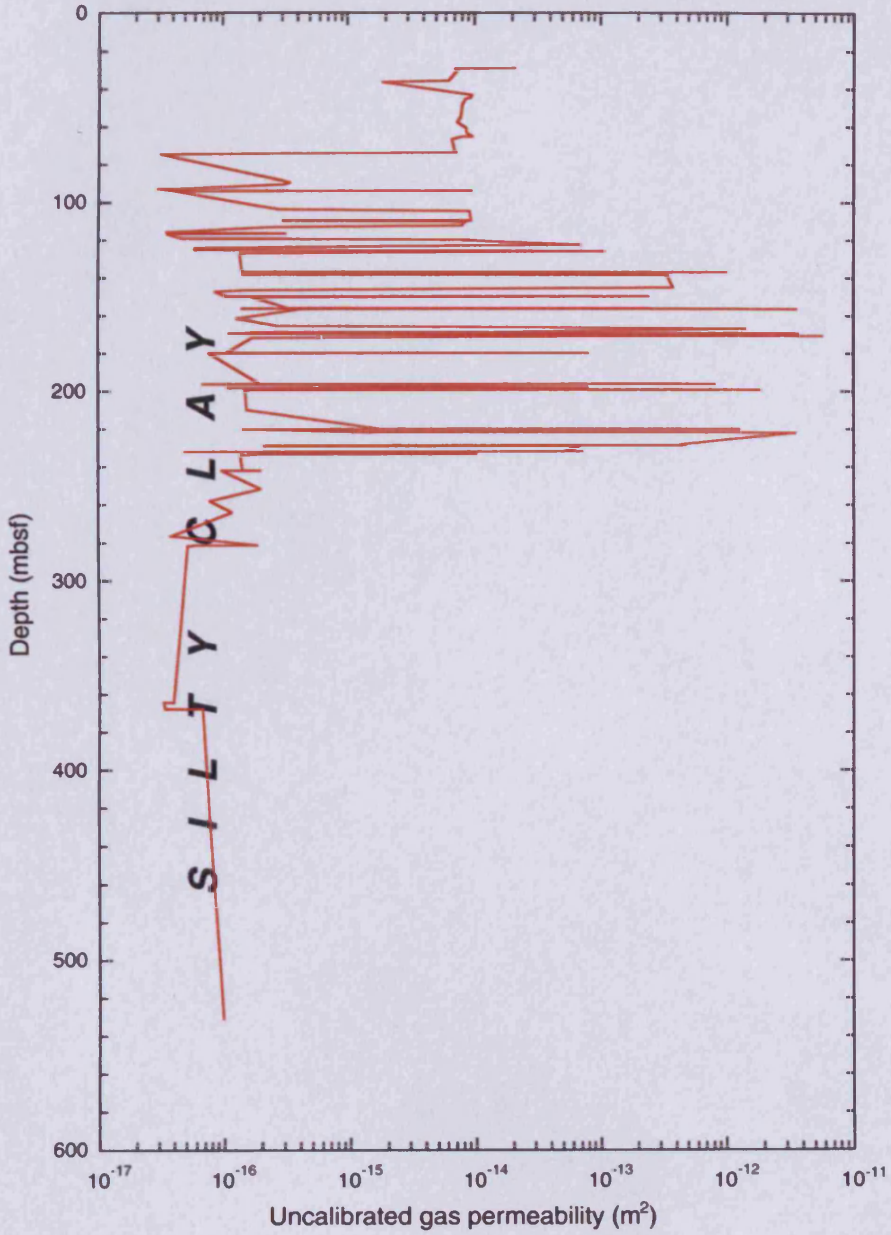

Figure 5.17 Depth plot showing gas permeability data from ODP Site 1173 at the Nankai Trough. Peak values above 250m depth are derived from relatively high permeability ash layers (taken from Moore et al, 2001).

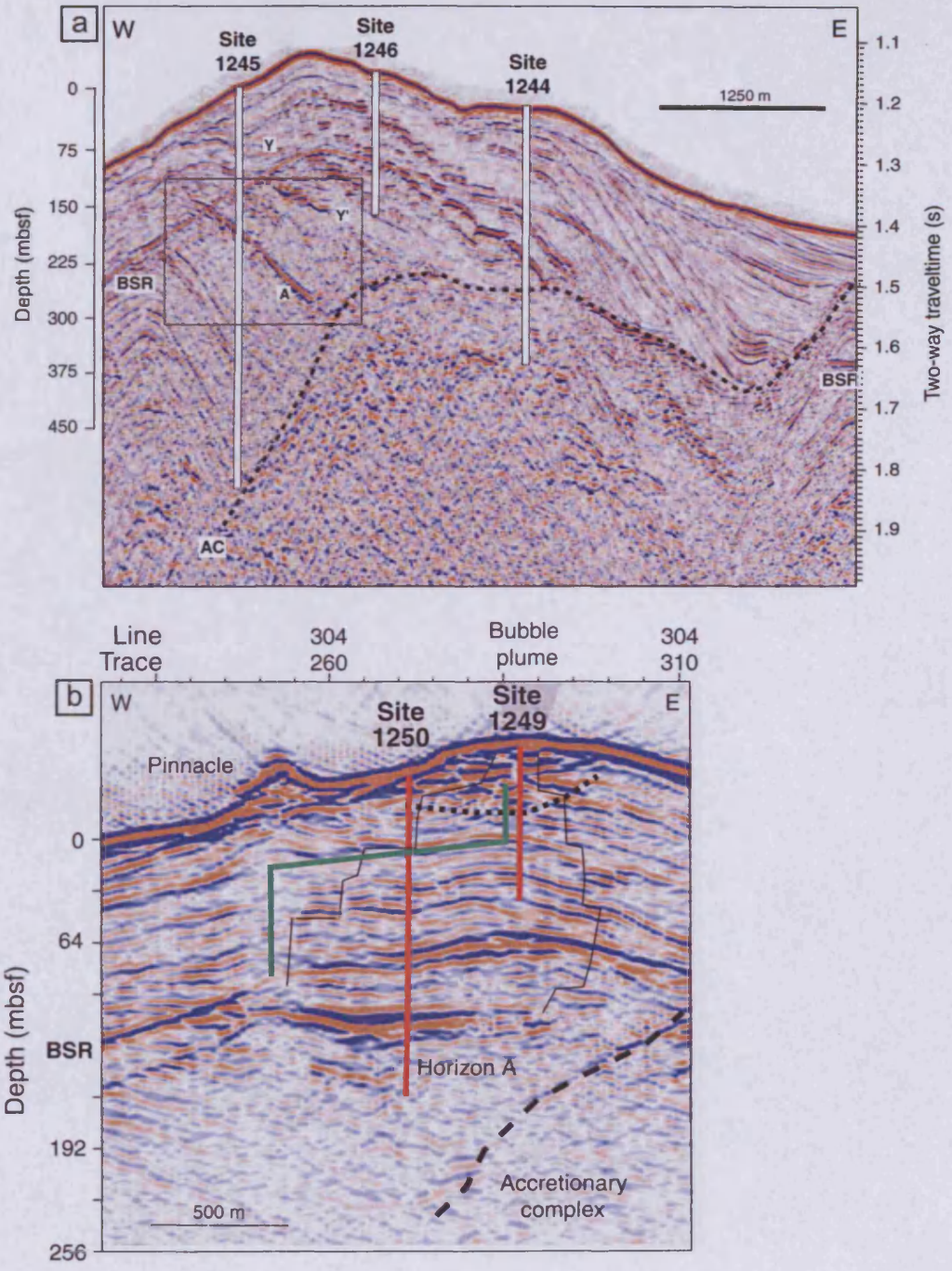

Figure 5.18 (a) Seismic profile across Hydrate Ridge on the Cascadia Margin. The high amplitude reflector marked 'A' was penetrated by Site 1245 and found to comprise a 2-4m thick unit of volcanic ash beds. This horizon is thought to provide a relatively high permeability conduit for migrating gas hydrates (image taken from Tréhu et al, 2003) **(b)** Seismic profile showing high amplitude reflector 'A' as it appears 2km south of Site 1245 where it was penetrated by Site 1250. Red, green, and black lines denote possible vertical migration pathways for gas hydrates reservoired in 'A', as proposed by Tréhu et al (2004).

Permeabilities in clay-rich sequences have also been shown to be significantly affected by certain pore fluid chemical chemistries known to exist in altered ash-bearing sequences. Experimental investigations by Kwon et al. (2004a, 2004b) investigated the impact of a range of pore fluid chemistries on the permeability of shale samples from the Wilcox shale. It was noted that permeabilities were as much as five times greater in clay samples for the flow of 1*M* solution of $CaCl_2$ than for either water, or solutions of NaCl, or KCl. The authors suggest that changes in permeabilities appear to be due to differential absorption and cation selectivity of clay surfaces, and that this sensitivity is likely to increase at shallower depths where sediments have a greater proportion of swelling clays such as smectites relative to illite (Kwon et al., 2004b). These findings have important implications for ash-bearing sequences where $CaCl_2$ brines are known to develop as a product of ash alteration, and where smectitic clays are found in high volumes e.g. Izu-Bonin and New Hebrides sequences (Egeberg et al., 1990; Martin, 1994).

On a basin scale, ash diagenesis also has implications for sediment compaction and fluid flow in volcaniclastic sequences. Laterally continuous smectite-rich layers which develop as a result of ash conversion are likely to exhibit markedly reduced permeabilities compared to ash material in its original, unaltered state. Where volumes of discrete ash beds are altered, the resulting low-permeability clay layers can act as barriers to vertical fluid migration and may slow the escape of pore fluids from surrounding sediments. This process is likely to be of particular importance where a high volume of ash material is interspersed with mud-rich sediments, likely to have high water contents and to undergo rapid de-watering, such as in the Columbia Basin (Sigurdsson et al., 1997). A potential implication of intraformational seal development is the development of overpressure cells with abnormally high pore fluid pressures (e.g. Schlomer and Krooss, 1997).

Discussions presented in previous sections suggest that typically, volcanic ash material will lose porosity and permeability as material becomes increasingly altered to secondary minerals. Several studies also highlight the complexities of shallow diagenetic reactions, and the sensitivity of sediment physical properties to pore fluid chemistries and early diagenetic precipitations (Kwon et al., 2004b; Dadey and Klaus, 1992). It is notable that the potential for ash-rich intervals to offer high permeability/low capillary pressure units compared to fine-grained host sediment will decrease with increasing glass alteration. The potential for ash layers therefore to function as seal bypass points in petroliferous sequences, in a similar way to that of sand and silt beds examined in previous chapters, is reduced significantly below depths of several hundred meters where alteration become pervasive (e.g. Shikoku basin, Moore et al., 2001).

In addition to considerations regarding the function of fresh and altered volcanic ash as capillary seals or flow conduits, ash diagenesis is also presented as a potential mechanism for the structural deformation of sedimentary units. Results of experiments examining the effect of insitu grain dissolution on the structural stability of granular media have recently been published by Shin et al. (2008). Their laboratory experiments were conducted by circulating warm fluids through aggregate mixtures of glass beads and soluble salt grains. Data suggests that volume contraction, associated with grain dissolution, causes a reduction in horizontal stress and the potential for internal shear failure conditions to develop (Shin et al., 2008). A similar reduction in volume, associated with the isovolumetric exchange of cations during diagenesis, has been suggested for volcanic glass alteration (Crovisier et al., 1987; Stroncik and Schmincke, 2001). The implications for such a mechanism potentially extend to the development of fracture networks and the propagation of faults nucleated in zones having undergone diagenetically induced volume contraction. Evidence for fracturing is seen in cores from all seven ODP sites examined here. High angle microfractures are common at Sites 792 and 792 from the Izu-Bonin fore-arc basin where fractures are often infilled with zeolites and gypsum (Fig 5.11). Similarly, sites from the New Hebrides are heavily fractured, particularly below depths of ~300 mbsf (Fig. 5.19 and 5.20). A polygonally faulted interval is also reported from ash-bearing mudstones of the Upper Shikoku Basin sequence from the Nankai Trough (Heffernan et al., 2004) (Fig. 5.21). Layer bound normal fault networks of this kind were first described from the North Sea Tertiary intervals (Cartwright and Lonergan, 1996) and have subsequently been identified from over 28 locations worldwide (Cartwright and Dewhurst, 1998). One hypothesis for the development of these fault networks, in the absence of any tectonic extension, has been the process of syneresis, or chemical dehydration, where three-dimensional contraction of smectite-rich sediment occurs through interparticle forces between clay particles and seawater (*see* Dewhurst et al., 1999c). The uptake of unbound water during incipient hydration of volcanic glass (e.g. Ross & Smith, 1955; Federman, 1984) represents another process where the dehydration of sediments may occur at shallow burial depths in smectitic sediments.

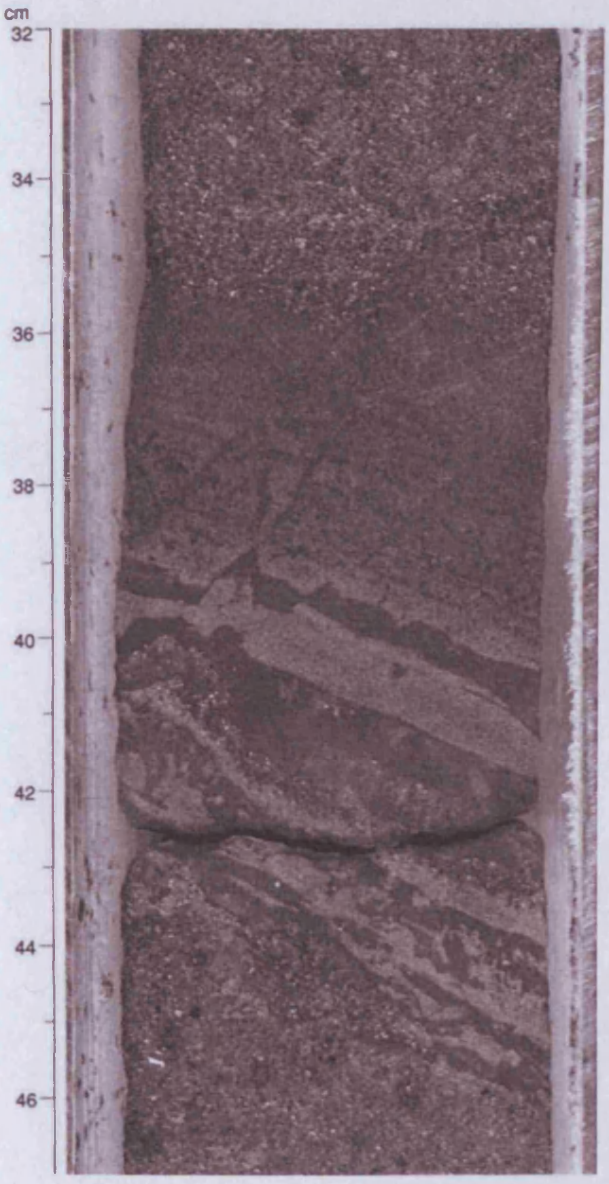

Figure 5.19 Core photograph from Site 832 from the New Hebrides Arc. High angle microfractures are seen cutting silts and vitric sandstone layers at 650m depth (image taken from Collot et al, 1992).

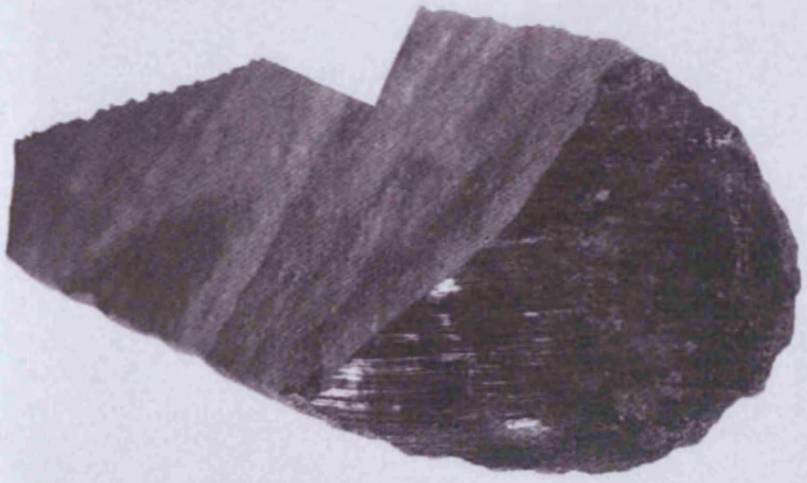

Figure 5.20 Photograph of fault surface showing slickensides with a normal sense of movement from core recovered at Site 832 (750m depth). Image taken from Collot et al (1992).

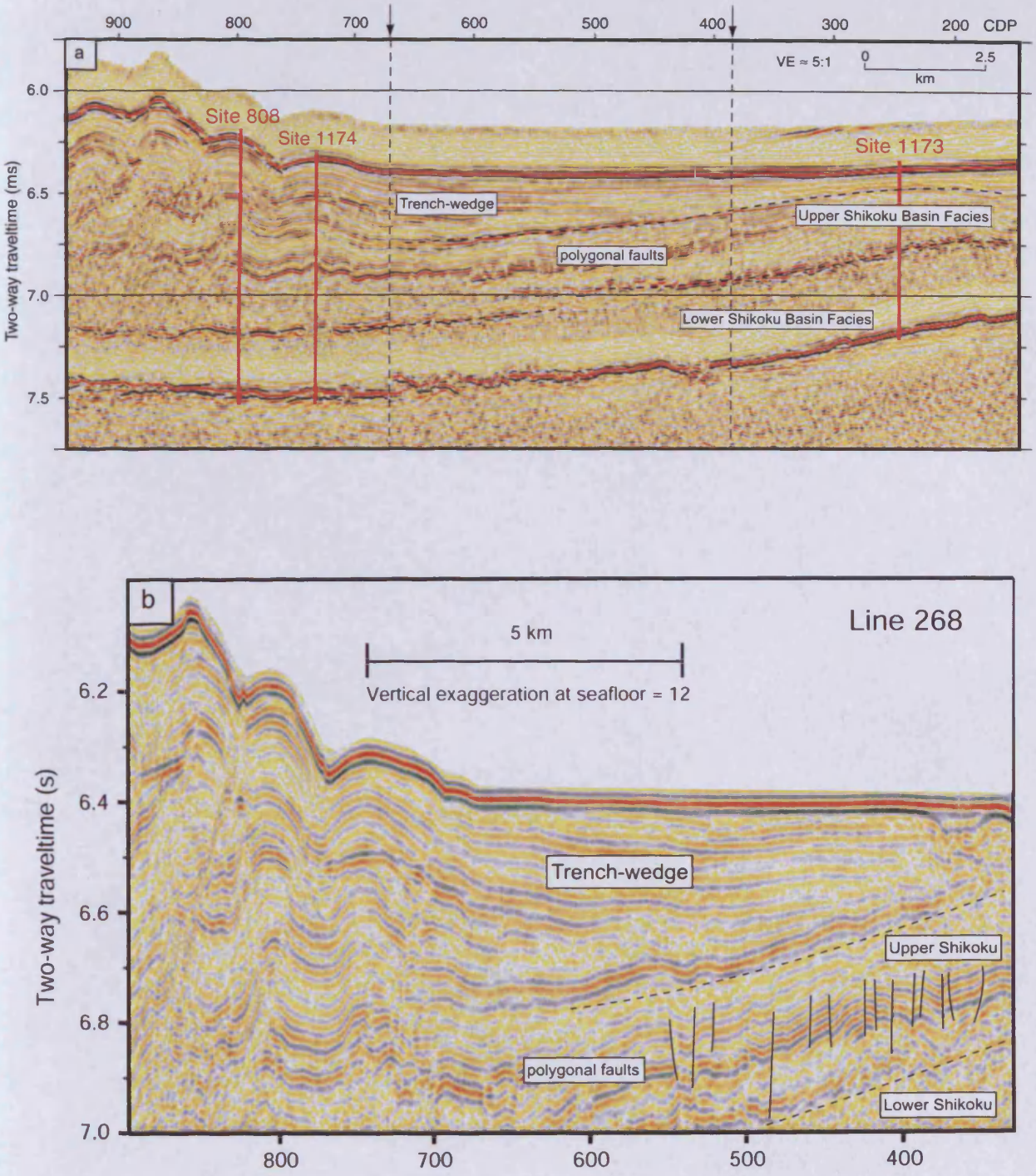

Figure 5.21 Seismic profiles from the Nankai Trough. (a) Seismic profile showing the positions of ODP Sites and the general stratigraphy of the Shikoku Basin. An interval of polygonally faulted mudstones is seen within the Upper Shikoku Basin Facies (grey shaded box). (b) Interpreted seismic profile showing the layer-bound nature of the polygonal fault network within the Upper Shikoku Basin Facies. Images adapted from Bangs and Gulick (2005).

5.6 Conclusion

1. Volcanic ash undergoes a particularly rapid and chemically complex diagenetic evolution at relatively shallow burial depths, contrasting with that of the majority of siliciclastic sediments.

2. Volcanic glasses are thermodynamically unstable and are readily altered to secondary minerals under shallow burial conditions through cation exchanges between glasses, authigenic phases, and pore fluids.

3. Ash-bearing units are likely to experience a reduction in porosities and permeabilities as glass shards are progressively replaced by clay minerals and pore volumes are infilled by authigenic minerals.

4. Evolving pore fluid brines which develop as a result of cations being leached from ash layers are likely to influence the fluid-flow properties of ash-bearing sequences and govern the mineralogy of precipitated phases.

5. The dehydration of volcaniclastic units in response to glass hydration is suggested as an addition mechanism to that published by Dewhurst et al. (1999c) for initiating syneresis and the volumetric contraction of sediment, potentially leading to fault nucleation.

Chapter 6

Chapter 6

Heterogeneities in fine-grained slope sequences: Predictability and implications for seal capacity

6.1 Introduction

This thesis comprises a series of 'pilot' studies designed to establish future avenues for research in a much longer term research program. The principal aim of this discussion chapter therefore is to evaluate how the main findings presented in this thesis can be applied to help better predict the seal quality of slope-drape sediments pre-drilling. Studies have aimed to highlight some of the lithological and physical heterogeneities that exist in fine-grained siliciclastic continental slope sequences, with particular emphasis on hemipelagites, and to address how these may impact fluid-flow pathways in the subsurface. My investigations have explored a number of research topics which all feed in to the overarching theme of the Caprocks Project which is tasked with providing petroleum explorers tools with which to more accurately predict the properties of mudstone sealing sequences. Within the Caprocks Project, I was given the task of establishing what kinds of processes influence the sealing integrity of hemipelagite dominated seals.

6.1.1 Seal capacity of fine-grained slope sequences

Seal integrity forms a critical, if relatively poorly studied, aspect of petroleum systems analysis. While the fundamental aspects of hydrocarbon trapping are well understood, the mechanisms and rate by which hydrocarbons migrate through seals remains poorly quantified (e.g. Grunau, 1987; Weber, 1997). In order for significant volumes of hydrocarbons to accumulate within a trap, fluid migration must be sufficiently retarded by a seal. In many cases, this seal is provided by a layer with low permeability, most commonly mudstones or evaporites (Grunau, 1987).

The critical importance of mudstones in the petroleum system is illustrated using a compilation of data in Figure 6.1. This figure helps explain the rationale behind examining these mudstone or claystone dominated sealing sequences. In Figure 6.1, I show the distribution of sealing lithologies from over 45,000 hydrocarbon fields around the world (*data source*, IHS Energy). This huge dataset clearly highlights the dominance of mudstones as seals to oil and gas accumulations worldwide, accounting for almost 80% of the fields

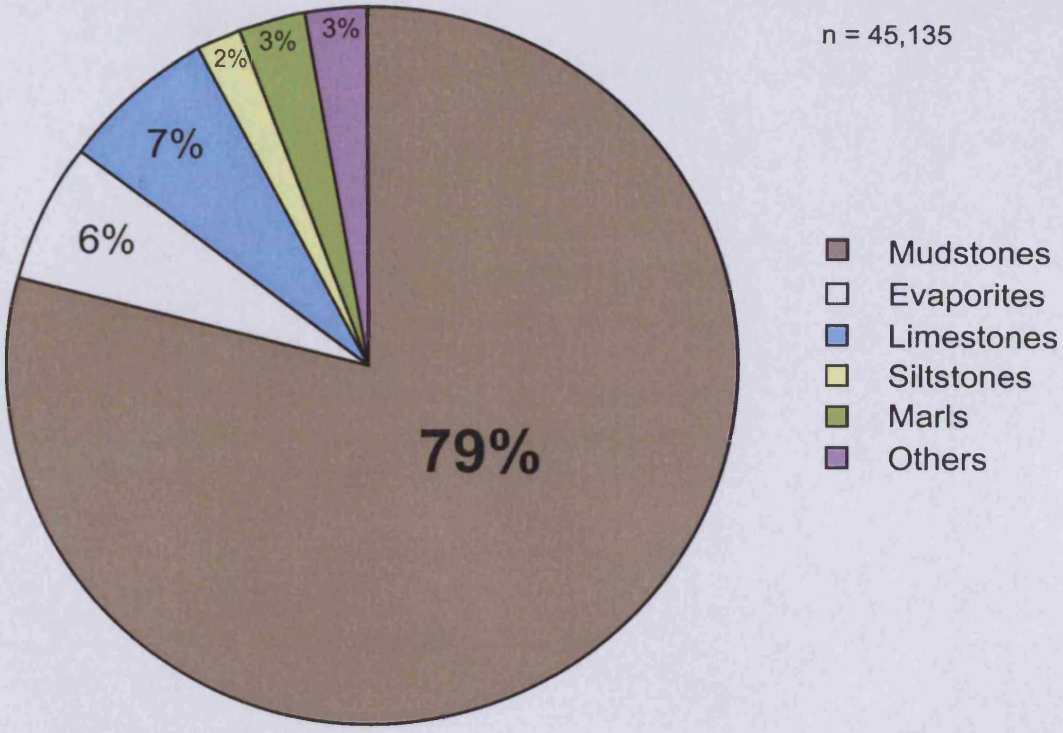

Figure. 6.1 Pie-chart showing the distribution of top seal lithologies from over 45,000 fields. Note the clear importance of mudstone sequences as seals in petroleum systems (*data source*, IHS Energy, 2009).

examined. This conclusion underpins the importance of improving our understanding of this type of sealing sequence, and documenting any factors that impact upon the sealing capacity of such sequences.

6.1.2 Global importance of hemipelagite sealing sequences

From a petroleum explorer's perspective, hemipelagic mudstones in particular typically represent favourable potential seal units, offering sequences of fine-grained sediment which can be 100's of metres thick and of enormous lateral extent (Downey, 1984). These slope drape mudstone deposits are proven hydrocarbon seals in many petroleum provinces. In the North Sea Basin for example, hemipelagic claystones of the late Palaeocene-aged Lista Formation are found widely distributed and are of significant economic importance (Mudge and Copestake, 1992). The Lista Formation provides the regional top seal to a number of fields in the East Shetland Platform area including the Balmoral (*see* Fig. 6.2) and Moira Fields and the Armada Field located on the southeast margin of the South Viking Graben (Tonkin and Fraser,199; Gluyas and Hichens, 2003). Another prolific hemipelagic seal in the northern North Sea Basin is the early Eocene-aged Sele Formation, which is dominated by hemipelagic silty claystones. The Sele Formation provides the regional seal over the Forties Field anticline, a structure with an oil column of 187m and an estimated initial in place oil volume of over 4.0 billion barrels, prior to initial production in 1975 (Wills, 1991; Mudge and Copestake, 1992; Gluyas and Hichens, 2003).

Globally, hemipelagic mudstones represent important sequences in many passive margin hydrocarbon provinces, and are becoming increasingly prevalent sealing units as hydrocarbon exploration moves basinward into deeper water environments. Table 6.1 presents data from 20 offshore oil fields where reservoired accumulations rely on regional hemipelagic top seals. Estimations of in-place oil volumes from these example fields range from accumulations of ~150 million barrels, such as the North Rankin Field (NW Australian shelf), to giant oil fields including the July Field in the Gulf of Suez, and the Minas Field in central Sumatra, which together have an estimated oil volume of close to 10 billion barrels (*data source*, C&C Reservoirs).

The relationships between hemipelagic seal thickness, in place oil volumes, column heights, and field areas from this dataset are plotted in Figs. 6.3. Plots 6.3a and 6.3b clearly show that, at least from this limited dataset, no clear systematic relationship exists between mudstone seal thickness and the two volumetric parameters. What can be taken from these plots however, is that it is possible to trap oil columns of up to 600m beneath relatively thin

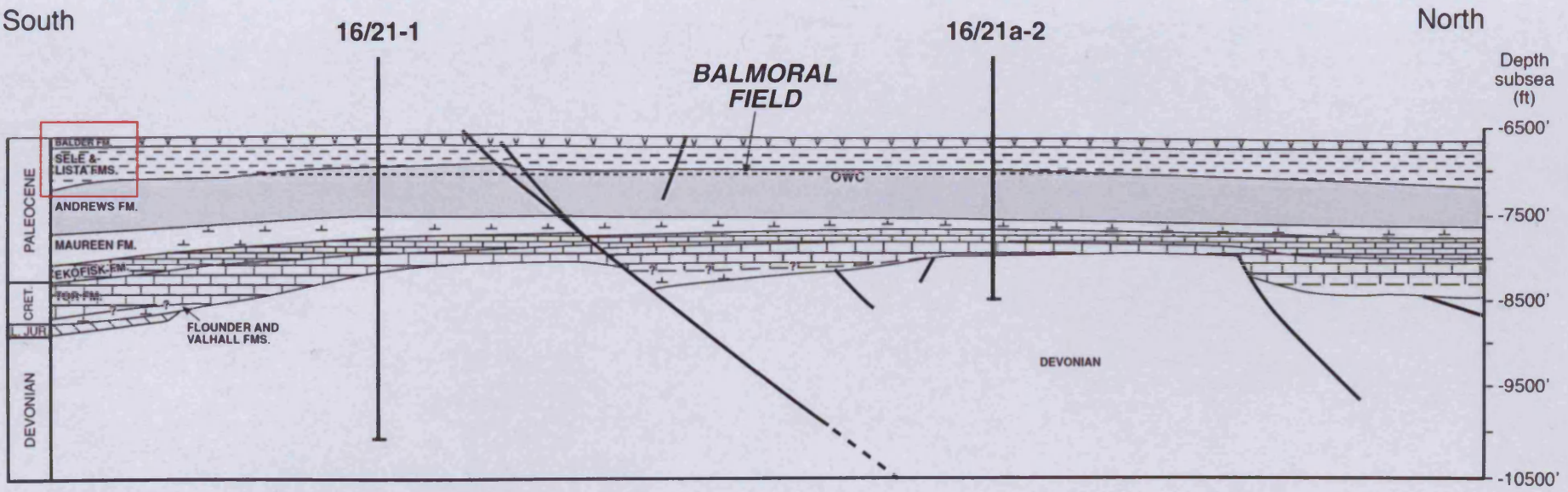

Figure 6.2 Schematic cross-section through the Balmoral Field, North Sea Basin. The Lista and Sele mudstone formations provide the top seal to a broad, anticlinal structure. Taken from Tonkin and Fraser, 1991.

Field		Seal					
Name	Location	Lithology	Age	Depositional process	Thickness (m)	Oil column (m)	Oil in place (MMbbl)
Bonga	Niger Delta Basin, Nigeria	Mudstone	Eocene	Hemipelagic on slope	>100	702	1470
Bullwinkle	Gulf of Mexico, U.S.A.	Mudstone	Pliocene	Bathyal hemipelagic	150	460	190
Draugen Field	Mid-Norway Shelf, Norway	Mudstone	Upper Jurassic	Anoxic marine	>100	40	1100
Emeraude Field	Congo Coastal Basin, Congo	Mudstone	Upper Cretaceous	Deep marine	>100	125	5750
Foinaven	Faeroe-Shetland Basin, U.K.	Mudstone	Upper Paleocene	Deep-marine basinal	N/A	158	337
Forties	Central North Sea, U.K.	Mudstone	Eocene - Recent	Slope hemipelagic	2000	187	4196
Girassol	Lower Congo Basin, Angola	Mudstone	Miocene	Hemipelagic	>100	221	1550
Gryphon	Northern North Sea, U.K.	Mudstone	Early Eocene	Slope and deep-marine basin	200	57	N/A
Jolliet	Gulf of Mexico, U.S.A.	Mudstone	Middle Pleistocene	Bathyal hemipelagic	3-60	upto 600	143
July	Gulf of Suez, Egypt	Mudstone	Middle Miocene	Slope hemipelagic	N/A	450	>5500
Lobster	Gulf of Mexico, U.S.A.	Mudstone	Pliocene	Deep-water slope	180	880 - 1325	210
Magnus	Northern North Sea, U.K.	Mudstone	Mid Cretaceous	Slope hemipelagic	>90	365	1652
Malampaya	Palawan Basin, Philippines	Mudstone	Middle Miocene	Slope hemipelagic	300	56	268
Marimba	Campos Basin, Brazil	Mudstone	Late Cretaceous	Upper-slope hemipelagic	>100	114	736
Mars	Gulf of Mexico, U.S.A.	Mudstone	Miocene	Hemipelagic & slope fan	15-180	N/A	>700
Minas	Central Sumatra, Indonesia	Mudstone	Middle Miocene	Open marine	120	146	>4000
Namorado	Campos Basin, Brazil	Mudstone	Mid Cretaceous	Upper-slope hemipelagic	>10	185	800
Nelson	Central North Sea, U.K.	Mudstone	Early Eocene	Basinal, deep-water	30	86	>500
North Rankin	Carnarvon Basin, Australia	Mudstone	Mid Cretaceous	Marine shelf	N/A	570m (gas)	162
Tiffany	Northern North Sea, U.K.	Mudstone	Late Jurassic	Anoxic marine basin	45-90	500	338

Table 6.1 This table contains data from 20 oil fields where hydrocarbon accumulations rely on regional hemipelagic top seals. This data is cross-plotted in Fig. 6.3.

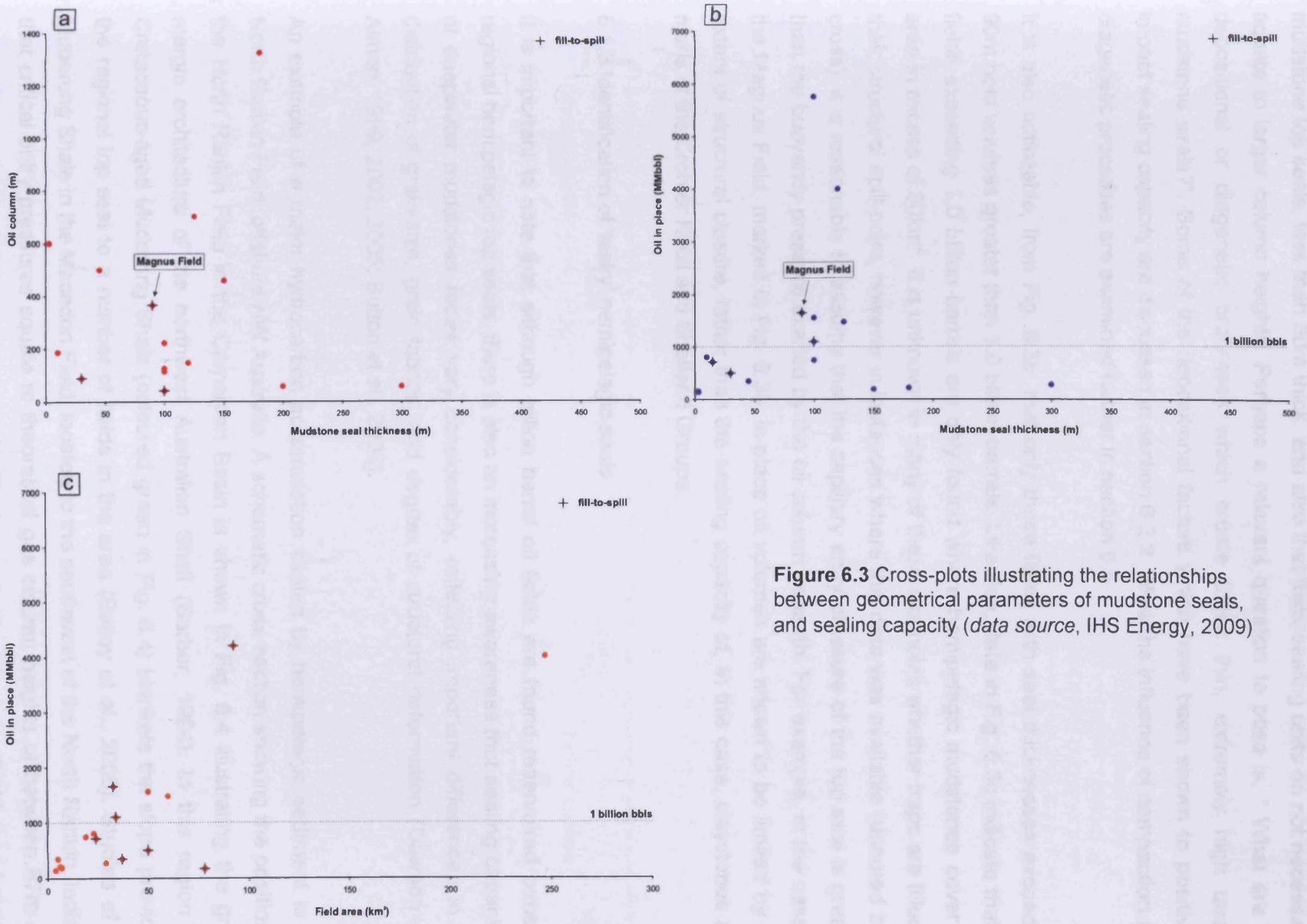

Figure 6.3 Cross-plots illustrating the relationships between geometrical parameters of mudstone seals, and sealing capacity (*data source*, IHS Energy, 2009)

mudstone top seals, less than 50m thick, and also that thick sealing units do not necessarily equate to larger column heights. Perhaps a relevant question to pose is, " What are the depositional or diagenetic processes which create these thin, extremely high quality mudstone seals?". Some of the depositional factors which have been shown to positively impact sealing capacity are discussed in section 6.2.2, while the influence of compaction and diagenetic processes are examined further in section 6.5.

It is also noticeable, from Fig. 6.3b, that only those fields with seal thicknesses exceeding 90m hold volumes greater than 1.0 billion barrels. Likewise, data in Fig. 6.3c indicate that oil fields exceeding 1.0 billion barrels are only found where hemipelagic mudstones cover an area in excess of 30km^2. It is unknown in many of these examples whether traps are filled to their structural spill-point, however in instances where this data was available (denoted by a cross), it is reasonable to assume that the capillary entry pressure of the top seal is greater than the buoyancy pressure exerted by the oil column beneath. For example, in the case of the Magnus Field, marked in Fig. 6.3b, in-place oil volumes are known to be limited by the extent of structural closure, rather than the sealing capacity of, in this case, claystones and marls of the Cromer Knoll and Shetland Groups.

6.1.3 Identification of 'leaky' hemipelagic seals

It is important to note that although billion barrel oil fields are found reservoired beneath regional hemipelagic top seals, there is also an increasing awareness that sealing capacities of deepwater mudstones facies vary considerably, reflecting important differences in the distribution of grain-size, grain fabrics, and degree of structural deformation (Dawson and Almon, 1999, 2002, 2005; Sutton et al., 2006).

An example of a major hydrocarbon accumulation sealed by hemipelagic sediment is the North Rankin Field, offshore NW Australia. A schematic cross-section showing the position of the North Rankin Field in the Carnarvon Basin is shown in Fig. 6.4 illustrating the gross margin architecture of the northwest Australian Shelf (Barber, 1994). In this region the Cretaceous-aged Muderong Shale (coloured green in Fig. 6.4) blankets the slope providing the regional top seal to a number of fields in the area (Bailey et al., 2006). Studies of the Muderong Shale in the Macedon Field, located to the southwest of the North Rankin, indicate that critical entry pressures equate to theoretical gas column heights of between 87m and 441m (Bailey et al., 2006). However, under-filled traps in the Macedon Field area have led Bailey et al. (2006) to suggest that leakage is occurring through the top seal sequence. They conclude that the Muderong Shale is indeed capable of retaining the observed column

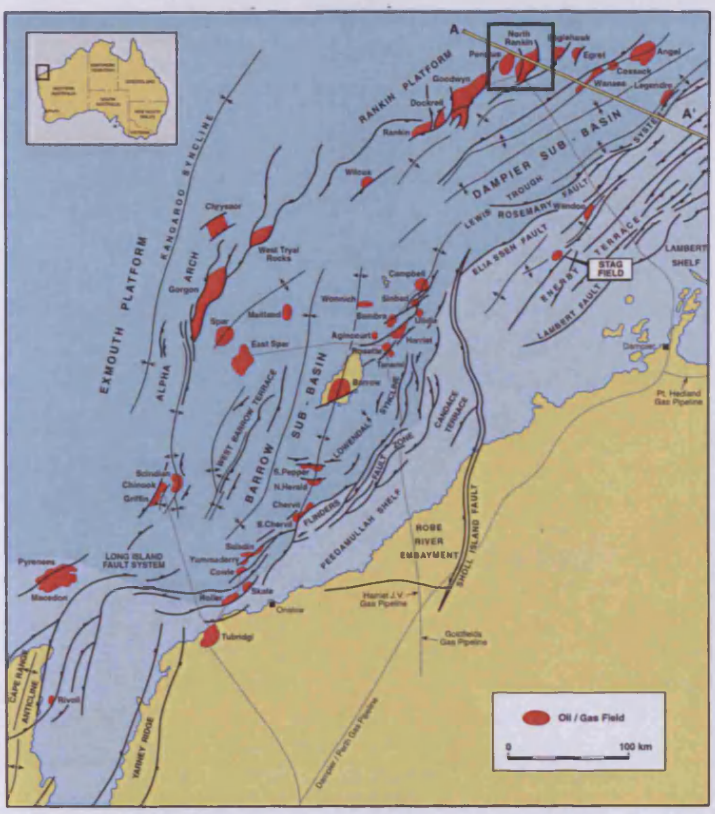

Figure 6.4 Location map (left) showing the location of the North Rankin Field in the Dampier Sub-basin, NW Australia (C&C Reservoirs, 2009). The cross-section (below) shows the Cretaceous-aged Muderong Shale draping the continental slope and providing the top seal in the North Rankin Field (Barber, 1994).

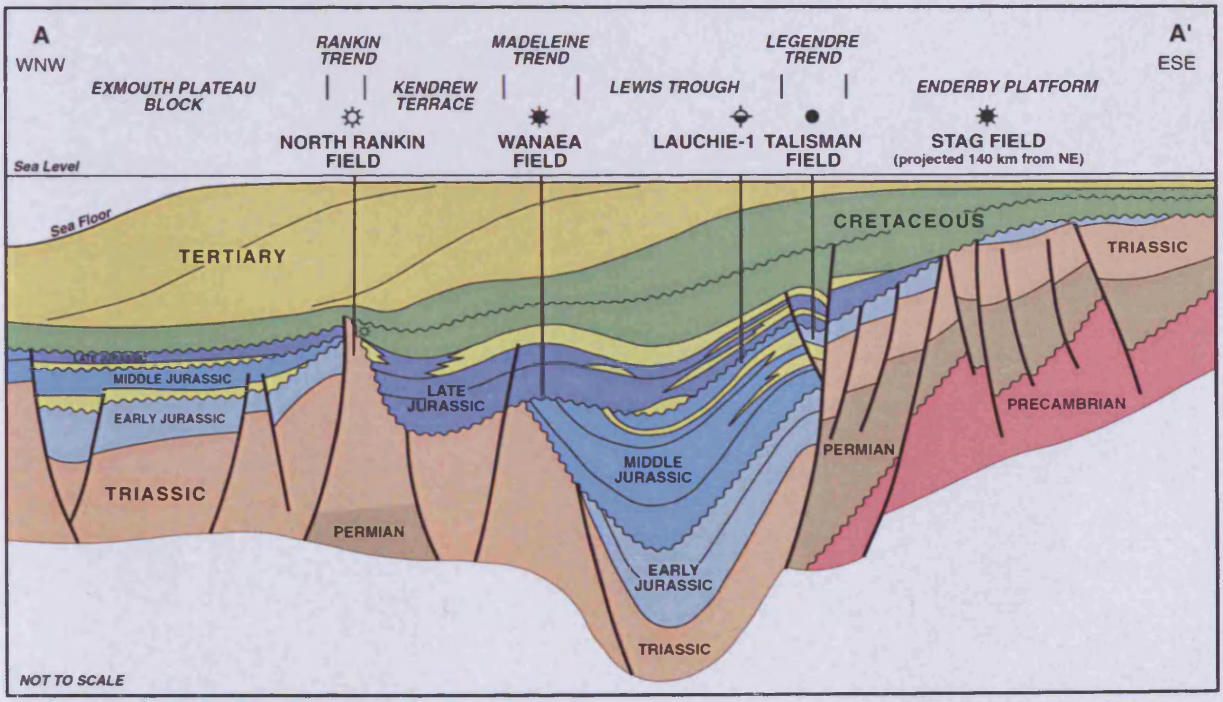

heights and propose that the reactivation of faults and the development of fractures has compromised the seal and led to the migration of gas out of trapping structures.

Similarly, leakage has also been documented from a number of North Sea Basin fields. Research conducted by Lilleng and Gundesø (1997) indicates that active hydrocarbon leakage is occurring in the Njord Field through top seal capillary leakage (membrane leakage of Watts, 1987). Unlike the tectonically compromised top seal proposed in the Macedon Field (Bailey et al., 2006), here the buoyancy pressure exerted by the hydrocarbon column is thought to have exceeded the seal's (Lower Cretaceous Viking Group) critical CEP, allowing fluids to displace pore-fluids within the water-wet seal and begin to migrate through the seal's pore network. This mechanism of leakage is thought to be the most common cause of mudstone top seal failure (Hall et al., 1997), and in petroleum systems where it is prevalent, such as the Njord Field, reservoired volumes of hydrocarbons may be significantly depleted or completely lost if the rate of leakage outpaces the rate of hydrocarbon generation and trap replenishment (Lilleng and Gundesø, 1997).

6.2 Quantifying seal capacity: The scale problem

6.2.1 Seismic and well-log data

Quantifying the likely capacity of seal sequences is a prerequisite to estimating in-place hydrocarbon volumes and assessing the economic viability of potential assets. Allocating numbers, typically CEP values, to seals, or portions of seals, also allows for comparisons of relative seal capacity to be drawn between different prospects. However, it has become clear during the course of this project that no single dataset is capable of capturing the spatial variations in seal physical properties, such that seal risking of hemipelagic drape sequences requires the integration of data from a range of scales.

Seismic data can aid the identification of large-scale (>15-20m) potential seal bypass features such as sand-injections, pipes and faults, and may alert explorers to possible active hydrocarbon leakage where amplitude anomalies exist in the overburden, or where acoustic 'dim zones' or 'bright spots' signify the vertical migration of gas (Cartwright et al., 2007; Løseth et al., 2008). Seismic-scale data can also be used to map the lateral continuity and thickness of sealing sequences allowing the distribution of potential 'weak' points to be identified, for example, highly faulted intervals or areas of reduced top seal thickness (e.g. Ligtenberg, 2005; Farseth et al., 2007; Bradbury et al., 2009). Subtle changes to the continuity, amplitude, and stacking pattern of seismic reflections may also reflect changes in

lithological facies (Brown and Fisher, 1977), however seal analysis at this scale provides little information regarding the detailed lithological properties of a seal unit, and is unlikely to resolve active pore-scale capillary leakage, if present (Løseth et al., 2008). The application of seismic data in predicting the likely location of thinly bedded units however may only be possible where larger scale architectural elements have been identified on the slope and likely facies associations can be recognised (Reading, 1996). For example, where mudstone units are proximal to potential sources of sand such as channel-levee complexes, or where mass-wasting scars suggest that coarser material may have been delivered down-slope.

Where wells have been drilled, a higher-resolution investigation of hemipelagic sequences utilising suites of wireline log data may indicate the position of meter-scale deep-water sand deposits, and may also confirm the presence of any leaked hydrocarbons in sediments overlying a reservoir (Rider, 1996). Wireline data will also provide more detailed physical property data with which to calibrate seismic facies within a potential mudstone seal (e.g. Aniekwena et al., 2003). Borehole investigations are however limited to a single dimension and determining the lateral extent of any identified sand bodies will require careful integration with three-dimensional seismic data. Where coarse layers thin laterally, or are below metre-scale, they will become increasingly difficult to identify in log data and may remain unidentified (*see* Chapter 2) (Rider, 1996). It follows therefore that gross seal architectures obtained using seismic and well logging tools must be meaningfully populated with physical property data to allow the determination of seal capacity and estimates of trapped fluid volumes. This was the rationale for the construction of the hemipelagite database presented in Chapter 3.

6.2.2 Measuring seal capacity directly: MICP analysis

Laboratory analysis of core samples and well-cuttings uses mercury injection capillary porosimetry (MICP) to directly measure the critical pressure at which a non-wetting phase, in this case mercury, enters the largest interconnected pore of a sample (Watts, 1987). MICP measurements can be used to estimate the height of a hydrocarbon column needed to initiate capillary leakage through a seal sample. Measured MICP data is also used in conjunction with determinations of sample grain-size distributions to provide useful insight into how critical entry pressure is linked to the distribution of grain sizes, porosities and sediment fabric (e.g. Neuzil, 1994; Dewhurst et al., 1998; Dawson and Almon, 1999, 2002; Lash, 2006; Yang and Aplin, 2007). Knowledge of seal CEP can also be used, as was the case in the Macedon Field (Bailey et al., 2006), to highlight likely underfilled traps, identified

where a discrepancy exists between the observed column height and the known top seal capacity.

A number of recently published articles have addressed how the detailed lithological and textural characters of various mudstone types relates to measured CEP and sealing capacity. Work conducted by Dawson and Almon (2002, 2005) and Lash (2006) on hemipelagic shales from the deep-water Gulf of Mexico and Devonian shale outcrops, respectively, indicate that subtle lithological and textural variability between studied samples plays a significant role in determining critical CEP values. Seal capacity was seen to be significantly reduced within shales containing abundant silt-sized siliciclastic or bioclastic grains (Dawson and Almon, 2002). Detrital silt-sized grains were seen to hinder the development of a compaction-generated clay fabric by 'shielding' pore spaces from mechanical rearrangement (Heling, 1970; Dawson and Almon, 2002), a mechanism also observed by Lash (2006) from the Upper Devonian Catskill Delta shales. Increases in the content of organic matter and/or early marine carbonate cementation were also seen to enhance seal capacity, while the disruption of grain fabric by bioturbation was seen to have a detrimental impact on seal capacity (Dawson and Almon, 2005; Lash 2006). Similar parameters were seen to impact seal capacities from outcropping shales in the United States and Spain as recorded by Sutton et al. (2004). In addition to parameters already mentioned, discrete micro layers of unaltered volcanic ash were seen to have a detrimental effect on seal capacity, while samples containing altered ash (bentonites) were typically excellent seals (*see* Chapter 5). Studies such as that by Sutton et al. (2004) prompted an appraisal within this thesis of the changes to sediment physical properties during ash diagenesis (*see* Chapter 5).

It is important to note, as several authors have pointed out, that while pore-scale MICP data are important for seal risking, collections of single 'point' measurements are of only limited value when assessing overall seal capacity and must be integrated into larger-scale top seal models which allow for spatial variability in parameters such as grain-size distribution, fault density, and depositional facies types (Downey, 1984; Grunau, 1987). This upscaling of measured properties for use in regional seal evaluations represents a major technical challenge, but remains the ultimate objective of the Caprocks Project.

6.3 Coarse-grained deposits in deep-water slope environments

6.3.1 Introduction

Given the difficulties of scaling-up directly measured physical property data, this section discusses an approach to preliminary seal characterisation which focuses on sedimentary processes capable of delivering and depositing coarser grained sediment to deep-water slope environments. In the absence of extensive subsurface datasets, an appreciation of these depositional systems, and their likely distribution, will allow for a more predictive approach to preliminary seal evaluations. Many of these processes were identified from the examination of ODP cores and outcrops (*see* Chapter 2 and 3) where they were responsible for increasing the overall proportion of coarse-grained material.

Grain-size heterogeneity studies present here indicate that variability in the grain-size distributions of deep-water clastic sediments result from the interaction of location-specific conditions, primarily sediment input sources, transport pathways, and remobilization processes (*see* section 3.5) (Bouma, 1981; Stow and Tabrez, 1998; Stow, 1996; Stow and Mayall, 2000). In these slope settings, sediments are dominated by hemipelagites, turbidity current deposits, mass-transport deposits, and contourites (e.g. Stow and Holbrook, 1984; Piper et al., 1985; Posamentier et al., 1988; Weaver et al., 1992; Piper and Savoye, 1993; Normark et al., 1993; Stow, 1996; Viana et al., 1998). These facies are often found in close association with one another but are likely to differ with respect to physical properties such as grain-size distribution, texture, and mineralogy (Stow and Tabrez, 1998). This in turn will create differences in fluid-flow properties such as porosity, permeability and pore-throat diameter (e.g. Yang and Aplin, 1998; Dewhurst et al., 1999b; Dawson and Almon, 2006). Differentiating these sedimentary units in cores on the basis of these characteristics is possible (e.g. Stow and Tabrez, 1998), however the often thinly-bedded nature and cyclic alternation of these facies means that this differentiation is extremely difficult using lower resolution datasets (i.e. well logs and seismic data). From a seal perspective, thin silt and fine-sand beds deposited by gravity driven flows or by sediment remobilisation, represent lower quality fluid barriers than clay-rich hemipelagic sediments (e.g. Dewhurst et al., 1999b; Dawson and Almon, 2002).

6.3.2 Gravity-driven sedimentation processes

The scale of deposits observed resulting from the introduction of coarse sediment to the slope and basin-floor vary significantly, ranging from mega-turbidite deposits >20m thick

(Reeder et al., 2000), to centimetre and millimetre scale silt beds and laminations such as those presented in Chapters 2 and 3 (e.g. Figs 2.1). The exact processes which lead to the deposition of thick sands in deep-water settings are the topic of much current research (e.g. Cronin et al., 2005; Shanmugam, 2008; Boyd et al., 2008 ; Davis et al., 2009; Haughton et al., 2009). Deposition from sandy debris flows, pulses of turbidity current and evolved slump and slide deposits are all suggested as processes capable of delivering large volumes of sand to the slope and basin-floor (Amy et al., 1998; Shanmugam, 2000; Lowe and Guy, 2000).

Shelves which are fed by major point sources, such as the Amazon Delta and the Pearl River Delta are major repositories for terrigenous sediment and act as the principal supply for coarse grained sediment being introduced to the slope (e.g. Kuehl et al., 1984; Wang et al., 1986; Flood et al., 1995). Margins without major riverine inputs, such as the NW African margin, may be relatively starved of terrigenous sediment and dominated by fine-grained hemipelagic sedimentation, laterally sourced material, and may record aeolian detrital input (Holz, 2005; Stow, 1996).

Transfer of coarse clastic material from the shelf into deep-water occurs by a number of processes. Slope canyon systems incise the shelf and upper slope, funnelling river-sourced sediment directly to lower reaches of the slope and basin-floor. In the case of the Lower Congo Basin system (*see* section 3.3.2), upper and mid-slope areas which flank the Congo canyon are bypassed by coarse clastic material evidenced by a 200m Pleistocene hemipelagic sediment column largely 'unpolluted' by silt and sand material (Wefer et al., 1998). This thesis study has also interpreted slope bypass in the Urenui Formation, Taranaki Basin, where coarse material is confined to incisional channel features and the accumulation of sand is restricted laterally (King et al., 1993) (*see* Fig. 2.45). Hemipelagic units truncated by deeply-incised submarine canyons are therefore unlikely to contain significant volumes of coarse material, although silty material may be deposited from the suspension cloud of large turbidity currents which over-top canyon margins (Cronin et al., 2005). In contrast, submarine channel-levee systems which develop at the base of canyon systems may provide shallower and less confined conduits for gravity flows, increasing the likelihood of sand material being introduced to laterally adjacent inter-channel units as overbank deposits (e.g. Pirmez et al., 1997; Hiscott et al., 1997; Keevil et al., 2006). Levees sequences immediately adjacent to channels, often identified in seismic data by a wedge geometry thinning away from the channel axis (Fig. 6.2), may contain appreciable volumes of thin sands. As examples of this process, intervals of cored mudstones examined from the Gulf of Mexico (*see* Figs. 3.35 and 3.37) and from outcrops in West Wales (Aber Rhigian, Fig. 2.9) record frequent alternations

of hemipelagic and non-hemipelagic sediment thought to result from the over-spilling of coarser sediment onto the slope adjacent to channel conduits.

In slope depositional regimes where channelised systems are not well established, silt and sand may also introduced to deep-water by gravity-driven sediment failures originating at the shelf-break and upper slope (e.g. Masson et al., 1997; Piper et al., 1999; Georgiopoulou et al., 2009). Sediment remobilised as a result of submarine slides and slumps is known to travel enormous distances downslope evolving into turbidity or debris-flows capable of delivering silt and sand material to abyssal depths (Cronin et al., 1998; Bryn et al., 2005). The recognition of failure scars and large-scale mass-transport complexes on seismic data may indicate an increased risk of silt and sand pollution in time-equivalent hemipelagic units in lower portions of the slope.

6.3.3 Contourites

Slope systems which are devoid of major terrigenous sediment inputs may accumulate coarse grained material through the remobilisation and lateral transfer of material by slope-parallel bottom currents (e.g. Faugères et al., 2002). Good examples of this may be found in the Faeroe Shetland Basin where otherwise fine grained hemipelagites are interbedded with coarser glacially fed material (Knutz and Cartwright, 2003; 2004). This coarser component can easily compromise seal quality in deep-water environments. Contour currents are known to be active on many continental margins but contourites remain poorly understood compared to downslope processes such as turbidite systems (Stow et al., 2002). Identification of fossil contourite deposits on land is helping to refine depositional models and characterise the sedimentology of these common slope elements (Duan et al., 1993; Stow et al., 1998). Contourite deposits examined in sediment cores indicate that the actions of bottom currents are capable of introducing sandy material to deep-water settings which may otherwise be at a low risk of coarse grained deposition (Viana et al., 1998). Sediments recovered from the Carolina Slope reveal contourite deposits containing silt- and sand-grade material together with intervals of hemipelagic and gravity-driven sedimentation (*see* section 3.3.1). Contourites represent an increased risk of encountering sandy material in slope setting and an important consideration for explorationists is therefore the recognition and mapping of contourite deposits in subsurface data (Marani, et al., 1993; Faugères et al., 1999). Sand or silt units within contourite drifts may have a much greater lateral extent than other forms of coarse clastic 'pollution' of hemipelagites, and are thus worthy of particular consideration during exploration.

6.3.4 Influence of slope morphology

Down-slope and slope-parallel sedimentation processes discussed above will be influenced by slope morphology and the geometry of sediment pathways. Basin margins with complex seafloor relief, such as convergent margins (e.g. Cascadia) or margins where diapirism has created slope-basins (e.g. Gulf of Mexico) will tend to direct and pond gravity-driven sedimentation in response to the position of structurally controlled relief (Smith, 2004). Recent sedimentation onto the Cascadia slope, presented in Chapter 3, reveals the existence of thin turbidites at the base of the Southern Hydrate Ridge whereas coeval hemipelagic sediments which drape the ridge itself have remained free of coarser grained deposits.

6.4 Grain-size heterogeneities in the wider context of seal risking

The discussion in section 6.3 outlines some of the mechanism and processes by which coarser sediment can be delivered to deep-water slope settings. With this in mind, this section will summarise the evidence for these processes as observed from outcrop and core investigation and address the question, "How can data this thin-bed data be practically used by explorationists to better predict seal quality, pre-drilling?".

6.4.1 Implications of thin-bed data in seal risking

Discrete beds of coarse grained material which punctuate clay-dominated sequences will generate preferential pathways for migrating fluids by creating more permeable and porous layers. Based on MICP analysis for example, silty mudstones indicate potential column heights of a much as two orders of magnitude smaller than for pure claystones (Darby, 2002; Hall et al., 1997; Aplin, A. C. *pers. comm.*). It follows from this that one distinct form of lithological heterogeneity which can significantly comprise seal quality is the interbedding of thin sands and silts in clay-dominated fine-grained sequences.

The characterisation of modern hemipelagic sediments with respect to the distribution of coarser-grained layers is presented in Chapter 3 from the investigation of 23 ODP and IODP sites. Tertiary sites examined were chosen to capture slope sedimentation away from identified or likely sources of coarser grained material (i.e. submarine channel-levee complexes). Variability in the grain-size distribution of these slope-drape facies is described in Chapter 3, and indicates that the margin settings examined contain up to 6% discrete coarser layers (silt and sand) which, from the 1023 thin-beds identified, show an average

thickness of 2.7cm. Though these thin-bed distributions may not be fully representative, they do provide explorers with a notion of the range of possible net-to-gross, thicknesses, and spacing values that can be expected in these sequences. The documentation here of a range of values, and a mean value for thin-bed thickness in hemipelagites is a potentially valuable input into stochastic modelling of sealing capacity where no local well calibration is possible. It is believed that this is the first such compilation of thin-bed data from this type of sequence.

Outcrop studies of Palaeozoic slope mudstones reveal a range of grain-size heterogeneities not seen in the cored slope sediments examined. Thinly bedded mudstones examined in West Wales contain as much as 40% discrete silt and fine sand horizons, indicating a fundamental difference in the availability of coarser sediment compared to core from the modern slope sites examined (*see* table 2.2). Lateral variability in the portion of silty layers within the Cwm-yr-Eglwys and Nantmel Mudstones Formations is thought to represent varying proximities to coarser sediment pathways in the Dinas Island Formation (Davies et al., 2003). Units containing appreciable volumes of coarse material are typically bedded on a centimetre scale (1-3cm) revealing cyclic alternations of silt- and clay-rich sediment (*see* Figs. 2.9; 2.25; 2.29), which from a seal perspective are likely to lead to a stratified distribution of permeabilities and capillary pressures. Individual beds display lateral continuities ranging from 10's of centimetres to in excess of 100m as well as evidence of secondary reworking processes including current winnowing and bioturbation (e.g. Figs. 2.13; 2.32). These centimetre-scale 'carrier' beds can, if vertically connected, by for example faults or pipes, be enough to compromise a seal, or significantly reduce expected column heights.

Variability in the grain-size distributions among ODP Sites and outcropping sections is thought to result from the interaction of location-specific conditions, primarily sediment input sources, transport pathways, and remobilization processes (Stow and Tabrez, 1998). The key learning points from these studies of fine-grained sequences are distilled into a practical work-flow in Fig. 6.5. This work-flow poses a series of questions for the consideration of those making 'first-pass' assessments of potential sealing capacities in this type of sequence. While the detailed characterisation of heterogeneities in a specific drape sequence will require the integration of available data of various scales, as discussed in section 6.1.3, appreciation of these principles is thought to be globally applicable.

Question	Consideration	Possible seismic evidence
Is there evidence for a major river/delta point source?	Hemipelagites away from major point sources are likely to be less polluted with coarser grained terrigenous sediments than those deposited proximal to major river deltas.	Can sigmoidal prograding seismic packages be identified within the sealing sequence?
Is there evidence of sediment bypass of the slope?	Slope deposition adjacent to deeply incised canyons is likely to be largely devoid of coarser grained material as a result of sediment bypass e.g. Lower Congo Basin	*Can a major incisional feature be identified in* seismic data?
Is there evidence of sediment ponding?	Coarser grained sediments may be concentrated in intra-slope basins and may be largely absent where palaeo-highs existed e.g. Brazos basin, Gulf of Mexico	Is it possible to identify palaeo-seafloor relief from the seismic reflection patterns e.g. onlap relationships?
Is there evidence of contourite deposition?	Contourites may introduce coarser grained material to the slope independent of local point sources e.g. Carolina Slope and Blake-Bahama Outer Ridge	Can contourite deposits be interpreted in seismic data i.e. broadly lenticular, upward-convex units?
Is there evidence for time-equivalent sediment failures up-dip? → Are drape sediments interbedded with mass-transport deposits?	Indicators of sediment failures, such as arcuate head scars, may indicate that sediment has been remobilised down-slope and may be interbedded with drape deposits.	Can failure surfaces be recognisable in the upper slope? Are drape sediments interbedded with seismic units of chaotic and discontinuous reflections?
What is the proximity of channel-levee systems? →Are drape sediments interbedded with levee deposits?	Levees are likely to contain considerably more coarse material compared to adjacent hemipelagites, resulting from channel over-spill.	Can channel-levee features be identified in seismic data? What is the extent of channel-levees?

Figure 6.5 Table containing a number of questions for the consideration of those making preliminary evaluations of the potential sealing quality of slope mudstone units. Based on the data presented in this thesis, questions such as these will aid the identification of zones where mudstone sealing quality may be reduced by the presence of coarser sediment.

6.5 Towards the better prediction of slope mudstone seal quality ahead of drilling

6.5.1 The Caprocks Project seismic genetic units approach

In addition to considering the potential grain-size heterogeneities within seismic facies considered as 'hemipelagites', the Caprocks Project has been working together with industry sponsors to try an develop a method which enables better characterisation of entire fine-grained slope systems using seismic data. The 'genetic units' approach aims to sub-divide potential sealing sequences into constituent, seismically mappable units.

Such a scheme has only been developed at a relatively large-scale (low-resolution), but this framework has the potential to be populated with increasingly detailed geological information, as data becomes available. My examination of hemipelagite-dominated sequences has aimed to collect relatively high-resolution data from outcrops and core analysis with which to 'geologically populate' seismically identifiable hemipelagite facies. The detailed characterisation of the other genetic units, for example mass-transport deposits, channel-levee systems, and contourites, was not the focus of this thesis and is work which is currently ongoing.

The applicability of this approach relies on the degree on accuracy to which depositional units can be ascribed to packages of seismic reflections, which is largely a function of seismic data resolution. Seismic datasets provided by sponsor companies have been interpreted by the Caprocks Project team, Aggeliki Georgiopoulou and Joe Cartwright, and different slope genetic units have been differentiated based on the geometry, amplitude and continuity of seismic reflections. Hemipelagic seismic facies are packages of continuous to semi-continuous reflections of low-to-moderate amplitude which do not show architectural features indicative of other genetic units (Fig. 6.6)(Brown and Fisher, 1977). Conversely, submarine channels appear in 3D seismic as low to very high amplitude features, with a distinctive concave up form that abruptly interrupts stratified slope sediments (Fig. 6.7). In mid-slope to lower slope settings they have been identified as being commonly accompanied by channel-levees that are readily identifiable when their wedge-shape tapering geometry has been maintained post-burial (Fig.6.7). However, often the characteristic 'wedge' shape of levees is altered during compaction, in these cases, overbank deposits are assumed to be present. Amplitudes in levees are similar to hemipelagites, although some high amplitude reflections may be observed where appreciable sand is present, commonly seen adjacent to channel meander bends, where flow-stripping is common (Hiscott et al., 1997). Mass transport complexes (MTC's) are characterised by a high variability of amplitude values and

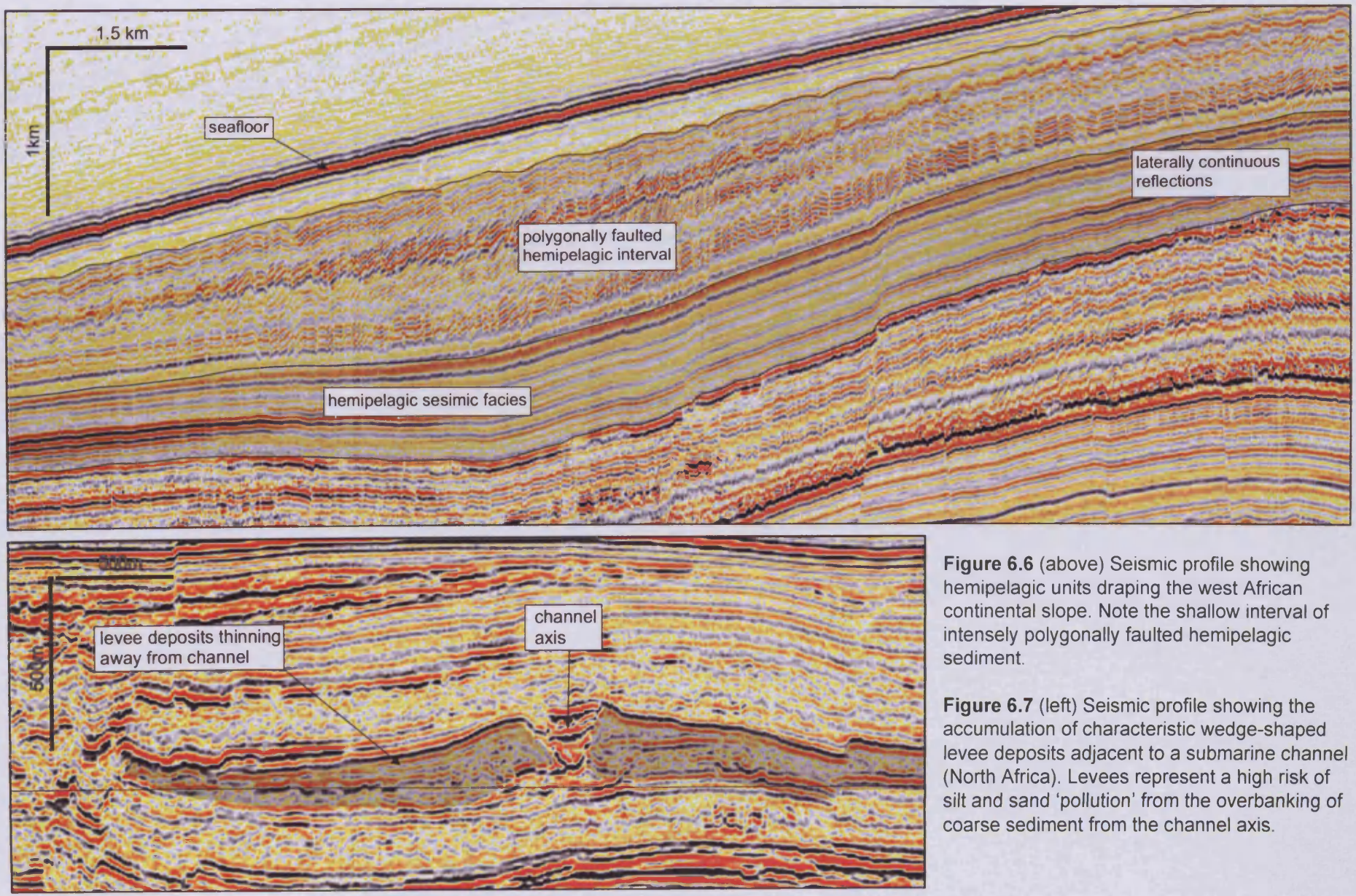

Figure 6.6 (above) Seismic profile showing hemipelagic units draping the west African continental slope. Note the shallow interval of intensely polygonally faulted hemipelagic sediment.

Figure 6.7 (left) Seismic profile showing the accumulation of characteristic wedge-shaped levee deposits adjacent to a submarine channel (North Africa). Levees represent a high risk of silt and sand 'pollution' from the overbanking of coarse sediment from the channel axis.

random internal distribution (Fig. 6.8)(Frey Martinez et al., 2006; Bull et al., 2009). This variability is in amplitude is thought to be directly related to the lithologies that have been incorporated in the MTD (Georgiopoulou *pers. comm.*, see also Flemings et al., 2006). Reflections within MTC packages are typically extremely discontinuous and abruptly truncated (Fig. 6.8).

An example of a continental slope which has been sub-divided into genetic units is shown in Fig. 6.9. (Georgiopoulou, unpublished work). This seismic slice through an active petroleum province reveals the variability in seismic facies, and the relative proportion of each genetic unit using a simple pie-chart. In the absence of any further data to constrain the distribution of facies, this approach already allows the seismic interpreter to say something about the distribution of seismically definable units, and the gross lithological make-up of a sequence.

Initial estimates of the relative sealing potential of these hemipelagic seismic facies should consider the work-flow presented in Fig. 6.5, and be aware of the range of net-to-gross values presented from outcrop and cores studies in these types of sediment, presented in Chapters 2 and 3.

An advantage of this seismic genetic units approach are that it allows sealing sequences to be mapped spatially, potentially providing a three-dimensional facies model for input into basin modelling software. However, this approach relies on accurate interpretation of genetic units with non-unique seismic attributes and geometries. Since this 'window of interpretability' is directly affected by the vertical stratigraphic resolution of the seismic data, the accurate and reproducible identification of seismic genetic units is effectively limited to unit thicknesses of greater than this resolution limit, typically 15-20m in the highest quality 3D surveys.

6.5.2 A sequence stratigraphic approach

An examination of the literature has revealed that tools and work-flows for estimating the sealing capacity of mudstones pre-drilling are rare. One plausible method which has recently been proposed by Dawson and Almon (2002, 2006). The authors have identified six end-member mudstone facies from the deep-water Gulf of Mexico which exhibit distinct compositional, textural and petrophysical properties. MICP analysis indicates that samples also reveal sealing capacities which vary systematically within a sequence stratigraphic framework, suggesting a certain level of predictability of relative seal capacity (Dawson and Almon, 2006).

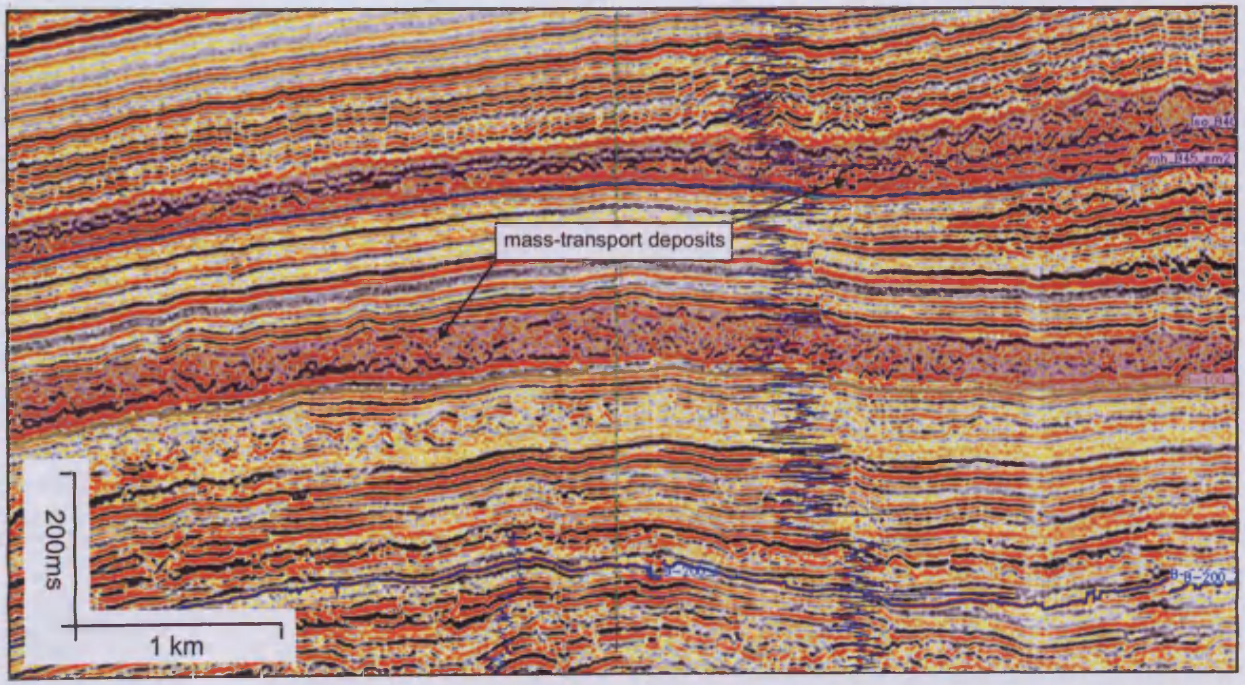

Figure 6.8 (left) Seismic profile showing chaotic and discontinuous seismic facies characteristic of mass-transport complex Image from the West African continental slope.

Figure 6.9 (below) Continental slope seismic panel which has been interpreted using the Caprocks Project genetic units approach (Georgiopoulou, *unpublished work*). The approximate distribution of the different genetic units in this particular profile is shown in the pie-chart.

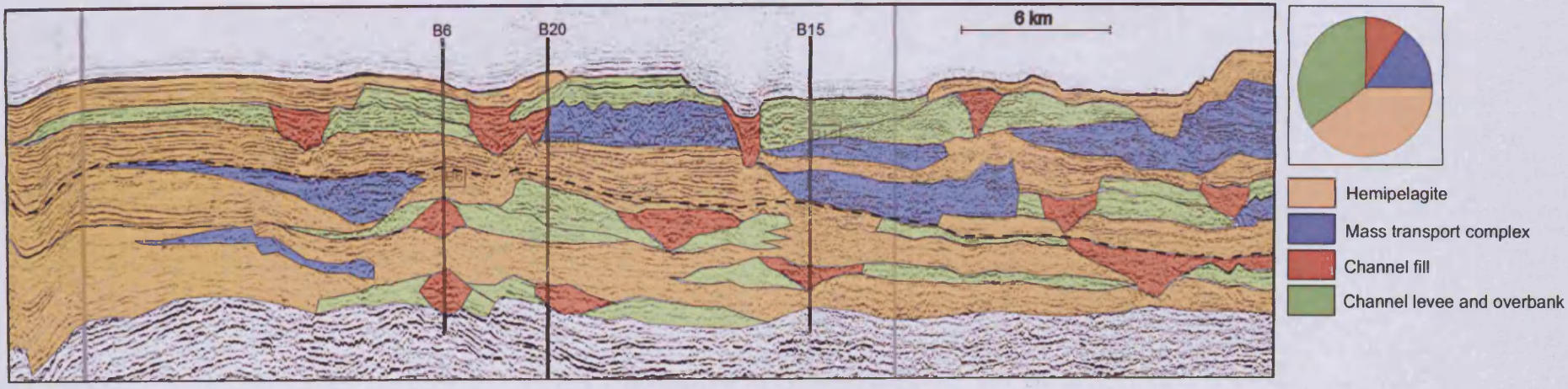

It is suggested that mudstones deposited during highstand systems tracts (HST) are less effective seals compared to those deposited during transgressive systems tracts (TST). It is shown that TST mudstones are silt-poor relative to HST mudstones and also show enhanced sealing potential resulting from a well-laminated microfabric. The highest potential sealing capacities were found to coincide with the latest parts of transgressive units, deposits characterised by reduced rates of sedimentation (Dawson and Almon, 2006). The position of these sequences within an idealised sequence stratigraphic model are shown in Fig. 6.10.

However, this approach relies on developing a robust sequence stratigraphic frame-work which requires high quality dataset and knowledge of basin evolution and regional stratigraphy. The Gulf of Mexico if one of the world's most explored petroleum provinces with a well-established sequence stratigraphic framework (e.g. Galloway, 1989; Mitchum et al., 1991; Prather et al., 1998; Beaubouef and Friedmann, 2000; Booth et al., 2000), during exploration in frontier basins, this approach may not be practical if little data is available.

6.6 Post-depositional processes: Hemipelagite compaction and ash diagenesis

There is an increasing recognition in published studies of the significant role that diagenetic processes play in altering the physical properties of fine-grained sequences during burial (*see* Chapters 4 and 5). This section discusses the implications of mechanical compaction and volcanic ash diagenesis on the prediction of sealing properties in mudstones. Other diagenetic processes considered important, but are beyond the scope of this thesis, and are not therefore discussed here in detail. These include reactions associated with the progressive alteration of opaline silica (e.g. Davies and Cartwright, 2007; Meadows and Davies 2009), and the chemical compaction of mudstones resulting from the transformation of illite clay minerals to smectite (e.g. Peltonen et al., 2008). From a sealing perspective, these processes certainly change sediment physical properties during burial and these changes are often abrupt and profound, with concomitant implications for modelling fluid-flow in the subsurface and predicting potential seal capacities (e.g. Meade, 1964; Weaver, 1989; Giles, 1997; MarcussenØ et al., 2009).

6.6.1 Hemipelagite compaction and overpressure development

A key observation from the examination of mudstone porosity trends in Chapter 4 is the considerable variability in the rates at which these sequences lose porosity as a function of burial depth. This in turn has highlighted the difficulty of fitting a single 'compaction curve' to the observed trends, as proposed by several authors (e.g. Baldwin, 1971; Sclater and

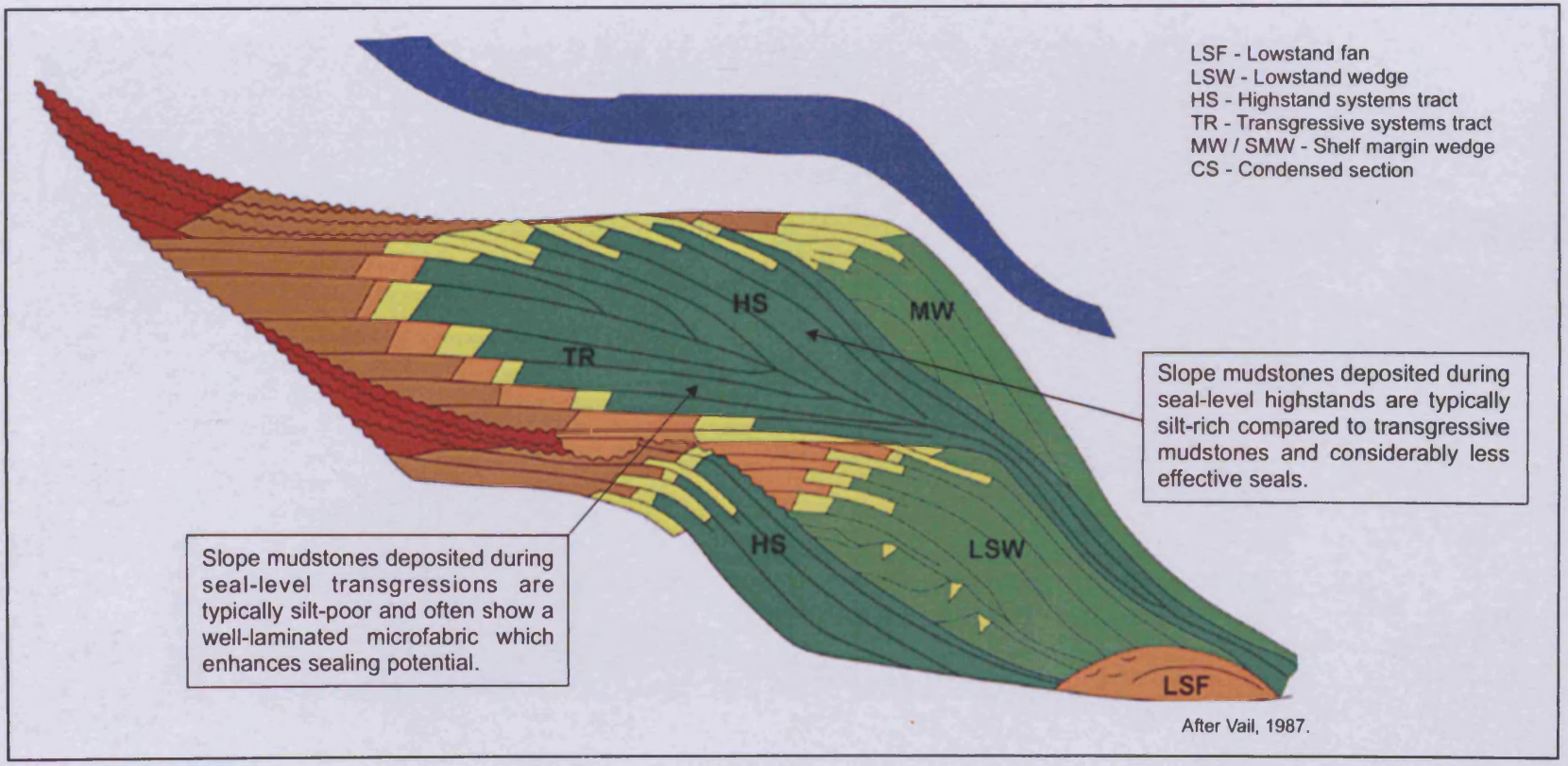

Figure 6.10 Schematic sequence stratigraphic framework model, after Vail et al (1897), showing the relative position of transgressive and highstand mudstone units.

Christie, 1980; Baldwin and Butler, 1985) (*see* Figs 4.8 and 4.9). Porosity-depth relationships from 16 fine-grained sequences (*see* Fig. 4.7) show considerable variability in both initial porosity values, which range from 64-82%, and the rate at which porosity decreases with depth (*see* Fig 4.6). A further database of 255 initial porosity measurements taken from the ODP, shown in Figs. 4.3 and 4.5, provide a clear picture of the variability in mudstone initial porosities, which are here ascribed to differences in primary lithology (*see* section 4.5). This systematic variability in mudstone physical properties resulting from lithological changes has recently been investigated by MarcussenØ et al. (2009) from the Cenozoic succession in the northern North Sea Basin. MarcussenØ et al. (2009) present velocity and bulk density data from 42 well logs characterising mudstones of the Rogaland, Hordaland, and Nordland Groups. They report that significant variability in p-wave velocities and sediment densities, at depths less than 2000m, can be largely attributed to changes in primary mudstone mineralogical composition. The authors suggest that the primary control on velocities and densities with depth is smectite content, a clay mineral derived from the alteration of volcanic ash. It is thought that the low permeability of smectite clay has resulted in the development of overpressures. This has in turn led to undercompaction in the Rogaland and Hordaland groups, resulting in the observed low measured bulk densities and velocities (Mondol et al., 2008; MarcussenØ et al., 2009). This work is in agreement with core-scale investigations of Sutton et al. (2004) who found the sealing capacity of bentonitic mudstones to be excellent. The development of significant overpressure in sealing sequences will have implications for seal integrity where fluid pressures exceed the strength of the formation (e.g. Gaarenstroem et al., 1993; Converse et al., 2000; Darby et al., 2000). Seal breaching through the development of hydraulic fracturing is thought to occur in a number of southern North Sea fields where otherwise well-defined traps have not retained any hydrocarbon column (Gaarenstroem et al., 1993).

From their examination of Cenozoic mudstones MarcussenØ et al. (2009) go on to suggest that different mudstone compaction trends, based on facies, should be employed in basin modelling so as to avoid "misrepresenting" these sequences. This is in agreement with findings presented in Chapter 4 where it is suggested that a simple classification scheme of fine-grained facies, such as the example given in 4.5, could be used to reduce the level of uncertainty in basin modelling calculations involving initial porosity values. Mudstone initial porosity values are a commonly used but rarely discussed input into basin models which are often given a generic value (e.g. Sclater and Christie, 1980; Mann and Mackenzie, 1990). The use of standard initial porosity values and standard porosity-loss trends for mudstone sequences ignores a large range of lithological heterogeneity and will not accurately predict the physical properties of subsurface units (MarcussenØ et al., 2009).

6.6.2 Effects of ash diagenesis on mudstone physical properties

As is noted by MarcussenØ et al. (2009), the alteration of volcanic ash is a little studied, but potentially very important diagenetic process in shallow buried mudstone sequences. The thermodynamic instability of glasses make them particularly susceptible to diagenesis, and in fine-grained sequences containing abundant ash, the products of alteration reactions may reduce porosities and permeabilities, alter pore-fluid chemistries, and dehydrate ash-bearing intervals (e.g. Ninkovich and Heezen, 1967; Egeberg et al., 1990; Dadey and Klaus, 1992; Lyons et al., 2000; MarcussenØ et al., 2009). Studies cited in Chapter 5 typically have focussed on the alteration of formation fluids as a result of ash alteration reactions and the associated authogenic minerals precipitated (e.g. Egeberg, 1992; Gérard and Person, 1994; Lyons et al., 2000), while studies examining the role of ash diagenesis in controlling and altering the physical properties of ash bearing sequences are rare (e.g. Tribble and Wilkens, 1994; MarcussenØ et al., 2009).

A recent study by Spinelli et al. (2007) examined the physical properties of ash bearing hemipelagic sediments known to be undergoing diagenesis in the Shikoku Basin, Japan (Tribble and Wilkens, 1994; Moore et al., 2001). Spinelli et al. (2007) examined ODP data from the Shikoku Basin collected during Leg 190 and have proposed a cause for the unusual physical properties exhibited by hemipelagic sediments approaching the Nankai Trough (the sedimentology of the Shikoku Basin have been introduced in section 3.3.4). Hemipelagic sediments of the Upper and Lower Shikoku Basin facies share similar lithological characteristics, both consisting largely of clay minerals and silt sized material along with minor amounts of biogenic material. The boundary between the two formations was picked by shipboard ODP scientists as the depth of the deepest clearly defined ash layer recognised in cored sections, which in the case of Site 1173 (*see* Fig. 5.10), is at a depth of 344mbsf (Moore et al., 2001). This boundary is thought to be at least in part diagenetic with ash beds within the Lower Shikoku Basin Facies completely altered to siliceous claystone (Moore et al., 2001).

Physical property data above and below the boundary of the Upper and Lower Shikoku basin Facies boundary indicate that these two units have behaved differently during burial and compaction, clearly visible in porosity measurements shown in Fig. 6.11. Sediments of the upper Shikoku basin facies appear to retain porosity despite increasing burial depth for the interval 100-350 mbsf, while porosities in the underlying lower Shikoku Basin clearly decrease with increased burial depth.

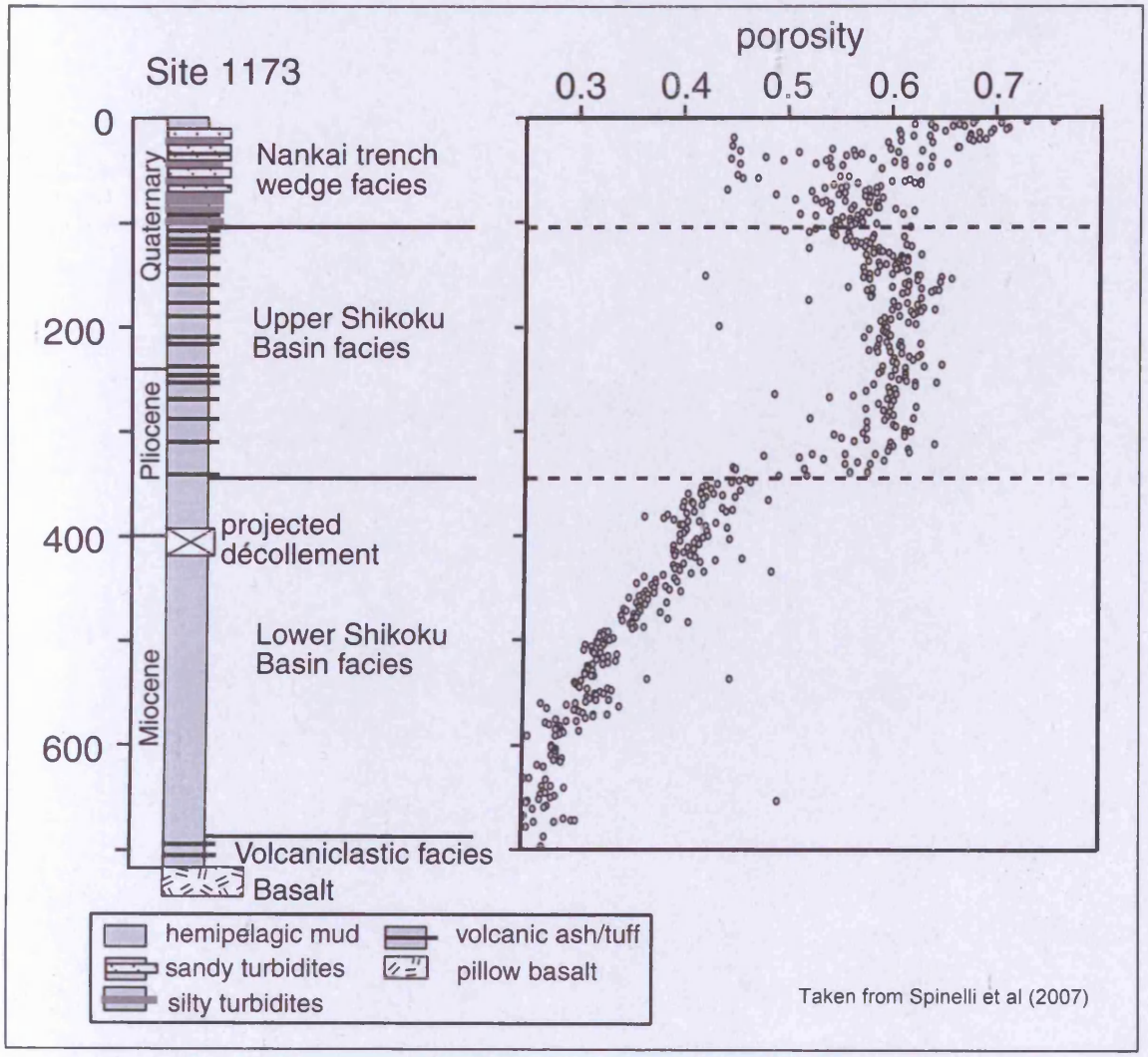

Figure 6.11 Stratigraphic column and porosity profile from ODP Site 1173, Nankai Trough. Porosity, which remain largely uniform throughout the Upper Shikoku Basin facies, is seen to begin falling rapidly once the Lower Shikoku Basin facies is reached at 344mbsf.

Spinelli et al. (2007) have examined physical property data from ODP Site 1173 and other nearby sites and have proposed a model which suggests that minute amounts of opal cement at grain contacts in the upper Shikoku Basin formation is responsible for increasing sediment strength and retarding the normal compaction of sediment (i.e. decreasing porosity with increasing depth, *see* Chapter 4). Measured opal cement volumes in the upper Shikoku Basin facies are reported to range from 0.76 to 1.25wt%, while values in the lower Shikoku are between 0.34 to 0.37 wt% (Spinelli et al., 2007). They propose that once sediments pass through a threshold where the rate of cement dissolution outpaces that of precipitation, inter-granular porosity is thought to collapse producing the significant drop in porosity values seen at approximately 350 mbsf in Fig. 6.11. (Spinelli et al., 2007)

Aside from the anomalous porosity trend of hemipelagic sediments Site 1173, P-wave velocities also appear to support the hypothesis of grain cementation. Data indicate that P-wave velocities increase over a depth range of 100-350m, coinciding with the zone of porosity retention within the upper Shikoku Basin facies. This parameter suggests a stiffening of the sediment, indicative of cementation, making other mechanisms of porosity retention such as over pressured pore fluids, less likely. The low abundances of diatoms (rarely exceeding 5 wt% in smear slides) would also appear to rule out the possibility that porosity retention is due to the high intra-test porosity which can be exhibited by diatomaceous sediments, as seen in Chapter 4.

Given the available data, it seems likely that the anomalous porosity and P-wave velocities exhibited by the Shikoku Basin facies sediments are indeed the result of cementation at the grain contacts within the upper Shikoku Basin facies, as hypothesised by Spinelli et al. (2007). In their model, opal cement is thought to be sourced from the dissolution of biosiliceous tests, based largely on the absence of preserved biosiliceous material in the lower Shikoku Basin facies (Moore et al., 2001; Spinelli et al., 2007). This model however does not consider the potential influence of ash diagenesis on sediments and pore fluids in the Shikoku Basin, despite the depth of the deepest recognisable ash horizon coinciding exactly with the proposed opal cement threshold at 344 mbsf. Discussions presented in Chapter 5 indicate that silica is one element liberated into pore fluids during the dissolution of volcanic glass. Given this, and the active ash diagenesis occurring in the Shikoku Basin, silica derived from dissolving volcanic material is likely a component of pore fluids silica concentrations, and may be linked to the observed cement precipitated at grain contacts.

One example of how ash diagenesis may facilitate this type of cementation is given by Altaner and Grim (1990) who examined the volcaniclastic Sucker Creek Formation of

Eastern Oregon. Their work indicates that silica-rich fluids liberated during the alteration of volcanic glasses in the Sucker Creek volcaniclastic sequence has leached into neighbouring siliciclastic layers and precipitated, creating opal C-T rich beds. Silica within these opal-rich beds was found to be chiefly derived from adjacent altered ash layers.

Similarly, ash alteration and silica liberation have been recognised as an important process governing early diagenesis and cementation in sandstones, a topic of particular importance for petroleum reservoirs (e.g. McBride, 1984; Jeans et al., 2000). Jeans et al. (2000) indicate that early cementation of sandstones of the Brent Formation (North Sea Basin) is likely to have been sourced from silica liberated during diagenesis of Middle Jurassic volcanic sediments. It follows therefore that one potential impact of ash diagenesis on sediment physical properties is that of a change in sediment stiffness resulting from ash-derived silica cement. Preferential cementation of sediments in proximity to ash-bearing intervals will alter sediment strength with implications for the nucleation and distribution of fractures and faults.

Chapter 7

Chapter 7

Conclusions

7.1 Conclusions

1. Studies carried out on outcropping mudstones in West Wales and Cornwall have identified heterogeneous slope facies containing upto 40% coarse thin-beds. These discrete layers of silt and sand are often laterally continuous, will increase the bulk permeability of mudstone units, and will be detrimental to seal effectiveness.

2. Further field studies examining the Miocene Taranaki Basin slope sequence indicate that thinly bedded siliciclastic grain-size heterogeneities (<20cm) are below the resolution of outcrop gamma-ray spectrometry and are likely to be undetectable in subsurface data.

3. Studies examining ODP and IODP cores recovered from modern hemipelagic slope settings reveal a range of mudstone types and grain-size distributions reflecting varying proportions of clay, silt, sand, and biogenic material. Work conducted suggests that sediment input sources, transport pathways, and remobilisation processes the most important controls on the sedimentology and distribution of coarser material in hemipelagic slope settings. A series of questions are posed in Fig. 6.5 which are designed to aid those making preliminary, pre-drilling, evaluations of mudstone seals by suggesting depositional systems where hemipelagic sediments are at a high risk of coarser grained input. When used in conjunction with available knowledge regarding location specific sedimentation controls (e.g. input sources, transport pathways, etc), these considerations will help formulate a better estimate of the character of hemipelagic sediments in the subsurface.

4. No 'type' hemipelagite lithofacies has been observed from ODP studies. Discrete coarse grained intervals comprise between 0-6% of the total sediment cored at the sites examined, while background facies show a range of lithologies and grain-sizes reflecting varying proportions of clay, silt, sand, and biogenic material.

5. Investigations into the porosity profiles of buried slope mudstones indicate that in shallow sequences, hemipelagic sediments do not consistently conform to trends of

exponentially decreasing porosity values with depth, as suggested by some authors (e.g. Baldwin and Butler, 1985; Bahr et al., 2001). Rather deviations from well constrained trends often appear to correlate with shifts in bulk lithology, suggesting that the inherent physical properties of particular intervals are responsible for varying porosity values with depth.

6. A second significant observation from porosity studies is that lithology, primarily grain-size, plays a significant role in determining the values of initial, or depositional porosities in hemipelagic sediments. It is suggested that the use of 'default' initial porosity values for hemipelagic sediments in basin models and decompaction analysis ignores a large range of natural variability, and could lead to significant analytical errors.

7. Ash diagenesis is presented here as a diagenetic mechanism capable of altering the physical properties of shallow ash-bearing hemipelagic sequences, with potential implications for mudstone sealing sequences. The alteration of volcanic glass has been shown to significantly impact the pore-fluid chemistries, porosities and permeabilities of host sequences with implications for fluid-flow. The dehydration of volcanic sediments in response to the incipient hydration of glass hydration during alteration is suggested as an addition mechanism to that published by Dewhurst et al. (1999c) for initiating syneresis and the volumetric contraction of sediment, potentially leading to fault nucleation.

Future Research

Chapter 8.

Future research

This section briefly covers some suggested future research topics which would build on the discussions presented in this thesis and advance our understanding of mudstones and their sealing potential.

8.1 Further characterisation of genetic units

The Caprocks genetic units approach to mudstone seal prediction requires the relatively detailed calibration of seismic facies with cored or outcropping slope sediments. Presently, this predictive method remains largely untested and is lacking detailed grain-size characterisations for levee, contourite, and mass-transport facies. Much future research is needed to better understand the ranges of physical properties which can be expected in these units and their capacity as seals to hydrocarbons. It is likely that core databases, such as the ODP, will remain a principal dataset for such studies, although examinations of these facies in outcrop will enable a better understanding of their sedimentology and grain-size variability.

In addition to the important sedimentological characterisation of the four genetic units, as suggested above, a critical knowledge gap remains regarding the identification of thinly bedded facies in well-log and core-log data. Discussions in Chapter 2 indicate that thinly bedded grain-size heterogeneities are not directly detectable at the resolution of well-log data, however further work may identify log signatures characteristic of heterolithic facies. This work may incorporate for example the use of micro-resistivity image logs (FMI) to better constrain the distribution of thinly bedded units in the absence of cored sections. The integration of FMI logs with lower resolution log data such as gamma-ray may provide information about how bedding and facies changes can be better predicted from bore-hole investigations.

8.2 Porosity-loss trends for fine-grained facies

Data presented in Chapter 4 indicates that fine-grained sediments do not necessarily compact according to well-known exponential trends, and that subtle changes in lithology may be responsible for this. Figures in Chapter 4 also indicate that the range of initial

porosities for a range of fine-grained facies varies considerably. An informative topic for future research would be the examination of compaction profiles for range of fine-grained facies in order to ascertain whether these facies (e.g. silty clay or siliceous clays) have characteristic porosity loss profiles.

8.3 The importance of ash diagenesis in mudstone seals

Discussions on the alteration of volcanic ash and the resulting implications for sediment physical properties have been touched on in this thesis. One possible avenue for future research would be to experimentally examine the alteration of volcanic glasses and the resulting changes to sediment properties and pore-fluid mineral concentrations. Under elevate temperatures and pressures it may be possible to observe changes to sediment grain-fabric and also the onset of palagonisation in the laboratory. In addition to this, a world-wide examination of mudstones rich in authogenic smectite would provide clues as to the importance of ash alteration to the development of high quality seals. A valuable dataset for this type of investigation would be petroleum industry well data from areas such as the North Sea Basin and South China Sea Basin, where smectitic clays are prevalent.

References

References

Aigner, T., Schauer, M., Junghans, W. - D., Reinhardt, L., 1995. Outcrop gamma-ray logging and its applications: examples from the German Triassic. Sedimentary Geology, 100, 47-61.

Alexander, J. and Morris, S., 1994. Observations on experimental, nonchannelized, high-concentration turbidity currents and variations in deposits around obstacles. Journal of Sedimentary Research, Section A: Sedimentary Petrology and Processes, 64, 899–909.

Allen, J.R., 1982. Sedimentary structures: Their character and physical basis, vol. 2. Elsevier, Amsterdam.

Allen, P.A. and Allen, J.R., 1990. Basin Analysis. Blackwell, Oxford.

Altaner, S.P. and Grim, R.E. 1990. Mineralogy, chemistry and diagenesis of tuffs in the Sucker Creek Formation (Miocene), Eastern Oregon. Clays and Clay Minerals, 38, 561–572.

Andersson, P. O. D. and Worden, R. H., 2004. Mudstones of the Tanqua Basin, South Africa: an analysis of lateral and stratigraphic variations within mudstones, and a comparison of mudstones within and between turbidite fans. Sedimentology, 54, 479-502.

Andrews, A. J., 1977. Low temperature fluid alteration of oceanic layer 2 basalts, DSDP leg 37. Canadian Journal of Earth Science, 14, 911-926.

Aniekwena, A. U., McVay, D. A., Ahr, W. M., Watkins, J. S., 2003. Integrated characterization of the thin-bedded 8 reservoir, Green Canyon 18, Gulf of Mexico. In: SPE 84051 Presented at the SPE Annual Technical Conference and Exhibition Held in Denver, Colorado, October 5–8, 2003.

Anketell, J. M., 1963. The geology of the Llangranog district, southwest Cardiganshire. Unpublished PhD thesis (Queen's University of Belfast).

Aplin, A. C., and Larter, S. R., 2005. Fluid flow, pore pressure and leakage in mudstone cap rocks. In: Boult, P. and Kaldi, J. (Eds), Evaluating fault and cap rock seals: AAPG Hedberg Series 2, 1– 12.

Aramaki, S. and Lipman, P. W., 1965. Possible leaching of Na2O during hydration of volcanic glasses. Proceedings of the Japanese Academy ,61, 467- 470.

Armstrong, H.A. and Coe, A.L., 1997. Deep sea sediments record the geophysiology of the end Ordovician glaciation. Journal of the Geological Society, 154, 929-934.

Athy, L.F., 1930. Density, porosity, and compaction of sedimentary rocks. American Association of Petroleum Geologists Bulletin, 14, 1–21.

Avseth, P., Mukerji, T. and Mavko, G., 2005. Quantitative seismic interpretation: Applying rock physics tools to reduce interpretation risk. Cambridge University Press.

Aydin, A., 2000. Fractures, faults, and hydrocarbon entrapment, migration and flow. Marine and Petroleum Geology, 17, 797–814.

Babonneau, N., Savoye, B., Cremer, M., and Klein, B., 2002. Morphology and architecture of the present canyon and channel system of the Zaire deep-sea fan. Marine and Petroleum Geology, 19, 445-467.

Bahr, D.B., Hutton, E., Syvitski, J., and Pratson, L., 2001. Exponential approximations to compacted sediment porosity profiles. Computers and Geoscience, 27(6), 691-700.

Bailey, W.R., Underschultz, J., Dewhurst, D.N., Kovack, G., Mildren, S. and Raven, M. 2006. Multi-disciplinary approach to fault and top seal appraisal; Pyrenees-Macedon oil and gas fields, Exmouth Sub-basin, Australian Northwest Shelf. Marine and Petroleum Geology, 23, 241–259.

Baillie, P.W., and Jacobson, E.P., 1997. Prospectivity and exploration history of the Barrow Subbasin, Western Australia: Australian Petroleum Production & Exploration Association Journal, 37, 117-135.

Baldwin, B. and Butler, C., 1985. Compaction curves. American Association of Petroleum Geologists Bulletin, 69(4), 622-626.

Baldwin, B., 1971. Ways of deciphering compacted sediments. Journal of Sedimentary Petrology, 41 (1), 293–301.

Barber, P., 1994. Late Jurassic-Early Cretaceous depositional systems of the Dampier Sub-basin - Quo Vadis?. Australian Petroleum Exploration Association Journal, 34, 566-585.

Beaubouef, R.T., and S. J. Friedmann, 2000. High resolution seismic/sequence stratigraphic framework for the evolution of Pleistocene intra slope basins, western Gulf of Mexico: Depositional models and reservoir analogs. In: Weimer, P., Slatt R. M., Coleman, J., Rossen, N. C., Nelson, H., Bouma, A. H, Styzen, M. J, and Lawrence D. T., (Eds.), Deep-water reservoirs of the world: Gulf Coast Section-SEPM Special Publication, 40-60.

Berger, G., Laparols, C., Guy, C., and Daux, V., 1994. Dissolution rate of a basalt glass in silica-rich solutions: Implications for long-term alteration. Geochimica et Cosmochimica Acta, 58 (22), 4875-4886

Bernaud, D., Dormieux, L., Maghous, S., 2006. A constitutive and numerical model for mechanical compaction in sedimentary basins. Computers and Geotechnics, 33 (6-7), 316-329.

Bertrand, C., Tonellot, T., Fournier, F., 2003. Seismic facies analysis applied to P and S impedances from pre-stack inversion, 72nd Annual International Meeting: Society of Exploration Geophysicists, 217.

Binns, R. A., et al, 2002. Proceedings of the Ocean Drilling Program, Initial Reports, 193, College Station, TX.

Bishop, R. S., Gehman, H. M., and Young, A., 1983. Concepts for estimating hydrocarbon accumulation and dispersion. American Association of Petroleum Geologists Bulletin, 67, 337-348.

Bjørlykke, K., 1999. Principal aspects of compaction and fluid flow in mudstones. In: Aplin, A.C., Fleet, A.J. & Macquaker, J.H.S. (Eds) Mud and mudstones: Physical and fluid flow properties. Geological Society of London, Special Publication 158, 73-78.

Bjorlykke, K., Hoeg, K.,1997. Effects of burial diagenesis on stresses, compaction and fluid flow in sedimentary basins. Marine and Petroleum Geology, 14, 267-276.

Bluck, B. J., Ward, J. D., Cartwright, J. and Swart, R., 2007. The Orange River, southern Africa: an extreme example of a wave-dominated sediment dispersal system in the South Atlantic Ocean. Journal of the Geological Society, 164(2), 341-351.

Blum, P., 1997. Physical Properties Handbook: A guide to the shipboard measurement of physical properties of deep-sea cores. Ocean Drilling Program Technical Note 26.

Boles, J. R., Eichhubl, P., Garven, G. and Chen, J., 2004. Evolution of a hydrocarbon migration pathway along basin-bounding faults: Evidence from fault cement: American Association of Petroleum Geologists Bulletin, 88, 947– 970.

Booth, J. R., DuVernay III, A. E., Pfeiffer, D. S., and Styzen, M. J., 2000. Sequence stratigraphic framework, depositional models, and stacking patterns of ponded and slope fan systems in the Auger basin: central Gulf of Mexico Slope. In: Weimer, P., Slatt R. M., Coleman, J., Rossen, N. C., Nelson, H., Bouma, A. H, Styzen, M. J, and Lawrence D. T., (Eds.), Deep-water reservoirs of the world: Gulf Coast Section-SEPM Special Publication, 82-103.

Boulay, S., Colin, C., Trentesaux, A., Frank, N. and Liu, Z., 2005. Sediment sources and East Asian monsoon intensity over the last 450 ky. Mineralogical and geochemical investigations on South China Sea sediments. Palaeogeography, Palaeoclimatology, Palaeoecology, 228(3-4), 260-277.

Bouma, A. H., 1962. Sedimentology of some Flysch deposits: A graphic approach to facies interpretation, Elsevier.

Bouma, A. H., 1981. Depositional sequences in clastic continental slope deposits. Gulf of Mexico. Geo-Marine Letters, 1-2, 115-121.

Bouma, A. H., and Moore, J. C., 1975. Physical properties of deep-sea sediments from the Philippine Sea and Sea of Japan. In: Karig, D. E., Ingle, J. C, Jr., et al, Initial Reports, Deep Sea Drilling Project, 31, 535-568.

Boyce, R.E., 1973. Appendix I. Physical property methods. Initial Reports, Deep Sea Drilling Project, 15, 1115-1128.

Boyd, R., Ruming, K., Goodwin, I., Sandstrom, M., and Schro¨der-Adams, C., 2008. Highstand transport of coastal sand to the deep ocean: A case study from Fraser Island, southeast Australia. Geology, 36, 15-18.

Bradbury, W., Freeman, S., Harris, S.D., Jones, P., Knipe, R., 2009. Fault seal risk maps and volumes - a tool for better understanding uncertainty and focusing interpretation effort for prospect and field development. Presented at American Association of Petroleum Geologists Annual Convention, , Denver, Colorado, June 7-10, 2009.

Broichhausen, H., Littke, R., Hantschel, T., 2005. Mudstone compaction and its influence on overpressure generation, elucidated by a 3D case study in the North Sea. International Journal of Earth Science, 94, 956-978.

Brown Jr., L.F. and Fisher, W.L., 1977. Seismic stratigraphic interpretation of depositional systems: examples from Brazilian rift and pull-apart basins. In: Payton, C.E. (Ed.), Seismic Stratigraphy - Applications to Hydrocarbon Exploration. American Association of Petroleum Geologists Memoir 26, 213–248.

Brown, A., 2000. Evaluation of possible gas microseepage mechanisms. American Association of Petroleum Geologists Bulletin, 84, 1775-1789.

Browne, G. H. and Slatt, R. M., 2002. Outcrop and behind-outcrop characterization of a late Miocene slope fan system, Mt. Messenger Formation, New Zealand. American Association of Petroleum Geologists Bulletin, 86, 841-862.

Browne, G.H., Slatt, R.M. and King, P.R., 2000. Contrasting styles of basin floor fan and slope fan deposition: Mount Messenger Formation, New Zealand. In: Bouma, A.H. and Stone, C.G. (Eds), Fine Grained Turbidite Systems, American Association of Petroleum Geologists Bulletin Memoir 72 / SEPM Special Publication 68, 143-152.

Bryant, W. R., Hottman, W., and Trabant, P., 1975. Permeability of unconsolidated marine sediments, Gulf of Mexico, Marine Geotechnology, 1(1), 1-14.

Bryant, W.R. and Rack, F.R., 1990. Consolidation characteristics of Weddell Sea sediments: results of ODP Leg 113. In: Barker, P.F., Kennett, J.P., O'Conell, S. and Pisias, N.G et al, Proceedings of the Ocean Drilling Program, Scientific Results, 113, College Station, TX, 201–223.

Bryn, P., Berg, K., Forsberg, C. F., Solheim, A., and Kvalstad, T. J., 2005. Explaining the Storegga Slide. Marine and Petroleum Geology, 22(1-2), 11-19.

Bull, S., Cartwright, J., and Huuse, M., 2009. A review of kinematic indicators from mass-transport complexes using 3D seismic data. Marine and Petroleum Geology, 26(7), 1132-1151.

Burland, J.B., 1990. On the compressibility and shear strength of natural clay. Géotechnique, 40, 329-378.

Burne, R. V., 1995. Return of 'The Fan That Never Was': Westphalian turbidite systems in the Variscan Culm Basin: Bude Formation (southwest England). In: Plint, A.G. (Ed.), Sedimentary Facies Analysis. Special Publication International Association of Sedimentologists, 22, 101-135.

Burne, R. V., 1998. Return of 'The Fan That Never Was': Westphalian turbidite systems in the Variscan Culm Basin: Bude Formation (south-west England). Reply. Sedimentology, 45, 971-975.

Busch, W.H., 1989. Patterns of sediment compaction at Ocean Drilling Program Sites 645, 646, and 647, Baffin Bay and Labrador Sea. In: Srivastava, S.P., Arthur, M.A., Clement, B., et al, Proceedings of the Ocean Drilling Program, Scientific Results, 105, College Station, TX, 781-790.

Caillet, G., 1993. The cap rock of the Snorre field, Norway: A possible leakage by hydraulic fracturing. Marine and Petroleum Geology, 10, 42-50.

Campbell, C. V., 1967. Lamina, laminaset, bed and bedset. Sedimentology, 8, 7-26.

Carey, S. N. and Sigurdsson, H., 1980. The Roseau Ash: deep-sea tephra deposits from a major eruption on Dominica, Lesser Antilles Arc. Journal of Volcanology and Geothermal Research, 7, 67-86.

Carlson, R. L., 1981. Acoustic properties of tuffaceous and calcareous sediments, Deep Sea Drilling Project Leg 60. In: Hussong, D.M., Uyeda, S., et al, Initial Reports, Deep Sea Drilling Project, 60, Washington, 803-804.

Carlson, R.L., Christensen, N.I., and Wilkens, R.H., 1980. Acoustic properties of volcaniclastic sediments recovered from the floor of the Philippine Sea, Deep Sea Drilling Project Leg 59. In: Kroenke, L., Scott, R., et al, Initial Reports, Deep Sea Drilling Project, 59, Washington, 519-522.

Cartwright J. A., Huuse, M. and Aplin, A. C., 2007. Seal Bypass Systems. American Association of Petroleum Geologists Bulletin, 91, 1141-1166.

Cartwright, J. A. and Dewhurst, D., 1998. Layer-bound compaction faults in fine-grained sediments. Geological Society of America Bulletin, 110, 1242-1257.

Cartwright, J. A. and Lonergan, L., 1996. Volumetric contraction during the compaction of mudrocks: a mechanism for the development of regional-scale polygonal fault systems. Basin Research, 8, 183-193.

Chevallier, J., Tréhu, A.M., Bangs, N.L., Johnson, J.E., and Meyer, H.J., 2006. Seismic sequence stratigraphy and tectonic evolution of southern Hydrate Ridge. In: Tréhu, A.M., Bohrmann, G., Torres, M.E., and Colwell, F.S. (Eds), Proceeding of the Ocean Drilling Program, Scientific Results, 204, College Station, TX, 1-29.

Chilingar, G., V., 1964. Relationship between porosity, permeability, and grain-size distribution of sands and sandstones. In: van Straaten, L. M. J. U., (Ed), Developments in Sedimentology, Volume 1, Deltaic and Shallow Marine Deposits, Elsevier, 71-75.

Clare, A.P., and Crowley, A.J., 2001. Qualitative analysis of spectral gamma ray data as a tool for fieldwide and regional stratigraphic correlation, Enderby Terrace, Carnarvon Basin, Western Australia. Australian Petroleum Production & Exploration Association Journal, 41, 449-462.

Cochran, J. R, et al, 1988. Proceedings of the Ocean Drilling Program, Initial Reports, 116, College Station, TX.

Collett, T, S., Riedel, M., Cochran, J. R., Boswell, R., Kumar, P. and Sathe, A.V., 2008. Indian continental margin gas hydrate prospects: results of the Indian national gas hydrate program (NGHP) expedition 01. Proceedings of the 6th International Conference on Gas Hydrates (ICGH 2008), Vancouver, British Columbia, Canada, July 6-10, 2008.

Collinson, J. D. and Thompson, D. B., 1989. Sedimentary Structures. Unwin Hyman, London.

Collot, J.-Y., et al, 1992. Proceedings of the Ocean Drilling Program, Initial Reports, 134, College Station, TX.

Comas, M.C., et al, 1996. Proceedings of the Ocean Drilling Program, Initial Reports, 161, College Station, TX.

Compton, J. S., 1991. Porosity reduction and burial history of siliceous rocks from the Monterey and Sisquoc Formations, Point Pedernales Area, California. Geological Society of America Bulletin, 103, 625-636.

Converse, D. R., Nicholson, P. H., Pottorf, R. J., and Miller, T. W., 2000. Controls on overpressure in rapidly subsiding basins and implications for failure of top seal. In: Mello M. R. and Katz, B. J., (Eds.), Petroleum systems of South Atlantic margins: American Association of Petroleum Geologists Memoir 73, 133–150.

Cope, R.N. and Reed, J.J. 1967. The Cretaceous paleogeography of the Taranaki-Cook Strait area. Australasian Institute of Mining and Mettalurgy proceedings, 222, 63-72.

Cope, R.N., 1965. The Taranaki Basin: a subsurface review. Shell, Bp and Todd Oil Services. EP Reports, 61.

Crisp, J. A., 1984. Rates of magma emplacement and volcanic output. Journal of Volcanology and Geothermal Research, 20, 177-211.

Cronin, B. T., Akhmetzhanov, A. M., Mazzini, A., Akhmanov, G., Ivanov, M., Kenyon, N. H. and TTR-10 Shipboard Scientists, 2005. Morphology, evolution and fill: implications for sand and mud distribution in filling deep-water canyons and slope channel complexes. Sedimentary Geology, 179, 71-97.

Cronin, B. T., Hartley, A. J ., Owen, D., and Kneller, B., 1998. Slumps, debris flows and sandy deep-water channel systems: implications for the application of sequence stratigraphy to deep water clastic sediments. Journal of the Geological Society of London, 155, 429–432.

Crovisier J. L., Honnorez J. and Eberhart J. P., 1987. Dissolution of basaltic glass in seawater: mechanism and rate. Geochimica et Cosmochimica Acta, 51, 2977–2990.

Crown Minerals Website, 2009a. Petroleum Basins, Facts and Figures. Available from http://www.crownminerals.govt.nz/cms/petroleum/facts-and-figures/#production [accessed 18/03/09]

Crown Minerals Website, 2009b. Taranaki Basin reservoirs. Available from http://www.crownminerals.govt.nz/cms/pdf-library/petroleum-basins-1/taranaki_reservoirs.pdf [accessed 19/03/09]

Dadey, K. A., and Klaus, A., 1992. Physical properties of volcaniclastic sediments in the Izu-Bonin area. In: Taylor, B., Fujioka, K., et al, Proceeding of the Ocean Drilling Program, Scientific Results, 126, College Station, TX, 543–550.

Darby, D., 2002. Seal properties, overpressure and stress in the Taranaki and East Coast Basins, New Zealand, 2002 New Zealand Petroleum Conference Proceedings, Crown Minerals, Ministry of Economic Development, Edmonton, Alberta.

Darby, D., Funnell, R. and Stagpoole, V., 2000. Overpressure , seal breaching and stress regimes in East Coast and Taranaki Basins, New Zealand [Abstract]. American Association of Petroleum Geologists International Conference and Exhibition, Bali, Indonesia.

Darling, H. R., Sneider, R. M., 1992. Production of low resistivity, low contrast reservoirs, offshore Gulf of Mexico basin. Gulf Coast Association of Geological Society Transactions, abstract, 42, 73-88.

Davies, J. R., Sheppard, T. H., Waters, R. A, and Wilson, D. 2006. Geology of the Llangranog district - A brief explanation of the geological map. Sheet explanation of the British Geological Survey. 1:50 000 Series Sheet 194 Llangranog (England and Wales).

Davies, J. R., Waters, R. A., Wilby, P. R., Williams, M. & Wilson, D. 2003. Geology of the Cardigan and Dinas Island district – a brief explanation of the geological map. Sheet explanation of the British Geological Survey. 1:50 000 Sheet 193 (including part of Sheet 210) Cardigan and Dinas Island (England and Wales).

Davis, C., Haughton, P., McCaffrey, W., Scott, E., Hogg, N., and Kitching, D., 2009. Character and distribution of hybrid sediment gravity flow deposits from the outer Forties Fan, Palaeocene Central North Sea, UKCS. Marine and Petroleum Geology, Article in Press, doi:10.1016/j.marpetgeo.2009.02.015.

Dawson, W.C. and Almon, W.R., 1999. Top seal character and sequence stratigraphy of selected marine shales in Gulf Coast style basins. Gulf Coast Association of Geological Societies Transactions 49, 190–197.

Dawson, W.C. and Almon, W.R., 2002. Top seal potential of Tertiary deep-water Gulf of Mexico shales. Gulf Coast Association of Geological Societies Transactions 52, 167–176.

Dawson, W.C. and Almon, W.R., 2005. Shale facies variability and sequence stratigraphy: Application to top seal prediction in deepwater depositional systems. Gulf Coast Association of Geological Societies Transactions, 55, 133-145.

Dawson, W.C. and Almon, W.R., 2006. Shale facies and seal variability in deepwater depositional systems. Poster presentation at American Association of Petroleum Geologists Annual Convention, Houston, Texas, April 9-12, 2006.

Dewhurst D. N. , Aplin A. C., Sarda J-P. and Yang Y., 1998. Compaction-driven evolution of porosity and permeability in natural mudstones: an experimental study. Journal of Geophysical Research, Solid Earth, 103/B1, 651-661.

Dewhurst, D. N ., Aplin, A. C., and Sarda, J. P., 1999a. Influence of clay fraction on pore-scale properties and hydraulic conductivity of experimentally compacted mudstones, Journal of Geophysical Research, Solid Earth, 104/B12, 29261-29274.

Dewhurst, D. N ., Yang Y. and Aplin A. C., 1999b. Fluid flow through natural mudstones. In: Aplin, A. C., Fleet, A. J. and Macquaker, J. H. S. (Eds), Muds and mudstones: physical and fluid flow properties. Geological Society of London Special Publication, 158, 23-43.

Dewhurst, D. N. and Hennig, A., 2003. Geomechanical properties related to top seal leakage in the Carnarvon Basin, Northwest Shelf, Australia. Petroleum Geoscience, 9, 255-263.

Dewhurst, D. N., Cartwright, J. A. and Lonergan, L., 1999c. The development of polygonal fault systems by syneresis of colloidal sediments. Marine and Petroleum Geology, 16(8), 793-810

Dickinson, G., 1953. Geological aspects of abnormal reservoir pressures in the Gulf Coast Louisiana. American Association of Petroleum Geologists Bulletin, 37 (2), 410–432.

Downey, M.W., 1984. Evaluating seals for hydrocarbon accumulations, American Association of Petroleum Geologists Bulletin, 68,1752-1763.

Duan, T., Gao, Z., Zeng, Y. and Stow, D. A. V., 1993. A fossil carbonate contourite drift on the Lower Ordovician palaeocontinental margin of the middle Yangtze Terrane, Jiuxi, Northern Huan, Southern China. Sedimentary Geology, 82, 271–284.

Dugan, B. and Flemings, P. B., 2000. The New Jersey margin: compaction and fluid flow. Journal of Geochemical Exploration, 69-70, 477-481.

Dzevanshir, R. D., Buryakovsskiy, L. A. and Chilingarian G.V., 1986. Simple quantitative evaluation of porosity of argillaceous sediments at various depths of burial, Sedimentary Geology, 46, 169–175.

Egeberg, P.K. and the Leg 126 Shipboard Scientific Party, 1990. Unusual composition of pore waters found in the Izu-Bonin fore-arc sedimentary basins. Nature, 244, 215-218.

Egeberg, P.K., 1992. Thermodynamic aspects of Leg 126 interstitial waters. In: Taylor, B., Fujioka, K., et al, Proceeding of the Ocean Drilling Program, Scientific Results, 126, College Station, TX, 519-530.

Esch, W. L. and Hanor, J. S., 1995. Fault and fracture control of fluid flow and diagenesis around the Iberia salt dome, Iberia Parish, Louisiana. Gulf Coast Association of Geological Societies Transactions, 45, 181-187.

Evans, R., Mory, A. J. and Tait, A. M., 2007. An outcrop gamma ray study of the Tumblagooda Sandstone, Western Australia. Journal of Petroleum Science and Engineering, 57 (1-2), 37-59.

Farseth, R. B., Johnsen, E., and Sperrevik, S., 2007. Methodology for risking fault seal capacity: Implications of fault zone architecture. American Association of Petroleum Geologists Bulletin, 91(9), 1231-1246.

Faugères J.-C., Zaragosi, S., Mezerais, M. L, and Masse, L., 2002. The Vema contourite fan in the South Brazilian basin. Geological Society of London Memoirs, 22(1), 209 - 222.

Faugères, J.-C., Stow, D. A. V., Imbert, P. and Viana, A., 1999. Seismic features diagnostic of contourite drifts. Marine Geology, 162, 1-38.

Federman, A. N., 1984. Hydration of abyssal tephra glasses. Journal of Non-crystalline Solids, 67, 323–332.

Felt, V. L., Reda, M., Easley, D., Montasser, S., Williams, T. R., and Fathy, M., 2004. Understanding thin bedded reservoirs in Pliocene slope channel levee complexes offshore West Nile Delta. Association of Petroleum Geologists International Conference, October 24-27, 2004; Cancun, Mexico.

Fiore, S., Huertas, F.J., Huertas F. and Linares, J., 2001. Smectite formation in rhyolitic obsidian as inferred by microscopic (SEM-TEM-AEM) investigation. Clay Minerals, 36, 489-500.

Fiore, S., Huertas, F.J., Tazaki, K., Huertas F., Linares, J., 1999. A low temperature experimental alteration of obsidian. European Journal of Mineralogy, 11, 455-469.
Fisher, R. V., Schmincke, H.-U., 1984. Pyroclastic rocks. Springer, Berlin Heidelberg, New York..

Flemings, P. B., Behrmann, J.H., John, C.M., and the Expedition 308 Scientists, 2006. Proceedings of the Integrated Ocean Drilling Project, 308. College Station TX.

Flemings, P. B., Long, H., Dugan, B., Germaine, J., John C. M., Behrmann, J. H., Sawyer, D. and IODP Expedition 308 Scientists, 2008. Pore pressure penetrometers document high overpressure near the seafloor where multiple submarine landslides have occurred on the continental slope, offshore Louisiana, Gulf of Mexico. Earth and Planetary Science Letters, 269 (3-4), 309-325.

Flint, L. E., and Selker, J. S., 2003. Use of porosity to estimate hydraulic properties of volcanic tuffs. Advances in Water Resources, 26, 661–671.

Flood et al, 1995. Proceedings of the Ocean Drilling Program, Initial Reports, 155, College Station, TX.

Freshney, E. C., Edmonds, E. A., Taylor, R. T. and Williams, B.J., 1979. Geology of the country around Bude and Bradworthy: Memoir for 1:50 000 geological sheets 307 and 308 Memoirs of the Geological Survey of Great Britain, England and Wales.

Frey Martinez, J., Cartwright J., and James D., 2006. Frontally confined versus frontally emergent submarine landslides: a 3D seismic characterisation, Marine and Petroleum Geology, 23, 585–604.

Friedman, I. and Long W. D., 1976. Hydration rate of obsidian, Science, 191, 347-352.

Friedman, I. and Smith, R. L., 1958. The deuterium content of water in some volcanic glasses. Geochimica et Cosmochimica Acta, 15, 218-228.

Friedman, I. and Smith, R. L., 1960. A new dating method using obsidian: part I, The development of the method. American Antiquity, 25, 476-522.

Friedman, I., Smith, R. L. and Long, W. D., 1966. Hydration of natural glass and formation of perlite. Geological Society of America Bulletin, 77, 323-328.

Friedmann, S. J. and Nummedal, D., 2003. Reassessing the geological risks of seals failure for saline aquifers and EOR projects. In: 2nd Annual Carbon Sequestration Conference, DOE/NETL, Alexandria, VA, May 5-8, 2003.

Fujii, N., 1975. Material and energy production from volcanoes. Bulletin of the Volcanological Society of Japan, 20, 197-204.

Furnes, H., 1984. Chemical changes during progressive subaerial palagonitization of a subglacial olivine tholeiite hyaloclastite – a microprobe analysis. Chemical Geology, 43, 271-285.

Gaarenstroem, L., Tromp, A. J., de Jong, M. C. and Brandenburg, A. M., 1993. Overpressures in the Central North Sea: implications for trap integrity and drilling safety. In: Parker, J. R., (Ed), Petroleum geology of northwest Europe: Proceedings of the 4th conference, The Geological Society of London, 1305 – 1313.

Galloway, W.E., 1989. Genetic stratigraphic sequences in basin analysis II: Application to Northwest Gulf of Mexico Cenozoic Basin. American Association of Petroleum Geologists Bulletin, 73(2), 143 – 154.

Gartrell, A., Lils, M. and Underschultz, J., 2002. Controls on the trap integrity of the Skua oil field, Timor Sea. In: Keep, M. and Moss, S. J., (Eds) The sedimentary basins of Western Australia 3, Proceedings of the Petroleum Exploration Society of Australia Symposium, Perth.

Georgiopoulou, A., Wynn, R. B., Masson, D. G., and Frenz, M., 2009. Linked turbidite–debrite resulting from recent Sahara Slide headwall reactivation, Marine and Petroleum Geology, Article in Press, doi:10.1016/j.marpetgeo.2009.02.013

Gérard, M., and Person, A., 1994. Low hydrothermal impact in volcaniclastic sediments of the north Aoba Basin: Sites 832 and 833. In: Greene, H. G., Collot, J.-Y., Stokking, L. B., et al, Proceeding of the Ocean Drilling Program, Scientific Results, 134, College Station, TX, 131–176.

Gibson, R. E., Schiffman, R. L. and Cargill, K. W., 1981. The theory of one-dimensional consolidation of saturated clays: II. Finite nonlinear consolidation of thick homogeneous layers. Canadian Geotechnical Journal, 18 (2), 280-293.

Gieskes, J.M. and Lawrence, J.R., 1981. Alteration of volcanic matter in deep sea sediments: evidence from Deep Sea Drilling cores. Geochimica et Cosmochimica Acta, 45, 1687-1703.

Giles, M. R., 1997. Diagenesis: A Quantitative Perspective - Implications for Basin Modelling and Rock Property Prediction, Kluwer Academic Publishers, Dordrecht.

Giles, M. R., Indrelid, S. L. and James, D. M. D, 1998. Compaction - the great unknown in basin modelling. Geological Society of London, Special Publication, 141, 15 - 43.

Glennie, K., W., 1998. Petroleum Geology of the North Sea: Basic Concepts and Recent Advances, Blackwell.

Glennie, K.W., 1958. Upper Miocene Formations of West Taranaki. Ministry of Commerce New Zealand, Unpublished Petroleum Report, PR419.

Gluyas, J.G. and Hichens, H.M., 2003. United Kingdom Oil and Gas Fields. Commemorative Millennium Volume. Geological Society Memoir 20.

Graber, K.K., Pollard, E., Jonasson, B., and Schulte, E. (Eds.), 2002. Overview of Ocean Drilling Program engineering tools and hardware. ODP Technical Note 31.

Gràcia, E., Martínez-Ruiz, F., Piñero, E., Larrasoaña, J. C., Vizcaino, A., and Ercilla, G., 2006. Data report: Grainsize and bulk and clay mineralogy of sediments from the summit and flanks of southern Hydrate Ridge, Sites 1244–1250, ODP Leg 204. In: Tréhu, A. M., Bohrmann, G., Torres, M. E., and Colwell, F. S. (Eds), Proceeding of the Ocean Drilling Program, Scientific Results, 204, 1-19.

Grauls, D., and Cassignol, C., 1992. Fluid pressure-induced open fracture anomaly characterization from well data and seismic velocities - Mechanisms and major implications: Bulletin des Centres de Recherches Exploration-Production Elf Aquitaine, 16, 275– 284.

Grim, R. E. and Güven, N., 1978. Bentonites: Geology, mineralogy, properties and uses; Developments in Sedimentology 24, Elsevier Publishing Company, New York.

Grunau, H.R., 1987. A worldwide look at the cap rock problem. Journal of Petroleum Geology 10, 245–266.

Gutierrez, M. and Wangen, M., 2005. Modeling of compaction and overpressuring in sedimentary basins. Marine and Petroleum Geology, 22 (3), 351-363.

Hall, D. M., Duff, B. A., Elias, M., and Gytri, S. R., 1997. Pre-cretaceous top-seal integrity in the greater Ekofisk area In: Moller-Pedersen, P., and Koestler, A. G., (Eds), Hydrocarbon Seals: importance for Exploration and Production. Norwegian Petroleum Society (NPF) Special Publication 7, Elsevier, 231-242.

Hamilton, E. L., 1976. Variations in density and porosity with depth in deep-sea sediments. Journal of Sedimentary Petrology, 46, 280-300.

Hansen, R. J. and Kamp, P. J. J., 2004. Late Miocene to early Pliocene stratigraphic record in northern Taranaki Basin: condensed sedimentation ahead of Northern Graben extension and progradation of the modern continental margin. New Zealand Journal of Geology and Geophysics, 47, 645-662.

Hart, B. S., Flemings, P. B., and Deshpande, A. 1995. Porosity and pressure: role of compaction disequilibrium in the development of geopressures in a Gulf Coast Pleistocene basin. Geology, 23, 45 - 48.

Haskell, B. J., Johnson, T. C., and Showers, W.J., 1991. Fluctuations in deep western North Atlantic circulation on the Blake Outer Ridge during the last deglaciation. Paleoceanography, 6, 21-31.

Haughton, P., Davis, C., McCaffrey, W., Barker, S., 2009. Hybrid sediment gravity flow deposits - Classification, origin and significance. Marine and Petroleum Geology, Article in Press, doi:10.1016/j.marpetgeo.2009.02.012.

Hay, R. F., 1967. Sheet 7 - Taranaki (1st Edition). Geological map of New Zealand 1:250000. Department of Scientific and Industrial Research, Wellington.

Hedberg, H. D., 1926, The effect of gravitational compaction on the structure of sedimentary rocks, American Association of Petroleum Geologists Bulletin, 10, 1035–1072.

Hedberg, H. D., 1936. Gravitational compaction of clays and shales. American Journal of Science, 31, 241–287.

Heezen, B. C., Hollister, C., 1964. Deep-sea current evidence from abyssal sediments. Marine Geology, 1(2), 141-174.

Heffernan, A. S., Moore, J. C., Bangs, N. L., Moore, G. F. and Shipley, T.H., 2004. Initial deformation in a subduction thrust system: polygonal normal faulting in the incoming sedimentary sequence of the Nankai subduction zone, southwestern Japan. In: Davies, R. J., Cartwright, J., Stewart, S. A., Underhill, J. R and Lappin, M. (Eds), 3D Seismic Technology: Application to the Exploration of Sedimentary Basins. Geological Society of London, Memoir 29, 143-148.

Heiken, G., 1974. An atlas of volcanic ash. Smithsonian Contributions to the Earth Sciences, 12, 1-101.

Heling, D., 1970. Micro-fabrics of shales and their rearrangement by compaction: Sedimentology, 15, 247-260.

Henderson, J., 1937. Petroleum in New Zealand. DSIR bulletin 60, Department of Scientific and Industrial Research, Wellington.

Henry, J. D., 1911. Oil fields of New Zealand. Oil fields of the Empire, Series 2. Bradbury, Agnew and Co. London.

Higgs, R. 2004 Ross and Bude Formations (Carboniferous, Ireland and England): reinterpreted as lake-shelf turbidites. Journal of Petroleum Geology, 27(1), 47-66.

Higgs, R., 1991. The Bude Formation (Lower Westphalian), SW England: siliciclastic shelf sedimentation in a large equatorial lake. Sedimentology, 38, 445-469.

Higgs, R., 1994. Lake Bude (Upper Carboniferous), southwest England. In: Gierlowski-Kordesch, E. and Kelts, K. (Eds), Global Geological Record of Lake Basins, volume 1. Cambridge University Press, 121-125.

Higgs, R., 1998. Return of 'The fan that never was': Westphalian turbidite systems in the Variscan Culm Basin: Bude Formation (south-west England). Discussion. Sedimentology, 45, 961-967.

Hiscott, R. N., Hall, F.R. and Pirmez, C., 1997. Turbidity current overspill from the Amazon Channel: Texture of the silt/sand load, paleoflow from anisotropy of magnetic susceptibility and implications for flow processes. In: Flood, R. D., Piper, D. J . W., Klaus, A. and Peterson, L. C., (Eds), Proceedings of the Ocean Drilling Program Scientific Results, 155, College Station, Texas, 53–78.

Hodder, A. P. W., Naish, T.R. and Nelson, C.S., 1993. A two-stage model for the formation of smectite from detrital volcanic glass under shallow-marine conditions. Marine Geology, 109, 279–285.

Holt, W. E. and Stern, T. A. 1994. Subduction, platform subsidence, and foreland thrust loading: The late Tertiary development of Taranaki Basin, New Zealand. Tectonics, 13(5), 1068-1092.

Holz, C., 2005. Climate-induced variability of fluvial and aeolian sediment supply and gravity-driven sediment transport off Northwest Africa. PhD Dissertation, Department of Geosciences, University of Bremen.

Huggett, J. M., 1992. Petrography, mineralogy and diagenesis of overpressured Tertiary and Late Cretaceous mudrocks from the East Shetland Basin. Clay Minerals, 27, 487–506.

Hurst, A., 1990. Natural gamma-ray spectrometry in hydrocarbon-bearing sandstones from the Norwegian Continental Shelf. In: Hurst, A., Lovell, M. A. and Morton, A. C. (Eds) Geological Applications of Wireline Logs. Geological Society of London, Special Publication 48, 211-222.

Hurst, A., Cartwright, J. A., Huuse, M., Jonk, R., Schwab, A., Duranti, D., and Cronin, B., 2003. Significance of large scale sand injectites as long-term fluid conduits: Evidence from seismic data. Geofluids, 3, 263–274.

Ingram, G. M., and Urai, J. L., 1999. Top seal leakage through faults and fractures: The role of mudrock properties. In: Aplin, A.C., Fleet, A.J. & Macquaker, J.H.S. (Eds) Muds and mudstones: Physical and fluid-flow properties: Geological Society of London, Special Publication 158, 125–135.

Ingram, G. M., Urai, J. L., and Naylor, M. A., 1997. Sealing processes and top seal assessment. In: Moller-Pedersen, P., and Koestler, A. G., (Eds), Hydrocarbon Seals: importance for Exploration and Production. Norwegian Petroleum Society (NPF) Special Publication 7, Elsevier, 165-174.

James, D. M. D., 1975. Caradoc turbidites at Poppit Sands (Pembrokeshire), Wales. Geological Magazine, 112, 295-304.

James, D. M. D., 1997. Llanvirn–Llandovery activity on the Llangrannog Lineament in southwest Ceredigion. Mercian Geologist, 14, 68-78.

Jansen, E., et al, 1996. Proceedings of the Ocean Drilling Program, Initial Reports, 162, College Station, TX.

Jeans, C.V., 2000. Mineral diagenesis and reservoir quality—the way forward: an introduction, Clay Minerals, 35 , 3–4.

Jezek, P. A. and Noble, D. C., 1978. Natural hydration and ion exchange of obsidian: an electron microprobe study. American Mineralogist, 63, 266–273.

Kamp, P. J. J., Vonk, A. J., Bland, K. J., Hansen, R. J., Hendy, A. J. W., McIntyre, A. P., Ngatai, M., Cartwright, S. J., Hayton, S. and Nelson, C. S., 2004. Neogene stratigraphic architecture and tectonic evolution of Wanganui, King Country, and eastern Taranaki Basins, New Zealand. New Zealand Journal of Geology and Geophysics, 47, 625-644.

Karig, D. E. and Hou, G., 1992. High-stress consolidation experiments and their geologic implications. Journal of Geophysical Research, B, Solid Earth and Planets, 97 (1), 289–300.

Karig, D. E., and Angevine, C. L., 1986. Geologic constraints on subduction rates in the Nankai Trough. In: Kagami, H., Karig, D. E., and Coulbourn, W. T., et al., Initial Reports, Deep Sea Drilling Project., 87, 789–796.

Kataoka, Y., Nagahashi, S. and Yoshikawa, S., 2001. An extremely large magnitude eruption close to the Plio-Pleistocene boundary: reconstruction of eruptive style and history of the Ebisutoge-Fukuda tephra, central Japan. Journal of Volcanology and Geothermal Research, 107 (1-3), 47-69.

Kawano, M., Tornita, K. and Kamino, Y., 1993. Formation of clay minerals during low temperature experimental alteration of obsidian. Clays and Clay Minerals, 41, 431-441.

Keevil, G. M., Peakall, J., Best, J. L., and Amos, K. J., 2006. Flow structure in sinuous submarine channels: Velocity and turbulence structure of an experimental submarine channel. Marine Geology, 229(3-4), 241-257.

Keigwin, L. D., et al., 1998. Proceedings of the Ocean Drilling Program, Initial Reports, 172, College Station, TX.

Khan, A., Horowitz, D., Liesch, A., Schepel, K., 1996. Semi-amalgamated thinly-bedded deepwater GOM turbidite reservoir performance modeled using object-based technology and Bouma lithofacies: SPE paper 36724, presented at the 1996 SPE ATCE, Denver, 6-9 October.

King, P. R, Browne, G. H. and Slatt, R. M., 1994. An outcropping Late Miocene basin floor fan to channel-levee complex in Taranaki Basin, New Zealand: sequence stratigraphic implications and subsurface correlations. In: Weimer, P., Bouma, A. H. and Perkins, B. F. (Eds), Submarine Fans and Turbidite Systems: Gulf Coast Section, SEPM 15th Annual Research Conference, Houston.177-193.

King, P. R. and Thrasher, G. P., 1996. Cretaceous-Cenozoic geology and petroleum systems of the Taranaki Basin, New Zealand. Institute of Geological and Nuclear Sciences monograph 13. Lower Hutt, New Zealand.

King, P. R., 1988. Well summary sheets, onshore Taranaki. New Zealand Geological Survey report G125.

King, P. R., Scott, G. H. and Robinson, P. H., 1993. Description, correlation and depositional history of Miocene sediments outcropping along the North Taranaki coast. Institute of Geological and Nuclear Sciences Monograph 5. Lower Hutt, New Zealand.

Kneller, B. C. and Buckee, C., 2000. The structure and fluid mechanics of turbidity currents: a review of some recent studies and their geological implications. Sedimentology, 47, 62-94.

Kneller, B. C., 1995. Beyond the turbidite paradigm: physical models for deposition of turbidites and their implications for reservoir prediction. In: Hartley, A. and Prosser, D. J. (Eds), Characterisation of Deep Marine Clastic Systems, Geological Society of London, Special Publications, 94, 29-46.

Knox, G. L., 1982. Taranaki Basin, structural style and tectonic setting. New Zealand Journal of Geology and Geophysics, 25, 125-140.

Knutz, P. C. and Cartwright, J. A., 2003. Seismic stratigraphy of the West Shetland Drift: implications for Late Neogene paleocirculation in the Faeroe–Shetland gateway, Paleoceanography, 18, 1093.

Knutz, P. C. and Cartwright, J. A., 2004. 3D anatomy of Late Neogene contourite drifts and associated mass flows in the Faroe–Shetland Basin. In: Davies, R. J., Cartwright, J. A., Stewart, S. A., Lappin, M. and Underhill, J. R., (Eds). 3D Seismic Technology: Applications to the Exploration of Sedimentary Basins. Geological Society of London Memoirs, 29, 63–71.

Kokelaar, P., 1988. Tectonic controls of Ordovician arc and marginal basin volcanism in Wales. Journal Geological Society of London, 145 (5), 759-775.

Kuehl, S. A., Nittrouer, C. A., Demaster, D. J., and Curtin, T. B., 1984. An overview of sedimentation on the Amazon continental shelf. Geo-Marine Letters, 4(3-4), 207-210.

Kwon, O., Herbert, B. E. and Kronenberg, A. K., 2004b. Permeability of illite-bearing shale: 2. Influence of fluid chemistry on flow and functionally connected pores. Journal of Geophysical Research, 109, B10206.

Kwon, O., Kronenberg, A. K., Gangi, A. F., Johnson, B., and Herbert, B. E., 2004a. Permeability of illite-bearing shale: 1. Anisotropy and effects of clay content and loading. Journal of Geophysical Research, 109, B10205.

Laine, E. P., Gardner, W. D., Richardson, M. J., and Kominz, M. A., 1994. Abyssal currents and advection of resuspended sediment along the northeastern Bermuda Rise. Marine Geology, 119, 159-171.

Laird, M. G., 1980. The late Mesozoic fragmentation of the New Zealand segment of Gondwana. In: Cresswell, M. M., and Vella, P. (Eds) Gondwana Five. Balkema, Rotterdam, Netherlands. 311-318.

Lash, G., 2006. Top seal development in the shale-dominated Upper Devonian Catskill Delta Complex, western New York State. Marine and Petroleum Geology, 23 (3), 317-335.

Lawrence, D. T., Doyle, M. and Aigner, T., 1990. Stratigraphic simulation of sedimentary basins: Concepts and calibration. American Association of Petroleum Geologists Bulletin, 74, 273-295.

Leckie, R.M. et al, 2000. Proceedings of the Ocean Drilling Program, Scientific Results, 165, College Station, TX.

Leith, T. L. and Fallick, A. E., 1997. Organic geochemistry of caprock hydrocarbons. In: Surdam, R. C. (Ed), Seals, traps and the petroleum system. American Association of Petroleum Geologists, Memoir 67, 115-134.

Leith, T. L., Kaarstad, I., Connan, J., Pierron, J. and Caillet, G., 1993. Recognition of caprock leakage in the Snorre Field, Norwegian North Sea. Marine and Petroleum Geology, 10, 29-41.

Lerche, J., 1990. Basin analysis. Quantitative methods, (Volume 2), Academic Press, San Diego, CA.

Ligtenberg, J. H., 2005. Detection of fluid migration pathways in seismic data: implications for fault seal analysis. Basin Research, 17(1) , 141-153.

Lilleng, T. and Gundesø, R., 1997. The Njord Field: a dynamic hydrocarbon trap In: Moller-Pedersen, P., and Koestler, A. G., (Eds), Hydrocarbon Seals: importance for Exploration and Production. Norwegian Petroleum Society (NPF) Special Publication 7, Elsevier, 217-229.

Lipman, P. W., 1965. Chemical comparison of glassy and crystalline volcanic rocks. U.S. Geological Survey Bulletin, I20I-D, DI-D24.

Lipman, P. W., Christiansen, R. L. and van Alstine R. E., 1969. Retention of alkalies by calc-alkalic rhyolite during crystallization and hydration. American Mineralogist, 54, 285-291.

Long, J. C. S., Aydin, A., Brown, S. R., Einstein, H. H., Hestir, K., Hsieh, P. A., Myer, L. R., Nolte, K. G., Norton, D. L., Olsson, O. L., Paillet, F. L., Smith, J. L. and Thomson, L., 1996. In: Rock fracture and fluid flow: contemporary understanding and applications, National Academy Press, Washington.

Løseth, H., Gading, M., and Wensaas, L., 2009. Hydrocarbon leakage interpreted on seismic data. Marine and Petroleum Geology, 26(7), 1304-1319.

Løseth, H., Wensaas, L., Arntsen, B., and Hovland, M., 2003. Gas and fluid injection triggering shallow mud mobilization in the Hordaland Group, North Sea. In: van

Rensbergen P., Hillis, R., Maltman, A., and Morley, C. (Eds). Subsurface sediment mobilisation: Geological Society of London, Special Publication, 216, 139-157.

Losh, S., Eglinton, L., Schoell, M. and Wood, J., 1999. Vertical and lateral fluid flow related to a large growth fault, Eugene Island Block 330 field, offshore Louisiana. American Association of Petroleum Geologists Bulletin, 83, 244-276.

Lowe, D. R. and Guy, M., 2000. Slurry-flow deposits in the Britannia Formation (Lower Cretaceous), North Sea: a new perspective on the turbidity current and debris flow problem. Sedimentology, 47, 31-70.

Lyons, T. W., Murray, R. W. and Pearson, D. G., 2000. A comparative study of diagenetic pathways in sediments of the Caribbean Sea: highlights from pore-water results. In: Leckie,

R. M., Sigurdsson, H., Acton, G. D. and Draper, G. (Eds), Proceedings of the Ocean Drilling Program, Scientific Results, 165, College Station, TX. 287–298.

Macgregor, D. S., 1996. Factors controlling the destruction or preservation of giant light oilfields. Petroleum Geoscience, 2, 197–217.

Madof, A.S., Christie-Blick, N., and Anders, M.H., 2009. Stratigraphic controls on a salt-withdrawal intraslope minibasin, north-central Green Canyon, Gulf of Mexico: Implications for misinterpreting sea level change. American Association of Petroleum Geologists Bulletin, 93, 535-561.

Maldonado, A., Barnolas, A., Bohoyo, F., Galindo, -Z. J., Hernandez, -M. J., Lobo, F., Rodriguez, -F. J., Somoza, L., Vazquez, J. T., 2003. Contourite deposits in the central Scotia Sea: the importance of the Antarctic Circumpolar Current and the Weddell Gyre flows. Palaeogeography, Palaeoclimatology, Palaeoecology, 198, 187-221.

Mandl, G. and Harkness, R. M., 1987. Hydrocarbon migration by hydraulic fracturing. In: Jones, M. E. and Preston, R. M. F. (Eds.) Deformation of sediments and sedimentary rocks. Geological Society of London, Special Publication 29, 39-53.

Mann, D. M. and Mackenzie, A. S., 1990. Prediction of pore fluid pressures in sedimentary basins. Marine and Petroleum Geology, 7, 55–65.

Marani, M., Argnani, A., Roveri, M. and Trincardi, F., 1993. Sediment drifts and erosional surfaces in the central Mediterranean: Seismic evidence of bottom current activity. Sedimentary Geology, 82, 207-220.

Marcussen, Ø., Thyberg, B.I., Peltonen, C., Jahren, K., Bjørlykke, K., and Faleide, J.I., 2009. Physical properties of Cenozoic mudstones from the northern North Sea: impact of clay mineralogy on compaction trends. American Association of Petroleum Geologists Bulletin, 93(1), 127–150.

Marsters, J. C., and Manghnani, M. H., 1993. Consolidation test results and porosity rebound of Ontong Java Plateau sediments. In: Berger, W. H., Kroenke, L. W., Mayer, L. A., et al, Proceedings of the Ocean Drilling Program, Scientific Results, 130, College Station, TX. 687-694.

Martin, J. B., 1994. Diagenesis and hydrology at the New Hebrides forearc and intra-arc basin. In: Greene, H. G., J.-Y. Collot, L. B. Stokking, et al., Proceedings of the Ocean Drilling Program, Scientific Results, 134, College Station, TX. 109-130.

Martinius, A. W., Geel, C. R. and Arribas, J., 2002. Lithofacies characterization and fluvial sandstones from outcrop gamma-ray logs (Loranaca Basin, Spain): the influence of provenance. Petroleum Geoscience, 8, 51-62.

Masson, D. G., Van Niel, B., and Weaver, P. P. E., 1997. Flow processes and sediment deformation in the Canary Debris Flow on the NW African Continental Rise. Sedimentary Geology,110(3-4), 163-179.

Masson, D. G., Watts, A. B., Gee, M. R. J., Urgeles, R., Mitchell, N. C., Le Bas, T. P. and Canals, M., 2002. Slope failures on the flanks of the western Canary Islands. Earth Science Reviews, 57, 1-35.

Masuda, H., O'Neil, J. R., Jiang, W. T. and Peacor, D. R., 1996. Relation between inter-layer composition of authigenic smectite, mineral assemblages, I/S reaction rate and fluid composition in silicic ash of the Nankai Trough. Clays and Clay Minerals, 44, 443–459.

Mayall, M., Jones, E. and Casey, M., 2006. Turbidite channel reservoirs-Key elements in facies prediction and effective development. Marine and Petroleum Geology, 23(8), 821-841.

McBride, E. F., 1984. Rules of sandstone diagenesis related to reservoir quality. American Association of Petroleum Geologists Bulletin, 68, 1215-1216.

McCann, T., 1992. The stratigraphy of the Ordovician rocks around Cardigan, Wales. Proceedings of the Yorkshire Geological Society, 49, 57-65.

Meade, R. H., 1964. Removal of water and rearrangement of particles during the compaction of the clayey sediments. U.S. Geological Survey Professional Paper 450-B, B1–B23.

Melvin, J., 1987. Upper Carboniferous fine-grained turbiditic sandstones from southwest England: a model for growth in an ancient, delta-fed subsea fan. Reply. Journal of Sedimentary Petrology, 57, 380-382.

Mitchum, R. M., Jr., Sangree, J. B., Vail, P. R., and. Wornardt, W. W, 1991. Sequence stratigraphy in the late Cenozoic expanded sections, Gulf of Mexico, In: Armentrout, J. M. and Perkins, B. F., (Eds), Sequence stratigraphy as an exploration tool, concepts and practices in the Gulf Coast: Gulf Coast Section, SEPM Foundation, Eleventh Annual Research Conference, 237–256.

Mondol, N. H., Bjørlykke, K. and Jahren, J., 2008. Experimental compaction of clays: Relationship between permeability and petrophysical properties in mudstones: Petroleum Geoscience, 14, 1–19.

Moore, G.F., et al, 2001. Proceedings of the Ocean Drilling Program, Initial Reports, 190, College Station, TX.

Moore, J. K. S., 2005. Integration of the sedimentological and petrophysical properties of mudstone samples. Unpublished PhD thesis, Newcastle University, UK.

Mudge, D.C. and Copestake, P., 1992. Lower Palaeogene stratigraphy of the northern North Sea. Marine and Petroleum Geology, 9, 287-301.

Myers, K. J. and Wignall, P. B., 1987. Understanding Jurassic organic-rich mudrocks - New concepts using gamma-ray spectrometry and Palaeoecology: Examples from the Kimmeridge Clay of Dorset and Jet Rock of Yorkshire. In: Leggett, J. K. and Zuffa, G. G. (Eds), Marine Clastic Sedimentology: Developments and Case Studies. Graham and Trotman, London.172-189.

Myers, K. J., 1989. The origin of the Lower Jurassic Cleveland Ironstone Formation of North-East England: evidence from portable gamma-ray spectrometry. In: Young, T. P. and Taylor, W. E. G. (Eds), Phanerozoic Ironstones, Geological Society of London, Special Publication 46, 221-228.

Nakamura, K., 1974. Preliminary estimate of global volcanic production rate. In: Furumoto, S., Minikami, T. and Yuhara, K. (Eds), The utilization of volcanic energy. Sandia Laboratories, Albuquerque, New Mexico, 273-284.

Nelson, P.H. and Anderson, L.A., 1992. Physical properties of ash flow tuff from Yucca Mountain, Nevada. Journal of Geophysical Research, 97, 6825-6841.

Neuzil, C. E., 1994. How permeable are clays and shales? Water Resources Research, 30 (2), 145-150.

Nichols, G., 1999. Sedimentology and Stratigraphy. Blackwell Science, Oxford UK.
Ninkovich, D. and Heezen, B. C., 1967. Physical and chemical properties of volcanic glass shards from Pozzolana ash, Thera Island, and from upper and lower ash layers in eastern Mediterranean deep-sea cores. Nature, 213, 582-584.

Ninkovich, D., 1979. Distribution, age and chemical composition of tephra layers in deep-sea sediments off western Indonesia. Journal of Volcanology and Geothermal Research, 5, 67-86.

Nobes, D. C., Mwenifumbo, C. J., Mienert, J., and Blangy, J. P., 1991. The problem of porosity rebound in deep-sea sediment cores: A comparison of laboratory and in-situ physical property measurements, Site 704, Meteor Rise. In: Ciesielski, RF, Kristoffersen, Y., et al, Proceedings of the Ocean Drilling Program, Scientific Results, 114, College Station, TX. 711-716.

Noble, D. C., 1967. Sodium, potassium and ferrous iron contents of some secondarily hydrated natural silicic glasses. American Mineralogist, 52, 280-286.

Nordgard Bolas, H. M. and Hermanrud, C., 2002. Rock stress in sedimentary basins - implications for trap integrity. In: Koestler, A. G. and Hinsdale, R., (Eds) Hydrocarbon Seal Quantification, Norwegian Petroleum Society (NPF), Special Publication, Elsevier, Amsterdam. 17-35.

Normark, W. R., Moore, J. G., and Torresan, M. E., 1993. Giant volcano-related landslides and the development of the Hawaiian Islands. In: Schwab, W. C., Lee, H. J., and Twichell, D. C. (Eds), Submarine Landslides: Selected Studies in the U.S. Exclusive Economic Zone. United States Geological Survey Bulletin 2002, 184-196.

North, C. P. and Boering, M., 1999. Spectral gamma-ray logging for facies discrimination in mixed fluvial-eolian successions: A cautionary tale. American Association of Petroleum Geologists Bulletin, 83 (1), 155-169.

NZOG, 1995. Cheal-1 well completion report PPL38707. Petroleum Report Series, PR 2179, Crown Minerals, New Zealand.

O'Brien, G. W., Lisk, M., Duddy, I. R, Hamilton, J., and Woods P.,1999. Plate convergence, foreland development and fault reactivation: Primary controls on brine migration, thermal histories and trap breach in the Timor Sea, Australia. Marine and Petroleum Geology, 16, 533-560.

Olson, R. E. and Mitronovas, F., 1962. Shear strength and consolidation characteristics of calcium and magnesium illite. Clays and clay minerals; 9th National Conference of Clays and Clay Minerals.

Ostermeier, R. M., Pelletier, J. H., Winker, C. D., and Nicholson, J. W., 2001. Trends in shallow sediment pore pressures. Proceedings of the Society of Petroleum Engineers/ International Association of Drilling Contractors Drilling Conference, 1-11.

Peltonen, C., Marcussen, Ø., Bjørlykke, K. and Jahren, J., 2008. Mineralogical control on mudstone compaction ; a study of Late Cretaceous to Early Tertiary mudstones of the Vøring and Møre basins, Norwegian Sea. Petroleum Geoscience, 14, 127-138.

Pilaar, W. F. H. and Wakefield, L. L., 1978. Structural and stratigraphic evolution of the Taranaki basin, offshore North Island New Zealand. Australian Petroleum Exploration Association Journal, 18, 93–101.

Piper, D. J. W. and Savoye, B., 1993. Processes of late Quaternary turbidity current flow and deposition on the Var deep-sea fan, north-west Mediterranean Sea. Sedimentology, 40, 557-582.

Piper, D. J. W., Cochonat, P., and Morrison, M. L., 1999. The sequence of events around the epicenter of the 1929 Grand Banks earthquake: initiation of debris flows and turbidity current inferred from sidescan sonar. Sedimentology, 46, 79–97.

Piper, D. J. W., Shor, A. N., Farre, J. A., O'Connell, S., and Jacobi, R., 1985. Sediment slides around the epicenter of the 1929 Grand Banks earthquake. Geology, 13, 538-541.

Pirmez, C., Hiscott, R. N., and Kronen, J. K., Jr., 1997. Sandy turbidite successions at the base of channel-levee systems of the Amazon Fan revealed by FMS logs and cores: unraveling the facies architecture of large submarine fans. In: Flood, R. D., Piper, D. J. W., Klaus, A., and Peterson, L. C. (Eds.), Proceedings of the Ocean Drilling Program, Scientific Results, 155, College Station, TX, 7–33.

Pittenger, A., Taylor, E., and Bryant, W.R., 1989. The influence of biogenic silica on the geotechnical stratigraphy of the Vøring Plateau, Norwegian Sea. In: Eldholm, O., Thiede, J., Taylor, E., et al, Proceedings of the Ocean Drilling Program, Scientific Results, 104, College Station, TX .923-940.

Posamentier, H. W., and Vail, P. R., 1988. Eustatic controls on clastic deposition. II. Sequence and systems tract models. In: Wilgus, C. K., Hastings, B. S., Kendall, C. G. St. C., Posamentier, H. W., Ross, C. A., Van Wagoner, J. C., (Eds), Sea Level Changes - An Integrated Approach, Society of Economic Paleontologists, Mineralogists, Special Publication, 42, 125-154.

Posamentier, H. W., Jervey, M. T and Vail P. R., 1988. Eustatic controls on clastic deposition, I. Conceptual framework. In: Wilgus, C. K., Hastings, B. S., Kendall, C. G. St. C., Posamentier, H. W., Ross C. A. and Van Wagoner, J. C. (Eds). Sea-Level Changes: an Integrated Approach, Society of Economic Paleontologists, Mineralogists, Special Publication, 42, 109-124.

Potter, P. E., Maynard, J. B. and Depetris, P. J., 2005. Mud and Mudstone: Introduction and Overview. Springer-Verlag.

Potter, P. E., Maynard, J. B. and Pryor, W. A., 1980. Sedimentology of Shale, Study Guide and Reference Source. New York: Springer-Verlag.

Powers, M. C., 1967. Fluid-release mechanism in compacting marine mudrocks and their importance in oil exploration. American Association of Petroleum Geologists Bulletin, 51, 1240-1254.

Prather, B. E., Booth J. R., and Steffens, G. S., and Craig P. A., 1998. Classification, lithologic calibration, and stratigraphic succession of seismic facies of intraslope basins, deep-Water Gulf of Mexico. American Association of Petroleum Geologists Bulletin, 82(5A), 701–728.

Pudsey, C. J., 2002. The Weddell Sea: contourites and hemipelagites at the northern margin of Weddell Gyre. In: Stow, D. A. V., Pudsey, C. J., Howe, J. A., Faugères, J.-C., Viana, A. R. (Eds), Deep-water contourite systems: Modern drifts and ancient series, seismic and sedimentary characteristics. Geological Society of London Memoir, 22, 289-303.

Reading, H. G., 1963. A sedimentological comparison of the Bude Sandstones with the Northam and Abbotsham Beds of Westward Ho! Proceedings of the Ussher Society, 1, 67-69.

Reading, H. G., 1996. Sedimentary Environments: Processes, Facies and Stratigraphy. Blackwell Science Ltd, London.

Reeder, M. S., Rothwell, G., and Stow, D. A. V., 2000. Influence of sea-level and basin physiography on emplacement of the Herodotus Basin Megaturbidite from the SE Mediterranean. Marine and Petroleum Geology, 17, 125-135.

Revil, A., Cathles, L. M., Shosa, J. D., Pezard, P. A., and De Larouziere F. D., 1998. Capillary sealing in sedimentary basins: A clear field example. Geophysical Research Letters, 25(3), 389-392.

Rhein, M., 1994. The Deep Western Boundary Current: tracers and velocities. Deep-Sea Research, 41, 263-282.

Rider, M. H. 1990. Gamma-ray log shape used as a facies indicator: critical analysis of an oversimplified methodology. In: Hurst, A., Lovell, M. A. and Morton, A. C. (Eds) Geological applications of wireline logs, Geological Society of London, Special Publication, 48, 27-37.

Rider, M. H., 1996. The geological interpretation of well logs, 2nd edition, Houston, Texas, Gulf Publishing.

Rieke, H. and Chilingarian, G. V., 1974. Compaction of argillaceous sediments. Developments in Sedimentology 16, Elsevier Scientific Publishing Company, Amsterdam.

Rollet, N., Logan, G. A., Ryan, G., Judd, A. G., Totterdell, J. M., Glenn, K., Jones, A. T., Kroh, F., Struckmeyer, H. I. M., Kennard, J. M., Earl, K. L., 2009. Shallow gas and fluid migration in the northern Arafura Sea (offshore Northern Australia). Marine and Petroleum Geology, 26(1), 129-147.

Ross, C. R. and Smith, R. L., 1955. Water and other volatiles in volcanic glasses, American Mineralogist, 40, 1071-1089.

Rubey W. W., and Hubbert, M. K., 1959. Role of fluid pressure in mechanics of overthrust faulting: overthrust belt in geosynclinal area of western Wyoming in light of fluidpressure hypothesis. Geological Society of America Bulletin, 70, 167-206.

Sawyer, D. S., et al, 1994. Proceedings of the Ocean Drilling Program, Initial Reports, 149, College Station, TX.

Scaglioni, P., Ruvo, L., and Cozzi, M., 2006. Implicit net-to-gross in the petrophysical characterization of thin-layered reservoirs. Petroleum Geoscience, 12, 325-333.

Schacht, U., Wallmann, K., Kutterolf, S. and Schmidt, M., 2008. Volcanogenic sediment-seawater interactions and the geochemistry of pore waters. Chemical Geology, 249, 321-338.

Schefuss, E., Versteegh G. J. M, Jansen, J. H. F, and Sinninghe Damsté, J. S., 2001. Marine and terrigenous lipids in southeast Atlantic sediments (Leg 175) as paleoenvironmental indicators: initial results. In: Wefer, G., Berger, W. H., and Richter, C. (Eds), Proceedings of the Ocean Drilling Program, Scientific Results, 175, 1-34.

Scheidegger, K. F., Jezek, P. A., and Ninkovich, D., 1978. Chemical and optical studies of glass shards in Pleistocene and Pliocene ash layers from DSDP Site 192, northwestern Pacific Ocean. Journal of Volcanology and Geothermal Research, 4, 99-116.

Schlomer, S. and Krooss, B. M., 1997. Experimental characterisation of the hydrocarbon sealing efficiency of cap rocks. Marine and Petroleum Geology, 14(5), 565-580.

Schneider, F., Potdevin, J. L., Wolf, S., and Faille, I., 1996. Mechanical and chemical compaction model for sedimentary basin simulators. Tectonophysics, 263(1-4), 307-317.

Schowalter, T. T., 1979. Mechanics of secondary hydrocarbon migration and entrapment. American Association of Petroleum Geologists Bulletin, 63, 723-760.

Sclater, J. G. and Christie, P. A. F.,1980. Continental stretching: an explanation of the post mid Cretaceous subsidence of the Central North Sea Basin. Journal of Geophysical Research, 85, 3711-3739.

Selley, R. C., 1998. Elements of Petroleum Geology, Academic Press, San Diego, CA.

Serra, O. and Sulpice, L., 1975. Sedimentological analysis of shale-sand series from well logs. Transactions of the SPWLA 16th Annual Logging Symposium, paper W.

Shanmugam, C., 2008. The constructive functions of tropical cyclones and tsunamis on deep-water sand deposition during sea level highstand: Implications for petroleum exploration. American Association of Petroleum Geologists Bulletin, 92(4), 443-471.

Shanmugam, G., 2000. 50 years of the turbidite paradigm (1950's to 1990's): Deep-water processes and facies model - a critical perspective. Marine and Petrology Geology, 17(2), 285-342.

Shanmugam, G., Spalding, T. D., and Rofheart, D. H., 1993. Process Sedimentology and reservoir quality of deep-marine bottom-current reworked sands (sandy contourites): An example from the Gulf of Mexico. American Association of Petroleum Geologists Bulletin, 77, 1241-1259.

Sharp, J. M., Jr., 1976. Momentum and energy balance equations for compacting sediments. Mathematical Geology, 8, 305-322.

Shepard, F. P. and Emery, K. O., 1973. Congo submarine canyon and fan valley. American Association of Petroleum Geologists Bulletin, 57, 1679-1691.

Shepard, F., 1954. Nomenclature based on sand-silt-clay ratios. Journal of Sedimentary Petrology, 24, 151-158.

Shew, R. D., Tiller G. M., Hackbarth C. J., Rollin D. R., White C. D., 1995. Characterization and modelling of channel and thin-bedded turbidite prospect in the Gulf of Mexico: integration of outcrops, modern analogs and subsurface data: SPE paper 30535, SPE ATCE, 1995, Dallas, 22-25 October.

Shin, H., J. Carlos Santamarina, and Cartwright, J. A., 2008. Contraction-driven shear failure in compacting uncemented sediments. Geology, 36, 931-934.

Sibson, R. H., 1981. Fluid flow accompanying faulting, field evidence and models. In: Simpson, D. W. and Richards, P. G., (Eds), Earthquake prediction an international review. American Geophysical Union Maurice Ewing Series, 4, 593–603.

Sigurdsson, H, et al, 1997. Proceedings of the Ocean Drilling Program, Initial Reports, 165, College Station, TX.

Skempton, A. W., 1970. The consolidation of clays by gravitational compaction. Quarterly Journal of the Geological Society of London, 125, 373–411.

Slatt, R. M., 2003. Importance of shales and mudrocks in oil and gas exploration and reservoir development. In: Scott, E. D., Bouma A. H., and Bryant W. R. (Eds), Siltstones, mudstones and shales: depositional processes and characteristics. SEPM/GCAGS Special Publication, SEPM, 1-22.

Smith, R., 2004. Silled sub-basins to connected tortuous corridors; sediment distribution systems on topographically complex sub-aqueous slopes. In: Lomas, S. A. and Joseph, P. (Eds), Confined turbidite systems. Geological Society of London, Special Publications, 222, 23-43.

Spinelli, G., Mozley, P., Tobin, H., Hoffman, N. and Bellew, G., 2007. Diagenesis, sediment strength, and pore collapse in sediment approaching the Nankai Trough subduction zone. Geological society of America Bulletin, 119, 377-390.

Springer, J., 1993. Decompaction and backstripping with regard to erosion, salt movement, and interlayered bedding. Computers and Geosciences, 19(8), 1115-1125.

Staudigel, H. and Hart, S. R., 1983. Staudigel and Hart, Alteration of basaltic glass: Mechanisms and significance from the oceanic crust-seawater budget. Geochimica et Cosmochimica Acta, 47, 337-350.

Stow, D.A.V. and Shanmugam, G., 1980. Sequence of structures in ancient and modern fine-grained turbidites. Sedimentary Geology, 25, 23-42.

Stow, D.A.V. and Piper, D.J.W., 1984. Deep-water fine-grained sediments: facies models. In, D.A.V. Stow and D.J.W. Piper, (Eds), Fine-grained sediments: deep-water processes and facies, Geological Society of London, Special Publication, 15, 611-646.

Stow, D. A. V. and Holbrook, J. A., 1984. North Atlantic contourites: an overview. In: Stow, D. A. V. and Piper, D. J. W. (Eds), Fine Grained Sediments: Deep-Water Processes and Facies. Geological Society of London, Special Publication, 15, 245-256.

Stow, D. A. V. and Mayall, M., 2000. Deep-water sedimentary systems: New models for the 21st century. Marine and Petroleum Geology, 17, 125-135.

Stow, D. A. V. and Tabrez, A.R., 1998. Hemipelagites; processes, facies and model. In: Stoker, M.S., Evans, D. and Cramp, A. (Eds.) Geological processes on continental margins; sedimentation, mass-wasting and stability. Geological Society Special Publications 129, 317-337.

Stow, D. A. V., 1996. Deep-sea clastics. In: Reading, H. G. (Ed.) Sedimentary Environments and Facies. Blackwell Scientific Publications, Oxford.

Stow, D. A. V., Faugères, J.-C., Howe, J. A., Pudsey, C. J. and Viano, A. R., 2002. Bottom currents, contourites and deep-sea sediment drifts: current state-of-the-art. In: Stow, D. A. V., Pudsey, C. J., Howe, J. A., Faugères, J.-C. and Viana, A.R. (Eds.), Deep-Water Contourite Systems: Modern Drifts and Ancient Series, Seismic and Sedimentary Characteristics. Geological Society of London, Memoir 22, 7–20.

Stow, D. A. V., Faugères, J.-C., Viana, A. and Gonthier, E., 1998. Fossil contourites: a critical review. In: Stow, D. A. V., Faugères, J.-C., (Eds), Contourites, Turbidites and Process Interaction. Sedimentary Geology, 115, 3–31.

Stroncik N. A. and Schmincke, H. U., 2001. Evolution of palagonite: Crystallization, chemical changes, and element budget. Geochemistry, Geophysics, Geosystems, 2, 2000GC000102.

Stroncik, N. A., Schmincke, H. U., 2002. Palagonite –a review. International Journal of Earth Sciences, 91, 680–697.

Sutton, S. J, Ethridge, F. G., Dawson, W. C, and Almon W.R., 2006. Parameters controlling mudstone sealing capacity. Poster presentation at American Association of Petroleum Geologists Annual Convention, Houston, Texas, April 9-12, 2006.

Sutton, S.J., Ethridge, F.G., Almon, W.B., Dawson, W.C., and Edwards, K.K., 2004. Textural and sequence-stratigraphic controls of lower and upper Cretaceous shales, Denver basin, Colorado. American Association of Petroleum Geologists Bulletin, 88, 1185–1206.

Talling, P. J., Amy, L. A., Wynn, R. B., Peakall, J., and Robinson, M., 2004. Beds comprising debrite sandwiched within co-genetic turbidite: origin and widespread occurrence in distal depositional environments. Sedimentology, 51, 163-194.

Tanaka, H. and Locat, J., 1999. A microstructural investigation of Osaka Bay clay: the impact of microfossils on its mechanical behaviour. Canadian Geotechnical Journal, 36, 493–508.

Taylor, B., et al, 1990. Proceedings of the Ocean Drilling Program, Initial Reports, 126, College Station, TX.

Tazaki, K. and Fyfe, W. S., 1992. Diagenetic and hydrothermal mineral alteration observed in Izu-Bonin deep-sea sediments, Leg 126. In: Taylor, B., Fujioka, K., et al, Proceeding of the Ocean Drilling Program, Scientific Results, 126, College Station, TX, 101-112.

Techer, I., Advocat, T., Lancelot, J., Liotard, J-M., 2001. Dissolution kinetics of basaltic glasses: control by solution chemistry and protective effect of the alteration film. Chemical Geology, 176, 235-263.

Terzaghi, K. and Peck, R. B., 1948. Soil Mechanics in Engineering Practice. Wiley, New York; Chapman and Hall, London.

Terzaghi, K., 1925. Erdbaumechanik auf bodenphysikalischer Grundlage. Deuticke, Leipzig.

Terzaghi, K., 1943. Theoretical soil mechanics. Wiley, New York.

Thrasher, G. P. and Cahill, J. P., 1990. Subsurface maps of the Taranaki Basin region, New Zealand. New Zealand Geological Survey report G142.

Tonkin, P.C., and Fraser, A.R., 1991. The Balmoral Field, Block 16/21, UK North Sea. In: Abbotts, I.L. (Ed) United Kingdom Oil and Gas Fields, 25 Years Commemorative Volume, Geological Society of London Memoir, 14, 237 – 243.

Tréhu, A. M., et al, 2003. Proceedings of the Ocean Drilling Program, Initial Reports, 204, College Station, TX.

Tréhu, A. M., Flemings, P. B., Bangs, N. L., Chevallier, J., Gràcia, E., Johnson, J. E., Liu, C. S., Liu, X., Riedel, M., and Torres, M. E., 2004. Feeding methane vents and gas hydrate deposits at south Hydrate Ridge. Geophysical Research Letters, 31, L23310.

Tribble, J. S., Mackenzie, F. T., Urmos, J., O'brien, D. K. and Manghnani, M. H., 1992. Effects of biogenic silica on acoustic and physical properties of clay-rich marine sediments. American Association of Petroleum Geologists Bulletin, 76(6), 792–804.

Tripsanas, E., Piper, D. J. W., Jenner, K. A., and Bryant, W. R., 2008. Submarine mass-transport facies: new perspectives on flow processes from cores on the eastern North American margin. Sedimentology, 46(1), 79-97.

Tucholke, B. E., et al, 2004. Proceedings of the Ocean Drilling Program, Initial Reports, 210, College Station, TX.

Vail, P.R., 1987. Seismic stratigraphy interpretation procedure. In: Bally, A.W. (Ed.), Atlas of Seismic Stratigraphy 27. American Association of Petroleum Geologists Studies in Geology, 1–10.

van der Klugt, S., van der Sijp, J. W. C. M., Geiger, M. E., 1959. Kapuni-1 (N119/03): Exploration well resume and well velocity survey. Ministry of Commerce New Zealand, Unpublished Petroleum Report, PR427.

van Olphen, H., 1977. An introduction to clay colloid chemistry (2nd edition), Wiley, New York.

Vasseur, G., Djeran, M. I., Grunberger, D., Rousset, G., Tessier, D. and Velde, B., 1995. Evolution of structural and physical parameters of clays during experimental compaction. Marine and Petroleum Geology, 12 (8), 941-954.

Velde, B., 1996. Compaction trends of clay-rich deep sea sediments. Marine Geology, 133, 193-201.

Viana, A. R., Faugères, J. -C, and Stow, D. A. V., 1998. Bottom-current-controlled sand deposits - a review of modern shallow- to deep-water environments. Sedimentary Geology, 115(1-4), 53-80.

Volpi, V., Camerlenghi, A., Hillenbrand, C. D., Rebesco, M., and Ivaldi, R., 2003. Effects of biogenic silica on sediment compaction and slope stability on the Pacific margin of the Antarctic Peninsula. Basin Research, 15, 339–363.

von Waltershausen, W. S., 1845. Über die submarinen Ausbrüche in der tertiären Formation des Val di Noto im Vergleich mit verwandten Erscheinungen am Ätna. Gottinger Studien Abteilung, 1, 371-431.

Wang, L., Sarnthein, M., Erlenkeuser, H., Grimalt, J., Grootes, P., Heilig, S., Ivanova, E., Kienast, M., Pelejero, C., and Pflaumann, U., 1999. East Asian monsoon climate during the late Pleistocene: high-resolution sediment records from the South China Sea. Marine Geology, 156, 245-284.

Wang, P., et al, 2000. Proceedings of the Ocean Drilling Program, Initial Reports, 184, College Station, TX.

Wang, Y., Ren Mei-e and Zhu, D. K., 1986. Sediment supply to the continental shelf by the major rivers of China. Journal of the Geological Society of London, 143, 935–944.

Watts, A. B. , Karner, G. D. and Steckler, M. S.,1982. Lithospheric flexure and the evolution of sedimentary basins. Philosophical Transactions of the Royal Society, London, 305, 249-281.

Watts, N. L., 1987. Theoretical aspects of cap-rock and fault seals for single and two phase hydrocarbon columns. Marine and Petroleum Geology, 4, 274-307.

Weaver, C. E., 1989. Clays, muds, and shales: Amsterdam, Elsevier Science Publishers. Developments in Sedimentology 44.

Weaver, P. P. E., Rothwell, R. G., Ebbing, J., Gunn, D., and Hunter, P.M., 1992. Correlation, frequency of emplacement and source directions of megaturbidites on the Madeira Abyssal Plain. Marine Geology, 109, 1-20.

Weber, K. J., 1997. A historical overview of the efforts to predict and quantify trapping features in the exploration phase and in field development planning. In: Moller-Pedersen, P. and Koestler A. G., (Eds), Hydrocarbon seals: Importance for exploration and production, Norwegian Petroleum Society (NPF) Special Publication, 7, 1-13.

Wefer, G., et al, 1998. Proceedings of the Ocean Drilling Program, Initial Reports, 175, College Station, TX.

Weimer, P. 1990. Sequence stratigraphy, facies geometries, and depositional history of the Mississippi Fan, Gulf of Mexico, American Association of Petroleum Geologists Bulletin, 74(4), 425 – 453.

Wentworth, C. K., 1922. A scale of grade and class terms for clastic sediments. Journal of Geology, 30, 377–392.

Williams, L. A. and Crerar, D. A., 1985. Silica diagenesis, II. General mechanisms. Journal of Sedimentary Petrology, 55, 312-321.

Wills, J.M., 1991. The Forties Field, Block 21/10, 22/6a, UK North Sea. Geological Society of London, Memoirs 14, 301-308.

Wilson, M. E. J., Hirano, S., Fergusson, C. L., Steurer, J., and Underwood, M. B., 2003. Data report: Sedimentological and petrographic characteristics of volcanic ashes and siliceous claystones (altered ashes) from Sites 1173, 1174, and 1177, Leg 190. In: Mikada, H., Moore, G. F., Taira, A., Becker, K., Moore, J. C., and Klaus, A. (Eds), Proceedings of the Ocean Drilling Program, Scientific Results, 190/196,1-9.

Worthington, P. F., 2000. Recognition and evaluation of low-resistivity pay. Petroleum Geoscience, 6, 77-92.

Yan, P., Deng, H., Liu, H., Zhirong, Z. and Jiang Y., 2006. The temporal and spatial distribution of volcanism in the South China Sea region. Journal of Asian Earth Sciences, 27, 647–659.

Yang, Y. L. and Aplin, A. C., 1998. Influence of lithology and effective stress on the pore size distribution and modelled permeability of some mudstones from the Norwegian margin. Marine and Petroleum Geology, 15, 163-175.

Yang, Y.L. and Aplin, A.C., 2004. Definition and practical application of mudstone porosity effective stress relationships. Petroleum Geoscience, 10(2), 153-162.

Yang, Y.L. and Aplin, A.C., 2007. Permeability and petrophysical properties of 30 natural mudstones. Journal of Geophysical Research, 112(B3), B03206.

Yao, Y.-J., Wu, N.-Y., Xia, B., Wan, R.-S., 2003. Petroleum geology of the Zengmu basin in the southern South China Sea. Geology in China, 35 (3), 503-513.

Yokokawa, M., 2001. Sedimentary structures of contourites and turbidites observed by X-radiographic prints: samples from Blake-Bahama Outer Ridge and Sohm Abyssal Plain. In: Keigwin, L.D., Rio, D., Acton, G.D., and Arnold, E. (Eds.), Proceedings of the Ocean Drilling Program, Scientific Results, 172, College Station, TX, 1-37.

Young, A., Low, P. F., and McLatchie, A. S., 1964. Permeability studies of argillaceous rocks. Journal of Geophysical Research, 69, 4237-4245.

Zhang, G., Mi, L., Wu, S., Tao, W., He, S., Lu, J., 2007. Deepwater area - The new prospecting targets of northern continental margin of South China Sea. Acta Petrolei Sinica, 28,15–21

Appendices

Appendices

Appendix 1 – Results of laboratory grain-size and porosity analysis on siltstone samples collected from the Urenui Formation, Taranaki Basin. Data are discussed in section 2.3.8. Analysis conducted by Newcastle University.

Appendix 2 – Digital copy of the Caprocks Hemipelagite Database (CD-ROM inside back-cover).

Appendix 1

Urenui Formation sample physical properties data

Onaero Beach - Upper weakly bedded unit

Sample	Clay	Cohesive Silt	Coarse Silt	Sand				
	2μm > X	10 μm >X> 2μm	63 μm >X> 10μm	X > 63 μm	Porosity	Mean Pore radius (nm)	Modelled Kx (m²)	Modelled Kz (m²)
2	19	23	55	3	0.33	1233	2.41E-18	2.05E-18

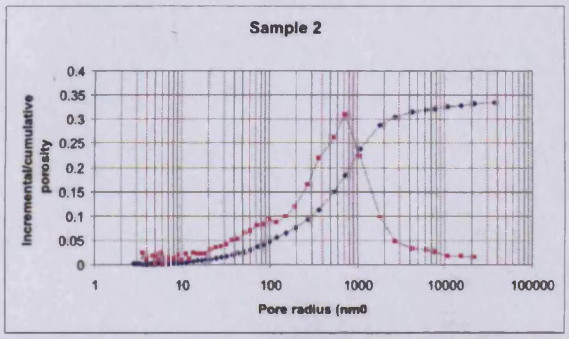

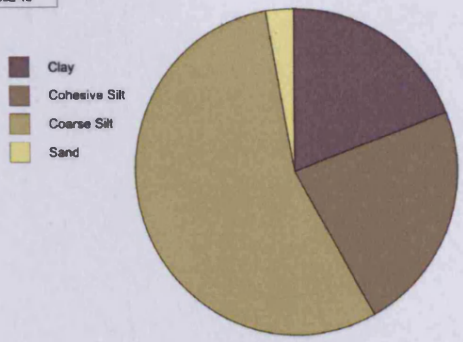

Urenui Formation sample physical properties data

Urenui Beach - Middle channelled and interbedded unit

Sample	Clay	Cohesive Silt	Coarse Silt	Sand				
	2μm > X	10 μm >X> 2μm	63 μm >X> 10μm	X > 63 μm	Porosity	Mean Pore radius (nm)	Modelled Kx (m²)	Modelled Kz (m²)
6	15	13	67	5	0.34	2476	4.88E-18	4.57E-18

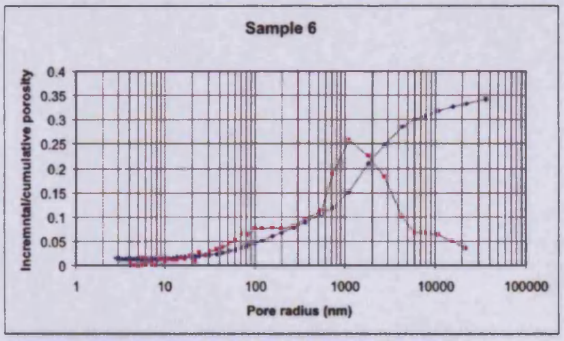

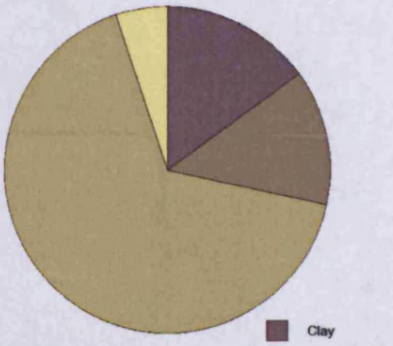

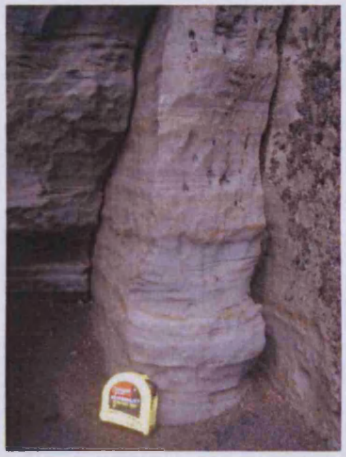

Urenui Formation sample physical properties data

Urenui Beach - Middle channelled and interbedded unit

Sample	Clay	Cohesive Silt	Coarse Silt	Sand				
	2µm > X	10 µm >X> 2µm	63 µm >X> 10µm	X > 63 µm	Porosity	Mean Pore radius (nm)	Modelled Kx (m²)	Modelled Kz (m²)
7	15	14	67	4	0.32	1655	3.17E-16	2.87E-16

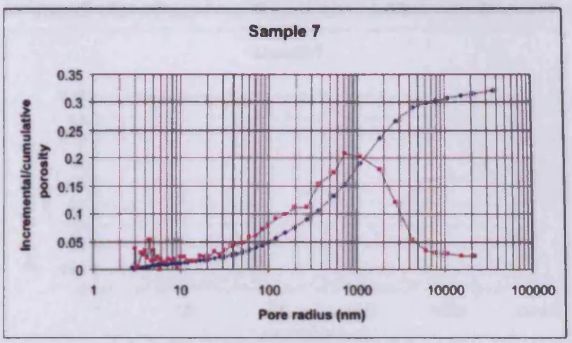

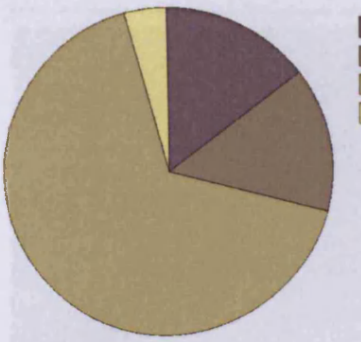

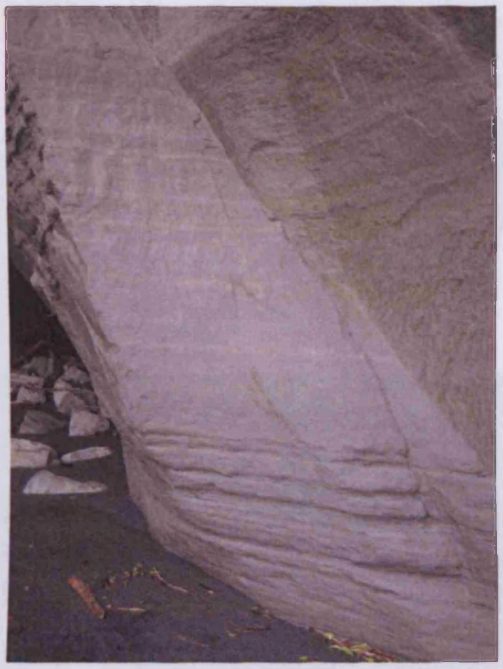

Urenui Formation sample physical properties data

Urenui Beach - Middle channelled and interbedded unit

Sample	Clay	Cohesive Silt	Coarse Silt	Sand				
	2µm > X	10 µm >X> 2µm	63 µm >X> 10µm	X > 63 µm	Porosity	Mean Pore radius (nm)	Modelled Kx (m²)	Modelled Kz (m²)
8	19	22	57	2	0.27	248	4.01E-18	3.11E-18

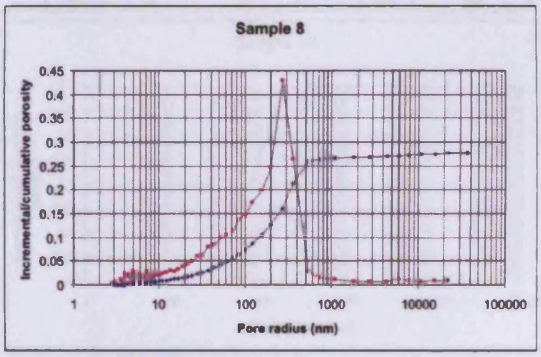

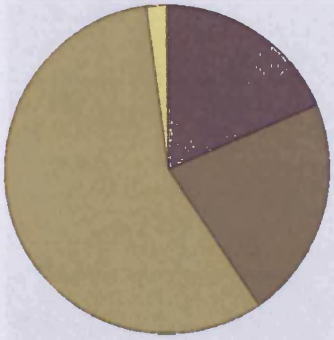

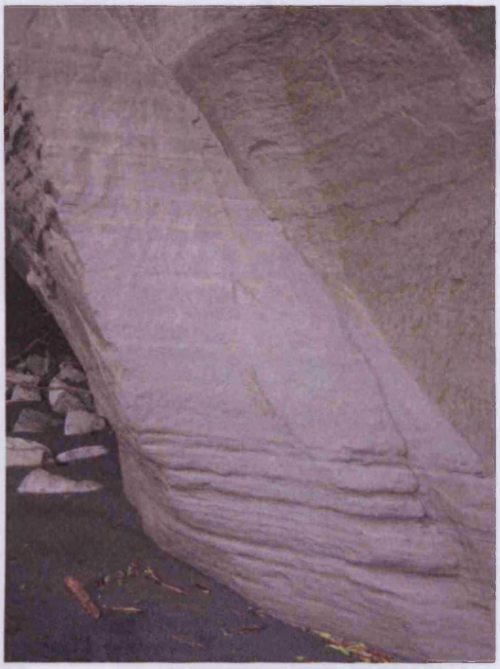

Urenui Formation sample physical properties data

North Wai-iti Beach - Lower weakly bedded unit

Sample	Clay	Cohesive Silt	Coarse Silt	Sand				
	2µm > X	10 µm >X> 2µm	63 µm >X> 10µm	X > 63 µm	Porosity	Mean Pore radius (nm)	Modelled Kx (m²)	Modelled Kz (m²)
9	20	26	49	4	0.26	162	2.51E-19	1.86E-19

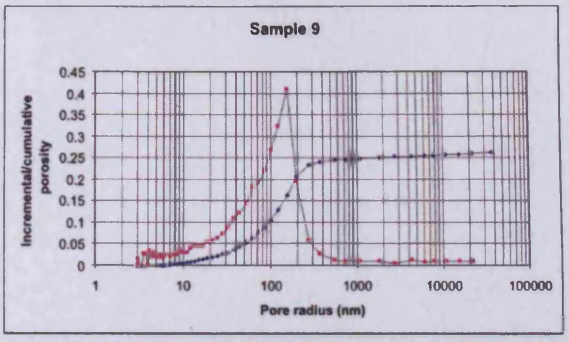

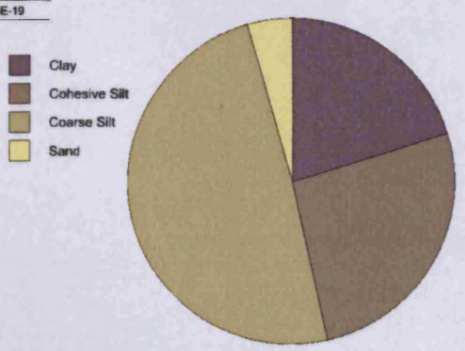

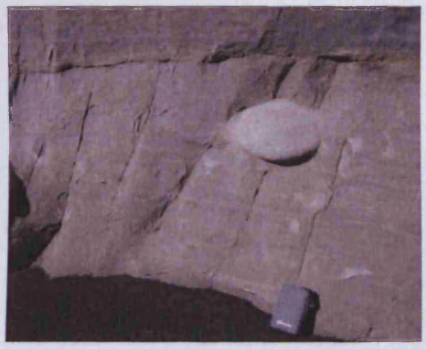

Urenui Formation sample physical properties data

Wai-iti Beach - Lower channelled unit

Sample	Clay	Cohesive Silt	Coarse Silt	Sand				
	2µm > X	10 µm >X> 2µm	63 µm >X> 10µm	X > 63 µm	Porosity	Mean Pore radius (nm)	Modelled Kx (m²)	Modelled Kz (m²)
16	20	28	45	7	0.26	286	4.65E-19	3.45E-19

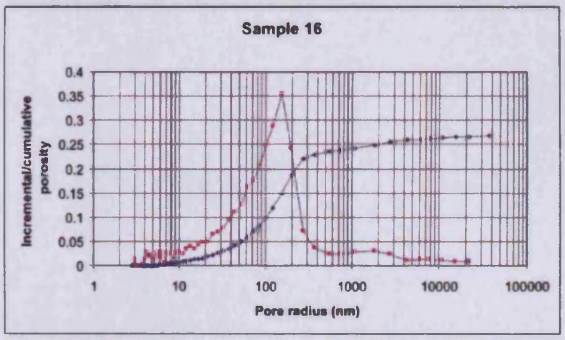

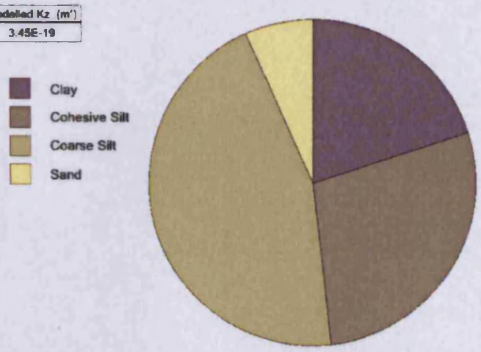

Urenui Formation sample physical properties data

South Wai-iti Beach - Middle weakly bedded unit

Sample	Clay	Cohesive Silt	Coarse Silt	Sand				
21	2µm > X	10 µm >X> 2µm	63 µm >X> 10µm	X > 63 µm	Porosity	Mean Pore radius (nm)	Modelled Kx (m²)	Modelled Kz (m²)
	21	29	48	2	0.26	148	2.30E-19	1.67E-19

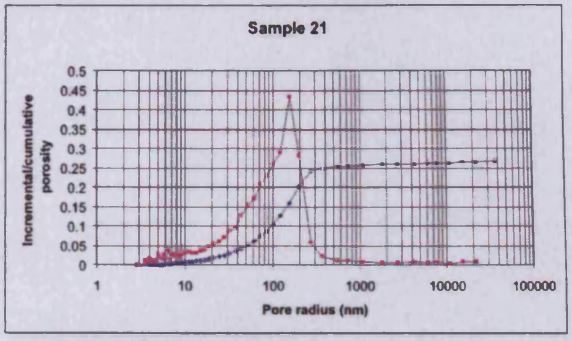

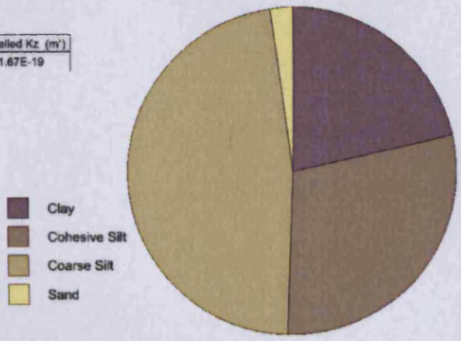

Urenui Formation sample physical properties data

South Wai-iti Beach - Middle weakly bedded unit

Sample	Clay	Cohesive Silt	Coarse Silt	Sand				
22	2µm > X	10 µm >X> 2µm	63 µm >X> 10µm	X > 63 µm	Porosity	Mean Pore radius (nm)	Modelled Kx (m²)	Modelled Kz (m²)
	25	38	37	1	0.25	114	1.74E-19	1.18E-19

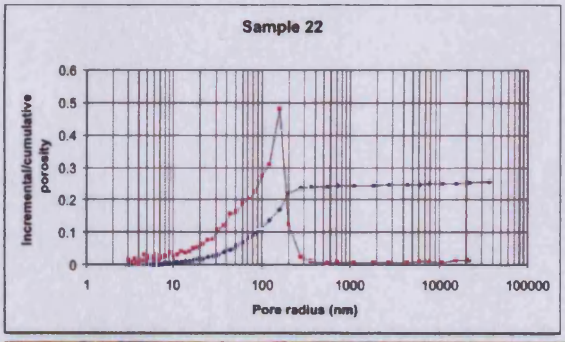

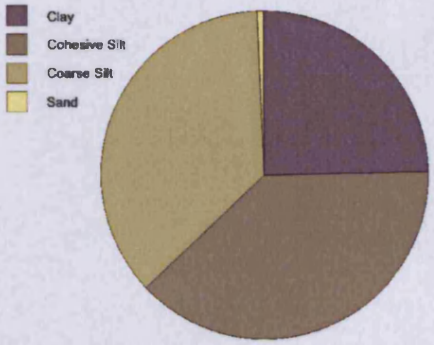

Urenui Formation sample physical properties data

Waiau Beach - Upper channelled unit

Sample	Clay	Cohesive Silt	Coarse Silt	Sand				
	2µm > X	10 µm >X> 2µm	63 µm >X> 10µm	X > 63 µm	Porosity	Mean Pore radius (nm)	Modelled Kx (m²)	Modelled Kz (m²)
25	16	21	57	6	0.3	276	4.62E-18	3.85E-19

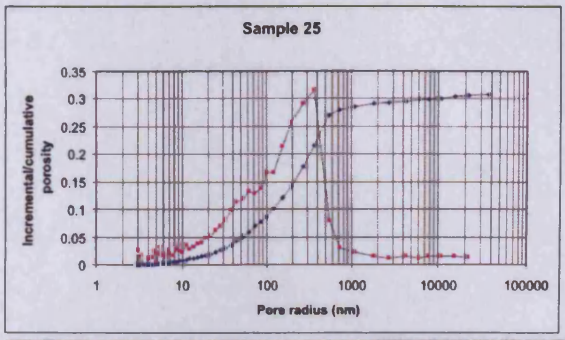

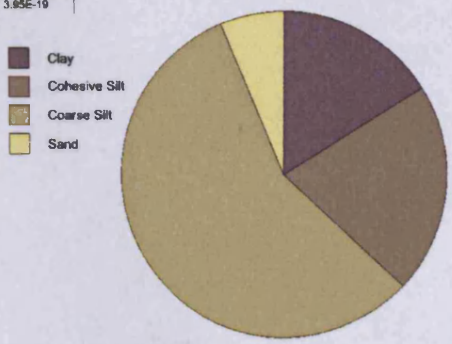

Urenui Formation sample physical properties data

Waiau Beach - Upper channelled unit

Sample	Clay	Cohesive Silt	Coarse Silt	Sand				
	2µm > X	10 µm >X> 2µm	63 µm >X> 10µm	X > 63 µm	Porosity	Mean Pore radius (nm)	Modelled Kx (m²)	Modelled Kz (m²)
26	18	28	45	9	0.25	274	4.18E-18	3.22E-19

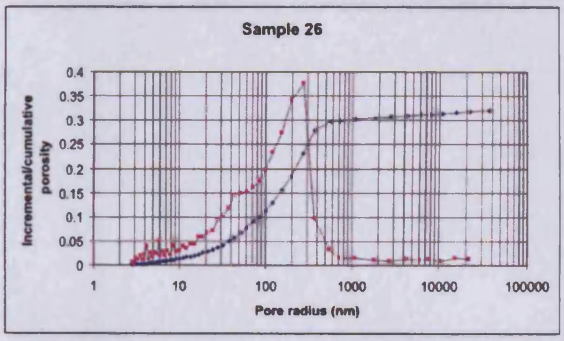

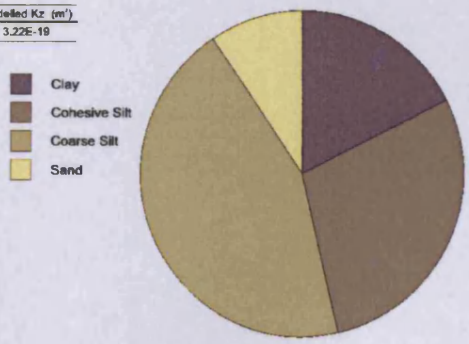

Urenui Formation sample physical properties data

Waiau Beach - Upper channelled unit

Sample	Clay	Cohesive Silt	Coarse Silt	Sand				
	2µm > X	10 µm >X> 2µm	63 µm >X> 10µm	X > 63 µm	Porosity	Mean Pore radius (nm)	Modelled Kx (m²)	Modelled Kz (m²)
29	18	36	44	2	0.32	274	4.74E-19	4.03E-19

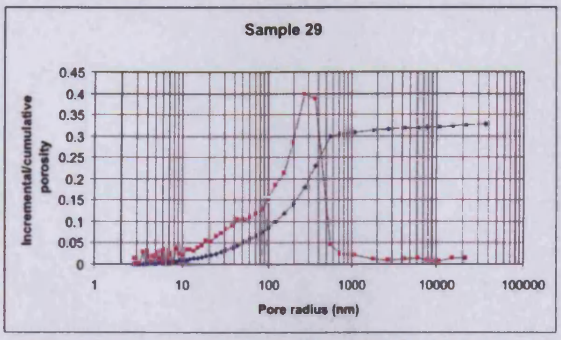

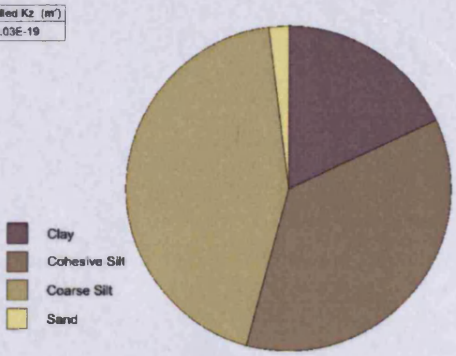

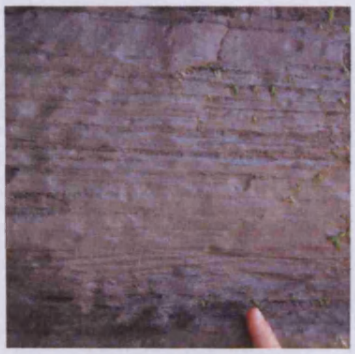

Urenui Formation sample physical properties data

Waiau Beach - Upper channelled unit

Sample	Clay	Cohesive Silt	Coarse Silt	Sand				
	2µm > X	10 µm >X> 2µm	63 µm >X> 10µm	X > 63 µm	Porosity	Mean Pore radius (nm)	Modelled Kx (m²)	Modelled Kz (m²)
29	18	36	44	2	0.32	274	4.74E-19	4.03E-19

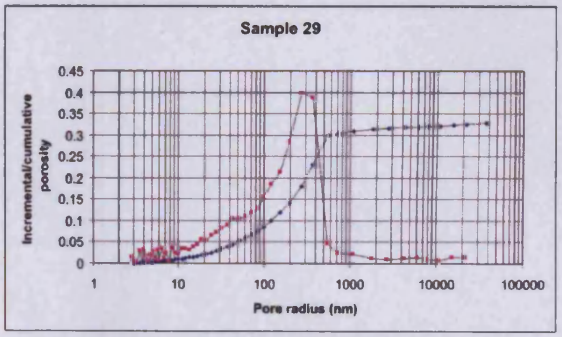

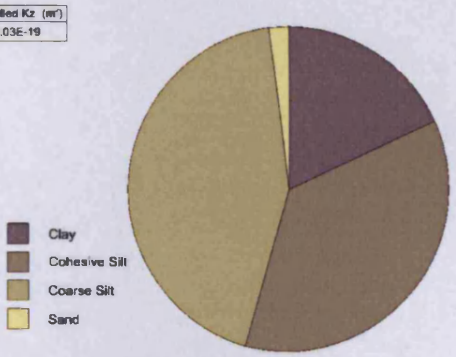

Urenui Formation sample physical properties data

Waiau Beach - Upper channelled unit

Sample	Clay	Cohesive Silt	Coarse Silt	Sand				
	2µm > X	10 µm >X> 2µm	63 µm >X> 10µm	X > 63 µm	Porosity	Mean Pore radius (nm)	Modelled Kx (m²)	Modelled Kz (m²)
30	16	32	43	6	0.31	210	3.55E-19	2.96E-19

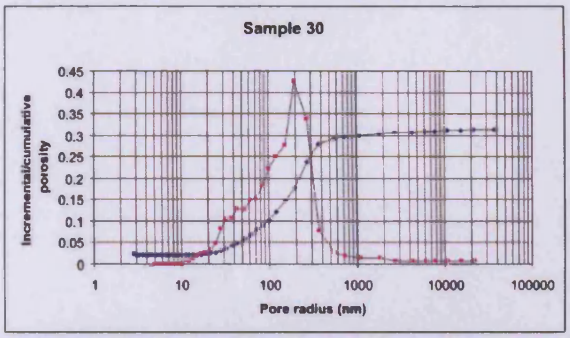

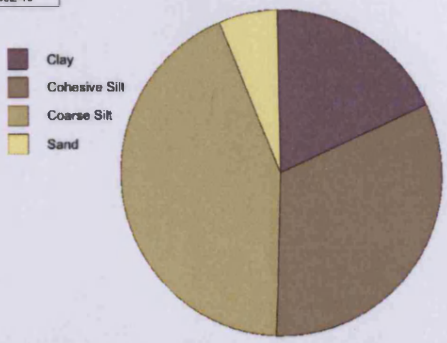

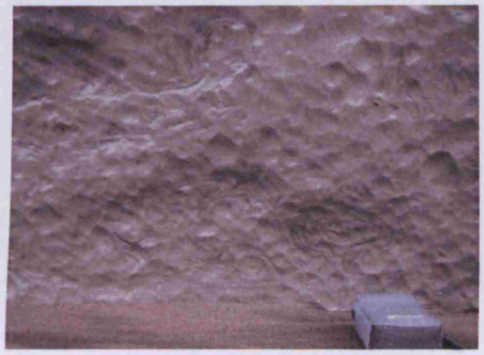

Urenui Formation sample physical properties data

Mimi Beach - Middle weakly bedded unit

Sample	Clay	Cohesive Silt	Coarse Silt	Sand				
	2µm > X	10 µm >X> 2µm	63 µm >X> 10µm	X > 63 µm	Porosity	Mean Pore radius (nm)	Modelled Kx (m²)	Modelled Kz (m²)
33	24	33	39	3	0.26	110	1.72E-19	1.17E-19

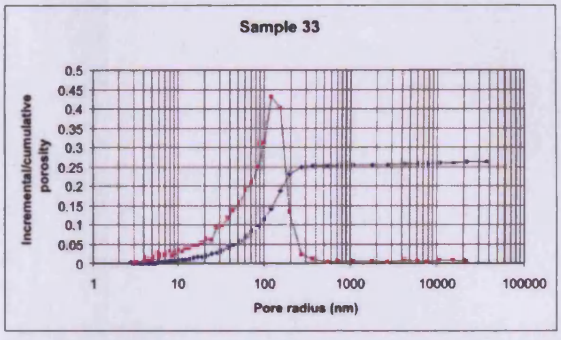

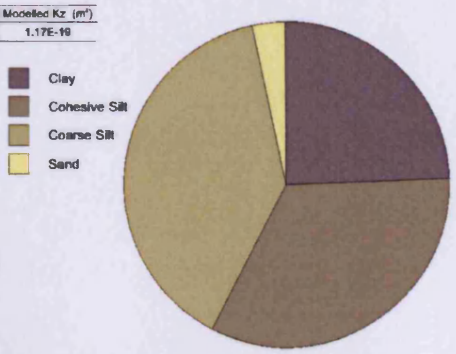

CARDIFF UNIVERSITY